



HAL
open science

Genetics and genomics of black spot disease resistance in garden roses

Diana Carolina Lopez Arias

► **To cite this version:**

Diana Carolina Lopez Arias. Genetics and genomics of black spot disease resistance in garden roses. Plants genetics. Agrocampus Ouest, 2021. English. NNT : 2021NSARC157 . tel-03518898

HAL Id: tel-03518898

<https://univ-angers.hal.science/tel-03518898v1>

Submitted on 15 Mar 2022

HAL is a multi-disciplinary open access archive for the deposit and dissemination of scientific research documents, whether they are published or not. The documents may come from teaching and research institutions in France or abroad, or from public or private research centers.

L'archive ouverte pluridisciplinaire **HAL**, est destinée au dépôt et à la diffusion de documents scientifiques de niveau recherche, publiés ou non, émanant des établissements d'enseignement et de recherche français ou étrangers, des laboratoires publics ou privés.

THESE DE DOCTORAT DE

AGROCAMPUS OUEST

ECOLE DOCTORALE N° 600

Ecole doctorale Ecologie, Géosciences, Agronomie et Alimentation

Spécialité : Génétique, Génomique et Bio-informatique

Par

Diana Carolina LOPEZ ARIAS

Genetics and genomics of black spot disease resistance in garden roses

Thèse présentée et soutenue à Angers, le 7 Juin 2021

Unité de recherche : UMR 1345 Institut de Recherche en Horticulture et Semences

Thèse N° : C-157 _ 2021-15

Rapporteurs avant soutenance :

Mathilde Fagard

Directrice de recherche – INRAE Centre de Versailles-Grignon

Valérie Geffroy

Directrice de recherche – INRAE - Institute of Plant Science - Paris Saclay

Composition du jury :

Président :

Emmanuel Geoffriau

Professeur – Institut Agro, Angers

Examineurs : René Smulder

Docteur – Wageningen University & Research (WUR)

Stan Hokanson

Professeur – University of Minnesota Department of Horticultural Science

Dir. de thèse : Fabrice Foucher

Directeur de recherche – INRAE Centre Pays de la Loire

Co-encadrants : Laurence Hibrand-Saint Oyant

Ingénieure de recherche – INRAE Centre Pays de la Loire

Vanessa Soufflet-Freslon

Maître de conférence – Institut Agro, Angers

Invitée

Sophie Paillard

Chargée de recherche – INRAE Centre Pays de la Loire

Genetics and genomics of black spot disease resistance in garden roses

Diana Carolina Lopez Arias

June 7, 2021

This dissertation is submitted for the degree of Doctor of Philosophy

L'institut Agro | Agrocampus Ouest

COPYRIGHTS

The author of this document authorizes you to share, reproduce, distribute and communicate it under the following conditions:

- You must give appropriate credit, provide a link to the license, and indicate if changes were made. You may do so in any reasonable manner, but not in any way that suggests the licensor endorses you or your use.
- You may not use the material for commercial purposes.
- If you remix, transform, or build upon the material, you may not distribute the modified material.

Consult the full creative commons license in English:

<https://creativecommons.org/licenses/by-nc-nd/2.0/fr/deed.en>

L'auteur du présent document vous autorise à le partager, reproduire, distribuer et communiquer selon les conditions suivantes :

- Vous devez créditer l'oeuvre, intégrer un lien vers la licence et indiquer si des modifications ont été effectuées à l'oeuvre. Vous devez indiquer ces informations par tous les moyens raisonnables, sans toutefois suggérer que l'offrant vous soutient ou soutient la façon dont vous avez utilisé son oeuvre.
- Vous n'êtes pas autorisé à faire un usage commercial de cette oeuvre, tout ou partie du matériel la composant.
- Dans le cas où vous effectuez un remix, que vous transformez, ou créez à partir du matériel composant l'oeuvre originale, vous n'êtes pas autorisé à distribuer ou mettre à disposition l'oeuvre modifiée.

Consultez la licence creative commons complète en français :

<https://creativecommons.org/licenses/by-nc-nd/2.0/fr/deed.fr>



ACKNOWLEDGMENTS

The department of INRAE 'Biologie et Amélioration des Plantes' and the RFI 'Objectif végétal' funded this research project. In particular, I would like to thank RFI 'Objectif végétal' for funding my research mobility to Germany. Thank you to Mathilde Fagard, Valérie Geffroy, Emmanuel Geoffriau, René Smulder and Stan Hokanson, for giving me the honor of being in my PhD jury.

Thank you to Charles-Eric Durel, Professor Thomas Debener and Elisabeth Dirlwanger for accepting to be part of my PhD committee. Your guidance and advice during the comity sessions were very helpful.

A tremendous thank you to Professor Thomas Debener for welcoming me in his laboratory in Hannover and for teaching me all that I needed to know about black spot disease and *Diplocarpon rosae*. Julia Schröter, thank you for your time, patience and teachings. You taught me everything about detached leafves assay and the staining techniques and, for that, me and my team are very grateful. Thank you to Helena and Jannis for their warm welcome and for integrating me in the lab with the other PhD students. And thank you to all the members of Pr. Debener's lab that helped me one way or another, you were all very kind to me.

Tout d'abord, je voudrais remercier la plateforme de génotypage ANAN et la plateforme de microscopie IMAC pour la mise à disposition du matériel et des compétences nécessaires au bon déroulement de cette thèse. Merci tout particulièrement à Fabienne et Aurélia, pour leur aide et leur bonne humeur. J'ai été chouchoutée par toutes les deux et cela me faisait vraiment plaisir d'aller sur le plateau même si c'était pour passer des heures et des heures dans la chambre noire à observer mes échantillons.

A mes encadrants de thèse (officiels et non-officiel),
Merci de m'avoir accueillie au sein de votre équipe et de m'avoir donné la chance de travailler parmi les roses. Vous avez toujours été là pour m'aider et nous avons affronté bien des soucis ensemble (on l'aime notre oïdium !). Merci pour l'autonomie que vous m'avez laissée et de la confiance accordée. Vous avez été les meilleurs encadrants de thèse qu'un doctorant puisse imaginer. J'ai non seulement beaucoup appris de vous mais j'ai aussi reçu beaucoup de bienveillance et de soutien tout au long de ces trois années et demie de thèse. Merci d'avoir rendu les réunions « TheRe » aussi drôles et décontractées. Je suis consciente de ma chance car vous avez contribué à faire de ces années de thèse un souvenir joyeux, pleins d'anecdotes et de bons moments.

Tout particulièrement, merci à mon directeur de thèse, Fabrice Foucher, pour son sang-froid à toute épreuve et pour les leçons (sans le vouloir) de management. Tu es mon exemple de manager idéal et j'espère un jour pouvoir montrer autant de leadership que toi. Et une de tes leçons que je n'oublierai jamais est de toujours revenir « au pourquoi on fait ceci ou cela » car maintenant je peux même prédire quand tu me demanderas : « mais alors Diana, quelle est la question ici ? ».

A Laurence, merci pour tes enseignements. De toi je retiendrais un mot : efficacité. Tu suis tellement de projets et tu connais tellement de choses que je me demande si tu n'es pas la Wonder Woman de GDO. Tu arrives à gérer tellement de choses en même temps, c'est tout bonnement épatant ! Et merci pour toutes ces fois où tu as pris du temps pour m'expliquer des choses quand je venais toquer à la porte de votre bureau en disant : « Boonjouuur » (je parie que tu viens de le lire avec le bon ton).

A Vanessa, merci d'avoir été là pour discuter de boulot mais aussi, et surtout, de tout et de rien. Parce que au-delà de ton rôle d'encadrante, tu as été une très bonne amie, toujours là pour écouter et pour me conseiller. Merci mille fois de m'avoir aidée avec toutes ces histoires de vacances... Sans toi, je ne sais ce que j'aurais pu faire. Et surtout merci à toi et à Pierre, pour avoir donné une chance à Brendan de décrocher ce contrat au GEVES. Cela a été la meilleure chose qui nous soit arrivée pour qu'il puisse rester en France à mes côtés. Je voudrais m'excuser de t'avoir fait souffrir avec l'anglais, ce n'était déjà pas évident d'encadrer ta première thésarde mais en plus une thésarde qui voulait tout faire en anglais ! Ne t'inquiètes pas la soutenance se passera très bien !

Enfin j'aimerais remercier mon encadrante officieuse qui est arrivée en cours de route mais qui a été d'une grande aide tant dans les expériences qu'à la correction de ce manuscrit. Sophie, merci pour tous ces mots d'encouragement, tu as toujours su me remonter le moral et dire exactement ce que j'avais besoin d'entendre. Ton empathie et surtout ta bonne humeur sont tes plus grandes qualités. Je suis contente que tu sois arrivée à GDO. J'espère que tu pourras t'épanouir avec cette superbe équipe car tu le mérites.

A mes collègues,
Merci pour tous ces beaux moments passés en votre compagnie et ce lors d'innombrables pauses cafés, déjeuner raclette et repas d'équipe, parce que je n'ai jamais autant et aussi bien mangé qu'avec vous. Faire partie de GDO et travailler à l'IRHS en général a été la meilleure des expériences de travail. J'aimerais tout particulièrement remercier nos acolytes notateurs (Annie, Jérôme, Tatiana et mes encadrants) avec qui nous avons passé des heures sous le soleil à regarder nos petits rosiers et à nous faire attaquer par les épines quand nous cherchions des feuilles avec des taches. Aux autres collègues et à mes encadrants, merci d'avoir mis la main à la patte pour les essais. C'était toujours un plaisir d'aller échantillonner, broyer et noter en votre compagnie. Enfin je voudrais remercier Julien et Annie pour leurs aides en biologie moléculaire. Un grand merci à Tatiana pour avoir fait les boutures et pour s'être occupée de tous nos bébés plantes en serre comme au champ ! Cela n'a pas été facile pour toi mais tu as toujours gardé un énorme sourire et ça fait plaisir.

A mes ami(e)s et ex-collègues du Groupuscule,
Un grand merci pour les bons moments passés avec vous, les fous rires et les aventures. Parce qu'au-delà du travail présenté dans ce manuscrit, ces trois ans et demi de thèse m'ont apporté des souvenirs que je n'oublierai jamais et surtout de précieux amis. En particulier, merci à Myriam Tiss, la petite sœur et coloc' de bureau. J'espère faire honneur à tes magnifiques photos avec ce manuscrit et qu'on se reverra bientôt. Anaïs et Julien, nous sommes allés dans la même école et pourtant ce n'est qu'à l'INRAE que nous sommes devenus amis. Je suis tellement contente que nous ayons tous travaillé ensemble mais aussi que vous ayez trouvé refuge dans notre bureau de temps en temps pour discuter. La chaise du Psy en a vu des gens : Anne, Annie, Anaïs, Aurélien, Julien Boboss', Alexandre et plein d'autres...

A mes camarades de Greenyd
(Justine, Juliette, Julie, Julia, Lili, Alexis, Matthieu, Wiwi, et plein d'autres !),
Merci pour tous ces bons moments. Nous avons créé une belle association et j'espère que nous pourrons continuer à travailler ensemble même si c'est de loin. Je vous souhaite tous bon vent !

To my sweet Briana,
Thank you so much for your help correcting my first published paper. I am so happy that I met you at that Latino night. You will be my best meeting for sure. Still dreaming to be your neighbor someday but until then let's meet in Colorado next fall!

A mes chers amis de longue date Kenneth, Marina et Maillys,

Merci de m'avoir fait penser à autre chose qu'à mes petits rosiers. Même de loin, vous avez toujours été là pour moi et pendant la rédaction, vous avez été d'une grande aide. J'espère qu'on se retrouvera tous pour fêter cela ou autre chose... À cet été!

Brendan, my love, my friend and my Jiminy cricket (Sorry I had to say it)! Thank you for always believing in me even when I thought I couldn't do it and for helping me find my way whenever I got lost or desperate. You are the best support I could ever have imagined during these years of PhD but mostly during these last months of writing. Thank you for listening to my excited speeches about this work and for always trying to understand whatever crazy theory I would come up with. You are the best part of my life and if this PhD-me did not drive you away, then nothing will!

A mi hermanito cachetón y a mi princesa Gaby,
Gracias por su apoyo y por ser los hermanitos más lindos (y cansones) del mundo. Ustedes dos son mi orgullo de hermana grande. ¿Saben? Sin saberlo me dieron mucho apoyo y el tiempo que pasábamos juntos (aunque poco por la distancia) siempre me permitió olvidar un poco el doctorado. Mi Gaby, gracias por tus lindos regalos, cartas y creaciones. ¡Y Nico, que alegría tener un hermano que siempre estará allí para "recochar" e ir de fiesta!

A mis padres,
Sin los cuales no hubiera tenido la oportunidad de estar donde estoy hoy en día. Quisiera decirles que todos esos sacrificios y momentos difíciles que pasamos cuando llegamos, aquí en Francia, no fueron en vano y este trabajo es la prueba de su suceso como padres. Tengo el orgullo de poder decir que mis padres lo dejaron todo para nosotros y que lucharon desde abajo para darnos las mejores oportunidades. Ustedes son mi ejemplo y mi motivación. El apoyo y amor incondicional que me han dado se refleja en mis conquistas y por eso de todo corazón: ¡Gracias papi y mami!

Encore merci et toutes mes excuses à tous ceux que j'aurais pu oublier dans ces quelques pages...

DEDICATION



CONTENTS

Copyrights	<i>i</i>
Non-plagiarism declaration	<i>iii</i>
Acknowledgments	<i>v</i>
Dedication	<i>ix</i>
Contents	<i>xi</i>
List of figures	<i>xvii</i>
List of Tables	<i>xxi</i>
List of Supplementary Figures	<i>xxii</i>
List of Supplementary tables	<i>xxvi</i>
Synthèse de la thèse en français	<i>xxviii</i>
Chapter 1 : General introduction	<i>38</i>
1. Synopsis	<i>4</i>
2. Plant disease resistance: concept, basis and applications	<i>5</i>
2.1. Plant immune response: from recognition to defense	<i>5</i>
2.1.1. Multilayered plant immunity: preformed and induced defenses in plant	<i>5</i>
2.1.2. The Zigzag model and beyond	<i>7</i>
2.1.3. Plant-pathogen coevolution: an endless arms race.....	<i>12</i>
2.2. Terminology and misconceptions behind plant disease resistance	<i>15</i>
2.2.1. Quantitative – qualitative disease resistance: not a strict duality.....	<i>16</i>
2.2.2. Plant resistance durability	<i>20</i>
2.2.3. The influence of plant Integrity and “age” on disease resistance	<i>21</i>
2.3. Investigating quantitative disease resistance (QDR) and its biological bases	<i>23</i>
2.3.1. Conceptual basis of QTL mapping and its progress over the years	<i>24</i>
2.3.2. Precision and limitations of QTL mapping	<i>25</i>
2.3.3. Mining the genes underlying quantitative resistance loci (QRLs)	<i>28</i>
3. Rose and humans, a long lasting history	<i>31</i>
3.1. Origin of roses and their importance in our society	<i>31</i>
3.1.1. Rose classification over the centuries.....	<i>31</i>
3.1.2. Roses and people	<i>32</i>
3.1.3. The horticultural importance of roses	<i>34</i>
3.1.4. A short history of rose breeding	<i>34</i>
3.1.5. Breeding strategies of yesterday, today and tomorrow	<i>38</i>

3.2.	Evolution of the breeding techniques.....	39
3.2.1.	Improvements in rose hybridization through embryo rescue and ploidy level manipulation	40
3.2.2.	Selection procedures nowadays	40
3.2.3.	Innovation without crossing?	42
4.	The beauty's beast: black spot disease on rose	44
4.1.	Rose nowadays: a threatened beauty?.....	44
4.1.1.	Pathogens threats.....	44
4.1.2.	New restrictions in phytochemical use.....	44
4.2.	Breeding for disease resistance	47
4.2.1.	Introgression programs.....	47
4.2.2.	Disease evaluation throughout the selection process.....	48
4.2.3.	Still room for improvement?	49
4.3.	Diplocarpon rosae, the causal agent of black spot disease on garden roses	51
4.3.1.	Disease symptoms and effect of the environment.....	51
4.3.2.	Hemibiotrophy and its role in the infectious cycle of <i>D. rosae</i>	54
4.3.3.	Diplocarpon rosae diversity and infection strategies	58
4.4.	Rose-Diplocarpon rosae interaction and disease resistance characterization	60
4.4.1.	Plant-pathogen interaction in rose- <i>D. rosae</i> pathosystem.....	60
4.4.2.	Different types of resistance to <i>D. rosae</i>	66
4.4.3.	Beyond categories: rose immune responses to <i>D. rosae</i> infection	69
4.4.4.	Field and laboratory/greenhouse disease assessments	70
5.	Research objectives	72

Chapter 2 : A multi-environment and multi-population quantitative trait loci study of black spot disease resistance in rose **74**

1.	Synopsis	76
2.	Article: Characterization of black spot resistance in diploid roses with qtl detection, meta-analysis and candidate-gene identification	78
2.1.	Key message.....	78
2.2.	Abstract.....	78
2.3.	Keywords.....	78
2.4.	Author contribution	78
2.5.	Introduction	79
2.6.	Material and methods.....	81
2.6.1.	Mapping populations	81
2.6.2.	Disease scoring and statistical analyses.....	82
2.6.3.	Genetic data and linkage mapping	83
2.6.4.	QTL mapping	83
2.6.5.	Meta-QTL analysis.....	84
2.6.6.	NB-encoding genes and candidate-gene mining	85

2.7.	Results	85
2.7.1.	Disease scoring and statistical analyses.....	85
2.8.	Linkage mapping of parental maps.....	86
2.8.1.	QTL analysis.....	89
2.8.2.	Meta-analysis	96
2.8.3.	Gene mining from meta-QTL intervals and NB-encoding genes in <i>Rosa</i> genome.....	97
2.9.	Discussion.....	101
2.9.1.	Importance of environmental effects on BSD scores	101
2.9.2.	New QTLs detected on parental genetic maps	101
2.9.3.	QTLs characterization and two-part model result interpretation	102
2.9.4.	Meta-analysis and gene mining	103
2.10.	Conclusion	105
3.	Additional results	105
3.1.	Disease evolution over years: environmental effects.....	105
3.1.1.	Supplementary explanation for two-part model results	108
3.1.2.	Interval mapping for binary traits.....	113
3.2.	Effects of putative QTLs	118
3.2.1.	Multiple-QTL models fit	119
3.2.2.	Estimated QTL and allelic effects	122
4.	Discussion and critical review.....	127

Chapter 3 : Phenotypic and microscopic study of rose-Diplocarpon rosae interaction during the infection **132**

1.	Synopsis	134
2.	Introduction	135
3.	Materials and methods.....	137
3.1.	Effects of putative QTLs	137
3.1.1.	Rose genotypes studied	137
3.1.2.	Fungal strain chosen	138
3.2.	Pathogen propagation, storage and inoculum preparation	138
3.3.	Plant cultivation	139
3.3.1.	Cuttings for whole plant assay.....	139
3.3.2.	Cuttings for detached leaf assay.....	139
3.4.	Inoculation procedure.....	140
3.4.1.	Whole plant inoculation.....	140
3.4.2.	Detached leaf inoculation	141
3.5.	Macroscopic disease assessment	141
3.6.	Microscopic investigations.....	142
3.6.1.	Microscopic observation of infected leaves from whole plant assay: sample preparation and aniline blue staining	142

3.6.2. Microscopic observation of infected leaves from detached leaf assay: sample preparation and double staining	142
3.7. Image processing and statistical analyses	143
4. Results	145
4.1. Black spot disease (BSD) evaluation on whole plant	145
4.2. Compatible interaction on ‘Old Blush’ leaves.....	145
4.2.1. Diplocarpon rosae infectious cycle on ‘Old Blush’ (OB).....	145
4.2.2. Comparison with another susceptible genotype: the hybrid tea rose ‘pariser charm’ (PC)	149
4.3. Diplocarpon rosae development on <i>Rosa wichurana</i> , a partial resistant genotype	151
4.3.1. Description of <i>R. wichurana</i> – <i>D. rosae</i> interaction over time	151
4.3.2. Leaf age related partial resistance to diplocarpon rosae in <i>Rosa wichurana</i> genotype	153
4.4. Comparison with genotypes exhibiting complete resistance to Diplocarpon rosae and strain characterization	160
4.4.1. A post-penetration resistance in the hybrid shrub cv ‘George Vancouver’ (GV) and the transgenic PC carrying the resistance gene <i>murdr1a</i> (<i>PC:muRdr1a</i>)	162
4.4.2. Pre-penetration resistance for both climbing rose Brite Eyestm (cv ‘radbrite’) (BE) and <i>Rosa majalis</i> (RM).....	165
4.4.3. Different types of callose response according to the interaction type	167
4.4.4. Strain characterization.....	169
5. Discussion	169
5.1. Diplocarpon rosae infectious cycle and important time points for later studies	169
5.2. Strain multiplication: a strategic choice.....	170
5.3. Age-related resistance to black spot disease in <i>Rosa wichurana</i> (RW)	171
5.3.1. Effect of the leaf age on the components of partial resistance.....	171
5.3.2. Difference of interaction type and host response according to leaf age in the partially resistant genotype RW	172
5.4. Cuticle integrity and its importance in partial resistance to black spot disease.....	174
5.5. different types of callose deposition according to the interaction	175
5.5.1. Late hypersensitive response and callose deposition upon epidermal cell invasion by haustorial structures	176
5.5.2. Early hypersensitive response and callose deposition at the penetration site	177
5.5.3. Other plant responses.....	178

<i>Chapter 4 : Comparative transcriptional analysis of compatible and incompatible interactions during Diplocarpon rosae infection</i>	182
1. Synopsis	184
2. Introduction	185
3. Material and methods	187

3.1.	Experimental work	187
3.2.	RNA preparation	188
3.3.	Transcriptome sequencing and computational analyses	189
3.3.1.	Library preparation and sequencing characteristics.....	189
3.3.2.	Illumina adapters trimming in samples and quality control	189
3.3.3.	RNA-seq read mapping and post-mapping quality	190
3.3.4.	Differential expression analysis of RNA-seq data	190
3.3.5.	Complementation of <i>Rosa chinensis</i> 'Old Blush' genome annotation and Functional enrichment analyses of RNA-seq data using gene Ontology	192
3.3.6.	Fungal read mapping for contamination analysis.....	193
3.3.7.	Statistical analyses	194
4.	Results part 1: Mapping and quality assessment.....	196
4.1.	Quality controls.....	196
4.2.	Mapping results	196
5.	Results part 2: Differential expression analysis using RNAseq	197
5.1.	Transcriptomic changes specific to the genotypes	197
5.2.1.	Clustering according to the time after inoculation for OB samples	199
5.2.2.	Number of differentially expressed genes over the infection for OB genotype	199
5.2.3.	Functional analysis using parametric gene set enrichment analysis (PAGE) of OB genes differentially expressed between inoculated and mock samples	202
5.3.1.	Clustering according to the time after inoculation for RW samples	205
5.3.2.	Number of differentially expressed genes over the infection for RW genotype.....	206
5.3.3.	Functional analysis using parametric gene set enrichment analysis (PAGE) of RW differentially expressed genes between inoculated and mock samples.....	207
6.	Results part 3: Investigation of powdery mildew contamination in RNAseq samples	209
6.1.	Quantification of fungal reads from <i>Diplocarpon rosae</i> and <i>Podosphaera pannosa</i>	209
6.1.1.	rRNA removal from rose unmapped reads and mapping to fungal genomes.....	209
6.1.2.	Statistical analyses of fungal read counts.....	210
6.2.	Separated time course analysis for inoculated and mock samples from the RNA-data .	212
6.2.1.	Gene expression profiles over the infection time points and associated enriched GO terms for OB genotype	212
6.2.2.	Gene expression profiles over the infection time points and associated enriched GO terms for RW genotype	220
7.	Discussion	227
7.1.	Validation of <i>Diplocarpon rosae</i> inoculation and assessment of limited presence of powdery mildew through fungal read mapping	227
7.2.	Responses to <i>D. rosae</i> and <i>P. pannosa</i> in an incompatible interaction (with <i>R. wichurana</i> , RW)	229
7.2.1.	PTI response:.....	230

7.3. Response to <i>D. rosae</i> and <i>P. pannosa</i> in a compatible interaction (with <i>R. chinensis</i> ‘Old Blush’, OB)233	
7.4. Limits of this study and perspectives.....	236
Chapter 5 : General discussion and perspectives	240
1. Different types of resistance to black spot disease in <i>Rosa</i> genus.....	242
2. <i>Rosa wichurana</i> resistance leads to a complex incompatible interaction	246
3. <i>Rosa chinensis</i> ‘Old Blush’, a susceptible not so susceptible	249
4. <i>Diplocarpon rosae</i> development in susceptible leaves, a mix of lifestyles?	252
5. Breeding for black spot resistance in garden roses.....	254
Appendix A : Supplementary figures and tables of chapter 2 - Article.....	258
Appendix B : Supplementary figures of chapter 2 – Additional results	270
Appendix C : Supplementary figures of chapter 3.....	284
Appendix D : Supplementary figures of chapter 4	298
References	316

LIST OF FIGURES

Figure 1: Zigzag model illustrating different phases in the plant immune system.....	8
Figure 2: Components of plant disease resistance mechanisms reviewed and presented in Andersen et al. (2018).....	11
Figure 3: Summary of plant-pathogen coevolution strategies adapted from (Anderson et al. 2010; Cook et al. 2015; Aoun 2017)	15
Figure 4: Two aspects of qualitative and quantitative disease resistances (split-up of phenotypic and genetic aspects) presented by Niks et al. in 2015 citing Niks and Kuiper 1983; Franckowiak et al. 1997; Qi et al. 1998; Jafary et al. 2006	17
Figure 5: Basic concept of quantitative trait loci (QTL) analysis for quantitative disease resistance investigation (adapted from Keller et al. 2000; Collard et al. 2005)	27
Figure 6: Illustration of different strategies for molecular dissection of QTLs from Salvi and Tuberosa (2005)	30
Figure 7: <i>Rosa</i> genus classification from morphological classification from Rehder (1940), revised by Wissemann (2003) and newly proposed classification by Debray et al. (2020), based on nuclear and chloroplastic markers	33
Figure 8: Hypothetical representation of the complex origin of the cultivated roses, from Liorzou PhD Thesis in 2016.....	36
Figure 9: Summary of the history of rose breeding in Europe	37
Figure 10: Proposed garden rose breeding scheme that includes disease and pest resistance selection and testing (adapted from Noak 2003, Zlesak 2007, Leus et al, 2007, Debener and Byrne 2014, Leus 2017 and french breeders recommandations).	43
Figure 11: Main diseases affecting rose plants.....	46
Figure 12: Example of scheme for introgression of black spot resistance from <i>R. multiflora</i> genetic background into a cultivated pool (adapted from Debener 2004)	48
Figure 13: Illustration of black spot disease symptoms on different garden roses.....	53
Figure 14: Taxonomic classification of <i>D. rosae</i> according to Brands (2020)	54
Figure 15: <i>Diplocarpon rosae</i> infectious cycle adapted from Drewes-Alvarez 2003, Gachomo 2005 and Horst and Cloyd 2007	55
Figure 16: Schematic representation of different structures built by <i>Diplocarpon rosae</i> during a compatible interaction	57
Figure 17: Updated rose host differential set identifying 13 races of <i>D. rosae</i> from Zlesak et al. (2020)	59
Figure 18: Diversity of symptoms observed in the compatible interactions between <i>D. rosae</i> and 10 rose varieties	62
Figure 19: Summary of the eight interaction types between rose species and <i>D. rosae</i> by Blechert and Debener (2005)	64
Figure 20: Black spot disease scoring data distribution for all years and locations for the three populations.....	88

Figure 21: Representation of individual QTLs and meta-QTLs associated with black spot disease resistance for OW, FW and HW rose populations on the male consensus map 99

Figure 22: Candidate R-genes placed on the pseudochromosomes of *Rosa chinensis* assembly and meta-QTL position..... 100

Figure 23: Overall rainfall during April-September (A) and cumulative rainfall (B) from April to September for the scoring period of three locations (in mm) 107

Figure 24: Histogram of survival time, following infection with *Listeria monocytogenes*, of 116 intercross mice. Approximately 30% of the mice recovered from the infection and survived to the end of the experiment (264 hr). Figure extracted from Broman 2003 109

Figure 25: Scoring data transformation to two types of binary trait (bn and bn1) and histograms of number of hybrids of FW and HW populations for three non-normal data after transformation to binary trait..... 112

Figure 26: QTL mapping associated with black spot disease (BSD) resistance on the male maps for non-normal data of FW and HW populations using interval mapping for binary traits..... 115

Figure 27: Co-localization of the QTL peaks detected with both binary methods (bn and bn1) with the metaQTLs published in Lopez Arias et al. 2020 and the QTL peak detected with the two-part model ... 116

Figure 28: QTL mapping associated with black spot disease (BSD) resistance on the female maps for non-normal data of FW and HW populations using interval mapping for binary traits 117

Figure 29: QTM mapping workflow followed in this study using Rqtl package and K. Broman recommendations in diverse discussions in google groups (<https://groups.google.com/g/rqtl-disc>) 131

Figure 30: Whole plant assay (A to E) and detached leaf assay (F-G) illustrations, picture credits: D. C. Lopez Arias (2019-2020)..... 140

Figure 31: Different types of spots observed in ‘Old Blush’ (OB) and *Rosa wichurana* (RW) infected leaves with *Diplocarpon rosae* from whole plant inoculation in the greenhouse at 28dpi..... 144

Figure 32: Black spot disease (BSD) scores on whole plant inoculated with DiFRA67 strain of *D. rosae* 145

Figure 33: Fluorescent microscope photographs of *Diplocarpon rosae* infectious cycle on the susceptible genotype ‘Old Blush’ 148

Figure 34: Multiscale comparison of *Diplocarpon rosae* infection in two susceptible genotypes (‘Old Blush’, OB and ‘Pariser Charme’, PC) at 9dpi 150

Figure 35: Callose vesicles in fluorescing cells and callose depositions on haustorial structures forming a collar around the haustorial neck on ‘Old Blush’ (OB) and ‘Pariser Charm’ (PC) young leaves infected by *D. rosae* at 9dpi 152

Figure 36: Components of partial resistance measured, at 15dpi, on leaves of different ages and inoculated with DiFRA67 in ‘Old Blush’ (OB) and *R. wichurana* (RW) genotypes 155

Figure 37: Characteristics of *R. wichurana* (RW) reaction to DiFRA67 with brown spots according to the leaf age 156

Figure 38: Macroscopic observations of *R. wichurana* (RW) leaves with different ages at the time of inoculation with DiFRA67 157

Figure 39: Fluorescence microscopy with a double staining of *R. wichurana* (RW) leaves from different ages at 9dpi 158

Figure 40: Different types of callose deposition on *R. x wichurana* (RW) old and young leaves at 9dpi in response to *D. rosae* infection 161

Figure 41: Multiscale investigation of ‘Georges Vancouver’ (GV) responses to infection by the strain DiFRA67 of *D. rosae*..... 163

Figure 42: Multiscale investigation of the transgenic PC::muRdr1A responses to infection by the strain DiFRA67 of *D. rosae*..... 164

Figure 43: Multiscale investigation of the responses on ‘Brite Eyes™’ (BE) (left) and *Rosa majalis* (RM) (right) leaves infected with the strain DiFRA67 of *D. rosae* at 9dpi 166

Figure 44: Co-localization of callose responses to *D. rosae* in different types of interaction at 9dpi 168

Figure 45: Summary of the compatible interactions between roses and DiFRA-67 investigated in this study 179

Figure 46: Summary of the incompatible interactions between resistant roses and DiFRA-67 investigated in this study..... 180

Figure 47: Experimental design for transcriptomic analyses using RNAseq..... 188

Figure 48: RNAseq analysis workflow followed for the host reads 195

Figure 49: Exploratory data analysis with principal component analysis (PCA) and sample hierarchical clustering for all the samples considering genotype, time, condition and repetition as factors of variation 198

Figure 50: Principal component analysis (PCA) of gene expression data in ‘Old Blush’ (OB) leaves challenged by DiFRA67 (I) or water-sprayed (N)..... 199

Figure 51: Number of genes differentially expressed (DEG_LFC1) between inoculated and mock samples at each time point of the infection by *Diplocarpon rosae* for both genotypes ‘Old Blush’ (OB) and *R. x wichurana* (RW) 200

Figure 52: Volcano plots of the genes differentially expressed during *Diplocarpon rosae* infection of the susceptible genotype ‘Old Blush’ (OB)..... 201

Figure 53: Example of enriched GO terms obtained with a PAGE analysis for the response of ‘Old Blush’ (OB) genotype to *Diplocarpon rosae* infection..... 204

Figure 54: Principal component analysis (PCA) of gene expression data in *R. x wichurana* (RW) leaves challenged by DiFRA67 or water-sprayed 205

Figure 55: Volcano plots of the genes differentially expressed during *Diplocarpon rosae* infection of the resistant genotype *R. x wichurana* (RW)..... 207

Figure 56: Example of enriched GO terms obtained with a PAGE analysis for the response of *R. x wichurana* (RW) genotype to *Diplocarpon rosae* infection..... 208

Figure 57: Summary of rRNA composition of unmapped reads (content, pie chart on the left) and the corresponding percent of rRNA aligning with each rRNA database (db_type, pie chart on the right) 209

Figure 58: Fungal read counts in RNAseq samples 211

Figure 59: Barplot of fungal read counts from *Diplocarpon rosae* (A) and *Podosphaera xanthii* (B) for ‘Old Blush’ (OB) and *R. x wichurana* (RW) according to time points and inoculation conditions..... 211

Figure 60: Cluster analysis of genes differentially expressed across time for the inoculated (A) and mock (B) samples for the genotype ‘Old Blush’ (OB)..... 212

Figure 61: Comparison of time course analyses between the group 1 for inoculated samples and the groups 1-8 for mock samples, all groups exhibiting a drop at 3dpi for the susceptible genotype ‘Old Blush’ (OB)..... 216

Figure 62: Comparison of time course analyses between the group 4 for inoculated samples and the group 2 for mock samples, both groups exhibiting a gradual decrease in expression for the susceptible genotype ‘Old Blush’ (OB) 217

Figure 63: Comparison of time course analyses between the group 3 for inoculated samples and the group 6 for mock samples, both groups exhibiting a large peak at 3dpi and stable expression between 5 and 7 dpi for the susceptible genotype ‘Old Blush’ (OB) 218

Figure 64: Comparison of time courses analyses between the group 5 for inoculated samples and the group 4 for mock samples, both groups exhibiting a large peak at 3dpi and an increased expression at 7dpi for the susceptible genotype ‘Old Blush’ (OB) 219

Figure 65: Clustering of genes differentially expressed across time for inoculated (A) and mock (B) samples for the genotype *R. x wichurana* (RW) 220

Figure 66: Comparison of time course analyses between the group 1 for inoculated samples and the group 1 for mock samples, both groups exhibiting a drop at 3dpi for the partial resistant genotype *R. x wichurana* (RW)..... 223

Figure 67: Comparison of time course analyses between the group 5 for inoculated samples and the group 3 for mock samples, both groups exhibiting a decrease of expression at 3dpi and an increased expression at 5 and 7dpi for the partial resistant genotype *R. x wichurana* (RW) 224

Figure 68: Comparison of time course analyses between the group 3 for inoculated samples and the group 4 for mock samples, both groups exhibiting an increase expression at 3dpi and 7dpi for the partial resistant genotype *R. x wichurana* (RW) 225

Figure 69: Comparison of time course analyses between the group 4 for inoculated samples and the group 5 for mock samples, both groups exhibiting an increased expression at 3dpi and a stable expression at 5-7dpi for the partial resistant genotype *R. x wichurana* (RW) 226

Figure 70: Diagram summarizing the interaction types between different rose genotypes and DiFRA67 observed microscopically 246

Figure 71: Proposed model of defense responses to *Diplocarpon rosae* for the susceptible genotype *Rosa chinensis* ‘Old Blush’ and the resistant genotype *Rosa wichurana* 251

Figure 72: Proposition of a spatial model of infection for the hemibiotroph fungus *Diplocarpon rosae* 253

LIST OF TABLES

Table 1: Cloned genes with partial effects contributing to QDR in plants from Pilet-Nayel et al. (2017) completed with recent studies.....	31
Table 2: Summary of black spot disease resistance genes identified to this day.....	68
Table 3: Comparison of <i>Rosa</i> RadRazz 'Knock out®' responses to different isolates from several races according to three studies.....	71
Table 4 Summary of the SSR and SNP-based linkage maps for OW population and the common markers with other populations.....	92
Table 5 : Summary of QTL for black spot disease resistance in OW, FW and HW populations across multiple environments (years and locations) for male maps	93
Table 6: Summary of QTL for black spot disease resistance in OW, FW and HW populations across multiple environments (years and locations) for female maps	95
Table 7: Meta-QTL genomic position and gene mining	96
Table 8: Summary of the analyses performed with a two-part model for non-normal phenotypic distributions	110
Table 9: Summary of QTLs linked to black spot disease resistance found with one dimensional scan with covariate (CIM) and multiple QTL mapping methods in OW, FW and HW populations across multiple environments (years and locations) for the male maps	121
Table 10: Summary of RW alleles contributing to the resistance for the markers at the QTL peaks detected on the male maps for OW, HW and FW populations	125
Table 11: Filter characteristics for each fluorescence microscope used	143
Table 13: Summary of disease responses to DiFRA67 expressed by the studied genotypes.....	169
Table 12: Summary of observations on RW leaves of different ages challenged with DiFRA67.....	174
Table 14: Summary of the separated analysis of mock (NI) and inoculated (I) samples with DiFRA67 for the susceptible genotype <i>Rosa chinensis</i> 'Old Blush' (OB)	215
Table 15: Summary of the separated analysis of mock (NI) and inoculated (I) samples with DiFRA67 for the partial resistant genotype <i>R. wichurana</i> (RW)	222

LIST OF SUPPLEMENTARY FIGURES

Supplementary figure 1: Evaluation zone and rating scale of black spot disease in rose	258
Supplementary figure 2: Overall mean of black spot disease (BSD) scores for three rose populations over several locations and years under natural infections in field	259
Supplementary figure 3: Genetic linkage map of the female parent, <i>Rosa chinensis</i> 'Old Blush', for OW population	260
Supplementary figure 4: Genetic linkage map of the male parent hybrid, <i>Rosa wichurana</i> , for OW population	261
Supplementary figure 5: QTL mapping associated with black spot disease (BSD) resistance using a normal model with an CIM analysis for OW population for the male map	262
Supplementary figure 6: QTL mapping associated with black spot disease resistance using a two-part model approach for non-normally distributed data of FW population for the male map	262
Supplementary figure 7: QTL mapping associated with black spot disease (BSD) resistance for normally distributed data of HW population using a normal model with CIM analysis for the male map	263
Supplementary figure 8: QTL mapping with black spot disease (BSD) resistance using a two-part model approach for non-normally distributed data of HW population for the male map	264
Supplementary figure 9: QTL mapping with black spot disease resistance using a two-part model approach for non-normally distributed data of FW and HW populations for the female maps	265
Supplementary figure 10: Co-localization of the <i>Rdr1</i> genes cluster with the QTLs on A1 from OW and FW female maps	266
Supplementary figure 11: Influence of rain and temperature upon build-up of infection in H.T. roses at Alphonington in 1963 and 1964	270
Supplementary figure 12: Heatmap of disease score evolution for hybrids of OW population (from 2014 to 2018)	271
Supplementary figure 13: Heatmap of disease score evolution for hybrids of FW population (for 2014 and 2018)	272
Supplementary figure 14: Heatmap of disease score evolution for hybrids of HW population planted in Angers (from 2012 to 2014 and for 2018)	273
Supplementary figure 15: Heatmap of disease score evolution for hybrids of HW population planted in Bellegarde (from 2012 to 2014 and for 2018)	274
Supplementary figure 16: Heatmap of disease score evolution for hybrids of HW population planted in Diémoz (from 2012 to 2014 and for 2018)	275
Supplementary figure 17: Example of the sequence of models visited by the forward/backward selection of the <i>stepwiseqtl</i> function for HW population scored in 2013 in Angers	276
Supplementary figure 18: Comparison of LOD curves for the simple interval mapping (SIM) and composite interval mapping (CIM) for HW population for the mean of the scored years in Diémoz	277
Supplementary figure 19: Example of interaction plots between detected QTLs to assess evidence for epistasis	277

Supplementary figure 20: Effect of putative QTLs detected on linkage groups 3, 4 and 5 of the male map for OW population.	278
Supplementary figure 21: Effect of putative QTLs detected on linkage groups 3 and 5 of the male map for FW population.	279
Supplementary figure 22: Effect of putative QTLs detected on linkage groups 3, 5 and 6 of the male map for HW population localized in Angers.....	280
Supplementary figure 23: Effect of putative QTLs detected on linkage groups 3, 5 and 6 of the male map for HW population localized in Bellegarde. The average BSD score for each scoring year was plotted against the genotype at the marker peak of each QTL using the <i>effectplot</i> function of R/qlt package ...	281
Supplementary figure 24: Effect of putative QTLs detected on linkage groups 3, 5 and 6 of the male map for HW population localized in Diémoz. The average BSD score for each scoring year was plotted against the genotype at the marker peak of each QTL using the <i>effectplot</i> function of R/qlt package ...	282
Supplementary figure 25: Callose deposition after <i>D. rosae</i> invasion in ‘Old Blush’ (OB) leaf tissue at 9dpi.....	284
Supplementary figure 26: Evolution of <i>D. rosae</i> hyphal network during the infection of a susceptible host and extent of the reacting area in host tissues upon infection by <i>D. rosae</i>	285
Supplementary figure 27: Fluorescence microscopy Z-stack of an acervulus in an old infection site at 15dpi on ‘Old Blush’ (OB) leaves	286
Supplementary figure 28: Epidermal cells fluorescing when invaded by haustorial structures of DiFRA67	287
Supplementary figure 29: Z-stack of an infection site on PC leaves inoculated with DiFRA67 using a double staining of WGA-Alexa Fluor™ 488 and Aniline blue.....	288
Supplementary figure 30: <i>Rosa wichurana</i> (RW) leaves infected with the strain DiFRA67 at 9dpi and 23dpi and effect of sampling on the resistance to <i>D. rosae</i>	289
Supplementary figure 31: <i>Rosa wichurana</i> (RW) young leaves inoculated with <i>D. rosae</i> at 23dpi ..	290
Supplementary figure 32: ‘George Vancouver’ (GV) leaves inoculated with <i>D. rosae</i> at 23dpi.....	291
Supplementary figure 33: Pc:: <i>muRdR1A</i> leaves inoculated with <i>D. rosae</i> at 23dpi	292
Supplementary figure 34: Callose deposition in incompatible interactions between rose and <i>D. rosae</i> at 9dpi.....	293
Supplementary figure 35: ‘Brite Eyes™’ (BE, right) and <i>Rosa majalis</i> (RM, left) leaves inoculated with <i>D. rosae</i> at 23dpi	294
Supplementary figure 36: Fluorescence intensity used to observe the signals on ‘Pariser Charme’ (PC) and ‘Old Blush’ (OB) leaves challenged with DiFRA6.	295
Supplementary figure 37: Fluorescence intensity used to observe the signals on <i>Rosa wichurana</i> (RW) leaves challenged with DiFRA67.....	296
Supplementary figure 38: Fluorescence intensity used to observe the signals on ‘Georges Vancouver’ (GV), Pc:: <i>muRdr1A</i> , Brite Eyes™ (BE) and <i>Rosa majalis</i> (RM) leaves challenged with DiFRA67	297
Supplementary figure 39: Library preparation by Novogene company using TruSeq™ RNA sample preparation kit from Illumina®	298
Supplementary figure 40: Alignment results and QC results after trimming and mapping.....	299
Supplementary figure 41: Summary of mapping results	300

Supplementary figure 42: Number of reads that did not map on rose genome (Hibrand et al. 2018) for all sequenced samples.....	301
Supplementary figure 43: Percentage of reads unmapped on the rose genome and aligning with the rRNA database (in blue, rRNA) and not aligning with it (in beige, no-rRNA)	312
Supplementary figure 44: Percentage of fungal reads out of the total number of reads for each sample	313
Supplementary figure 45: Plot by sample of fungal read counts for both genotypes.....	314

LIST OF SUPPLEMENTARY TABLES

Supplementary table 1: Common marker list for all populations for the female and male maps.....	267
Supplementary table 2: NB-encoding genes information and position in Rose genome.....	268
Supplementary table 3: Information concerning the eight databases of SortMeRNA software	301
Supplementary table 4: Example of the most highly up-regulated genes according to their $-\log_{10}(\text{padj})$ and their mean \log_2 fold change at each time point for 'Old Blush' (OB) genotype.....	302
Supplementary table 5: Example of the most highly down-regulated genes according to their $-\log_{10}(\text{padj})$ and their mean \log_2 fold change at each time point for 'Old Blush' (OB) genotype	304
Supplementary table 6: Example of the most highly up-regulated genes according to their $-\log_{10}(\text{padj})$ and their mean \log_2 fold change at each time point for <i>R. x wichurana</i> (RW) genotype	307
Supplementary table 7: Example of the most highly down-regulated genes according to their $-\log_{10}(\text{padj})$ and their mean \log_2 fold change at each time point for <i>R. x wichurana</i> (RW) genotype	309

SYNTHESE DE LA THESE EN FRANÇAIS

Si Jupiter voulait donner une reine aux fleurs, la rose serait la reine de toutes les fleurs. Elle est l'ornement de la terre, la plus belle des plantes, l'œil des fleurs, l'émail des prairies, une beauté toujours suave et éclatante ; elle exhale l'amour, attire et fixe Vénus : toutes ses feuilles sont charmantes ; son bouton vermeil s'entrouvre avec une grâce infinie et sourit délicieusement aux zéphirs amoureux.

– Sappho, traduit par Ernest Falconnet. Les petits poèmes grecs.



Descendant OW du croisement entre *Rosa wichurana* et *Rosa chinensis* 'Old Blush' par M. Tisserand

Les fleurs font partie intégrante de notre vie et ont été utilisées tout au long de l'histoire humaine comme symbole et objet de représentation pour l'art et la poésie. Mais parmi les fleurs, une reine comme dirait la poétesse Sappho, la Rose, se détache de par son importance historique, artistique et symbolique. Par ailleurs, les rosiers sont les plantes ornementales les plus importantes dans le monde. La "reine des fleurs" peut prendre de nombreuses formes mais n'est pas entièrement à l'abri des attaques de pathogènes. Comme pour les autres plantes, les rosiers interagissent constamment avec des micro-organismes qui peuvent être des agents pathogènes potentiels. En effet, de nombreux pathogènes pouvant infecter les rosiers ont été décrits et ont plus ou moins d'impacts sur eux. Le pathogène le plus important infectant les rosiers de jardin qui a été décrit jusqu'à présent est *Diplocarpon rosae*, l'agent causant la célèbre maladie des taches noires. Cette maladie n'est pas seulement une menace pour la plante elle-même, mais représente aussi une menace tant pour l'environnement que pour l'homme car elle ne peut être contrôlée que par des applications de fongicides. De plus, la maladie des taches noires représente une menace importante pour l'attractivité des rosiers et, par conséquent, pour l'ensemble de l'industrie de la rose.

La maladie des taches noires est rarement observée dans les productions sous serre car l'humidité peut y être régulée. En revanche, elle est présente en milieu extérieur. La multiplication et le greffage des rosiers de jardin se font principalement sur le terrain, et les rosiers sont généralement utilisés dans les jardins et les aménagements paysagers pour leur valeur esthétique. En raison du caractère pérenne des rosiers de jardin et la capacité de *D. rosae* à survivre l'hiver sur les feuilles mortes, de nouvelles infections peuvent apparaître chaque année si la maladie n'est pas correctement gérée (Münnekhoff et al. 2017). De ce fait, l'impact sur les consommateurs finaux tels que les jardiniers privés et les gestionnaires de jardins publics est important. Cette maladie est traditionnellement gérée par des applications de fongicides préventives qui permettent un bon contrôle des infections. Cependant, pour réduire le risque d'exposition aux produits chimiques, les coûts supplémentaires et la main d'œuvre associés à ce type de gestion, les consommateurs d'aujourd'hui sont davantage demandeurs de variétés de rosier présentant une résistance naturelle (Harp et al. 2009 ; Zlesak et al. 2010, 2017 ; Waliczek et al. 2015b ; Byrne et al. 2019). De plus, les pays européens ayant adopté de nouvelles lois visant à préserver la santé et l'environnement en diminuant l'utilisation des produits agrochimiques, il est nécessaire que la filière s'adapte. Par exemple, en France, des mesures telles que le plan Ecophyto et plus particulièrement la loi Labbé (2014) ont interdit l'utilisation de produits chimiques dans les aménagements paysagers publics et les jardins privés depuis janvier 2017 et 2019, respectivement. Cette nouvelle tendance chez les consommateurs a amené les sélectionneurs et chercheurs à étudier cette maladie dans le but de développer des connaissances, des outils ainsi que des variétés présentant des niveaux de résistance plus élevés mais aussi des résistances plus durables. Depuis les années 1900, la résistance aux maladies a connu un regain d'intérêt dans les programmes de sélection. Malgré cela, peu de variétés cultivées présentent aujourd'hui une réelle résistance face aux différentes maladies : une étude allemande conduite par Schulz et al. en 2009 a montré que seulement 8% des accessions cultivées qui avaient été évaluées (de 6,7% à 8,5%) présentaient une résistance à la maladie des taches noires tandis que 31,5% des accessions de rosiers sauvages étaient résistants à cette maladie. Une autre étude américaine plus récente (Byrne 2015) a également conclu que seulement 6% des rosiers cultivés et commercialisés présentaient une résistance à la maladie des taches noires. Ces études montrent que les variétés cultivées restent encore peu résistantes à la maladie des

taches noires alors que le pool sauvage semble contenir plus d'espèces résistantes. Enfin, une dernière étude française, menée par mon équipe d'accueil (GDO) en collaboration avec sept entreprises de sélection et/ou de production, a évalué la résistance à cette maladie de 45 variétés de rosier en cours de commercialisation en 2016. Ils ont démontré qu'entre 10% et 60% des nouvelles variétés (variation selon les obtenteurs) présentaient moins de 25% de taches noires (Soufflet-Freslon et al. 2021). On voit à travers ces études une sélection de rosiers plus résistants ; toutefois, il reste encore une marge de progression. En effet, le gain de la sélection est généralement plus faible pour des caractères tels que la résistance aux maladies et, souvent, davantage de ressources sont nécessaires pour évaluer la performance d'une plante lorsqu'elle est confrontée à un large éventail de pathogènes (Zlesak 2007).

Dans ce contexte, de nombreux travaux ont été menés sur la résistance totale, avec plusieurs articles décrivant des génotypes qui ne présentent aucun symptôme visible. Dans le cas d'une infection fongique, la résistance totale résulte d'une interaction incompatible entre l'agent pathogène et son hôte durant laquelle aucune sporulation n'est observée et pour laquelle la croissance mycélienne du pathogène est fortement limitée. Ce type de résistance est généralement contrôlée par des gènes majeurs. Pour le pathosystème rosier-*Diplocarpon rosae*, quatre gènes majeurs conduisant à une résistance totale race-spécifique ont été identifiés : *Rdr1* et *Rdr2* sur le chromosome 1 (Malek et Debener 1998 ; Yokoya et al. 2000 ; Malek et al. 2000 ; Kaufmann et al. 2003, 2010 ; Hattendorf et al. 2004 ; Whitaker et al. 2010a ; Terefe-Ayana et al. 2011 ; Menz et al. 2018, 2020), *Rdr3* sur le chromosome 6 (Whitaker et al. 2010a ; Zurn et al. 2020) et *Rdr4* possiblement situé sur le chromosome 5 (Zurn et al. 2018). Outre la résistance totale, la littérature suggère l'existence d'une résistance partielle à la maladie des taches noires (BSD) chez le rosier qui ne semble pas être spécifique d'une race donnée (Xue et Davidson 1998 ; Whitaker et Hokanson 2009 ; Dong et al. 2017). Ce type de résistance n'empêche pas le pathogène d'infecter une plante mais il réduit la sévérité des symptômes (taille des lésions, étendue de la sporulation et dégâts sur la plante entière) en retardant la pénétration du pathogène, son développement mais aussi en réduisant la sporulation (Parlevliet 1985 ; Xue et Davidson 1998 ; Whitaker et Hokanson 2009 ; Dong et al. 2017). La résistance partielle semble réduire la pression épidémique d'un agent pathogène. Il est reconnu qu'il est plus difficile pour les populations pathogènes de s'adapter à ce type de résistance, ce qui la rend donc plus durable et d'autant plus intéressante pour les jardiniers et sélectionneurs (Parlevliet 1993, 2002 ; Johnson 2000 ; Pilet-Nayel et al. 2017). Par conséquent, l'étude de la résistance partielle à la BSD a fait l'objet d'une attention accrue ces dernières années. *Rosa wichurana* Crép. est une espèce semblant présenter ce type de résistance. Il s'agit d'une espèce diploïde originaire de l'est de la Chine et du Japon qui a été introduite au début des années 1880 en Europe et ce, pour sa résistance au froid, sa résistance aux maladies et ses feuilles glabres. *R. x wichurana* a été largement utilisée dans les programmes de sélection en Europe mais aussi sur le continent américain (Lammerts 1945 ; Swim 1948 ; Wylie 1955 ; Xue et Davidson 1998 ; Blechert et Debener 2005 ; Shupert 2006 ; Byrne et al. 2007, 2010 ; Dong et al. 2017). Jusqu'à présent, la résistance partielle de *R. x wichurana* et des génotypes qui en sont dérivés (populations diploïdes et tétraploïdes) a été évaluée suite à des inoculations contrôlées (sur feuilles détachées et sur plante entière) en laboratoire (Whitaker et Hokanson 2009 ; Dong et al. 2017) ou lors d'infections naturelles au champ (Shupert 2006 ; Dong 2014). Les études sur le déterminisme génétique de cette résistance restent cependant limitées. D'une part, Whitaker et Hokanson (2009) ont démontré que, pour les populations diploïdes et tétraploïdes dérivées de *R. x wichurana*, la résistance était caractérisée par un fort effet additif et une bonne capacité

de combinaison générale. D'autre part, Dong et al. (2017) ont calculé l'héritabilité au sens stricte de la résistance partielle à la BSD : elle varie de 0,28 à 0,43. Sur la base de ces résultats, l'intégration d'une résistance partielle stable à la BSD dans des cultivars de rosier semble être faisable et une solution prometteuse pour la filière du rosier. Afin d'identifier les déterminants génétiques contrôlant cette résistance partielle, des analyses QTL (Quantitative Trait Loci) peuvent être menées dans des populations en ségrégation par exemple. La résistance partielle à la maladie des taches noires a été décrite comme ségrégeant de façon quantitative. Une analyse QTL sur plusieurs années et localisations utilisant trois populations en ségrégation connectées par le parent RW (un hybride de *Rosa wichurana*) vous sera présentée dans ce manuscrit ; ces résultats ont fait l'objet d'une publication dans le journal *Theoretical and Applied Genetics*. Par ailleurs, cette étude vient compléter une autre étude QTL menée par le laboratoire de Yan et al. (2019) sur un autre génotype de l'espèce *Rosa wichurana* : le cultivar *R. wichurana* 'Basye's Thornless'.

Il reste difficile d'étudier le déterminisme génétique des caractères tels que la résistance aux maladies. En effet, les gènes qui contrôlent la résistance peuvent agir à différentes étapes de l'infection et être impliqués dans différents mécanismes biologiques : reconnaissance du pathogène par le biais de ses PAMP (acronyme pour Pathogen-Associated Molecular Pattern) ou ses effecteurs, transduction du signal au sein de la plante, mise en place de la résistance. Une connaissance précise de ce qui se passe à un niveau microscopique peut alors apporter plus d'informations sur la façon dont une plante donnée résiste à l'infection. L'hybride de *R. x wichurana* utilisé dans ce projet de thèse a été décrit comme résistant dans différentes localisations et sur plusieurs années (Lopez Arias et al. 2020). De nombreuses divergences peuvent être observées dans la littérature concernant le type de résistance des membres de l'espèce *Rosa wichurana*. En effet, différents auteurs ont proposé plusieurs hypothèses et ne semblent pas s'accorder sur le type de résistance, à savoir pré-pénétration (avant que le pathogène ne pénètre la cuticule) ou post-pénétration (résistances mise en place suite à la pénétration de la cuticule par le pathogène). Il existe plusieurs raisons pouvant expliquer ces divergences comme par exemple les contraintes dues aux techniques microscopiques utilisées, les différences entre les isolats (nature, agressivité et composition) ainsi que des différences de matériel végétal (individus différents représentant l'espèce *R. wichurana* ou type de feuilles évaluées). Ces résultats dénotent une grande variabilité au sein de l'espèce *R. wichurana* ; cette observation a été confirmée par Debener et al. (1998) qui a mis en évidence deux comportements distincts entre deux accessions appartenant à cette même espèce (un génotype complètement résistant aux cinq isolats testés et un autre complètement sensible à ces mêmes isolats). Il était donc nécessaire de mener une étude détaillée au niveau microscopique et macroscopique de la résistance présentée par le génotype de *R. x wichurana* utilisé dans cette étude.

Outre l'identification de gènes majeurs et/ou de QTL de résistance du rosier à la maladie des taches noires, l'étude des mécanismes biologiques impliqués dans cette résistance enrichit la connaissance de ce pathosystème et améliore les chances d'une résistance durable à cette maladie. Ces études moléculaires restent néanmoins peu étayées. Neu et al. (2019) ont étudié les réponses activées suite à l'infection par *Diplocarpon rosae* au cours des premières phases d'une interaction compatible avec le rosier 'Pariser Charme'. L'infection par *D. rosae* semble induire l'expression de gènes codant pour des homologues de PR1, PR5 et PR10, des chitinases et des facteurs de transcription comme WKRY et ERFs (ETS domain-

containing transcription factor) et, de la même manière, l'expression de gènes des voies des phénylpropanoïdes et des flavonoïdes a augmenté. Jusqu'à présent, aucune étude n'a été menée sur les changements transcriptomiques au niveau des feuilles d'un génotype partiellement résistant à la suite d'une infection par *D. rosae*. Comprendre le mécanisme contrôlant ce type de résistance est crucial pour mieux comprendre la réponse des rosiers à une infection par *D. rosae*. La dernière partie de ce manuscrit s'attachera à comprendre les mécanismes de défenses mis en place chez le génotype RW partiellement résistant à la maladie des taches noires (interaction incompatible), et ces mécanismes seront comparés à ceux mis en place dans un contexte sensible, ici, représenté par le génotype sensible *Rosa chinensis* 'Old Blush' (interaction compatible). De plus, étant donné l'importance de la signalisation systémique dans la résistance des plantes (Orłowska et al. 2013) et afin de rester plus proche des conditions naturelles dans lesquelles les plantes sont infectées, nous avons étudié la réponse immunitaire à *D. rosae* sur plantes entières.

L'objectif principal du présent manuscrit est de fournir une étude multi-échelle d'une résistance quantitative à la maladie des taches noires affectant les rosiers de jardin :

(1) identification de loci de résistance quantitative (QRL) stables dans trois populations interconnectées partageant le même parent mâle résistant, apparenté à *Rosa wichurana* (RW), qui a été décrit comme présentant une résistance partielle à la maladie des taches noires sur plusieurs années et dans plusieurs localisations (échelles de la population, de l'individu et du gène) ;

(2) études phénotypique et microscopique de la résistance partielle de RW à *D. rosae* en comparaison à des génotypes complètement sensibles et à des génotypes porteurs de gènes de résistance spécifique afin d'évaluer les interactions entre les différents hôtes et le pathogène au cours du processus d'infection et d'identifier les facteurs influençant la résistance partielle pour l'interaction RW-*D. rosae* (échelles de l'organe et de la cellule) ;

(3) les réponses de défense à *D. rosae* pendant les deux étapes du cycle d'infection (biotrophe et nécrotrophe) pour une interaction compatible et une interaction incompatible (RW) afin d'identifier les réponses immunitaires conduisant à une résistance partielle chez le rosier (échelle du gène).

Tout d'abord, le chapitre 1 de ce manuscrit constitue une synthèse bibliographique qui me permettra de : (i) clarifier des concepts clés de la résistance des plantes aux agents pathogènes, (ii) présenter l'histoire du rosier et de sa sélection ainsi que des enjeux que la filière rencontre, (iii) faire un état de l'art des connaissances sur la maladie des taches noires chez le rosier de jardin. Une présentation succincte du contexte de l'étude a été proposé précédemment ; pour plus d'informations, je vous invite à lire le chapitre 1. Ensuite, les principaux résultats des trois chapitres suivants vous seront brièvement présentés dans cette synthèse ; pour de plus amples explications, vous êtes invité à lire les chapitres correspondants. Enfin, le dernier chapitre (chapitre 5) est une discussion générale permettant de rapprocher tous les résultats obtenus lors de ce projet de recherche et de proposer des hypothèses et modèles explicatifs tout en mettant en perspective les principaux résultats. Ce chapitre ne fera pas l'objet d'un résumé en tant que tel mais certains éléments de la réflexion seront apportés au regard des principaux résultats de ce projet de recherche.

Le chapitre 2 présente la recherche de QTL de résistance à la maladie des taches noires. L'étude génétique a été réalisée sur la base d'une évaluation phénotypique sur des plantes entières lors d'une infection naturelle ; l'échelle d'évaluation repose sur le pourcentage d'infection et le degré de défoliation. L'utilisation d'un jeu de données conséquent (plusieurs années, plusieurs localisations et trois populations connectées par le parent résistant RW) nous a permis d'identifier deux principaux QTL liés à la résistance partielle observée chez RW et de caractériser ces loci et leur effet sur le phénotype. D'une part, ces deux QTL ont montré une grande stabilité et se retrouvaient quel que soit le fond génétique avec lequel le parent résistant était croisée. Comme dans beaucoup de recherches de QTL liés à la résistance aux maladies, les données de phénotypage obtenues pour certaines années et localisations ne présentaient pas de distribution normale. Nous avons donc appliqué des modèles spécifiques comme le modèle « two-part » ou le modèle binaire proposé dans le package R/qtl (Broman 2003 ; Broman and Sen 2009). Les QTL sur le groupe de liaison (GL) B3 affectent à la fois la pénétrance et la sévérité de la maladie tandis que ceux situés sur le GL B5 impactent spécifiquement la pénétrance. Cette connaissance sera utile pour l'exploration des gènes sous-jacents aux QTL ; en effet, elle peut nous aider à être plus critiques quant à l'implication ou non d'un gène dans la résistance à *D. rosae*. D'autre part, nous avons pu montrer que le fond génétique avait une influence sur l'expression de la résistance partielle puisque l'incidence de la maladie sur les trois populations était différente. La détection de QTL spécifiques aux populations sur le GL B4 pour OW et le GL B6 pour HW va également dans ce sens. Suite à l'identification des QTL, une analyse méta-QTL a été menée afin de réduire les intervalles de confiance de ces régions d'intérêt de sorte à ce que la recherche des gènes causaux soit plus efficace et que la sélection des marqueurs pour la sélection assistée par marqueurs (SAM) soit plus précise. Deux méta-QTL ont ainsi été déterminés sur le chromosome 3 et le chromosome 5 (figure 21 reprise ci-dessous). Plusieurs hypothèses peuvent être formulées pour expliquer la présence de deux méta-QTL sur le chromosome 3 lors de la combinaison des QTL avec l'analyse méta-QTL : (1) il est possible que le double méta-QTL soit un artefact dû à un grand réarrangement sur le chromosome 3 ; (2) des données supplémentaires ainsi que l'étude des pics de LOD et des courbes semblent confirmer l'existence de deux méta-QTL sur ce groupe de liaison qui pourraient avoir des effets différents sur le phénotype. En ce qui concerne le GL B5, de nombreux résultats tendent à confirmer de la même manière l'existence de deux méta-QTL. Par ailleurs, une étude expertisée des gènes NLR (nucleotide-binding domain leucine-rich repeat containing) sur le génome 'Old Blush' a permis d'étudier la co-localisation des méta-QTL avec ces gènes NLR. De la même manière, d'autres gènes connus pour intervenir dans la résistance aux pathogènes ont été trouvés dans ces intervalles et peuvent aussi être considérés comme des candidats contrôlant la résistance observée chez RW.

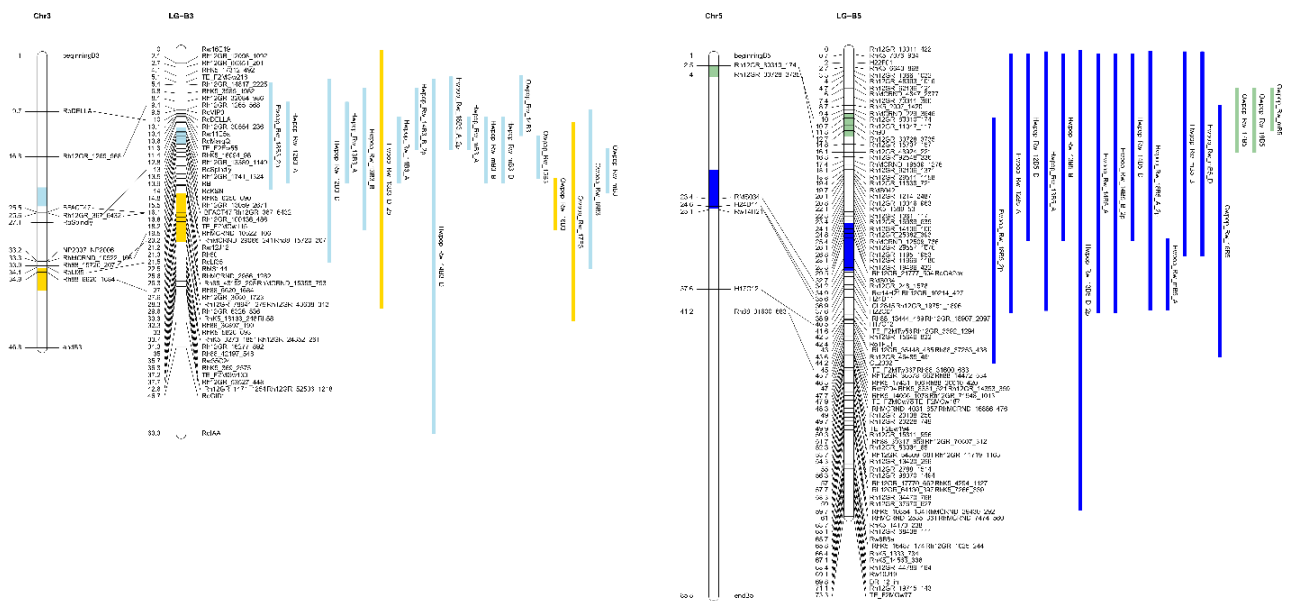


Figure 21 (Chapitre 2) : Représentation des QTL individuels et des méta-QTL associés à la résistance à la maladie des taches noires pour les populations OW, FW et HW sur la carte consensus mâle

Les noms des marqueurs sont à droite et les distances génétiques (en cM) à gauche. Les 19 et 17 QTLs détectés sur B3 et B5, respectivement, dans les trois populations sont projetés sur une carte consensus nouvellement construite. Les noms des QTL sont codés comme suit : NomPop_carte_AnnéeGL_Localisation_méthode. Les intervalles de confiance bayésiens à 95% sont affichés avec des barres verticales dont la longueur est proportionnelle à la largeur de l'intervalle, et le pic du QTL est représenté par une ligne. Les méta-QTL sont représentés en couleur unie sur les GL.

L'environnement a une forte influence sur le développement de la maladie des taches noires au champ. Contrairement à d'autres maladies, l'infection par *D. rosae* ne semble pas s'accumuler année après année. Même si les conditions environnementales d'une année peuvent affecter l'incidence de la maladie l'année suivante, en particulier sur les génotypes résistants, le niveau de résistance semble se maintenir au fil des années. Cependant, une accumulation des infections a été observée, mais seulement au cours de la même année. Ce sont à la fois les précipitations lors des périodes proches de la notation et tout l'historique des pluies entre le début de l'infection au printemps et la période de notation qui semblent affecter le taux d'infection final. Nous avons montré que, dans les populations avec un parent résistant, la pluie accumulée pendant la période d'infection semble affecter grandement les notes de maladie finales tandis que la température moyenne et l'humidité ne semblent pas avoir d'effet sur l'infection.

La compréhension de l'interaction entre *R. x wichurana* et *Diplocarpon rosae* constitue une étape importante pour mieux caractériser la résistance partielle qui ségrège dans les trois populations étudiées. L'objectif du chapitre 3 était donc de présenter de nouvelles connaissances sur l'interaction entre *R. x wichurana* (RW) et *D. rosae* et de préparer l'expérience transcriptomique qui est présentée au chapitre 4. Se concentrer sur « le champ de bataille » qui se déroule au niveau de la feuille et analyser comment l'interaction fonctionne à un niveau microscopique peut nous aider à mieux comprendre l'effet des loci que nous avons détectés et à expliquer ensuite les changements transcriptomiques qui peuvent être observés. De plus, la réaction de RW face à *D. rosae* a été comparée à la réaction de génotypes porteurs de gènes *Rdr* face à ce même pathogène. Tout d'abord, des différences tant au niveau macroscopique que microscopique ont été observées chez RW, ce qui nous a conduits à envisager l'existence d'un effet de

l'âge de la feuille sur l'efficacité de la résistance partielle observée chez ce génotype. Le pourcentage de feuilles infectées, la surface de la feuille avec des symptômes, le pourcentage de la feuille présentant des taches nécrotiques et le nombre de folioles chlorosées se sont avérés significativement différents entre les jeunes et les vieilles feuilles de RW. En revanche, lorsque des taches noires étaient présentes, aucun acervule n'a pu être observé à l'œil nu et la longueur de la plus grande lésion n'était pas significativement différente entre les deux âges des feuilles. Chez le génotype sensible 'Old Blush', aucune différence n'a pu être décrite entre les feuilles d'âge différent. De même, les génotypes portant des gènes majeurs *Rdr* sont restés complètement résistants même lorsque des jeunes feuilles étaient inoculées. Ainsi, pour le pathosystème rosier-*D. rosae*, nous avons démontré, pour la première fois, un effet de l'âge de la feuille sur la résistance partielle. Ces résultats suggèrent également que la résistance spécifique médiée par des gènes majeurs est déjà mise en œuvre et opérationnelle dans les feuilles jeunes alors que la résistance partielle est acquise avec la maturité des feuilles. Par ailleurs, nous avons pu démontrer que la résistance partielle observée dans les feuilles âgées de RW était corrélée, d'une part, à un dépôt précoce de callose au niveau du site de pénétration du champignon, et d'autre part, à une réponse hypersensible (HR) rapide au moment de la pénétration du pathogène.

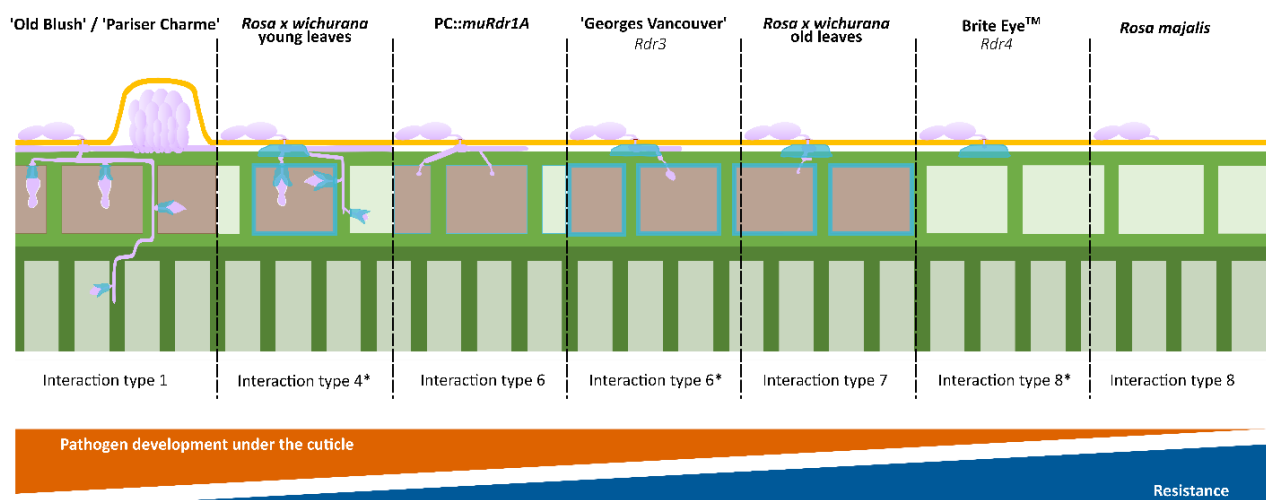


Figure 70 (Chapitre 5) : Diagramme résumant les types d'interaction entre les différents génotypes de rosier et la souche DiFRA67, observés au microscope

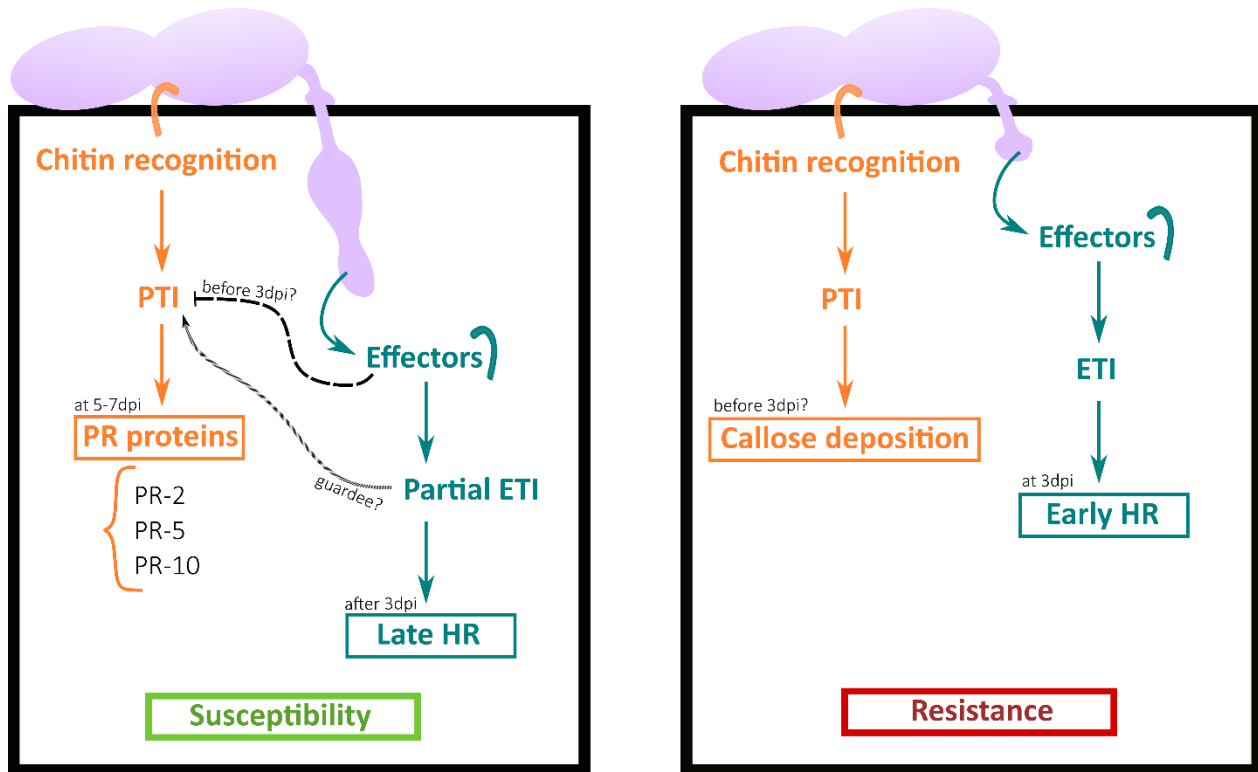
Les génotypes sont classés en partant des sensibles qui présente un développement important de structures fongiques sous la cuticule et pour lesquels une sporulation se produit jusqu'aux très résistants qui ne montrent aucune croissance fongique sous la cuticule. Le dépôt de callose est représenté en bleu. La cuticule est en orange. Les cellules nécrotiques sont représentées en brun et les cellules saines en vert. Les structures fongiques sont en rose. Le type d'interaction est indiqué sous chaque diagramme. Le diagramme regroupe les observations faites à 9 et 23dpi.

NB (*) : Pour les jeunes feuilles de *Rosa wichurana*, la sporulation a été observée dans très peu de cas après 9dpi et pour 'George Vancouver', une croissance fongique supplémentaire sous la cuticule a été observée après 9dpi et pour Brite Eye™, des dépôts de callose aux sites de pénétration ont été observés dans certains cas à 9dpi et dans tous les échantillons à 23dpi.

Enfin, le chapitre 4 décrit l'approche transcriptomique qui a été menée afin de mieux comprendre les mécanismes à l'origine de la résistance présente chez RW et de mieux décrire l'interaction compatible avec *Rosa chinensis* 'Old Blush' (OB). Pour cela, nous avons procédé à une étude comparative des changements transcriptomiques qui se produisent au cours du processus d'infection pour ces deux génotypes, en utilisant une approche temporelle avec une étude multi-séries. Les expériences ont été réalisées en serre en utilisant un test sur plante entière avec quatre points de cinétique (30 minutes, 3 dpi,

5 dpi et 7 dpi) et trois répétitions biologiques indépendantes. Les feuilles vieilles ont été choisies pour mener cette étude étant donné que nous avons montré (chapitre 3) que la résistance partielle de RW s'exprimait dans ces feuilles et non dans les feuilles jeunes. Des résultats étranges ont été obtenus en comparant les échantillons inoculés aux échantillons non inoculés (mocks). Nous avons émis l'hypothèse qu'une infection limitée par l'oïdium, tant dans les échantillons inoculés que dans les échantillons mocks, était la raison pour laquelle nous avons obtenu ces résultats. Les limites de l'étude transcriptomique sont amplement discutées dans le chapitre 4 du manuscrit (pages 211 à 213). Partant de l'hypothèse d'une infection par l'oïdium, j'ai alors considéré que les échantillons inoculés présentaient une réponse à *D. rosae* et une réponse à la présence limitée de *Podosphaera pannosa* (agent pathogène causant l'oïdium chez le rosier) tandis que les échantillons mocks présentaient une réponse à *P. pannosa*. Les analyses transcriptomiques ont permis d'identifier plusieurs centaines de gènes dont l'expression est modulée dès 30 minutes après infection et à chacun des points de cinétique. Nous avons ainsi pu démontrer que la réponse des feuilles vieilles de RW est caractérisée par une réponse rapide de type PTI (immunité basale) qui conduit à l'activation de gènes impliqués dans le dépôt de callose, puis une réponse ETI (immunité déclenchée par des effecteurs fongiques) qui conduit à une HR. Très brièvement, dans les vieilles feuilles de RW, la reconnaissance de la chitine par les protéines PRR (pattern recognition receptor) conduit à une réponse PTI rapide qui consiste à déposer précocement de la callose au niveau des points de pénétration mais aussi au niveau de la paroi cellulaire épidermique. Nous supposons que cette réponse est activée avant 3dpi. Cependant, les papilles de callose au niveau du site de pénétration ne sont pas suffisantes et le pathogène est capable d'envahir une seule cellule. Pendant cette invasion, la callose est encore déposée et des effecteurs sont produits par l'agent pathogène. L'un de ces effecteurs est reconnu par une protéine R à 3dpi, ce qui active une réponse ETI complète qui conduit à une HR rapide de la cellule envahie et parfois des cellules voisines. Cette réponse rapide entraîne une résistance et est caractérisée par l'activation de plusieurs gènes codant pour des récepteurs kinases, des facteurs de transcription (WRK29, 40 or 48), des protéines de résistance comme ACD6 (encoding protein ACCELERATED CELL DEATH 6) qui intervient dans l'activation des voies métaboliques de l'acide salicylique et entraîne la mort cellulaire. Contrairement au génotype résistant RW, la réponse PTI du génotype sensible OB est inhibée dès les premiers stades de l'infection, et une ETI partielle se met en place, impliquant probablement une reconnaissance spécifique d'effecteurs fongiques. En effet, même si de nombreux récepteurs kinases liés à la membrane (protéines PRR) étaient activés à 0 et 3dpi, les gènes associés à la réponse PTI comme les protéines PR ont montré une faible expression pour ces points de cinétique et leur expression n'a augmenté qu'après 5dpi. Ces résultats suggèrent donc une inhibition de la réponse PTI et nous pouvons supposer que l'agent pathogène a libéré des effecteurs qui peuvent modifier/inhiber cette PTI. Pourtant, en même temps que la PTI était inhibée, nous avons observé une augmentation de l'expression de gènes codant pour des protéines impliquées dans la reconnaissance directe et indirecte des effecteurs de l'agent pathogène à 3dpi (protéines de type NBS-LRR par exemple). Ces gènes sont impliqués dans l'activation de la mort cellulaire programmée de l'hôte et des réponses de type HR. Il est intéressant de noter que les cellules épidermiques envahies par les haustoria étaient nécrosées après 3dpi, ce qui est en accord avec les résultats de l'étude transcriptomique. En outre, certains des gènes codant pour des protéines impliquées dans le modèle de garde (protéines NBS-LRR gardant les protéines PRR comme RPM1) sont également fortement exprimés à 3dpi (Anderson et al. 2010 ; Cook et al. 2015). A partir de ces résultats, nous supposons que la reconnaissance de l'inhibition de la PTI par la plante à travers ce modèle de garde pourrait avoir conduit à

la restauration de la PTI ultérieurement (figure 71). De plus, la réponse tardive de type HR observée lorsque le champignon a déjà envahi les cellules épidermiques ainsi que l'expression d'analogues de gènes de résistance (RGA) suggèrent l'existence d'une réaction ETI partielle qui serait initiée plus tardivement chez ce génotype sensible que chez un génotype résistant comme RW. Neu (2018) a également proposé qu'une réaction ETI partielle existait chez 'Pariser Charme' lorsque celui-ci était infecté par la souche allemande DortE4.



***Rosa chinensis* 'Old Blush'**

Rosa x wichurana

Figure 71 (Chapitre 5) : Modèle proposé résumant les réponses de défense à *Diplocarpon rosae* pour le génotype sensible *Rosa chinensis* 'Old Blush' et le génotype résistant hybride de *Rosa wichurana*

Les résultats obtenus dans ce projet de thèse permettent d'envisager de futurs travaux de recherche au sein de l'équipe. Les collaborations avec des équipes étrangères ont été renforcées et de nouvelles techniques ont été développées et seront utiles dans cette quête de compréhension du pathosystème rosier-*D. rosae*. Plusieurs points restent à valider, en particulier dans l'analyse RNAseq. Néanmoins, ce projet de thèse a apporté des connaissances sur les bases génétiques et génomiques des interactions compatible et incompatible entre le rosier et *D. rosae*. Dans le contexte d'évolution constante des attentes des consommateurs et des législations de plus en plus strictes, il est indispensable que la filière du rosier s'adapte et puisse mettre sur le marché des variétés présentant des niveaux de résistance plus élevés et durables. Aider les sélectionneurs est le but final de tous ces projets de recherche et nous espérons pouvoir leur fournir dans un futur proche des marqueurs liés aux gènes majeurs et aux loci contrôlant des résistances quantitatives comme celle observée chez RW.

Chapter 1 : General introduction

There are always flowers for those who want to see them.

– Henri Matisse



'The Fairy' flowers by M. Tisserand

1. SYNOPSIS

Flowers have been around mankind for as long as History can remember. But among the countless flowers that exist in the world, roses have been chosen to be part of our art, our poetry, our happy days as well as the hard ones. Not only are they a part of our History, they are also part of our daily lives. Wherever you look, you see roses: in your parent's/grandparent's garden, your family memories or the small square of nature around the corner. In that way, roses are the most important ornamental plants worldwide. From the wild roses to the roses of our gardens, many centuries of evolution and breeding have happened giving them all the characteristics that we know as of today. From the flower shape, color or sent to the plant architecture, an incredible diversity of characters is available in the complex genus *Rosa* (Liorzou et al. 2016; Debray et al. 2019). The "queen of flowers" can take many forms but is not entirely safe from pathogen attacks. Like for other plants, roses interact constantly with microorganisms that can be potential pathogens. Indeed, many pathogens that can infect roses were described and have more or less impact on them. The most important pathogen in garden roses described so far is *Diplocarpon rosae*, the causal agent of the well-known black spot disease. This disease is not only a threat to the plant itself but is also an immense threat to the rose attractiveness and, therefore, to the whole rose industry.

But disease development is only possible when a pathogen breaks the host barriers. However, plants have learnt to evolve and surround themselves with complex defense responses. Throughout the years, researchers have studied the plant responses to a wide variety of infections. Many terms have been defined and models elaborated to qualify the phenomena behind plant response to pathogen infection. The evolution of this knowledge has accelerated with modern techniques allowing us to understand more deeply the interactions between plants and pathogens. Terms and models have, therefore, evolved and some are being corrected, completed or even completely dropped.

In this chapter, I would like to begin by clarifying the concepts behind plant disease resistance as they are the bases of the work outlined in this manuscript. Then, I will present the roses through their history and the evolution of their breeding throughout the years. I will also present the threats and challenges that the rose industry is facing nowadays so I can introduce the implication for the research area working on disease resistance as knowledge and tools need to be developed to help breeders in their work of improving disease resistance in rose. Subsequently, I will focus my review on the resistance to black spot disease by making a state-of-the-art of the knowledge we have acquired on this disease so far. Finally, I will conclude with a presentation of the rationales and objectives of my thesis.

2. PLANT DISEASE RESISTANCE: CONCEPT, BASIS AND APPLICATIONS

Because of the impact of disease on crops and related economical losses, plant disease resistance has been of principal concern for centuries. Countless studies have investigated plant immune responses and disease resistance for very different pathosystems. Research on plant-pathogen interactions has enlightened us on mechanisms shared or not between different pathosystems and the more we know the more the terminology that has been associated with them evolves and changes. When trying to understand and describe plant immunity and resistance, one can easily get lost in the amount of concepts, definitions and contradictory visions and findings. This is why I will try to unravel the existing concepts in plant-pathogen interactions in light of up-to-date knowledge in the following section. I do not mean to provide definitions carved in stone nor say which concept should be used instead of what but I would like to discuss their applicability in an always more complex vision of interactions between plants and their parasites.

2.1. PLANT IMMUNE RESPONSE: FROM RECOGNITION TO DEFENSE

2.1.1. *MULTILAYERED PLANT IMMUNITY: PREFORMED AND INDUCED DEFENSES IN PLANT*

Although lacking an adaptable immune system like in the animal kingdom, plants have developed a well-organized innate immunity expressed by all cells (not only by specialized immunity cells like in mammals) and rely on systemic signals transported from the infection sites. This innate immunity comprises several structural, chemical and protein-based defenses used to detect but also to stop the invading organisms (Hammond-Kosack and Jones 1996; Nürnberger et al. 2004; Ausubel 2005; Jones and Dangl 2006; Bent and Mackey 2007; Boller and Felix 2009; Cook et al. 2015; Keller et al. 2016). The mechanisms involved in plant immunity can be divided into two categories: (1) preformed or constitutive defense mechanisms and (2) induced defense mechanisms. Constitutive defense responses are expressed at all-time even with no pathogen attack and, therefore, are costly in the absence of disease while induced defenses are expressed upon infection and are only costly when the host responds to infection (Huot et al. 2014; Boots and Best 2018). Although secondary costs may emerge in an immunity that only/mainly relies on induced defenses as damage can occur due to the infection before the immune response takes place, induced defenses are generally favored in response to a virulent parasite or attacker (Agrawal and Karban 1999; Boots and Best 2018). Indeed, a trade-off between constitutive and induced defenses is observed with induced defenses favored particularly in crop plants as valuable agronomic characteristics (growth, reproduction, overall plant fitness, etc.) may be compromised if a plant is constantly defending itself (Moreira et al. 2014, 2018; Huot et al. 2014; Rasmann et al. 2015; Karasov et al. 2017; Agrawal and Hastings 2019). Scientific studies and breeding efforts have, therefore, been concentrated in induced defense responses over constitutive ones.

Despite the recent focus on induced defense responses, constitutive defenses seem to be a major component of host and nonhost resistance (Heath 1997, 2000; Zhang et al. 2008; Niks and Marcel 2009; Vergne et al. 2010; Teixeira 2019). These preformed defenses in plants can take several forms and are the first line of immune defense before pathogen colonization or pest attack happens. They are often found on the plant surface as physical barriers but also as biochemical defenses produced outside and within plant cells and tissues. Preformed defenses provide a natural protection to the entry of a large spectrum of invading organisms (microbes, pests and herbivores). Physical barriers include wax layers, rigid cell walls

or cuticular lipids, cutin, bark, prickles, etc. while biochemical defenses can be preexisting antimicrobial compounds, toxic inhibitors, phytoanticipins, phytohormones, etc. (Doughari 2015). The role of preformed defenses in plant resistance to adapted pathogens (host interaction) has been investigated in several pathosystems and it seems that they play an important role in partial resistance (Ranathunge et al. 2008; Vergne et al. 2010; Lanubile et al. 2015; Zhu et al. 2017). For instance, regarding physical barriers as constitutive defenses, Ranathunge et al. (2008) demonstrated that pre-formed aliphatic suberin in soybean root may delay *Phytophthora sojae* infection leading to strong partial resistance in the cultivar 'Conrad'. Preformed expression of defense-related genes is likely to be responsible for a part of partial resistance against *Magnaporthe oryzae* causing rice blast but not against *Xanthomonas oryzae* pv. *oryzae* causing bacterial blight in rice (Vergne et al. 2010). The authors suggested that constant pressure by *M. oryzae* on rice might have selected towards the maintenance of preformed defenses and in that case, in a recurrent disease pressure setting, preformed defense benefits to rice might outweigh the cost to implement them, which is supported by Hulten et al. study (2006) in *Arabidopsis*. Finally, a comparative analysis of transcriptomes of two apple rootstock cultivars that were not challenged with any pathogen revealed that the resistant genotype exhibited a constitutive expression of defense-related genes such as R proteins, pattern recognition receptors (PRR), proteins for defense hormone biosynthesis and signaling (Zhu et al. 2017). The other layers of plant immunity are defenses that are induced upon pathogen attack. This system of defense is based on a large number of receptors that perform a constant surveillance and are able to detect pathogen presence as well as to transmit the signal of attack. The receptor proteins are strategically located on host membranes to detect pathogen features or factors produced by them. Induced defenses represent a specific response to pathogens as hosts are capable of recognizing the presence of pathogens at different levels during the infection (Jones and Dangl 2006; Dodds and Rathjen 2010). Host and nonhost resistance may result from these induced defenses. A multilayer set of responses is triggered during plant induced immunity upon pathogen recognition that activates a signaling cascade leading to genetic and physiological changes in the hosts. These changes can be divided into (1) induced histological defenses and (2) induced cellular defenses (Doughari 2015). After establishment of infection and to prevent further colonization of the surrounding tissues, host cells induce histological defense systems such as lignification of cell wall which provides an impermeable physical barrier to prevent hyphal penetration and enhance pathogen starvation, suberization to isolate infected cells from healthy ones, abscission of part or whole infected tissues to get rid of infected or invaded tissues or plant parts, tyloses to block the spread of pathogen in vascular organs, and gum and vascular gel deposition to surround feeding structures like haustoria for biotrophic fungi which may cause pathogen starvation and ultimately its death (Doughari 2015). On the other hand, induced cellular defenses include a wide range of cellular changes that aim to stop or kill the invader. Several means can be used by the host plant like induction of cellular defense structures (such as carbohydrate and callose deposition), structural proteins or induced cytoplasmic defense, production of toxic substances for the pathogen, phenolic compounds, phytoalexins, protein and enzyme synthesis, alteration of biosynthetic pathways and activation of programmed cell death leading to hypersensitivity response (Vergne et al. 2010; Doughari 2015). These induced defenses are also subjected to selection because of the constant adaptation on the pathogen/invader side which certainly brings another layer of complexity in the whole immune system of plant (Jones and Dangl 2006).

2.1.2. THE ZIGZAG MODEL AND BEYOND

Countless biochemical changes operate within a cell when a pathogen attacks and this sophisticated defense system is difficult to conceptualize due to its complexity (multilayers, many actors of the immunity, links between them and constant evolution). To capture and describe the complexity of the plant immune system, various conceptual models have been developed. In general, models and in particular 'expository' models find their utility in the integration of restricted empirical data and a set of assumptions to explain complex systems and are an abstract representation of reality (Pritchard and Birch 2014; Cook et al. 2015).

In the 1940s, Harold Flor determined that plants and pathogens interacted with particular combinations of genes (Flor 1942) and, therefore, the first model that tried to explain the plant immune system was proposed by Flor (1971) and was based on a 'gene-for-gene' hypothesis. He proposed that a single dominant host-resistance gene (*R*) would recognize a single dominant avirulence gene (*Avr*) expressed by the pathogen, and this recognition would lead to disease resistance phenotype (Flor 1942, 1955, 1971). Separated studies identified so-called "general elicitors" from microbes that did not allow race specificity determination and were detected by various plant species (Darvill and Albersheim 1984). Later, general elicitors' nature was identified in vertebrate immunity and helped to better characterize concepts in plant immunity (Janeway 1989). Microbes were then considered to possess pathogen-associated molecular patterns (PAMPs) whereas pathogenic ones possess MAMPs (Microbe-associated molecular patterns) and these features were believed and latter demonstrated to be recognized by host pattern recognition receptors (PRRs) as nonself (Janeway 1989; Nürnberger et al. 2004; Ausubel 2005). For a long time, general elicitors and particular *Avrs* were separate and disparate actors of the immunity until an important conceptual advance was proposed with the now well-known zigzag model, which organized both actors around a single multilayered but very comprehensive model (Jones and Dangl 2006).

The zigzag model defines a dichotomy between PTI (PAMP-triggered immunity) and ETI (effector-triggered immunity) with separated immune responses to PAMPs and effectors. It has, therefore, incorporated the discovery of *Avrs* with the gene-for-gene model and the existence of general elicitors, unifying them into a model that discriminates different layers of pathogen recognition while considering the pathogen side and its need to bypass these layers of immunity, which results in an evolutionary pressure on both organisms to fight each other in an endless arms race (see [section 4.1.3](#)). This model includes four phases that can be described as a sequence of actions, each one following each other and involving both host and pathogen responses (see Figure 1). First, PAMPs are recognized by cell surface-localized PRRs during PTI, which leads to a broad-spectrum resistance against a wide range of microbes (in orange in Figure 1). Then, some adapted microbes can produce effectors that allow them to overcome PTI, which results in an effector triggered susceptibility (ETS). Thereafter, intracellular receptors (*R* proteins) may recognize these effectors, activating ETI (in turquoise in Figure 1). As a result, pathogens may evade ETI and restore ETS by evading the recognition through loss or mutation of the recognized effectors or by suppressing ETI with novel effectors. In return, plants may evolve as well and restore ETI by evolving new *R* genes which again can be overcome by the pathogens (Jones and Dangl 2006). The model proposes a

continued co-evolution between hosts and pathogens with natural selection on both sides providing new variability in Avr and R genes (Jones and Dangl 2006; Cook et al. 2015).

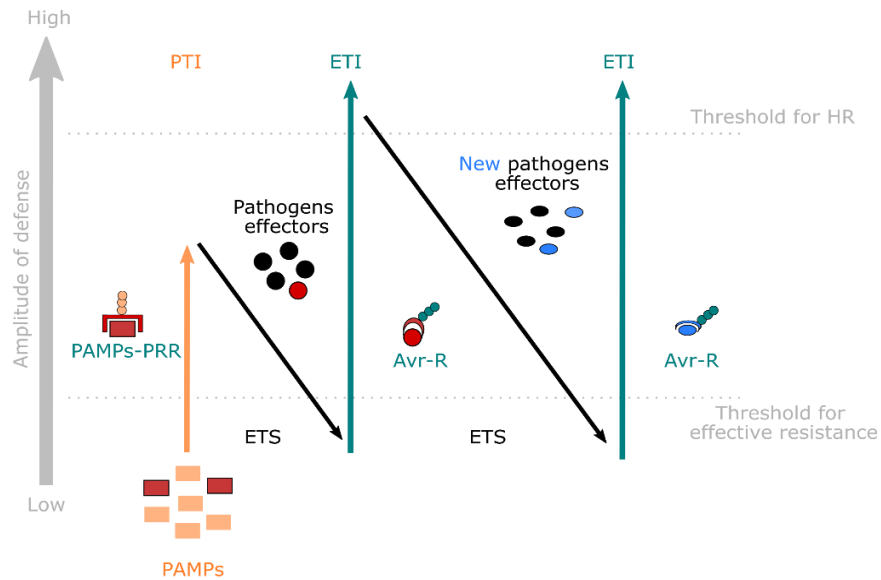


Figure 1: Zigzag model illustrating different phases in the plant immune system

PAMPs: pathogen-associated molecular patterns; PRR: pattern recognition receptor; PTI: PAMP-triggered immunity; ETS: effector triggered susceptibility; ETI: effector-triggered immunity; Avr: avirulence effectors; R: R protein or NB-LRR protein; HR: hypersensitive response; Amplitude of defense is proportional to [PTI-ETS+ETI]. Successful pathogens produce effectors (represented by black circles) or new effectors (represented by black ellipses), which leads to ETS. In some cases, pathogen effectors can be recognized by NB-LRR proteins and form “Avr-R” complexes (recognized pathogen effectors are represented by red circles and new ones by blue ellipses).

Used over a decade now, the zigzag model has become the foundation of plant immunity investigation, and countless reviews and articles have used this concept and the associated terms to describe new and exciting mechanisms in plant immunity. However, some authors have pointed out several missing considerations, misconceptions and drawbacks that appeared to be linked to the PTI-ETI dichotomy and that were taken far beyond the model’s original description and aim (Pritchard and Birch 2014; Andolfo and Ercolano 2015; Cook et al. 2015).

Like any other models, the zigzag model was based on the available observations and knowledge at that time and these observations were also made from a limited number of systems. First, the zigzag model did not take into account the existence of host endogenous elicitors or damage-associated molecular patterns (DAMPs) that may serve as danger signals and activate plant immunity (Boller and Felix 2009). These authors explained that PAMPs or more generally MAMPs, DAMPs and effectors were one and the same type of signal that indicated to the plant a situation of danger. Attempts have been made to incorporate DAMPs in immunity models (Hein et al. 2009; Karban 2011; Cook et al. 2015). Later, it was suggested that adapting the “Danger model” or “Danger theory” (Matzinger 1994, 2001) for plants would broaden the applicability to other systems like necrotrophic/hemibiotrophic behaviors, insects/herbivores or oomycetes (Hein et al. 2009; Karban 2011; Cook et al. 2015; Gust et al. 2017).

As a matter of fact, one of the most obvious problems is that the zigzag model is more adapted to plant immune responses to biotrophs, which makes sense as the observations used to build this model

were mainly done on biotrophic systems. Jones and Dangl (2006) said that they did not consider further or more complex issues such as small RNA-base immunity against viruses in plants or specific immune responses targeted against herbivores. But beyond these specific branches, the zigzag model did not consider the feeding behavior of many foes like fungi (Andolfo and Ercolano 2015; Cook et al. 2015). Plant immune responses will have more or less success if the induced response provides favorable nutritional conditions for the pathogen. Indeed, a response with hypersensitivity might not be adequate for a necrotrophic fungus that feeds on dead cells (Thomma et al. 2001). In that sense, necrotrophic microorganisms produce nonspecific toxins, cell wall degrading and defense suppressing enzymes that aim to kill and macerate host tissues but also to control host responses (Andolfo and Ercolano 2015). It is hard to position responses to necrotrophic pathogens as host-specific toxin effectors are released and counteract host immune defenses by using their machinery in an “inverse gene-for-gene” relationship (Cook et al. 2015). Detection of effectors here does not lead to immunity but rather triggers the host susceptibility. And it gets even more complicated when it comes to hemibiotrophic pathogens as they combine both strategies with an initial biotrophic phase suppressing the host immune system and subsequent necrotrophic phase enhancing it to induce host cell death (Koeck et al. 2011). For such pathogens, hypersensitive reaction (HR) leading to cell death may be beneficial to the host early in the interaction and a fine control of hypersensitive response by NLRs (nucleotide-binding site-leucine-rich repeats) is important in the distinction between different pathogen lifestyles (Balint-Kurti 2019). Some PAMPs and effectors such as NLPs (necrosis and ethylene-inducing peptide 1 like proteins or Nep1-like proteins) seem to play an important role in facilitating the transition to the necrotrophic phase of fungi and oomycetes (Qutob et al. 2006; Hein et al. 2009). Existence of these infectious strategies raises the question of how plants that resist necrotrophs or hemibiotrophs do to distinguish them from plain biotrophs. Andolfo and Ercolano (2015) have proposed a multicomponent model that includes the PTI/ETI defense response activation but also considers the plant ability to distinguish the pathogen lifestyle as a second component that modulates immunity.

Several misconceptions have risen in particular from the strict dichotomy between PTI and ETI since they are considered as two separate layers of plant immunity in the zigzag model. Indeed, authors like Thomma et al. (2011) or Cook et al. (2015) have warned the community of the reduced view of plant immunity if PTI and ETI are considered as separated mechanisms because plant immunity “is a continuous system that evolves to detect invasion”. Since the zigzag model was proposed, new insights have come to light revealing this blurred border between both branches of the model. First, MAMPs have for a long time been believed to not induce HR responses but latter studies have reported MAMPs involved in activation of HR responses, for example in tomato with the fungal elicitor ethylene-inducing xylanase (EIX) (Ron and Avni 2004) or the elicitors responsive genotypes of *Nicotiana* species as well as *Raphanus sativa* showing stronger cell death (Takemoto et al. 2005). Second, the model supposes as well a strong dichotomy MAMP-effector but are they so different or are there shades between these two terms? New findings have reported a widespread occurrence of effectors that can actually be qualified as MAMPs. NEPs like proteins (NLPs), for example, seem to have a conserved region of 20-24 amino acids that can induce plant immune responses. Similarly, BcSpl1 effector has two conserved 40 amino acid regions that interact with each other on the protein surface and that are necessary and sufficient for cell death induced responses in hosts. Both effectors previously described contain patterns that may act as conserved MAMP-like regions while

serving virulence functions. It is, therefore, difficult to include them into the MTI-ETI classification of the zigzag model (Cook et al. 2015). Third, PTI is often described as a static phase and strict separation of PTI and ETI has led to erroneous assumption that PRRs are old defense systems that evolve slower and that are highly conserved unlike *R* genes. Indeed, as MAMPs are often taught to be conserved features acting in important parts of the pathogen survival like chitin for fungus cell walls or flagellin for bacterium movement, misleading conclusion can arise and therefore, one can believe that MAMPs are stable and detected broadly whereas effectors are more variable and detected by specific hosts. However, several studies showed quite the opposite as MAMPs may exhibit variable epitopes that can fail to activate plant immunity and receptors may be subjected to independent evolution allowing them to recognize different epitopes, which suggests a host-pathogen coevolution rather than a general perception. In that case, pattern recognition receptors (PRRs) seem to have a dynamic nature that has evolved under selection pressures leading to pathosystem-specific variations similarly to *R* genes (Cook et al. 2015). Finally, the model fails to consider possible broad recognition of effectors by *R* genes. It was demonstrated that NLRs can detect pathogen effectors broadly outside the inner circle of strains from a single pathosystem. For example, the NLR immune receptor of tomato Mi-1.2 confers resistance to phloem-feeding insects as well as root-knot nematodes (Rossi et al. 1998; Vos et al. 1998). Some *R* genes can also detect elicitors from very different foes like the tomato cell surface receptor-like protein (RLP) Cf-2 that guards the apoplastic papain-like cysteine protease Rcr3pim, activates resistance when Rcr3pim is suppressed by Avr2 from the leaf mold fungus *Cladosporium fulvum* or by the nematode effector Gr-VAP1 (Lozano-Torres et al. 2012). These results imply a conserved recognition protein that recognizes directly or indirectly effectors from different and separated pathosystems similarly to MAMP recognition (Cook et al. 2015).

Pritchard and Birch (2014) pointed out several other limitations like misunderstandings of plant immunity due to time-scale, events ordering (are the phases in the zigzag model sequential or stepwise?) and physical-scale ambiguities. The zigzag model intended to present plant immunity from an evolutionary point of view rather than a sequence of events occurring during a single plant-pathogen interaction and in a single cell/tissue/organism. In addition, the authors mentioned an absence of environmental context that may influence plant immune responses, and expressed their concern on the possibility of inclusion of these parameters in the model as it is currently described.

Many models have been proposed to embrace all the limitations reported above and a few examples can be mentioned here. Pritchard and Birch (2014) proposed a dynamic and quantitative model of the plant immune system that means to actually respond to the 'quantitative output of the plant immune system' originally proposed by the zigzag model. Andolfo and Ercolano (2015) proposed a circular model taking into account the plant ability to distinguish and correctly respond to the feeding behavior of the invader. Cook et al. (2015) proposed the invasion model that considers the continuity between PTI and ETI and aims to be applicable to necrotrophs, endophytes and mutualists (symbioses), viruses, nematodes and insects. Lastly, other authors proposed to use the zigzag model as a base to explain plant immunity and to add up new ramifications when findings report particularities in plant-pathogen interaction that do not fit the proposed zigzag model such as miRNAs as determinant regulators of PTI and ETI or specific plant responses to necrotrophs (Alizadeh and Askari 2014; Keller et al. 2016). Perhaps it has been difficult to fit the complex multicomponent system in a single model because countless components, actors,

mechanisms are involved in disease resistance in plants. Andersen et al. (2018) conducted an extensive literature search (around 350 references were used) to review the major components of plant immune systems and elegantly presented a state of art knowledge that our scientific community has acquired so far. By presenting plant defense systems through pathogen detection, signal transduction and defense responses, Andersen et al. (2018) illustrated very well how complex, dynamic and communicating plant-pathogen interactions can be (see Figure 2).

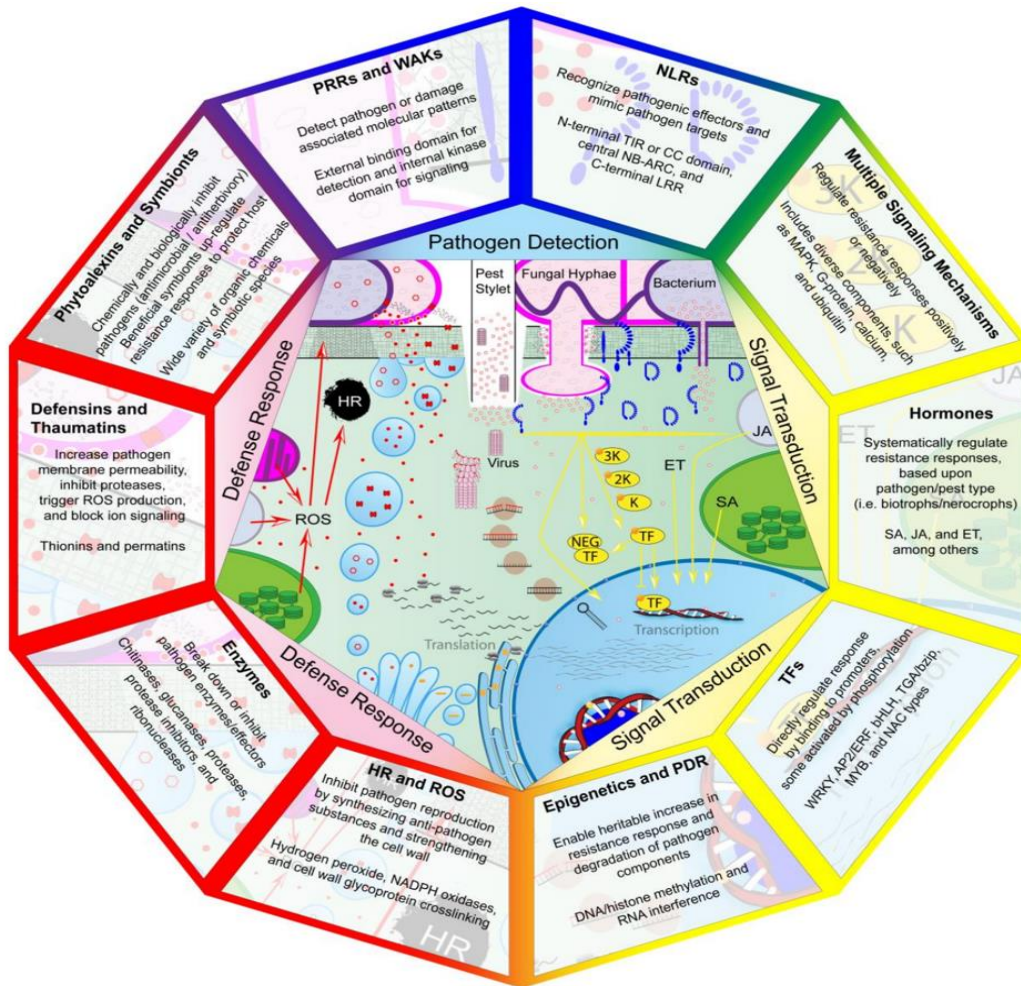


Figure 2: Components of plant disease resistance mechanisms reviewed and presented in Andersen et al. (2018)

Components of plant disease resistance mechanisms involved in pathogen detection, signal transduction, and defense response (detection in the upper center and progressing around clockwise, ending in defense response in the upper left). Pathogenic elicitors (cell components or effectors) produced by bacteria, fungi, insects, nematodes or viruses trigger plant receptors to initiate signaling cascades. Activated receptors (blue) then initiate one of many signal transduction pathways or directly act as transcription factors (TFs). Signal transduction pathways (yellow) include mitogen-activated protein kinase (MAPK) cascades, calcium ion signaling, hormone production, TF activity, and epigenetic regulation. These factors trigger the expression of genes associated with defense responses, such as those regulating the production of reactive oxygen species (ROS), antimicrobial enzymes, defensins, and phytoalexins. These defense-related compounds (red) actively inhibit pathogen reproduction or make further infection more difficult. Breakdown of pathogenic cell components by defense compounds leads to further release of receptor-triggering elicitors, increasing the resistance response. Multiple organelles are involved in defense response, including chloroplasts and peroxisomes for hormone production as well as the nucleus, endoplasmic reticulum, and Golgi apparatus for antimicrobial protein production. PRR: pattern recognition receptors; WAK: wall-associated kinases; NLR: nucleotide-binding domains and leucine-rich repeats; PDR: pathogen-derived resistance; HR: hypersensitive response; TIR: N-terminal Toll/interleukin-1 receptor-like; CC: coiled-coil; SA: salicylic acid; JA: jasmonic acid; ET: ethylene.

2.1.3. PLANT-PATHOGEN COEVOLUTION: AN ENDLESS ARMS RACE

In that sense, with the ‘expository’ zigzag model, one can easily grasp the complexity of the plant-pathogen coevolution and the endless arms race to which they dedicate themselves. There are different selection pressures on the actors of the immunity for the plant and the pathogenicity for the pathogen that lead to a combined evolution. Plants have learnt to evolve and modify responses according to pathogen pressure, and vice versa pathogens evolve to be able to infect plants and survive. In order to discuss this matter, I will take the zigzag model as a base for the following explanations but information about recent findings such as knowledge on necrotrophic lifestyle and DAMP recognition will also be considered.

The occurrence of disease on an individual is relatively low even if plants are constantly in contact with several potential pathogens. Indeed, beyond preformed defenses, induced defenses like PTI are undoubtedly efficient over a large set of microbes as plants are able to detect diverse types of microbe associated signals (MAMPs/PAMPs/DAMPs) with such a strong degree of redundancy that one pathogen may trigger linked or independent PTI pathways through PRR recognition, which contributes to broad spectrum effectiveness (Anderson et al. 2010). For their own sake, pathogens must bypass this first layer of surveillance to be able to infect the host plant (Figure 3). Therefore, PAMPs and host PRRs are under diversifying selection pressure to evade (for the pathogen) and facilitate (for the plant) recognition (Anderson et al. 2010). For example, on one hand, the flagellin flg22 epitope is recognized by many plants all over the taxa but flagellin-host perception has a dynamic nature as some species have evolved to recognize other epitopes in the protein. Clarke et al. (2013) demonstrated that a recent evolution within *Solanaceae* family has enabled some species (including tomato plants) to recognize the flgII-28 epitope (28–amino acid immunogenic region at C terminal of flagellin) from *Pseudomonas syringae*. On the other hand, after several studies, it was shown that, in addition to sequence diversification, posttranslational modifications such as glycosylation in virulent *Pseudomonas avenae* flagellin can affect its perception by rice plants (Cook et al. 2015 and references therein). Same as for flagellin-PRR pair, independent evolution of receptor to bacterial elongation factor EF-Tu (EF-Tu receptor) has enabled *Brassicaceae* members to respond to elf18 from *P. syringae* (Cook et al. 2015 and references therein). Both plants and pathogens exhibit specific evolution towards a better recognition of PAMPs or towards their avoidance. On one side, pathogens can diversify their PAMPs (see (1) in Figure 3), and on the other side, plants can respond by exhibiting new or slightly different proteins that are able to recognize altered PAMPs (see (a) in Figure 3).

Pathogens can also produce effectors to counter PTI responses and establish effector triggered susceptibility (ETS) leading to disease development. There are several possibilities that I tried to summarize in Figure 3 (four possibilities in brown from (2) to (5)).

First possibility, pathogens could arm themselves with effector shields protecting them from PTI responses (see (2) in Figure 3). For example, the fungal effector Avr4 is used to protect from chitinase produced during PTI as it lowers the accessibility to chitin by the plant chitinase (Anderson et al. 2010). Another strategy that can be mentioned is the posttranslational modification of chitin like its deacetylation leading to the formation of polymer chain of chitosan into fibrils that become less accessible to chitinase and remain attached to the hyphal cell wall (Aoun 2017 and the references therein). Some pathogens were described to escape PRR recognition by excluding chitinase from cell walls of specialized fungal

structures or by releasing effectors or chitin fragments that compete for binding with PAMP recognition proteins (Aoun 2017 and the references therein). Conversely and like previously explained, plants evolve and new PRR proteins are able to detect the pathogen presence (see (a) in Figure 3). Both PAMPs and PRRs are under diversifying selection (Anderson et al. 2010).

The second possibility is the degradation of bioactive products of PTI through a wide range of detoxification pathways (see (3) in Figure 3). For example, some pathogens like *P. syringae* can produce effectors (AvrPtoB) that can mimic host E3 ubiquitin which ubiquitinates host defense proteins leading to their degradation (Anderson et al. 2010). Others can degrade or prevent the accumulation of phytoalexins (from crucifers for example) through the activity of enzymes (oxidation, reduction or hydrolysis) like *Alternaria brassicicola*, *Botrytis cinerea*, *Nectria haematococca*, *Leptosphaeria maculans* (canola and mustard virulent isolates), *L. biglobosa*, *Rhizoctonia solani* and *Sclerotinia sclerotiorum* (C. Pedras and Abdoli 2017; Aoun 2017). Another strategy is to produce enzymes that directly inhibit activity of some PR proteins like the protease inhibitor EPI10 from the oomycete *P. infestans* that completely inhibits P69b, a PR-7 protein with protease activity (Aoun 2017).

The two last possibilities depend on the lifestyle of pathogens. Indeed, for biotrophs, it was described that they produce effectors suppressing PTI (see (4) in Figure 3) and these effectors are under diversifying selection pressure to avoid detection by host R proteins (Anderson et al. 2010).

For instance, effectors from *P. infestans* like AvrPto, AvrPtoB and HOPAI1, suppress PTI by blocking mitogen-activated protein kinase (MAPK) pathway from *Arabidopsis thaliana*. On one hand, AvrPtoB can inhibit the kinase domain of proteins of the PTI response including FLS2, BAK1 and CERK1. On the other hand, this oomycete can avoid stomatal closure (essential for its penetration) by targeting RIN4 with AvrRpm1 and AvrB to cause hyperphosphorylation of RIN4 or with AvrRpt2 protease that degrades RIN4 (Anderson et al. 2010 and reference therein). Necrotrophs are known for their capacity to produce toxin type effectors to bypass PTI response and especially induce HR for successful infection (see (5) in Figure 3) and this by the use of host specific toxins (HSTs) that target host R proteins to induce HR (Horbach et al.; Friesen et al. 2008; Anderson et al. 2010; Tsuge et al. 2013; Wang et al. 2014; Chowdhury et al. 2017). Several HSTs were described such as the *Alternaria alternata* toxin AM-toxin (I to III) affecting apple resistance, or AF-toxin (I to III) affecting strawberry among many others (Tsuge et al. 2013; Wang et al. 2014). The effectors from biotrophs and the HSTs from necrotrophs are under opposite selection pressure as, for biotrophs, effectors are selected towards detection avoidance while for necrotrophs the selection pressure is for detection maintenance (Anderson et al. 2010).

Different evolutionary mechanisms were described to participate in the pathogen evolution such as convergent evolution, cryptic genetic variation, chromosomal instability giving variation, hybridization and introgression (sexual recombination, lateral gene transfer through cytoplasmic or nuclear factor exchanges and whole genome exchange through somatic hybridization) and host jumps (Anderson et al. 2010; Teixeira 2019). To adapt their “effector arsenal”, pathogens may use two types of strategies: (1) gain-of-function mutation to diversify the effectors and MAMPs contributing to their pathogenicity or (2) loss-of-function mutation to prevent the host from recognizing them and initiating programmed cell death in the case of biotrophs (Niks et al. 2015), and to prevent direct toxin effector recognition for necrotrophs.

A continued coevolution of plant-pathogen systems has led plants to be able to recognize these effectors and mount a rapid targeted defense response like HR. The pathogen presence can be detected

via (a) direct recognition by R proteins or (b) indirect recognition through a sophisticated guard system (additional R proteins guarding R proteins). An elegant example of a guard system is the one for PRR protein RIN4 that is guarded by R proteins RPM1 and RPS2. Indeed, when RIN4 is targeted by AvrRpm1 or AvrB, RPM1 is activated and signal transduction leads to HR response. Also, RIN4 degradation by AvrRpt2 activates the guard R protein RPS2 which subsequently activates ETI. Protein degradation can be seen as DAMPs detection by the guard system. Moreover, there are evidences that NLR immune receptors guarding RIN4 have a conserved ability to detect AvrB and AvrRpm1 and that RIN4 modification sites are conserved across a wide taxonomic distribution. These findings point out that guarding RIN4 is a conserved host immune strategy (Anderson et al. 2010). In the case of ETI establishment, host R proteins are under different selection pressures according to the type of interaction with the pathogen effector (see (b) in Figure 3). If there is direct interaction, the R protein is under diversification pressure for detection of changing biotroph effectors and avoidance of HSTs whereas if there is an indirect interaction through the guard system, then, stabilizing selection pressure happens to maintain interaction between R protein and guard R protein. In that case, a pressure on R protein is maintained to coevolve with its guard protein while this one may be under selective pressure to avoid interaction with the pathogen effectors (Anderson et al. 2010; Cook et al. 2015). Cook et al. (2015) propose that this coevolution between R proteins and guard proteins is either an ancient defense mechanism that has been conserved all through evolution on a broad range of taxa or separated evolution that has led to the development of similar defense systems for different pathogens.

It is now clear that the pathogen capacity to infect the host is essential to its survival. Parameters like pathogen lifestyle (biotrophic, hemibiotrophic or necrotrophic), life cycle (polycyclic or monocyclic in one growing season/year), “recolonization-extinction dynamics” (host range, spore stage, dormant stage and capacity of saprophytism) as well as its dispersal ability (wind, water, animal/insect, contact, etc.) will determine the relative selective impact of migration and gene flow (Anderson et al. 2010; Brown and Tellier 2011; Vries et al. 2020). Other factors like frequency of virulence and frequency of resistant hosts, combined with the capacity of the pathogen to produce many cycles (polycyclic) and to its dispersal capacity, can greatly affect pathogen fitness through what Brown and Tellier (2011) call a negative direct frequency-dependent selection (ndFDS). This ndFDS results from the concept of gene-for-gene relationship that implies a coevolution of plants and their pathogens in the familiar boom-and-bust cycle. This cycle is described by a resistance selection when virulence is rare and virulence selection when resistance is common. Brown and Tellier (2011) also mentioned a possible stability in polymorphism in both sides when ecological and epidemiological factors cause ndFDS on the host, the pathogen or both leading to a lower fitness of a trait if its frequency increases. Stability in polymorphism can also be reached by overdominance, i.e. when heterozygous have greater resistance than homozygous to different pathogens but also when host and pathogen life cycles are partially decoupled. However, agricultural systems have lost some of the factors promoting stability in host-pathogen interactions (increase homozygosity in crops through the use of lines and single varieties, pathogen life cycle coupled with crop cultural calendar, fields with only resistant phenotypes, use of pesticides putting a high pressure on pathogens, etc.) leading to a constant acquisition of novel traits that increase fitness for the pathogen, thus, resistance is broken and a new breeding cycle is needed to release new resistant varieties (Brown and Tellier 2011; Münnekhoff et al. 2017; Vries et al. 2020). Allele’s span life in both pathogens and plants

is then short and constantly changing, which makes pathogen evolution unstable and disease control unpredictable (Brown and Tellier 2011).

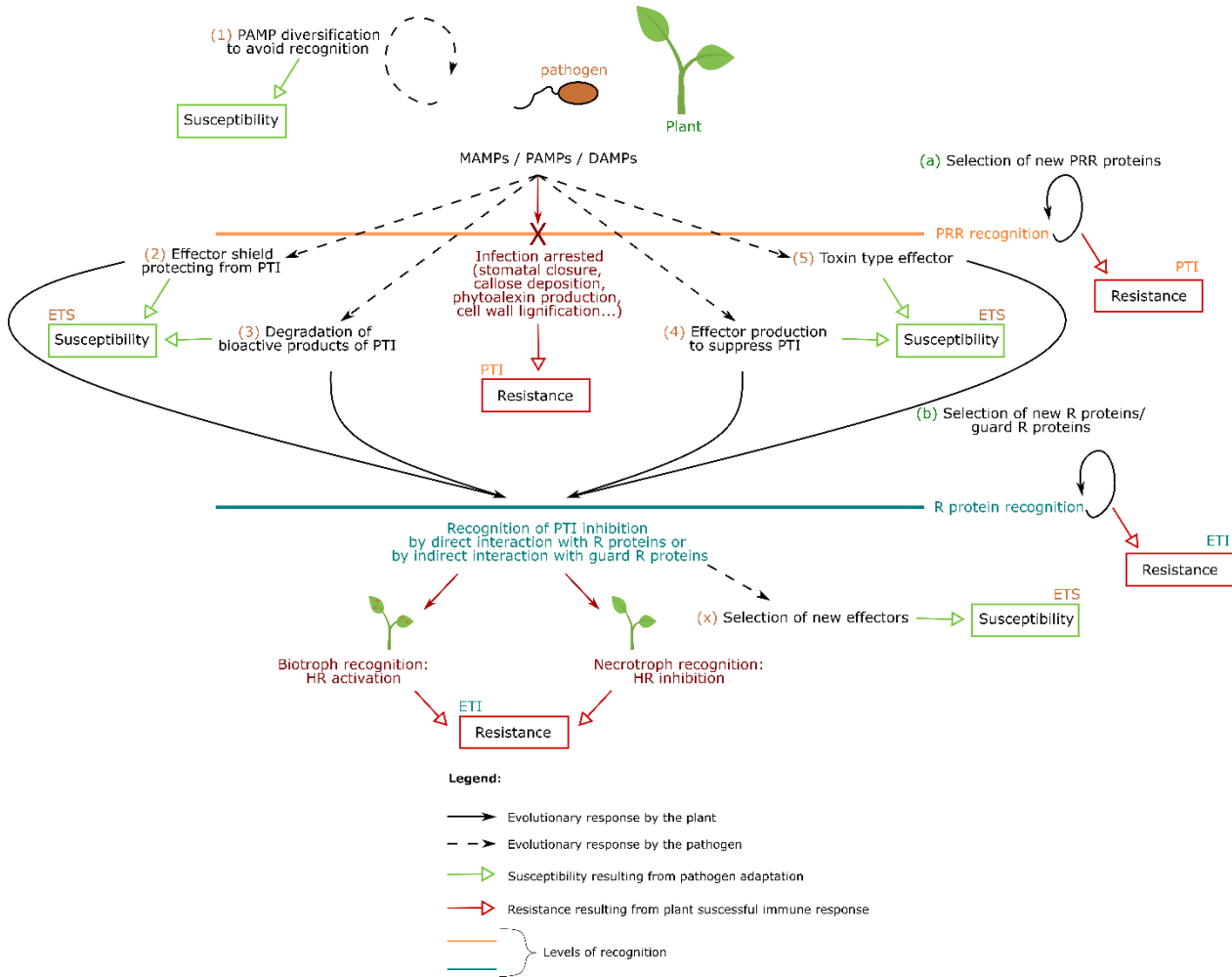


Figure 3: Summary of plant-pathogen coevolution strategies adapted from (Anderson et al. 2010; Cook et al. 2015; Aoun 2017)

Pathogen possible evolution represented by brown numbers in parentheses (1-5) and plant possible interaction by green letters in parentheses (a-b); PAMPs: pathogen-associated molecular patterns; PRR: pattern-recognition receptor; R protein: resistance protein; PTI: PAMP-triggered immunity; ETI: effector-triggered immunity; ETS: effector-triggered susceptibility - il y a aussi le x = new effectors

2.2. TERMINOLOGY AND MISCONCEPTIONS BEHIND PLANT DISEASE RESISTANCE

The aim of this part is to discuss the different concepts used to define and characterize plant disease resistance and I would like to point out some misconceptions that have arisen in the field of disease resistance applied to plants. Again, I do not intend to give set definitions but rather present and discuss concepts like quantitative and qualitative resistance in relation to durability. First, I would like to address the existing duality that is so often described between qualitative and quantitative disease resistances as well as the concept of durability of disease resistance. This section will present the concepts but the tools

used to investigate these types of disease resistance (especially quantitative disease resistance) will be detailed in the next [section 4.3](#). Finally, I would like to point out the importance of plant integrity and the effects of the environment in the expression of disease resistance.

2.2.1. *QUANTITATIVE – QUALITATIVE DISEASE RESISTANCE: NOT A STRICT DUALITY*

Disease resistance is generally defined using two categories: (1) complete resistance that totally prevents pathogen propagation and is characterized by the absence of pathogen development beyond early stages of infection (Heitefuss 1997), and (2) incomplete resistance that allows some sporulation and is often linked to a reduction of symptoms and a limited pathogen development (Keller et al. 2000; Roux et al. 2014) (see definition box 1). A wide variety of terms exists in the literature and aims to describe this perceived dichotomy in the terminology referring to disease resistance. The diversity of terms reflects the interests and assumptions made by scientists over the years and has often been used in different ways by the scientific community which has increased the confusion around disease resistance. Indeed, throughout the years, shortcuts have been made which have led to often mistaken the observed phenotypes with the genetic bases as well as considering a strict dichotomy between terms referring to disease resistance (St Clair 2010). Terms like vertical, major-gene, narrow-spectrum, monogenic, qualitative and not durable are often used to qualify complete resistance while terms like horizontal, minor-gene, broad-spectrum, polygenic, quantitative and durable are used to qualify incomplete resistance. These terms have sometimes been used one for another like they have similar meanings or like they are synonymous referring to the same concept (Johnson 1981; Keller et al. 2000; Poland et al. 2009; St Clair 2010). However, if we look closer at the list of terms used to qualify disease resistance, we can see a mix of terms referring to either the observed disease phenotypes (quantitative/qualitative and complete/incomplete) or the genetic interaction between the host and the pathogen (horizontal/vertical and broad-spectrum/narrow-spectrum) or the genetic bases underlying them (monogenic/polygenic and major-gene/minor-gene) (Keller et al. 2000; Poland et al. 2009; St Clair 2010). Durability or not has also been associated with these two types of resistance and many authors have implied that horizontal, partial or generalized resistance is more durable. But it actually does not refer to either of these aspects (Johnson 1981) and will be further discussed in the following section. In addition, assumptions about the relationships between the observed phenotypes and the genetic bases were often made and can lead to erroneous conclusions and ambiguous teachings. St Clair (2010) proposed to describe the observed disease resistance phenotypes separately from “untested hypotheses about the underlying genetic basis”. Indeed, it is difficult to determine the genetic basis with a simple glance at the phenotype.

Phenotypically, one can define disease resistance as qualitative when binary phenotypes are observed, i.e. either resistant or susceptible, and as quantitative when a continuous distribution of disease phenotypes from susceptible to resistant is observed in host populations (see definition box 1). Quantitative resistance is also described to be expressed as disease symptom reduction instead of a complete absence of disease symptoms which refers to qualitative resistance (Poland et al. 2009; Niks et al. 2015). However, Roux et al. (2014) pointed out that qualitative and quantitative resistances may not necessarily be exclusive because phenotypes may seem one way or another according to different parameters such as our ability to read, score or interpret disease phenotypes, the environmental conditions, the host population size, the accuracy and resolution of the phenotyping. It is, therefore,

important to choose the phenotyping strategy and to use methods and measurements that allow both an accurate phenotyping and ease of interpretation of the disease phenotype. Moreover, the wider the populations are, the more chances of observing a great variability of phenotypes there are.

Quantitative and qualitative duality in plant disease resistance is even more blurred when the genetic bases underlying them are considered. Niks et al. (2015) defined two different aspects of quantitative and qualitative disease resistances: (1) the phenotypic aspect that I explained in the last paragraph, and (2) the genetic aspect that implies the mode of inheritance. Indeed, they considered that qualitative disease resistance in terms of inheritance is based on one or two major genes that segregate according to discrete phenotypic classes following the Mendelian principles, and that quantitative disease resistance in terms of inheritance is based on several genes contributing to a small proportion of the resistance level and is, therefore, polygenic. The authors explained that resistance for which the phenotypic nature is quantitative may have a qualitative inheritance and vice versa, a qualitative phenotypic nature of disease resistance may be the result of quantitatively inherited genes (see Figure 4).

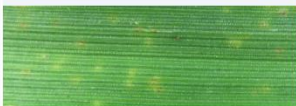

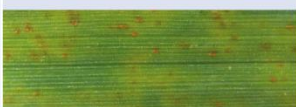
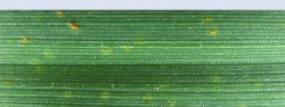
	Genetically qualitative	Genetically quantitative
Phenotypically qualitative	a <i>R</i> genes causing complete resistance ^a 	b Nonhost resistance based on minor genes ^b 
Phenotypically quantitative	c <i>R</i> genes causing incomplete resistance ^c 	d Partial resistance ^d 

Figure 4: Two aspects of qualitative and quantitative disease resistances (split-up of phenotypic and genetic aspects) presented by Niks et al. in 2015 citing Niks and Kuiper 1983; Franckowiak et al. 1997; Qi et al. 1998; Jafary et al. 2006

There are four categories of qualitative or quantitative nature of resistance with two aspects (genetic and phenotypic) being considered for each type of resistance (qualitative and quantitative). Niks et al. illustrated each category with an example of rust fungus (*Puccinia*) on barley. The picture at the top left corner is presented as comparison with a very susceptible barley genotype named L94 infected by *Puccinia hordei* isolate 1.2.1; (a) illustration of a major *R* gene, *Rpb7g*, causing complete resistance on the cultivar ‘Cebada Capa’ when challenged with the avirulent isolate 1.2.1. of *P. hordei*; (b) example of nonhost resistance of the cultivar ‘Vada’ against an isolate of the rye grass stem rust fungus *Puccinia graminis* f. sp. *lolii* showing a complete resistance but that is based on the combined effect of minimum three quantitative resistance genes of minor effects; (c) the cultivar ‘Trumpf’ exhibiting an incomplete resistance to an avirulent isolate of *P. hordei* named Israel 202 that is conferred by one major gene *Rph9.z*. Some sporulation occurred despite a hypersensitive reaction; (d) illustration of high level of partial resistance to *P. hordei* isolate 1.2.1 on the cultivar ‘Vada’ that is known to be conferred by several quantitative resistance genes.

In Figure 4, both examples (a) and (d) are the most common cases where qualitative inherited genes give a qualitative type of phenotype and where the combination of several genes with quantitative effect induces partial resistance. The case (c) also gives an example of *R* gene (*Rph9.z*) that is inherited in a Mendelian fashion but that does not fully impede pathogen multiplication (as sporulation occurs), which leads to partial resistance. Other genes like this were described to give a large effect on resistance at the adult stage, for example in wheat for leaf rust, stripe rust and powdery mildew (*Lr34*) or the *MILa* gene for powdery mildew resistance in barley or the recessive nonhypersensitive *mlo* gene of barley against

Blumeria graminis, the causal agent of powdery mildew, which complies to the partial resistance definition given by Parlevliet (1978) but is qualitatively inherited rather than quantitatively (Niks et al. 2015). Another interesting example is the nonhost interaction exhibiting complete resistance that are due to combined effects of several genes with quantitative effects (Figure 4) like for barley challenged with different grass or cereal *Puccinia* rust fungi or for *Lactuca saligna* to the lettuce downy mildew *Bremia lactucae* (Niks et al. 2015). St Clair (2010) also mentioned some examples of deviations from the strict duality between quantitative and qualitative disease resistances. For example, a gene controlling a trait with low heritability might in certain environmental conditions present a continuous phenotypic distribution. Furthermore, a combination of genes with small effects might lead to complete resistance and yield binomial distribution. In addition, some resistances may appear incomplete because of degenerated alleles of single genes reacting to specific environmental conditions lived by the plant (Poland et al. 2009). The biology underlying quantitative resistance will be further discussed in [section 2.3.3](#). In the end and with all these examples, one can easily understand that the genetic basis of a trait cannot be correctly determined by simply considering the phenotypic observation but must be established by adequate genetic analysis to determine the relationship between genotype and phenotype (St Clair 2010).

Quantitative and qualitative disease resistances are often considered to be non-race-specific and race-specific, respectively. Other concepts like vertical and horizontal resistances are used to define whether or not a resistance is effective against some of the existing pathogen races and for which there is a known “gene-for-gene relationship” (vertical) or effective against all known races of the pathogen and, therefore, characterized by “the absence of genetic interactions between” the host and pathogen genotypes (horizontal) (Keller et al. 2000, p. 24-25). However, recent studies have demonstrated that quantitative disease resistance can be isolate- or race-specific and, in contrast, qualitative disease resistance can extend over a large variety of races and pathogens (Zhao et al. 2004; Reignault and Sancholle 2005; Poland et al. 2009; Narusaka et al. 2009). Poland et al. (2009) pointed out evidence for narrow-spectrum quantitative resistance loci (QRLs, see definition box 1) that involved a gene-for-gene interaction in quantitative disease resistance, but also for broad-spectrum QRLs giving resistance to multiple disease resistances. On one hand, race-specificity of QRLs was reported for rose black spot disease (Whitaker et al. 2007b), rice blast, leaf rust, vascular wilt in melon, black stem in sunflower, etc. (Poland et al. 2009 and references therein). Several authors have speculated that quantitative disease resistances were weaker forms of race-specific (*R* gene-mediated) resistance (Parlevliet and Zadoks 1977; Li et al. 2006; Poland et al. 2009) or due to “minor-gene-for-minor-gene interaction” where a minor pathogenicity gene interacts with a minor effect resistance gene (QRL) (Poland et al. 2009). On the other hand, co-localisation between QRLs conferring resistance to different pathogens were also described, suggesting, according to the authors, a common genetic basis (Wisser et al. 2005, 2006; Lanaud et al. 2009; Wang et al. 2010).

In the end and as Poland et al. (2009) stated “... qualitative and quantitative disease resistances might only be two ends of a continuum, with *R*-genes tending to lie toward one end of the spectrum and QRLs toward the other”, many shades between these two concepts might exist.

Definition box 1:

Complete resistance: multiplication of the pathogen is totally prevented, no spore production (Keller et al. 2000)

Incomplete resistance: refers to all type of resistance that allow some spore production and includes partial resistance that is a form of incomplete resistance reducing spore production even if host plants are susceptible to infection (Keller et al. 2000)

Qualitative disease resistance: binary phenotype observed with either susceptible or resistant phenotype (Roux et al. 2014)

Quantitative disease resistance (QDR): disease phenotype follows a continuous distribution from susceptibility to resistance in host populations (Roux et al. 2014). Often described as host plant resistance that confers a reduction in disease, not the absence of disease (Poland et al. 2009; St Clair 2010)

Quantitative trait: trait exhibiting a continuous (noncategorical) distribution of phenotypic values in a genetically variable population that does not have Mendelian segregation ratios (St Clair 2010)

Quantitative trait locus (QTL): a genomic region, containing one or more genes, that exhibits a statistically significant association between marker polymorphisms and quantitative trait variation, i.e. that shows a continuous variation in phenotypes (Poland et al. 2009; St Clair 2010)

Quantitative trait nucleotide (QTN): the causal molecular variant that affects variation in a quantitative trait (Mackay2009)

Quantitative resistance locus (QRL): a locus with an effect on QDR (Poland et al. 2009)

Vertical resistance: existence of a gene-for-gene interaction between the host and the pathogen (Keller et al. 2000)/if the resistance is effective against some of the existing pathogen races (race-specific) (Van Der Plank 1963)

Horizontal resistance: absence of genetic interaction between the host and the pathogen (Keller et al. 2000)/if the resistance is effective against all known races of the pathogen (race-non-specific) (Van Der Plank 1963)

2.2.2. PLANT RESISTANCE DURABILITY

The term “durability” has been used in many ways to describe plant resistance. The first definition of durability was perhaps given by Johnson (1981, 1983) who stated that a durable resistance is the plant resistance that remains effective over a prolonged period of widespread use under conditions conducive to the disease. However, as Lo Iacono et al. (2013) well pointed out, although conceptually simple, this definition uses terms that can be misinterpreted. What do ‘remains effective’ and/or ‘prolonged period’ actually mean? Does it mean complete resistance or is tolerance accepted? To what extent can a cultivar be considered to be ‘widely cultivated’? Later with the polygenic vs monogenic paradigm, some authors suggested that polygenic resistance is expected to be more durable than monogenic one (Young 1996; Keller et al. 2000; Leach et al. 2001; Palloix et al. 2009) but experimental evidence supporting this hypothesis remained scarce for a long time. Nevertheless, some exceptions were found where disease resistance controlled by genes with monogenic inheritance such as *mlo* recessive gene for powdery mildew resistance in barley, *Rpg1* for resistance to stem rust in barley and the dominant *I* gene giving resistance to mosaic virus in common bean have been associated with resistance to multiple isolates/races and have been providing durable resistance over decades (St Clair 2010; Lo Iacono et al. 2013 and references therein). Recently, evidence for selection of pathogen genotypes capable of overcoming quantitative resistance has been observed (Burdon et al. 2014; Niks et al. 2015; Pilet-Nayel et al. 2017) and the speed at which the pathogens overcome QRLs seems to depend on genetic background in which they are introduced (Fournet et al. 2013).

Durability is no longer a matter of which type of resistance is used but rather opinions on its “longevity” have changed and it seems that durability cannot only be based on the genetic basis of the host resistance but multi-criteria like population genetics and size, pathogen’s degree of host specialization, cultural practices, deployment of resistance in the field (variety and species mixture, gene pyramiding, etc.) need to be taken into account (Finckh et al. 2000; McDonald and Linde 2002a, b; Michelmore 2003; Bent and Mackey 2007; St Clair 2010). Indeed, a larger population will likely present a wider genetic diversity and population size can, therefore, influence the “so-called random genetic drift” that occurs when populations encounter a bottleneck of selection or when small portions of a pathogen population start infecting a new host (i.e. the change in the frequency of alleles randomly chosen in parts of pathogen population) (McDonald and Linde 2002a, b). Niks et al. (2015) pointed out an interesting fact about Johnson’s definition of durability. Johnson (1981) defined the period of effectiveness with two forms “while a cultivar possessing it is widely cultivated” or “while cultivars containing it are widely used.” These two ways to define durability imply very different matter as the first one reduces the durability to the amount of area occupied by a single cultivar possessing a certain resistance while the second one takes into account that newly introduced resistance or *R* genes are deployed in several released and grown cultivars at the same time, which implies that resistance effectiveness is not only linked to the area occupied by that one cultivar possessing it but also to the area where different cultivars with the same resistance are cultivated. Therefore, Niks et al. (2015) suggested that *R* gene effectiveness should “preferably be longer than the commercial lifetime of the first cultivar” and vegetable crops with a high variety turnover needed the same time requirement for durability than cereal crops. For them, the *R* genes or their combination should be the relevant unit to be considered when assuming durability rather than the variety itself.

As explained in [section 2.1.3](#), the use of single varieties in fields or several varieties but carrying the same resistance can only participate in the boom-and-bust cycle by increasing the resistance allele frequencies in the host population (boom phase), which subsequently selects for virulent pathogens (bust phase) (Schumann 1991; Keller et al. 2000; Brown and Tellier 2011; Niks et al. 2015). Combination of different strategies for disease resistance gene deployment can be used: (1) gene pyramiding, i.e. the incorporation of several resistance genes and QRLs into the same plant, (2) multiline or variety mixtures exhibiting similar agronomic traits but with different levels and/or resistance genes within the same field or differential landscape deployment at a farm level or at a regional level, i.e. cultivation of different varieties at the same time bearing different resistance genes in different fields, (3) rotations, i.e. periodic alternation of different resistance genes at the same site, and (4) sequential usage/release of varieties, i.e. use of each resistance gene until resistance breakdown and replacement with a new resistance. The latter has been the most used but contributes in maintaining the boom-and-bust cycle. The other strategies aim to reduce the selection pressure on pathogen population and delay evolution of virulent pathogen genotypes, which protects plants from resistance breakdown (Finckh et al. 2000; Papaix et al. 2011; Mundt 2014; Delmotte et al. 2016). Recent studies have suggested that pyramiding of disease resistance genes within a plant is the most durable strategy particularly if quantitative resistance is added (Brun et al. 2010; Vu et al. 2014; Delourme et al. 2014; Delmotte et al. 2016; Pilet-Nayel et al. 2017), which validates Nelson's poetic statement about disease resistance breeding (1978):

“Go back young man and gather up your weary and defeated genes of the past, take your currently successful genes, find some new ones if you can, and build yourself a genetic pyramid”.

Finally, it has been suggested that practices for pathogen control like pesticides, biological control, beneficial organism, and other agricultural practices (prophylactic methods, crop rotation, soil preparation etc.) can be combined with disease resistance gene deployment strategies to build a relevant management strategy that could greatly slow down pathogen evolution and, therefore, increase disease resistance durability. Unfortunately, as of today, limited information is available on the power and limitations of such combinations (Delmotte et al. 2016), and pesticide use being more and more criticized by consumers and prone to strict regulations, there is an increased need to find better solutions to reduce their need. Delmotte et al. proposed to updated Nelson's advice cited above to better fit disease resistance managements with today's challenges:

“Go back once more young man and gather up not only your most efficient genes, but also molecules, natural enemies and practices, and build a highly durable strategy... and be wise enough to make this strategy economically and ecologically sustainable.”

2.2.3. THE INFLUENCE OF PLANT INTEGRITY AND “AGE” ON DISEASE RESISTANCE

Plant-pathogen interactions have been studied in fields and laboratory/greenhouse settings for several centuries. Laboratory/greenhouse tests are often preferred because they are easily implemented and conditions are better controlled. Excised parts of plants are used in laboratory tests such as leaves, leaf discs, stems, roots, etc. Even if a majority of publications have reported good correlations between detached leaf assays (DLA) and whole plant assays (WPA) at the phenotypic level (Abubakkar et al. 2013; Dong et al. 2015; Miller-Butler et al. 2018; Aregbesola et al. 2020), some studies have reported differences in defense responses between detached organs and whole plants. Most of the time, these differences are

attributed to variation in experimental setup or the presence of specific *R* genes like for *Solanum tuberosum-Phytophthora infestans* interaction (Wang et al. 2004; Rietman 2011). However, authors like Orłowska et al. (2013) believe that these differences might be the results of a compromised plant integrity. The definition of plant integrity is difficult to find but it seems to involve a holistic view of the plant that integrates the plant in its complexity with the above and below ground compartments that work synergistically but also consider the plant throughout its life cycle (Pazderů and Bláha 2013). Orłowska et al. (2013) reviewed the role of plant integrity in disease resistance and showed that defense responses to infection differ between whole intact plants and detached leaves but also that above- and below-ground defense signaling are important for plant resistance to pathogen attack. For example, infection of *A. thaliana* with the hemibiotroph fungus *Collectotrichum* led to rather different symptoms and pathogenesis-related gene expression when the leaves were detached compared to the infection of attached leaves (Liu et al. 2007). Similarly, in potato-*P. infestans* interaction, differences in visual symptoms as well as in the induction of pathogenesis-related genes like acidic and basic chitinases (*ChtA* and *ChtB*) and *PR-1* were observed between detached and attached leaves. These genes were more induced in whole plants than in detached leaves (Orłowska et al. 2012a) and were also induced earlier in the infection in resistant plants compared to susceptible ones (Orłowska et al. 2012b). Finally, Lieberei (2007) discussed the importance of leaves being attached to the rubber tree when inoculated with the necrotrophic fungus *Microcyclus ulei* because leaves are metabolic sink tissues that are dependent on the energy balance of the mother plant. Disrupting this communication and assimilate transport by detaching the leaves could lead to different results between whole plants and detached leaves since processes involved in defense responses like cinnamic acid, scopoletin, lignin and glycoside synthesis can be delayed or halted in detached leaves because of lack of "energy-delivering compounds" (Lieberei 2007; Orłowska et al. 2013). In the end, detached leaf assays can be a rapid and reliable tool to assess disease resistance phenotypically in most cases but when it comes to the study of the genes and mechanisms underlying disease resistance, it is important to consider plant integrity as a major component in plant defense response and, therefore, whole plants should be used in priority instead of detached organs.

Lieberei's observation about "energy-delivering compounds" transport disruption in detached leaves being linked to differences in resistance can be related to the fact that known adult plant resistance genes (APR) giving partial resistance in cereals (*Lr34*, *Lr46* and *Lr67*) mediate resistance by modifying sugar regulation or signaling (Burdon et al. 2014; Moore et al. 2015; Krattinger et al. 2016; Rinaldo et al. 2017; Boni 2017; Milne et al. 2019). For example, *Lr67* seems to be involved in pathogen starvation by limiting nutrient transport to the pathogen or may indirectly trigger defense response by altering hexose/sucrose balance or it may reduce pathogen growth through unknown mechanism due to its altered function (Milne et al. 2019). Then, plant age seems to be important in disease resistance implementation especially if the genes giving the resistance are development stage-dependent (Niks et al. 2015). Indeed, quantitative disease resistance can sometimes be effective only at adult plant stage, and they can induce nonhypersensitive reactions like *Rph20* in barley and *Rph4* in cucumber (Hickey et al. 2012; Schouten et al. 2014) as well as hypersensitive reactions like *Lr22a* and *Lrr22b* in wheat (Dyck 1979). Constitutive expression of resistance genes was also demonstrated to increase with plant age like for the *R* genes *Xa3/Xa26* and *Xa21*. These findings can explain that genes like that were only effective in adult plants but not in juvenile ones (Vergne et al. 2010). But beyond the plant age importance reviewed above, organs of

different ages can also exhibit different immune responses and degrees of resistance. Developmental acquired defense or resistance was described in several organs and pathosystems such as grape powdery mildew (Ficke et al. 2002), apple leaves resistance to *Venturia inaequalis* (Li and Xu 2002; Gusberti et al. 2013), rice leaves resistance to *Xanthomonas campestris*, wheat leaves resistance to *P. sorghi* (Develey-Rivière and Galiana 2007 and references therein), *Phytophthora capsici* resistance in cucumber (Ando et al. 2009), onion resistance to *Fusarium oxysporum* (Galeano et al. 2014), etc. Leaf age was also demonstrated to be involved in non-host resistance against *Pyricularia oryzae* in *Arabidopsis thaliana* (Yamauchi et al. 2017). Because of the diversity of host species, host age, infected organs and causal agents, many terms have been used to qualify the age acquired resistance like age-related resistance (ARR), ontogenic resistance, developmental resistance, mature seedling resistance or adult plant resistance (APR) (Panter and Jones 2002; Develey-Rivière and Galiana 2007; Hu and Yang 2019). ARR is directly related to plant age that can be defined by different aspects such as developmental progression of individual organs also known as ontogenesis, exact chronological age (the time post planting/propagation or post organogenesis) and physiological age described by both morphological and physiological features (transition between different stages such as embryonic stage, flowering stage, vegetative stage, etc.) (Hu and Yang 2019). Hu and Yang (2019) suggested that multiple mechanisms might be involved in this type of resistance, which could explain such diversity of terms and ways to express plant age. Many other genes involved in age-dependent defense responses were identified in different hosts and are well described in Hu and Yang's review (2019). We can see from the list of candidate genes that age-dependent resistance can be controlled by genes of very different nature like sugar transporters (*Lr34-46-67*), miRNAs (miR172 and miR156 also called *Corngrass1*), floral inducers like SOC1 or transcription factors like SPL9.

Plant integrity and “age” are important as they can greatly influence disease resistance in many ways and need to be considered when investigating plant-pathogen interactions. Therefore, the choice of disease assessment with whole or part of plants used, on which developmental stage, organ or timing is essential and needs to be carefully decided as it can lead to biased results and erroneous assumptions.

2.3. INVESTIGATING QUANTITATIVE DISEASE RESISTANCE (QDR) AND ITS BIOLOGICAL BASES

Quantitative disease resistance (QDR) relies on multiple quantitative traits that can be measured with different phenotypic assessments such as disease index, lesion size and length, number of organs infected, time to defoliation for resistance against biotrophs, latency period and sporulation for fungal pathogens, number of colonies forming units *in planta* for bacterial pathogens, enzyme-linked immunosorbent assays for viral pathogens, etc. (Roux et al. 2014; Dong et al. 2017a; Willocquet et al. 2017). The loci having an effect on QDR are called quantitative resistance locus (QRL) (Poland et al. 2009). QTL mapping is a powerful tool for genetic analysis of quantitative traits (Young 1996; Broman and Sen 2009; Mackay et al. 2009; St Clair 2010) that can be used to investigate the genetic bases of a quantitative resistance trait (see definition box 1). In the first part of this section, I will present the conceptual basis of QTL mapping with a focus on QTL mapping for highly heterozygous species. Then, I will discuss QTL mapping precision and its limitations. However, QRLs are not all necessarily QTLs as QRLs might as well produce disease phenotypes that are continuously distributed but they are “not necessarily due to multiple loci segregating in a population” (St Clair 2010). Therefore, biological bases underlying QRLs will be discussed in the last part as well as

investigations on causal genes and causal quantitative trait nucleotide (QTN) polymorphisms underlying QRLs (see definition box 1).

2.3.1. CONCEPTUAL BASIS OF QTL MAPPING AND ITS PROGRESS OVER THE YEARS

Economically important traits like yield and disease resistance are inherited quantitatively and scientists have presumed that they are under polygenic control for which the exact number, mode of action and location are difficult to be assessed through analyses relying on Mendelian hypothesis (Muluaem and Bekeko 2016). Quantitative trait loci mapping has been widely used to investigate these traits with a special interest in disease resistance. To perform linkage-based QTL mapping, segregating populations (i.e. populations derived from sexual reproduction) need to be developed by crossing parents that differ for one or more traits (see Figure 5). Many species like forest trees or ornamental plants, are highly heterozygous and have a strong inbreeding depression when self-fertilized. In that case, outbred crosses are performed and the resultant progeny will have individuals that will be homozygous at some loci and heterozygous at others just like the parents. When populations are generated, the following step is the identification of polymorphism, i.e. the identification of DNA markers that reveal genetic differences between the parents (Keller et al. 2000; Collard et al. 2005). Sufficient polymorphism between the parents is necessary to build a linkage map (Young 1996). The type of DNA markers has greatly evolved in the last decades which has led to the development of many types of markers like RAPD, EST, ISSR, SSR, AFLP, SCAR, SNP among many others (see). Their choice is often limited to their availability and costs (Collard et al. 2005). Genetic markers are used to genotype the whole populations, i.e. to determine which alleles from the parents at a specific marker have been inherited by the individuals and that for each one of the markers. The next step is then to build a linkage map with these markers and the genotyping associated with it for each individual of the mapping population (see Figure 5). Briefly, linkage map construction is based on three main steps: (1) calculation of all pairwise distances by testing for linkage between “close” markers and calculating recombination frequencies in the population (distances in linkage maps are measured in terms of frequency of recombination between genetic markers, Paterson 1996), (2) grouping all markers with less than 50% recombination frequencies in the same linkage group, and (3) marker ordering in each linkage group. Two commonly used mapping functions are Kosambi and Haldane mapping functions that convert recombination fractions into genetic distances expressed in centiMorgans (cM) (Paterson 1996a; Keller et al. 2000; Collard et al. 2005). In outbred crosses, a procedure is necessary to determine the correct linkage phase before linkage estimation which can be rather difficult. Most of the time, “two-way pseudo-testcross mapping” strategies are used to exploit the high levels of heterozygosity in outbred individuals and “test-cross markers”, i.e. markers heterozygous in one parent and considering the other parent homozygous are used. Therefore, a linkage map is constructed for each parent (Grattapaglia and Sederoff 1994; Plomion and Durel 1996). When both linkage map(s) and phenotyping are done, QTL mapping can be carried out (see Figure 5). QTL analysis is based on detection of a statistically significant association between a phenotype exhibiting a quantitative trait variation and an allelic variation (polymorphism) at a marker genotype (Young 1996; Collard et al. 2005; Broman and Sen 2009). Simply put, individuals from a segregating population are divided into different genotypic groups (different alleles) for each considered marker or interval, phenotypic mean for each genotypic group is calculated, and a significant difference between the phenotypic means indicates that for that specific marker/interval a link between its allelic variation and the phenotypic differences exists, which means that the marker is linked

to a QTL controlling the studied trait (Paterson 1996b; Young 1996; Keller et al. 2000; Collard et al. 2005). There are three methods for detecting QTLs that have been widely-used: single-marker analysis (very simple method based on single-point analysis but not that used anymore), simple interval mapping (SIM, that analyses intervals between pairs of linked markers) and composite interval mapping (CIM, that combines interval mapping with linear regression and uses markers near large-effect QTLs as covariates to reduce residual variance and increase power to detect further QTLs) (Zeng 1993; Jansen and Stam 1994; Tanksley et al. 1996; Liu 1997; Broman and Sen 2009). Recently, increase interest has been given to multiple interval mapping (MIM) approaches that tackle the multidimensionality problem when several QTLs are detected (Zeng 1993; Kao et al. 1999; Zou and Zeng 2008; Broman and Sen 2009; Kao and Zeng 2010; Broman and Wu 2019). Indeed, MIM allows us to define QTL locations and infer them between markers, account for missing genotype data and investigate interaction between QTLs (Broman and Sen 2009; Muluaem and Bekeko 2016). This will be further discussed in chapter 2. Finally, the most recent method for multiple QTL mapping uses Bayesian QTL mapping approaches that are based on the Markov chain Monte Carlo algorithm (Yi et al. 2005; Yi and Shriner 2008; Yi and Xu 2008).

2.3.2. PRECISION AND LIMITATIONS OF QTL MAPPING

QTLs are statistically inferred from genotypic and phenotypic data generated during an experiment. Even though interval mapping is more reliable than single-marker analysis because of the use of two flanking markers instead of one, the statistic test for SIM or CIM used to locate a QTL is presented using a logarithm of odds (LOD) giving “the most likely position” for a QTL in relation to the specific linkage map. But to say if a specific locus is actually linked to observed phenotypic variation, the LOD peak of a QTL needs to exceed a specific threshold (level of significance) that is now calculated by a permutation test (Doerge and Churchill 1996). This permutation test mixes the phenotypic values while holding the genotyping data constant, runs once more the QTL analysis and assesses the amount of false positives detected after the permutation. This is repeated several times (minimum 500 times) and then, significance levels can be calculated based on the amount of false positives. Data for which phenotypic value permutations yield an important amount of QTLs linked to the phenotypic variation will therefore have a higher threshold and only statistically significant loci will be reported (Collard et al. 2005; Broman and Sen 2009). However, one can get to see that with these methods, many factors inherent to the experiment itself may influence QTL detection.

Indeed, the main sources of experimental errors come from mistakes in marker genotyping and errors in phenotypic evaluation. On one hand, genotyping errors as well as missing data can greatly affect the linkage map precision and the order of the markers in it but can also affect the power to detect QTLs if they are too important (Collard et al. 2005; Broman and Sen 2009). The type of markers as well as the density and coverage of the linkage map are important features that can be improved to increase the power for QTL detection. In particular, as missing genotype information can compromise multiple QTL fitting and the calculation of QTL effect on the phenotype, methods like multiple imputation that “fill in all missing genotype data even at sites between markers” are used and this helps to reduce the QTL model fitting to an ANOVA (for single-QTL models) or multiple regression (for multiple-QTL models) (Broman and Sen 2009). On the other hand, mistakes in phenotyping and accuracy of measurement can yield unreliable results and reduce the power to detect QTLs. Replicating phenotypic measurements or using clones can

also reduce the background noise and errors as well as take into account the genotype variability (Chandra and Bidinger 2002; Collard et al. 2005; Broman and Sen 2009). In addition, repeated evaluation in time and in different sites can give more insights in the influence of environmental conditions on QTLs affecting the trait of interest since environmental conditions and pathogen population for natural infection evaluations can greatly influence the expression of quantitative traits (Paterson 1996b; Collard et al. 2005; St Clair 2010; Pilet-Nayel et al. 2017; Willocquet et al. 2017).

Another important factor limiting the power to detect QTLs is the population size that both influences the map precision (Ferreira et al. 2006) and the QTL detection. Charmet (2000) showed that bias in QTL position estimations is important for small population size and in particular when QTLs seem to be located near the end of a linkage group. Moreover, the larger the population is, the more likely it is that QTLs with small effects will be detected (Collard et al. 2005; Vales et al. 2005; Li et al. 2006a) but also the more power there will be to detect QTLs that are closely linked (Broman and Sen 2009; Kao and Zeng 2010). So, increasing the population size can allow one to gain statistical power, estimate of locus effects and accuracy of confidence intervals of the QTL locations (Collard et al. 2005). The type of populations was also demonstrated to have an effect on the power of QTL mapping because the genetic diversity is directly linked to choice of the two founders, especially in bi-parental populations. Indeed, the higher the complexity of the population (several generations of crosses or multi-parent populations) is, the more recombination can be captured to generate more accurate genetic maps (Huang et al. 2015; Scott et al. 2020).

Finally, additional factors can limit the detection of QTLs but that cannot be improved as they are intrinsic and specific to the trait studied. For example, the heritability of the trait or the distribution of genetic effects as well as the existence of genetic interactions can greatly affect the power of QTL mapping (Charmet 2000; Collard et al. 2005; Tong et al. 2012; Li et al. 2012).

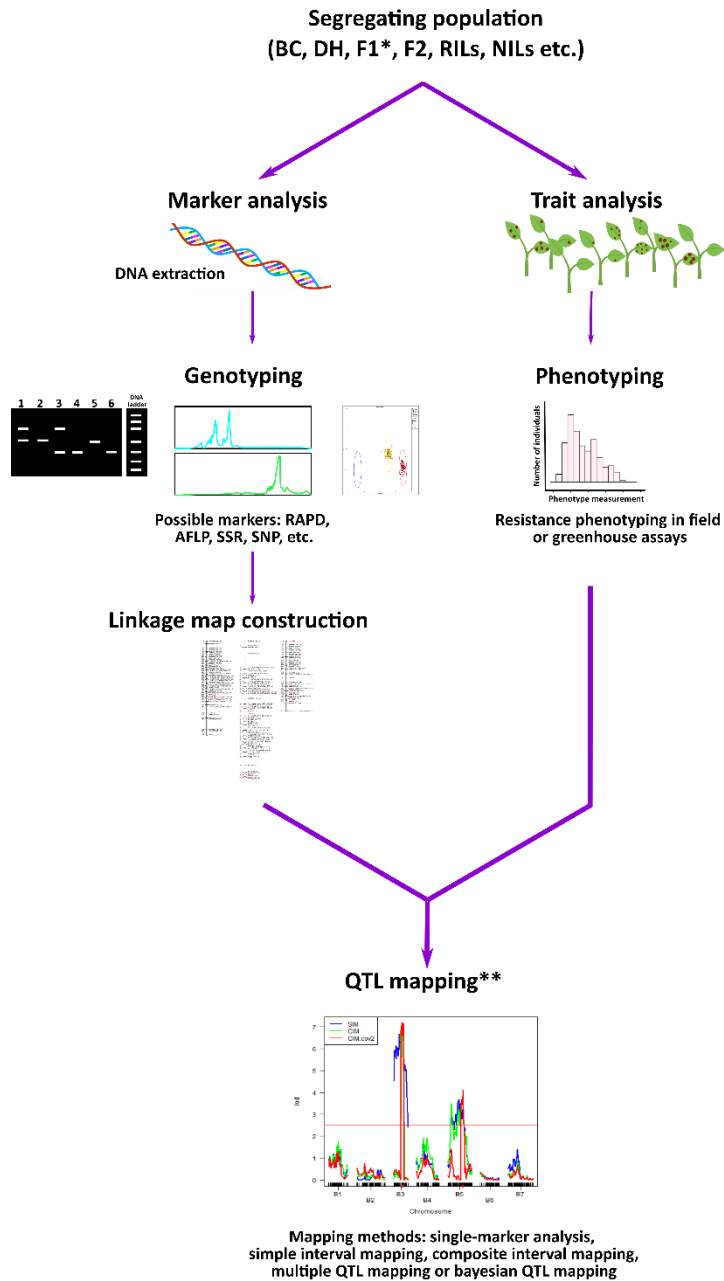


Figure 5: Basic concept of quantitative trait loci (QTL) analysis for quantitative disease resistance investigation (adapted from Keller et al. 2000; Collard et al. 2005)

Segregating population names: BC for backcross, DH for dihaploid population, F1 for filial 1, i.e. first generation of individuals resulting from a cross of distinct parent types (Khan 2017), F2 for filial 2 that is the product of the cross between F1 individuals, RILs for recombinant inbred lines, NILs for near isogenic lines; F1* can be obtained by crossing either two homozygous lines that are different or by crossing two heterozygous parents; DNA markers cited: RAPD for random amplified polymorphic DNA, AFLP for amplified fragment length polymorphism, SSR for simple sequence repeat or microsatellite, SNP for single nucleotide polymorphism; resistance phenotyping is tested in field or in laboratory/greenhouse and needs to be replicated to determine resistance phenotype of each individual. Infection can be the result of natural or artificial infections. Different measurements can be used like disease index, lesion size and length, number of organs infected, time to defoliation for resistance against biotrophs, latency period and sporulation for fungal pathogens, number of colonies forming units in planta for bacterial pathogens, enzyme-linked immunosorbent assays for viral pathogens, etc. (Roux et al. 2014; Dong et al. 2017a; Willcoquet et al. 2017); QTL analysis uses both phenotypic resistance data and genotyping data to determine the location of the QTLs that are involved in the expression of the resistance. An illustration of QTL mapping results using simple interval mapping and composite interval mapping is presented using black spot disease scoring on hybrids from the cross between resistant and susceptible rose genotypes. QTL mapping** will be further discussed in chapter 2.

2.3.3. MINING THE GENES UNDERLYING QUANTITATIVE RESISTANCE LOCI (QRLs)

Several strategies can be adopted for the molecular dissection of detected QRLs and some were reviewed by Salvi and Tuberosa (2005, 2007) and presented in Figure 6. The initial step to investigate QDR is to identify QRLs by either performing a linkage-based QTL mapping using a segregating population like previously explained or association mapping using a germplasm collection presenting different degrees of resistance. Most of the time the first mapping only locates loci within an interval ranging from 10 to 30cM when biparental or multiparental populations are used for linkage-based QTL mapping or collections with high linkage disequilibrium (LD) for association mapping (see Figure 6). Hundreds of genes can be found in such wide intervals, which makes mining for causal genes or causal QTN polymorphisms difficult. Further studies are then needed to clone QTLs and discover genes underlying them. First, for association mapping, low LD collection can be used to reduce confidence intervals. Then, for positional cloning (linkage-based method), several steps are necessary to reduce confidence intervals to less than 1cM (QTL fine mapping) which greatly reduces the list of causal genes to be tested. In order to map the QTL more accurately, nearly isogenic lines (NILs) can be created as they harbor a specific QTL (and no other ones) as the major source of variation. The QTL is considered to be “mendelized” and that way the cM distances between a QTL and the nearby molecular markers can be estimated more precisely (Salvi and Tuberosa 2005). When the confidence interval is sufficiently reduced, one can use molecular genotyping using expressed sequence tags (ESTs) to cover the QTL region using the closest markers as anchors (see Figure 6). QTL tagging can also be used to investigate the molecular bases underlying QRLs. This technique employs different approaches that aim to functionally modify or inactivate genes within the QTL using T-DNA-based methods as well as DNA-transposons and retrotransposons (see Figure 6). However, for this technique to be efficient, a complete screening of a high number of plants is needed as well as callus culture or direct regeneration. Finally, transcriptomic, metabolomic and proteomic approaches can be used to help identify the causal genes underlying QRLs and more widely QTLs. After a gene or sequence is identified to be linked to a quantitative trait (for example QDR), the candidates need to undergo functional testing by, for example, overexpressing or down-regulating the target gene through genetic engineering, RNAi techniques, CRISPR-Cas9 or if available reverse genetics tools like T-DNA or transposon-tagged populations and targeted induced local lesions in genomes (TILLING) (Salvi and Tuberosa 2005, 2007). Validation of QTNs in non-coding regions (like promoters or far to the regulated gene like enhancers or silencers, miRNA loci, regions controlling chromatin methylation and organization, etc.) remains a major challenge.

Even though many QTL-based studies trying to investigate quantitative disease resistance were published in the last century, relatively few QRLs were cloned. St Clair (2010) mentioned that it is difficult to assess the number of QRLs that were cloned because of the “proliferation of conflicting and confusing terms used to describe QDR in the literature”. Indeed, depending on how authors decide to define QDR and QRLs, distinguishing between major-effect QRLs and qualitative resistance mapped as QRL with a high LOD score and a narrow chromosomal region can be complicated. In 2017, Pilet-Nayel et al. tried to report the genes that were cloned and that gave partial effects contributing to quantitative resistances. A total of 15 genes were identified until 2017 (French et al. 2016; Pilet-Nayel et al. 2017), and after 2017, two additional cloned QTLs were published for potato late blight field resistance and wheat fusarium head blight resistance (Jiang et al. 2018; Gadaleta et al. 2019). The investigation and validation of the recently published QRLs revealed a wide diversity of mechanisms and causal genes underlying QDR. In 2009, Poland

et al. listed some hypotheses about the mechanisms underlying QRLs. As of today, with the cloned QTLs that have been published since the review of Poland et al., some of these hypotheses can be validated and new ones proposed (French et al. 2016; Pilet-Nayel et al. 2017). First, Poland et al. hypothesized that genes regulating morphological and developmental phenotypes could condition QDR by having pleiotropic effects in disease resistance. This hypothesis has not yet been validated but some QRLs were demonstrated to be developmental stage- and environment-dependent. Some of the cloned genes were, indeed, expressed at specific developmental stages like *Lr34* (resistance of wheat to leaf rust) and *ZmWAK*, or under specific environmental conditions like *Yr36* (resistance of wheat to stripe rust) that gave resistance at high temperatures (25-35°C) and susceptibility at low temperatures (under 15°C) (French et al. 2016 and references therein). Another hypothesis was that QRLs might intervene as components of chemical warfare, i.e. genes involved in the production of enzymes working in detoxification pathways like phytoalexins. The clubroot resistance QRL *PbAt5.2* from *A. thaliana* was demonstrated to be associated with an enhanced clubroot-triggered induction of camalexin biosynthesis (Lemarié et al. 2015). Similarly, the QRL associated with *A. thaliana* resistance to botrytis was correlated with different camalexin levels (Poland et al. 2009). However, a good correlation does not mean that genes controlling phytoalexins levels are behind QRLs, so further studies need to be undertaken to validate or not this hypothesis. QRLs also seem to participate in defense signal transduction as many cloned QRLs have kinase domains (six loci out of the 15 cloned encode for kinase protein domains) (See Table 1) and one locus (*STV11*) encodes for an enzyme involved in the catalysis of salicylic acid (SA) transformation into sulphonate SA (SSA) which is believed to be a signal that triggers increased SA biosynthesis giving rice stripe virus resistance (Wang et al. 2014a). Poland et al. (2009) mentioned the hypothesis that QRLs can be involved in defense signal transduction but at that time no evidence supporting it has been demonstrated. Another hypothesis was that QRLs could be 'weak' or 'defeated' forms of *R* genes. Indeed, many studies reported coincidence of QRLs with *R* genes (Poland et al. 2009; Roux et al. 2014; French et al. 2016; Pilet-Nayel et al. 2017), and three of the cloned QRLs exhibited a NB-LRR domain (See Table 1). But Vásquez et al. (2018) asked a relevant question: "How to explain that a *R* protein confers only partial resistance?" One possibility is that the presence of the weak allele coding for a slightly different *R* protein can lead to a reduced affinity between the *R* protein and the pathogen effector which would not be sufficient to activate a full response and would result in a residual resistance (Vásquez et al. 2018). An example of 'defeated' *R* gene is the rice bacterial blight resistance gene *Xa4* that gives around 50% less of the level of resistance against strains containing *avrXa4* locus (CR6 *Xoo* strain) than when the *R* gene resistance is not broken (French et al. 2016 and reference therein). QDR could also be due to mutation or different alleles of genes involved in basal defense (Poland et al. 2009). For instance, the gene *Pi35* presents altered forms in its NBS and LRR domains and *Pi35* alleles give moderate levels of resistance with no HR against multiple races of *M. oryzae*. It was demonstrated that *Pi35* encoded a different allele of *Pish* that is a gene known to produce HR response against *M. oryzae* leading to race-specific qualitative resistance to blast. With this example one can see that allelic differences at the same locus can be responsible for two different types of resistance with either complete resistance or partial resistance (French et al. 2016). It was also demonstrated that QDR can be the result of loss-of-function susceptibility alleles like for *Pi21* that is known to be a *S* allele in rice blast disease and that lost a large portion of sequence in the proline consensus motif. This motif participates in the protein-protein interaction domain and this could mean that the resistant protein is unable to interact with the pathogen effector, probably leading to the slower HR observed in lines carrying the deletion

(French et al. 2016). An additional mechanism underlying QRLs was proposed by French et al. 2016: it is a variation in host metabolism as a basis for QDR. They gave the example of *Rhg4* that encodes for a serine hydroxymethyltransferase domain (SHMT) known to play a major role in folate-dependent one-carbon (C1) metabolism. C1 metabolism is extremely important for the development of nematode feeding cells (syncytia) in plant roots and disrupting the conversion and transfer of C1 groups in the folate metabolism may be detrimental for the nematode life cycle (French et al. 2016).

With the recent progress in QTL cloning, more and more QRLs were cloned in different pathosystems. Their nature informs us on the possible biological bases underlying QRLs, and at first glance with existing discoveries, it is clear that many different types of genes and mechanisms lead to QDR. Given the wide range of actors possibly implicated in QDR from kinases, metabolic enzymes, transporters to altered *R* genes, it is likely that additional and even unique set of unidentified genes may be found to participate to the establishment of QDR type of resistance (Poland et al. 2009; French et al. 2016; Vásquez et al. 2018).

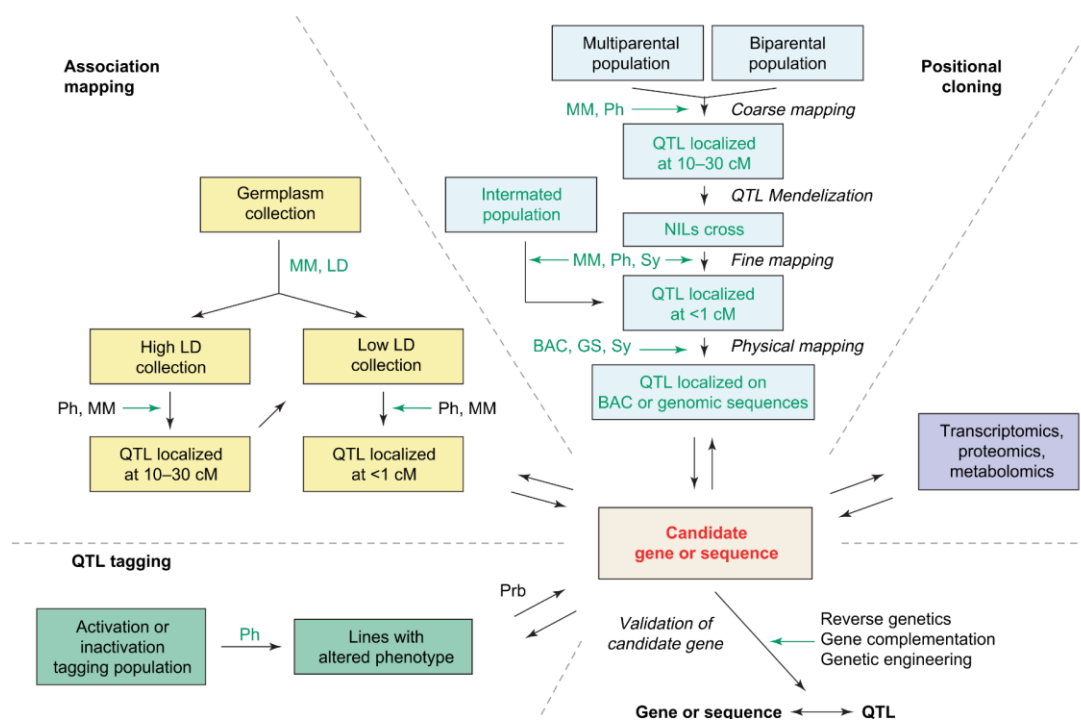


Figure 6: Illustration of different strategies for molecular dissection of QTLs from Salvi and Tuberosa (2005)

Boxes indicate starting material or major milestones. Major experimental processes are indicated in black italic font. For each experimental process, relevant genetic, molecular or analytical tools are indicated in green font. Abbreviations: BAC, library of bacterial artificial chromosomes; GS, genomic sequence; LD, data on linkage disequilibrium; MM, molecular markers; NILs, nearly isogenic lines; Ph, phenotyping; Prb, probing with tagging agent, for example, transposon; Str, data on population structure; Sy, synteny. Reverse genetics includes transposon and T-tagging, activation tagging, TILLING and RNAi.

Table 1: Cloned genes with partial effects contributing to QDR in plants from Pilet-Nayel et al. (2017) completed with recent studies

Plant/pathogen pathosystem	Locus	Protein domain(s)	Mechanims underlying QDR	Reference
Arabidopsis thaliana/Xanthomonas campestris	RKS1 RRS1/RPS4	Atypical kinase NB-LRR pair	Defense signal transduction and R gene	Huard-Chauveau et al., 2013; Debieu et al., 2016
Arabidopsis thaliana/Fusarium oxysporum	RFO1	Wall-associated receptor-like kinase	Defense signal transduction	Diener and Ausubel, 2005
Maize/Setosphaeria	Htn1	Wall-associated receptor-like kinase	Defense signal transduction	Hurni et al., 2015
Maize/Setosphaeria turcica, Cochliobolus heterostrophus, Cercospora zeae-maydis	qMdr9:02	Caffeoyl-CoA O-methyltransferase	Host metabolism variation	Yang et al., 2017
Maize/Sporisorium reilianum	qHSR1	Wall-associated receptor-like kinase	Defense signal transduction (Developmental stage-specific expression)	Zuo et al., 2015
Rice/Magnaporthe oryzae	Pi21	Heavy metal-transport detoxification	Loss-of-function susceptibility allele	Fukuoka et al., 2009
Rice/Magnaporthe oryzae	Pi35	NB-LRR	R gene (polyallelic variation)	Fukuoka et al., 2014
Rice/Tenuivirus	STV11	Sulfotransferase	Defense signal transduction via SA hormone	Wang et al., 2014
Soybean/Heterodera glycines	Rhg1	Amino acid transporter – a-SNAP protein- wound inducible protein	Unusual disease resistance locus	Cook et al., 2012; Liu et al., 2017
Soybean/Heterodera glycines	Rhg4	Serine hydroxymethyltransferase	Host metabolism variation	Liu et al., 2012
Wheat/Puccinia triticina, P. striiformis, Blumeria graminis	Lr34	ABC (Adenosine triphosphate - Binding Cassette) transporter	Sugar regulation or signaling (Developmental stage-specific expression)	Krattinger et al., 2009
Wheat/Puccinia striiformis	Yr36	Kinase-START	Defense signal transduction (Environment-specific expression)	Fu et al., 2009
Wheat/Puccinia triticina, P. striiformis, P. graminis, Blumeria graminis	Lr67	Hexose transporter	Sugar regulation or signaling	Moore et al., 2015
Wheat/Fusarium graminearum	Fhb1	Pore-forming toxin-like	Detoxification	Rawat et al., 2016
Potatoe/Phytophthora infestans	R8	NB-LRR	R gene	Jiang et al. 2018
Wheat/Fusarium graminearum	QFhb.mgb-2A	Wall-associated receptor-like kinase (WAK2)	Defense signal transduction	Gadaleta et al. 2019

3. ROSE AND HUMANS, A LONG LASTING HISTORY

There is probably no other flower like the rose that has been so loved and popular throughout the History. The “so called” queen of flowers holds a strong symbol and carries an invaluable cultural importance. Mention of roses can be found in countless legends, myths and tales. However, roses are known to have thrived on earth long before the existence of humans.

3.1. ORIGIN OF ROSES AND THEIR IMPORTANCE IN OUR SOCIETY

3.1.1. ROSE CLASSIFICATION OVER THE CENTURIES

Rose belongs to the family of *Rosaceae* that groups together several genera of well-known horticultural crops such as *Malus* (apple), *Pyrus* (pear), *Prunus* (cherry, plumb, peach or apricot), *Rubus* (blackberry or raspberry) and *Fragaria* (the famous strawberry). The *Rosa* genus is large and is divided into four subgenera according to the morphological classification presented by Rehder 1940 and revised by

Wissemann 2003 (Figure 7). The subgenus *Rosa* comprises between 150 to 200 species distributed in nine sections (Wissemann and Ritz 2007). Hybridizations between different species in the *Rosa* genus have led to a complex classification where many bridges between species can be found, which makes it even more difficult to distinguish the species in the genus (Wissemann and Ritz 2007; Tomljenovic and Pejić 2018). Recently, some studies have attempted to unravel the complexity of the *Rosa* genus using modern techniques of phylogenetics and phylogenomics like genomic markers (AFLP, SSR etc.), chloroplast DNA sequences or whole genome sequences (Bruneau et al. 2007; Koopman et al. 2008; Fougère-Danezan et al. 2015; Debray et al. 2019). As a result, a modification of the classification has been proposed with several taxonomic modifications based on recent discoveries (Debray 2020). The genus would no longer be divided into four subgenera but instead, Debray (2020) suggests to divide it into sections as the subgenus *Rosa* is not monophyletic and the other subgenera seem to be scattered at different positions within the subgenus *Rosa* (Figure 7).

3.1.2. ROSES AND PEOPLE

The earliest evidence of roses was found in a fossil bed in Idaho (USA) dating it back to the Paleocene (55Mya – 35Mya) (Becker 1963 citing Hollick 1936). From then, wild roses evolved and colonized all of Asia and North America. Later on, traces of roses during the Eocene were found in Europe (reviewed by Debray 2020). Roses are endemic to the northern hemisphere and can be found in a wide variety of environments (from Alaska to Mexico but also northern Africa). It is only around 7,000 B.P. that evidence of rose (seed heaps) being used by mankind was found in German (Debray 2020 citing Elburg 2010) and British sites (Debray 2020 citing Brown and Murphy 1997). It remains unclear where rose cultivation really started 5,000 years ago (either China or Mesopotamia) but it is during the Roman empire that its popularity gained a larger public (Bombarely 2018). The passion for roses only grew stronger with time until it became one of the greatest symbols in our history. The first evidence of rose used in human representation was found to be dated from 3,500 B.P. during the Greek civilization (Widrlechner 1981; Bombarely 2018). Thousands of representations have used roses as a symbol of purity, love, beauty, friendship, sexuality and secrecy but also as a symbol of war (Ole Becker et al. 2007). Royalties have used roses as an emblem of their power and have declared wars “in the name of roses” like with the well-known “War of the Roses” in England (1455-1485). Roses are often associated with a civilization's prosperity. But it is in the literature and paintings that we can see the greatest representations of roses. Countless poets, writers, artists have tried to capture and portray their fragile beauty associating roses with particular emotions. Emotional connection to roses and their link to human history may have given an undoubtable prominence to these flowers (Ole Becker et al. 2007). In addition, beyond their symbolic importance, roses have solely gained in value as trade material mainly as ingredients for perfumes, unguents and remedies of all sorts (Bombarely 2018).

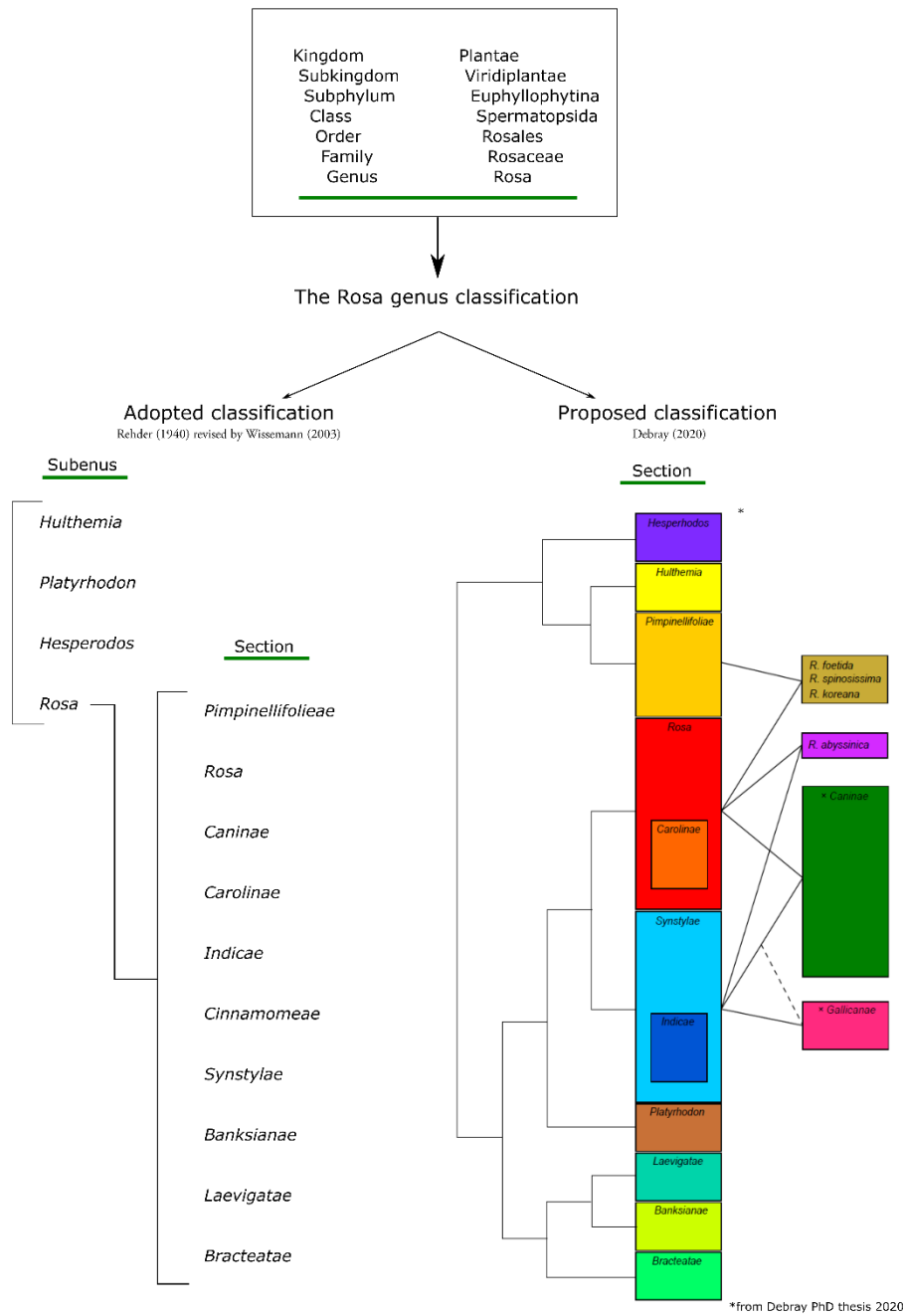


Figure 7: Rosa genus classification from morphological classification from Rehder (1940), revised by Wissemann (2003) and newly proposed classification by Debray et al. (2020), based on nuclear and chloroplastic markers

3.1.3. THE HORTICULTURAL IMPORTANCE OF ROSES

Nowadays, rose represents the most important ornamental plant with a high economic value and has been entitled as the world's favorite flower (Zlesak 2007). In 2008, the value of world rose production was estimated at € 24 billion (Heinrichs 2008). Three main usages can be pointed: cut roses, garden roses and extract of fragrance as well as the new niche market of potted roses as houseplants (Marriott 2003).

On one hand, roses for cut flowers dominate the ornamental market and have been ranked at the first place of worldwide trade for many years by the world's biggest auction company for ornamentals, Royal FloraHolland. Indeed, total exportations of cut roses reached 3.337 billion sold units with a value of € 746 million (Neu 2018 citing FloraHolland) with The Netherlands being the top exporter (1.2 billion USD in 2016), followed by Kenya (700 million USD) and Ecuador (600 million USD) (Royal Floral Holland 2018). France is one of the biggest importers with € 376.3 million spent on cut flowers by 7.3 million homes in 2018 (VAL'HOR 2018). Cut roses are offered on many occasions but they are often related to important life events like birthdays, weddings and funerals as well as specific festive days in the modern calendar (Valentine's Day or Mother's day) (VAL'HOR 2017; Benoit 2019).

More and more customers have chosen to offer pot roses instead of cut flowers. In France, 2.8 million rose pots, worth € 23.2 million, were bought in 2018 (VAL'HOR 2018) and 5.9 million of potted roses, worth 25.9 million USD, were bought in the U.S. in 2019 (USDA National Agricultural Statistics Service 2020).

On the other hand, the garden rose market is losing importance in many countries. Two examples can be presented: in France, garden rose value and volume have been divided by two with 10.3 million of rose shrubs in 2008 against only 4.7 million in 2018 (VAL'HOR 2018), and in the U.S., rose shrub sales have decreased between 2014 and 2019 with 36.6 million roses sold in 2014 (worth 203.5 million USD) versus 25.1 million in 2019 (worth 168.1 million USD) (USDA National Agricultural Statistics Service 2015, 2020).

Finally, roses have been used for their scent to produce amazing fragrance throughout the years (Gudin 1999; Zlesak 2007). As of today, it is a product of luxury as perfumery uses three to five tons of rose flowers to produce one kilo of rose attar (Baudino et al. 2013). Lastly, roses are used in restricted amounts for culinary purposes (flavors in the food industry for example, Gudin 1999) but also for medicinal purposes (for example, the medicinal benefits of rose hips from dogrose, species from *Rosa* section *Caninae*, Nybom and Werlemark 2016).

3.1.4. A SHORT HISTORY OF ROSE BREEDING

Roses have been part of our history for centuries and continue to be used in our modern society in many ways. From the wild roses of our lands to the beautiful roses in our vases or our gardens, there have been years and years of breeding to shape the roses that we know today.

In Europe, cultivation of roses increased during the Roman empire with the cultivation of many hybrids such as *Rosa x richardii*, *Rosa x damascena*, and *Rosa x bifera* (Bombarely 2018). In the meantime, roses were widely cultivated during the Han Dynasty, 3.000 years ago (Wang 2007). It is believed that two centers of rose cultivation (China and Europe) remained separated until the late eighteenth century when *cultivated old Chinese roses* were introduced in Europe (See summary on Figure 9). Thus, rose breeding in the western world can be divided into two periods (pre-1800 and post-1800) separated by the introduction

of Chinese roses in European background (Wylie 1955; Marriott 2003; Liorzou et al. 2016). Chinese rose introduction brought new characters into the European pool with the most important and revolutionary being the continuous flowering (Marriott 2003).

This introduction marked the beginning of the Modern roses that we know today. Modern roses are known to have originated from a small set of seven to ten species but the introduction of Chinese roses increased the primarily genetic pool (Zlesak 2007). Before the 1800s, European roses were exclusively bred from species belonging to the *Rosa* section with groups like Gallica, Damas, Alba, Centifolia and Moss roses. Ancient European roses were known for their hardiness and were in majority once flowering plants (except for the variety 'Quatre saisons'). All seem to have a common ancestor *Rosa gallica* sp. that is known to have pink or white flowers. Therefore, more exotic colors and true red were not known. After the 1800s and with the introduction of Chinese roses, new colors were available such as true red, yellow and apricot-color (Marriott 2003). Pink roses like 'Pink China' or 'Old Blush' as well as red genotypes like 'Slater's Crimson China' (*Rosa chinensis* 'Semperflorens') were introduced in Europe at the end of the eighteenth century. Later, during the nineteenth century, two additional Chinese varieties were introduced in England ('Hume's Blush Tea-Scented China' and 'Parks Yellow Tea-Scented China'). These Chinese varieties were crossed with old European roses and numerous hybrids were obtained during the nineteenth century as Noisette, Bourbon, Tea, Chinese Hybrids, Reblooming Hybrids... leading to the Modern roses (Figure 8) (Wylie 1955; Marriott 2003; Liorzou 2016). It is worth mentioning that the introduction of Chinese roses revolutionized rose breeding but left in oblivion the ancient European roses causing the disappearance of an important number of them (Liorzou et al. 2016).

The genus *Rosa* is particularly complicated because of the remarkable ability of roses to cross between species of the same genus. This characteristic has been used for a long time and many interspecific hybrids have been developed over the centuries. Countless combinations can be made with this incredible diversity to create new varieties. But, rose breeding, as for many other plants, has been driven by different strategies that have evolved along with society.

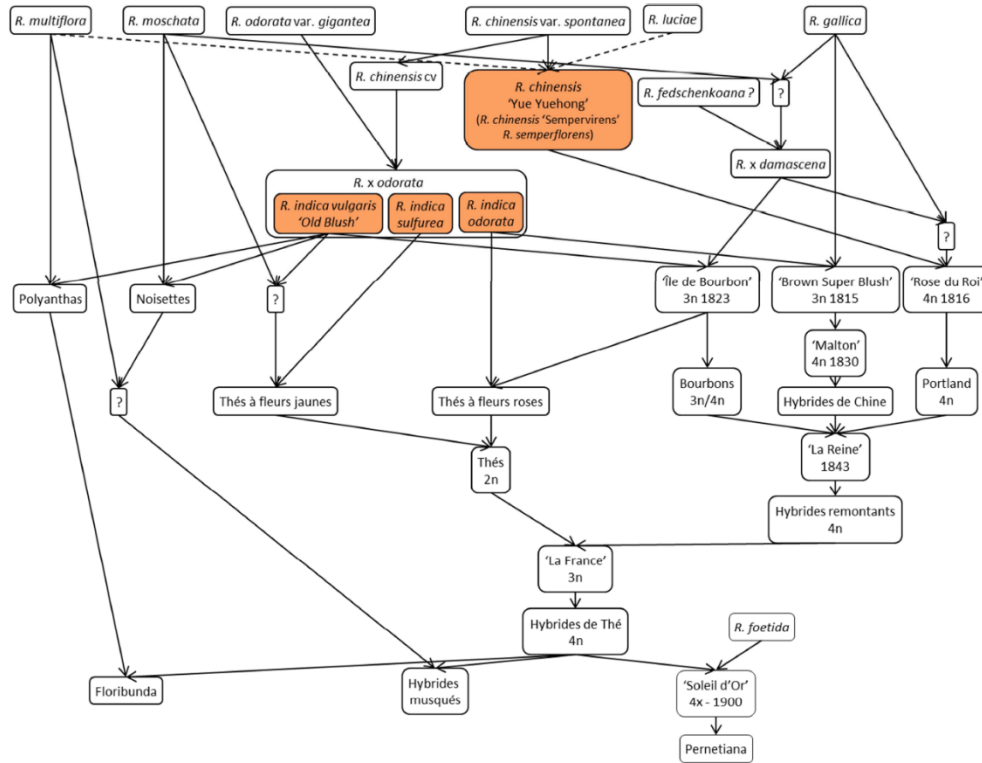


Figure 8: Hypothetical representation of the complex origin of the cultivated roses, from Liorzou PhD Thesis in 2016

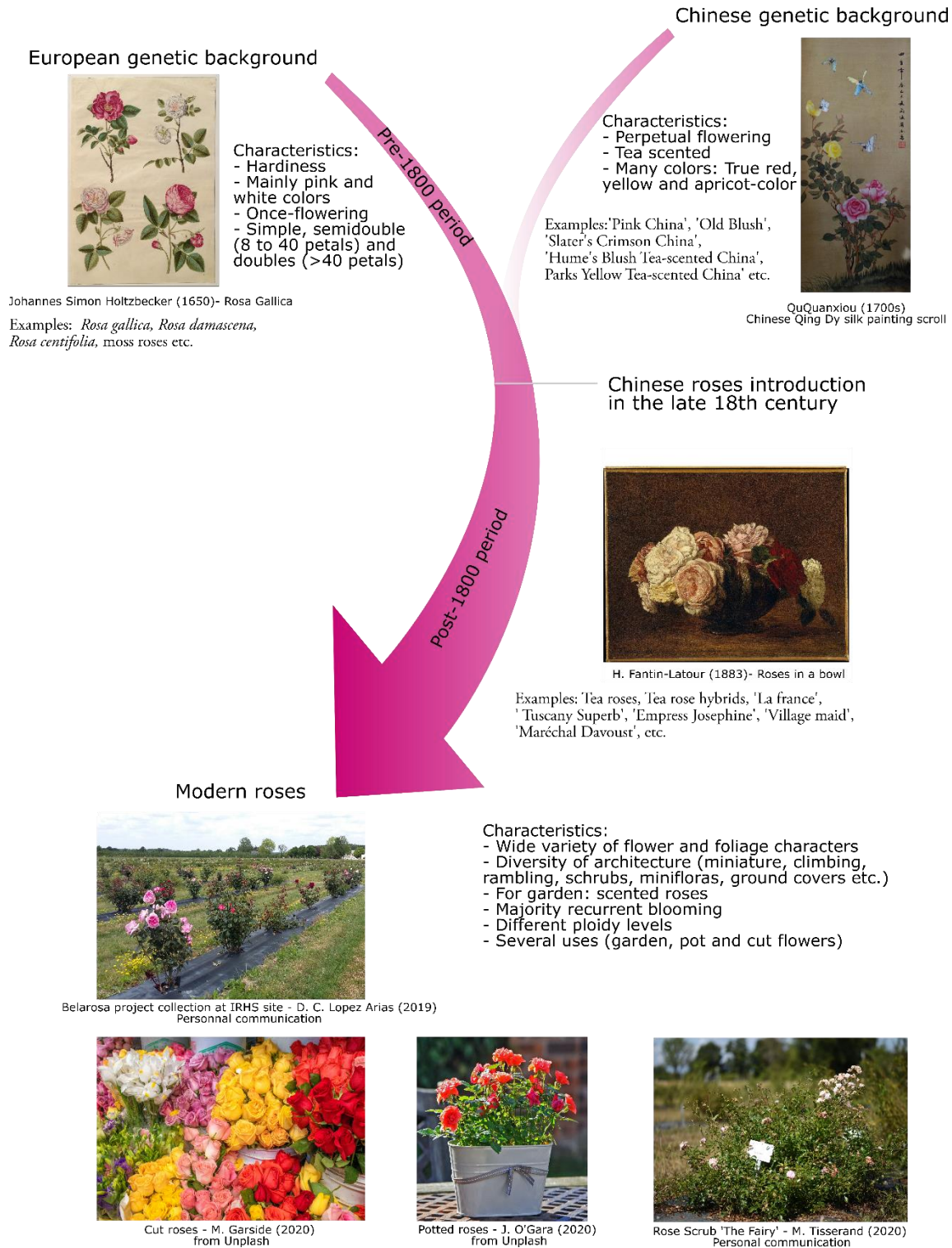


Figure 9: Summary of the history of rose breeding in Europe

Summary adapted from Wylie 1955, Marriott 2003 and Liorzou 2016. Picture credits for Johannes J. S. Holtzbecker painting: Statens Museum for Kunst, <http://www.smk.dk/en/copyright/creative-commons/>; for Qu Qanxiu silk painting: Image found in Etsy and copyright granted by the owner Dragondynasty-EtsyShop; Picture credits for H. Fantin-Latour painting donated by Metropolitan Museum of Art to Wikimedia (<https://www.metmuseum.org/art/collection/search/437995>). Photo credits are indicated under each photo and photos from unplash are copyright free.

3.1.5. BREEDING STRATEGIES OF YESTERDAY, TODAY AND TOMORROW

During the nineteenth century, increasing interest was given to recurrent blooming hybrids which led to the creation of Tea rose Hybrids, the first group of Modern roses. The purpose of Tea rose Hybrids breeding was to produce the perfect flower leaving behind the improvement of other characters. Characters such as flower color, blooming period, floribundity, double flower, flower scent and hardiness were the most important breeding criteria during the 1800s (Oghina-Pavie 2015). For example, 'Soleil d'Or' was the first variety to have a real yellow color on the rose flowers but was not vigorous and very susceptible to disease (Marriott 2003). Prevalence of the flower character and the blooming over the disease resistance was observed until the middle of the twentieth century. Indeed, English rose breeders aimed to combine characteristics and growth habits of the old European roses (flower delicacy and fragrance) with the recurrent-blooming habit and wide color range of the modern roses (Marchant 1994). With this breeding strategy and because one can only follow a few characters in progeny, it was difficult for them to develop and sometimes retain other important characters like disease resistance and hardiness (Marchant 1994). Nowadays, rose breeding has shifted to a more specialized breeding, having very different criteria and goals according to the final horticultural use of the product. I will review the breeding strategies for the main outlets of the rose industry.

First, traditional breeding objectives for cut roses were increased productivity, post-harvest vase life and tolerance to pests and diseases (Gudin 1999). For many years, long stems and post-harvest characteristics like transporting qualities or vase-life have prevailed over the flower scent. Today, fragrance is absent in most modern cut rose varieties but to meet the increasing demand of cut roses with a strong smell (Özzambak et al. 2009; Berki and Menrad 2019), breeders need to adapt and select for roses with stronger scent. In his book, Gudin mentioned that increased fragrance in roses was under selection in 1999 and that the expression of "real rose" fragrance was incompatible with a good postharvest life. In general, the average vase-life of a variety needs to be between 12 and 14 days, with some varieties having up to 18 days, and varieties with fragrance have, indeed, a lower vase life (8-10 days) (Chaainin 2003). However, evidence for fragrance not being directly related to short vase life has been demonstrated (Borda et al. 2007). New prospects on cut rose breeding have arisen with the isolation and characterization of several genes responsible for the rose floral scent like the well-known Nudix hydrolase RhNUDX1 or the two fragrance related genes OOMT1 and OOMT2 (Guterman et al. 2002; Joichi et al. 2005; Baudino et al. 2013; Roccia 2013; Magnard et al. 2015; Roccia et al. 2019; Sun et al. 2020). For instance, engineering floriculture crops to produce fragrant roses with a long vase life has, now, become a possibility (Clark 2007).

Another example is one of the potted roses. Breeding for pot roses is mainly focused on selecting "miniature" roses and varieties with a good rooting capacity. Dwarfism seems to be quantitatively inherited when Dwarf Polyantha, Koster roses or Compactas are crossed with Floribunda or Hybrid Tea varieties, which reduce the number of possible candidates selected in populations. But for *R. roletii* crosses, the character was shown to be controlled by the single dominant gene *D* (De Vries 2003). More than simply small roses, increasing interest in "small roses with large flowers" has led breeding strategies to evolve with, for example: crosses between "miniatures" and large roses, retaining "accidental" dwarf

individuals that can be discarded in “large roses” breeding programs or genetic engineering of desired large roses with the *IPT* gene to shorten the internodes while maintaining the flower size (De Vries 2003).

Nowadays, garden roses have been awarded with multiple uses. Indeed, beyond their utilization in our garden, increased interest in landscape roses has led breeders to breed for very different criteria. For instance, Hybrid Tea roses are used for their decorative features and, therefore, careful attention is paid to the flower (floribundity, recurrent blooming, scent, color, fragrance, etc.), the foliage, the architecture and the disease and pest resistance. Additionally, climbing roses have been developed since the late nineteenth century, mainly from naturally occurring sports (spontaneous mutations) of pre-existing rose varieties such as Hybrid Tea and Floribunda roses (Marriott 2003; T.O. Buidina et al. 2019). Such roses are known for their increased growth rate (20-56cm in height), continuous flowering (even if some varieties can flower in spring and then one time in autumn) and floribundity (Marriott 2003; Iwata et al. 2012; Vukosavljev et al. 2013). Climbing roses produce primary shoots with indeterminate vegetative growth allowing them to “climb” and blooming happens in axillary secondary shoots that do not terminate the principal shoot growth (Iwata et al. 2012). More and more shrubs and ground -covers have been bred to satisfy the increased demand from landscape professionals (towns, highway companies or landscape architects). These specific roses are selected for their floribundity, hardiness, disease and pest resistance and their low maintenance (Gudin 1999; Marriott 2003). Moreover, a new trend of “all-season” decorative roses has arisen and roses are, then, selected for their hip esthetics during the winter period (color, number and size) as well (Gudin 1999). The same way as for cut roses, increased demand for fragrant varieties has led breeders to breed for new fragrance or blends like anis, lemon, peach, pear, apple, etc. (Gudin 1999). However, fragrance seems to be linked to unwanted characters like black spot and botrytis susceptibility (Gudin 1995 citing unpublished results from Gudin and Mouchotte). Specific breeding for disease resistance will be further reviewed in the following sections. Finally, some people feel nostalgic for the beauty of the old garden roses but because of their fragility and susceptibility to various diseases/pests and environmental stresses, constant care is needed. As much as a regular garden would like to own old garden roses, in our society’s era, less time is spent gardening, which makes it difficult to have healthy old rose varieties in our gardens. Breeders are, then, trying to select for roses with similar characteristics than the old varieties but with an increased resistance to diseases and other stresses (Gallais and Bannerot 1992; Liorzou 2016).

We can see that the criteria used in rose breeding have evolved over the centuries adapting more and more to the consumer’s demands. Breeding has gone from a simple hobby in someone’s garden to a well-organized institution following rules (patents, catalogue inscription of varieties, etc.) and trends (surveys and market simulation) (Zlesak 2007). Evolution of rose genetics has led to the evolution of breeding perspectives with new techniques now within our reach.

3.2. EVOLUTION OF THE BREEDING TECHNIQUES

Rose breeding is no longer just observing the rose and hoping to get the desired traits but it aims to control every inch of the rose to adapt to the consumer’s demands, new challenges and threats. At the beginning of the nineteenth century, rose breeding was performed via open-pollination and breeders only considered the traits of the seed parent (Zlesak 2007; Oghina-Pavie 2015). It was around 1830-1840 that breeders started to use artificial crossings and, therefore, to control the fertilization by deciding which

cross to perform. When artificial crossing started, crosses were more or less controlled as they were mainly done by shaking the flower of one plant over another one (Oghina-Pavie 2015). Thereafter, techniques gained in sophistication so crosses could be better controlled (emasculatation and flower isolation among others). Rose breeding has been marked by the shift between traditional hybridization like mentioned above to breeding programs combining traditional hybridization and several other techniques that I will briefly review.

3.2.1. IMPROVEMENTS IN ROSE HYBRIDIZATION THROUGH EMBRYO RESCUE AND PLOIDY LEVEL MANIPULATION

Limiting factors such as pollen fertility, pollination, seed maturation and germination as well as inner incompatibilities can greatly affect the breeding efficiency of traditional hybridization. Therefore, during the late 1900s, increased interest has been given to define the best conditions and practices during pollination and fertilization so traditional breeding can be improved (Gudin 1995, 2001; Gudin and Mouchotte 1996).

Interspecific crosses are often performed by breeding companies to bring new characters from other species of the genus into the current genetic pool. Nevertheless, some crosses can be harder than others with limited success of seed production or sometimes not at all. It is after the twentieth century that traditional hybridization was combined with modern techniques such as embryo rescue, ploidy level manipulation and protoplast fusion. Embryo rescue in rose was successfully performed in the late 1900s to prevent early abortion during traditional hybridization (Gudin 1994, 1995; Marchant 1994). For example, an original interspecific hybrid *R. rugosa* x *R. foetida* was successfully produced via this technique (Gudin and Mouchotte 1996). Ploidy level manipulation aims to help breeders to successfully perform crosses between species or varieties of different ploidies while producing fertile varieties. Two possibilities exist: polyploidization that increases the ploidy level with colchicine treatment or *in vitro* seedling culture in liquid medium (for example, chromosome doubling of diploid varieties/species so they can be crossed with tetraploids), and haploidization that reduces the ploidy level of tetraploid varieties for example, so they can be crossed with diploids (Meynet et al. 1994; Crespel 2001; Gudin 2001). For example, the genotype H190 used in several studies for QTL mapping including in the present work was obtained by haploidization of the 4x *R. hybrid* 'Zambra' (Crespel et al. 2002a, b) using irradiated pollen. However, some interspecific or intergeneric crosses are impossible because the abortion happens too early and the embryo cannot be rescued or because the fertilization does not happen due to incompatibilities between species or genera. In these cases, protoplast fusion can help to obtain hybrids from difficult crosses or impossible sexual crosses (Gudin 1999; Zlesak 2007). The first attempt was made by Matthews et al. in 1991 and hybrids between *Rosa persica* x *xanthina* and *Rosa wichurana* were obtained. In addition, intergeneric hybrids were also obtained using this technique like for example hybrids between rose and blackberry or cherry (*R. hybrida* 'Frensham'/*Prunus avium* x *Prunus pseudocerasus* 'Colt' and 'Frensham'/*Rubus laciniatus* 'Thornless Oregon', Mottley et al. 1996).

3.2.2. SELECTION PROCEDURES NOWADAYS

Beyond the problems of unsuccessful crosses, rose breeding is a long process that can take up to ten years (in general between 7-8 years) from the first hybridization to the commercialization of a new variety (Noack 2003; Zlesak 2007; Vukosavljev 2014; Leus 2017). According to a survey in 2015, 135 out of 1,800

participants indicated that they bred roses. The majority of them are part-time breeders (mostly older than 50 years old) that were retired. Another significant part of the rose breeders was represented by nursery professionals that indicated to breed and release varieties to provide new products for their business. Finally, the vast majority of released roses are done by full-time breeders from breeding companies that follow specific breeding programs adapted to their market and commercializing regions (Byrne 2015). In the next steps, I will only focus on the presentation of breeding programs for garden roses.

Before proceeding with a breeding program, breeders screen for potential parents in the cultivated pool but they can also choose parents within wild roses. An intensive observation of roses characteristics is performed for several years under a wide variety of environmental conditions to identify candidates with higher traits. The parents are then selected for their innovative traits but also for their disease and pest resistance. Rose breeding programs are divided in two phases: (1) selection among a large number of seedlings in the greenhouse during the first two years and (2) performance testing and selection in the field from the third year and on (Chaanin 2003; Noack 2003; Zlesak 2007). Most recurrent flowering roses bloom within several weeks after germination (around 30 days from germination to first flower bud appearance, De Vries 1976), which enables selection for floral traits relatively early compared to most woody plants (Zimmerman 1972). During the first year, breeders select against weak growth, for innovative traits that are not found in the released varieties (Noack 2003; Leus 2017) and for floral traits like color attractiveness and longevity, wilted flowers that do fall properly and bloom shape (Zlesak 2007). The first selection step is crucial and several strategies can be adopted by breeders. A breeder can either perform a strong selection on floral traits from the first blooming which allows for more rapid progress in these traits or keep more seedlings after first blooming to observe them more critically as they mature (Zlesak 2007). Selection for disease and pest resistance at this stage is not often performed as more resources are needed to perform controlled inoculations, and knowledge on the disease or pest system tested is also necessary (Chaanin 2003; Noack 2003; Zlesak 2007). Nonetheless, authors like Debener and Byrnes (2014), Leus (2017), as well as Soufflet-Freslon et al. (2019) presented bioassays to test disease resistance in laboratory and greenhouse settings. Disease resistance inclusion in breeding programs will be further discussed in [section 2.1.3](#) (Figure 10). It is during this first phase that marker assisted selection (MAS) can be applied and it can help to perform early selection of seedlings with characters not yet visible at this stage. This reduces the number of selected seedlings for the next steps and, therefore, reduces the costs related to clone propagation and planting. The second step of selection can last several years and is mainly done in the field. Selection for floral traits, plant development and adaptability, disease and pest resistance, tolerance to diverse abiotic stresses and multiplication capacity is done from year 2 to the end. The first year of field testing is done in one breeding station but for the following years, different locations are chosen to test for adaptability and tolerance to different stresses. Throughout the years, offspring performance is tested on different settings: planted on their own roots (a trend in the U.S. and progressively more and more common in Europe) and grafted onto different rootstocks (Noack 2003; Zlesak 2007; Leus 2017). The most common rootstocks are *R. canina*, *R. indica major*, *R. multiflora*, 'Manetti' and 'Dr. Huey'. The choice of rootstock will depend on the use of the variety as well as the environmental conditions, the pests and root diseases known for the locations of commercialization and also on the date of commercialisation (for example, *R. multiflora* is often used to produce plants in pots for the spring). That is why most breeders test the compatibility of selected offsprings with different

rootstocks (Noack 2003; Zlesak 2007). At the end of the fifth year, three to five candidates are selected for official variety testing and patenting abroad. Further field trials are conducted during two to three more years and more candidates can be selected again following these trials (Figure 10). Variations of breeding schemes exist according to the usage of the new varieties. For example, for cut roses selection, the flower traits selected are different from the ones for garden roses or shrubs (long and strong stems, long vase life, multiple blossoms for spray varieties, etc.) and require additional testings (for example, vase-life trials) (Zlesak 2007). Specific traits are selected for other usages like mentioned at the beginning of this section.

3.2.3. INNOVATION WITHOUT CROSSING?

In addition to classical selection procedures, innovative traits of high commercial interest for both growers and consumers can be introduced or found in commercial varieties without needing to perform hybridizations and selection procedures. Indeed, the market of ornamental plants is very competitive and innovation is extremely important to satisfy the consumer's demand for novelties.

On one hand, an important source of new varieties is the mutation of preexisting roses. Natural mutation can occur on commercialized varieties leading to the selection of sports and it can allow breeding companies to commercialize product lines with different colors and aspects. Two examples can be cited: (1) spontaneous mutations (somaclonal variations inducing sport) in petals leading to different colors, petal variegation or double color blossoms, and (2) mutations producing climbing versions of bush roses or more compact bushes (Arene et al. 1993; Marriott 2003; Zlesak 2007). Mutation rate can also be increased through radiation (Gupta and Shukla 1971), chemical mutagens and somaclonal variations using callus cultures but it is not widely used in commercial rose breeding (Gudin 1999; Marriott 2003; Zlesak 2007). Genotypes obtained following mutations (natural or induced) are also integrated into breeding programs and used as progenitors for subsequent selection programs.

On the other hand, genetic engineering of rose plants can introduce innovative traits that are not normally found in the genetic pool and offer opportunities for rapid advancement. Furthermore, like mentioned in [section 2.3](#), knowledge on genes controlling ornamental traits of interest has opened new possibilities to introduce specific features in roses. Fragrance, flower color or plant architecture have been mentioned as potential traits that can be introduced in rose varieties. Roses represent 6.7% of the genetically modified (GM) ornamental plants in scientific publications (Boutigny et al. 2020). So far, plant attributes like morphological aspects, enhanced adventitious rooting, flower anatomy, perfume as well as longevity and prolonged vase life for cut roses have been genetically modified on roses. Resistance to fungi (black spot and powdery mildew), drought and cold have also been modified in roses (Zlesak 2007; Boutigny et al. 2020). However, only flower color-modified roses have been commercialized in some countries. The success of transgenic rose commercialization greatly depends on the consumer's acceptance and the country's regulation for genetically modified plants. For instance, no GM roses are commercialized in Europe due to strong interdictions of the European Union. Techniques of *Agrobacterium*-mediated transformation and biolistic transformation have been successfully implemented in diploid and tetraploid roses (Zlesak 2007; Boutigny et al. 2020). Genetic transformation of roses is mostly used in research to evaluate important ornamental genes. Yet, tissue culture regeneration as well as successful gene integration remain challenging and need further improvement but as for now, transformation efficiency is between 2 and 15%, which is encouraging for the future (Dong et al. 2017).

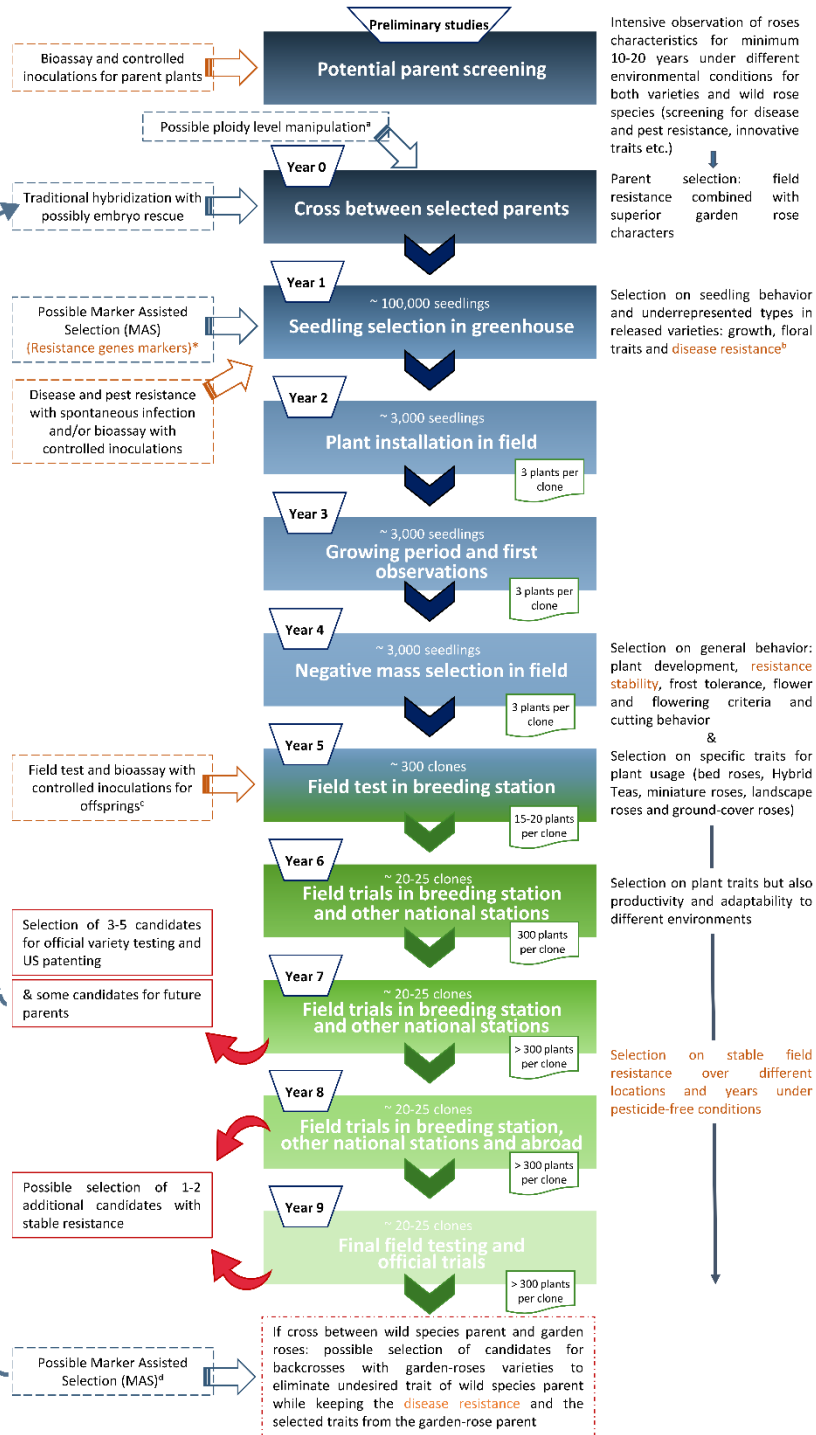


Figure 10: Proposed garden rose breeding scheme that includes disease and pest resistance selection and testing (adapted from Noak 2003, Zlesak 2007, Leus et al, 2007, Debener and Byrne 2014, Leus 2017 and french breeders recommendations).

^a Done if selected parents have different ploidy levels. Two options: haploidization and polyploidization (Crespel 2001, Crespel et al. 2002a-b, Zlesak et al. 2005). For example, 4n rose variety crossed with 2n wild species rose.

^b Depends on the breeder belief of young seedling resistance reflective of older plant resistance (Debener and Byrne 2014).

^c Disease resistance is tested in the field each year from Year 3 and bioassay/controlled inoculations can be done any time after that year.

^d MAS in introgression projects done to decrease the number of backcross cycles by reducing the genetic background of the donor genotype.

* Use of markers closely linked to resistance genes like *Rdr* type genes (*Rdr1* and *Rdr3*) for resistance to black spot disease or *Rpp1* gene developed for powdery mildew resistance.

4. THE BEAUTY'S BEAST: BLACK SPOT DISEASE ON ROSE

In the previous sections, we have seen that increased interest has been given to breed varieties with higher resistance. First, I would like to present the different diseases affecting roses and their impacts for the rose industry. Then, I would like to review the solutions proposed to breeders to face the new challenges as well as the implications of breeding for disease resistance for the research area.

4.1. ROSE NOWADAYS: A THREATENED BEAUTY?

4.1.1. PATHOGENS THREATS

The esthetic appearance is particularly important for rose marketability and consumer acceptance. Several pathogens can cause leaf and flower mosaic, distortion, spotting, discoloration, necrosis and early abscission (Debener and Byrne 2014). The main fungal diseases affecting rose leaves are black spot (*Diplocarpon rosae*), powdery mildew (*Sphaerotheca pannosa* var. *rosae*), rust (*Phragmidium* spp.), leaf spot (*Cercospora* spp.), and verticillium wilt (*Verticillium alboatrum* or *Verticillium dahliae*) (Figure 11). Another important disease that is not caused by a fungus is downy mildew (*Peronospora sparsa*) that causes leaf spots. One virus, the rose rosette virus (RRV), also known as witches' broom of rose, causes important damages to roses in Canada and the United States (Byrne et al. 2018). Finally, some diseases can affect indirectly the upper part of the plant like crown gall disease, a bacterial disease caused by *Agrobacterium tumefaciens* or nematodes, causing reduced vigor, wilting and chlorosis by infecting the roots (Horst and Cloyd 2007; Zlesak 2007; Debener and Byrne 2014; Leus 2017). The diseases caused by these pathogens mainly affect leaves and flowers and can drastically affect the ornamental value of the plant (Figure 11). They are the principal concern of growers and breeders and require a high degree of control. Some diseases can be specific to a certain area: RRV occurs mainly in Canada and the U.S; brown rot, caused by *Ralstonia solanacearum* (Smith), was reported for the first time in The Netherlands in 2015. Other diseases can be specific to a cultivation method. For instance, the major disease affecting roses in greenhouse settings is powdery mildew (*Podosphaera pannosa*) whereas the major one in outdoor-grown roses is black spot disease. However, in favorable conditions, downy mildew and black spot disease can affect cut-roses production in tropical areas (Leus 2017). Pests can also greatly affect rose production and commercialization but are not the main focus of breeding strategies nowadays and will not be detailed here. Unfortunately, losses due to the diseases described above are poorly documented (Debener and Byrne 2014), but diseases like black spot can lead to plant's death within a few years in the most susceptible cases (Smith et al. 1989; Black et al. 1994).

4.1.2. NEW RESTRICTIONS IN PHYTOCHEMICAL USE

The major diseases affecting roses are generally controlled in rose production by preventive chemical sprays every seven to 14 days when the conditions are favorable for disease development, which can lead to more or less 20 sprays per year (Debener and Byrne 2014). It is believed that 40% or more of the pesticides are used to control powdery mildew (Tjosvold and Koike 2001). For growers, half of the disease and pest control budget is allocated to disease control which represents between \$16,000 to \$35,000/ha/year. In addition to the high costs, worker safety, environmental contamination as well as the development of pesticide resistant pathogens and pests have encouraged growers to use integrated pest and disease management in their control protocols (Debener and Byrne 2014). Moreover, restricted access and use of chemicals make it difficult to control disease development when the rose product is used by

final consumers. Indeed, recent restrictions in the use of chemicals in Europe have led to a problematic situation as the most devastating diseases for outdoor-grown roses (garden roses, landscape roses etc.) are efficiently controlled by fungicide spray. European governments intend to reduce the use of chemicals by half before 2025 (European Parliament 2009; ECOPHYTO II et al. 2015). As a matter of fact, the use of chemicals has been prohibited in France since 2017 for landscape professionals (towns, landscape architects, public forest, roads and highways) and since 2019 for home-gardeners (Labbé 2014; Pothier 2017).

Beside the restrictions in European countries, gardeners have expressed an increased concern about using chemicals in their gardens not only because of the cost but also for their safety (Zlesak 2007; Eurobarometer 314/71.1 2009). Therefore, today's consumers are less willing to grow pesticide-dependent landscape plants and are leaning more towards lower maintenance landscape or shrub roses (Harp et al. 2009; Pemberton and Karlik 2015; Zlesak et al. 2017). Indeed, disease resistance has been ranked as the most desired trait worldwide by many studies the last ten years (Harp et al. 2009; Waliczek et al. 2015, 2018; Byrne et al. 2019).



Figure 11: Main diseases affecting rose plants

A and B: Black spot disease on garden roses; **C and D:** Powdery mildew on cut roses; **E and F:** Rust on garden roses; **G and H:** Cercospora or leaf spot on garden roses; Photo credits: **[A-G]** M. Tisserand (2020), **[B-C-D]** D. C. Lopez Arias (2019), **[E-F]** Nightflyer in Wikimedia (2009) and **[H]** B. Mulrooney (2008) found in <https://sites.udel.edu/ornamentals-hotline/tag/cercospora-leaf-spot/> website.

4.2. BREEDING FOR DISEASE RESISTANCE

In the 1990s, disease resistance started to be considered in breeding programs when breeders stopped using pesticides during selection of rose varieties. Indeed, before that, breeders used pesticides in line with cultivation practices in nurseries during the selection cycles. However, once in the final consumer's hands, these selected roses started exhibiting more and more disease symptoms as the spraying decreased (Leus 2017). As of today, a survey among 16 breeders indicated that they did not spray or at least use pesticides in minimal quantities (Debener and Byrne 2014). Breeding programs need to give emphasis to disease resistance during the selection cycles, especially for garden roses that are today threatened by pesticide interdictions like mentioned above. Propositions of breeding programs including disease resistance in the selection procedure were published (Noack 2003; Debener et al. 2004; Zlesak 2007; Leus 2017; Byrne et al. 2019) and I decided to include them in orange in Figure 10.

4.2.1. INTROGRESSION PROGRAMS

Increasing efforts have been made to exploit the genetic resources available outside the cultivated pool. Several introgression programs have been carried out to introduce disease resistance from wild species in cultivated backgrounds. Two examples of introgression programs of black spot resistance from a donor genotype to a cultivated rose can be cited here. First, the cross between the dihaploid genotype H190 (haploidized 4x *R. hybrid* 'Zambra') and *R. wichurana* aimed to introgress the black spot disease resistance from the wild diploid species into a cultivated tetraploid with high susceptibility to it (Crespel 2001; Crespel et al. 2002a, b). A segregating population called HW was produced and linkage studies have been carried out since then including the one presented in this manuscript. Second, in the late 1990s, Pr. Debener's team started to introgress the resistance to black spot disease from the diploid *Rosa multiflora* hybrid 88/124-46 (carrying *Rdr1* resistance gene) into the genetic background of the tetraploid rose *R. multiflora* 'Caramba' (Malek and Debener 1998; Debener et al. 2003, 2004). Several steps were needed with polyploidization of the donor genotype (88/124-46), hybridization with the cultivated variety to give a F1 population and then two backcrosses with both cultivated *R. multiflora* 'Heckenzauber' and 'Caramba' to reduce the genetic background of the donor genotype (see Figure 12). Association between modern techniques of ploidy level manipulation and traditional hybridization can help breeders to introduce new sources of resistance from outside their genetic pools. However, crosses like that can lead to loss of desirable characters as the progeny shares genes from both parents. In that case, MAS can help to reduce the number of backcross cycles in introgression projects by helping to identify, in the offsprings expressing the disease resistance of the wild species, the ones with the least genetic background from that donor genotype (wild species) and more of the genetic background of the cultivated rose (see Figure 10) (Noack 2003; Debener et al. 2003, 2004; Zlesak 2007).

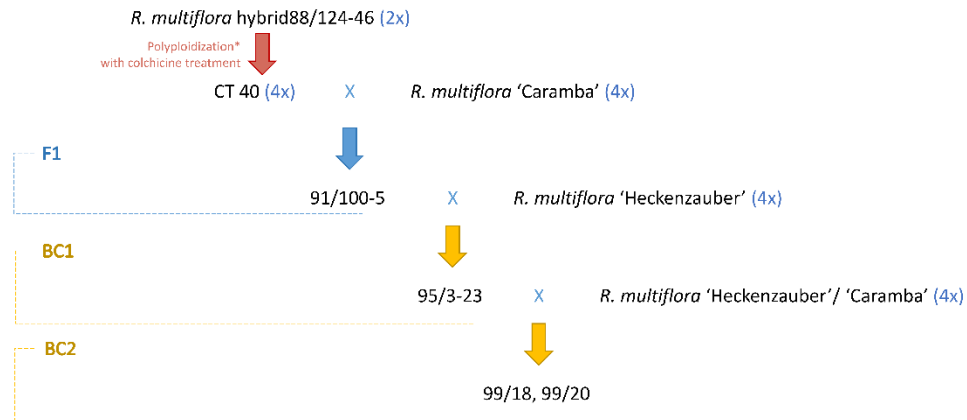


Figure 12: Example of scheme for introgression of black spot resistance from *R. multiflora* genetic background into a cultivated pool (adapted from Debener 2004)

* Chromosome doubling of the diploid genotype prior hybridization with tetraploid variety

4.2.2. DISEASE EVALUATION THROUGHOUT THE SELECTION PROCESS

On one hand, since disease resistance gained interest in the late 1900s, research programs have focused on the development of tools that could help breeders to screen for disease resistance at several moments of the selection process. Several institutes have been working on providing bioassays and controlled inoculations to either (1) screen the gene pool of breeding companies or additional rose species to help them identify potential parents for their new breeding programs (Leus 2017) or to (2) perform disease resistance tests for early selection of rose seedlings (Leus et al. 2007) and/or selected individuals from progenies (Leus 2017) (see Figure 10). Several bioassays for powdery mildew resistance screening like inoculation tower, conidia suspension for greenhouse inoculation or ventilator inoculation have been developed by research institutes in the last 15 years (Linde and Debener 2003; Leus et al. 2008; Leus and Huylenbroeck 2009). Similarly, some bioassays to test for black spot disease resistance on detached leaves in laboratory (Debener et al. 1998; Carlson-Nilsson 2001; Dong et al. 2015) or whole-plant tests in semi-controlled setting in greenhouse (Leus et al. 2007; Dong et al. 2015; Soufflet-Freslon et al. 2019) have been developed in the last years. However, up to date, bioassays are not widely used by professional rose breeders as the tests can be difficult to implement because they need pathogen culture, laboratory facilities and they can be costly (Debener and Byrne 2014; Leus 2017).

On the other hand, disease resistance is mostly evaluated in the field during the selection process (Debener and Byrne 2014; Leus 2017). Resistance to powdery mildew can be easily tested during seedling selection as spontaneous infection may happen in the greenhouse (see Figure 10). Nowadays, breeders test the genotypes selected after year 4 over several carefully chosen locations. For instance, breeders in the U.S. may choose cool humid regions in the west coast to test for resistance to powdery mildew, downy mildew and rust whereas locations with warmer and humid weather may be chosen to test resistance to black spot and cercospora. That way, most of the American commercial testers and testing programs evaluate varieties on both sides of the country (Debener and Byrne 2014). Similarly, in France, regions like the south Mediterranean coast tend to have greater rust infections than black spot disease, and more humid and rainy regions like the west coast will have good natural field inoculum levels (Hibrand-Saint

Oyant, personal communication?). As more and more roses are distributed internationally, breeders have to test for disease resistance abroad with international collaborators for multiple-site testing before sending the selected roses to final variety registration (Debener and Byrne 2014).

When candidate varieties have been selected, breeders send them to variety trials and patenting abroad. On one hand, rose patenting has decreased in the last 30 years with, for example, 50 US rose patents in 1992 down to 13 cultivars patented in 2013 in North America (Byrne 2015). Nowadays, half of the roses are released without patenting with 74 rose patents worldwide against 155 rose cultivars introduced in 2020 according to HelpMeFind database. On the other hand, variety trials have started to flourish all around the world and aim to test the performance of roses in several locations, so roses with greater climatic adaptability, disease resistance and tolerance to a wide range of soil types can be identified. Variety trials like Earth-kind® trials (<https://aggie-horticulture.tamu.edu/earthkindroses/field-trials/>) and American Garden Rose Selection (<https://www.americangardenroseselections.com/#>) in the United States (Harp et al. 2009; Zlesak et al. 2010, 2015), the General Examination for New Roses (ADR) trials in Germany (http://www.adr-rose.de/html_english/adr_wasist.htm), Excellence Roses in the Netherlands and Belgium or SNHF trials (<https://www.snhf.org/roses/>) in France undertake performance trials based on years field testing over several locations within a specific country and all around the world. Special designations are bestowed by these organizations and give a prestigious label for newly released varieties with significant commercial advantages.

4.2.3. STILL ROOM FOR IMPROVEMENT?

Several studies have evaluated rose resistance to different pathogens to identify varieties exhibiting resistance and also to have an idea about the resistance in the cultivated pool as well as among wild species. I would like to mention three studies that evaluated the resistance to black spot disease as an example. In Germany, Schulz et al. in 2009 evaluated the disease resistance of a germplasm of 581 accessions in two locations as well as in detached leaf assays. Between 6.7% and 8.5% of the accessions were found to be resistant to black spot disease in both field and laboratory evaluations in both locations whereas assessment of black spot resistance in wild species showed that 31.5% were found resistant (Schulz et al. 2009). In the United States, RHA-TAMU Rose Survey on commercial variety performance in 2015 concluded that only 6% of the 413 cultivated roses tested in the field were resistant to black spot disease when considering 10% of disease damage as the dividing point between resistant and susceptible genotypes (Byrne 2015). Both of these surveys show a lack of resistance in the cultivated pool while more wild species seem to be resistant to black spot disease. In the French project Belarosa, gathering seven breeding companies, the resistance to black spot disease of 45 varieties, which have not yet been commercialized or that were in process of commercialization in 2016, was tested using artificial inoculation of several monosporial inoculation in the greenhouse (Soufflet-Freslon et al. 2019; Marolleau et al. 2020). Depending on the breeding company, between 10% and 60% of the new varieties showed less than 25% of black spot symptoms (Belarosa Project results not published). These results are promising as they show an increased resistance to black spot disease in the future released varieties. Thus, even if in the last 30 years, breeders have started to release new rose varieties with higher degrees of resistance, there is still room for improvement so that more resistant varieties can be released. Indeed, gain from selection is

generally lower for traits like disease resistance and often, more resources are needed to assess a seedling's performance when challenged with a wide range of pathogens and strains (Zlesak 2007).

One of the easiest ways to better integrate disease resistance screening is making the different bioassays that already exist more available for breeders (be it for potential parents screening like proposed in Figure 10 or for early seedling screening in a greenhouse). Collaborative projects between breeding companies and research institutes, like in the French Belarosa project, or commercial services for disease screening from organizations or research institutes can be options to improve breeding for disease resistance in the rose industry. For example, Schulz et al. 2009 survey screened for resistance in the wild rose species to identify resources for resistance introgression from wild species, and Vegepolys Valley service in France offers to test the resistance of varieties from breeding companies.

Like mentioned in [section 2.4.3](#), genetic engineering can be another option to introduce disease resistance not naturally present within cultivated roses. Different resistance mechanisms can be transferred or existing ones enhanced through this technique while keeping the important ornamental value intact. For instance, a chitinase transgene was successfully integrated in the floribunda 'Glad Tidings' leading to the reduction of 13% to 43% of black spot disease (Marchant et al. 1998a, b). Similarly, other antifungal proteins (chitinase, glucanase, wheat signal peptide and lysozyme) were integrated into the susceptible hybrid tea 'Pariser Charme' which reduced black spot disease severity (Dohm et al. 2002; Debener et al. 2004). *Ace-AMP1*, an antimicrobial protein gene, was also transferred into the shrub 'Carefree Beauty™' and was found to enhance resistance to powdery mildew (Li et al. 2003). Moreover, research programs have allocated budget on the search of genes responsible for the main disease resistance like *Rdr* genes for black spot disease (markers were developed for *Rdr1* and *Rdr3*) and *Rpp1* as well as *MLO* genes for powdery mildew (Malek et al. 2000; Linde and Debener 2003; Debener et al. 2004; Biber et al. 2010; Zurn et al. 2020). Resistance genes could also be used in genetic engineering to introduce resistant genes in susceptible rose varieties from wild species or for functional alteration of *MLO* genes with zinc finger nucleases (ZNFs), Talens or CRISPR/Cas to introduce powdery mildew resistance (Leus 2017). But again, these techniques can be costly and they require high technicity for sometimes very limited results (especially genetic engineering). Besides, the social acceptance is still low in Europe. Thus, they are not often used and are limited to research topics so far (Dong et al. 2017; Boutigny et al. 2020).

Finally, the development of new information and tools for rose breeding and genetics has accelerated in recent years with the availability of sequencing techniques at lower costs. On one hand, several genetic maps for diploids and tetraploids are now available with markers like RGAs, PKs, CAPs, SCARs, etc. (Byrne 2009; Debener and Byrne 2014). Recently, next-generation sequencing has facilitated the discovery of a large number of single-nucleotide polymorphism (SNP) markers as well as transcriptomes (Smulders et al. 2019). With these genetic maps, several linkage studies were carried out to study traits like date of flowering, petal color, petal number, architecture, fragrance and prickles among many others (Dugo et al. 2005; Hibrand-Saint Oyant et al. 2007; Kawamura et al. 2015; Leus et al. 2015; Roman et al. 2015; Magnard et al. 2015, Sun et al., 2020, Bourne et al., 2017, Zurn et al. 2018; Yan et al. 2019; Zhou et al. 2020). In addition, markers linked to quantitative disease resistance have been investigated in recent studies (Leus et al. 2015; Yan et al. 2019; Soufflet-Freslon et al. 2019) and they could be used in marker assisted selection (see Figure 10). On the other hand, transcriptomes of several rose genotypes belonging to different species

were released and have allowed scientists to get more insights on the genetic control of different mechanisms such as petal abscission and development, drought stress tolerance, blooming, disease responses, etc. (Yan et al. 2014; Gao et al. 2016; Han et al. 2017; Neu et al. 2019; Lu et al. 2020; Li et al. 2020). Transcriptomes have also contributed to identify patterns of selection (Li et al. 2018), transcripts and peptides (Dubois et al. 2012) or SNP markers (Koning et al. 2015) among other things. Recently, two rose genome sequences of high quality were released, which will considerably help in the identification of candidate genes for traits of interest (Raymond et al. 2018; Hibrand-Saint Oyant et al. 2018). These new tools and techniques can be used to study the resistance to diseases in depth and that way more knowledge on disease resistance can be obtained to ultimately help breeders to select for durable resistance to diseases.

Disease in roses is an immense threat in particular today with the increasing environmental concerns. Trends have shifted to a more responsible way of growing plants (production and gardening). The rose industry has had to adapt to these changes and even if efforts have been made to release varieties with higher degrees of disease resistance, major diseases like black spot disease remain a problem today. Deeper knowledge of diseases is needed to be able to meet the challenges of tomorrow while breeding beautiful and innovative roses.

4.3. DIPLOCARPON ROSAE, THE CAUSAL AGENT OF BLACK SPOT DISEASE ON GARDEN ROSES

Due to the importance of rose in the ornamental market, black spot disease is the major disease affecting garden roses worldwide (Horst and Cloyd 2007; Byrne et al. 2019). Since it was first reported back in the nineteenth century in Europe (Sweden between 1815 and 1844), black spot disease has been observed in both northern and southern hemispheres. Indeed, global trade of roses has enabled its dispersal in the entire world and its occurrence in private gardens as well as public spaces, has made it one of the most recognized plant diseases by common people (Wolf 1912; Debener 2019). It is also one of the most studied diseases affecting ornamental plants with 250 peer-review publications (Debener 2019). A state of art of the knowledge we have acquired on the major disease of garden roses, black spot disease, will be presented so I can introduce the principal axes of research developed in this dissertation.

4.3.1. DISEASE SYMPTOMS AND EFFECT OF THE ENVIRONMENT

Black spot disease is caused by an hemibiotrophic ascomycete referred as *Diplocarpon rosae* (Wolf) in its imperfect stage (asexual state) or *Marssonina rosae* in its perfect stage (sexual state). Its multiplication is mainly done asexually even though the sexual state has been reported in North America (Wolf 1912; Aronescu 1934), Great Britain (Knight and Wheeler 1977; Cook 1981) and Russia (Gachomo 2003 citing Dubin 1972). Black spot is particularly devastating in outdoor-grown roses where it occurs in epidemic proportions (Horst and Cloyd 2007) but is a minor concern in the greenhouse as humidity is carefully regulated. Typical symptoms of this disease include dark rounded spots with fringed-like margins on the upper-side of the leaves. Spots can grow up to 15mm but as they grow bigger single spots may merge and form larger spots (see Figure 13) (Gachomo and Kotchoni 2007). In susceptible cases, leaves exhibit chlorosis but the area around the dark spot can remain green forming what is called ‘green islands’ by Gachomo and Kotchoni (2007) (see Figure 13). Premature defoliation follows leaflet chlorosis and can cause reduced plant vigor (Smith et al. 1989) and, in the most susceptible cases, leads to plant death (Black et al. 1994). Defoliation causes weakening of the plant which can make it less resistant to other stresses

(Drewes-Alvarez 2003). Therefore, the damages caused by *D. rosae* are greater than the simple leaf spots and chlorosis as premature defoliation does not only affect the aesthetic appearance of the plant but also its vigor and its ability to respond to other stresses (Gachomo 2005). In general, the whole shoot from the buds, leaves, petioles to the young stems can be infected by *D. rosae*. A difference in susceptibility has been observed between organs of different ages. In particular, young leaves are more susceptible than old ones, and inoculation on leaves that have finished their growth (old leaves) yield very few acervuli (Aronescu 1934). Nevertheless, infection always spreads from the bottom to the top of the plant, which can be explained by the fact that lower leaves are more exposed to water splashes and if fallen infected leaves are already covering the ground, infections will start from there (see Figure 15). Once established on rose plants, black spot infection is difficult to control without using chemical control. Prophylactic measures can be taken to reduce disease incidence like removing fallen infected leaves from the ground, pruning canes with infected leaves to reduce potential overwintering, adequate pruning and sparse planting to reduce leaf canopy density and allow air circulation so leaves dry faster as well as avoiding foliar watering (Saunders 1966; Gachomo 2005; Horst and Cloyd 2007). But authors have demonstrated that leaf removal is only effective when it is done immediately after the symptoms appear and does not prevent the seasonal build-up observed in black spot infection in the field (Saunders 1966).

D. rosae is a water-born pathogen that is mainly spread by raindrops splashing onto lesions (Wolf 1912; Frick 1943; Saunders 1966), even though spread by wind and direct contact with man or animal vectors including insects and arachnids (Saunders 1966; Palmer et al. 1978). Very small amount of rain splash is needed to release most of the conidia from lesion according to Saunders (1966). However, several hours of imbibition and high humidity are required to obtain conidium germination on rose leaves (Aronescu 1934; Palmer et al. 1978). Disease symptoms only occur between 10°C and 29°C because fungal structure development is arrested above 29°C whereas conidium germination can happen between 0 and 33°C (Palmer and Semeniuk 1962; Gachomo and Kotchoni 2007). Initial infections begin during the first rains in spring and come from overwintering conidia in fallen leaves and/or canes. Further spread occurs mainly in late summer and the logarithmic pattern of disease development is triggered by heavy rainfall combined with average daily temperatures above 14°C. August has been described as a critical month in south-west England where appropriate preventive sprays can greatly reduce the total inoculum (Saunders 1966). Knight (1975) suggested that the same basis as for apple scab forecasting (mills periods) could be used for black spot symptoms forecasting as both pathogens need water for dispersal and germination.



Figure 13: Illustration of black spot disease symptoms on different garden roses
(Picture credits: D. C. Lopez Arias and M. Tisserand, 2019-2020)

A: Leaflet with small black spots with no chlorosis; **B:** Expanded spots after single spot merging and beginning of chlorosis; **C:** Large black spot that is probably the result of individual spot merging and advanced chlorosis leading to leaflet death; **D:** Different stages of infection in a single leaf with one leaflet exhibiting small spots and no chlorosis, another one with larger spots and beginning of chlorosis, and a last one with spread chlorosis; **E:** Premature defoliation in July of the susceptible cultivar *R. chinensis* 'Old Blush'.

4.3.2. HEMIBIOTROPHY AND ITS ROLE IN THE INFECTIOUS CYCLE OF *D. ROSAE*

Diplocarpon rosae is an ascomycete that belongs to the *Drepanopizizaceae* family (see Figure 14). Its host range is restricted to the genus *Rosa* and there is no report of its capacity to infect members of other genera (Horst and Cloyd 2007). *D. rosae* has been described as a hemibiotrophic fungus with a biotrophic phase during which host cells remain alive and a subsequent necrotrophic phase involving killing of host cells (Wolf 1912; Palmer et al. 1978; Gachomo et al. 2006). *D. rosae* can also grow saprophytically in fallen leaves (Frick 1943) and in different artificial media (Wolf 1912; Shirakawa 1955; Saunders 1967; Gachomo and Kotchoni 2007).

Kingdom	Fungi
Subkingdom	Dikarya
Phylum	Ascomycota
Subphylum	Pezizomycotina
Class	Leotiomycetes
Order	Helotiales
Family	Drepanopizizaceae
Genus	<i>Diplocarpon</i>
Species	<i>Diplocarpon rosae</i> F. A. Wolf

Nauta and Spooner (2000) revised by Johnston et al. (2019)

Figure 14: Taxonomic classification of *D. rosae* according to Brands (2020)

Many definitions of fungal life-styles have been reported but an attempt to define biotrophy, hemibiotrophy and necrotrophy was done by De Silva et al. (2016). Biotrophs are fungi with a narrow host range and they derive their nutrients from living host cells (for example rusts, smuts, powdery mildews and other biotrophic oomycetes). Necrotrophic fungi (like *Botrytis*, *Sclerotinia* or *Alternaria*) cause host cell death by secreting hydrolytic enzymes and specific toxins in order to be able to absorb nutrients from dead cells. In the middle, there are hemibiotrophic fungi that group fungi with more than one life-style. Hemibiotrophs are initially biotrophic and form association with living cells of the host the same way obligate biotrophs do, and later on switch to a necrotrophic life-style and kill host cells to obtain nutrients. These fungi are capable of producing appressoria and haustoria during the initial biotrophic phase but they can also synthesize hydrolytic enzymes and toxins during their late necrotrophic phase. Moreover, obligate biotrophs are difficult to grow and obtain sporulation in artificial media and are known to be very hard to maintain in the laboratory. They also lose their pathogenicity and change in morphology when grown in artificial media (Gachomo et al. 2006; De Silva et al. 2016; Debener 2019). An extended study conducted by Gachomo et al. in 2006 aimed to demonstrate the hemibiotrophic life-style of *D. rosae*. Detailed description of the infectious cycle of *D. rosae* was done in Gachomo PhD thesis and will be summarized here. The role of hemibiotrophy in *D. rosae* infection will also be discussed.

In temperate regions, initial infections start in spring with the germination of two-celled conidia released from overwintering acervuli that were formed subepidermally the year before (Figure 15 and Figure 16). Like mentioned in the previous section, conidia are moved by water splash from infected material and spread to healthy tissues of the same plant or adjacent plants. If there is enough water to germinate and compatibility between the strain and the rose genotype, conidia will penetrate the cuticle and haustorial structures can be formed within about 48 hours (Figure 15) (Gachomo 2005). During penetration, a well-defined appressorium at the end of the germ tube is not always observed and

penetration may happen underneath the conidia without production of the germ tube (Aronescu 1934; Gachomo 2005). However, melanization of the appressorium is important for the fungus pathogenicity and contributes to an increased pressure in the appressorium which helps to break the host cuticle (Figure 16). Lack of melanized appressorium ring formation is typical of growth on an artificial surface and of non-host interactions (Gachomo et al. 2010). Furthermore, lytic enzymes seem to be involved in host penetration by *D. rosae* as well as further development under the cuticle.

Once the fungus breaches the cuticle, an infection vesicle is formed and is believed to serve as a holding center for all fungal cellular content from which the first subcuticular and intercellular hyphae are formed (Gachomo 2005). Subcuticular hyphae spread from the entry point (infection vesicle) and away from it with regular strands that branch into new strands, which give to the spot this particular snowflake/star-like shape (Figure 16). The origin of the black color on the spots has been subjected to many hypotheses throughout the years (Wolf 1912; Dodge 1931; Aronescu 1934; Frick 1943). However, Gachomo (2005) reported that the initial hyphae are colorless but that the brown/black color at the infection site comes from the browning of the mesophyll cells followed by a browning of subcuticular hyphae and acervuli. Soon after subcuticular hyphae begin to form, intercellular hyphae are formed, that penetrate epidermal and mesophyll cells where the first haustoria are formed within the first 24h (Figure 16).

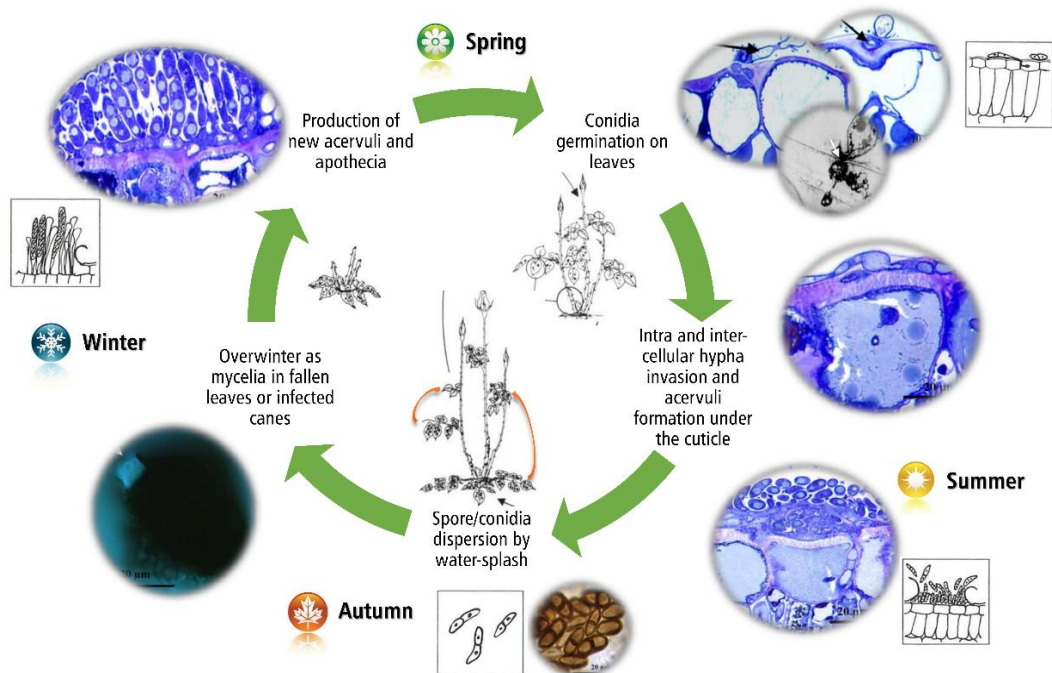


Figure 15: *Diplocarpon rosae* infectious cycle adapted from Drewes-Alvarez 2003, Gachomo 2005 and Horst and Cloyd 2007

Development of haustoria is the sign of the biotrophic stage in the fungus development, which allows it to feed on alive cells through a close interfacial matrix between the fungal cell wall and the invaginating plasma membrane (Gachomo 2005; Gachomo et al. 2006). Haustoria are formed from a base at the cell periphery and are characterized by a thin hypha (haustorial neck) surrounded by collar material and bottle-shape extremity that is surrounded by the cell membrane (Figure 16). Collar material is a mixture of callose and other unknown substances (Knight 1975; Knight and Wheeler 1977; Kuklinski 1980; Gachomo and

Kotchoni 2007). Such callose depositions in compatible interactions are interesting to point out as highly specialized obligate biotrophs like rust fungi rarely lead to such reactions (Littlefield 1979). Gachomo et al. (2006) suggest that *D. rosae* is unable to completely suppress the host defense reaction during its biotrophic phase and that it can, therefore, be considered as a primitive form of biotrophic interaction.

The length of the biotrophic phase is variable but is assumed to be halted once the fungus forms necrotrophic intracellular mycelia. Under favorable conditions, a necrotrophic phase is reached after six days. These intracellular mycelia are observed at the onset of asexual reproduction (just before the acervulus base is formed) (Gachomo et al. 2006). However, there are discrepancies between authors observing these intracellular mycelia in living tissues still attached to the plant (Wolf 1912; Frick 1943; Gachomo et al. 2006) and others only reporting them in infected fallen leaves (Dodge 1931; Frick 1943). In addition, Debener (2019) expressed his doubts on the necrotrophic phase described by Gachomo as a clear correlation between cell death and the presence of these hyphae has not yet been demonstrated. Indeed, as long as molecular biology studies (transcriptomics and proteomics) combined with adequate histochemical staining of fungal structure and cell death are not conducted, it is hard to rule out the possibility that cell death is not due to intracellular hyphae but is a consequence of massive invasion, unspecific toxic metabolites or other indirect effects of the fungal invasion (Debener 2019). But one thing's for sure, *D. rosae* does not have a typical biotrophic life-style and is capable of living on dead tissues as well as on artificial media.

Further development of the fungus leads to the development of acervuli from older subcuticular hyphal structures (Figure 15 and [Ac] in Figure 16). Conidiogenesis can start after only three to five days after the penetration and hyphal structures with finger-like projections are formed to build the bottom of the acervuli. The development of newly formed conidia and the upward growth of the acervuli pushes it against the cuticle that is eventually breached leading to conidium release (Gachomo 2005). The dispersion happens again with water splashed when the rain comes. In general, one to two weeks are needed to complete a cycle. Therefore, several pathogenic cycles happen during the plant growing period (from spring to autumn) leading to an infection build-up all along that period (Saunders 1966; Gachomo and Kotchoni 2007).

Finally, the fungus overwinters as saprophytic mycelium in dormant stems, prickles, fallen leaves and buds (Cook 1981; Gachomo and Kotchoni 2007). The next spring, conidia are formed from overwintered mycelia that feed saprophytically on dead cells of fallen leaves and are the main sources of primary infection (Figure 15). Some authors described the formation of apothecia from overwintered material in the U.S., Canada and Great Britain (Wolf 1912; Knight and Wheeler 1977; Cook 1981).

Hemibiotroph nature of *D. rosae* allows it to invade and feed from host cells (biotrophy) until a switch happens and it starts feeding from dead cells like a necrotroph. Its capacity to get nutrients from dead cells plays an important part in its re-emergence from overwintered hyphal structures as it is capable of feeding saprophytically from fallen overwintered leaves that have started their decomposition. However, even if its capacity to feed from dead cells has been demonstrated, no clear indication that it produces lytic enzymes and toxins with the goal of killing cells to get its nutrients like a real necrotroph has been shown (Debener 2019).

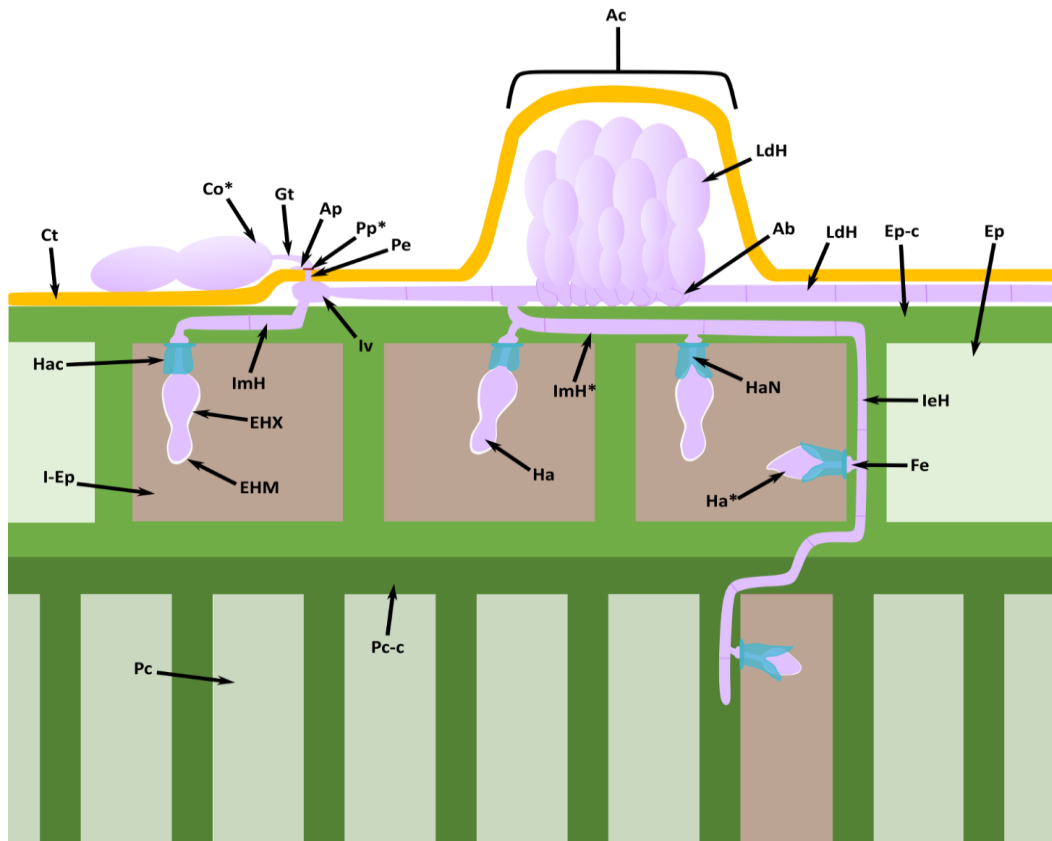


Figure 16: Schematic representation of different structures built by *Diplocarpon rosae* during a compatible interaction (adapted from Kuklinski 1980, Gachomo 2005 and Debener 2019)

The two-celled conidium [Co*] germinates and produces a germ tube [Gt] with variable length. Sometimes appressoria [Ap] can be observed. At the penetration point, the fungus breaks the cuticle [Ct] and a round penetration pore [Pp*] can be observed. A thin penetration peg [Pe] grows under the cuticle and produces infection vesicles [Iv] from which long distance hyphae or subcuticular hyphae [LdH] are produced. The hypha enlarges before penetrating the epidermal cell wall [Ep-c] and forming short intramural hyphae [ImH] and longer ones [ImH*]. From these intramural hyphae, the haustoria [Ha] are produced with the fungal hyphae that enlarge [Fe] before invaginating the host plasma membrane or also called extrahaustorial membrane [EHM] by Gachomo (2005). The extrahaustorial membrane is found around the haustorial body forming a larger extrahaustorial matrix [EHX] around it but lies close to the haustorial neck [HaN] when no extrahaustorial matrix [EHX] is observed. Haustorial collar [Hac] around the haustorial neck is deposited by the plant and is composed of callose. Haustoria were observed to lie close to the host nucleus of the invaded epidermal cells [I-Ep]. The invaded epidermal cells [I-Ep] turn necrotic (represented by the brown color) and appear fluorescent when stained with aniline blue. Intramural hyphae can grow between the cells and inside palisade cell walls [Pc-c]. They are called intercellular hyphae [IeH] from which further haustoria are produced in between levels of the epidermal cells and also inside palisade cells [Pc]. During the advanced state of disease development, intracellular hyphae can be observed but are not represented here. During fructification, finger-like projections are formed at intervals along the subcuticular hyphae and these projections grow to form pseudoplectenchymatic hyphae that constitute the acervulus base [Ab]. Conidia are produced inside the acervulus [Ac] and the roof of the acervulus is the host cuticle that is pushed upwards when the acervulus grows. Eventually, when the acervulus is mature, the cuticle is breached releasing the new formed conidia [Co].

4.3.3. *DIPLOCARPON ROSAE* DIVERSITY AND INFECTION STRATEGIES

Black spot disease evaluations on rose species and varieties that are performed in different countries do not yield the same results probably because of the occurrence of different races of the fungus in different areas of the world and also various climates (Carlson-Nilsson and Davidson 2000). Very early, authors started to notice a variation in pathogenicity of isolates taken in different geographic regions (Frick 1943; Jenkins 1955; Palmer et al. 1966; Knight and Wheeler 1977; Wenefrida and Spencer 1993). But these authors used polyconidial isolates so no clear identification of physiological races and pathovars could be done. The first authors to have used monoconidial isolates were Bolton and Svejda in 1979, which allowed them to identify three races in Canada. Since then, existence of different races within *D. rosae* has been widely reported (Black et al. 1994; Wiggers et al. 1997; Debener et al. 1998; Yokoya et al. 2000; Carlson-Nilsson and Davidson 2000; Leus 2005; Whitaker et al. 2007a, b, 2010; Zurn et al. 2018; Zlesak et al. 2020). As of today 13 pathogenic races have been described on a standard set of nine rose cultivars (see Figure 17) (Whitaker et al. 2010; Zlesak et al. 2020). Isolates from these races denote a variation in pathogenicity on different rose cultivars but unpublished observations may indicate that there are far more races than the ones already differentiated (Debener 2019). In addition, investigations on the genetic diversity of *D. rosae* using molecular markers seem to confirm the high variability of *D. rosae* strains. For instance, Whitaker et al. (2007a) used Amplified Fragment Length Polymorphism (AFLP) markers on 50 monoconidial isolates sampled on cultivated roses and could differentiate 49 of them. A large genetic diversity was demonstrated but no clear correlation between the host origin, pathogenic race or geographical location was found. In contrast, Werlemark et al. (2006) used Random Amplified Polymorphic DNA (RAPD) markers on 11 isolates and found correlation between the race structure and geographic origin. Later, Münnekhoff et al. (2017) used Single Sequence Repeat (SSR) markers to characterize a large collection of isolates from geographical locations in Europe and outside of Europe. They also found a high genetic diversity of *D. rosae* and showed that it can be correlated with the age of rose bushes (time they were planted) and application of fungicides. Recently, Marolleau et al. (2020) investigated the genetic structure among 77 monoconidial isolates sampled from both cultivated and wild rose backgrounds using 27 SSR markers. A strong genetic differentiation was found between isolates from cultivated roses and wild species with a lower diversity among isolates from cultivated roses compared to wild species. Again no differentiation on the geographical origin (Europe or Asia) was observed. One may hypothesize about the lack of genetic differentiation according to geographical origin being explained by the worldwide trade of garden roses that can transport and/or select for the same fungal population even miles away (Whitaker et al. 2007a). Moreover, these results are very interesting since they raise the question of the origin and spread of *D. rosae* worldwide as well as a question of pathogen specialization. Indeed, are the well-separated isolates from wild species capable of infecting cultivated roses and *vice versa*? If yes, how virulent can they be? And if not, is the fungus diversity (or fungus pathogenicity) linked to the rose domestication? Another question is worth to be mentioned here: what can explain the genetic diversity observed within fungal populations from cultivated roses when the asexual propagation is predominant and the fungus has a low capacity for long-distance dispersal (only water splash)? Debener (2019) gave two hypotheses to explain this inherent contrast: (1) sexual cycles might happen more often than described in the literature or (2) genetic variation can come from side mechanisms such as mutations, mitotic recombination or genome evolution (as WGD). Similarly, according to the results presented by Marolleau et al. in 2020, an even higher genetic diversity of *D. rosae* populations is present in the wild

roses compared to cultivated ones and the authors have also hypothesized a higher frequency of sexual reproduction in the wild compared to garden settings.

Host ^z	Race												
	1	2	3	4	5	6	7	8	9	10	11	12	13
	Isolate												
	HSN	2402 E1	GVH	Dü A3	B 005	Dort E4	R6	ACT	IGWA	KOMN	CW1	BEP	PAP
'Pariser Charme'	-	+	+	+	+	+	+	+	+	+	+	+	+
Honeybee™ ('ZLEhoney')	-	-	+	+	+	+	+	-	-	+	-	+	+
Sexy Rexy® ('MACrexy')	-	-	-	+	+	+	+	+	+	+	+	+	+
Surrey ('KORlanum')	-	-	-	-	-	+	+	+	+	+	+	+	+
Love and Peace™ ('BAIpeace')	-	-	-	-	-	-	+	+	+	+	+	+	+
'George Vancouver'	-	-	+	-	-	-	-	-	+	+	+	-	-
Knock Out® ('RADrazz')	-	-	-	-	+	-	+ ^y	-	-	+	-	+ ^y	+
Baby Love™ ('SCRivlulv')	-	-	-	-	-	-	-	-	-	-	+	-	+
'Hansa'	+	-	-	-	-	-	-	-	-	-	-	-	-
Lemon Fizz™ ('KORfizzlem')	-	-	-	-	-	-	+	-	-	-	-	-	-

Figure 17: Updated rose host differential set identifying 13 races of *D. rosae* from Zlesak et al. (2020)

Disease response of the studied varieties is labeled as susceptible (+) or resistant (-); ^zHost names reported as cultivar name (trade name); ^yKnock Out® was originally scored as resistant to isolate R6 (race 7) by Whitaker et al. (2010), however, it was found to be inconsistently susceptible in this study and susceptible in Rouet et al. (2020) study. 'Knock Out®' displayed a similarly inconsistent susceptible reaction with BEP (race 12) in Zlesak et al. 2020 study.

Significant advances on the knowledge of the *D. rosae* genome and transcriptome have been made in the last years. Neu et al. (2017) released a draft genome of a strain called DortE4 that was previously used to isolate and characterize the resistance gene *Rdr1*. Several genes could be predicted but one interesting result is the whole genome duplication that was observed for this strain. On the contrary, two other strains from cultivated and wild rose genotypes (called DiGER-003 and DiKAZ-180) were sequenced and no (or partial) duplication was observed (Marolleau et al. 2020). The blast of 27 SSR markers (provided by Marolleau et al. 2020) on DortE4 also confirmed the genome duplication but when these markers were used on both DiGER-003 and DiKAZ-180, no duplication was seen. Neu et al. (2017) hypothesized that a recent event of genome duplication had occurred followed by a deletion of some duplicated genes while others diverged in sequence. These findings suggest a large variability in genomes for *D. rosae* strains and give rise to several questions related to importance of total or partial genome duplication in *D. rosae* populations and its role on the pathogen's aggressiveness and virulence (Marolleau et al. 2020). Neu and Debener, in 2019, showed that some effector candidates involved in penetration and haustorium development were found in pairs, which suggests their duplicated state. However, a low percent of predicted proteins and corresponding mRNA sequences shared more than 70% identity which would indicate that diversification among duplicated sequences has already started. It is believed that the process of whole-genome duplication and function diversification of retained duplicated genes play an important role in emergence of diversity within a species (Lynch and Conery 2000; Lynch and Katju 2004; Crow and Wagner 2006; Escalera-Fanjul et al. 2019) and, therefore, in fungus acquisition of new functions or effectors enabling an easier adaptation or conferring a significant fitness advantage (Skamnioti et al. 2008). Neo-functionalization of retained duplicated genes participates in the acquisition of novel functions which can indirectly be involved in the formation of pathogenic races infecting hosts differently (Neu and Debener 2018). DortE4 sequencing has also revealed a surprising contrast between its alleged biotrophic phase and the secretion of an effector related to necrosis inducers. Among 52 fungal effector sequences detected during the biotrophic phase (0 to 72 hours), one protein was detected and was only found in

obligate biotrophic fungi but two other sequences were homologous to necrosis inducing proteins (Neu and Debener 2019).

A transcriptomic study compared the interaction between a susceptible rose genotype ('Pariser Charme') and two fungi with different life-styles (the biotroph *Podosphaera pannosa* causing powdery mildew and the hemibiotroph *Diplocarpon rosae* causing black spot disease). By comparing the genes induced by the infection of both pathogens, specific induction of genes on the host was observed during the infection by *D. rosae*. For example, *D. rosae* infection (with DortE4) leads to significant downregulation of two WRKYs (WRKY33 and 53), known to support the resistance to an attacking pathogen, and to significant upregulation of four WRKYs (WRKY 27, 40, 50, and 51), known to repress resistance (Birkenbihl et al. 2017; Neu et al. 2019). These findings seem to indicate that DortE4 infectious strategy includes inhibition of some defense reactions in the susceptible variety ('Pariser Charme'). Another example is the specific induction of genes during *D. rosae* infection that were not found to be induced in *P. pannosa* infection (phenylpropanoid and lignin biosynthesis as well as genes involved in the salicylic acid signaling pathway and specific PR genes such as *PR-1* and *PR-5*) (Neu et al. 2019).

The existence of races, the high genetic diversity within *D. rosae* populations and the capacity of the fungus to acquire new effectors indicate a wide range of interactions between this pathogen and roses. Researchers have studied and described rose-*D. rosae* interactions in the hope to identify varieties and wild species that are able to resist the infection but also to understand and characterize resistance to black spot disease.

4.4. ROSE-DIPLOCARPON ROSAE INTERACTION AND DISEASE RESISTANCE CHARACTERIZATION

4.4.1. PLANT-PATHOGEN INTERACTION IN ROSE-D. ROSAE PATHOSYSTEM

For a long time, members of the genus *Rosa* have been classified into susceptible and resistant genotypes. In field investigation as well as in laboratory or greenhouse assessments, it has been easy to clearly discern genotypes that developed spots on their leaves following *D. rosae* infection, called susceptible genotypes, from the ones showing no symptoms at bare eye, called resistant genotypes. The distinction between susceptible and resistant genotypes has been used to identify the 13 pathogenic races mentioned before (see Figure 17) in laboratory assessments (Debener et al. 1998; Yokoya et al. 2000; Leus 2005; Whitaker et al. 2007a, 2010; Zurn et al. 2018; Zlesak et al. 2020) but also to select individuals during breeding programs (see section 3.2). On one hand, a compatible interaction between *D. rosae* and rose genotype results in an infection where the fungus is able to complete its life cycle and, therefore, produce conidia. On the other hand, an incompatible interaction results in the impossibility for the fungus to develop in the host because of resistance mechanisms that were implemented successfully by the host. A short cut would be to say that incompatible interactions yield no symptoms at all whereas compatible interactions lead to symptom development that are visible to the bare eye. However, examples in the literature showed that there is a wide diversity of compatible interactions (Knight 1975; Kuklinski 1980; Blechert and Debener 2005; Marolleau et al. 2020) but also that even if genotypes may exhibit some symptoms (rapid defoliation, strong cell death or chlorosis), the infection can be successfully halted (Bolton and Svejda 1979; Blechert and Debener 2005).

4.4.1.1. COMPATIBLE INTERACTIONS

The diversity in compatible interactions is expressed macroscopically with spots of varying size and shape (unpublished results from Belarosa Project), but also microscopically with differences in the overall colonization and the fungal structure development (Blechert and Debener 2005). To support this evidence, I will present some unpublished results obtained by my team during the project Belarosa in 2015 as well as some studies on chlorosis and leaf abscission. Then, I will show this variability in compatible interactions from a microscopic side with Blechert and Debener's study (2005).

In the framework of the Belarosa project, a total of 40 genotypes were artificially inoculated with 10 fungal strains (monoconidial isolates at 10^4 conidia per ml) to assess their resistance using a whole plant assay in greenhouse (personal communication of L. Hibrand-Saint Oyant and V. Soufflet-Freslon). From these 40 genotypes, nine were chosen as controls and published by Marolleau et al. (2020). Eight genotypes out of the nine controls developed symptoms with at least one strain and some of them presented atypical symptoms compared to the round black spot symptoms with fringed margins (unpublished results). Differences in the shape of the black spots but also in the chlorosis around them were observed (see Figure 18). For example, genotypes like *Rosa* 'Amandine Chanel'® MASamcha, *Rosa* 'Paul Bocuse'® MASpaujeu, *Rosa* 'Jazz Festival'® MEIzizany, *Rosa* 'Génération Jardin'® DELparviro, *Rosa chinensis* 'Old Blush', and *Rosa* 'Prince Jardinier'® MEItroni presented typical round symptoms with fringed margin associated with the so-called 'green islands' when chlorosis is observed (Figure 18 A-B-E-F-G*J). Others like *Rosa* 'Fragonard'® DELparviro and *Rosa* 'Martine Guillot'® MASmabay did not exhibit a strong chlorosis (Figure 18 H*-I). A strong necrosis in the middle of the black spot was observed in both *Rosa* 'Paul Bocuse'® MASpaujeu and *Rosa* 'Velasquez'® MEImirtilus (Figure 18 B-C-). The variety *Rosa* 'Utopia'® JALtopia presented star-like symptoms instead of round homogenous black spots (Figure 18 D). Both *Rosa* 'Fragonard'® DELparviro and *Rosa* 'Martine Guillot'® MASmabay presented atypical symptoms as well with black rings and a light colored center (almost yellow). Looking up-close there seems to be an HR-like response in the center of the ring with cell browning and a light chlorosis (Figure 18G*-H*). The latter results are rather interesting as it seems that these varieties responded to the infection trying to contain it to the penetration point but failed as symptoms showed up a little further.

According to the genotype, chlorosis was observed around the black spots but it can also rapidly spread to the whole leaf (Figure 18) and leaf abscission can also happen relatively quickly or not. These physiological changes may be an important component of the infection response by susceptible genotypes and attempts have been made to explain them. For example, it was demonstrated that ABA is produced by *D. rosae* when grown in potato dextrose broth and by infected rose leaves but not by uninfected ones (Wani et al. 1980). This indicates that ABA is produced by *D. rosae* and it is believed to play a role in both chlorosis and leaf abscission in compatible interactions. Ethylene production by *D. rosae* as well as auxin degradation by an unidentified enzyme produced by *D. rosae* may contribute to leaf yellowing and abscission (Kazmaier 1960; Horst 1983; Drewes-Alvarez 2003). These results show that *D. rosae* manipulates the plant physiology by producing hormones and enzymes that can help to complete its infectious cycle. However, some rose genotypes present low chlorosis or none and also different degrees of defoliation, which implies that in some cases the pathogen fails to manipulate the host or we can also think that the host develops an insensitivity to these hormones. Thus, from the macroscopic point of view,

the wide variety in spot size, shape and color as well as the speed of chlorosis and leaf abscission occurrence display the incredible diversity in interactions among the compatible group.

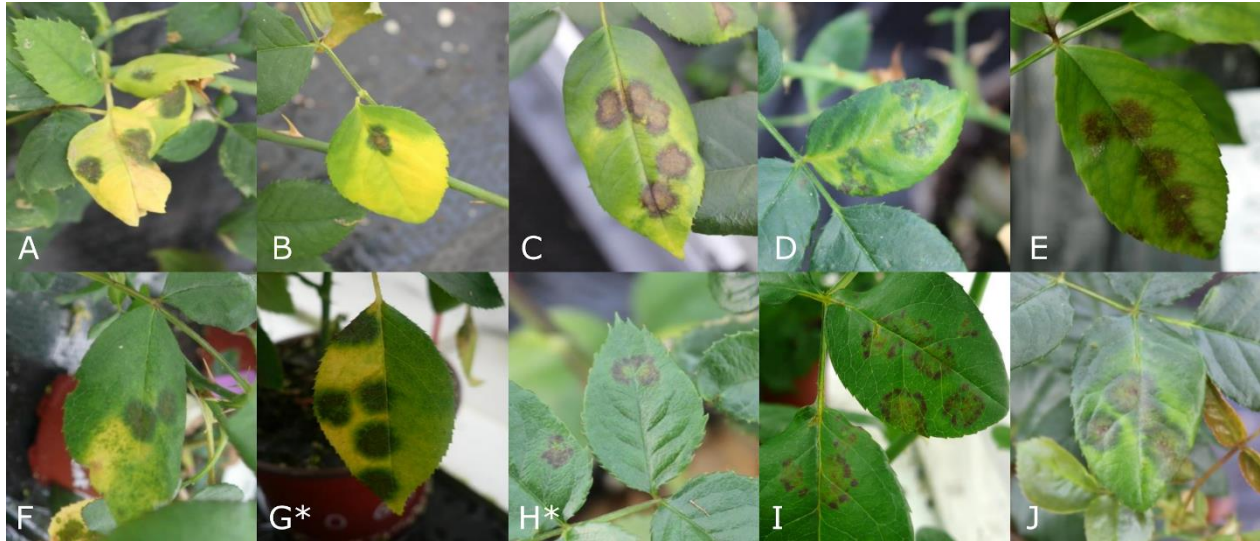


Figure 18: Diversity of symptoms observed in the compatible interactions between *D. rosae* and 10 rose varieties

A: Symptoms on *Rosa* 'Amandine Chanel'® MASamcha; B: Symptoms on *Rosa* 'Paul Bocuse'® MASpaujeu; C: *Rosa* 'Velasquez'® MEIirtylus; D: *Rosa* 'Utopia'® Jaltopia; E: *Rosa chinensis* 'Old Blush'; F: *Rosa* 'Jazz Festival'® MEIizany; G: *Rosa* 'Génération Jardin'® DELparviro; H: *Rosa* 'Fragonard'® DELparviro; I: *Rosa* 'Martine Guillot'® MASmabay; J: *Rosa* 'Prince Jardinier'® MEItroni ; * Varieties not included in the controlled set published by Marolleau et al. 2020

Blechert and Debener in 2005 conducted macro- and microscopic analyses of 34 rose species inoculated with the strain DortE4 in order to characterize morphologically the interaction between *D. rosae* and various rose species. Eight types of interactions were characterized with five being compatible interactions that can be subdivided into strong and weak susceptibilities (Blechert and Debener 2005). In the most susceptible cases, all the fungal structures described by other authors (Wolf 1912; Aronescu 1934; Frick 1943; Gachomo 2005) can be observed microscopically with long distance hyphae, haustorial colonization of epidermal cells, intercellular hyphae that colonize the palisade mesophyll where additional haustoria are produced as well as an important number of acervuli (see infection type 1 in Figure 19). This type of interaction was described for very susceptible genotypes like cv. Pariser Charme and *R. tomentosa* (*Caninae* section). For the compatible interaction type 2, a less-developed hyphal network was observed with no colonization of lower cellular levels. Long distance hyphae developed radially from the entry point with production of acervuli, and lateral short-distance hyphae with low branching were formed. Haustoria were only visible inside epidermal cells (see infection type 2 in Figure 19) of *R. hugonis* and *R. foetida* (*Pimpinellifoliae* section) and of *R. longicuspis* (*Synstylae* section). Weaker infections were described for interactions 3, 4 and 5 with reduced sporulation and fungal colonization. The third compatible interaction was described on *R. blanda* (*Cinnamoneae* section) and *R. foliolosa* (*Carolinae* section). This interaction was characterized by a poor colonization of long distance hyphae, but well-developed short-distance hyphal structures colonizing the palisade mesophyll were observed (see infection type 3 in Figure 19). Interaction type 4 was found in several species of the *Caninae* section, such as *R. canina* and *R. obtusifolia*, as well as *R. acicularis* and *R. nutkana* from the *Cinnamoneae* section. A weak subcuticular colonization was observed as long-distance hyphae were shorter than for the other compatible interactions and only epidermal cells were colonized by haustorial structures (see infection type 4 in Figure 19). Finally,

interaction type 5 was described with the least hyphal development but a strong development of pseudoplectenchymatic cells (acervulus base) (see infection type 5 in Figure 19). This type of interaction was observed in *R. arkansana* and *R. pendulina* (*Cinnamomeae* section). The authors assumed that a reduction of pathogen fitness might be happening for interactions with weak susceptibility (3, 4 and 5) and that the observation of weak susceptibility with different colonization patterns of the fungus and specific reduction of hyphal structures might be a sign of partial resistance acting against different structures of developmental stages of the fungus.

In general, it is easy to see the occurrence of acervuli after a successful infection of host tissues either by looking at the leaf or observing it under low magnifications with stereomicroscopes (Blechert and Debener 2005). But to conclude whether or not it is a true incompatible interaction or a weak susceptibility in a compatible interaction, Blechert and Debener demonstrated that further inspections were critical. For example, weak susceptibility can yield small symptoms with sparse and slow sporulation that can be missed with macroscopic investigations like in the case of *R. acicularis*, *R. carolina* and *R. rubiginosa*. No acervuli were macroscopically observed seven days after inoculation but under the microscope, non-mature acervuli were observed, which indicates that the fungus was able to produce acervuli but at a slower rate than on strong susceptible genotypes. Thus, checking for symptoms appearance or acervulus production at later time points under a stereomicroscope could also help to know if these structures developed into mature acervuli bearing conidia.

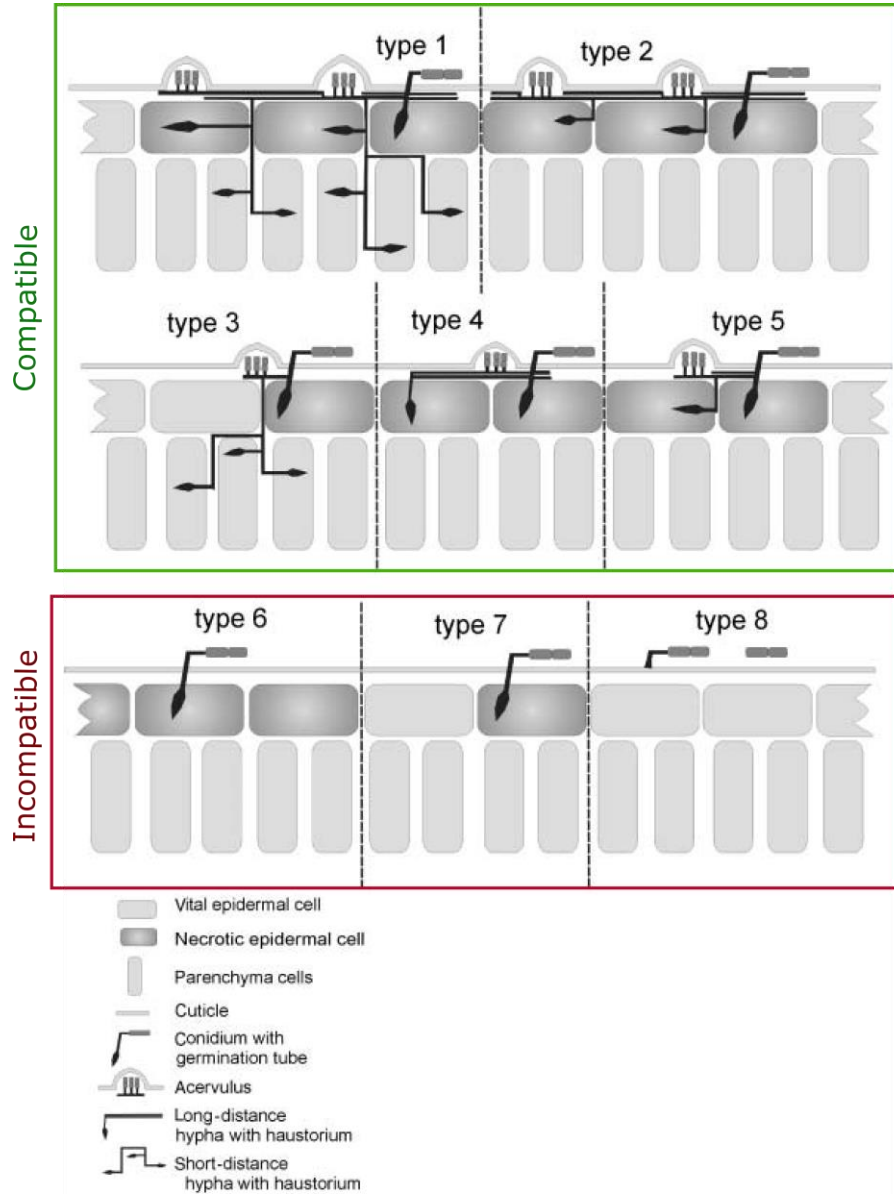


Figure 19: Summary of the eight interaction types between rose species and *D. rosae* by Blechert and Debener (2005)

4.4.1.2. INCOMPATIBLE INTERACTIONS

Macroscopically, incompatible interactions are characterized by either no visible symptoms or more or less necrosis with no development of black spots (unlike *Rosa* ‘Paul Bocuse’[®] MASpaujeu and *Rosa* ‘Velasquez’[®] MEImirtylus or *Rosa* ‘Fragonard’[®] DELparviro and *Rosa* ‘Martine Guillot’[®] MASmabay in Figure 18 that show necrosis associated with black rings). Different shades of incompatible interaction were also described microscopically (Kuklinski 1980; Wiggers et al. 1997; Blechert and Debener 2005). Incompatible interactions are the result of resistance mechanisms that completely stop the pathogen entrance or its development, and they can be divided in two types: (1) interaction associated with penetration of the cuticle and hypersensitive response (HR) at the infection site and (2) interaction associated with an absence of fungal structure development under the cuticle.

The latter incompatible interaction can be characterized macroscopically by either necrotic spots at the infection site or no visible symptoms. Blechert and Debener (2005) described two types of interaction during which more or less cells responded with HR. On one hand, for interaction type 6, once penetrated the fungus can form some structures such as short hyphal strands but no long distance hyphae or mature reproductive structures are observed (see infection type 6 in Figure 19). Plant reactions can also be observed with fluorescent cell-wall appositions around the fungal invasion. This type of resistance was observed on *R. caudata* (*Cinnamomeae* section) and on *R. gallica* (*Gallicanae* section) (Blechert and Debener 2005). Such resistance was also documented in ‘Allgold’ by Kuklinski (1980). Indeed, haustorial structures could be observed in these genotypes but further development was arrested by localized cell death at the sites of penetration. Kuklinski (1980) mentioned a continued increase in the amount of cell death (“browned cells”) in ‘Allgold’ leaves challenged with *D. rosae* and suggested that the fungal growth was not entirely limited. These observations are typical of a delayed HR that was triggered upon pathogen recognition perhaps when haustoria colonized the host cells. On the other hand, for interaction type 7, HR is restricted to single cell or maximum two to three cells right underneath the penetration site so, apart from penetration hyphae, no fungal structures were observed (see infection type 7 in Figure 19). This type of interaction was described on *R. wichurana* and *R. roxburghii* by Blechert and Debener (2005) and was also reported by Wiggers et al. (1997). These authors concluded that the resistance observed in these two species was due to a post-penetration defense response. Macroscopically, necrotic areas were observed on detached leaves (Kuklinski 1980; Wiggers et al. 1997; Blechert and Debener 2005) but, in field evaluations, these genotypes showed high degrees of resistance to black spot disease and very low defoliation ratings (Knight 1975; Black et al. 1994; Xue and Davidson 1998; Carlson-Nilsson 2001). Another remarkable example is the mode of resistance of the genotype H71 from Svejda and Bolton’ study (1980). When inoculated with a *D. rosae* isolate from the floribunda cultivar ‘Arthur Bell’, hypersensitivity reactions were described on H71 leaves that were dropped within only 12 hours, and the new shoots did not exhibit any symptoms. Rapid defoliation at low disease intensity can be seen as a mechanism for quantitative resistance against biotrophs as such pathogens cannot survive on dying tissues (Willcoquet et al. 2017). However, for hemibiotrophs, this mechanism needs to occur before the pathogen is able to switch to the necrotrophic stage to be efficient.

The other incompatible interaction is the most extreme form of resistance and is characterized by the absence of visible symptoms and the lack of fungal structures that penetrate below the leaf cuticle (see

infection type 8 in Figure 19). Bleichert and Debener (2005) described fluorescence of single epidermal cells as well as fluorescing papillae in *R. moyesii*. But in some cases, like for *R. multibracteata*, no reaction could be observed at the microscopic scale and only a few conidia remained on the leaves after the leaf treatments and staining. It was then difficult to conclude whether the absence of fungal structure under the cuticle was due to the inhibition of conidium germination or to a failed penetration (Bleichert and Debener 2005). Previous studies reported an inhibition of conidium germination on some resistant genotypes. Indeed, Reddy et al. (1992) observed the death of conidia on the leaf surface of resistant species and assumed that the conidium germination was stopped by germination inhibitors exuded from the leaf epidermis. Similar observations were made on 'Alberic Barbier' (a hybrid of *Rosa wichurana*) for which resistance mechanism was believed to be based on unidentified diffusible substance from leaves as well as on 'Allgold' that was shown to produce an exudate (most likely phytoalexins) in response to *D. rosae* that inhibit spore germination (Saunders 1970; Knight 1975; Knight and Wheeler 1978). Knight and Wheeler also indicated that the production of inhibitors was relatively slow as some conidia germinated within the first 24h but no additional germination was observed after 48h. Other works demonstrated that in some incompatible interactions with no symptoms, the conidia germinated but failed to penetrate the cuticle. For a long time, resistance has been associated with thick and tough leaves (Green 1931), with the physical nature of the leaf surface (Frick 1943) and the cuticle (Dodge 1931). Indeed, several studies demonstrated the importance of the cuticle as a barrier to the fungus by removing it with abrasion or chemicals (Dodge 1931; Castledine et al. 1981; Walker et al. 1996). An increase in infection severity was observed in leaves without a cuticle or with a compromised cuticle compared to intact leaves. Further investigations on leaf surface properties (epidermal structures and extent of wax apposition) as well as cutin monomers or cuticular waxes did not reveal any link with the infection intensity (Reddy et al. 1992; Goodwin et al. 2007). However, these studies used a small set of genotypes and, therefore, lack of power to demonstrate a causal relationship between these leaf surface features and the levels of black spot infection (Debener 2019).

Whether it is compatible or incompatible interaction, a wide diversity of responses to *D. rosae* infection were reported in this section. From the weak susceptibility to the most extreme form of resistance, rose hosts are capable of establishing various resistance mechanisms with more or less success. A multitude of strategies ranging from preformed to induced mechanisms, resistance based on single genes or quantitative resistance exist and have been of high interest the last few decades.

4.4.2. DIFFERENT TYPES OF RESISTANCE TO *D. ROSAE*

Over the years, efforts have been made to better characterize the interaction between rose hosts and *Diplocarpon rosae*. In the same way as the other pathosystems, several terms have been used to describe the resistance observed in this pathosystem. For example, as early as 1976, Knight presented his study on the general pattern of black spot disease development in different rose cultivars over two years. One of his conclusions was that the resistance observed in the genotypes he studied operated within two components: (1) vertical or race-specific resistance and (2) horizontal or race-non-specific resistance because particular strains were selected on the cultivars between 1974 and 1975. The terms used by Knight were based on Van der Plank's statement that horizontal or race-non-specific resistance can be discerned from vertical or race-specific resistance by testing several host genotypes against different

pathogen isolates (Van Der Plank 1963). However, the terminology used in host-pathogen interactions is inconsistent and has been revised over the years as explained in [section 1.2.1](#). Literature suggests the existence of two main forms of resistance in the rose-*D. rosae* pathosystem: complete resistance (that prevents pathogen multiplication and for which conidium production is nonexistent) and partial resistance (that is incomplete with reduced pathogen development and for which low conidium production can be observed). In order to review the types of resistance to *D. rosae* that have been described in rose genotypes, I will present to you the current knowledge on black spot disease resistance in light of the two main forms of observed resistant phenotypes.

4.4.2.1. COMPLETE RESISTANCE

Extensive work on complete resistance was carried out with numerous papers describing genotypes that show no visible symptoms. Complete resistance is found in incompatible interactions where there is no sporulation and mycelial growth of the pathogen is severely restricted. It is usually controlled by major genes. Four dominant genes for complete resistance to specific races of *D. rosae* were identified and referred as *Rdr* genes (Malek and Debener 1998; Yokoya et al. 2000; Malek et al. 2000; Hattendorf et al. 2004; Whitaker and Hokanson 2009; Whitaker et al. 2010a, b; Terefe-Ayana et al. 2011; Menz et al. 2018, 2020; Zurn et al. 2018, 2020) (see Table 2). The first and most studied black spot resistance gene is *Rdr1* that is race specific (races 3 and 6) and was derived from a *Rosa multiflora* background (Malek and Debener 1998; Malek et al. 2000; Kaufmann et al. 2003, 2010; Terefe-Ayana et al. 2011; Menz et al. 2018). It is located on linkage group 1 of the genetic maps developed for this study (chromosome 1) and was later cloned by Kaufmann et al. (2010). A cluster of nine genes (*muRdr1* gene family) was found in *Rdr1* locus after sequencing with *muRdr1A* being the active form (Menz et al. 2018). Further experiments demonstrated that *Rdr1* is effective against several isolates and is only broken by isolates R6 and AB13 from race 7 (Menz et al. 2018). Blechert and Debener (2005) indicated a HR response in *R. multiflora* against DortE4 (race 6), and microscopic analyses of *Rdr1* donor genotype (88/124-46) and a transgenic line of 'Pariser Charme[®]' with *mudRdr1A* showed that conidia could germinate, form an appressorium and penetrate the cuticle but only a few short hyphae were developed with no establishment of fully-developed haustoria and reproductive structures (Menz et al. 2018). This study also indicated that the effect of *Rdr1* is independent of the genetic background. Then, a second resistance gene was identified, (*Rdr2*) which gives resistance to race 4 and appeared to be tightly linked to *Rdr1* (Hattendorf et al. 2004). *Rdr3* locus, giving resistance to race 8, was identified from 'George Vancouver' and was later localized on chromosome 6 (Whitaker et al. 2010a; Zurn et al. 2020). Finally, the last resistance locus discovered was *Rdr4* from the climbing rose *Rosa hybrida* 'Radbrite' (Brite Eyes[™]) and was localized on chromosome 5. This resistance locus had broad resistance and was only broken by the isolate BEP (from North America) representing race 12 (Zurn et al. 2018). The resistances conferred by these genes/loci were described with segregation of 1:1 in rose populations, typical of monogenic resistances, and genotypes carrying these major resistance genes/loci showed no sporulation or mycelial growth. The discovery of single dominant genes along with the identification of 13 different races of *D. rosae* that cause differential reactions among the genotypes tested (Debener et al. 1998; Whitaker et al. 2010b; Zlesak et al. 2020) have led to consider the existence of a "gene-for-gene" type of interaction in the rose-*D. rosae* pathosystem. Authors have defined the complete resistance as vertical or race-specific. However, further proof is still required with,

for example, the identification of avirulence genes on *D. rosae* genome that would be recognized by these major genes (Malek and Debener 1998).

Race-specific resistance is often more easily selected for and introgressed in susceptible backgrounds as it generally has a high expression. Therefore, to increase probability of durable resistance, breeders can take the available resistance genes (R-genes) and use multiple race-specific resistance alleles with complementary pathogen recognition patterns into a single variety by using marker-assisted R-genes pyramiding. However, the threat of resistance being broken down by the pathogen that acquires the corresponding virulence alleles is still present (Zlesak 2007; Debener 2019).

Table 2: Summary of black spot disease resistance genes identified to this day

Gene	Background	Isolate tested*/ Race-specificity	Location	Linked marker (distance to gene in cM)	References
<i>Rdr1</i>	<i>Rosa multiflora</i>	Isolate DortE4 – All races except race 7	Chr1	155(0cM), 69E24(0,1cM) and RMS015(2,26cM)	Whitaker2010
<i>Rdr2</i>	<i>Rosa multiflora</i>	Isolate DüA 3 – Race 4	Chr1	NA	Hattendorf et al. 2004
<i>Rdr3</i>	<i>Rosa hybrida</i> cv. George Vancouver	Isolate ACT - Race 8	Chr6	ND5E (9,1cM), RMISA004_132(0cM) and RMISA010_248(0cM)	Whitaker et al. 2010 and Zurn et al. 2020
<i>Rdr4</i>	<i>Rosa hybrida</i> cv. Radbrite ('Brite Eyes™')	Isolate 2402 E1, GVH, ACT, IGWA, KOMN, CW1, and PAP – All races except race 12	Chr5	Rh12GR_258_2610(3,77cM)	Zurn et al. 2018

4.4.2.2. PARTIAL RESISTANCE

Partial resistance was described in other host-pathogen interactions involving roses, such as rose-powdery mildew interaction, and seems to delay the infection, reduce pathogen growth and reproduction (Temmen et al. 1980; Schlösser 1990; Yan et al. 2006). As mentioned in [section 4.4.1.1](#), weak susceptibility in compatible interactions can indicate the existence of partial resistance acting against different components of the infection and structures of the pathogen. Early investigation of resistance to black spot disease revealed quantitative variation in resistance phenotypes as presented in Figure 19 (Jenkins 1955; Palmer et al. 1966b; Saunders 1967; Knight and Wheeler 1978; De Vries 2000; de Vries and Dubois 2001; Allum et al. 2010). Partial resistance to black spot disease was first investigated by Xue and Davidson in 1998. Ten of the 11 studied genotypes showed different degrees of infection and differed in various measured components. These genotypes were, therefore, considered as partially resistant. Five components of partial resistance were scored such as incubation period (IP), leaf area with symptoms (LAS), number of lesions (NL), lesion length (LL), and sporulation capacity (SC). If resources are limited, one could use LAS and SC as they were considered the most efficient components to score (easy and a lot of information gained). Later studies reported other genotypes with partial resistance to black spot disease

(Whitaker and Hokanson 2009; Whitaker et al. 2010a; Dong et al. 2017a). In particular, Whitaker and Hokanson (2009) studied partial resistance in absence of major resistance genes by choosing 12 parents with low lesion lengths (LL between 0 and 4 mm). Their study suggested the possibility of breeding for partial resistance as both diploid and tetraploid populations segregating for partial resistance ability showed strong additive genetic effects and significant general combining ability. This type of resistance is known to be mainly polygenic and race-non-specific, which is believed to be more durable (Shaik 1985; Parlevliet 1993, 2002; Vale et al. 2001). However, Whitaker et al. (2007b) noted that partial resistance to black spot disease appeared to be race-specific for some rose genotypes, which proves that quantitative disease resistance can also behave in a race-specific manner (see [section 2.2](#)). The polygenic control of this trait was suggested by different authors as their studies revealed a normal and continuous distribution of phenotypes in segregating populations from field evaluation (Carlson-Nilsson and Davidson 2000; Uggla and Carlson-Nilsson 2005; Shupert 2006; Whitaker and Hokanson 2009). Another study revealed a partial resistance against race 9 for 'Applejack' segregating in a quantitative fashion (Whitaker et al. 2010a). Nonetheless and as explained in [section 2.2](#), it is difficult to know with certainty if the partial resistance observed in rose genotypes is conferred by multiple genes of small effects or if it is the result of major genes conferring incomplete resistance. For this, it would be necessary to perform the adequate analyses to explain the relationship between the observed partial resistance phenotype and the genetic bases underlying it (St Clair 2010). Only recently and thanks to advances in SNP markers, by using SNP chips or next-generation sequencing (Koning et al. 2015), researchers have been able to use molecular markers to provide further information on the genetic loci controlling such traits. So far, two mapping studies were conducted using two genotypes related to *Rosa wichurana* sp. as a resistant parent, and they mapped quantitative resistance loci (QRLs) on chromosomes 3 and 5 (Yan et al. 2019; Soufflet-Freslon et al. 2019). But before concluding on the genetic bases of partial resistance in roses, one must remember that what is discovered in a genotype might be different in another one. Therefore, we can only say that the partial resistance observed in the genotypes of *Rosa wichurana* used in these studies seem to be mainly controlled by two QRLs. These types of resistance might bring an additional layer if combined with complete resistance which could help to release varieties with higher and more durable resistance.

4.4.3. BEYOND CATEGORIES: ROSE IMMUNE RESPONSES TO *D. ROSAE* INFECTION

Although one can divide rose resistance responses to black spot disease into two categories that seem clearly different according to the authors, vertical or race-specific versus horizontal or race-nonspecific, it does not directly describe the underlying biology of plant defense. Rose immune responses to pathogen attacks such as *D. rosae* involve a multitude of mechanisms and actors from pathogen receptors and signal transduction pathways to defense-related gene products directly participating in the resistance (complete or not). Some defenses are constitutive like the cuticle as physical barrier (Dodge 1931; Castledine et al. 1981; Walker et al. 1996) and others can be compounds that are induced upon pathogen attack like phytoalexins (Knight 1975; Knight and Wheeler 1978) and polyphenol production (Saunders 1967). For the latter, additional induced compounds were described such as β -1,3-glucanase and chitinase that contributed to the reduction of black spot symptoms on *in vitro* rose plants. These antifungal compounds degrade fungal cell walls into short oligosaccharides that can play the role of signals for additional downstream defense responses (Suo and Leung 2001). These authors also noticed an accumulation of pathogenesis-related (PR) proteins (PR-1, PR-2, PR-3, and PR-5) in infected leaves with a systematic

induction of PR-2, PR-3, and PR-5 in uninfected upper leaves, which suggests that systemic acquired resistance (SAR) and induced systemic resistance (ISR) might be involved in black spot infection responses. Indeed, PR proteins can be induced within three days of acibenzolar-S methyl (BTH) treatment (known to induce SAR), which seems to reduce black spot symptoms in *in vitro* grown roses (Suo and Leung 2002).

It is only lately, with the rise of sequencing methods, that we have been able to access such detail in response to *D. rosae* infection through the study of transcriptomic changes operated upon infection and during the early phases of pathogen development (most likely during the biotrophic phase of its cycle). However, this study was conducted on a completely susceptible genotype which did not allow us to characterize an immune response that could eventually lead to partial or complete resistance. Neu et al. (2019) demonstrated that a conserved but insufficient pathogen associated molecular pattern (PAMP) triggered immunity (PTI) was expressed by the susceptible genotype ‘Pariser Charme®’ through the expression of PR proteins (like PR-10 homologs), chitinases and defense-related transcription factors (such as WRKY genes). Similarly, as in Suo and Leung study (2002), paralogs of *PR-1* and *PR-5* were differentially expressed along with genes from the phenylpropanoid and flavonoid pathways. Additional factors acting in the salicylic acid signaling pathway such as phytoalexin deficient 4 (*PAD4*) and six senescence-associated carboxylesterase 101 (SAGs 101) genes were upregulated (Neu et al. 2019). Interesting sequence of defense responses was studied here but it lacks information about the genes activated when the fungus switches to its necrotic life-style and there is also a need to investigate the disease responses that can lead to an efficient resistance.

4.4.4. FIELD AND LABORATORY/GREENHOUSE DISEASE ASSESSMENTS

As mentioned in [section 3.2.2](#), black spot evaluation in commercial breeding programs is commonly carried out in fields (Noack 2003; Leus 2017). However, it is a long process because, to ensure sufficient disease pressure, plants need to be left in fields for at least two to three years before being evaluated for disease resistance (Carlson-Nilsson and Davidson 2000; Noack 2003; Debener and Byrne 2014) (see Figure 10). In order to speed up this process, it has been suggested that greenhouse or laboratory controlled inoculations could be used as a substitute for field trials (Carlson-Nilsson and Davidson 2000; Drewes-Alvarez 2003). However, low correlations between disease ratings in fields among years were mentioned by Leus (2005) probably due to nonuniform spread of inoculum and climatic differences. Artificial inoculation in the field is rarely done but a common practice is to plant new trials with already established ones, insert susceptible genotypes among the tested individuals and plant them at high density so sufficient disease pressure and spread can be guaranteed (Debener and Byrne 2014). Greenhouse tests (Leus et al. 2007; Soufflet-Freslon et al. 2019; Marolleau et al. 2020) as well as laboratory screening have been proposed the last years for breeders but have also been used in black spot disease resistance studies for a long time now (Dodge 1931; Jenkins 1955; Palmer et al. 1966a; Knight 1975; Knight and Wheeler 1977; Kuklinski 1980; Castledine et al. 1981; Walker et al. 1996; Carlson-Nilsson 2001, 2002; Linde and Debener 2003). Laboratory screenings with artificial inoculations have been done on either leaf discs or detached leaves but a natural question that arises is whether or not these systems reflect the whole plant or field situations. As a matter of fact, some breeders prefer not to perform selection among young rose seedlings as they do not consider the resistance of these to be reflective of full grown plants (Debener and Byrne 2014; Debener 2019). Several studies have, indeed, demonstrated an effect of the leaf age on the

expression of disease resistance for different pathosystems such as apple-*Venturia inaequalis*, broccoli-*Hyaloperonospora parasitica*, cauliflower-*Alternaria brassicicola*, wheat-*Puccinia striiformis* among many others (Li and Xu 2002; Doullah et al. 2006; Coelho et al. 2009; Deep and Sharma 2012; Farber and Mundt 2016). In rose-*Diplocarpon rosae* pathosystem, some authors have mentioned a difference in susceptibility to black spot disease and even sometimes a resistant genotype might get infected if young leaves were inoculated, which was the case with ‘Red Radiance’ genotype (Dodge 1931; Aronescu 1934; Knight 1975). In another study, leaf disc assays were demonstrated to deviate from field situations (Walker et al. 1996) while detached leaf assays were found to reflect the situation in potted plants and field situations (Jenkins 1955; Carlson-Nilsson 2002; Dong et al. 2015). A recent study also demonstrated a good correlation between greenhouse disease assessment on whole potted plants and resistance scoring in fields (Marolleau et al. 2020). Regarding these results, detached leaf assay in laboratory settings and whole plant assays in greenhouse conditions seem to be the best option to assess resistance to black spot disease in an easier and fastest way. However, repeated inoculations (at least two or three repetitions) in greenhouse seedling selection need to be done to ensure the reproducibility of results as recommended by Leus (2005). Finally, in my opinion, artificial inoculations (whether it is in a greenhouse or laboratory) are tools that can come as supports to assess disease resistance but cannot completely replace field assessment in breeding programs. Some genotypes express very different behaviors between field and greenhouse/laboratory assessments and are even sometimes found to react very differently between artificial inoculations; it is the case for the field resistant variety *Rosa Radrazz* ‘Knock Out®’ (see Table 3). This genotype was found to be resistant in studies performing artificial inoculation as well as in field assessment (Whitaker et al. 2010b; Zlesak et al. 2010) but a recent study found it susceptible to tested races (Rouet et al. 2020) even the ones previously tested by Whitaker et al. (2010b). A latter study found inconsistent results for the same genotype using the same isolates and proposed to remove it from the standard set of genotypes used to differentiate *D. rosae* races (Zlesak et al. 2020). In this study, differences in infection within the same experiment (differences between boxes, see Table 3) were observed with some leaves exhibiting symptoms and sporulation by day 14 but no expansion was observed on day 25. Inconsistencies in infection incidence as well as lesion development might be related to the resistance mechanisms operating in ‘Knock Out®’ as it is dependent on the isolates’ nature but further investigations need to be done to explain these inconsistencies.

Table 3: Comparison of *Rosa RadRazz* ‘Knock out®’ responses to different isolates from several races according to three studies

	Whitaker et al. 2010				Rouet et al. 2020				Zlesak et al. 2020				
Race	10	8	7	5	10	8	7	5	10	8	7	5	12
Isolate	ACT/ KOMN	DA-1	R6	B005	ACT /DA-1	R6	B005		ACT/ KOMN	DA-1	R6	B005	BEP
‘Knock Out®’	+	-	-	+	+	+	+	+	+	-	+ ^y	+	+ ^y

^y Inconsistent susceptible reactions (infection occurrence and lesion growth) observed for different boxes when challenged with R6 and REP isolates

Furthermore, these studies were conducted by different research teams and differences in isolates, leaf selection (age) and experimental conditions might have affected the success of artificial inoculations on detached leaves as well as the outcome. Detached leaf assay is an interesting tool but may yield rather inconsistent results if the resistance observed in a genotype is linked to the leaf age (Dodge 1931; Aronescu 1934; Knight 1975) or the integrity of cuticle like shown by Castledine et al. (1981). In order to obtain reproducible and homogenous results, attention must be paid to these parameters (leaf age and leaf integrity) as well as stable virulence of the isolates used (shown to decrease when the fungus is propagated in artificial media, Frick 1943; Palmer et al. 1966a, a; Knight and Wheeler 1978; Drewes-Alvarez 2003).

5. RESEARCH OBJECTIVES

The actual context of reduction, even elimination of phytochemical use and the increasing demand for roses with higher degrees of resistance expressed by the final consumers have led scientists of the rose community to investigate more and more disease resistance in rose species and varieties. The most important and widespread disease in garden roses is black spot disease caused by the hemibiotrophic fungus *Diplocarpon rosae*. Even if increased efforts have been made to release varieties with higher degrees of resistance to this disease, there is still a lot of improvement to do. Garden rose breeding programs have now started selecting for disease resistance under conditions favorable for disease development. But with breeding cycles being very long, MAS could be a promise to select individuals from the seedling stage instead of waiting for three years for the disease to build up and be sufficient for resistance assessment in fields. Markers linked to disease resistance loci are, therefore, an increased need for efficient selection of disease resistant varieties.

So far, research has focused on the study of major genes controlling disease resistance in rose but a whole branch of disease resistance has been omitted until recently. Indeed, over the years, partial resistance has been described in several rose species and commercialized varieties but research about its genetic bases remains scarce. In order to avoid the release of varieties only exhibiting resistance controlled by major genes that have been described to be less durable in most cases, it is necessary to start investigating other sources of resistance that apply less selection pressure on the pathogen like for example partial resistance, which can be used in combination with major genes. Partial resistance to black spot disease in rose has been described to segregate quantitatively, which has led us to consider QTL mapping to investigate the genetic bases underlying such trait. To map loci linked to the partial resistance quantitatively inherited in rose segregating populations, we used the disease scoring of three populations connected by the male resistant parent related to *Rosa wichurana*, which was described to exhibit partial resistance to black spot disease over seven years and in different locations. In the meantime, an American team started developing 15 inter-related diploid rose populations using the black spot resistance cultivar *Rosa wichurana* 'Basye's Thornless'.

The main objective of the present manuscript is, then, to provide a multiscale study of a quantitative resistance to black spot disease on garden roses. In order to present the first insights in the genetics and genomics of the partial resistance to black spot disease in rose, the main objective will be declined in three studies each one corresponding to a thorough study of partial resistance at different scales:

- (1) stable quantitative resistance loci (QRLs) identification in three interconnected populations sharing the same resistant male parent related to *Rosa wichurana*, which has been described to exhibit partial resistance to black spot disease over several years and locations (**population, individual and gene levels**);
- (2) phenotypic and microscopic study of the partial resistance of *R. wichurana* to *D. rosae* in comparison to completely susceptible genotypes and genotypes carrying *R* genes to assess the interactions during the infection process and to identify factors influencing partial resistance (**organ and cell levels**);
- (3) defense responses to *D. rosae* during both stages of the infection cycle (biotrophic and necrotrophic) for a compatible interaction and an incompatible interaction to identify immune responses leading to partial resistance in rose (**gene level**).

With this study, we would like to bring complementary QTL mapping results to the one under work in the U.S. and to study more in detail the partial resistance observed in the hybrid of *Rosa wichurana* background with microscopic and transcriptomic approaches.

Chapter 2 : A multi-environment and multi-population quantitative trait loci study of black spot disease resistance in rose

It's the time that you spent on your rose that makes your rose so important...People have forgotten this truth, but you mustn't forget it. You become responsible forever for what you've tamed. You're responsible for your rose.

– Antoine de Saint-Exupéry



Hybrid from the cross between *Rosa wichurana* with white simple flowers and *Rosa chinensis* 'Old Blush' with pink double flowers
by M. Tisserand

1. SYNOPSIS

The literature suggests the existence of partial resistance to black spot disease (BSD) in rose hosts (Xue and Davidson 1998; Whitaker and Hokanson 2009; Dong et al. 2017). This type of resistance does not prevent pathogen infection but rather reduces the symptom severity (lesion size, sporulation and whole plant damage) by delaying pathogen penetration, development and also by reducing sporulation (Parlevliet 1985; Xue and Davidson 1998; Whitaker and Hokanson 2009; Dong et al. 2017). So, unlike a susceptible type of infection, partial resistance seems to reduce the epidemic pressure of a pathogen. It is believed that it is more difficult for pathogen populations to adapt to this type of resistance, which makes it, therefore, more durable and interesting for breeders (Parlevliet 1993, 2002; Johnson 2000; Pilet-Nayel et al. 2017). Consequently, increased attention has been given to study partial resistance to BSD in the past years. One rose species in particular has been reported to exhibit a partial resistance to BSD: *Rosa wichurana* Crép. It is a diploid species that was introduced from the east of China and from Japan in the early 1880's for its winter hardiness, disease resistance and glabrous leaf character. *R. wichurana* has been widely used in breeding programs (Lammerts 1945; Swim 1948; Wylie 1955; Xue and Davidson 1998; Blechert and Debener 2005; Shupert 2006; Byrne et al. 2007, 2010; Dong et al. 2017). So far, the partial resistance of *R. wichurana* and genotypes derived from it (diploid and tetraploid populations) have been assessed in controlled inoculations (detached leaf assay and whole plant assay) in laboratory (Whitaker and Hokanson 2009; Dong et al. 2017) as well as in fields (Shupert 2006; Dong 2014). However, the study of the genetic basis controlling this type of resistance remains limited. Indeed, all what we knew about the genetic basis of partial resistance to BSD when my team's projects started nine years ago was that: (1) (Whitaker and Hokanson 2009) had reported a strong additive genetic effect as well as a general combining ability for diploid and tetraploid populations derived from *R. wichurana*, *R. chinensis* and *R. multiflora*, and (2) Dong et al. (2017) had calculated the narrow-sense heritability of partial resistance to BSD in population derived from *R. wichurana*. It varies from 0.28 to 0.43 with a genetic variance analysis and from 0.76 to 0.86 with offspring-midparent regression. Based on these findings, integration of a stable partial resistance to BSD in rose cultivars seems to be feasible and is a promising possibility for the rose industry.

The goal of this chapter of my dissertation is to present the first insights on the genetic basis controlling the partial resistance to BSD observed in a hybrid of *R. wichurana* (RW). This work has only been possible thanks to the tremendous work provided by the GDO team. Several years of data collected over several locations from three populations connected by the resistant male parent RW were used to investigate the genetic basis of the partial resistance carried by this genotype.

I think that it is essential to explain the origin of the material used in this chapter so you, reader, can understand that the work behind this chapter did not only start with my PhD project but has been carried on for almost two decades now. Indeed, material development for field assessment of perennial plants takes several years from the hybridizations to plants ready to be assessed in the fields. And of course as we wanted to study the plant resistance under natural infection, we had to ensure sufficient disease pressure by scoring the plants after at least three years in the field, which added more time to have plants ready to be assessed (Debener and Byrne 2014). Two of the three populations used in this study (FW and HW populations) have already been developed by Meilland breeding company during L. Crespel PhD project (2001) in order to study the introgression of recurrent blooming and disease resistance to

commercial varieties. The crosses behind these populations will be detailed in the material and method of the section XX. Then, two collaborative projects between rose breeding companies and the research institute of the IRHS were carried out before my arrival to install plant material and perform the disease assessments. In 2010, the GDO team decided to develop a third population, called OW population, with the aim of using it to build a high density genetic map to anchor the 'OB' genome sequence. This new population was also used to study several traits such as recurrent flowering, date of flowering, color, prickles determinism, fragrance, double-flowers, architecture and disease resistance. In addition to the plant material, tools and genetic maps were developed throughout the years (Hibrand-Saint Oyant et al. 2007, 2018; Kawamura et al. 2011; Roman et al. 2015; Soufflet-Freslon et al. 2019; Marolleau et al. 2020) without which this study could have not been carried out.

The conclusion of all these years of data collection and research was published in the journal *Theoretical and Applied Genetics* (TAG) and is presented in the first part of this chapter. The contributing authors are listed below:

D. C. Lopez Arias¹, A. Chastellier¹, T. Thouroude¹, J. Bradeen², L. Van Ech², Yannick De Oliveira³, S. Paillard¹, F. Foucher¹, L. Hibrand-Saint Oyant¹ and V. Soufflet-Freslon¹

¹ IRHS-UMR1345, Université d'Angers, INRAE, Institut Agro, SFR 4207 QuaSaV, 49071, Beaucouzé, France

² Department of Plant Pathology and The Stakman-Borlaug Center for Sustainable Plant Health, University of Minnesota, St. Paul, MN, USA

³ Génétique Quantitative et Évolution - Le Moulon, INRAE - Université Paris-Sud - CNRS - AgroParisTech, Ferme du Moulon, F-91190 Gif-sur-Yvette, France

The contribution of each author is specified in section 2.2 at the beginning of the article.

The second part of this chapter will present supplementary results from different analyses performed during the first part of my PhD project that were not included in the publication. First, I would like to present a reflection on the effect of the environmental conditions on the BSD incidence as we have had the possibility to follow the same individuals for several years and, for some of them, in several locations. Then, I would like to focus my dissertation on the QTL analysis for non-normal phenotypes as biological data are not often normally distributed. In that part, I would like to further discuss the implication of using a two-part model for spike-like data as well as introducing results for binary QTL analysis performed on these non-normal scoring years. Furthermore, complex traits like disease resistance are controlled by many genes and, therefore, one cannot restrict the QTL search to a one-dimensional scan as the search of multiple QTLs is essentially a multidimensional problem. Thus, I would like to go a little further in the QTL analysis that was already published by exploring multiple QTL model fitting using the functions provided by the R/qtl package. These additional analyses will help us discuss the effect of the QTLs detected on the phenotype and to better estimate the allelic effect of the QTLs detected in the publication. Both multiple QTL models fit and estimated allelic effects will be presented in the last section.

The supplementary data for the article that is mentioned in the text can be found in Appendix 1 and the supplementary data for the additional analysis can be found in Appendix 2.

2. ARTICLE: CHARACTERIZATION OF BLACK SPOT RESISTANCE IN DIPLOID ROSES WITH QTL DETECTION, META-ANALYSIS AND CANDIDATE-GENE IDENTIFICATION

2.1. KEY MESSAGE

Two environmentally stable QTLs linked to black spot disease resistance in the *Rosa wichurana* genetic background were detected, in different connected populations, on linkage groups 3 and 5. Co-localization between *R*-genes and defense response genes was revealed via meta-analysis.

2.2. ABSTRACT

The widespread rose black spot disease (BSD) caused by the hemibiotrophic fungus *Diplocarpon rosae* Wolf. is efficiently controlled with fungicides. However, in the actual context of reducing agrochemical use, the demand for rose bushes with higher levels of resistance has increased. Qualitative resistance conferred by major genes (*Rdr* genes) has been widely studied but quantitative resistance to BSD requires further investigation. In this study, segregating populations connected through the BSD resistant *Rosa wichurana* male parent were phenotyped for disease resistance over several years and locations. A pseudo-testcross approach was used, resulting in six parental maps across three populations. A total of 45 individual QTLs with significant effect on BSD resistance were mapped on the male maps (on linkage groups (LG) B3, B4, B5 and B6), and 12 on the female maps (on LG A1, A2, A3, A4 and A5). Two major regions linked to BSD resistance were identified on LG B3 and B5 of the male maps and were integrated into a consensus map built from all three of the male maps. A meta-analysis was used to narrow down the confidence intervals of individual QTLs from three populations by generating meta-QTLs. Two “hot spots” or meta-QTLs were found per LG, enabling reduction of the confidence interval to 10.42 cM for B3 and 11.47 cM for B5. An expert annotation of NBS-LRR encoding genes of the genome assembly of Hibrand et al. was performed and used to explore potential co-localization with *R*-genes. Co-localization with defense response genes was also investigated.

2.3. KEYWORDS

Rosa, quantitative resistance, natural infection, *Diplocarpon rosae*, QTL mapping, meta-analysis

2.4. AUTHOR CONTRIBUTION

DCLA participated in the phenotyping, performed the genetic and statistical analyses and wrote the paper. VSF, FF and LHSO conceived the AC provided a technical support in the SSR genotyping and participated in the phenotyping. TT coordinated the field trials and participated in the phenotyping. LVE and JB performed the manual annotation and provided revision of the manuscript. YDO provided support in software Biomercator and the meta-analysis approach. FF provided extensive revisions of the manuscript. SP, LHSO and VSF participated in the phenotyping and provided extensive revisions of the manuscript. All authors read the final version of the manuscript and approved its publication.

2.5. INTRODUCTION

Cultivated roses are among the most popular garden plants (Waliczek et al. 2015a; Wang et al. 2017). In France, 16% of shrubs bought by the final consumers are garden roses, with a market value of 50.6 million Euros in 2017. Due in part to susceptibility to BSD, sales of garden roses in France declined 10% in 2017 compared with 2016 (VAL'HOR 2017). As such, BSD causes large economic losses and is, therefore, considered the most serious disease of cultivated roses grown outdoors.

BSD in roses, caused by the hemibiotrophic fungus *Diplocarpon rosae* Wolf, is globally distributed and affects nearly all modern varieties. To date, 13 races have been reported (Carlson-Nilsson 2001; Gachomo et al. 2006; Whitaker et al. 2007, 2010b; Zlesak et al. 2010; Zurn et al. 2018). Typical symptoms of this disease include dark rounded spots with fringed margins on the adaxial side of the leaves followed by chlorosis around the lesion and premature defoliation (Blechert and Debener 2005; Gachomo et al. 2006; Horst and Cloyd 2007). Reduced vigor in susceptible varieties can be observed, sometimes leading to death due to increased susceptibility to other stresses, like frost (Smith et al. 1989; Black et al. 1994). It is, then, important to study the rose-*Diplocarpon rosae* pathosystem.

The BSD fungus is obligate to the genus *Rosa*, though other *Diplocarpon* species are pathogenic on different crop species in the *Rosaceae* genus (Horst and Cloyd 2007). *Diplocarpon rosae* is spread mainly through asexual spores that are water-borne. During the infection process, the spores germinate, develop a germ tube with a melanized appressorium and penetrate the leaf cuticle (Gachomo 2005; Gachomo et al. 2006, 2010; Gachomo and Kotchoni 2007). During the biotrophic phase, subcuticular hyphae are formed followed by intercellular hyphae. Haustoria can be observed in this first stage of infection (Gachomo 2005; Gachomo and Kotchoni 2007). Then, the pathogen switches from a biotrophic lifestyle to a necrotrophic one and forms necrotrophic intracellular hyphae, followed in short order by a production of acervuli and second-generation conidia. On susceptible plants, a new generation of conidia is produced within nine days after inoculation (Gachomo 2005; Gachomo et al. 2006; Gachomo and Kotchoni 2007). Conidia are then spread by water-splash to start a whole new infection process on other leaves. Effective infection requires free water and humid conditions (Saunders 1966; Wiggers et al. 1997). Consequently, BSD is especially problematic in areas with high annual precipitation and humidity (Debener 2017).

BSD is rarely observed in greenhouse production as humidity can be carefully regulated. Garden rose multiplication and grafting are mainly done in the field, and rose bushes are generally used in gardens and landscaping for aesthetic value and low maintenance requirements. Due to the perennial habit of garden roses and *D. rosae* overwintering in fallen leaves, new infections can appear each year if the disease is not well managed (Münnekhoff et al. 2017) and can impact final consumers such as private gardeners and public garden managers. BSD is traditionally managed with fungicide applications. To reduce risk of chemical exposure, added costs and labor associated with this type of management, today's consumers are increasingly asking for natural resistance in rose plants (Harp et al. 2009; Zlesak et al. 2010, 2017; Waliczek et al. 2015b; Byrne et al. 2019). Moreover, European countries have adopted new laws to preserve the environment that aim to decrease agrochemical use. For example in France, measures such as the Ecophyto Plan (Labbé 2014) have forbidden the use of chemicals in public landscaping and private gardens since January 2017 and 2019, respectively (Labbé 2014). These concerns have encouraged

breeders and researchers to study BSD and to develop varieties with sustainable and higher levels of resistance.

Indeed, genetic resistance is a critical challenge to successful disease management in an environmentally friendly and cost-effective manner. Researchers have studied the genetic resistance to BSD, helping to identify modern rose varieties and wild species with high levels of resistance (Wiggers et al. 1997; Carlson-Nilsson 2001; Boontiang 2003; Bleichert and Debener 2005; Uggla and Carlson-Nilsson 2005; Harp et al. 2009; Schulz et al. 2009; Soufflet-Freslon et al. 2019). However, breeding for BSD resistance is complex due to the development of new pathogenic races and different ploidy levels in the genus *Rosa* (Debener et al. 1998; Uggla and Carlson-Nilsson 2005; Whitaker et al. 2007; Debener 2017). Four major loci associated with BSD resistance were identified mostly using detached leaf assays: *Rdr1* and *Rdr2* on chromosome 1 (Malek and Debener 1998; Yokoya et al. 2000; Malek et al. 2000; Kaufmann et al. 2003, 2010; Hattendorf et al. 2004; Whitaker et al. 2010a; Terefe-Ayana et al. 2011; Menz et al. 2018, 2020), *Rdr3* recently found to be located on chromosome 6 (Whitaker et al. 2010a; Zurn et al. 2020) and *Rdr4* possibly located on chromosome 5 (Zurn et al. 2018). Evidence of partial resistance to BSD was reported in several cases and seems to be race-non-specific (Xue and Davidson 1998; Shupert 2006; Whitaker and Hokanson 2009; Whitaker et al. 2010b; Allum et al. 2010; Dong et al. 2017). Quantitative resistance often confers a partial level of resistance to the plant by reducing pathogen multiplication, plant colonization, disease spread or symptom severity (Pilet-Nayel et al. 2017). This type of resistance is usually controlled by several genes and is associated with genomic regions termed Quantitative Trait Loci (QTLs). Over the last 20 years, many QTL experiments for disease resistance have been carried out on major crops (Lacape et al. 2010; Qi et al. 2011; Holland and Coles 2011; Yadava et al. 2012; Hamon et al. 2013; Semagn et al. 2013; Said et al. 2013; Pilet-Nayel et al. 2017). More recently, QTL analyses have been conducted on ornamental crops such as carnations, gerberas or roses (Yagi et al. 2006, 2012; Leus et al. 2015; Fu et al. 2017; Yan et al. 2019). On-going research suggests QTLs conferring resistance to BSD. Yan et al. (Yan et al. 2019) have identified a possible major QTL on LG 3, based on one year of phenotypic data and a pedigree based map of 15 diploid genotypes while Soufflet-Freslon et al. (Soufflet-Freslon et al. 2019) identified possible QTLs in two populations in France. These emerging studies aside, quantitative resistance to BSD has not been extensively studied, yet it remains a powerful tool to identify genomic regions involved in complex traits such as disease resistance.

The validity of QTL mapping results is influenced by many factors, including experimental conditions, choice of parents, rating scale, environmental conditions during the scored years, type and size of mapping populations, map density and statistical methods (Lanaud et al. 2009; Liu et al. 2009; Vasconcellos et al. 2017; Guo et al. 2018). Thus, QTL mapping of one trait across multiple populations and environments can frequently yield heterogeneous results comprising different genomic positions and large confidence intervals. Further refinement of these intervals and synthesis of all QTL information are difficult but necessary steps prior to QTL cloning attempts and MAS breeding application. Meta-analysis is an effective approach to combine QTL results from independent studies and refine QTL positions on a consensus genetic map (Goffinet and Gerber 2000; Veyrieras et al. 2007). This method was useful in characterizing the genetic determinants of complex traits for a variety of crops such as drought stress in rice (Khowaja et al. 2009), ear emergence in wheat (Griffiths et al. 2009), yield and anthesis silking in maize (Semagn et al.

2013), yield associated traits in *Brassica juncea* (Yadava et al. 2012), seed weight and resistance to soybean cyst nematode in soybean (Guo et al. 2006; Qi et al. 2011), partial resistance to *Aphanomyces euteiches* in pea (Hamon et al. 2013) or fiber quality, yield, drought tolerance and disease resistance in cotton (Lacape et al. 2010; Said et al. 2013). With plant genome sequences becoming increasingly available, it is now possible to apply comparative analysis between genetic and physical maps to identify candidate genes underlying MetaQTLs. This approach has not yet been explored for an ornamental crop such as roses.

The main objective of our study was to explore the genetic determinants of BSD resistance in *Rosa wichurana* (RW). We identified QTLs linked to BSD resistance in RW using three different populations phenotyped over several years and locations. We next evaluated the stability of these QTLs and their inheritance in different genetic backgrounds. Finally, we explored sets of candidate genes at BSD resistance QTL locations using one of the recently published rose genome assembly from Hibrand-Saint Oyant et al. in 2018.

2.6. MATERIAL AND METHODS

2.6.1. MAPPING POPULATIONS

We used *R. wichurana* (RW) as a source of resistance. Indeed, RW was described to be highly resistant to BSD (Debener et al. 1998; Yan et al. 2019). RW was crossed with different cultivars to develop three F1 progenies:

- OW population (151 individuals) was obtained from a cross between *R. chinensis* 'Old Blush' (OB), susceptible to BSD, and RW (Lopez Arias et al. 2020; Hibrand-Saint Oyant et al. 2018; Soufflet-Freslon et al. 2019),

- HW population (209 individuals) was generated from a cross between a dihaploid rose named H190 (Meynet et al. 1994), susceptible to BSD, and RW (Soufflet-Freslon et al. 2019),

- FW population (96 individuals) resulted from a cross between the cultivar 'The Fairy' (TF) and RW (Kawamura et al. 2015). In the Earth-Kind® Trials using detached leaf assay, TF was shown to be susceptible to pathogen races 3, 8 and 9 (Zlesak et al. 2010).

The OW and FW populations were planted on their own roots in the field at INRA Horticulture Experimental Facility (Beaucouzé, France). The HW population was grafted on to *Rosa canina* 'Laxa' rootstock and planted in three French sites (Soufflet-Freslon et al. 2019):

- Nursery France Pilté (45270 Quiers-sur-Bezonde, Loiret, France), henceforth referred to as Bellegarde,

- Nursery/Breeder Meilland Richardier (Diémoz, Isère, France), henceforth referred to as Diémoz,

- Horticulture Experimental Facility (Beaucouzé, France), henceforth referred to as Angers.

Pruning was performed in November followed by a copper treatment to protect against canker. One to two applications of the fungicide NIMROD® were made according to manufacturer's recommendations in

the Spring to prevent powdery mildew development, and an aphicide spray was used if necessary. NIMROD® is not effective against *D. rosae* and no broad-spectrum fungicide was used.

For the HW and FW populations, field trials were performed in a randomized complete block design with three replicates. Due to production problems, only one replicate per individual for the OW population was used.

2.6.2. DISEASE SCORING AND STATISTICAL ANALYSES

BSD was visually scored for each population two years after planting them in the field and at the peak of disease (between July and September depending on the year). BSD was scored on the lower part of the plant using a visual rating scale from 0 to 5 presented in Supplementary figure 1 (Marolleau et al. 2020; Soufflet-Freslon et al. 2019). These scores correspond to a percentage of infected leaves and a degree of defoliation (scores 4 and 5). Disease resistance or susceptibility on field trials was assessed using the visual rating scale described above. First, plants with a score lower than 1 were considered “resistant”. Indeed, the response to the *D. rosae* infection seemed to prevent pathogen development on the leaves or considerably reduce pathogen growth on the plant, leading to no visible symptoms (score 0) or to the infection of a small portion of leaves (less than 25% of the lower part of the plant). Then, plants with a score lower than 4 were considered “intermediate” as less than 75% of the lower part of the plant was infected but no defoliation had yet occurred. Finally, susceptible plants were scored 4 to 5 with more than 75% of the lower part of the plant showing symptoms and/or a severe defoliation at that time, meaning that the response to the infection did not efficiently impair pathogen development.

The OW population was scored from 2014 to 2018 (Lopez Arias et al. 2020), the HW population was scored from 2012 to 2014 (Soufflet-Freslon et al. 2019) and in 2018, and the FW population was scored in 2014 and 2018.

All phenotypic data were analyzed with Rstudio interface (version 1.1.463, <http://www.rstudio.com/>) of R software (<http://www.r-project.org/>), version 3.5.1 (2018-07-02).

An overall mean for each population was calculated for each year of scoring to assess whether or not the disease incidence was uniform over the years using a Kruskal-Wallis test (for OW and HW populations) and a Wilcoxon test (for FW population).

The normality of residuals was tested using a Shapiro-Wilk test and the homogeneity of variance was assessed with a Bartlett’s test. However, in field situations, plants can die or disease scoring can be missing, resulting in unbalanced experimental designs. Unlike analysis of variance (ANOVA), maximum likelihood methods, such as Restricted Maximum Likelihood (REML), provide unbiased estimators without any demand on the design and balance of data (Patterson and Thompson 1971; Corbeil and Searle 1976; Harville 1977; Lynch and Walsh 1998; Holland et al. 2010). Based on the data distribution, REML was used in place of ANOVA to estimate variance components using the package ‘sommer’ (Covarrubias-Pazarán 2019) in R. The broad-sense heritability was calculated for each population based on the following formula:

$$H^2 = \sigma_g^2 / (\sigma_g^2 + \frac{\sigma_{gxe}^2}{a} + \frac{\sigma_e^2}{ar})$$
, where σ_g^2 is the genotypic variance among populations, σ_{gxe}^2 is the variance of the interaction between genotype and environment (year/location for HW and year for FW

and OW), σ_{ε}^2 is the residual variance, a is the number of scoring years and r the number of replicates in each population.

2.6.3. GENETIC DATA AND LINKAGE MAPPING

It is not possible to obtain homozygous parental lines in rose by self-fertilizing due to strong inbreeding depression. As such, a “double pseudo-testcross strategy” developed for highly heterozygous plants (Grattapaglia and Sederoff 1994; Weber et al. 2003; Fischer et al. 2004; Hibrand-Saint Oyant et al. 2007; Roman et al. 2015; Zurn et al. 2018; Bourke et al. 2018; Yan et al. 2019) was used in the current study. This strategy involves a controlled cross between two genotypes, with heterozygous genetic markers originating from either parents, followed in their F1 generation. Multiple maximum likelihood mapping was conducted using JoinMap V4.1 (Van Ooijen 2011) using the CP (Cross population = outbreed full-sib family) population setting. In this analysis, molecular markers can segregate in one or both parents, with maps comprising dominant and co-dominant markers calculated separately for each parent followed by construction of an integrated consensus map.

Parental linkage maps for FW and HW populations were constructed from previously published data (Kawamura et al. 2015; Roman et al. 2015). Constructed maps were checked for apparent genotyping errors and/or poor fitting loci by looking at aberrant number of double crossing, high values of ‘Nearest Neighbor fit’ (N.N fit) and genotype probabilities (-Log₁₀(P)). When outstanding loci were found, genotyping was controlled either with SNP/probeset categories according to cluster properties or raw genotyping from GeneMapper software and removed when necessary. Maps were then re-calculated. The consensus map released by (Spiller et al. 2011) was used to check LG names and whole LG inversions for consistency. Parental linkage maps for the OW population were developed using previously reported single nucleotide polymorphism (SNP) marker data (Hibrand-Saint Oyant et al. 2018). Short sequence repeat (SSR) markers previously genotyped in this population were also included (Lopez Arias et al. 2020) and used as common markers for the Meta-QTL analysis. Parental maps were calculated using JoinMap 4.1 (Van Ooijen 2011) but due to insufficient “anchor loci” (i.e. markers heterozygous in both parents) an integrated map could not be obtained for this population. Following calculation of pair-wise recombination frequencies, seven LGs were identified using the logarithm of odds (LOD) score of independence between pairs of loci at a threshold of 4. Due to a large number of markers per LG (from 171 to 1,134 markers), the maximum-likelihood mapping algorithm method was used to order markers on LGs. Indeed, this method is more suitable than regression mapping for large marker datasets (Cheema and Dicks 2009). The maximum-likelihood mapping algorithm method was carried out under default JoinMap calculation settings (i.e. simulated annealing chain length of 10,000 with an acceptance probability threshold of 0.25, Gibbs sampling for estimation of multipoint recombination frequencies with a burn-in chain length of 10,000 and a chain length per Monte Carlo EM algorithm of 1,000). The same procedure previously described was carried out to identify and remove markers with genotyping errors and poor fitting.

2.6.4. QTL MAPPING

QTL mapping was performed using the parental maps for each population (OW, FW and HW) and data from different years were analyzed separately. The R/QTL package (Broman and Sen 2009; Broman and Wu 2019) was used to map QTLs and specific analyses were carried out for each set of phenotypic data according to the distribution of disease scores. For all populations, scoring years and locations, a “one

dimensional QTL scan” was carried out using different specific models that best fit the data using the package R/QTL on the Rstudio interface (Broman and Sen 2009).

For data distributed normally, a three-step strategy was employed using a normal model for simple interval mapping (SIM) and composite interval mapping (CIM). First, the multiple imputation method was used to overcome issues with missing data as it fills in all missing genotype data even at sites between markers on a defined grid along LGs (Broman and Sen 2009). For this, the function ‘sim.geno’ was used with 200 imputations and a step size of 1cM. Next, using the previous simulated data, a genome scan with a single QTL model (SIM) was performed with the function ‘scanone’ (parameters: normal model and imputation method). Finally, a permutation test with 1,000 permutations of the data was used to identify genome-wide significance thresholds for declaring the presence of a QTL (Doerge and Churchill 1996). When QTLs were identified, CIM was performed to improve further QTL detections by including a marker at the peak of QTL with large effect as covariate (Broman and Sen 2009).

For data exhibiting a substantial peak at zero, the mapping strategy was based on a two-part model used to better characterize the influence of a QTL presence on BSD (Broman 2003; Broman and Sen 2009; Holland and Coles 2011). For this approach, the phenotypic data were analyzed in two parts. First, individuals with scoring values above zero were analyzed using a normal phenotype model. Second, the trait was considered as binary (0 and >0) (Broman 2003; Broman and Sen 2009). The two-part model performs the following three calculations, each with a resulting LOD score: (1) the hypothesis that a given QTL increased the probability that an individual had a null phenotype (LOD_{π}), and so was resistant (which can also be referred as the penetrance of the disease); (2) the hypothesis that a detected QTL influenced the average phenotype among individuals with non-null phenotypes (LOD_{μ}), so it affected the severity of the disease; (3) the probability of having a QTL at a given position ($LOD_{\mu,\pi}$) (simply the sum of LOD scores from the preceding analyses).

To characterize detected QTLs, approximate 95% Bayesian credible intervals, phenotypic variation and QTL effects were estimated using the functions bayesint, makeqtl/fitqtl and effectplot respectively.

2.6.5. META-QTL ANALYSIS

The meta-QTL analysis was conducted with Biomeqator v4.2.2 software (Arcade et al. 2004; Sosnowski et al. 2012). The total number of QTLs per LG for all three populations was recorded. LGs with more than three QTLs and with QTLs from all the populations were considered for the meta-analysis. Input map files and QTL files for Biomeqator v4.2.2 were prepared for the male parent map of each population according to its requirements. Using the male map of OW population as the reference linkage map to fix locus order, a consensus male map was constructed using ConsMap (based on a weighted least square (WLS) strategy). To identify meta-QTLs, we pursued the approach proposed by Goffinet and Gerber in 2000. Due to the fact that our mapping populations share a common male parent and because the same plants were phenotyped across years, our data are not completely independent. In simulation tests, the Goffinet approach proved to be robust, obviating the need for further manipulation of non-independent data (Goffinet and Gerber 2000). The method first tests the likelihood of QTL grouping in maximum four groups and then selects the optimum number of groups using an ‘Akaike’ information criterion (AIC) (Arcade et al. 2004; Sosnowski et al. 2012). Estimated positions and confidence intervals (CI) of all

consensus QTLs were provided and the resulting meta-QTLs were projected on the previously constructed consensus map using QTLProj.

2.6.6. NB-ENCODING GENES AND CANDIDATE-GENE MINING

In version 4.2.2 of BiomeRCator, genetic maps can be linked to genome annotation using anchor markers. Genes underlying QTL or meta-QTL confidence intervals (CI) can be listed and basic gene ontology (GO) term representation within CI, chromosome or whole genome can be applied. In this study, we compared the lists of genes underlying meta-QTLs for the recently released rose genome sequence (Hibrand-Saint Oyant et al. 2018).

To detect potential candidate-genes, a detailed analysis of NBS-LRR genes was performed. Protein sequences from *Rosa chinensis* (Hibrand-Saint Oyant et al. 2018) were scanned for the presence of R-gene-related domains using the hmmscan algorithm in HMMER v3.1b2 (Finn et al. 2015). These domains included NB-ARC (PF00931), TIR (PF01582, PF13676) and LRR (PF00560, PF07723, PF07725, PF12799, PF13306, PF13516, PF13855, PF14580) domains as defined in the Pfam database (Finn et al. 2016). Only proteins with an NB-ARC domain hit longer than 20 amino acid residues and with E-value $< 1 \times 10^{-05}$ were retained for subsequent analysis. These sequences were scanned for the presence of additional, non-canonical domains. The presence of coiled-coil domains was determined for each protein using ncoils with the arguments “-c -w -win 21 -min_P 0.75” and “-c -w -win 28 -min_P 0.75” (Lupas et al. 1991). Custom python scripts were developed to parse, tile and filter the scan output to obtain detailed domain configuration for each protein sequence. NB-ARC domains were extracted from each sequence according to the hmmscan results, and used for subsequent phylogenetic analysis. NB-ARC sequences were coalesced into homology groups using USEARCH with the arguments “-cluster_agg %s -id 0.8 -linkage min” (Edgar 2010). A multiple sequence alignment was constructed for each homology group using MUSCLE (Edgar 2004), and consensus sequences obtained using HMMBUILD and HMMEMIT in HMMER v3.1b2. A multiple sequence alignment was constructed from all consensus sequences using MUSCLE and converted to the PHYLIP format (Felsenstein 1989). RaxML was used to construct the phylogeny (Stamatakis 2014), using 100 bootstrap replicates and an NB-ARC consensus sequence from *Arabidopsis thaliana* as outgroup, with the arguments “-m PROTCATDAYHOFF -T 24 -f a -x 98 -p f -N 100”. Chromosomal positions for candidate R-genes were used to construct a physical map of R-gene distribution within the genome, using CIRCOS (Krzywinski et al. 2009).

2.7. RESULTS

2.7.1. DISEASE SCORING AND STATISTICAL ANALYSES

BSD was recorded in all three studied populations over several environments (years and locations) under natural infection in fields with no chemical treatment. Across all scoring years, the parents RW and TF were found resistant to BSD with a mean score of 0.50 and 0.33, respectively. The H190 female parent was classified as intermediate with a mean score of 3.44 for all locations whereas OB had a mean score of 4.7 and was classified as susceptible to BSD.

For the OW population, the mean annual BSD scores from 2014 to 2018 were not significantly different from each other ($H=7.2759$, 4 d.f., $P=0.122$, see Supplementary figure 2) indicating that the disease impact on the OW population was homogeneous over 2014-2015-2016-2017 and 2018. The disease scores in the

OW population ranged from 0 to the maximum score 5. The median of 2018 scoring was higher than for other years. Residuals for the OW population showed a distribution close to normal ($W=0.99509$, $P=0.02045$) but the homogeneity of variance across years was not validated by a Bartlett's test ($K=298.1$, 9 d.f., $P<0.001$). For the FW population, BSD scores in 2014 were significantly different from those in 2018 ($Z=-12.648$, 5 d.f., $P<0.001$, see Supplementary figure 2). In general, the FW population was more resistant than the two other populations with scores ranging from 0 to 4. Additionally, FW was the only population showing no defoliation due to disease. The phenotypic distribution of the FW population showed a peak at 0 and the residuals did not follow a normal distribution ($W=0.93557$, $P<0.001$). However, homogeneity of variance across years was validated ($K=298.1$, 9 d.f., $P<0.001$). For the HW population, the mean of BSD scores in different locations was significantly different ($H=476.52$, 2 d.f., $P<0.001$, data not shown), so all three locations were considered separately. In the three locations (Angers, Bellegarde and Diémoz), BSD was scored over several years (four, three and three years respectively) and infection levels for each year within a location were significantly different from each other ($H_a=346.74$, 3 d.f., $P<0.001$; $H_b=308.8$, 2 d.f., $P<0.001$ and $H_d=212.43$, 2 d.f., $P<0.001$; respectively, see Supplementary figure 2). BSD scores ranged from 0 to 4 for Angers and Bellegarde, and no individual was found completely resistant in Diémoz in all scoring years with BSD scores ranging from 0.67 to 4. A spike-like distribution was observed in 2018 in Angers, 2014 in Bellegarde and 2013 in Diémoz. Normality of residuals as well as homogeneity of variance were not validated (respectively $W=0.99618$, $P<0.001$ and $K=35.799$, 9 d.f., $P<0.001$). Interestingly, scoring year 2012 was lower than 2013 and 2014 for all three locations, and for Angers in 2018, many individuals presented a high resistance. However, the mean of BSD over the three years (2012, 2013 and 2014) was always the lowest in Angers, intermediate in Bellegarde and the highest in Diémoz.

Since normality and variance homogeneity assumptions were not validated for all three populations, the calculation of variance components was obtained using the REML method. The broad sense heritability of BSD resistance was estimated to be 0.79, 0.86 and 0.65 for the OW, HW and FW populations, respectively, indicating that BSD resistance is mainly controlled by genetic factors in all three populations. Moreover, the proportion of phenotypic variance due to genetic effects, here the variance in response to *D. rosae* infection due to genetic background of the individuals, seems to be higher for HW than for OW and lower for FW.

2.8. LINKAGE MAPPING OF PARENTAL MAPS

Parent-based maps were constructed for the HW and FW populations using previously published data (Kawamura et al. 2011, 2015; Roman et al. 2015). For both populations, seven LGs were defined and named according to the rose integrated consensus map of (Spiller et al. 2011). For the HW population, the male map comprised 56 markers covering 418.58 cM, and the female map comprised 37 markers covering 313.89 cM. On LG6 of the female map, only two markers were found heterozygous and were mapped. For the FW population, the male map comprised 94 markers covering 457.94 cM and the female map comprised 75 markers with a coverage of 369.91 cM.

For the OW population, we generated linkage maps with already published data by (Hibrand-Saint Oyant et al. 2018) and SSR markers selected to facilitate meta-analysis. A total of 497 SNP and 36 SSR markers were mapped on the male map. The resulting map comprises 402 unique loci assigned to seven LGs, designated B1-B7. The average marker interval was 1.14 cM (Table 4 and Supplementary figure 4) and

the entire map covered 453.62 cM. LGs range in size from 42.6 (B3) to 84.34 cM (B2). A total of 692 SNP markers, 31 SSR markers and one gene (*NP* also known as *RoAP2*, see Table 4 and Supplementary figure 3) were mapped in the female of the OW population. The resulting map included 513 unique loci assigned to seven LGs (named A1-A7). The average distance between markers is 0.96 cM and LGs range in size from 33.42 (A2) to 97.65 cM (A5). The female map for the OW population is 473.85 cM in total length.

Common markers were the ones shared by at least two populations. In total, 72 markers (41 common markers found for the male maps and 31 for the female maps) were used as “bridge markers” to connect the OW, FW and HW linkage maps (Table 4, listed on Supplementary table 1). The number of common markers per LG ranged from three (B1-B6 and A1-A6-A7) to nine (B3) (Table 4). Of 41 markers shared by at least two of the male linkage map, 21 were shared by all three male maps. Only eight markers were shared by the three female maps (Supplementary table 1). There was at least one common marker between the three populations for all LGs of the male and the female (except for A1) maps.

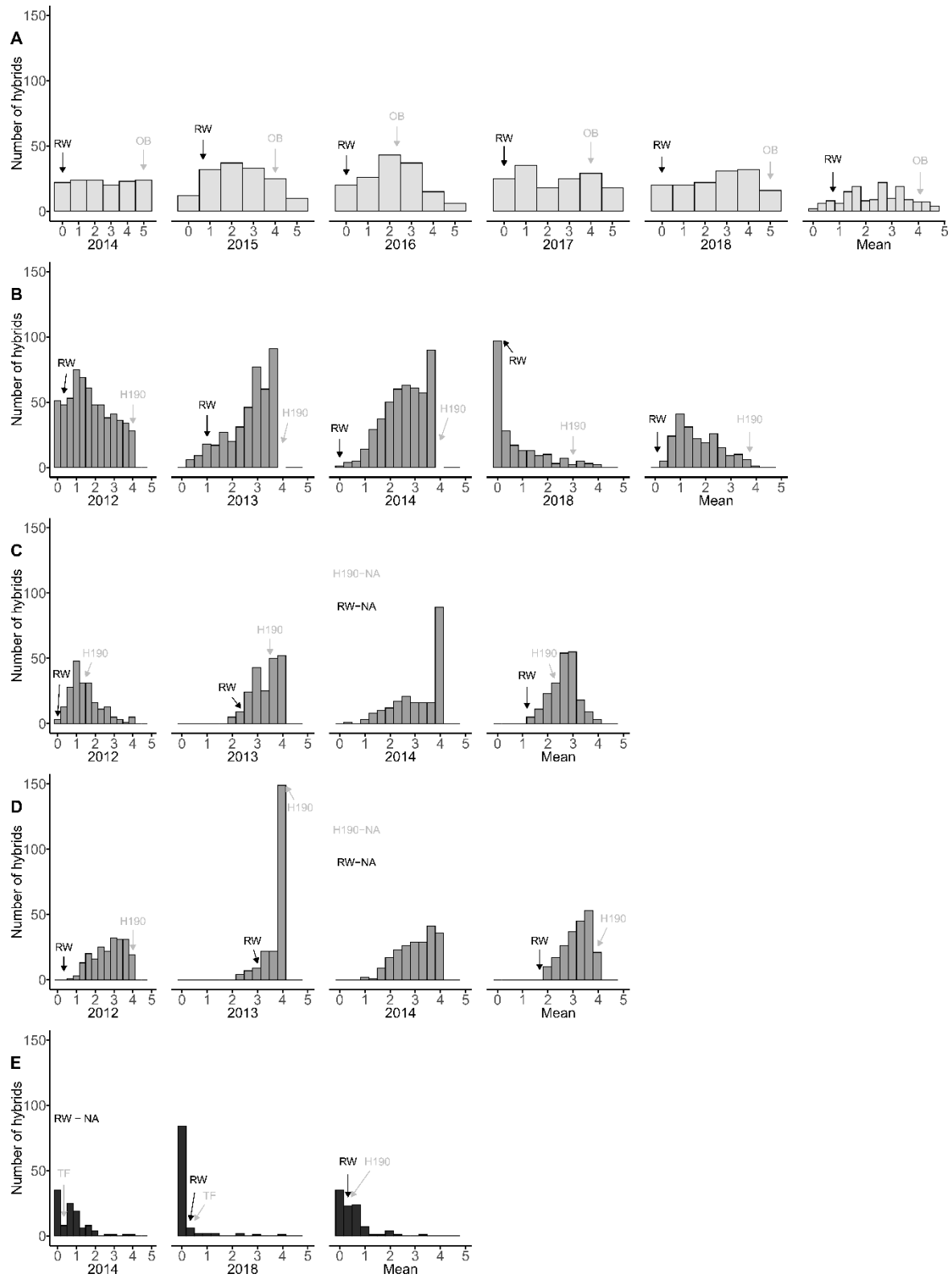


Figure 20: Black spot disease scoring data distribution for all years and locations for the three populations

2.8.1. QTL ANALYSIS

First, QTL detections within populations were performed using the parental genetic maps and phenotypic data of BSD resistance from the OW, HW and FW populations. In each population, individuals showed variable resistance responses across environments and years, so locations and years were considered separately in QTL analysis (Supplementary figure 2).

Two methods were adopted to perform QTL detection according to data distribution. Phenotypic data for the OW population and the HW population, with the exception of Angers 2018, Bellegarde 2014 and Diémoz 2013 phenotypic data (Figure 20) were analyzed using a normal model for simple interval mapping (SIM) and composite interval mapping (CIM). All other data exhibiting spike-like distribution were analyzed with a two-part model, henceforth referred as “2p” (Broman 2003). In addition, a mean across years was applied for each population (and for the HW population for each location separately). Then a normal method for QTL detection was used.

In total with the method for normally distributed phenotypes, 35 QTLs associated with BSD resistance were detected for the male maps, and eight QTLs were detected for the female maps. For spike-like distributions, ten QTLs were detected with the male maps and four with the female maps.

2.8.1.1. MALE MAPS

For all three populations, across years and locations combined, a total of 45 QTLs with significant effects on BSD resistance were identified on LGs B3, B4, B5 and B6 (Table 4, Supplementary figure 5, Supplementary figure 6, Supplementary figure 7 and Supplementary figure 8). QTLs on B3 and B5 were found for all three populations, whereas QTLs on B4 and B6 were population-specific (OW and HW, respectively).

QTLs on B3 were identified for all years and locations with both detection methods. Phenotypic variance within-population explained by individual QTLs on B3 varied from 3.9% to 23.6% and the LOD values varied from 2.73 to 15.23 (Table 5). For the OW population, five marker peaks were found in a region from 4cM to 26cM for the different years (Supplementary figure 5 and Table 5); for the HW population, five marker peaks were also found in a region from 3 to 19cM for all scoring years and locations (Supplementary figure 7 and Supplementary figure 8). For spike-like distributions, 2p model provides more information on the effect of the QTLs found. Indeed, for 2018 BSD scores of FW and HW in Angers and 2014 BSD scores of HW in Bellegarde, both LOD scores calculated for the 2p model exceeded their respective LOD thresholds (respectively Supplementary figure 6B, Supplementary figure 8A-B and Table 5). This means that the QTLs found on B3 affects the penetrance (appearance of the symptoms) as well as the severity of the disease. However, for HW Diémoz 2013, only the LOD π reached its corresponding threshold meaning that the QTL found on B3 for 2013 affected only the penetrance. The 2p model gave a better precision on the QTL location on B3 from the beginning of the LG to 9.67cM (Table 5).

QTLs on B5 were found repeatedly for each scoring year and location in the HW population (Supplementary figure 7 and Supplementary figure 8), and were year dependent in the OW population (detected for scoring years 2016, 2017 and 2018, see Supplementary figure 5). A QTL on B5 was also detected on FW for scoring year 2018. The LOD peak values varied from 3.43 to 12.14, and the phenotypic

variance ranged from 2.89% to 19.82% (Table 5). For the OW population, two close peaks were found for scoring years 2017, 2018 and the mean in a region from 8.71cM to 10cM. For all scoring years and locations for the HW population, four marker peaks were found in a region from 23cM to 41cM (Supplementary figure 7 and Supplementary figure 8). Interestingly, in the OW population in 2016, the FW population in 2018, and for all years and locations for the HW population, a second peak on the distal end of B5 can also be observed (Supplementary figure 5, Supplementary figure 6B, Supplementary figure 7 and Supplementary figure 8).

Two QTLs were identified on B4 in 2017 and with the mean across years for the OW population, explaining 5.1 to 7.6% of the phenotypic variance. The location of the B4 QTL was defined more precisely using BSD scores averaged across years (10cM region) than a single year scores (entire LG based on 2017 data, see Table 5).

QTLs with significant but small effects on BSD resistance were mapped on B6 in most years and locations for the HW population as well as for the average BSD scores. These QTLs were population-specific and were only detected when RW was crossed with H190 (Supplementary figure 7 and Supplementary figure 8). The LOD peaks ranged from 2.6 to 5.92 explaining 3.6 to 4.63% of phenotypic variance (Table 5). For data from HW Angers 2018 and HW Bellegarde 2014, the QTL on B6 affected the penetrance of the trait (Supplementary figure 8). No interactions between QTLs were observed across years and locations (data not shown). As B6 and B4 QTLs had small effects on BSD resistance and were population-specific and year-specific, they were not considered for the subsequent meta-analysis.

2.8.1.2. FEMALE MAPS

No QTL common across all three populations was identified on the female maps (Table 6), but QTLs were shared by pairs of populations. The OW and FW populations displayed a common QTL on A1, while for the HW and FW populations displayed two common QTLs, both on A4. In the OW population, a significant QTL on A1 was identified in 2017, explaining 6.53% of the total phenotypic variance and was located at the end of the LG (Lopez Arias et al. 2020). For the FW population, three QTLs were detected with 2018 data using 2p method. These QTLs, located on A1, A2 and A4, explained 4.06%, 2.57% and 3.61% of the phenotypic variance, respectively (Table 6). Interestingly, QTLs on A1 and A4 had an effect on the penetrance of the trait (LOD 2.59 and 4.09 respectively; see Table 6) whereas the QTL on A2 had an effect on both severity and penetrance (Supplementary figure 9A).

To position the QTL detected in the OW and FW populations on LG A1, markers at the confidence interval limits and markers at the peak of the QTLs were positioned on a physical map (Supplementary figure 10). TIR-NB-LRR (*TNL*) genes and cluster of genes from this regions identified by Menz et al. in 2020 were also mapped. Two clusters of *TNL* genes, named cluster 1 (genes OB2_C to OB2_H) and cluster 2 (genes OB2_J to OB2_S), were localized near the end of chromosome 1 (Supplementary figure 10). The *Rdr1* resistance gene from *Rosa multiflora* is part of cluster 2 (Malek et al. 2000; Kaufmann et al. 2003; Hattendorf et al. 2004; Terefe-Ayana et al. 2011; Menz et al. 2020). Importantly, the QTLs derived from the female parents TF and OB co-localized with both clusters of *TNL* genes (Supplementary figure 10).

For the HW population, QTLs were identified on LG A3 in 2012 and 2014 in Angers, 2013 in Bellegarde, 2014 in Diémoz and the averages across years for each location explaining 4.4% to 5.8% of the phenotypic variation (Table 6). One QTL explaining 5.91% of phenotypic variation was also identified on A3 in Bellegarde in 2014 using the 2p model. This QTL had an effect on the penetrance of the trait (Supplementary figure 9B). Also in Bellegarde, a QTL explaining 5.39% of the phenotypic variance was identified on A5 in 2012. In Diémoz, a QTL explaining 5.77% of the phenotypic variance was identified on A4 in 2014 (Table 6).

For both male and female maps, further QTLs and epistasis between QTLs were investigated using a two dimensional genome scan and no epistasis was significantly detected for any scoring year with normal distribution (data not shown). The percent explained by all QTLs is, then, the sum of all the phenotypic variance explained by the individual QTLs of each scoring years (Table 6).

Table 4 Summary of the SSR and SNP-based linkage maps for OW population and the common markers with other populations

LG	Female map							LG	Male map						
	Length (cM)	Number of markers			Number of loci	Average marker interval (cM)	Number of common markers*		Length (cM)	Number of markers			Number of loci	Average marker interval (cM)	Number of common markers*
		SNP	SSR	Total (identicals)						SNP	SSR	Total (identicals)			
A1	71.71	115	2	117 (690)	79	0.91	3	B1	57.44	66	2	68 (171)	50	1.15	3
A2	33.42	69	3	72 (1100)	45	0.74	8	B2	84.34	90	7	97 (266)	65	1.30	8
A3	53.75	61	5 (+1)	68 (520)	53	1.01	5	B3	42.6	37	5	42 (518)	35	1.22	9
A4	58.79	41	5	46 (220)	40	1.47	4	B4	66.82	73	7	80 (371)	66	1.01	6
A5	97.68	148	7	155 (1007)	115	0.85	5	B5	71.12	83	7	90 (318)	74	0.96	8
A6	70.15	133	4	137 (1134)	91	0.77	3	B6	55.89	65	3	68 (210)	48	1.16	3
A7	88.36	126	5	131 (841)	90	0.98	3	B7	75.41	83	5	88 (217)	64	1.18	4
Total	473.85	692	31 (+1)	726 (5512)	513	0.96	31	Total	453.62	497	36	534 (2072)	402	1.14	41

Linkage groups (LG) names for the female map (A1 to A7) and for the male map (B1 to B7) were assigned according to Spiller et al. 2011. Several makers were mapped at the same locus so the number of unique loci is displayed and in the total number, the number of markers with different phases (called identicals) are displayed in parenthesis. One gene marker was used for the female map and is represented with (+1) on the table.

*Marker was count as common when minimum two of the three populations shared this same marker.

Table 5 : Summary of QTL for black spot disease resistance in OW, FW and HW populations across multiple environments (years and locations) for male maps

Population	Method ^a	Location	Year	PT ^b	LG ^c	LOD ^a	Lod.π ^a	Lod.μ ^a	R ² (%) ^d	95% Bayes CI (in cM) ^e		Peak		
										Interval start	Interval end	Closest marker	Position (cM)	
OW	normal	Angers	2014	2.6	B3	3.16				10.1	4.07	13.5	Rh12GR_1265_568	9.34
					B3	8.72			23.6	13.5	20.2	Rh12GR_367_6432	1613	
					B3	6.79			17.9	20.2	28.3	Rh88_6620_1684	26.96	
			2017	2.6	B5	4.11			9.8	8.71	48.3	Rh88_31600_683	44.99	
					B3	4.65			10.2	11.4	42.6	Rh88_15720_207	20.19	
					B4	3.55			7.6	2	65.4	Rh12GR_14039_541	14.2	
			2018	2.6	B5	5.26			11.4	6.03	16.1	Rh12GR_80310_174	10.04	
					B3	3.17			8.8	9.44	34.3	RhMCRND_10522_106	19.52	
					B5	3.43			9.3	6.03	16.1	Rh12GR_80310_174	10.04	
			Mean	2.6	B3	11.18			22.1	15.46	22.49	Rh12GR_367_6432	16.33	
					B4	3.02			5.1	13.95	23.6	Rh88_49087_478	20.9	
B5	5.42					11	6.03	12.74	Rh12GR_30728_3735	8.71				
FW	2p	Angers	2018	2.15	B3	4.74	4.13	0.60	11.44	0	16.8	BFACT47	7.01	
					B5	2.91	2.74	0.17	0.89	10.4	49	RoGA2ox	29.34	
HW	normal	Angers	2012	2.32	B3	7.67			15.74	3.97	16.7	RB	9.67	
					B5	3.6			6.23	0	40.7	Rw14H21	25.13	
					B3	8.56			16.02	3.97	16.7	RB	9.67	
					B5	9.94			14.82	0	40.7	RMS034	32.18	
					B6	2.87			3.6	0	62.5	CTG623	8.28	
					B3	7.54			12.99	6.3	16.7	RB	9.67	
			2014	2.23	B5	6.36			9.66	0	40.7	RMS034	25.13	
					B6	3.12			4.22	0	20.88	CTG623	8.28	
					B3	15.23			21.43	6.3	11.5	RB	9.67	
			Mean	2.14	B5	12.14			16.76	29.34	40.69	RMS034	32.18	
					B6	3.92			4.63	0	20.88	CTG623	8.28	
B3	5.08					8.52	0	22.2	RoRGA/RoDELLA	3.97				
Bellegarde	2013	2.30	B3	5.08			8.52	0	22.2	RoRGA/RoDELLA	3.97			
			B5	9.86			19.6	0	29.3	Rw14H21	25.13			

Table 5 (continued)

Population	Method ^a	Location	Year	PT ^b	LG ^c	LOD ^a	Lod.π ^a	Lod.μ ^a	R ² (%) ^d	95% Bayes CI (in cM) ^e			Peak
										Interval start	Interval end	Closest marker	Position (cM)
HW	normal	Bellegarde	Mean	2.33	B3	5.23			8.41	6.3	16.66	RoMarQ	6.3
					B5	4.99			5.35	0	32.18	Rw14H21	25.13
					B6	2.6			4.15	0	20.88	CTG623	8.28
		Diémoz	2012	2.25	B3	3.72			7.19	0	28.7	BFACT47	11.5
					B5	4.21			9.14	0	29.3	Rw14H21	25.13
					B6	2.73			3.9	0	60.6	BFACT47	11.5
		2014	2.21	B3	2.73			3.9	0	60.6	BFACT47	11.5	
					B5	4.64			8.72	0	29.3	Rw14H21	25.13
					B6	2.96			4.17	0	38.3	CTG623	8.28
	Mean	2.08	B3	5.55			9.7	6.3	16.66	BFACT47	11.5		
				B5	8.43			12.78	0	32.18	Rw14H21	25.13	
				B6	8.19	0.77	7.42	15.66	0	11.5	RoSpindly	8.96	
	2p	Angers	2018	3.03	B3	8.19	0.77	7.42	15.66	0	11.5	RoSpindly	8.96
					B5	9.92	0.7	9.22	19.82	0	40.69	H24D11	30.08
					B6	3.13	0.64	2.48	2.35	0	62.5	CTG623	8.28
Bellegarde		2014	2.96	B3	12.55	9.62	2.95	13.69	0	9.67	RoRGA	3.97	
				B5	6.39	4.84	1.59	8.17	0	40.69	Rw14H21	25.13	
				B6	4.87	4.7	0.17	2.76	0	20.88	CTG623	8.28	
Diémoz	2013	3.06	B3	4	0.87	3.13	8.96	0	60.63	RoLf35	19.08		
			B5	5.98	0.16	5.82	11.93	0	72.49	H17C12	40.69		

^a Normal indicates a QTL mapping using a normal model with CIM analysis and 2p indicates a two-part model that studies consecutively a binary model and a normal one, so three LOD were calculated: LOD.π (penetrance, equivalent to binary model), LOD.μ (severity, equivalent to normal model for non-spike phenotypes) and LOD.π.μ (sum, complete model).

^b Permutation test giving the LOD threshold calculated using 1,000 permutations over which a QTL was significant.

^c Linkage group number with B for the male map.

^d Proportion of phenotypic variation explained by the QTL.

^e Confidence interval calculated with the 95% Bayesian credible interval.

Table 6: Summary of QTL for black spot disease resistance in OW, FW and HW populations across multiple environments (years and locations) for female maps

Population	Method ^a	Location	Year	PT ^b	LG ^c	LOD ^a	Lod.π ^a	Lod.μ ^a	R ² (%) ^d	95% Bayes CI (in cM) ^e		Peak	
										Interval Start	Interval End	Nearest marker	Position (cM)
OW	normal	Angers	2017	2.71	A1	4.12			6.53	42.89	60.3	Rh12GR_100474_250	54.3
FW	2p	Angers	2018	2.10	A1	2.6	2.59	0.01	4.06	15.92	44.87	Rw34L6	35
					A2	5.86	3.16	2.63	2.57	1.12	14.64	Rw59A12	1.12
					A4	4.18	4.09	0.01	3.61	32.53	44.28	Rw53O21	44.28
HW	normal	Angers	2012	2.04	A3	2.77			5.8	23.73	41.37	NP2007	33.71
			2014	2.09	A3	2.3			4.44	23.73	41.37	NP2007	33.71
		Bellegarde	2012	2.05	A5	2.51			5.39	0	36.04	H24D11	27.09
		Bellegarde	2013	1.95	A3	2.47			5.1	12.35	33.71	RoLf35H	23.73
		Diémoz	2014	2.08	A3	2.63			5.74	23.73	41.37	NP2007	33.71
						2.87			5.77	0	37.36	Rw20I17	12.6
		Diémoz	Mean	2.09	A3	2.17			4.4	23.73	41.37	NP2007	33.71
	2p	Bellegarde	2014	2.73	A3	3.02	2.15	0.91	5.91	12.35	51.19	NP2006	33.71

^a Normal indicates a QTL mapping using a normal model with CIM analysis and 2p indicates a two-part model that studies consecutively a binary model and a normal one, so three LOD were calculated: LOD.π (penetrance, equivalent to binary model), LOD.μ (severity, equivalent to normal model for non-spike phenotypes) and LOD.π.μ (sum, complete model).

^b Permutation test giving the LOD threshold calculated using 1,000 permutations over which a QTL was significant.

^c Linkage group number with B for the male map.

^d Proportion of phenotypic variation explained by the QTL.

^e Confidence interval calculated with the 95% Bayesian credible interval.

2.8.2. META-ANALYSIS

A meta-analysis of B3 and B5 QTLs was conducted. First, a consensus male map across all populations was constructed using 41 common markers (Table 4 and Supplementary table 1). In total, B3 comprised nine markers common across the OW, FW and HW male maps and B5 comprised eight markers common across all male maps (Table 4). LG3 and LG5 of the consensus map were represented in Figure 21. Secondly, QTLs of the original maps were projected on the chosen reference map (OW population map) by the map-projection function of Biomercator 4.2.2. In total, 20 QTLs of BSD resistance were projected on the reference LG3 and 17 QTLs on the reference LG5 (Figure 21). The meta-QTL optimum number was ensured by the AIC. Two meta-QTLs were identified on both LG3 and LG5 (represented by two different colors on the LGs of figure 2). For LG3, the first meta-QTL (named Meta_1_3) had a confidence interval (CI) of 2.72 cM and the second meta-QTL (named Meta_2_3) had a CI of 7.70 cM (Table 7 and Figure 21). The CI for the meta-QTL on LG5 (named Meta_1_5) was 3.95 cM and 7.52 cM for the second one (Meta_2_5). The average CI of the 20 individual QTLs found in B3 was 20.1 cM whereas for both predicted meta-QTLs together it was 10.42 cM. For B5, the individual QTL average CI was 26.62 cM and only 11.47 cM for both predicted meta-QTLs (Figure 21 and Table 7). The CI were approximately twice as small with the meta-analysis, which allowed us to be more precise in the location of QTLs linked to BSD resistance.

Table 7: Meta-QTL genomic position and gene mining

Meta_QTL ^a	Chr ^b	Genetic position (cM)		Interval position (bp) ^c		Number of genes in the interval		
		start	end	start	end	RGAs_auto ^d	RGAs_manual ^e	Total ^f
Meta_1_3	3	12.17	14.89	21605249	24567362	11	4	291
Meta_2_3	3	22.51	30.21	34220246	37772912	4	3	450
Meta_1_5	5	9.68	13.63	2414969	4219224	3	3	271
Meta_2_5	5	27.14	34.66	18827666	24889549	5	9	557

^a Meta-QTL names using all the QTLs found with the normal and 2p method results.

^b Chromosome numbers from *Rosa chinensis* genome (Hibrand Saint-Oyant et al. 2018).

^c Genomic positions of the meta-QTLs after projection on *Rosa chinensis* genome (Hibrand Saint-Oyant et al. 2018).

^d Genes coding for disease resistance proteins from the automatic annotation of the genome.

^e Resistance gene analogs with NB-domain found with protein sequence scan (manual annotation).

^f Total number of annotated genes under meta-QTL intervals with Goffinet et al. (2000) method.

When looking at the meta-QTL contributions, we can see that the first meta-QTL (Meta_1_5) was represented exclusively by OW population QTLs that showed large peaks at the beginning of the LG (except OWpop_RW_16B5 QTL that showed two distinct peaks separated by 30cM, see Supplementary figure 5) whereas the QTLs of HW and FW populations contributed to the second meta-QTL (Meta_2_5). Curiously, individual QTLs with a wide interval and double peaks separated by 10 to 30cM were detected on B5 (Supplementary figure 5 to Supplementary figure 8). The configuration suggests the presence of linked QTLs, requiring additional or alternative analytical approaches (Nakamichi et al. 2001; Kao and Zeng 2010). Accordingly, we attempted a two-dimensional analytical approach for normally distributed data but failed to separate more precisely the putatively linked QTLs in this region (data not shown).

2.8.3. GENE MINING FROM META-QTL INTERVALS AND NB-ENCODING GENES IN ROSA GENOME

All SNP markers were mapped to the *Rosa chinensis* reference genome of Hibrand-Saint Oyant et al. (2018) and were used to project the consensus genetic map onto the reference genome. The first meta-QTL on LG3, Meta_1_3, corresponds to an approximately 2.86 Mb genome region encompassing 291 annotated genes. The second one, Meta_2_3, represents a 3.5 Mb genome region comprising 450 annotated genes. On LG5, the first predicted meta-QTL, Meta_1_5, represents 1.80 Mb comprising 271 annotated genes, while the second meta-QTL, Meta_2_5, represents 6.06 Mb comprising 557 genes (Table 7). We explored genes associated with predicted meta-QTLs, focusing specifically on potential disease resistance genes. First, we annotated the predicted NB-encoding (Nucleotide Binding) genes in the rose genome, identifying 493 candidate R-genes (Supplementary table 2). Candidate NB-LRR genes were mapped onto the assembled pseudochromosomes of *R. chinensis* (Figure 22). NB-encoding genes mapped to every chromosome of the rose genome. Only nine genes mapped onto the unassembled scaffolds (rc00). Chromosome 1 contained the largest number of NB-encoding genes (106). Overall, the mean number of R-genes per chromosome was 69. However, NB-encoding genes were not homogeneously distributed across chromosomes, with clustering evident, especially on the distal end of chromosomes 1, 5 and 7 (Figure 22).

On LG3, 11 automatically annotated R-genes and four manually annotated NBS-encoding genes (*RC3G0136400*, *RC3G0136500*, *RC3G0136600*, *RC3G0145900*) co-localized with the first meta-QTL, Meta_1_3 (Table 7, Figure 22 and Supplementary table 2). The manual and the automated annotations identified nearly the same number of NBS-encoding genes in the interval of the second B3 meta-QTL (Meta_2_3) encompassing four RGAs for the automated annotation and three NB-coding genes (*RC3G0272000*, *RC3G0277900*, and *RC3G0280800*) for the manual annotation (see table 4). In addition to these NBS-encoding genes, we investigated co-localizations of defense response genes with the Meta-QTLs. Interestingly, a gene involved in response to fungal infection (*RC3G0142400*) is associated with the meta-QTL Meta_1_3. This gene encodes an EMSY-LIKE 1 protein that is known to contribute to RPP7-mediated and basal immunity against a specific strain Hiks1 of *Peronospora parasitica* in *Arabidopsis* (Tsuchiya and Eulgem 2011), possibly by regulating chromatin states. Two genes encoding for P450 cytochrome also co-localized with the first meta-QTL Meta_1_3. Cytochromes P450 monooxygenases (CYP) are known to be involved in plant defense mechanisms as they mediate secondary metabolism compounds of the xenobiotic detoxification pathway. For example, the CYP gene *CYP736B* in grapevine is involved in defense responses against *Xylella fastidiosa* and the wheat *CYP72A* is involved in the defense responses to *Fusarium graminearum* (Schuler and Werck-Reichhart 2003; Schuler et al. 2006). Similarly, in the Solanaceae, two cytochromes P450 participate in fungal pathogen resistance (Morant et al. 2003) and a *Phytophthora infestans*-induced cytochrome P450 is associated with quantitative resistance to late blight in potato (Trognitz et al. 2002). Moreover, a transcription factor from the WRKY family (*RC3G0261500*) upstream of the NBS-encoding gene (*RC3G0261700*) also co-localize with the Meta_2_3. WRKY transcription factors are known to play an important role in plant immunity and have been identified as major components of the resistance to fungi (Yang et al. 2009; Pandey and Somssich 2009; Lui et al. 2017). A pathogenesis-related (PR) thaumatin gene (*RC3G0264400*) was also found to co-localized with Meta_2_3. This gene codes for a PR-5 type protein (also called TLP for thaumatin-like protein) that has

been reported for its antifungal activity against various filamentous fungi (Chu and Ng 2003; Ho et al. 2007; Singh et al. 2013; Zhang et al. 2018).

For LG B5, 17 QTLs were mapped on the consensus LG and two meta-QTL clusters were identified. The same genes (*RC5G0059300*, *RC5G0061300*, and *RC5G0061600*) were annotated as *R*-genes with the expert annotation and the automatic one for Meta_1_5 (Table 7). However, in Meta_2_5 region, five genes were not found to be *NB*-encoding genes (*RC5G0227800*, *RC5G0228700*, *RC5G0231700*, *RC5G0232700*, *RC5G0245000*) with the expert annotation. Interestingly, Meta_2_5 is close to the region where the newly identified *Rdr4* gene giving resistance to all races of *D. rosae*, except the race 12, was located (Zurn et al. 2018). The meta-QTL, Meta_2_5, did not co-localize with the possible location of *Rdr4* but the marker peak of the QTL found in 2016 for OW population co-localized with it (Lopez Arias et al. 2020) as well as the marker peak of the QTL found in Diémoz 2013 scoring year of HW population. Moreover, a glucan synthase like gene (*RC5G0249400*; *GLS4* gene or also called *CalS8*), known to be involved in the formation of callose-containing papillae in response to pathogen attack (Dong 2005; Enns et al. 2005; Dong et al. 2008; Voigt and Somerville 2009; Enrique et al. 2011; Ellinger et al. 2013; Voigt 2014, 2016), co-localized with Meta_2_5. Finally, a cluster of ten genes coding for cytochrome P450 also co-localized with Meta_2_5.

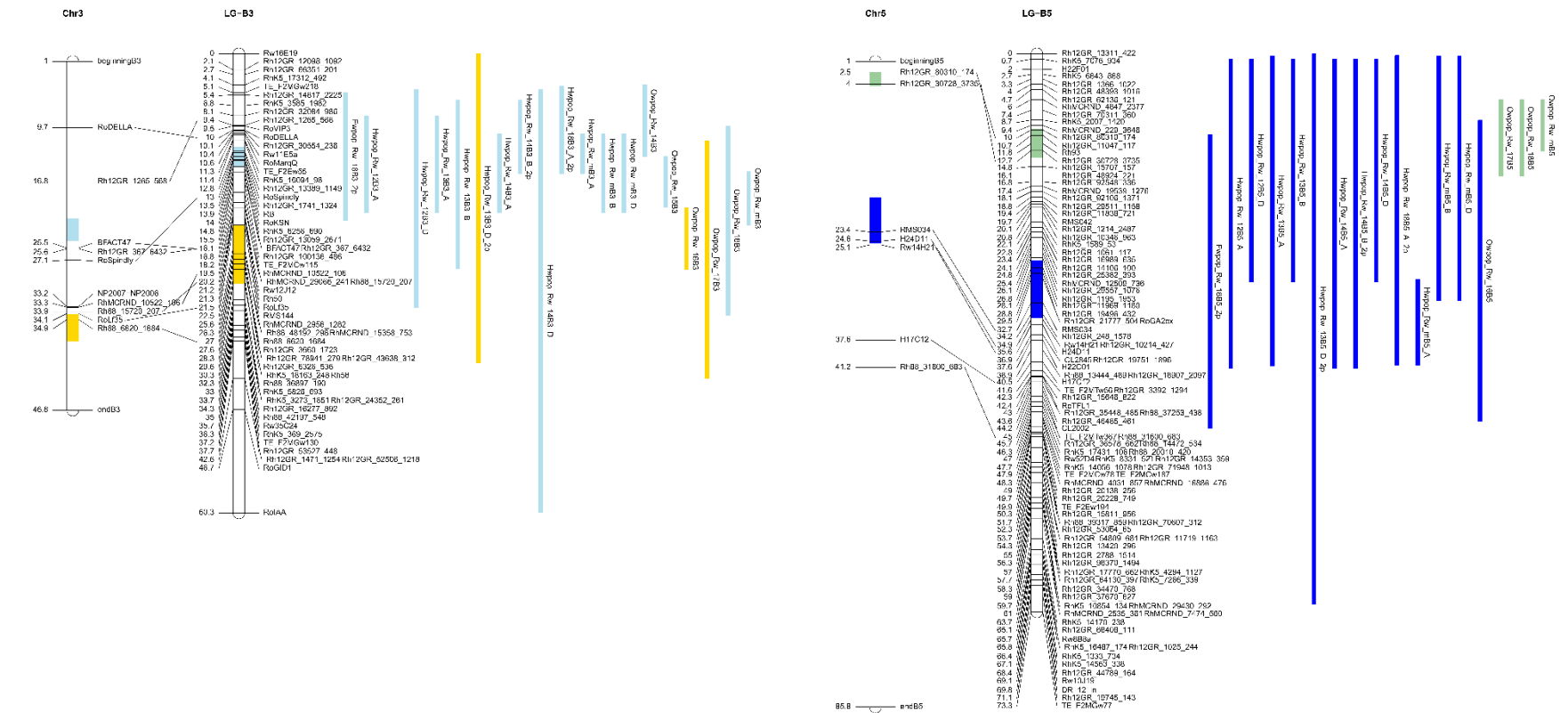


Figure 21: Representation of individual QTLs and meta-QTLs associated with black spot disease resistance for OW, FW and HW rose populations on the male consensus map

Names of markers are on the right and the genetic distances (in cM) on the left. The 19 and 17 QTLs detected on B3 and B5, respectively, on all three populations are projected onto a newly built consensus map. QTL names are coded as follows: PopName_map_YearLG_Location_method. 95% Bayesian confidence intervals are displayed with vertical bars where the length is proportional to the interval width, and the QTL peak is represented by a line. Meta-QTLs are represented in plain color on the LGs.

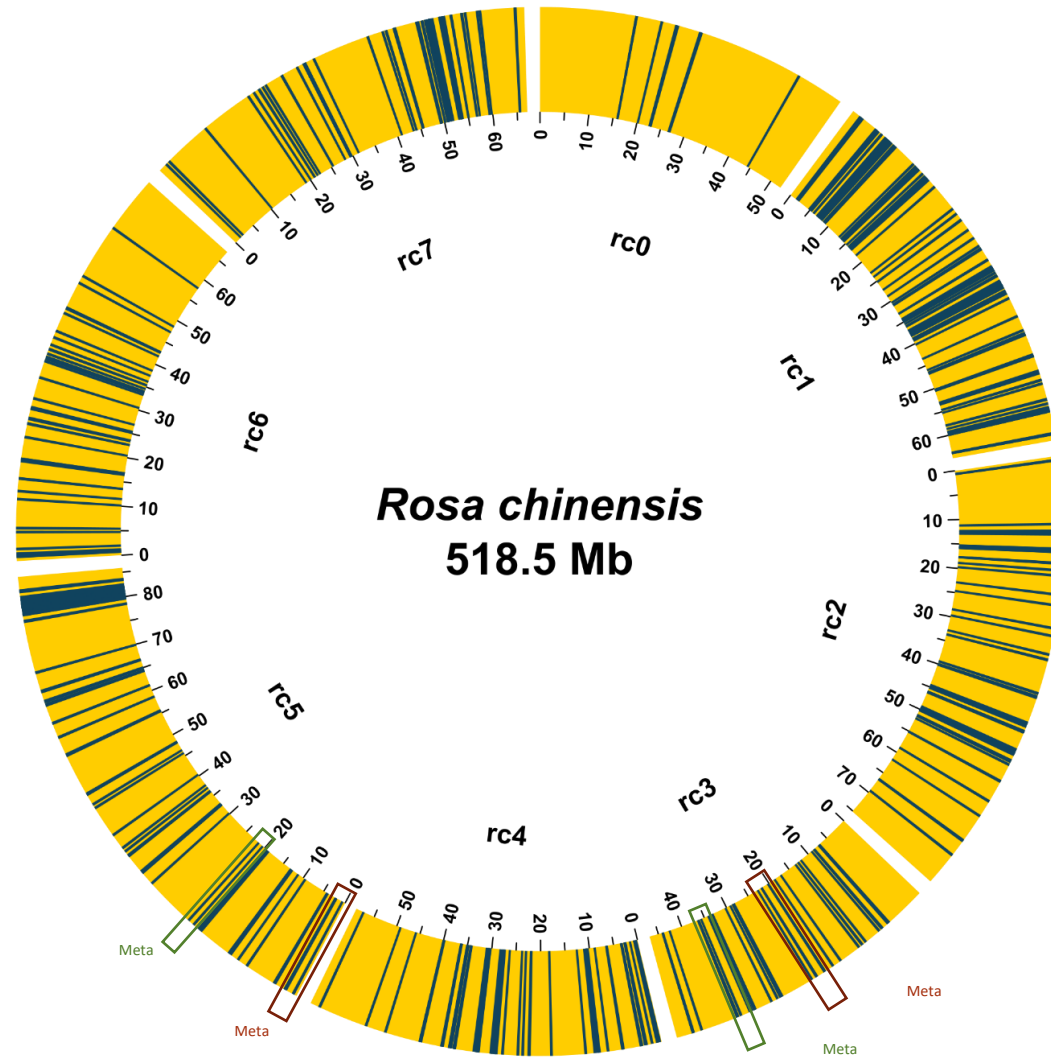


Figure 22: Candidate R-genes placed on the pseudo-chromosomes of *Rosa chinensis* assembly and meta-QTL position
Each pseudo-chromosome is represented by a yellow bar, with the positions of the R-genes indicated as blue lines.

2.9. DISCUSSION

2.9.1. IMPORTANCE OF ENVIRONMENTAL EFFECTS ON BSD SCORES

Since the expression of quantitative resistance can be affected by the environment, quantitative disease resistance (QDR) is best studied under field conditions with phenotypic measurements collected over different locations and years (Kelly and Vallejo 2006; Niks et al. 2015; Corwin and Kliebenstein 2017). In the current study, a difference of inoculum pressure or fungal strains between locations (Soufflet-Freslon et al. 2019) could explain why, for the HW population, the disease incidence was generally lower in Angers than in Bellegarde and Diémoz for a given year (Supplementary figure 2C). On the other hand, the effects of environmental conditions such as temperature, humidity or rainfall on BSD development in fields are well documented (Saunders 1966; Knight 1975; Gachomo 2005). In particular, (Saunders 1966) showed that climatic conditions play a critical role in the accumulation and spread of *D. rosae* inoculum. Heavy rainfalls and temperature above 14°C during trigger inoculum accumulation and spread of conidia from infected leaves (Saunders 1966). During the scoring period from 2012 to 2018, average precipitation in August and September of a given year was consistently lower in Angers and Bellegarde than in Diémoz. Similarly, for all populations, variation in disease impacts between years was observed, with low rainfall in August-September correlating with lower BSD scores. Conversely, in wetter locations or years (e.g., Diémoz in 2013 and Bellegarde in 2014), more individuals presented disease symptoms with BSD score distributions skewed to the left (with a lot of individuals presenting more symptoms than normal) like Diémoz. Specifically, the year 2013 (with a spike at score 4) could be explained by heavy rainfalls in August-September. Similarly, Bellegarde in 2014 presenting similar rainfall than Diémoz (97.25 mm) also showed a spike at score 4 and a distribution skewed to the left (Figure 20C).

2.9.2. NEW QTLs DETECTED ON PARENTAL GENETIC MAPS

Our main objective was to identify genomic regions conditioning resistance to *D. rosae*. We generated and analyzed phenotypic BSD data gathered across seven years, three locations, and three genetic populations.

The three populations used in this study were originated from interspecific crosses. The highly heterozygous nature of *Rosa* species is a complicating factor when it comes to genetic mapping. The pseudo-test cross mapping approach (Grattapaglia and Sederoff 1994; Kirst et al. 2004; Adam-Blondon et al. 2016), developed for highly heterozygous species, allows development of parental maps that are then combined into an integrated map. However, (Gartner et al. 2013) showed that, although integrating homologous chromosomes that have been rearranged can produce mathematically and statistically correct maps, they do not necessarily reflect the biological reality of chromosomal rearrangements and meiotic recombination that had happened during the outbred cross. Therefore, even if the gene position is highly conserved between species, genome rearrangements may exist in interspecific crosses. This can lead to significant changes in collinearity between parental genomes (Lespinasse et al. 2000; Gartner et al. 2013). For example, recently released, independently generated rose genome assemblies suggest chromosome rearrangements (Raymond et al. 2018; Hibrand-Saint Oyant et al. 2018; Smulders et al. 2019). In the current study, we observed rearrangements between the parents OB and RW, especially on chromosome 3. For these reasons, we decided to apply pseudo-test cross mapping approach without

integrating the parental maps at the end. QTL analyses were then carried out using two different methods of detection on separated parental maps.

Overall, many QTLs for resistance to BSD were detected in this study. Consistent with natural variation in inoculum pressure, pathogen race, and environmental conditions encountered in field studies over several years, some QTLs identified in this study were only found in a given population, location or year. For example, BSD resistance QTLs on B6 were found specifically on the male map of the HW population across all environments (Table 5). Since all three populations share the RW male parent, identification of the B6 QTLs only in the HW population for several years and locations suggests that expression of these QTLs also depends on genetic background that is crossed with *R. wichurana*. Moreover, the marker peak CTG623 of B6 QTL was found to co-localize with the possible location of *Rdr3* (Zurn et al. 2020).

Importantly, other QTLs were more consistently detected across populations, locations, and years, suggesting a more robust impact on disease resistance. First, a QTL on LG A1 was mapped in two populations (FW and OW) (Supplementary figure 10), originating from the female parents TF and OB. This QTL co-localizes with a cluster of NB-LRR genes, including the previously reported BSD resistance gene *Rdr1* (Lopez Arias et al. 2020; Hattendorf et al. 2004; Terefe-Ayana et al. 2011). This observation suggests the intriguing possibility that the underlying genetic basis of the A1 QTL might be a canonical NB-LRR gene, in whole or in part. In addition, regarding the difference of BSD score between both female parents (with OB very susceptible to BSD and TF resistant to it), we can hypothesize that an allelic variation in the causal gene could originate a difference in the observed phenotype. Then, a QTL conditioning BSD resistance on LG B4 was identified for two different environments and two different populations: the OW population in Angers in 2017 (male map) and the HW population in Diémoz in 2014 (H190 female map; Table 5 and Table 6). Resistance conditioned by this QTL may be environment- and pathogen race-dependent. Finally, QTLs on LGs B3 and B5 were found for all populations, years and locations in the male resistant parent RW but also in the H190 female map (Table 5 and Table 6). At the moment, the apparent mapping of QTLs from these two parents, with a clear difference in BSD resistance, on the same linkage groups could be explained by one of these two hypothesis: (1) RW and H190 QTLs co-localized meaning that both parents shared the same resistance source and the difference observed in the phenotype could be due to an allelic variation between them or (2) the QTLs originated from both parents do not co-localize meaning that the resistance source is different. Unfortunately, the maps quality did not allow us to determine precisely if the male and female QTLs on linkage group 3 and 5 co-localized (data not shown). However, consistent expression of QTLs on linkage groups 3 and 5 across environments and genetic backgrounds suggest that they are stable enough to be useful in the genetic improvement of rose resistance to *D. rosae*. In the end, we can see with this study that separated maps allowed us to identify two main QTLs on B3 and B5 with large effect on the resistance to BSD as well as small effect QTLs on parents that were considered tolerant or susceptible.

2.9.3. QTLs CHARACTERIZATION AND TWO-PART MODEL RESULT INTERPRETATION

Substantial peaks in the distribution of genotype mean values are fairly common and represent one of the principal departure from the assumption of normality required to perform QTL analysis (Lander and Botstein 1989). When working with disease resistance, individuals may show high resistance so a peak at 0 can be observed. In this case, the standard QTL detection approach behave poorly and can detect spurious QTLs in regions with low genetic information (Broman 2003; Feenstra and Skovgaard 2004). To

deal with this problem, Broman proposed in 2003 a “Two-part model” that combines a binary analysis (absence vs presence) and a normal analysis for individuals with non-null phenotype. The trait is divided in two components: penetrance and severity (Broman 2003; Broman and Sen 2009). That way, more information about the part of trait that is affected by the QTL can be obtained. This model has so far been applied for reproductive barriers with male sterility in house mouse and ear tip masculinization in maize (White et al. 2011, 2012; Holland and Coles 2011). In our study, we adapted when necessary the model used to perform the QTL analyses, so data distributions with a substantial spike were analyzed with the two-part model. When both the penetrance and the severity of the trait were affected by the QTLs, it meant that these positions have an effect on the appearance of the BSD symptoms or penetrance (when treated as binomial; with no symptoms vs symptoms) as well as the severity of symptoms (BSD score > 0).

The 2p model provided interesting information for the B3 and B5 QTLs found on the male parent maps. For Angers 2018 data from the HW and FW populations, both the penetrance and the severity of the trait were affected by the B3 QTLs, meaning that these regions impact both appearance of BSD symptoms and symptom severity. Interestingly, for the B5 QTLs in both populations, only penetrance (absence/presence of the symptoms) was impacted. For the resistant female parent TF, the A2 QTL impacts both the penetrance and the severity of the trait whereas the A1 and A4 QTLs impact only penetrance.

2.9.4. META-ANALYSIS AND GENE MINING

With recent progress in mapping algorithms and models that can handle a wide diversity of phenotypic data, quantitative trait mapping has become the first step in the dissection of the genetic factors underlying complex and quantitative traits such as disease resistance (Zhu and Zhao 2007; Rawat 2016). That way, many studies mapped quantitative disease resistance loci of crop plants over the past decades (Lacape et al. 2010; Qi et al. 2011; Holland and Coles 2011; Yadava et al. 2012; Hamon et al. 2013; Semagn et al. 2013; Said et al. 2013; Pilet-Nayel et al. 2017). Cloning and functional validation of causal gene(s) or quantitative trait nucleotide polymorphism underlying QTLs has been accomplished in maize (Yang et al. 2017) but remains a long and difficult process. Indeed, the biological bases of QDR in the defense responses are still unknown, so several reviews proposed hypotheses of mechanisms underlying Quantitative resistance loci (QRL) (Poland et al. 2009; St Clair 2010; Roux et al. 2014; Corwin and Kliebenstein 2017).

First, one crucial step facilitating cloning and validation of causal genes is the QRL position refinement. Towards this goal, in this study, we narrow the confidence interval of the most phenotypically stable and reproducible QTLs on a common consensus map and perform a meta-analysis of the corresponding LGs, B3 and B5. Two meta-QTL clusters were identified for both LG B3 and B5 (Figure 21 and Table 7). This method allowed us to refine the genomic regions linked to BSD resistance and to study the influence of genetic background and environment on QRL detection (Table 7). However, combination of QTL mapping results across several studies that differ with marker density, linkage, sample size, etc. is still a challenge. Even though Goffinet and Gerber’s method aims to resolve the number of QTL and their location using a model selection, questions on the real number of QTL subsist. On one hand, for LG B3, both clusters found during the meta-analysis can be either two real QTLs or an artefact due to the possible rearrangement that happened in this region. For instance, not far from the meta-QTL Meta_1_3 on B3, a large rearrangement was described between the two alleles in OB (corresponding to recurrent blooming locus and the

rearrangement of *copia*-like retrotransposon, Hibrand-Saint Oyant et al. 2018). On the other hand, on LG B5, uncertainty remains on whether or not the QTLs located within the same genomic region are the same QTLs. Specially, because individual QTLs present double LOD peaks characteristic of linked QTLs. Increasing the sample size of the populations in future experiments may provide a better power to separate closely linked QTLs on LG B5. Therefore, at this moment, only hypotheses can be made. For example: both clusters being completely new QTLs different from the newly identified *Rdr4* resistance gene (Zurn et al. 2018) or the first meta-QTL Meta_1_5 being a new QTL and the Meta_2_5 being *Rdr4* locus that did not co-localize with it due to map imprecisions.

Second, elucidating the molecular mechanisms underlying QTLs can assist breeders in developing cultivars with more durable levels of resistance by “making more informed and prudent decisions” (Kelly and Vallejo 2006). Indeed, it has been shown that QTLs can co-localize with major R-genes as well as defense response genes (Poland et al. 2009; St Clair 2010; Roux et al. 2014; Corwin and Kliebenstein 2017). In this study, we used the meta-QTL physical positions to inform gene mining efforts based on whole genome sequence data (Hibrand-Saint Oyant et al. 2018), specifically searching for associations between defined genetic regions and NBS-LRR and defense response genes. However, the resistance loci originated from RW and the genomic differences between both genotypes could impact our efforts. Nevertheless, the use of the haploid OB genome sequence to identify candidate genes underlying BSD resistance meta-QTLs has promise. Genes involved in pathogen recognition, signal transduction, transcription modulation and detoxification pathways were identified in the chromosomal regions linked to BSD resistance. Interestingly, Bleichert and Debener in 2005 classified the interaction between *D. rosae* and the wild type *R. wichurana* as type 7 meaning that the fungus germinates and penetrates the cuticle but is not capable of producing hyphal structures on the host. Indeed, cell-wall appositions were observed on one to three cells resulting in visible necrotic areas akin to hypersensitivity reactions (HR). Genes involved in the activation of cell death (WRKY, PR-proteins, ROS pathway, etc.) as well as in detoxification pathways (with cytochrome P450) seem to be good candidates.

Thus, the possibility of RGAs being responsible for the observed resistance on RW is also not to be ruled out as they are in the first line of biotic stress responses like the one observed for RW by Bleichert and Debener (2005).

In this study, confidence intervals of chromosomal regions conditioning quantitative resistance to *D. rosae* were reduced thanks to the meta-analysis approach. Unfortunately, at this stage of the study, no consistent markers linked to BSD resistance have been identified as the CI regions and peaks of detected QTLs vary slightly over the years and locations. A refinement of the QTL location of stable QTLs on B3 and B5 is needed prior to marker detection for marker assisted breeding and/or causal gene identification. Using the genomic resources now available such as the rose genome and the data provided in this article such as the manually annotated RGAs, the first hypothesis on the genetic basis of QDR in Rose-*D. rosae* pathosystem were made. However, at this stage, only a large number of candidate genes were identified. Further evidence supporting their involvement in the observed resistance of RW genotype need to be provided so the potential candidate genes can be narrowed down to a number that can allow experimental validation through qPCR expression profiles and/or gene inactivation. Finally, the large number of QTL detected in this study, together with the fact that some QTL did not co-localize with known *Rdr* genes,

suggests that the number of QTL could be even larger than what has been detected with these limited populations, offering the promise of wide spectrum of resistance sources to rose breeder and scientists.

2.10. CONCLUSION

In this study, we report the first discovery and genetic characterization of quantitative resistance to BSD. We examined the contributions of a common resistant parent over several years, locations, and genetic populations. We confirm the presence of a strong effect QTLs on LG B3 and B5 from the genotype *R. wichurana*, consistent with complementary on-going research (Yan et al. 2019). The LG B3 and LG B5 QTLs are stable over years and effective against a wide range of *D. rosae* races and across various environments (Lopez Arias et al. 2020; Yan et al. 2019; Soufflet-Freslon et al. 2019). We demonstrate a method to leverage meta-analyses to reduce CI of single QTLs. This method was specifically chosen for its robustness to non-full independency and it allowed us to integrate data from three different populations of perennial rose bushes. BSD data collected over seven years and multiple locations, provided validation of QTLs on B3 and B5, demonstrating their stability and robustness. Genes underlying these QTLs are potential breeding targets for the development of BSD resistant rose cultivars.

3. ADDITIONAL RESULTS

3.1. DISEASE EVOLUTION OVER YEARS: ENVIRONMENTAL EFFECTS

In this part, I would like to further discuss the implication of the environment in the disease evolution observed for all three populations. Two aspects will be addressed here. First, I would like to introduce a reflection on the influence of the rainfall in the symptom distribution shifts observed over the years. Then, I would like to mention the particular case of a resistant population (FW).

The disease incidence was demonstrated to be population-dependent in the article ([section 2.2](#)) with FW population presenting the lowest disease incidence. However, clear differences between years and locations were observed as well. In general, wetter years/locations produced higher disease scores (2014 or all the years in Diémoz) than dryer years (2014 and 2016, for example). *D. rosae* is polycyclic as it can produce several infectious cycles in one year (Saunders 1966). The heavy rains in early spring triggers the infection and sets a minimum of inoculum that will increase each time that a heavy rain happens as it allows this water-born pathogen to disseminate thanks to rain drops and infect new leaves, which leads to an exponential increase in the incidence of infected leaves (Supplementary figure 11). Saunders stated that the weather in August was favorable for spore dissemination as the rainfall was high just before the first marked increase of infection was observed in September. However, the difference of percentage of infection between 1963 and 1964 in September (less than 10% and 20% of infection, respectively) could also be explained by a higher rainfall observed in May-June in 1964 with 60mm for both months than in 1963 with only 20mm in May and 40mm in June (Supplementary figure 11).

Considering that when a rose bush is infected, the ultimate stage of the infection is the premature defoliation, the build-up not only starts in August but begins with the first leaves that fall due to the infection. In susceptible cases, the fallen leaves exhibit spots with mature lesions that bear newly produced conidia and that will contribute to increase the inoculum from which the next infection will happen. In that case, the more rain there is, the more dispersion there will be and therefore, more areas can be infected and will ultimately fall to increase even more the inoculum for the next cycles. For instance, high rainfall

at the beginning of the pathogen spread (in May-June 1964 for Saunder's study) will lead to a larger inoculum and, therefore, stronger visible infection. In light of these observations, I would like to illustrate and complete the discussion on the influence of the rainfall in the score distribution that was mentioned in the article by considering two aspects in the rainfall: the average rainfall and cumulative rainfall between the first infection and the scoring month. The average and cumulative rainfall from April (beginning of the infection according to Saunders) to September (when the scoring was done) for each location over the scored years is presented in Figure 23.

Diémoz had a much higher average rainfall and cumulative rainfall than Bellegarde and Angers for 2012, 2013 and 2014 which correspond to the three years of scoring in the framework of the Rosa Fortissima project. This is consistent with a high average BSD score observed in the HW population for all years and the absence of completely resistant phenotypes scored at this location (see Supplementary figure 16, only one genotype, HW559, was resistant in 2012). Interestingly, Angers had a low average rainfall in 2013 compared to the other years but a high cumulative rainfall, and this year was characterized by a strong infection exhibiting a score distribution with a lot of individuals with high scores (). Looking in more detail, Angers had a particularly dry August in that year with only 8.6mm of rain which decreased the average value but had a really high rainfall in May (90mm) which increased the cumulative value. The strong infection that year can, therefore, be explained by these heavy rainfalls in May. Moreover, some contradictory results can be observed for Bellegarde. A low average and cumulative rainfall was associated with a strong infection and a phenotypic distribution with a lot of individuals exhibiting high scores in 2013 when one would think that a weaker infection would be associated with low rainfall (Figure 23 and Supplementary figure 15). Again looking at the detailed rainfall for each month in 2013, March had an extremely high rainfall (166.6mm) which could have triggered an important spread of the fungus from the beginning leading to a significant inoculum by April. For OW population, we can see that more individuals were scored 0 and 1 in 2017 and it corresponds to a low average and cumulative rainfall (Supplementary figure 12). Conversely, 2018 was characterized by a high average and cumulative rainfall and in that year, a lot more individuals scored 3 or 4 than in 2017 (Supplementary figure 12). In light of these observations, we can say that for populations with only one resistant parent, the cumulative rainfall (or more globally the climate, including temperature, rain and hygrometry) during the infectious period had an important effect on the disease final scores and therefore, on the overall symptoms distribution. However, we have to consider the fact that each year and location is different and that the beginning of the infection might happen before April like in March for Bellegarde in 2013 so one should probably consider to use the cumulative rain over the period from March to the scoring period instead of using April as the beginning of the infection like recommended by Saunders.

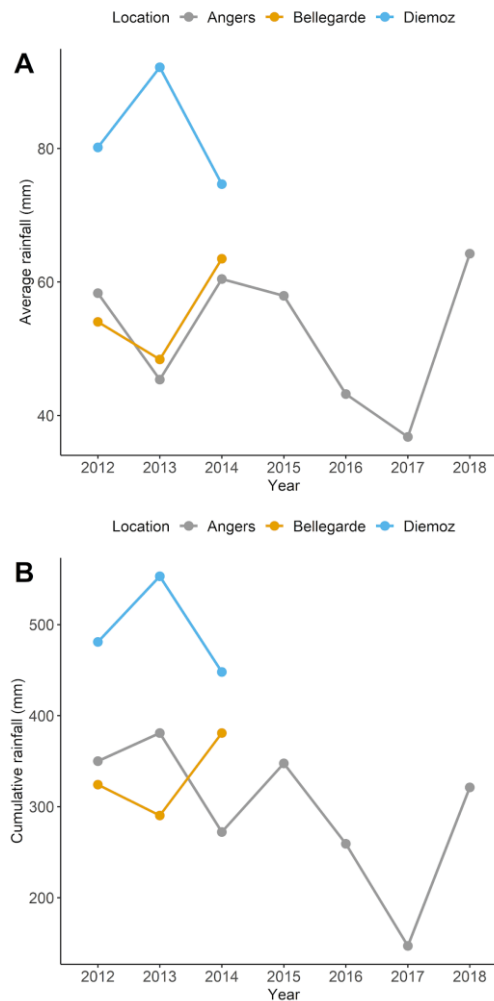


Figure 23: Overall rainfall during April-September (A) and cumulative rainfall (B) from April to September for the scoring period of three locations (in mm)

On the other hand, for the resistant population FW, only two scoring years were available but an interesting observation can be made that allows me to introduce another aspect in the study of natural infection in fields. The average and cumulative rainfall in 2014 and 2018 in Angers were similar. However, an important difference in the disease distribution was observed with more than 80% of the hybrids showing no symptoms at all in 2018. Individuals that were scored 1 to 2 in 2014 were found completely resistant (scored 0) in 2018 (see Supplementary figure 13). For perennial plants like rose bushes, it is important to study the disease evolution over several years as they are planted in a garden and kept in the same place for several years. Indeed, considering an epidemic over a period of many growing seasons is particularly important for perennial plants and for annual crops that are grown in monoculture. In most cases, the inoculum produced within the first year will be carried over to the next and the next and so on leading to a build-up of inoculum after several years for this type of plant as the pathogen overwinters in fallen leaves. For rose-*D. Rosae* pathosystem, this build-up year after year is possible as the fungus has the capacity to overwinter in dead leaves and rose canes. However, in the case of many resistant phenotypes with possibly different genes participating in the resistance, the inoculum produced during one year can

be greatly reduced (or selected) as the pathogen can complete a cycle and produce spores in only a few individuals. It has been observed that a combination of resistant QTLs with strong effect can lead to complete resistance like observed in FW population (Niks et al. 2015; Pilet-Nayel et al. 2017). Moreover, it has been demonstrated that *D. rosae* spread and survival is particularly affected by environmental conditions (Saunders 1966; Knight 1975; Gachomo 2005). Then, we can imagine that unfavorable conditions like a dry summer can greatly affect the survival of some *D. rosae* strains present in the fields and therefore select some strains or even reduce the pressure for the next year. In our case, 2017 was a very dry year with very low average (36.8mm) and cumulative (147.2mm) rainfall compared to 2018 (64.24mm and 321.2mm, respectively). Thus, a dry year combined with a resistant population for which only some individuals can produce new spores could explain that the following year (2018) exhibited less disease incidence even if the environmental conditions were favorable for pathogen development (Figure 23). Finally, it is interesting to notice that even after four years, no virulent strains have been able to break the resistance brought by both parents which might be related to the polygenic nature of the resistance studied here. Indeed, three QTLs with small effects were detected on the female map in 2018 and two QTLs were detected on the male map the same year. The combination of resistance QTLs (with strong and small effects) from the male and the female parents can make it harder for the pathogen to adapt (Parlevliet 1989; Niks et al. 2015; Pilet-Nayel et al. 2017). Perhaps, the fungi can take more time to circumvent the resistance. It would be interesting to study the field population of the fungi (diversity) in order to follow the evolution, selection and fitness adaptation throughout the years. QTL analysis for non-normal phenotypic distribution

Interval mapping methods often assume that the residual variation in the phenotypes follows a normal distribution. However, some phenotypes can show a clear departure from normality. It is possible to transform a phenotype to obtain a distribution closer to normality and interval mapping applied to such phenotypes performs reasonably well. Yet, there are alternatives when one cannot get close to normality even applying the appropriate transformation. Nonparametric interval mapping, interval mapping for binary traits or a more specific method using a two-part model perform well and can give more insights on the part of the trait linked to a QTL (Broman and Sen 2009). QTL mapping for non-normal phenotypes using a two-part model was used for the first time in rose and was published in our article (section 2.2). Indeed, as explained in 2.3.3.1, scoring data for 2014 and 2018 of FW population as well as for Angers in 2018, Bellegarde in 2014 and Diémoz in 2013 of HW population exhibited a particular distribution and did not follow the normality of residuals. These scoring data were therefore analyzed with a two-part model. Firstly, as the data distribution was very different with either peaks at score 0 or score 4, the interpretation for the results of the two-part model needs to be further explained. Secondly, I would like to present additional analyses using an interval mapping model for binary traits presented by Broman and Sen (2009).

3.1.1. SUPPLEMENTARY EXPLANATION FOR TWO-PART MODEL RESULTS

As previously presented, some scoring years of the three populations exhibited non-normal phenotypes with either peaks at 0 or 4. Interval mapping assuming normality could be applied but when the peak is far from the rest of the phenotypes and holds a large number of individuals, the maximum likelihood under normal model assumption can yield spurious LOD peaks in regions of low genotype information. Therefore, this type of distribution fits well the two-part model prerequisites presented by

Broman (2003). However, for HW population, scoring data for Bellegarde 2014 and Diémoz 2013 had a peak at score 4 which leads us to a rather different interpretation than the ones with a peak at score 0 like for this population in Angers 2018 or for FW population in 2014 and 2018 (Figure 20 from the article). It is important to understand how the model works to be able to interpret the results. As a reminder, two-part model (2p) combines a two-step analysis by denoting two types of phenotype: the “binary phenotype” and the “quantitative phenotype”. According to Broman (2003), assuming the spike in the distribution is at 0, an individual with a QTL genotype g has a probability π_g of presenting a phenotype different from zero (binary phenotype analysis) and if its phenotype is among the nonzero ones, the value is supposed to follow a normal distribution with a mean μ_g and standard deviation σ (conditional analysis of the quantitative trait). This model can be generalized to a spike at the largest phenotype like for the *Listeria* data used to illustrate the 2p model in Broman 2003 (see Figure 24 extracted from the publication). The extreme and maximum value was at 264 hours. The analysis can be performed with `*scanone*` function of the R/qtl package using `*model = “2part”*` and spikes for the smallest phenotype or the largest phenotype can be analyzed by setting the argument `*upper=FALSE*` or `*upper=TRUE*` respectively. In our case, scoring data of 2014 and 2018 for FW population and 2018 for HW population in Angers, exhibiting a peak at 0, were analyzed with `*upper=FALSE*`. The ones of Bellegarde 2014 and Diémoz 2013 for HW population, exhibiting a peak at 4, were analyzed with `*upper=TRUE*` (Table 8).

First, in the case of spike (maximal peak) at the smallest phenotype (here score 0), the 2p model performs an analysis for the binary trait (no symptoms vs symptoms) and a conditional analysis of the quantitative trait (for the phenotypes that showed symptoms, i.e. strictly above 0). Three LOD scores are, then, calculated as well as three corresponding LOD thresholds using data permutations:

- $\text{LOD}(\pi)$ to assess the evidence for QTL specifically influencing the chance that a hybrid shows symptoms, i.e. influencing the penetrance of the disease;
- $\text{LOD}(\mu)$ to assess the evidence for a QTL that influences the average phenotype when they show symptoms, i.e. influencing the severity of the disease;
- $\text{LOD}(\pi, \mu)$ is the LOD score of the 2p model that corresponds to the sum of $\text{LOD}(\pi)$ and $\text{LOD}(\mu)$.

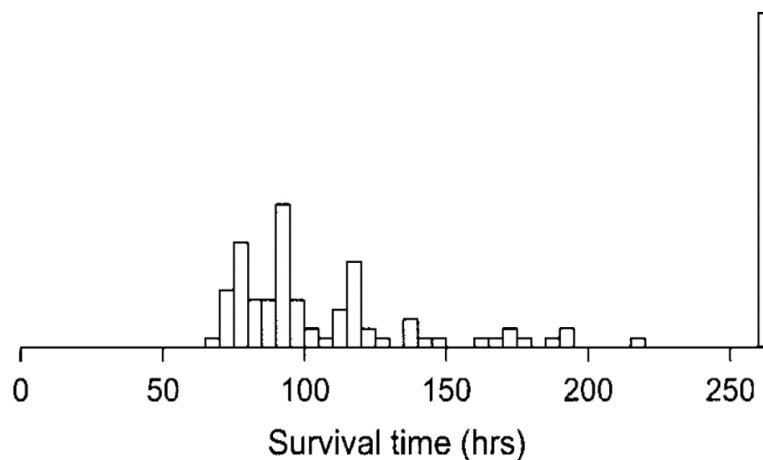


Figure 24: Histogram of survival time, following infection with *Listeria monocytogenes*, of 116 intercross mice. Approximately 30% of the mice recovered from the infection and survived to the end of the experiment (264 hr). Figure extracted from Broman 2003

Table 8: Summary of the analyses performed with a two-part model for non-normal phenotypic distributions

	Angers		Bellegarde*		Diémoz*	
	Phenotypic distribution (parameter for 2p model)	LG detected with a two-part analysis	Phenotypic distribution (parameter for 2p model)	LG detected with a two-part analysis	Phenotypic distribution (parameter for 2p model)	LG detected with a two-part analysis
2013	Normal	NA	Normal	NA	HW: peak at score 4 (upper=TRUE)	B3/B5
2014	FW: peak at score 0 (upper=FALSE)	no QTL	HW: peak at score 4 (upper=TRUE)	B3/B5/B6 & A3	Normal	NA
2018	FW: peak at score 0 (upper=FALSE)	B3/B5 & A1/A2/A4	NA	NA	NA	NA
	HW: peak at score 4 (upper=TRUE)	B3/B5/B6	NA	NA	NA	NA

For each population and for each year, the parameter used to decide if the peak was the smallest (upper=FALSE) or the largest (upper=TRUE) phenotype is mentioned in parenthesis; QTLs detected with the 2p model are summarized and the ones found with the normal model were omitted in this section (they can be found in Figure 21).

*Only HW population was scored in Bellegarde and Diémoz in 2013 and 2014.

If we consider the peak at 0 as the spike of the analysis and the overall LOD score ($LOD(\pi, \mu)$), no QTL was detected for FW population in 2014, two QTLs were found on B3 and B5 for FW in 2018 and three QTLs on B3, B5 and B6 for HW in 2018 for the male map (Table 5). The QTLs on B3 influence both penetrance and severity of the disease whereas the QTLs on B5 influence specifically the penetrance, i.e. the absence or presence of symptoms. An interpretation of these results was proposed in the discussion of the article (section 2.9). Additionally, one can only consider the LOD scores separately and in this case, the locus at 60.9cM on linkage group B2 seems to affect the severity of the disease given that an individual showed black spot symptoms (large $LOD(\mu)$ in green exceeding the corresponding threshold and low $LOD(\pi)$ in blue, see supplementary figure 9 of the article). Similarly, two QTLs on A1 and A4 affecting specifically the penetrance of the disease as well as one QTL on A2 affecting both apparition and severity of symptoms were detected on the female map of FW in 2018 (see supplementary figure 9 of the article).

Second, in the case of spike at the largest phenotype (here score 4), the 2p model performs an analysis for the binary trait too but this time, when the data is treated as binary, it is $BSD < 4$ vs $BSD \geq 4$ (Supplementary figure 6B and Supplementary figure 8B-8C). A hybrid was scored 4 when $75 < x \leq 100\%$ of leaflets were infected and the defoliation started (Supplementary figure 1). With the binary model, we can say that we are studying the effect of a QTL on premature defoliation more specifically. The conditional analysis of the quantitative trait, here, uses the phenotypes that showed no symptoms and the ones with symptoms but that had not defoliated. We can define the three LOD scores as follows:

- $LOD(\pi)$ to assess the evidence for QTL specifically influencing the defoliation when a hybrid is affected, i.e. influencing the penetrance of the trait;
- $LOD(\mu)$ to assess the evidence for a QTL that influences the average phenotype when they show no defoliation yet, i.e. influencing the severity of the disease;
- $LOD(\pi, \mu)$ is the LOD score of the 2p model that corresponds to the sum of $LOD(\pi)$ and $LOD(\mu)$.

With these assumptions in mind, we can imagine that QTLs only affecting specifically the penetrance, like B5 and B6 on the male map and A3 on the female map for Bellegarde in 2014, have an effect on the appearance of defoliation when the BSD scores are treated as binary (BSD<4 vs 4) and indicate that RW and H190 alleles at these positions increase the probability that a hybrid will not start defoliating. In addition, the QTL on B3 for Bellegarde 2014 also affects the severity of the symptoms, among those hybrids that did not defoliate (BSD<4). Similarly, both QTLs on B3 and B5 on the HW male map only affect the penetrance and therefore the appearance of the defoliation. Premature defoliation is an important aspect for the disease assessment in rose-*Diplocarpon rosae* pathosystem and seems to occur at the last step of the primal fungal infection (Gachomo 2005). Premature defoliation is then considered to be the result of an excessive infection where the fungus, feeding on the leaves' nutrients, gut it during its necrotrophic stage and is particularly important for susceptible genotypes (Gachomo 2005; Gachomo and Kotchoni 2007). Then, it is easy to understand that QTLs on B5, which were found to affect the appearance of symptoms for Angers 2018 scoring year, would also affect indirectly the occurrence of premature defoliation as, if the pathogen is not arrested at the entrance, the leaves would show symptoms that can probably lead to defoliation in the end. Similarly, QTLs on B3, which were found to affect the appearance of symptoms as well as their severity for Angers 2018 scoring year, still affect the severity of symptoms and indirectly the final point of the infection that is defoliation.

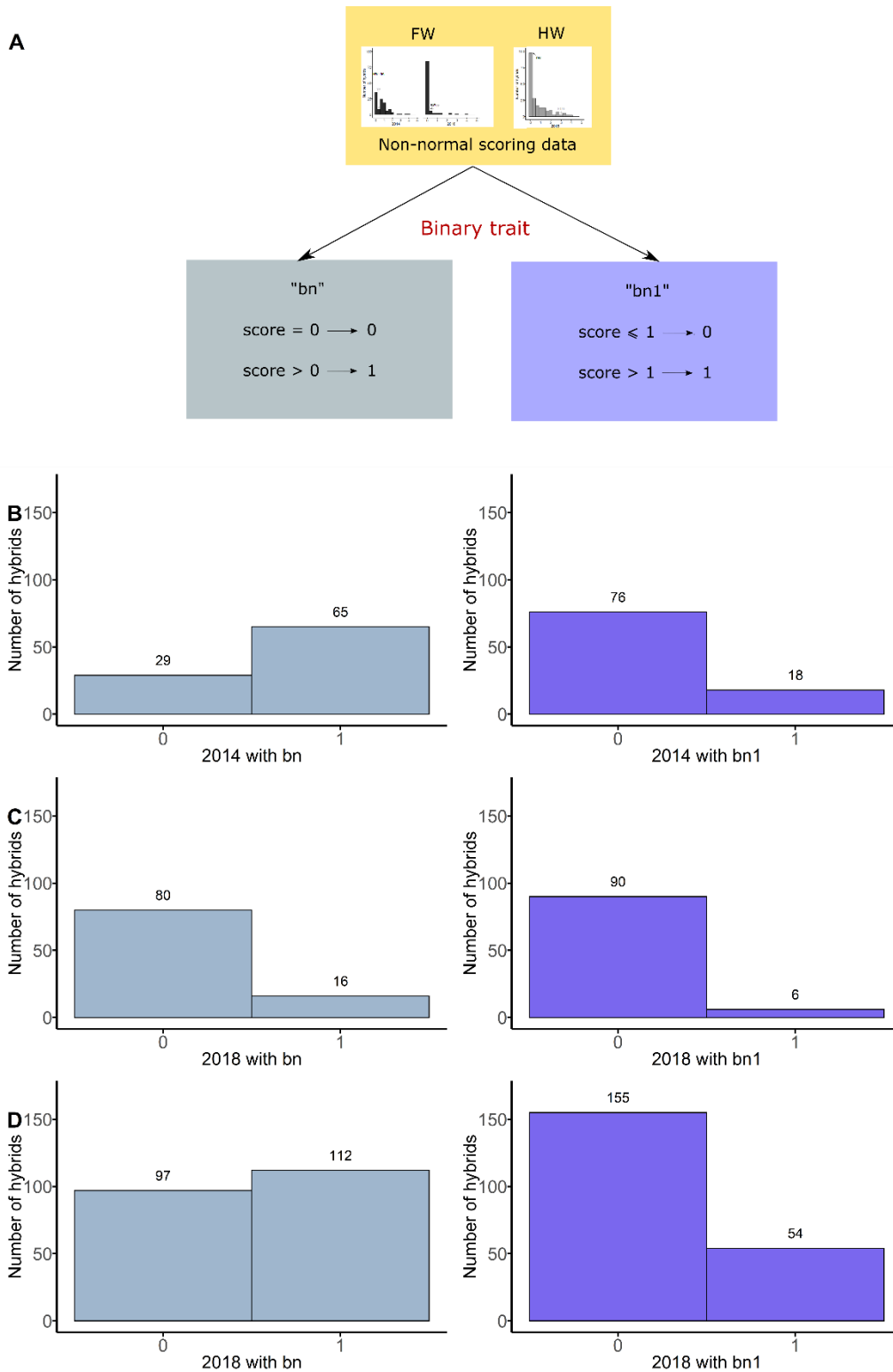


Figure 25: Scoring data transformation to two types of binary trait (bn and bn1) and histograms of number of hybrids of FW and HW populations for three non-normal data after transformation to binary trait

A: Summary of the binary transformation for the spike-like data with a peak at 0; **B:** 2014 scoring year for FW population, **C:** 2018 scoring year for FW population, **D:** 2018 scoring year for HW population

3.1.2. INTERVAL MAPPING FOR BINARY TRAITS

As described in the previous sections, scoring data for 2014 and 2018 of FW population as well as Angers in 2018 for HW population presented an interesting distribution with a large peak at the score 0. Then it is interesting to analyze this data with an interval mapping for binary traits (Broman and Sen 2009). The use of interval mapping for binary traits is another strategy to handle the non-normal distribution for these scoring years. The genotypic probabilities were calculated before running a “one dimensional QTL scan” with the binary model implemented in the R/QTL package. Two types of binary traits were created using the scoring data for HW in 2018 and FW in 2014 and 2018. Indeed, in our case, it is interesting to consider these scores as a binary trait with phenotypes taking values of either 0 for unaffected hybrids (no symptoms with score of 0) and 1 for affected hybrids (exhibiting symptoms, scores from 1 to 5). The analyses with these new phenotypes will be called “bn” for binary (see Figure 25A). Assigning hybrids to these two types of values allows us to investigate the genomic locations linked to absence/presence of the symptoms. Another option would be to consider phenotypes of 0 for hybrids exhibiting a certain resistance (scores of 0 or 1) and 1 for hybrids with less resistance (scores greater than 1). This second analysis is referred to as “bn1” for binary traits separating hybrids with a score below and above 1 (see Figure 25). In this case, we do not investigate the absence/presence of symptoms but rather scan for loci linked to the weak infection and not necessarily its complete stop. The new datasets created for this binary trait analysis are summarized in Figure 25 (B to D).

For FW in 2014, 29 hybrids showed no symptoms (value of 0) and the other 65 showed symptoms (value of 1) for bn. It is interesting to notice that for bn1 analysis more than 75% of the hybrids in this population showed no symptoms or less than 25% of infected leaves (see bn1 in Figure 25B). For 2018, most of the hybrids showed no symptoms (bn) or less than 25% of infected leaves (bn1) and just a few of them were greatly affected by the disease (Figure 25C). This confirms the high resistance present in this population which can be explained by the fact that both parents are resistant. On the other hand, HW population scored in 2018 showed a similar number of affected and unaffected hybrids when considering bn option (in Figure 25D). However, half of the hybrids that were assigned to the value 1 showed less than 25% of infected leaves (score 1). Overall, the disease had less incidence on HW population in 2018.

Again, no significant QTL was detected in 2014 on the male map of FW population neither for bn nor bn1. LOD scores on B5 spiked at 49cM for bn1 analysis but failed to reach the corresponding LOD threshold. LOD scores for bn analysis remained lower than 1.2 (Figure 26A). For FW population, two QTLs in B3 and B5 were detected in 2018 when bn was used whereas only one QTL on B3 was detected when bn1 was used (Figure 26B). It is interesting to notice that the peak was different for both analyses on B3, with a peak at 7cM (BFACT47) for bn and a peak at 12.89cM (TE_F2MCw115) for bn1 (Figure 26B). Indeed, the peak at 7cM was the same as the one detected with the two-part model when the LOD(π) was considered, and the one at 12.89cM for bn1 corresponded to the LOD(μ) peak (Supplementary figure 6B from the article and Figure 27). On one hand, we can say that the results found with the binary analysis of the 2p model are consistent with the binary trait analysis bn (symptoms vs no symptoms) and that the locus at 7cM largely affects the chance of presenting symptoms. On the other hand, the locus at 12.89cM seems to be linked to the infection reduction when analyzed with bn1 and was shown to affect the severity of the symptoms when analyzed with the 2p model. Moreover, after projecting the markers on the genome,

we can see that the locus detected with the bn method co-localized with the metaQTL Meta_1_3 whereas the locus detected with bn1 co-localized with the metaQTL Meta_2_3 (see Figure 27), which can confirm the existence of two loci on B3 linked to BSD resistance and that seem to affect different parts of the trait. However, we have to keep in mind that the precision of the male map for FW population did not allow us to fully separate these potential QTLs as confidence intervals overlapped (Figure 21). For HW, two QTLs were detected in 2018 on B3 and B5. The QTL on B5 detected with bn exhibited an important LOD score compared to the one detected with bn1 (Figure 26C). Both QTL peaks on B5 correspond to the peak found using the 2p model. The QTL on B5 from the 2p analysis was found affected the penetrance of the disease which reflects the high LOD score observed with the bn1 analysis. For the QTLs found on B3, we observed that the LOD scores obtained with bn and bn1 analysis were similar (Figure 26C). Indeed, the QTL found on B3 using the 2p analysis that year was found to affect both the penetrance and the severity of the disease.

For the female maps, no QTL was detected for FW in 2014 and HW in 2018 with neither of binary analysis. For FW in 2018, three QTLs were detected on A1, A2 and A4 with bn analysis and corresponded to the QTLs found with the 2p (Figure 28). Both QTL on A1 and A4 were described to affect the penetrance of the disease which fits well with the fact that we detected the QTL at the same location using bn analysis. The QTL on A2 detected with the 2p model seemed to affect both penetrance and severity but was only detected with the bn analysis and not the bn1. However, it is difficult to draw any conclusion for the female maps as the marker density was very low, which reduced the power of detection of QTL and the precision of their mapping.

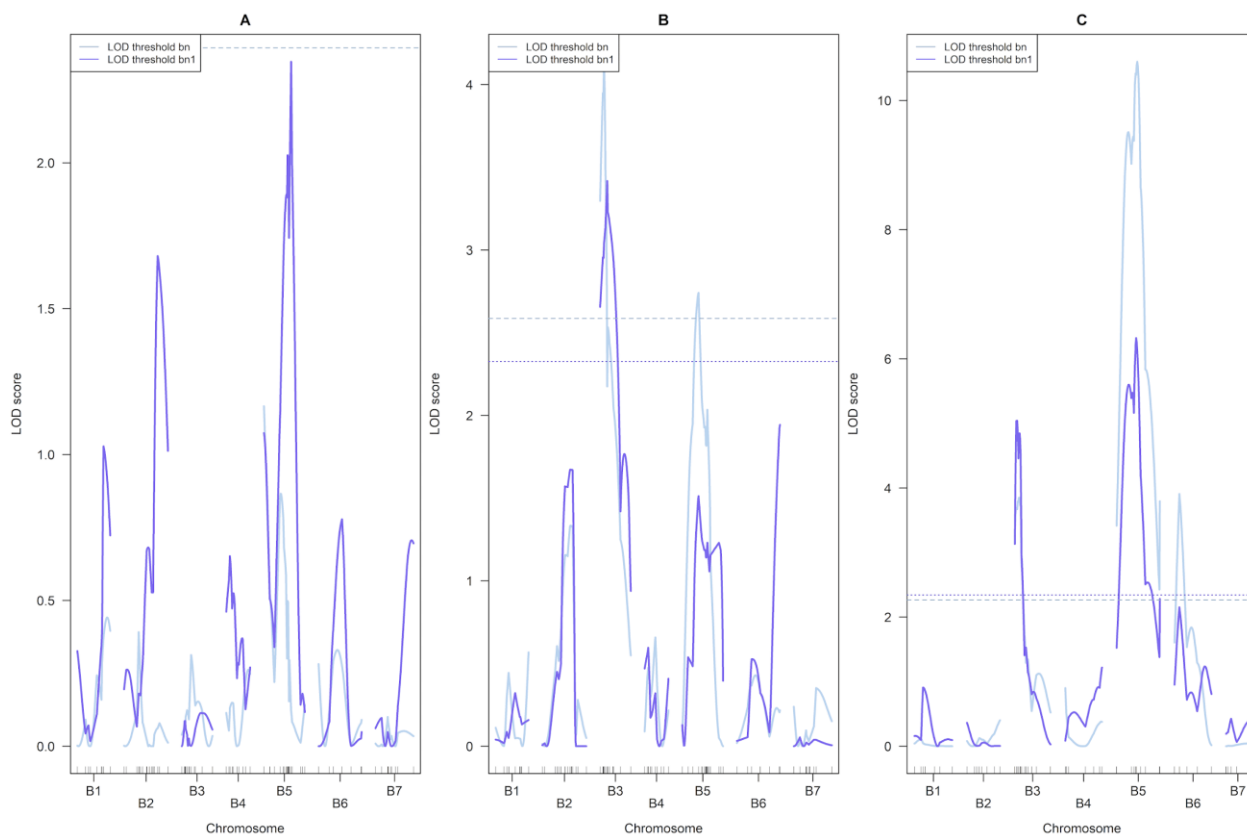
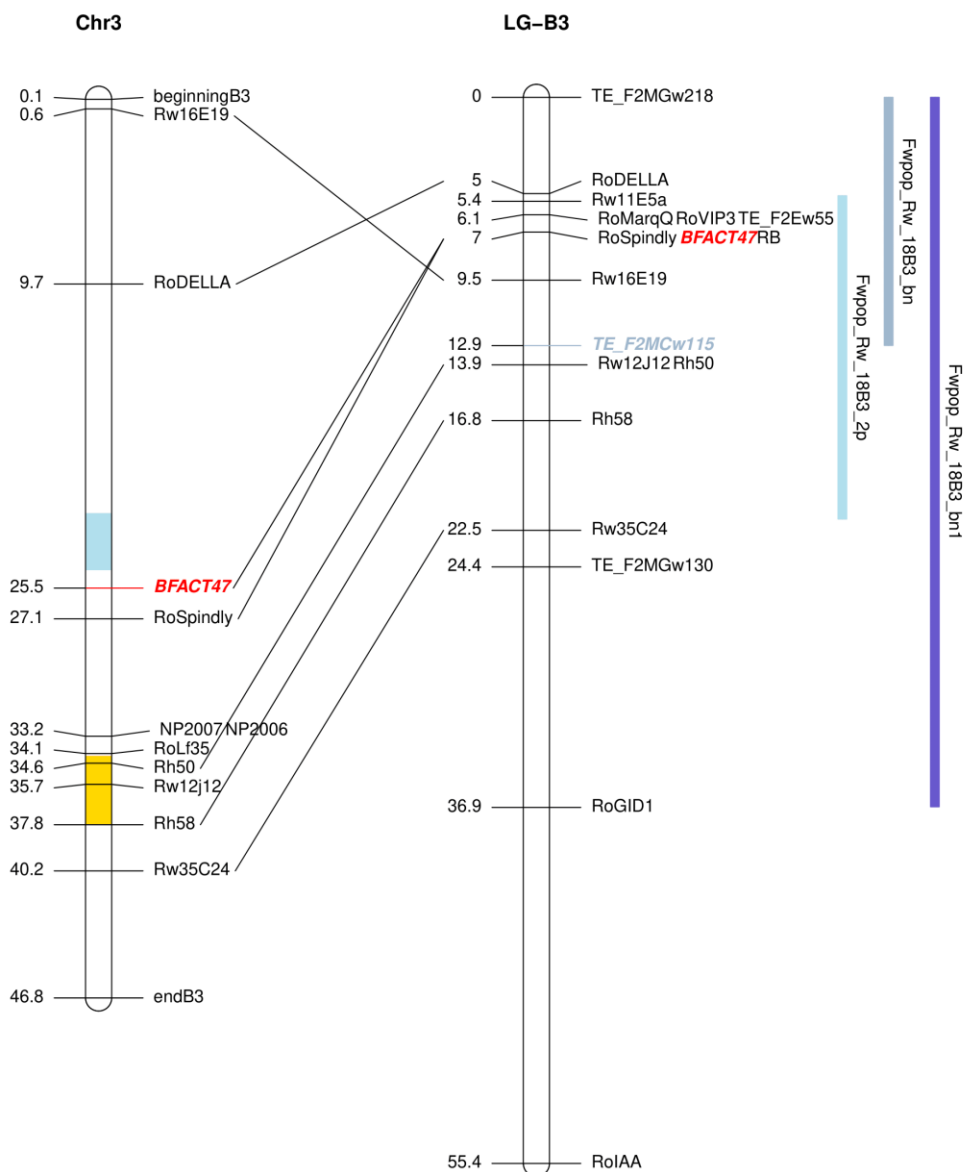


Figure 26: QTL mapping associated with black spot disease (BSD) resistance on the male maps for non-normal data of FW and HW populations using interval mapping for binary traits

Linkage groups are named as follows: “B” for the male map and the number of the linkage group. **A to C:** LOD curves of the binary model analysis for FW in 2014 (**A**), for FW in 2018 (**B**) and for HW in 2018 (**C**) for bn (in slate blue, scores = 0 vs scores > 0) and bn1 (in purple, scores < 1 vs scores > 1). The respective LOD thresholds of each type of analysis are displayed in the same color with $\alpha=0.05$ for declaring significant QTL based on 1,000 permutations.



Rendered by LinkageMapView

Figure 27: Co-localization of the QTL peaks detected with both binary methods (bn and bn1) with the metaQTLs published in Lopez Arias et al. 2020 and the QTL peak detected with the two-part model

Names of markers are on the right and the genetic distances (in cM for the linkage groups and in Mbp for the chromosome) are displayed on the left. Meta-QTLs are represented in plain color on the chromosome (Chr3) with Meta_1_3 in blue et Meta_2_3 in yellow. The markers at QTL peaks published in Lopez Arias et al. 2020 were localized on the genome. The QTLs detected on linkage group B3 for FW population with interval mapping for binary trait (bn in gray and bn1 in purple) as well as the QTL detected with the two-part model (in blue) are projected onto the FW male map (LG-B3). QTL names are coded as follows PopName_map_YearLG_Location_method. 5% Bayesian confidence intervals are displayed with vertical bars where the length is proportional to the interval width, and the markers at the QTL peaks are highlighted in a different color (the same color than the QTL bar or red if more than one method detected).

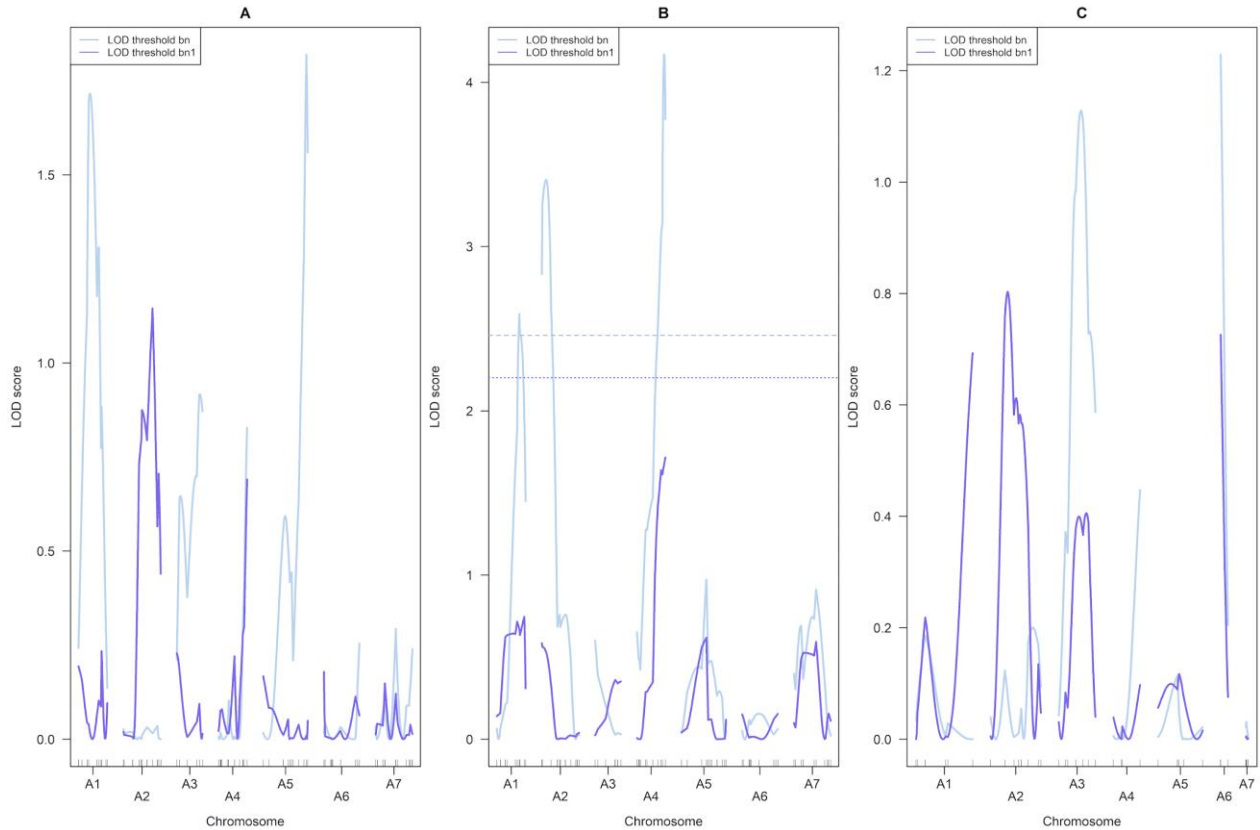


Figure 28: QTL mapping associated with black spot disease (BSD) resistance on the female maps for non-normal data of FW and HW populations using interval mapping for binary traits

Linkage groups are named as follows: “A” for the female map and the number of the linkage group. **A to C:** LOD curves of the binary model analysis for FW in 2014 (**A**), for FW in 2018 (**B**) and for HW in 2018 (**C**) for bn (in slate blue, scores = 0 vs scores > 0) and bn1 (in purple, scores < 1 vs scores > 1). The respective LOD thresholds of each type of analysis are displayed in the same color with $\alpha=0.05$ for declaring significant QTL based on 1,000 permutations.

3.2. EFFECTS OF PUTATIVE QTLs

For breeding purposes in agriculture as well as causal gene investigation, it is important to consider QTL effects. QTL effect can be characterized by two components according to Broman and Sen (2009): (1) the proportion of the phenotypic variance explained by the QTL and (2) the difference in the phenotype averages among groups with specific QTL genotypes. On one hand, when selecting a QTL in marker assisted selection (MAS), it is essential that such QTL accounts for a large portion of phenotypic variance of the desired trait. On the other hand, knowledge of the allele responsible for the improvement of the studied trait is also essential in the causal gene investigation following a QTL discovery, and that information is given by (2). But before determining the effect of putative QTLs published in the article, it is necessary to further investigate the class of QTL models that will be fit. Three main types of models exist: a model that is strictly additive (i.e. the effect of QTL is constant and independent of the genotype at other loci meaning that each allele contributes independently to the genetic variation), a model that allows epistasis between QTLs (i.e. the effect of a QTL is dependent on the genotype at another locus) and a model with dominance effects (i.e. the genetic variation is caused by an interaction between two alleles at a same locus). In some cases, models can combine dominance, additivity and epistasis. However, as we worked on pseudo backcross, we had to consider the genetic background of each parent independently, which did not allow us to identify QTLs with dominant effects.

The QTLs published in the article were detected with a single-QTL analysis (one dimensional scan) that controlled for the variation of strong effect QTLs by adding markers near large-effect QTLs as covariates (CIM). This method allowed us to seek for additional QTLs while performing a one-dimensional scan. The well-known interval mapping method was used. It is a method that performs a single-QTL analysis by performing a one dimensional scan on a dense grid across the genome and considers it as a putative QTL location. It, therefore, scans the genome for a single QTL at the time (Broman and Sen 2009). As it has been widely used, several methods have been developed to handle very different phenotype data like proposed in the article and [section 2.3.2](#) (normal model as well as two-part model and binary model for non-normal phenotypes). Several limitations arise, as when one searches for multiple QTLs explaining a complex trait, it goes beyond the consideration of one dimensional analysis. Most of the time, the single-QTL models perform reasonably well when the phenotypic data is supported by QTLs with large marginal effects and that are located on separated linkage groups. However, when QTLs of smaller effects also contribute to the trait as well as linked QTLs on a same linkage group, the one dimensional scan fails to identify them. Therefore, with a two dimensional genome scan, all possible two-loci QTL models are considered, which allows us to search for interaction between QTLs as well as to separate linked QTLs (see [Annex 1](#) for further explanation on the use and interpretation of two-dimensional scan). However, even if the two dimensional scan tests the fit of different types of models, it is restricted to the fit of maximum two QTLs in a model. Therefore, the next step, after testing for pairs of QTLs influencing the phenotypic data, is to find the best model that can explain our data by fitting several QTLs taking into account the possible evidence of interaction between QTLs (epistasis).

To investigate the QTLs explaining the data, I adopted a workflow with multiple steps to better explore the potential QTLs and their effect on each other. Both one and two-dimensional scans give us insights on the number of QTLs and their effect on each other. But then and only if several QTLs were detected with

these two methods, multiple-QTL models can be fitted. The results of the one-dimensional scans with CIM were presented in the article and the results of the two-QTL scans are not presented here but rather are used to discuss the results found during multiple-QTL models fitting that will be presented in the following section. Finally, after exploring the potential models and fitting them using multiple-QTL models, I would like to discuss the effect of the published QTLs.

3.2.1. MULTIPLE-QTL MODELS FIT

A wide range of methods exists to fit multiple-QTL models. During my PhD, I used two methods: a completely automatized method using the *stepwiseqtl* function, and “by hand” method using a range of functions provided by R/qtl such as *makeqtl*, *refineqtl* and *fitqtl*. The *stepwiseqtl* function performs a forward/backward stepwise search algorithm that optimizes a penalized LOD score criterion (pLOD). The penalized LOD score is used to control for false positives and is derived from the data permutation of the *scantwo* function. *Stepwiseqtl* can only visit a small portion of the existing models but is an interesting tool to identify the set of QTLs and epistatic interactions that best support the data. This automatized function was used to validate the models already found with the *scanone* and *scantwo* models. In most cases, the same observations were made than with the *scanone* and *scantwo* functions. The models were then fitted using *fitqtl* to get the estimated effects. In this part, I would like to briefly present the multiple-QTL model fit with the automatized function *stepwiseqtl*. An example of a sequence of models visited by the function for the scoring data of Angers in 2013 for HW population is presented in Supplementary figure 17. The function fits several models step by step performing two types of model selection. First, it starts running a single-QTL scan and fixes a QTL in the model by adding as covariate. Then, it starts adding loci to the model and testing for further additive QTLs, additional QTLs interacting with the ones already present in the model, and scans for additional additive QTLs or interactions beyond the set of QTLs already described (by performing a two-QTL scan). QTL locations are then recalculated in the current model. The function compares the new model to the one visited before and calculates the pLOD. If the pLOD is higher than for the previous model, it chooses the current model as the “new best” and starts again a new step. Once a large model is constructed (setting the parameter *max.qtl*), the backward selection begins and the functions drop loci and interactive loci from the model one at the time. The loci resulting in the smallest decrease in LOD is the one drop at each step and it is followed by refinement of the QTL locations in the current model. In the end, the final model chosen is the one that maximizes the penalized LOD score (in red in the Supplementary figure 17).

The results of all analyses performed for each year and location for all three populations are summarized in Table 9. The non-normal data was not analyzed with multiple QTL mapping as only a normal model is available. In general, the results of the *stepwiseqtl* search were consistent with the results found with the one dimensional scan except for five scoring years (mean in Angers, as well as 2012, 2014 and the mean in Diémoz for HW population, Table 9). On one hand, the additional QTL detected on B6 for the mean scores in Diémoz (HW population) using the multiple QTL mapping was also detected with a simple interval mapping (SIM) but no with the composite interval mapping (CIM) (Supplementary figure 17). On the other hand, *stepwiseqtl* finds epistasis between QTLs on B3 and B5 for only the mean in Angers, 2012 and 2014 in Diémoz for HW population. No interaction was detected when scanning for pairs of QTLs with the two-dimensional scan (results not shown). In the Rqtl manual, it is recommended to explore the

interaction plots between two markers at QTL peaks to assess if there is strong evidence for epistasis. In Supplementary figure 19, we can see that the QTLs on B3 and B5 act approximately additively as the effect of the marker on linkage group B3 (RB or BFATC47) is approximately the same for each one of two genotypes at the linkage group B5 (RMS034 or RW14H21). Epistatic interactions are shown when the effect of a QTL at a given linkage group is dependent on the presence of a specific allele at another locus which corresponds to lines that intersect. In our case, whether RB or BFATC47 on B3 are AA or AB, RMS034 or RW14h21 on B5 will have an effect on the disease scores. The evidence for epistasis using additional investigations with the two-dimensional scans and the observation of the interaction plots cannot be clearly demonstrated here. Therefore, the interaction between B3 and B5 was not fitted in the final models for these scoring years.

Table 9: Summary of QTLs linked to black spot disease resistance found with one dimensional scan with covariate (CIM) and multiple QTL mapping methods in OW, FW and HW populations across multiple environments (years and locations) for the male maps

Population	Location	Year	Phenotypic distribution	One dimensional scan with covariate (CIM ^a)	Multiple QTL mapping with <i>Stepwiseqtl</i>	Interaction plot indication ^b	Multiple QTL model fitted with <i>fitqtl</i>
OW	Angers	2014	Normal	B3	B3		$y \sim B3$
		2015	Normal	B3	B3		$y \sim B3$
		2016	Normal	B3 + B5	B3 + B5		$y \sim B3 + B5$
		2017	Normal	B3 + B4 + B5	B3 + B4 + B5		$y \sim B3 + B4 + B5$
		2018	Normal	B3 + B5	B3 + B5		$y \sim B3 + B5$
		Mean	Normal	B3 + B4 + B5	B3 + B4 + B5		$y \sim B3 + B4 + B5$
FW	Angers	2014	Spike-like	Null QTL model			$y \sim 0$
		2018	Spike-like	B3 + B5			$y \sim B3 + B5$
HW	Angers	2012	Normal	B3 + B5	B3 + B5		$y \sim B3 + B5$
		2013	Normal	B3 + B5 + B6	B3 + B5 + B6		$y \sim B3 + B5 + B6$
		2014	Normal	B3 + B5 + B6	B3 + B5 + B6		$y \sim B3 + B5 + B6$
		Mean	Normal	B3 + B5 + B6	B3 + B5 + B6 + B3:B5	No epistasis	$y \sim B3 + B5 + B6$
		2018	Spike-like	B3 + B5 + B6			$y \sim B3 + B5 + B6$
	Bellegarde	2012	Normal	Null QTL model	Null QTL model		$y \sim 0$
		2013	Normal	B3 + B5	B3 + B5		$y \sim B3 + B5$
		2014	Spike-like	B3 + B5 + B6			$y \sim B3 + B5 + B6$
		Mean	Normal	B3 + B5 + B6	B3 + B5 + B6		$y \sim B3 + B5 + B6$
	Diémoz	2012	Normal	B3 + B5	B3 + B5 + B3:B5	No epistasis	$y \sim B3 + B5$
		2013	Spike-like	B3 + B5			$y \sim B3 + B5$
		2014	Normal	B3 + B5 + B6	B3 + B5 + B6 + B3:B5	No epistasis	$y \sim B3 + B5 + B6$
		Mean	Normal	B3 + B5	B3 + B5 + B6		$y \sim B3 + B5 + B6^*$

^a CIM stands for composite interval mapping, interval mapping with the markers at the largest peaks as covariates.

^b When an epistatic effect was described, the interaction plots were verified before validating or not the evidence for interaction between two QTLs (see Supplementary figure 19).

* New models defined after evidence for additional QTL on B6.

3.2.2. ESTIMATED QTL AND ALLELIC EFFECTS

Unlike single marker analysis, interval mapping allows a better estimation of QTL effects as they are not confounded with recombination frequencies (Lander and Botstein 1989; Broman and Sen 2009). In R/qtl package, after detecting the QTLs with the *scanone* function and exploring two-QTL and multiple QTL models to assess the presence of additivity and epistasis, the *fitqtl* function is used to fit the multiple-QTL models with the detected QTLs and ultimately to obtain the estimates of QTL effects. Two types of models are handled by this function: the “normal” model used for data distributed normally and the “binary” model used for binary traits. Unfortunately, the two-part model is not yet available. The proportion of the phenotypic variance explained by each QTL individually is calculated as well as its importance (as a p-value) in the explanation of the phenotypic variation (Broman and Sen 2009). The individual effects of each QTL detected were reported in Table 5 and Table 6 of the article as “R² (%)” and all QTLs were found to have a significant p-value. Another use of *fitqtl* function is to get the estimated QTL effects. The estimated effect for a given QTL in a backcross is the difference between the phenotype average for the heterozygotes (AB) and homozygotes (AA). However, as reported in the article, some scoring years were analyzed with a two-part model due to their data distribution and therefore, the “normal” model of *fitqtl* might not be suited to calculate the estimated effects. Therefore, I tried to use both models to calculate separately the estimated effects when the two-part model was used to identify the QTLs and the estimated effects from them were both indicated in the effect plots (see Supplementary figure 20, Supplementary figure 21, Supplementary figure 22, Supplementary figure 23, Supplementary figure 24). Only scoring data with a large peak at 0 was analyzed with the “binary” model of *fitqtl* (i.e. 2018 for HW population based in Angers and 2018 for FW population).

In R/qtl package, the function *effectplot* is used to plot the phenotype average for genotype groups (heterozygous or homozygous in the case of backcross) and uses the multiple imputation method to better estimate the genotype-specific phenotype average while taking into account the missing genotype data (Broman and Sen 2009). I decided to manually add the estimated effects of each QTL onto its corresponding effect plot for ease of interpretation as the function does not provide this information on the effect plot (see Supplementary figure 20, Supplementary figure 21, Supplementary figure 22, Supplementary figure 23, Supplementary figure 24). As we are interested in the QTLs brought by the resistant male parent, only the effects of QTLs mapped on the male map were investigated here. For a pseudo-backcross, only markers heterozygous in one parent are used, which means that the male map was built with a <aaxab> type of marker. In this context, phases for one parent are known and calculated with JoinMap® (see section 2.6). To enter the genotyping information (marker genotyping and phases) in Rqtl, a specific encoding is used (see Annex 2). It is important to consider the phase of the marker at a QTL peak to properly determine the allele contributing to the resistance.

For OW population, the estimated effects of QTLs detected on B3 and B5 are higher than for the other populations and ranged from -0.7 to -1.3 (see Supplementary figure 20A-C). The effect of the QTLs on B4 varied much more (from 0.5 to 0.9, see Supplementary figure 20B). QTLs on linkage groups B3 decreased the BSD score by about 1 when the hybrids are heterozygous AB at the QTL location for 2014 (Rh12GR_1265_568), for 2015 and the mean (Rh12GR_367_6432) and for 2018 (Rh12GR_10522_106) whereas for 2016 (Rh88_6620_1684) and 2017 (Rh88_15720_207), the BSD score decreased when the

hybrids were AA at the QTL location (see Supplementary figure 20A). Indeed, markers Rh12GR_1265_568 (2014), Rh12GR_367_6432 (2015 and mean) and Rh12GR_10522_106 (2018) are on phase {-0} while Rh88_6620_1684 (2016) and Rh88_15720_207 (2017) are on phase {-1}. This indicates that, for 2014, 2015, the mean and 2018, the B allele at the QTL locations brings the resistance whereas the A allele is the one bringing the resistance for the QTLs detected in 2016 and 2017. Similar interpretation can be done for the QTLs detected in B4 and B5. For the QTLs on B4, being heterozygous AA at the QTL peak in 2017 leads to lower BSD (0.9 less than being AB at this locus), which means that the A allele brings the resistance while for the mean, being AA decreased the BSD score by 0.5 compared to being AB, which indicates that the A allele is the one bringing some resistance to BSD (see Table 10). For the QTLs detected on B5 in 2017, 2018 and the mean, it is the B allele that brings some resistance (0.9 less than having the A allele from RW) and conversely, it is the A allele that brings some resistance for the QTL detected in 2016 (see Supplementary figure 20C). For instance, in 2014 and 2015, the individuals exhibiting the B allele on B3 had less symptoms. The individuals combining the B allele from RW at the QTL peak on B3 and the A allele from RW at the QTL peak for 2016 had a high resistance to BSD while for 2018, combining B alleles from RW at the QTL locations on B3 and B5 led higher disease resistance. Finally, for 2017, the combination of the A allele at the QTL peak on B3 and the B alleles at the QTL peaks on B4 and B5 led to a strong resistance to BSD (21 hybrids presented these alleles at the QTL locations and exhibited an average BSD score of 0.9).

For FW population, only 2018 scoring data enabled the discovery of two QTLs on B3 and B5 when the two-part model was used. Both models in *fitqtl* function were used to calculate the estimates as the two-part model is not yet handled by this function. We can see that when the “normal” model was used to fit the QTL model, the estimated effects were very different than when the “binary” model was used. Indeed, on one hand, for the QTL linked to BFACT47 on B3, the estimated effect was -0.50 with the “normal” model and +0.05 with the “binary” model (see Supplementary figure 21A). This QTL was identified to have an effect on both penetrance (absence/presence of symptoms) and severity of symptoms. On the other hand, for the QTL linked to RoGA2ox on B5, the estimated effect was -0.13 and -0.40 with the “normal” and “binary” model, respectively (see Supplementary figure 21B). This QTL was identified as affecting the penetrance of the disease and therefore having a stronger effect on the binary part of the trait, which can explain that using a model that fits well a binary phenotype, we can get a better estimate of its effect. However, I would recommend to consider the estimated effects obtained for spike-like data such as FW and HW scoring data with caution as the model does not fully fit the phenotype data. With these results, we can say that an individual carrying the B allele at both QTLs (B3 and B5) is more likely to exhibit no symptoms at all (see Table 10).

Finally, for HW population, environmental locations were separated for a better visualization of the effect plots. For Angers, the estimated effects of the QTLs located on linkage group B3 varied from -0.78 to -0.89 (see Supplementary figure 22A) which is less than in OW background. The estimated effects of the QTLs on B5 varied a lot more than for the ones on B3 and went from -0.49 in 2012 to -0.9 in 2018 (see Supplementary figure 22B). For the QTLs on B6, the estimated effects were much smaller than for the other locations and varied from -0.31 to -0.45 (see Supplementary figure 22C). However, the effect of the QTLs on B5 was very variable over the years. I would like to point out that using the “binary” model gave, here, rather odd results, which confirms the inability to estimate precisely the effects of QTLs detected

with non-normal data. For Bellegarde, no QTLs were identified in 2012. Three QTLs were detected on B3 and three others on B5 with the estimated effects varying from -0.3 to -0.8 and from -0.3 to -0.6, respectively (see Supplementary figure 23A-B). However, the effects for 2013 and the mean were much smaller than for 2014 for both linkage groups. It is important to remember that the phenotypes for 2014 did not follow a normal distribution and the QTL analyses were performed with a two-part model which could explain that difference. Again, we were confronted with the incapacity of *fitqtl* to fit models with non-normal phenotypes (here a spike-like distribution). Two QTLs on B6 were detected with small estimated effects. Finally, for Diémoz in 2014, the estimated effects of the detected QTLs at this location were generally much lower than for Angers or Bellegarde. The QTLs detected on B3 had estimated effects varying from -0.27 to -0.45, the ones on B5 had estimated effects ranging from -0.30 to -0.51, and the ones on B6 around -0.25 (see Supplementary figure 24). For the mean, the additional QTL on B6 found thanks to previous analyses was fitted in a three-QTL model, the estimated effects were calculated and found to be lower than for the other QTLs found on B6 for the other locations and years. These results indicate that for all the QTLs detected on B3, B5 and B6, the presence of a B allele at these QTL locations decreased the BSD score except for Diémoz in 2013 and Angers in 2018 for which the A allele at the QTL peaks on B3 and B5, respectively, was linked to a better resistance (see Table 10).

In addition, the QTLs expressed individually help to reduce the disease incidence (making the hybrids less susceptible and more resistant) but none of them was seen to completely stop the pathogen (by decreasing the BSD score completely to 0). However, acting together these QTLs can drastically reduce the pathogen infection. Indeed, whenever a hybrid combined the right alleles at the QTL locations (AB for B3, B5 and B6 or AA for B4), the BSD score observed for that specific hybrid was lower than 1, which means that the infection was absent or at least restricted to a few leaves. Interestingly, we can see that both the genetic background in which the QTLs are expressed and the scoring year can influence the effects of all QTLs. However, it is hard to separate the effect of the genetic background and the effect of the environment (climate, fungal pressure, diversity of fungal strains, etc.) as the populations do not have the same age and the individuals of each population are separated by population (and not mixed in one big field).

In view of the QTL effects on the resistance to BSD, the stability of expression over different environments and the confidence intervals, we should choose in priority the QTLs on B3 and B5 to be further studied and maybe considered for breeding programs. That is why we decided to focus on the QTLs on B3 and B5 and we applied the meta-analysis method on these two QTLs only.

Table 10: Summary of RW alleles contributing to the resistance for the markers at the QTL peaks detected on the male maps for OW, HW and FW populations

	B3				
	Location-Year	JoinMap phasing	Position (cM)	B3-1	B3-2
OW	Rh12GR_1265_568	Angers-2014	{-0}	9.437	A B
	Rh12GR_367_6432	Angers-2015/mean	{-0}	16.131	A B
	RhMCRND_10522_106	Angers-2018	{-0}	19.519	A B
	Rh88_15720_207	Angers-2017	{-1}	20.186	B A
	Rh88_6620_1684	Angers-2016	{-1}	26.966	B A
	B4				
	Location-Year	JoinMap phasing	Position (cM)	B4-1	B4-2
	Rh12GR_14039_541	Angers-2017	{-1}	14.242	B A
	Rh88_49087_478	Angers-mean	{-0}	20.934	A B
	B5				
	Location-Year	JoinMap phasing	Position (cM)	B5-1	B5-2
	Rh12GR_80310_174	Angers-2017/2018	{-0}	10.043	A B
	Rh12GR_30728_3735	Angers-mean	{-0}	12.737	A B
	Rh88_31600_683	Angers-2016	{-1}	44.987	B A

The phases for each marker are coded according to JoinMap[®] codification and the marker positions are reported in cM. BX-1 (orange) carries the alleles that are not linked to BSD resistance whereas BX-2 (green) carries the alleles bringing the resistance (with X being the linkage group where QTLs were detected).

Table 10 (continued)

	B3						
		Location-Year	JoinMap phasing	Position (cM)	B3-1	B3-2	
HW	RoRGA	Bellegarde-2013/2014	{-0}	3.97	A	B	
	RoMarQ	Bellegarde-mean	{-0}	6.3	A	B	
	RoSpindly	Angers-2018	{-0}	8.96	A	B	
	RB	Angers-2012/2013/2014/mean	{-0}	9.67	A	B	
	BFACT47	Diémoz-2012/2014/mean	{-0}	11.5	A	B	
	RoLf35	Diémoz-2013	{-1}	19.08	B	A	
		B5					
			Location-Year	JoinMap phasing	Position (cM)	B5-1	B5-2
		Rw14H21	Angers-2012; Bellegarde-2013/2014/mean; Diémoz-2012/2014/mean	{-0}	25.13	A	B
		H24D11	Angers-2018	{-1}	30.08	B	A
		RMS034	Angers-2013/2014/mean	{-0}	32.18	A	B
		H17C12	Diémoz-2013	{-0}	40.69	A	B
		B6					
			Location-Year	JoinMap phasing	Position (cM)	B6-1	B6-2
	CTG623	All	{-0}	8.28	A	B	
FW	B3						
		Location-Year	JoinMap phasing	Position (cM)	B3-1	B3-2	
		BFACT47	Angers-2018	{-0}	7.01	A	B
		B5					
		Location-Year	JoinMap phasing	Position (cM)	B5-1	B5-2	
	RoGA2ox	Angers-2018	{-1}	29.34	B	A	

The phases for each marker are coded according to JoinMap[®] codification and the marker positions are reported in cM. BX-1 (orange) carries the alleles that are not linked to BSD resistance whereas BX-2 (green) carries the alleles bringing the resistance (with X being the linkage group where QTLs were detected).

4. DISCUSSION AND CRITICAL REVIEW

The partial resistance to BSD is a complex trait and its genetic basis has not yet been elucidated. Thus, the aim of this chapter was to present the first insights on the genetic basis controlling the partial resistance to BSD brought by the male resistant parent RW. To better characterize it, several analyses were carried out on an extensive dataset. The main results were published but additional analyses helped us to further investigate the effect of the environment on the disease development and to better characterize the loci that were detected to be linked to BSD resistance.

The importance of the environment on the development of BSD in fields was demonstrated in both the article and the additional results. Unlike other diseases, BSD infection does not seem to build-up year after year leading to an increased infection. The disease incidence seems to be linked to the environmental conditions and the resistance observed in some phenotypes seems to hold on throughout the years. Indeed, environmental conditions within one year can affect the disease incidence observed the following year especially on resistant genotypes. However, a build-up of infection was definitely observed but only during the immediate year. Not only rainfalls close to the scoring period seem to affect the final scores but also all the history of rain between the beginning of the infection in early spring and the scoring period. Indeed, with the additional results, we showed that, in populations with one resistant parent, the cumulated rain during the infectious period seems to greatly affect the final scores. The average temperature and the humidity did not seem to have an effect on BSD infection (data not shown). However, one cannot exclude an additional effect of pathogen population evolution and distribution in the fields. Unfortunately, no data was recorded neither during the plant installations in the fields nor during the years that were scored. To further investigate the evolution of the pathogen population over the years and its repartition in the field, we can imagine sampling conidia from susceptible and resistant (when possible) genotypes every time a scoring is performed and at different places in the field.

In the article, we decided to present the results obtained with a one dimensional scan using markers near large effect QTLs as covariates (CIM). However, complex traits like disease resistance are known to be controlled by many genes and the search of multiple QTLs is essentially a multidimensional problem that needs to be addressed like it. Therefore, multiple-QTL model fitting is necessary to get a grasp of the real nature of complex traits (Zou and Zeng 2008; Broman and Sen 2009; Han et al. 2016; Broman and Wu 2019). The additional results of the two-dimensional scan combined with multiple QTL mapping approaches allowed us to conclude that the effects of the detected QTLs were mainly additive effects and no epistatic effect was clearly demonstrated. In my opinion, it is important to explore the QTLs that best support our data by performing successively several analyses. One dimensional scans (SIM and CIM) are tools that help us to explore the possible QTL locations with low computational effort. But the analysis should not be restricted to that because when one detects more than one QTL for a dataset, the assumption of one dimensional scans are no longer met as they scan for a single QTL. Therefore, additive and epistatic effects cannot be detected. But combining the use of one and two dimensional scans can help us to better identify the QTLs explaining our data as well as their effect on each other (additivity, dominance and epistasis). Finally, the last step of a QTL analysis for a complex trait is the fit of a multiple-QTL model that best supports the data. Automatized search algorithms can help us to identify additional QTLs and even help to separate linked QTLs. The results gathered with all these analyses as well as

descriptive plots (interaction plots or effect plots) can help us to decide which loci would best fit the model. Investigation of QTLs linked to complex traits such as disease resistance needs to follow several steps so one can get better insights on the amount of loci controlling these types of trait, their relationship to each other and their effect on the phenotype. The steps followed in this study are summarized in the Figure 29. Many algorithms have been described throughout the years to help researchers in the study of QTL underlying a quantitative trait, but one cannot forget the limitations of each one of the proposed methods. So in the end and after crossing the results of several exploratory approaches and model fitting approaches, the researcher is the one deciding which results are the most consistent regarding the studied trait.

With this extensive study on BSD resistance, we are able to show that the genetic background has an influence in the expression of the partial resistance as the disease incidence on the three populations was different. The detection of population-specific QTLs on B4 for OW and B6 for HW also goes in this direction. But as two main QTLs were detected on B3 and B5 in all three populations and were stable over several years and locations, we believe that the partial resistance to black spot disease is mainly controlled by these two QTLs in *R. x wichurana*. Investigation on the effect of the detected QTLs allowed us to identify the effect of each QTL on the observed phenotypic variability and the allele associated with more BSD resistance for each marker. As we worked on pseudo-backcrosses, we were virtually looking at each parent side separately, so we were not able to identify dominant effects in the progeny. So when the estimated effects were calculated, we were only able to identify the alleles bringing the resistance from one parent separately. However, identifying the alleles responsible for less symptoms is important if we want to develop markers linked to BSD resistance in rose. In addition, the percent of phenotypic variance explained per QTL did not change drastically between crosses for a specific QTL, and the sum of the percent of phenotypic variance of all the QTLs for a specific year was close to the overall percent of phenotypic variance explained by the QTL model for that same year. These results are consistent with the absence of epistasis observed between these loci (Awata et al. 2019). Similarly, the study of non-normal phenotypes with both two-part and binary models helped us to better characterize the effect of the QTLs. QTLs on B3 seem to influence the penetrance as well as the severity of BSD infection whereas the QTLs detected on B5 with these methods seem to impact specifically the penetrance of the disease. This knowledge will be useful for gene mining under QTL locations as it can help us to be more critical of whether or not a gene is involved in the resistance to *D. rosae*.

The next step after identifying the locations linked to the partial resistance to BSD is to reduce the confidence intervals, so the causal gene investigation is more efficient and the selection of markers for MAS more precise. In that prospect, I tried to reduce the confidence interval by performing a meta-analysis of all the detected QTLs. The starting idea at the beginning of my PhD was to use the data of the three populations connected by the male parent by assuming that we had a whole population with half-sib individuals from the three crosses. This would increase the population size (for us it would have been 456 hybrids) and the individual's pedigree was then known for at least one generation. Methods like identity by descent could be applied in a QTL mapping context and it is known that the power of QTL detection is greatly increased that way (Crepieux et al. 2005; Hitzemann et al. 2008; Li et al. 2011; Muktar et al. 2015; Ogut et al. 2015; Han et al. 2016; Maurer et al. 2017). However, to perform these methods, all individuals

need to either be genotyped with the same markers (for example the same SNP array) or share a considerable amount of markers to build a consensus map that will be used for QTL mapping. In our case, the genetic maps only shared 41 markers for the male maps and 31 markers for the female maps (mainly SSRs), and for the OW maps, we had ten times more markers than for the other two maps. The markers that are not genotyped in the other populations would be considered as missing genotypes during the QTL mapping. One of the factors affecting QTL mapping is the missing genotype information according to Broman et al. 2009 and in our case more than 80% of the markers would have been missing for the HW and FW populations. In addition, only two years of scoring were common for all populations (2014 and 2018), which would have reduced the QTL mapping to two years instead of seven years of data. Considering that the reliability of the map would have been low and that the data would have been reduced to two scoring years, I decided to combine all the individual QTL mappings using a meta-analysis to make the best use of the data in my possession. Indeed, that way, no problem with missing genotypes was encountered as a consensus map was created without using the genotype information and all the years scored could be used. Many other systems have used this type of analysis (Khowaja et al. 2009; Griffiths et al. 2009; Lanaud et al. 2009; Yadava et al. 2012; Hamon et al. 2013; Semagn et al. 2013; Vasconcellos et al. 2017; Guo et al. 2018). More and more researchers have adopted this method to combine data from related populations like the recently published paper on QTL mapping of low temperature germination capacity in three connected populations of corn (Li et al. 2018). As discussed in the article, two meta-QTLs were found on B3 and two others on B5 with reduced confidence intervals. Several hypotheses were made to explain the presence of two meta-QTLs when combining the QTLs. In the article, we mentioned the possibility that the double meta-QTL was the result of large rearrangement on chromosome 3. However, additional data as well as the investigation of the LOD peaks and the curves seem to support evidence for two meta-QTLs in that linkage group that might have different effects on the phenotype. With respect to linkage group B5, many results tend to support the evidence for two different meta-QTLs. If we look at the QTL contributions, we can see that several scoring years for OW population seem to support the evidence for a QTL at the beginning of the linkage group whereas FW and HW populations seem to express another QTL located 10cM further. And in the middle, the scoring year 2016 exhibited a LOD curve typical of linked QTLs. Unfortunately, two dimensional scans as well as multiple QTL analyses did not allow us to identify two linked QTLs instead of one for that scoring year. Therefore, there is still doubt about the reality of two meta-QTLs in both chromosomes 3 and 5.

To increase the power to detect linked QTLs, we need to increase the population size. For that matter, an extension of the OW population (approximately 1,000 individuals) was prepared and will soon be ready for scoring. That way, fine mapping of the selected zones can be performed to reduce the confidence intervals and hopefully assess whether or not there are two linked QTLs in both B3 and B5. Another limiting factor in our study is the use of a reduced scoring scale. The importance of the accuracy and precision of field phenotyping on the power to detect reliable QTL has been largely demonstrated (Chandra and Bidinger 2002; Broman and Sen 2009) and represents a limiting factor in QTL mapping approaches. One possibility can be to score the additional individuals with the existing scoring scale as well as another one with more classes, so a better mapping of the QTLs could possibly be done. The latter has actually been implemented in our investigations for the last scoring year (2020) and will be used in comparison with the small rating scale to map QTLs. Another solution would be to combine multitrait QTL mapping by

phenotyping the entire population with different components of the partial resistance studied by Xue and Davidson in 1998 such as lesion length (LL), leaf area with symptoms (LAS), chlorosis, number of lesions (NL), sporulation capacity (SC), etc. However, considering the time needed to score a population of 151 individuals, it would take a great deal of time to phenotype a population of 1,000 hybrids using many components. A compromise can be found in the form of selective phenotyping. The selective phenotyping method is applied when the genotyping is less expensive and time consuming than phenotyping. It involves the selection of individuals to phenotype while maximizing their genotypic dissimilarities (Jin et al. 2004; Lee et al. 2014). Selective phenotyping is very effective when the genetic architecture has already been investigated as researchers can focus on specific regions and select the individuals that maximize the genetic difference in the regions of interest, but it can also bring some improvement when the selection is applied to the whole genome. That way, only the set of individuals that maximize the genetic difference in the QTL regions need to be phenotyped. This can allow us to perform additional disease assessments directly in the field by using several components like mentioned above to better characterize the genetic basis underlying the partial resistance to black spot disease.

Moreover, in order to effectively respond to breeders' demand for genes linked to partial resistance (believed to be more durable), a new project called KASPORO was initiated in 2018. The QTL mapping results obtained in this study for OW population were used to select a set of ten markers each million pair bases within the QTL region (i.e. 10 million bp) and to transform them into Kompetitive allele specific PCR (KASP) markers that are easier to use. These markers were used to genotype the hybrids with the most contrasted phenotypes (selective genotyping) and the results will soon be obtained, which should help us to narrow down the location of the causal genes as well as to propose usable markers for breeders if a marker close enough to the causal gene is identified.

Finally, the study like it is right now does not enable us to conclude on the specificity of the detected QTLs as we have no information about the strains present in our fields. Another perspective would be to collect monoconidial strains in the fields from plants with different degrees of resistance. This approach was initiated last year and, with the knowledge about the alleles responsible for the resistance at each detected QTL, we selected individuals that carry one or two specific QTLs (similar to a selective phenotyping approach) and sampled conidia from their infected leaves.

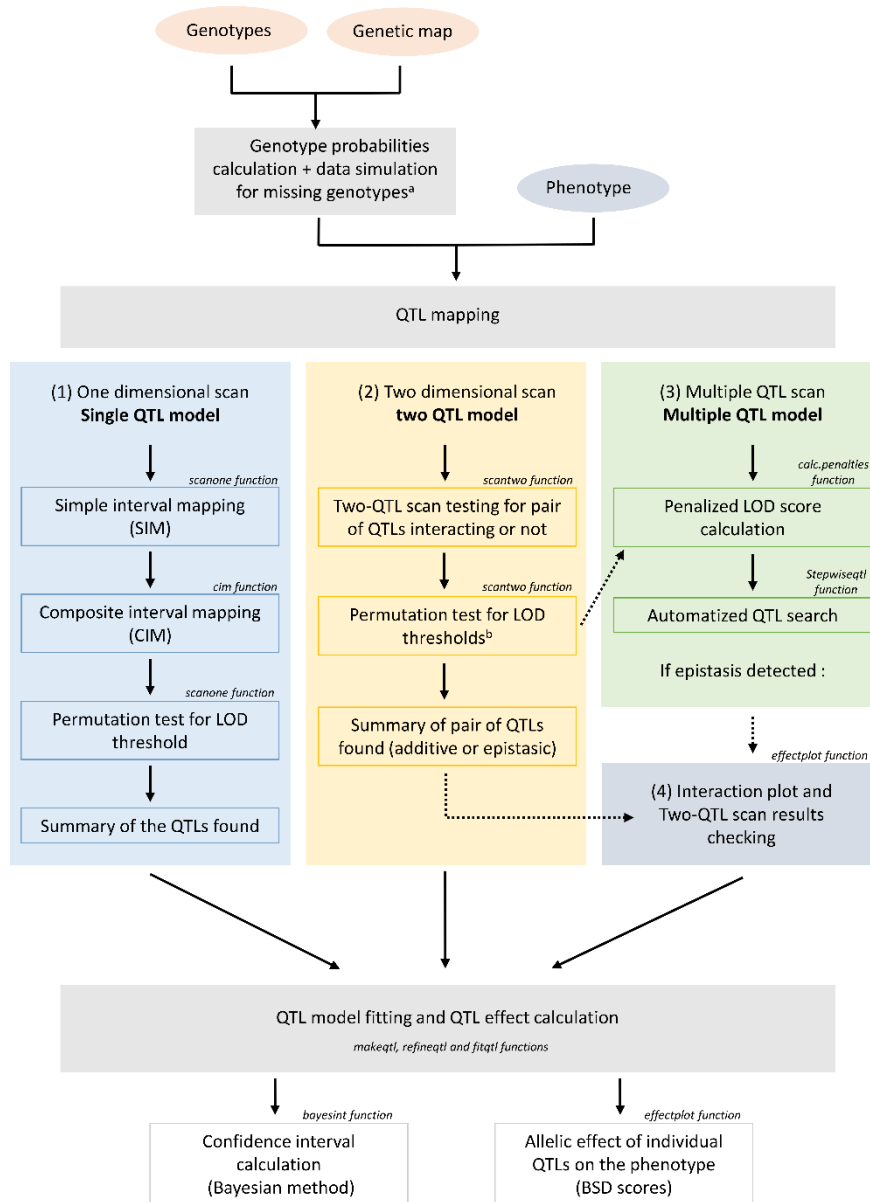


Figure 29: QTM mapping workflow followed in this study using Rqtl package and K. Broman recommendations in diverse discussions in google groups (<https://groups.google.com/g/rqtl-disc>)

^a Data simulation performed to fill in missing genotype information and necessary for the single QTL mapping with *scanone* function using the multiple imputation method.

^b Six LOD thresholds are calculated corresponding to the LOD for the different models tested (full model, additive model, interactive model, single QTL model and null model) during the two dimensional scan (see Annex 1).

Chapter 3 : Phenotypic and microscopic study of rose-*Diplocarpon rosae* interaction during the infection

A rose dreams of enjoying the company of bees, but none appears. The sun asks: 'Aren't you tired of waiting?' 'Yes,' answers the rose, 'but if I close my petals, I will wither and die'.

– Paulo Coelho



A bee visiting *Rosa wichurana* flower by T. Thouroude

1. SYNOPSIS

Investigation of the genetic determinism behind traits such as resistance is very difficult as genes controlling it can act at different moments of the infection and be involved in different mechanisms, from the pathogen recognition through its PAMPs or effectors, to signal transduction and resistance implementation. Therefore, precise knowledge of what is happening at a microscopic level can bring more insights on how a given plant resists. In the previous chapter, we were able to identify quantitative trait loci linked to partial resistance to black spot disease but also to characterize these loci and their effect on the phenotype. QTLs on B3 were found to influence both the penetrance and the severity of the disease while the ones on B5 impacted specifically the penetrance. The genetic study was carried out based on a phenotypic assessment on whole plants that used a rating scale with percentage of infection and degree of defoliation under natural infection. Focusing on the battlefield that happens at the leaf level and understanding how the interaction works at a microscopic level may help us to make better sense of the effect of the loci that we detected and subsequently to explain transcriptomic changes that can be observed.

During the Belarosa project (2015-2016), a large collection of fungal strains from different parts of Europe and Asia was built. Twenty of the 77 strains of the Eurasian collection were tested on the parents of OW population: *Rosa chinensis* 'Old Blush' (OB) and *Rosa wichurana* (RW). This study revealed that the strains' aggressiveness varied a lot as some of them have been able to cause large necrosis on the resistant genotype RW and others did not yield any symptoms on OB. For this purpose, our laboratory has developed a whole plant assay in semi-controlled conditions (greenhouse) to assess the resistance of rose genotypes (Soufflet-Freslon et al. 2019; Marolleau et al. 2020). In addition, to choose one strain with contrasted effects on OB and RW for the transcriptomic assay, I tested three of the strains from the collection that exhibited different aggressiveness based on a previous study. The results of this study will not be presented in this chapter. Moreover, unlike detached leaf assay, whole plant inoculation enables the study of different components of partial resistance such as leaf chlorosis due to the infection as well as premature defoliation that is characteristic of this disease. Besides, to well understand the interaction between a host and its pathogen and proceed with a transcriptomic assay, it was necessary to describe the main steps of the infectious cycle on the parents of OW population (OB and RW). The initial objective was then to define the time points during the infection that would be sampled for the transcriptomic experiment on the whole plant assay. In order to guarantee enough infection on OB plants, I decided to increase the inoculum concentration compared to what had previously been done in my team (from 10^4 conidia per milliliter to 10^5 conidia per milliliter like seen in the literature).

In this context, surprising observations both macroscopically and microscopically were made on RW plants which led me to schedule further experiments to study this phenomenon in more detail. In addition, because of its ease of implementation, I decided to consider the detached leaf assay to further characterize the effect of the leaf age that was observed. To learn the technique from a team that has been using it for several years, a collaboration was initiated with the university of Hannover, and Professor Thomas Debener from my PhD comity kindly accepted to welcome me in his laboratory for a research mobility of three months founded by the Objectif Végétal - RFI. During my stay, I had access to their expertise in

fluorescence microscopy and in rose-*D. rosae* interaction as well as their rose genotypes to conduct more experiments to compare the responses of the partial resistant genotype RW to responses of genotypes known to carry specific resistance genes. Unfortunately, due to current pandemic, not all what was planned could be achieved and this is how the study presented in this chapter was born and the results shed light on a phenomenon that has not yet been investigated in rose: the effect of leaf age on partial resistance to black spot disease.

2. INTRODUCTION

Many studies have been carried out to better understand black spot disease on rose. Symptoms expressed in roses have been reported to differ according to different parameters such as environment, genotypes and isolate. Symptoms occurrence has been described around 10 days after inoculation in detached leaf assay (Franck 1896) and in whole plant (Wolf in 1912) under controlled environment. However, symptoms apparition in fields seem more variable and have been reported between 10 and 15 days' post infection (Dodge 1931, Aronescu 1934, Sanders 1966). Kuklinski (1980) carried out several experiments to investigate the effect of growing plants at different temperatures on the susceptibility of two genotypes 'Frensham' and 'Allgold'. Not only the growth conditions affected the susceptibility of the varieties he studied, but differences of reaction to infection were observed between the genotypes themselves when grown under different temperatures. In addition, Gachomo and Kotchoni (2010) reported differences in symptom apparition on the variety 'Frensham' between strains G1 and K1, with symptoms appearing at 9 and 7dpi, respectively. Beyond the symptom expression, the timing of the main steps in the pathogen development was also reported to differ in the literature. Germination was described to happen between nine hours and one-day post inoculation. Penetration of the host cuticle varied between nine hours and three days (Wolf 1912; Aronescu 1934; Knight 1975; Kuklinski 1980; Blechert and Debener 2005). Haustorium formation was reported as early as 15 hours by Aronescu (1934) and usually followed the penetration of cuticle by a penetration peg. Subcuticular hyphae were seen after 3dpi in some cases (Gachomo and Kotchoni 2010) and "radiating strands" of subcuticular hyphae were also described after 4dpi by Wolf (1912). The development of acervuli was also described with different timing between studies and seemed to take place between 5dpi and 10dpi (Knight and Wheeler 1977; Kuklinski 1980; Blechert and Debener 2005). Mature acervuli were observed after 8 up to 17 days' post-inoculation (Wolf 1912; Blechert and Debener 2005). These non-exhaustive examples show that studying rose-*D.rosae* pathosystem with different genotypes probably belonging to different species, with strains of different nature (monosporial or polysporial) and origins as well as under different environments can yield divergent results in symptom occurrence and in the timing of pathogen development in the leaves. Therefore, it is necessary to describe the pathogen life cycle in our conditions and for the rose genotypes selected.

Field resistance has been reported for genotypes from *R. wichurana* species in many studies (Black et al. 1994; Shupert 2006; Byrne et al. 2010; Dong 2014). Similarly, RW has been found resistant in different locations and over several years in our field assessments (see chapter 2 and Lopez Arias et al. 2020). However, many discrepancies can be observed in the literature about the resistance of *Rosa wichurana* sp. members. Indeed, authors have proposed different hypotheses on the mechanism of resistance in *R.*

wichurana species and do not seem to agree if the resistance is pre-penetration or post-penetration. On one hand, Reddy et al. in 1992 reported a failed germination on *Rosa roxburghii* and *Rosa wichurana* leaves with conidia that appeared collapsed and apparently dead after two days. They speculated that the germination was impeded because of inhibitors produced on the leaf surface conferring a resistance to both genotypes. On the other hand, several authors reported the existence of a post-penetration resistance since reduced fungal growth was observed under the cuticle (Palmer et al. 1966; Castledine et al. 1981; Wiggers et al. 1997). Recently, Blechert and Debener (2005) classified the interaction type found in *R. wichurana* as type 7, i.e. the fungus germinates, penetrates the cuticle and forms small and underdeveloped haustoria but no further development of fungal structures is reported. Finally, Debener et al. (1998) also reported the existence of an intraspecific variability in *R. wichurana* resistance as two accessions belonging to this same species were found to be either completely resistant or susceptible to five single conidial isolates of *Diplocarpon rosae*. There are several possible reasons for these discrepancies like limitation due to the microscopic techniques used, differences in isolates (nature, aggressiveness and composition) as well as differences in the plant material used (individuals representing *R. wichurana* species or type of leaves assessed). Before proceeding any further in the study of the genetic mechanisms underlying the partial resistance observed on *R. x wichurana*, it is crucial that we characterize the interaction between our genotype and *Diplocarpon rosae*.

Bioimaging has always played an important role in studying fungal biology and plant pathology and allows elucidation of fungal growth in host cells. Fluorescence microscopy complements the application of bright-field microscopy when studying plant-pathogen interactions (Dunst and Tomancak 2019) as specific staining methods enable the visualization of both pathogen structures and plant reactions. Aniline blue, for instance, has long been employed to stain callose deposition in plant tissues specially to detect pathogen-associated molecular pattern (PAMP)-induced papillae (Zavaliev and Epel 2015) and it also stains glucans found in fungal cell walls. Callose in papillae acts as a physical barrier that is supposed to retard invading pathogens and to contribute to plant innate immunity in early defense responses (Jones and Dangl 2006; Voigt and Somerville 2009; Ellinger et al. 2013). Papillae formation is believed to give time to the host to initiate subsequent defense reactions that require more time like gene activation and expression in hypersensitive responses, phytoalexins and pathogenesis-related protein production and export (Brown et al. 1998; Ellinger et al. 2013; Voigt 2014). It has also been demonstrated that callose can strongly support penetration resistance if deposited at a very early stage of the infection and in elevated amounts (Ellinger et al. 2013). In the rose-*Diplocarpon rosae* pathosystem, partial resistance can affect one or several components of the pathogen infectious cycle like spore germination, penetration, colonization, incubation period and sporulation (Xue and Davidson 1998). The resistance based on specific resistance genes (*R*-genes) like the *Rdr* genes can also arrest pathogen development at specific stages of its infectious cycle. However, no characterization of the interaction between *D. rosae* and rose genotypes carrying *Rdr* genes have been carried out so far. Indeed, in rose-*D. rosae* pathosystem, Blechert and Debener (2005) reported fluorescing papillae in 21 out the 33 wild species investigated and the presence of fluorescing papillae was often associated with fluorescing cells that were reported to be necrotic by the authors. All the compatible and incompatible interactions described by these authors yielded very different pathogen developments and plant reactions. We can, then, wonder what differences in pathogen

development and plant reactions exist between genotypes carrying *R*-genes and partial resistant ones like *Rosa wichurana*. The use of fluorescence microscopy with specific staining can help us to answer this question.

Given the importance of finding new more durable sources of resistance to black spot disease in rose, we decided to investigate the genetic mechanisms underlying the partial resistance observed in *Rosa wichurana* (RW). In the previous chapter, we conducted an evaluation in the field at a whole plant level in different progenies in which RW partial resistance segregated. However, to better dissect the genetic mechanisms underlying such resistance, it is crucial to carry out a detailed study of the interaction between the fungal pathogen *Diplocarpon rosae* and the partial resistant genotype *Rosa wichurana* used in this project as well as describe the pathogen life cycle under our conditions using the susceptible parent of the OW population *Rosa chinensis* 'Old Blush'. In addition, a comparative study with another susceptible genotype 'Pariser Charm®' as well as four genotypes exhibiting complete resistance to certain strains and carrying *R*-genes (*Rdr1*, *Rdr3* and *Rdr4*) was carried out. Artificial inoculation on whole plants and detached leaves allowed us to undertake a detailed study of RW resistance at macroscopic and microscopic levels as well as to investigate the importance of leaf age in partial resistance to black spot disease. These results unveiled the mechanism behind the observed field resistance of our genotype belonging to *R. wichurana* species and helped us to select the material and design the transcriptomic experiment, presented in the next chapter.

3. MATERIALS AND METHODS

3.1. EFFECTS OF PUTATIVE QTLs

3.1.1. ROSE GENOTYPES STUDIED

The choice of genotypes was made according to their different type of resistance (field, greenhouse and laboratory) as well as the knowledge of resistance genes they carry (if available). The following genotypes were then used to study different interactions between rose and *D. rosae* since they were described in the literature and in previous experiments to have different degrees of resistance and susceptibility to black spot disease:

- *Rosa chinensis* 'Old Blush', called OB, was used because it has been described to be susceptible in our field assessments (see chapter 2, section 2.7) as well as in whole plant assays to a wide range of strains (not published results from Belarosa project). OB is also the female parent of one of the populations (OW population) used in chapter 2 to detect QTL linked to partial disease resistance.
- The hybrid tea rose Pariser Charm®, called PC, was used as susceptible control in the detached leaf assay. PC has been described as a susceptible genotype to many strains in several publications (Debener et al. 1998; Blechert and Debener 2005; Whitaker and Hokanson 2009).
- A hybrid of *Rosa wichurana*, called RW, was used as a partial resistant genotype and it has been described to be resistant in field assessments (see chapter 2, section 2.7), whole plant assays to a wide range of strains (not published results from Belarosa project) and other genotypes of *R.*

wichurana species were also tested using detached leaf assays (Castledine et al. 1981; Reddy et al. 1992; Wiggers et al. 1997; Debener et al. 1998; Blechert and Debener 2005).

- The hybrid shrub cv ‘George Vancouver’, called GV, was used because it presents a resistance to nine of the 13 races described by Zlesak et al. (2020) and it carries *Rdr3* resistance gene that gives the resistance to race 8 (Whitaker et al. 2010a; Zlesak et al. 2015; Zurn et al. 2020).
- The climbing rose ‘Brite EyesTM’ (cv ‘RADbrite’), called BE, was used because it exhibited resistance to three races (3, 8 and 9) in a detached leaf assay (Zlesak et al. 2010) and was later found to be resistant to 12 races out of the 13 described so far. BE was susceptible to isolate BEP from North America that represents race 12. It carries *Rdr4* resistance gene (Zurn et al. 2018).
- The stable transgenic clone PC::*muRdr1A* (PC background transformed with *muRdr1A*, the active *Rdr1* gene from the cluster), described to display similar interaction pattern that the donor genotype of *Rdr1*, was used in the detached leaf assay (Menz et al. 2018).
- *Rosa majalis* sp., called RM, was used in the detached leaf assay. It has been described to be completely resistant (Schulz et al. 2009) and its interaction type with DortE4 according to Blechert and Debener (2005) is 8, i.e. no penetration observed and lack of fungal structure beneath the cuticle.

3.1.2. FUNGAL STRAIN CHOSEN

The pathogen used was *Diplocarpon rosae* Wolf. A preliminary test was carried out (and will not be developed here) to choose the strain that was used for the inoculations. Differences of aggressiveness of three monoconidial strains (DiFRA18, DiFRA67 and DiFRA33) tested at 100,000c/ml (conidia per milliliter) were observed and confirmed the results obtained during the Belarosa project that had used a lower concentration (10,000c/ml). DiFRA67 belongs to the French collection of *Diplocarpon rosae* strains that counts 77 strains with 50 strains sampled from Eurasian cultivated roses and 27 from wild rose species in Kazakhstan (Soufflet-Freslon et al. 2019). DiFRA-67 was sampled from a cultivated rose variety in 2014 in Saint-Lambert-la-Potherie, France. It was found to be intermediate in terms of aggressiveness and gave the most contrasted results between the susceptible genotype OB and the partial resistant RW. It was, therefore, chosen for the subsequent experiments.

3.2. PATHOGEN PROPAGATION, STORAGE AND INOCULUM PREPARATION

The strain DiFRA67 was propagated on cellophane sheets overlaid onto malt agar (10 g/L chromomalt, 15 g/L agar). Petri dishes with the media and the cellophane sheets were incubated at 17-18°C with 16hr of light per day. Between seven and 10 days were necessary to obtain a good sporulation (checked under a binocular magnifier). Before the spores started germinating and producing hyphae, the cellophane sheets were removed from the media and dried during 24 to 96hr under a laminar flow hood in an empty sterile Petri dish. The cellophane sheets can then be stored at -20°C Marolleau et al. (2020). This technique enables the production of a high amount of inoculum because the cellophanes contain a strong

concentration of conidia, which is particularly important when inoculating whole plants. Inoculum was produced by rehydrating the cellophane sheets with distilled water. To ensure the maximum collection of conidia from the cellophane sheets, the mix of cellophanes and water was well agitated. The obtained solution was then filtered to remove the maximum hyphal structures and then the concentration was adjusted to 10^5 conidia per ml. For this strain, on average, one cellophane sheet in 10ml of deionized water can yield a concentration of $4 \cdot 10^5$ conidia per ml.

3.3. PLANT CULTIVATION

3.3.1. CUTTINGS FOR WHOLE PLANT ASSAY

Cuttings for the whole plant assay were cultivated at IRHS (PHENOTIC platform) in Beaucouzé, France. Cuttings were sampled on mother plants of OB and RW grown in the greenhouse. They were placed at 20-22°C under a plastic cover with mist to ensure saturated relative humidity during their rooting. Four to five weeks were required to obtain good rooting, and the rooted cuttings were then potted in 10.5cm pots using Klasmann® RHP 15 substrate. Rooted cuttings were pruned to homogenize the growth after two weeks of cultivation in the greenhouse and, then, were left to grow for four to five weeks before using them in inoculation assay. The plants were isolated to prevent development of other diseases and pest attacks. Fertilization was performed with the sub-irrigation (NPK balance of the fertilization was 1-1-2 and conductivity 0.5/0.8 EC) and irrigation was activated twice a day. Ten days before the inoculation assay, Nimrod® fungicide was applied to prevent powdery mildew infection during the assay.

3.3.2. CUTTINGS FOR DETACHED LEAF ASSAY

Cuttings for detached leaf assay (DLA) were cultivated in a growth chamber at Prof. Debener's lab in Hannover, Germany, as the DLA was performed in his lab. Clones of the genotypes OB, PC, GV, BE and PC::*muRdr1A* were obtained from sanitized rooted shoots grown *in vitro*. The *in vitro* plants were placed in rooting media for four to six weeks and then transferred into 7cm pots for adaptation (4-6 weeks) in a climate cabinet. The adapted plants were then potted in 14cm pots and were fertilized with the granulated fertilizer Floranid®^{Twin} from Compo expert added in the substrate ('Einheitserde' basic soil) during potting. Plants were watered three times a week and were kept in semi-controlled conditions with 16hr light at 23°C and 8hr dark at 21°C with a relative humidity varying from 30 to 80% (not controlled). After four to six weeks, plants were ready for leaf harvest for DLA.

Cuttings from our mother plants of OB and RW in France were sent to Germany for greenhouse cultivation before my arrival. Plants were grown in semi-controlled conditions and isolated from other plants. Plants were kept in the greenhouse under 18°C with 16hr light and 80% relative humidity. Constant mist was used to avoid powdery mildew development as well as pest attacks. Additional pest and disease control (mostly Cumulus fungicide) was applied when necessary but was avoided two weeks before I started using the leaves for DLA.

3.4. INOCULATION PROCEDURE

3.4.1. WHOLE PLANT INOCULATION

4.1.1.1. PATHOGEN LIFE CYCLE SETTING IN WHOLE PLANT ASSAY

Inoculation of DiFRA67 was performed on three months old cuttings in the greenhouse with 50ml of inoculum at 10^5 conidia/ml using a water mister (see Figure 30C). The experimental design was composed of two randomized blocks (see Figure 30A): one block for the strain application and one for the water-control (or Mock). Six plants were used per genotype and per strain/control and, in each block, genotypes were randomized. After inoculation, the plants were kept 72hr under a plastic film with 100% of humidity to ensure optimal conditions for *Diplocarpon rosae* germination (see Figure 30B). Air humidity was maintained at 80% using a fogging system and air temperature was set to 20 °C during the day and 18 °C at night like described in Marolleau et al.(2020). Sampling and disease assessment will be detailed in the following sections.

4.1.1.2. LEAF AGE EFFECT ASSAY

The experimental design consisted of fully randomized block design with three independent inoculations (replicates) performed with one day of interval and two conditions (Inoculated and Mock). Twenty clones per genotype were used for the inoculated condition and 16 clones for the mock. Plastic rings were positioned in each shoot at the first fully expanded leaf (or penultimate leaf) a day before the inoculation to mark off the leaves that received the inoculum/water (inoculated zone). Per replicate, 300ml of inoculum were prepared from cellophanes sheets like explained in section 3.2). After inoculation, plants were kept under a plastic film for 72hr like previously explained (see Figure 30). After that, the plastic film was removed and the plants were kept at 22°C with 80% of relative humidity.



Figure 30: Whole plant assay (A to E) and detached leaf assay (F-G) illustrations, picture credits: D. C. Lopez Arias (2019-2020)

A: Plant organization in randomized blocks before inoculation; **B:** Inoculated zone delimitation with colored rings before inoculation; **C:** Water mister pump used for whole plant inoculations; **D:** Plastic film covering the inoculated plants and mock during 72hr; **E:** OB plants at 18 days post-inoculation (dpi); **F:** Drops on RW leaves and sampling after 2dpi; **G:** Black spots on OB at 15dpi for DLA.

3.4.2. DETACHED LEAF INOCULATION

For the detached leaf assay, the first fully expanded leaves were sampled on the plants available in the growth chamber. Four leaves per genotype were used for each independent inoculation and three leaves were treated with water. Leaves were prepared for the inoculation by gently rubbing the leaflets surface with a wet paper towel (distilled water) to remove the leaf wax so the drops can adhere better. Three leaves were placed on a wet towel (15ml of tap water) in one box and were used for the inoculation with the DiFRA-67 as described by Debener et al. (1998). The inoculum was prepared (re-suspended) from cellophane sheets as well but only 25ml of inoculum were needed. Four to six drops of 10µl of inoculum were placed on each adaxial leaflet surface (see Figure 30F) of three leaves for each genotype. The fourth leaf was used as a mock, and distilled water droplets were placed on the leaf surface. Three independent inoculations were performed with one-week interval.

3.5. MACROSCOPIC DISEASE ASSESSMENT

For infection cycle investigation on whole plant assays, five inoculated plants and three mocks were assessed 28 days after inoculation using the rating scale described in chapter 2. At 16 days' post-inoculation (dpi), plants were thoroughly assessed by grading different components of partial resistance described by Xue and Davidson (1998). In the inoculated zone, two groups of leaves were considered according to their position on the shoot: group 1 consisted of the last three leaves at the tip of the shoot (these younger leaves were softer with a smaller leaf area and light green colour) and group 2 was composed of the first three leaves at the base of the shoot (these older leaves were harder, well developed and with a dark green colour). The aspects observed were the following:

- number of leaves per shoot,
- absolute leaf rank,
- number of leaflets per leaf,
- number of infected leaflets per leaf,
- LAS per infected leaflet (leaflet area with black spot symptoms with five classes of percentage comprising 1 = 0-10%, 2 = 10-25%, 3 = 25-50%, 4 = 50-75% and 5 = 75-100%),
- LL per leaf (largest lesion length in mm),
- acervuli (presence/absence),
- NC (number of leaflets with chlorosis),
- NF (number of fallen leaflets),
- number of reacting leaflets (with brown spots),
- number of brown spots per leaflet,
- maximum length of largest brown spot (mm).

Brown spots correspond to the reaction observed in RW inoculated leaves (see the white arrows in Figure 31) and black spots to either the “normal” spots observed in a compatible interaction (see [section 4.3.1](#) in chapter 1 and Figure 31A-B) or the small black spots with a star-like shape observed in RW (see the red arrows in Figure 31C).

For the detached leaf assay, a close investigation of the inoculated zones was carried out by taking pictures of the zone under a stereomicroscope (reference: Carl Zeiss Stemi 2000-C with an AxioCam MRc Zeiss camera) for each leaf at 0.65x, 2x and 5x magnification for all seven genotypes tested at 9dpi. Leaves were checked every day to determine the first day of symptom appearance for each genotype at bare eye. The presence of mature (acervuli releasing conidia) and non-mature acervuli was assessed with the pictures as well as the presence of brown spots to assess resistance (no acervuli observed) or susceptibility for each genotype. When no symptoms were observed at 9dpi, an additional observation was made at 23dpi to check whether or not further symptoms with or without acervuli were later developed.

3.6. MICROSCOPIC INVESTIGATIONS

3.6.1. MICROSCOPIC OBSERVATION OF INFECTED LEAVES FROM WHOLE PLANT ASSAY: SAMPLE PREPARATION AND ANILINE BLUE STAINING

To study the life cycle of *Diplocarpon rosae* on whole plant using a moderate aggressive strain (DiFRA67), three leaflets per plant were sampled at 12hpi (hours post-inoculation), 1dpi (day post-inoculation), 2dpi, 3dpi, 7dpi, 9dpi and 15dpi. The different time points of sampling during *D. rosae* infectious cycle were chosen according to the literature (Aronescu 1934; Saunders 1967; Wiggers et al. 1997; Carlson-Nilsson and Davidson 2000; Gachomo 2005; Blechert and Debener 2005; Gachomo et al. 2006; Gachomo and Kotchoni 2007). The sampling was carried out on OB as this genotype has been shown to be susceptible to black spot disease. Samples were placed in KOH at 1M, then directly discolored in the autoclave for 15min at 120°C and 1-2bar, rinsed twice in distilled water and stained with a solution of 0.05% aniline blue + 1M K₂HPO₄ for one hour in the dark (Hood and Shew 1996; Blechert and Debener 2005). Each whole leaflet was washed two times with distilled water and placed on slide and observed under an epifluorescence microscope (reference: Olympus BH2 fluorescence) using a U excitation filter cube unit (BH2-DMU; Olympus) with an excitation filter (UG-1; Olympus) for 4',6-diamidino-2-phenylindole (DAPI) observations. The characteristics of the DAPI filter used are summarized in Table 11. Observation with this filter will be referred to as “DAPI-BH2” in this manuscript. Images were captured using a camera Q-Imaging, MicroPublisher 5.0 RTV (10 bits). Aniline blue fluorochrome binds with various glucans and plant polysaccharides so it was used to color callose in plant as well as glucans in fungal cell wall (Smith and McCully 1978; Hood and Shew 1996; Blechert and Debener 2005; Bhadauria et al. 2010). With this staining both pathogen and host resistance reactions can be observed.

3.6.2. MICROSCOPIC OBSERVATION OF INFECTED LEAVES FROM DETACHED LEAF ASSAY: SAMPLE PREPARATION AND DOUBLE STAINING

To study differential host response to DiFRA67, ten discs per leaf were sampled on the seven genotypes (OB, RW, GV, BE, PC::*muRdr1A*, RM and PC) for each independent replication at 9dpi. When genotypes did not develop symptoms at 9dpi, additional sampling at 23dpi was carried out to investigate if further fungal growth was observed and if acervuli were produced with a delay.

The sampled leaf discs were stored in a fixing solution (25% acetic acid + 75% EtOH absolute). To help the samples to clear, the fixing solution was changed every day until the tissues were white. When cleared, four out of the ten discs were randomly chosen and then washed two times with distilled water, and KOH at 1M was added. The samples were cooked at 60°C in a water bath for 30 min to 1 h according to the leaf

thickness. Autoclaving was not used because the young leaves were too fragile and leaf discs were very difficult to handle after autoclaving them. After material destaining with KOH, samples were washed two times with distilled water and stained in the dark for 24 h at room temperature (RT) using a solution of wheat germ agglutinin (WGA)-Alexa Fluor™ 488 with PBS-Tween buffer (20µg/ml i.e. 1:200 dilution of stock solution). WGA-Alexa Fluor™ 488 binds to N-acetylglucosaminy residues that are the monomers composing chitin found in fungal cell walls and was therefore used to stain *D. rosae* cell walls. The samples were again washed two times with distilled water and stained in the dark for 1 h at RT using a solution of 0.05% aniline blue + 1M K₂HPO₄. After that, the discs were washed two times with distilled water and placed on a slide to be observed using two different epifluorescence microscopes: Olympus BH2 and the microscope Zeiss Axio Imager Z2. Images with the microscope Zeiss Axio Imager Z2 were captured using a camera Hamamatsu, Orca Flash 4.0. Two GFP filters specific to each machine but with the same characteristics were used to visualize the fluorochrome WGA-Alexa Fluor™ 488, and two other DAPI filters also specific to each machine with different characteristics were used to visualize the fluorochrome aniline blue (See Table 11).

Table 11: Filter characteristics for each fluorescence microscope used

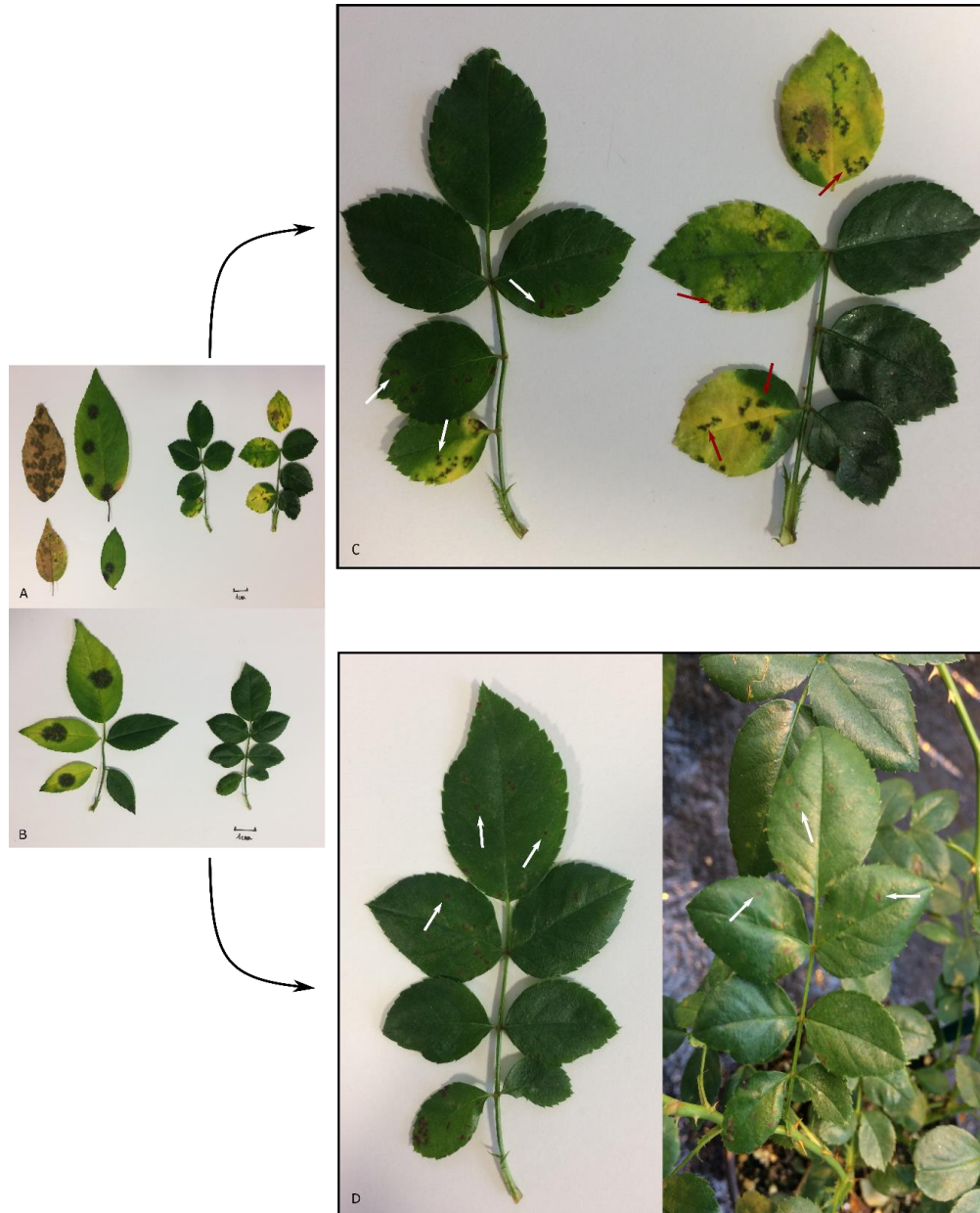
	Excitation filter	Dichromatic mirror	Emission filter
DAPI-BH2	330-385nm	400nm	LP420 (long pass)
DAPI-Axio	365nm	395nm	420-470nm
GFP-BH2/GFP-Axio	450-490nm	495nm	500-550nm

3.7. IMAGE PROCESSING AND STATISTICAL ANALYSES

No image processing other than scale bar adding was done for the fluorescence images obtained with the microscope Olympus BH2. For these images, manual Z-stack was done to visualize several layers of the fungal structures inside the rose leaves. Two pictures of the same zone and the same Z value were taken with both filters successively when the double staining was used. The microscope Zeiss Axio Imager Z2 was used to produce automated image acquisitions on a determined Z range that was chosen according to the structure observed (Z-stack image) for each channel (filter DAPI-Axio or GFP-Axio) separately. A Z-stack image contained between 10 and 50 single images that were processed using the iterative deconvolution algorithm provided by the software ZEN® 3.2 (with default parameters) and the Nearest-Neighbors method was selected as well as the Extended Depth of Focus processing with the maximum projection method. The signals obtained from both filters (GFP-Axio and DAPI-Axio) were then merged to co-localize the pathogen structures and the plant responses with callose deposition/production. The fluorescence profile of both signals was determined along a line to visualize the co-localization of the signals. Finally, the figures presented in this manuscript were produced using Inkscape software (version 1.0).

Statistical analyses were carried out with Rstudio interface (version 1.3.959, <https://www.rstudio.com/>) of R software (<https://www.r-project.org/>) version 3.6.3 (2019-03-11). Wilcoxon and Kruskal-Wallis tests were used to test significant differences between treatments for each leaf group for each genotype separately and significant differences between replicates for inoculated plants, respectively. Using the data obtained on 15dpi scoring, and for each leaf position, a proportion of the leaf that appeared

infected (number of infected leaflets on the total number of leaflets per leaf at that shoot position) was calculated and an average of these proportions was applied for each leaf group. The same procedure was done with the proportion of reacting leaflets in a leaf (number of leaflets with brown spots on total number of leaflets per leaf). Plots were generated using the packages *ggplot2*, *ggpubr*, *grid* and *wesanderson*.



**Figure 31: Different types of spots observed in ‘Old Blush’ (OB) and Rosa wichurana (RW) infected leaves with *Diplocarpon rosae* from whole plant inoculation in the greenhouse at 28dpi
photo credits: D. C. Lopez Arias (2018)**

A: Black spots with fringed margin on OB on the left (single leaflets), and brown spots on RW associated or not with small black spots with star-like shape and sometimes chlorosis can be observed on the right (whole leaves); **B:** Black spots with fringed margin on OB on the left, and on the right, RW infected leaf exhibiting small brown spots with no chlorosis; **C:** Zoom on RW leaves showing the brown spots with white arrows and the brown spots associated with star-like shape black spot symptoms with red arrows; **D:** Zoom on RW leaves showing the brown spots with white arrows and no black spot or chlorosis is observed.

4. RESULTS

4.1. BLACK SPOT DISEASE (BSD) EVALUATION ON WHOLE PLANT

Each plant of OB and RW genotypes was scored at 28dpi using the evaluation scale described in chapter 2 (see section 2.6.2) for each independent inoculation. No significant differences were observed between the replicates A, B and C for OB and for RW (See Figure 32B). Mock plants (NI in blue) did not exhibit any black spot symptoms. OB plants were scored on average 4.7 while RW plants were scored on average 1.1 (See Figure 32A). On one hand, the BSD scores observed for OB plants were similar to the ones assessed in the field (4.7 in the fields, see section 2.7.1 in chapter 2). As OB plants were found susceptible in both field and greenhouse assessments, we decided to describe the infectious cycle of *Diplocarpon rosae* on OB leaves. On the other hand, RW plants had a higher score in greenhouse conditions than in the fields with 1.1 instead of 0.5 (see section 2.7.1 in chapter 2), and in some cases, RW plants exhibited more than 25% of infected leaves (score 2) which was rarely observed in fields. Then, RW plants seem to exhibit a lower resistance overall when challenged with an artificial inoculation of DiFRA-67 in the greenhouse.

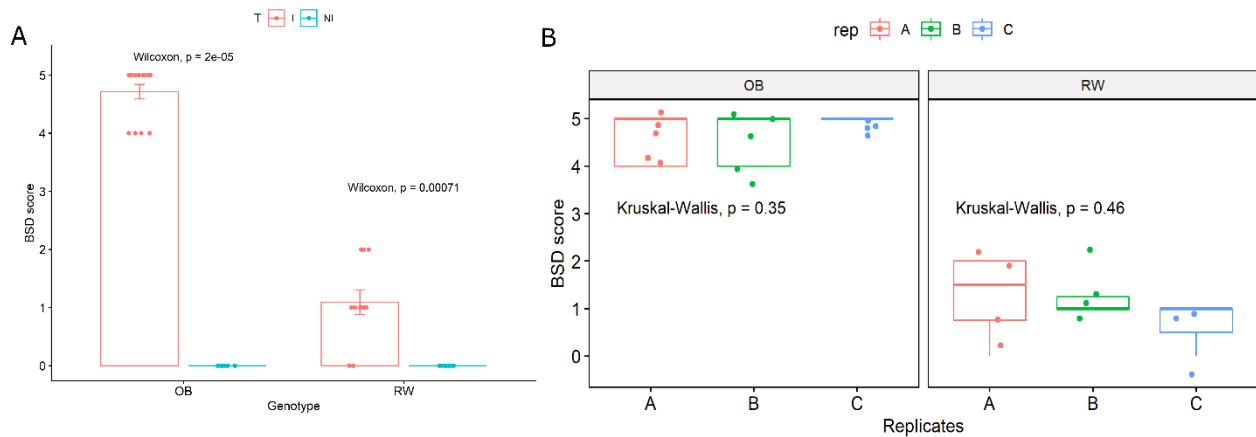


Figure 32: Black spot disease (BSD) scores on whole plant inoculated with DiFRA67 strain of *D. rosae*

A: Average BSD scores for OB and RW plants inoculated with DiFRA67 (I) or sprayed with water (mock, NI); **B:** Average BSD scores for OB and RW plants for each replicate (independent inoculations, from A to C). Significant differences were assessed using Wilcoxon non-parametric test (A) and Kruskal-Wallis non-parametric test (B). The package *ggpubr* (A) and the package *ggplot2* (B) were used to plot the results.

4.2. COMPATIBLE INTERACTION ON 'OLD BLUSH' LEAVES

4.2.1. DIPLOCARPON ROSAE INFECTIOUS CYCLE ON 'OLD BLUSH' (OB)

The purpose of this section is 1) to describe the main steps of *Diplocarpon rosae* growth cycle in our conditions for whole plant assay and 2) to determine the time points for the transcriptomic assay. The infectious cycle was described on the susceptible genotype OB. Disease symptoms on whole plants of OB inoculated with DiFR-A67 were first observed at 9dpi and well developed symptoms with visible mature acervuli were observed at 15dpi. At 15dpi, chlorosis was already observed on infected leaves and the first leaves started falling. Almost all the infected leaves were dropped by 28dpi.

Non germinated two-celled conidia were observed on OB leaves at 12hpi and 1dpi like illustrated in Figure 33A. Some germinated conidia were observed at 2dpi but no sign of cuticle penetration was assessed. At 3dpi, a brown ring was observed at the site of penetration either directly under the conidia

or at the surface of the appressoria (see [Pp] Figure 33B-C). Gachomo (2005) described these rings to be around the penetration pore from which further fungal growth took place under the cuticle. We can therefore say that the penetration happened at 3dpi on OB. The infection vesicle from which further fungal structures were developed could be observed at 3dpi underneath the penetration pore (brown ring, see [lv] in Figure 33B).

Then, long distance hyphae as well as short distance hyphae were observed with haustorium-like structures at 7dpi (see Figure 33D-E). Long distance hyphae [LdH] (subcuticular hyphae) were observed under the cuticle and above the epidermal cells (see Figure 33D) whereas short distance hyphae like intercellular hyphae ([IeH] in Figure 33E) grew into lower level of the leaf tissue (between epidermal cells towards the palisade parenchyma). Long distance hyphae grew away from the penetrating point and the first haustorial structures were observed right underneath the penetration point (see [LdH] in Supplementary figure 25C and [Ha] in Supplementary figure 25D). Fluorescing cells were observed at the cell penetration point right where the haustoria were formed but not where the long distance hyphae were growing (see [Fl-c] and [Ha] in Supplementary figure 25B). Callose depositions around the haustorium-like structures were also observed, which sometimes made difficult the observation of the fungal hyphae because of the brightness of callose depositions (see [Ca] Figure 33E and Supplementary figure 25B). Well-developed haustoria were observed in epidermal cells directly from the long distance hyphae (subcuticular mycelia) at 7dpi with an enlargement of the hyphal cell to form the penetrating hypha just before the host cell invasion (see [e] in Supplementary figure 25A). Subsequently, the penetration hyphae developed into haustoria by invaginating the host cell wall (Gachomo 2005). In response to that, the plant deposited callose around the invading structures (see [Ca] in Supplementary figure 25B and in Figure 33E). Gachomo (2005) observed this callose deposition around the hyphae penetrating the host cell and described a thick callose deposition on the inner side of the cell wall just below the invasion point. In susceptible cases, the haustoria were capable of growing through the callose deposition and expanded into the haustorial body with a bottle shape (see [Ha] in Figure 33I and Supplementary figure 25B). The callose deposition remained around the haustorial neck forming a collar surrounding it but was not found around the haustorial body (see [Ca] in Supplementary figure 25B-D and in Figure 33E). A granular texture could be described inside the fluorescing cells and it became brighter and smoother around/near a fungal structure (see Supplementary figure 25D-E).

With a closer look, vesicles carrying callose could be observed in epidermal cells neighboring the ones that were invaded by the fungus (see [CaV] in Supplementary figure 25A), and well defined callose depositions could be observed around invading fungal structures (here haustoria, see [Ha] and [Ca] in Supplementary figure 25B). The extent of the fungal network under the cuticle was hard to assess with only the aniline blue staining, since callose depositions appeared brighter than the glucans in the fungal cell wall. However, the largest length of the reacting area (with bright callose depositions) at 7dpi was around 0.77mm (see Supplementary figure 26A-B) while at 9dpi, it was around 1.6mm (see Supplementary figure 26C-D).

The fungal network at 9dpi was much more complex (reached lower levels of the leaf tissues) and extended (see Supplementary figure 26E) than at 7dpi. The spots at this time could reach 2mm of diameter

and were mostly star-like shaped. At the center of the irradiating hyphal network, small size acervuli could be observed (see Supplementary figure 26E). Looking up closer, the acervuli were under development either with finger-like projections that grew in a radial pattern from the long distance hyphae building the acervulus base stroma (see Figure 33G) or with conidia being produced above the acervulus base stroma, slowly forming a dome under the cuticle (see Figure 33F). No mature acervuli ripping the cuticle were observed at 9dpi. Again, collar callose deposition around the haustorial neck was observed (see [Ca] in Supplementary figure 25A-B) but a more developed short distance hyphae network could be observed with intercellular hyphae further colonizing the leaf mesophyll. Some intracellular hyphae could also be observed at this point (see [IaH] in Supplementary figure 25A).

Finally, at 15dpi, the fungal network was extensive (see Supplementary figure 26E) and around the penetration point, the secondary fungal hyphae were observed in a dense grid (see Figure 33J-K and Supplementary figure 27) accompanied by mature acervuli that ripped the host cuticle releasing newly produced conidia (see Figure 33H-I). The cuticle unfolded to release the content of the acervuli. Mature acervuli were found at the center of the infection site (near the penetration point) and new acervuli were produced further away (see Supplementary figure 26F). Fungal structures like intracellular hyphae were observed but with the present staining and microscopic view (for the top and through the cleared cells), it was difficult to assess in which type of cells they were found (see Supplementary figure 27). Gachomo (2005) found that intracellular hyphae mainly colonized epidermal cells and that very few intracellular hyphae were found in the palisade cells. Further intercellular hyphae developed to reach the palisade parenchyma (see Z6 to Z8 in Supplementary figure 27). At that point, the largest lesion length could reach 7mm in some cases.

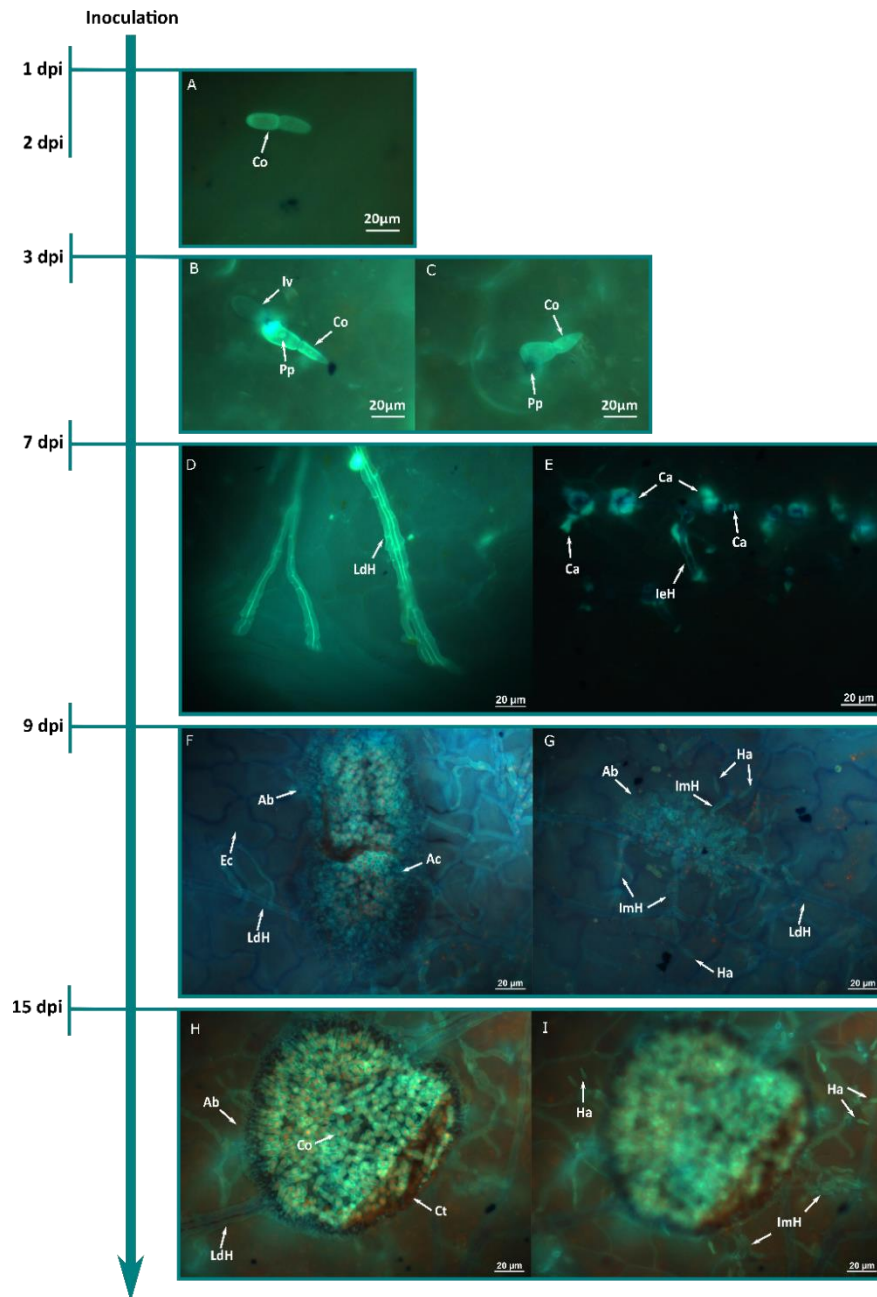


Figure 33: Fluorescent microscope photographs of *Diplocarpon rosae* infectious cycle on the susceptible genotype 'Old Blush'

Aniline blue staining was visualized with the DAPI-BH2 filter. **A:** A non-germinated conidium [Co] at 1dpi; **B:** A germinated conidium [Co] at 3dpi, no germ tube, penetration directly below the conidium with presence of a penetration pore [Pp] giving a brown ring and presence of an infection vesicle [Iv] under the cuticle right after the penetration point; **C:** Another germinated conidium at 3dpi, short germination tube and a direct penetration of the host cuticle (penetration pore or [Pp]) without a well-developed appressorium, **D:** Extremity of subcuticular hyphae (long distance hyphae or [LdH]) growing in a fascicle of parallel hyphae that divide into new branches (7dpi); **E:** Callose appositions [Ca] around fungal structures like haustoria and intercellular hyphae [IeH] growing from subcuticular hyphae (7dpi); **F:** Acervuli in development at 9dpi with a well formed acervulus base stroma [Ab] on top of the host epidermal cells [Ec] and a dome where conidiogenesis is happening [Ac], subcuticular hyphae [LdH] around the acervuli; **G:** Acervulus base stroma [Ab] formed from finger-like projections growing from subcuticular hyphae [LdH] at 9dpi, intramural hyphae [ImH] growing from the subcuticular hyphae (usually wider and on a slightly lower level on the Z-axis) and haustoria [Ha] produced from them in the host epidermal cells; **H-I:** Two levels on the Z-axis showing, in the first level, a mature acervulus [Ac] at 15dpi produced on top of long distance hyphae [LdH] from which the acervulus base stroma [Ab] was formed, the cuticle unfolds to release the acervulus content (two-cell conidia [Co]), and in lower levels, mature haustoria [Ha] growing from well-developed intramural hyphae [ImH].

4.2.2. COMPARISON WITH ANOTHER SUSCEPTIBLE GENOTYPE: THE HYBRID TEA ROSE ‘PARISER CHARM’ (PC)

PC was used as a susceptible control because it has already been used in detached leaf assay (DLA) in many studies and has been found to be susceptible to many fungal isolates from different races (Debener et al. 1998; Blechert and Debener 2005; Menz et al. 2018). Using DLA, at 9dpi, PC exhibited typical round black spot symptoms with a fringed margin while OB exhibited star-like symptoms (see Figure 34C-D). Clear branches irradiating from the penetration point could be observed on OB leaves and, interestingly, cells around the hyphae appeared brownish/black and seemed to collapse because they appeared at a different level than the green tissue neighboring the infected one (see [LdH] and [Cc] in Figure 34 and at 5x magnification in Figure 45). The cells collapsing in PC leaves extended between the long distance hyphae which gave the black center of PC symptoms at 9dpi (Figure 34D). The size of the symptoms was already important on PC (between 4 and 6mm) while this size of symptoms was only observed on OB leaves after 15 days. Acervuli could be observed at the center of the black spots developed on PC. Most of the acervuli were mature [Ac*] and were already ripped out the cuticle [Ct] releasing the newly produced conidia [Co*] (see [Ac*] and [Co*] in Figure 34J and [Ac*] in Figure 45). Unlike PC, mostly non-mature acervuli were observed at the center of the infection sites on OB leaves (Figure 34C Figure 45). No chlorosis was observed at 9dpi on OB and PC leaves.

Microscopically, the same fungal structures were observed on OB and PC leaves. Long distance hyphae [LdH] growing under the cuticle could be observed with intramural hyphae [ImH] growing from them. For both genotypes, haustorium production along the subcuticular hyphae was not regular and no haustorium was observed in portions or at the extremities of subcuticular hyphae [LdH*]. Combining both stainings (WGA-Alexa Fluor™ 488 for fungal cell wall staining and Aniline Blue for callose deposition), we were able to clearly distinguish the fungal structures and co-localize them with fluorescing cells (see Supplementary figure 28). Interestingly, the presence of long distance hyphae alone [LdH*] was not associated with fluorescing cells, which probably means that they do not activate a response that ultimately leads to fluorescing cells. However, as soon as the epidermal cell invasion started with the growth of haustoria in them, the cells reacted and appeared fluorescent (see Supplementary figure 28). In addition, we can hypothesize that the fluorescing cells around the long distance hyphae corresponded to the brown tissue that collapsed [Cc] around them when looking up close at a symptom. It is worth noticing that OB epidermal cells reacted less intensively than PC epidermal cells at this time point (see [Fl-c] in Figure 34G-H). Also, numerous haustoria with short intramural hyphae were observed on OB leaves (see [ImH] for OB in Figure 34) while *D. rosae* produced more and longer intramural hyphae in PC leaves (see [ImH] in Figure 34). This observation could explain that the area with brown cells around the subcuticular hyphae was wider on PC leaves than on OB leaves.

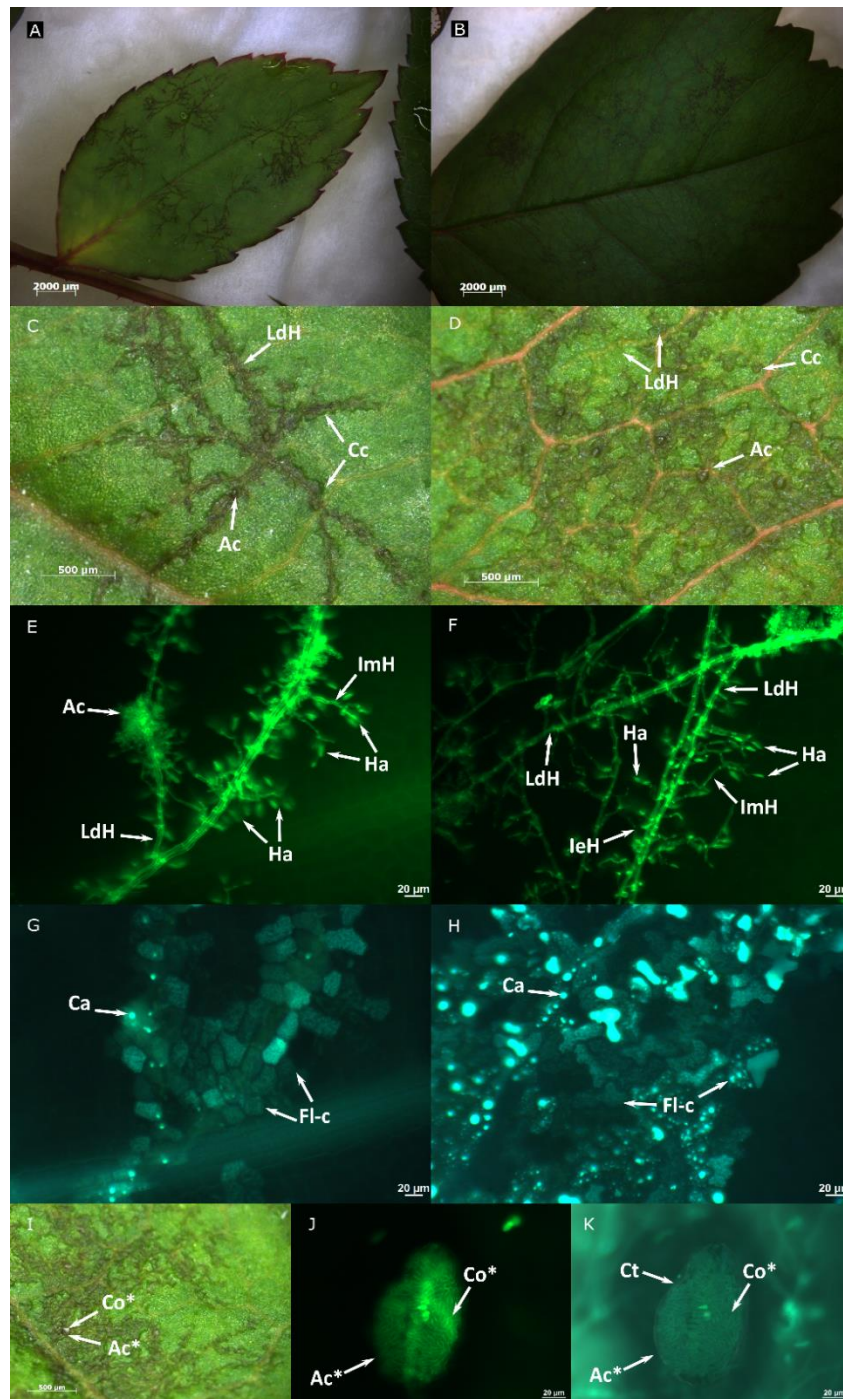


Figure 34: Multiscale comparison of *Diplocarpon rosae* infection in two susceptible genotypes ('Old Blush', OB and 'Pariser Charme', PC) at 9dpi

A: OB leaflet infected by DiFRA67 at 9dpi using the magnification 0.65x (leaf from the greenhouse); **B:** PC leaflet infected by DiFRA67 at 9dpi using the magnification 0.65x; **C-D:** Close up of OB (C) and PC (D) symptoms revealing subcuticular hyphae [LdH] and cells around them browning and collapsing [Cc]. The brown area around the hyphae on OB is smaller than for PC. **E-G and F-H:** Fluorescence microscopy of the same region with GFP filter (F-G) and DAPI filter (E-H) to visualize both fungal structures (long distance hyphae [LdH], intramural hyphae [ImH], intercellular hyphae [IeH] and haustoria [Ha]) and callose depositions for OB (E-G) and PC (F-H) leaves. **I-J-K:** Macroscopic view and fluorescence microscopy using a double staining of mature acervuli [Ac*] on PC leaf surface with conidia [Co*] release. On J, staining with aniline blue allows us to see the ripped cuticle [Ct] uncovering the acervuli content. Both non-mature [Ac] (C-D) and mature [Ac*] (I) acervuli can be observed in OB and PC but more mature acervuli whereas observed on PC leaves than on OB leaves.

We can then imagine that the area colonized by the fungus between the long distance hyphae growing radially from the penetration point was more important at 9dpi in PC leaves with longer secondary hyphae than in OB leaves. This can, therefore, explain that the symptoms at 9dpi on PC leaves appeared black and round with a full black center whereas symptoms on OB leaves had a star-like shape. However, later at 23dpi, OB symptoms were similar as the ones found on PC at 9dpi, which suggests that some resistance was implemented on OB leaves at the early stages of infection but was not efficient later as symptoms reached the same size as on PC leaves.

Moreover, when zooming on the fluorescent cells, two types of epidermal cells reacting to the infection can be described for both susceptible genotypes: the ones exhibited granular texture with what seemed to be callose vesicles [CaV] (see Figure 34) and others harbored well defined callose structures [Ca] (see Supplementary figure 29). By merging the visualization obtained with both filters from the Axio microscope, we were able to visualize the callose deposition around the haustorial neck and at the penetration point of the invaded epidermal cell wall forming a tube with a round base (see Figure 34).

4.3. DIPLOCARPON ROSAE DEVELOPMENT ON *ROSA WICHURANA*, A PARTIAL RESISTANT GENOTYPE

4.3.1. DESCRIPTION OF *R. WICHURANA*-*D. ROSAE* INTERACTION OVER TIME

The disease assessment on whole plants of RW was difficult, and interestingly, an evolution in the intensity of disease responses was observed along RW shoots. Indeed, the degree of infection varied between leaves at different levels in the shoot with either small black spot symptoms associated with brown HR-like spots (illustrated with the red arrows in Figure 31C or with the white arrows in Figure 34D) or no visible symptoms. In general, black spot symptoms appeared around 9dpi, but by 28dpi they were much smaller than for OB as they did not exceed 3mm. Chlorosis was observed in some of them at 28dpi and some leaves fell as well.

Microscopic observations were also made on RW genotype at different time points after the inoculation to assess whether or not the entry was delayed compared to the susceptible genotype OB. But when the samples were taken, we did not know about the differences in leaf reaction along the shoot and leaves were sampled randomly on OB and RW shoots. Therefore, after realizing that differences could be observed between leaves, we observed the samples critically and determined if differences in pathogen development were observed at the microscopic level as well. Overall, no delay on the conidia germination on RW leaves compared to the susceptible OB was observed since germinated conidia could be observed at 2dpi in all the leaves sampled (see Annex 3). Attempt of penetration was also observed at 3dpi on RW with a brown ring like for OB. Until 3dpi, the sampled leaves showed similar reactions and the fungus was found to germinate and some attempts of penetration were observed. After that time point, fungal growth in RW leaves was very variable and the observation of the later time points yielded inconsistent results from one leaf to another. Examination at 5dpi showed that, in the majority of leaves, the signs of penetration as well as a callose deposition around the penetration pore could be observed. However, some leaves exhibited further fungal growth under the cuticle at 5dpi (see Annex 3). At 6dpi, the presence of reduced fungal growth under the cuticle on RW was observed on several leaves but some others only presented germinated conidia that penetrated the cuticle and were associated with callose deposition.

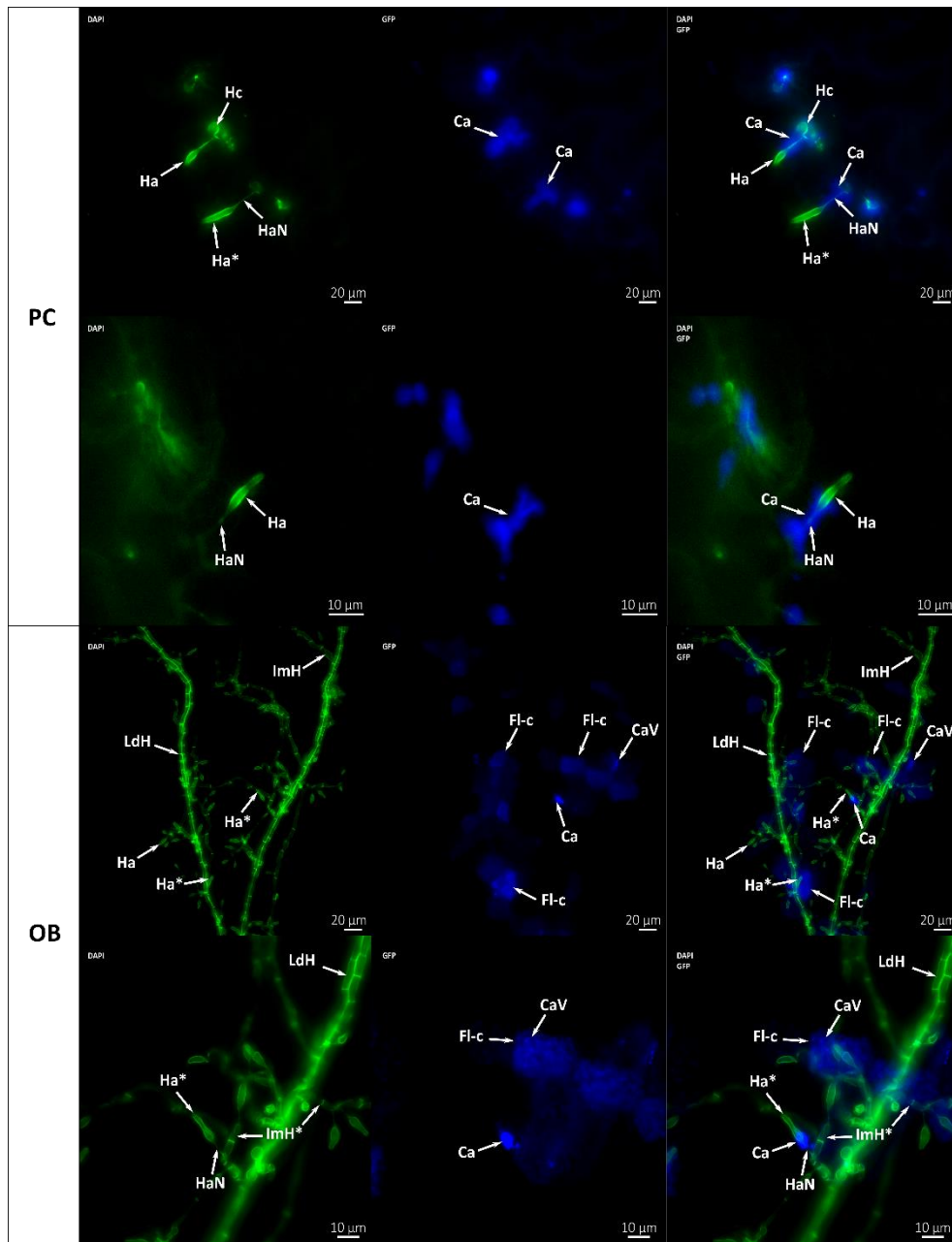


Figure 35: Callose vesicles in fluorescing cells and callose depositions on haustorial structures forming a collar around the haustorial neck on 'Old Blush' (OB) and 'Pariser Charm' (PC) young leaves infected by *D. rosae* at 9dpi

Fluorescence microscopy of OB and PC leaves inoculated with DiFRA67 at 9dpi and double stained with WGA Alexa Fluor™ 488 that binds to fungal cell wall and aniline blue that visualizes callose deposits. Two filters were used: GFP filter to visualize WGA Alexa Fluor™ 488 and DAPI filter to visualize the aniline blue. Pictures from these separated channels (filters) were merged to localize the callose deposition. Similar observations for OB and PC leaves inoculated with DiFRA67 were made. Long distance hyphae grew under the cuticle above the cell wall and short [ImH*] and long intramural hyphae [ImH] grew from them inside the cell wall towards the epidermal cell membrane. Callose deposition [Ca] formed a collar around the haustorial neck [HaN] and callose was also deposited on the epidermal cell wall at the penetration point forming the round base. Haustoria [Ha] under formation were capable of growing through the callose collar [Ca] and mature haustoria [Ha*] exhibited a bottle shape and measured between 10 and 20μm. The hyphal cell swelled before penetrating the epidermal cell [Hc] to form the haustorium. Fluorescence associated with callose was observed inside epidermal cells invaded by haustoria [Fl-c] and small vesicles of callose could be observed [CaV].

At 7dpi, two different situations were observed: (1) some leaves exhibited a fungal development that was arrested at the penetration point showing conidia associated with callose deposition around the penetration pore as well as fluorescing cells around the penetration site, and (2) other leaves presented further fungal growth under the cuticle with short subcuticular hyphae and haustoria close to the penetration point (see Annex 3). The invasion by haustoria of epidermal cells was associated with fluorescence like observed in susceptible cases, and callose deposition around the haustorial neck was also observed. At 9dpi, both situations were observed but longer subcuticular hyphae were found in the leaves exhibiting fungal growth. On the contrary, leaves with arrested fungal development like observed at 7dpi were also observed (see Annex 3). At 15dpi, in some leaves, the fungal network was more extended and reached lower levels of the mesophyll but remained less important than for OB. In other leaves, no fungal development under the cuticle was observed and instead brown areas were observed. At this point, no acervuli were formed on the leaves of RW that developed fungal structures (see Annex 3).

Differences between leaves at different levels of the shoot were then observed for RW partial resistant genotype but not for the susceptible genotype OB. Leaves at different levels presented different ages at the moment of inoculation. We observed that the younger the leaf was at the moment of inoculation (near the apex), the more BSD symptoms and brown spots typical of a HR-like response were observed. Leaves close to the base (that finished growing) did not exhibit any visible reactions (brown spots) or BSD symptoms. To study this phenomenon, we conducted an evaluation of different components of partial resistance described by Xue and Davidson (1998) on two groups of leaves on both genotypes: group 1 with leaves close to the apex (or “young” leaves) and group 2 with leaves close to the base of shoot (or “old” leaves). Macroscopic and microscopic observations were carried out for the two groups separately to confirm the observations made in this section.

4.3.2. LEAF AGE RELATED PARTIAL RESISTANCE TO DIPLOCARPON ROSAE IN ROSA WICHURANA GENOTYPE

4.1.1.3. INFLUENCE OF LEAF AGE ON THE COMPONENTS OF PARTIAL RESISTANCE

No major differences in several measured components were observed between young (group 1) and old (group 2) leaves of OB plants. Only the largest lesion length (LL) was significantly larger in young leaves than in old ones at 15dpi with in average 6.1mm and 4.6mm, respectively (see Figure 36C). In addition, OB leaves systematically presented acervuli associated with the black spots. However, more young leaves of OB presented acervuli (95.1% of them) while only 71.1 of the old leaves showed acervuli.

Unlike OB leaves, the leaves of RW reacted differently according to the age they were at the inoculation moment. Indeed, on one hand, old leaves did not exhibit any black spot symptoms but some exhibited brown spots (HR-like spots) that were considered as areas with symptoms (LAS) but they never exceeded 10% of the leaflet. An average of 16.5% of the leaf for group 2 (old) were found to exhibit these brown spots and were considered as “reacting leaflets” (see Figure 36A-D). But on the other hand, we observed that young leaves exhibited both types of spots (brown spots and black spots) and that brown spots could be found alone whereas black spots were always associated with a brown spot in the middle. Indeed, a significant difference in the percent of the leaf reacting to the infection was found between both

leaf groups: only 16.5% of the leaf reacted when the leaves were old at the inoculation moment (see group 2 in Figure 36D) while for younger leaves, 60% of the leaf exhibited both brown and black spots (see Figure 36A-D). The length of the largest (LL) black spot on young leaves was 1.74mm whereas the brown spot found associated with it did not exceed 0.9mm in average (see Figure 36C and figure Figure 37Q). The length of the largest brown spot was significantly different between leaf groups and the largest length measured on old leaves had an average of 0.2mm (figure Figure 37A). The number of brown spots found on young leaves was significantly higher than on old leaves with an average of five spots and two spots, respectively (see Figure 37B).

Two additional components were observed: the number of leaves with chlorosis and the number of fallen leaflets. Interestingly, at 15dpi no leaves were prematurely dropped on RW plants for both young and old leaves (see Figure 36F). However, a high amount of leaflets from young leaves (group 1) exhibited chlorosis, with four leaflets in average. The leaflets with chlorosis were often associated with the development of small black spots but no chlorosis was observed on leaves only exhibiting brown spots.

Finally, the absence or presence of acervuli at bare eye was assessed for each leaf group and rose genotype. The percentage of leaves with or without acervuli out of the total number of infected leaves assessed for each group and genotype was calculated and is reported on Figure 36G. Interestingly, no acervuli were visible at bare eye on all the leaves of RW that exhibited small black spot symptoms.

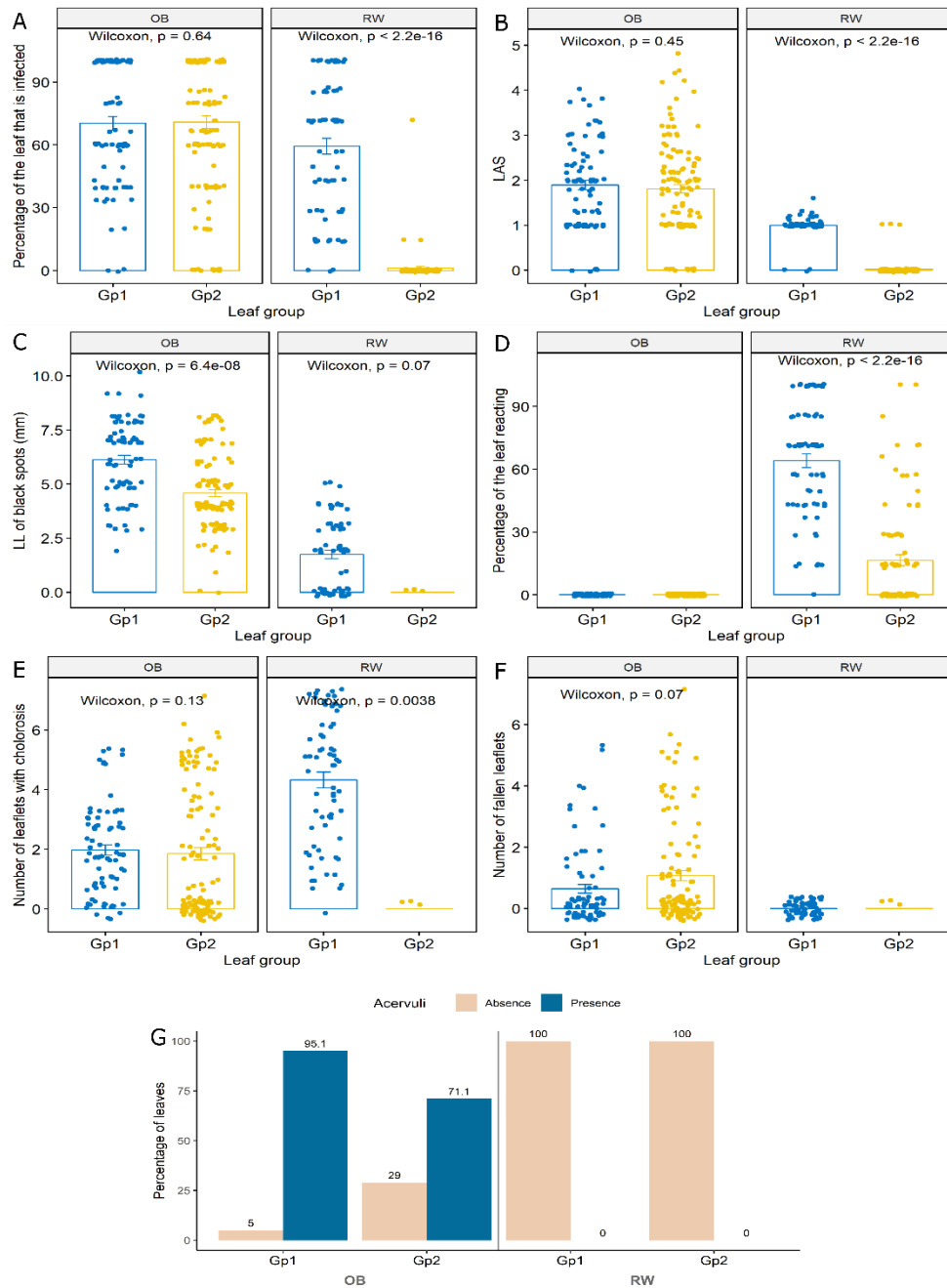


Figure 36: Components of partial resistance measured, at 15dpi, on leaves of different ages and inoculated with DiFRA67 in ‘Old Blush’ (OB) and *R. x wichurana* (RW) genotypes

RW is a partially resistant genotype and OB a susceptible genotype. Leaves were classified in two groups according to their position on the shoot: group 1 (Gp1) corresponds to young leaves at the apex of the shoot (four first leaves after the fully expanded one) and group 2 (Gp2) corresponds to old leaves on the shoot (four last leaves before the one entering in senescence).

A: Percentage of the leaf that was infected (number of leaflets infected out of the total number of leaflets per leaf) for each genotype and each leaf group; **B:** Mean of the leaflet area with symptoms (LAS) to all infected leaflets of a leaf; **C:** Largest lesion length of black spot symptoms in mm; **D:** Percentage of the leaf reacting to the infection, i.e. that exhibited brown spots (HR-like spots); **E:** Number of leaflets with chlorosis; **F:** Number of leaflets dropped prematurely; **G:** Percentage of leaves exhibiting or not acervuli at bare eye.

Significant differences were assessed using Wilcoxon non-parametric test and the package *ggpubr* was used to plot the results for A to H and the package *ggplot2* to plot the results for G.

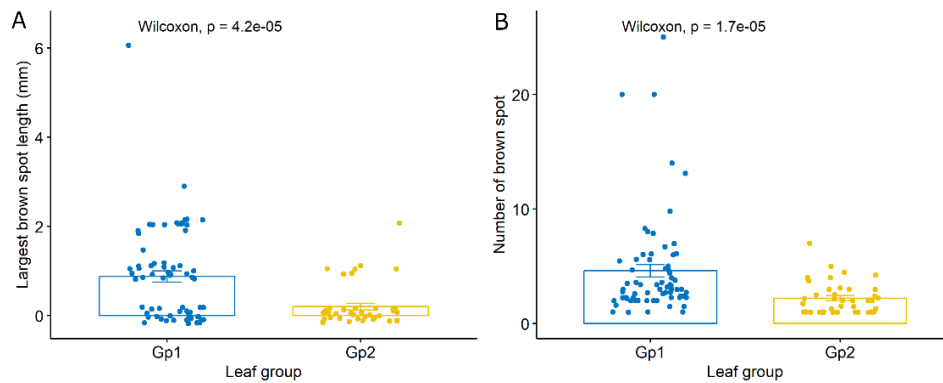


Figure 37: Characteristics of *R. x wichurana* (RW) reaction to DiFRA67 with brown spots according to the leaf age

Leaves were classified in two groups according to their position on the shoot: group 1 (Gp1) corresponds to young leaves at the apex of the shoot (four first leaves after the fully expanded one), and group 2 (Gp2) corresponds to old leaves on the shoot (four last leaves before the one entering in senescence). **A:** Length of the largest brown spot in mm; **B:** Number of brown spots per leaflet. Significant differences were assessed using Wilcoxon non-parametric test and the package *ggpubr* was used to plot the results.

4.1.1.4. DIFFERENT REACTION TYPES BETWEEN *R. X WICHURANA* AND *D. ROSAE* ACCORDING TO THE LEAF AGE

In order to investigate the different types of reaction observed on whole plants inoculated with DiFRA67, we conducted a multiscale investigation on detached leaves of RW with different ages (either young and still growing or old and fully developed) at 9dpi. Similar study was carried out on OB leaves but, as the differences between young and old leaves were limited, only the results for RW genotype will be presented in this chapter. For more information about the results found for OB genotype, please refer to the [Annex 4](#).

The same observations as the whole plant assay were made on RW detached leaves inoculated with DiFRA67. On one hand, old leaves (group 2) did not exhibit any visible symptom at bare eye (see Figure 38B-C), and very small brown spots, which appeared to be like a hypersensitivity reaction to the infection [HR], could be observed at a stronger magnification but the size did not exceed 0.5mm (see Figure 38E-H-F-I). On the other hand, young leaves (group 1) exhibited larger brown spots (HR-like spots) visible at bare eye (see Figure 38A). Looking closer, the HR-like symptoms on young leaves were limited to the infection sites and single spots never exceeded 1mm but sometimes several spots merged forming longer brown spots (Figure 38I-J). At this stage (9dpi), only brown spots were observed.

No fungal structure could be observed on the small brown spots of old leaves (group 2) whereas the brown spots of young leaves (group 1) could measure up to 3mm and long distance hyphae [LdH] could be observed at magnification 5x (see Figure 38A). The tissue around the extended spots with hyphae appeared with a lighter green color (see Figure 38F-J and Supplementary figure 30A-B-C-D). It is worth mentioning that one leaf of the group 1 (young) exhibited extended black spot symptoms with non-mature acervuli but some leaflets of this leaf were broken and scratched. In addition, the leaves from which the discs were sampled at 9dpi were kept until the end of the study and developed more and bigger black spot

symptoms with acervuli than the ones left untouched for both types of leaves (see Supplementary figure 30E-F-G-H).

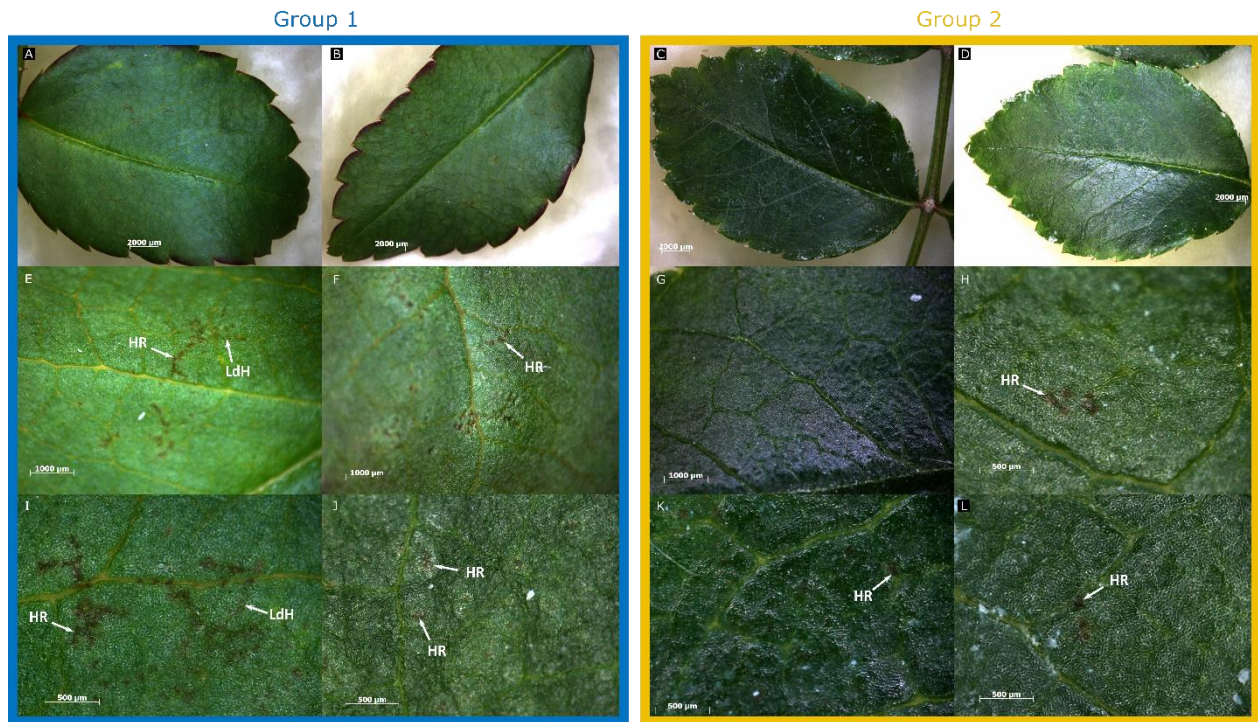


Figure 38: Macroscopic observations of *R. x wichurana* (RW) leaves with different ages at the time of inoculation with DiFRA67

A: Extended brown spots with hypersensitive response-like areas [HR] on young leaves (group 1) at magnification 0.65x; **B:** Close up of an infection site revealing HR-like symptoms on young leaves at 9dpi; **C-D:** Old leaves (group 2) with no visible symptoms at 0.65x; **E-I:** Close up of extended brown spots with a star-like shape on young leaves where long distance hyphae [LdH] can be observed inside HR-like spots [HR] (brown spots); **F-J:** Close up of small brown spots on young leaves where no fungal structure can be observed; **G-H-K-L:** Close up of infection sites of old leaves where no or some small brown spots (HR-like spots [HR]) can be observed at magnification 5x. No fungal structure can be observed.

The pathogen development on RW leaves was very different between young leaves and old ones. The fungus seemed to have been stopped at the penetration point at 9dpi in old leaves (see Figure 39A-B). Restricted fungal structures (infection vesicles and very short hyphae) were observed under the cuticle (see Figure 40). Germinated conidia [Co*] with long germ tubes [Gt] or with appressoria [Ap] were observed (see Figure 39A-B). The plant response in old leaves was characterized with a localized callose deposition at the penetration point [Ca] (see Figure 39C-D). Interestingly, the fungal development on old leaves of RW was consistent between leaf discs and area investigated but for young leaves two different types of fungal development could be observed on the same leaf disc. Therefore, two types of response could be described in RW young leaves: (1) an early response associated with fluorescing epidermal cells at the penetration site and callose deposition at the cell walls, and (2) a late response associated with callose deposition on haustorial structures and invaded cells appeared fluorescent (see Figure 39I-K). Here, early response with callose deposition refers to response that happened early in the pathogen development i.e. at the penetration moment and late response to response that occurred later on the pathogen development when it has already penetrated the cuticle.

First, in the early response, non-germinated [Co] and germinated conidia [Co*] trying to penetrate the host cuticle could be observed and the host epidermal cells under the penetration site appeared fluorescent [Fl-c] whereas the cells under the non-germinated conidia remained normal (see Figure 39A-C and Figure 40). Moreover, strong fluorescence at the entry point was found for several cells around the penetrating conidia. This suggests the deposition of callose on the cell walls of the epidermal cells situated under the conidia trying to penetrate (see Figure 39C-D and Figure 40)). No callose deposition was observed around the penetration pore like for the old leaves and further fungal growth under the cuticle could be observed (see Figure 40)).

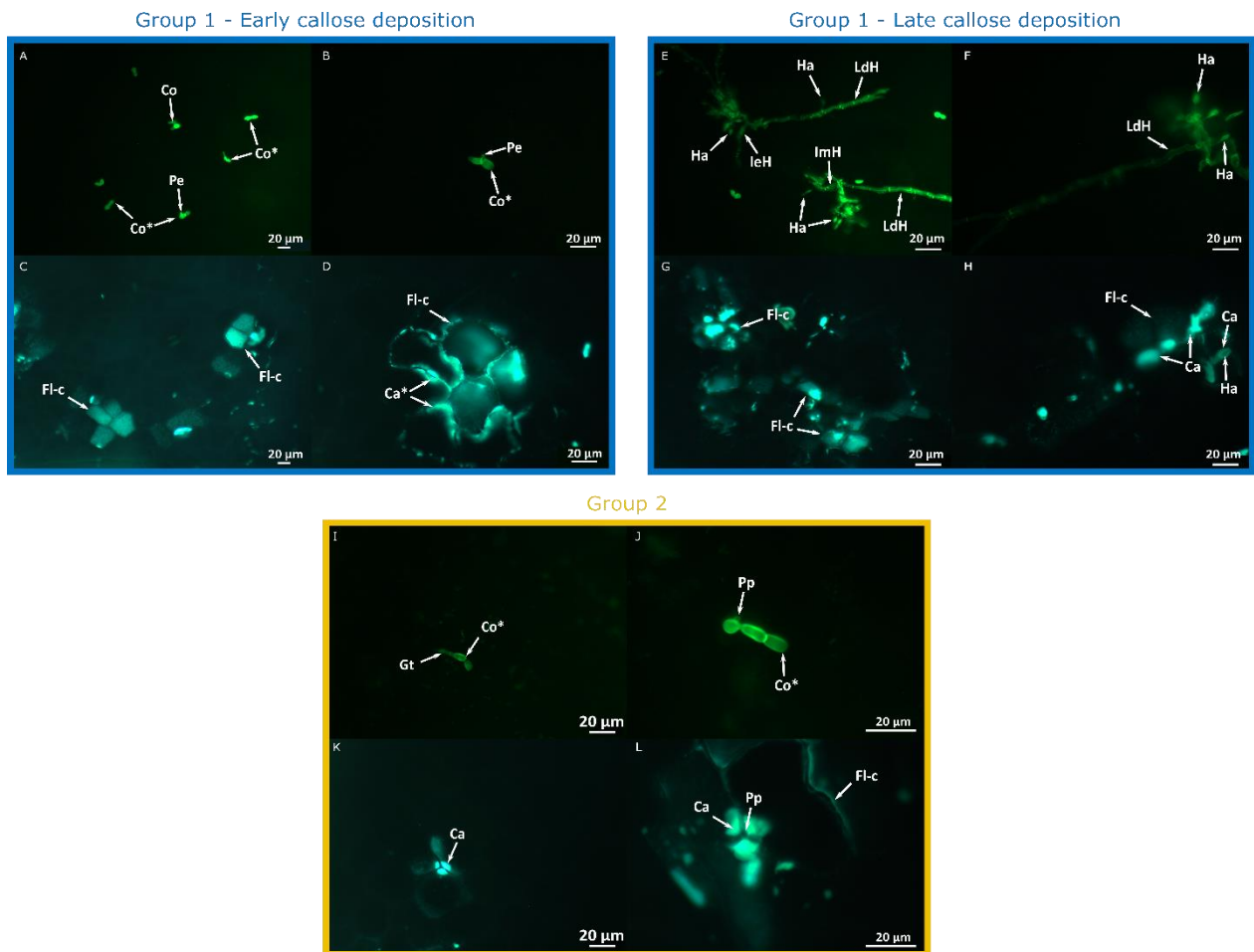


Figure 39: Fluorescence microscopy with a double staining of *R. x wichurana* (RW) leaves from different ages at 9dpi

For both groups, the pictures on the top (A-B, E-F and I-J) correspond to photographs of fluorescence microscopy using the GFP-BH2 filter to visualize fungal structures and the pictures on the bottom (C-D, G-H and K-L) correspond to photographs of the exact same zone with the DAPI-BH2 filter that shows the plant response with callose deposition and fluorescing cells. **A-B:** Conidia successfully arrested at the penetration point on young leaves (Group 1) with germinated conidia [Co*] showing penetration peg [Pe]; **C-D:** Fluorescing cells [Fl-c] with granular texture right under the germinated conidia that are penetrating the rose cuticle, and the fluorescing cells exhibit callose deposition on the cells walls [Ca*]; **E-F:** Visualization of fungal development under the cuticle after infection of young leaves (Group 1). Different fungal structures can be observed like long distance hyphae (or subcuticular hyphae) [LdH], intercellular hyphae [IeH], intramural hyphae [ImH] and haustoria [Ha]; **G-H:** Callose deposition [Ca] around the haustoria [Ha] and haustorial neck were observed as well as fluorescing epidermal cells [Fl-c]; **I-J:** Germinated conidia [Co*] on old leaves (Group 2) with germ tubes [Gt] and penetration peg [Pp]; **K-L:** Photographs of the exact same zone with the DAPI-BH2 filter that shows a callose deposition [Ca] at the penetration point [Pp] and fluorescent cells [Fl-c].

Second, in the late response, the fungus already penetrated the cuticle and fungal structures could be observed inside the leaf like short subcuticular hyphae [LdH] from which short intramural hyphae [ImH] were formed, and these hyphae rapidly grew between epidermal cells (intercellular hyphae, [IeH]) to colonize lower levels of the leaf. Haustorial structures [Ha] were also observed at specific points along the subcuticular hyphae (see Figure 39E-H). Cell invasion by haustoria [Ha] was associated with fluorescence of the epidermal cells [Fl-c] (see Figure 39G). Looking closer, these fluorescing cells also contained small vesicles of callose [CaV] (see Figure 39H). Callose depositions [Ca] were also observed around the haustorial structures either with a collar shape (see Figure 39) or callose completely encapsulated the haustoria under development (see Figure 39I-J). In the end, the late responses observed in RW young leaves that have been successfully infected were similar to the ones observed on OB and PC. However, the extent of long distance hyphae colonization and the haustoria size and number were greatly reduced on RW. These results suggest the existence of a complete resistance in old leaves and a partial resistance in young leaves in RW that may act at several levels and at different time points of the infection reducing therefore the pathogen development.

In addition, we checked if the fungus grew more after 9 dpi by observing the leaves at 23dpi under the microscope. At 23dpi, no black spot symptoms nor brown spots could be observed at bare eye on old leaves. However, some small black spot symptoms could be observed macroscopically on young leaves so we decided to investigate *D. rosae* development and RW responses on these leaves after 23 days (see white arrow in Supplementary figure 31A). For infection sites that were described exhibiting a late callose response, the extent of the leaf colonization by the fungus was greatly reduced compared to the susceptible genotypes OB and PC with long distance hyphae [LdH] harboring very short intramural hyphae and many intercellular hyphae [IeH] limited to some zones. Like for 9dpi, few haustoria [Ha] were found along the subcuticular hyphae [LdH]. The size of the haustoria remained small compared to the size of the ones found in OB and PC leaves (see in Supplementary figure 31B-C). Very few fluorescing cells were found at 23dpi compared to OB and PC leaves but instead bright callose deposition [Ca] around haustoria was observed (see in Supplementary figure 31D-E). Indeed, the callose was no longer found in vesicles inside the invaded epidermal cells but was specifically located around haustorial structures. In other cases, the early response seemed to have definitely limited the development of fungal structures under the cuticle. Again germinated conidia [Co*] penetrating the cuticle with a short germ tube [Gt] were observed. Underneath the penetration pore [Pp], callose deposition on the cell walls [Ca*] with immediate contact with infection vesicle [Iv] and other fungal structures were observed. Thick callose deposition [Ca] around the small haustoria [Ha] that were formed was observed with either a collar shape or a complete encasement like at 9dpi (see in Supplementary figure 31D-E).

To better localize the callose deposition around the penetration point observed on old leaves of RW, we used the fluorescence microscope Axio Imager Z2 with the selective DAPI-Axio filter. We observed that the callose co-localized with the penetration pore and around the short hyphae growing under the cuticle on old leaves (see Figure 44A). For young leaves, the callose was found to co-localize with the haustorial neck like in susceptible cases, and callose vesicles inside the cells invaded by haustoria could be observed (see Figure 40).

4.4. COMPARISON WITH GENOTYPES EXHIBITING COMPLETE RESISTANCE TO DIPLOCARPON ROSAE AND STRAIN CHARACTERIZATION

The interaction between the strain DiFRA67 and four genotypes were investigated with three of them that were described to exhibit a resistance based on specific *R*-genes in the literature and one that was completely resistant to all strains tested. Young leaves were used for this study to determine if the genotypes described as resistant exhibited this resistance even in growing leaves unlike the partial resistant RW. For practical issues, the detached leaf assay was used to investigate these interactions. Macroscopic and microscopic investigations were made at 9dpi for all the genotypes and later disease assessment was performed at 23dpi to assess if further fungal development happened. With all the interactions studied in this chapter, we characterized further the strain DiFRA67. The hybrid shrub cv 'George Vancouver' (GV), the climbing rose 'Brite Eyes™' (BE), the transgenic PC::*muRdr1A* and *Rosa majalis* exhibited all an incompatible interaction when challenged with DiFRA67. However, the fungus was arrested at different moments of its development: after it penetrated the leaf cuticle (post-penetration resistance) and before the penetration even happened (pre-penetration resistance).

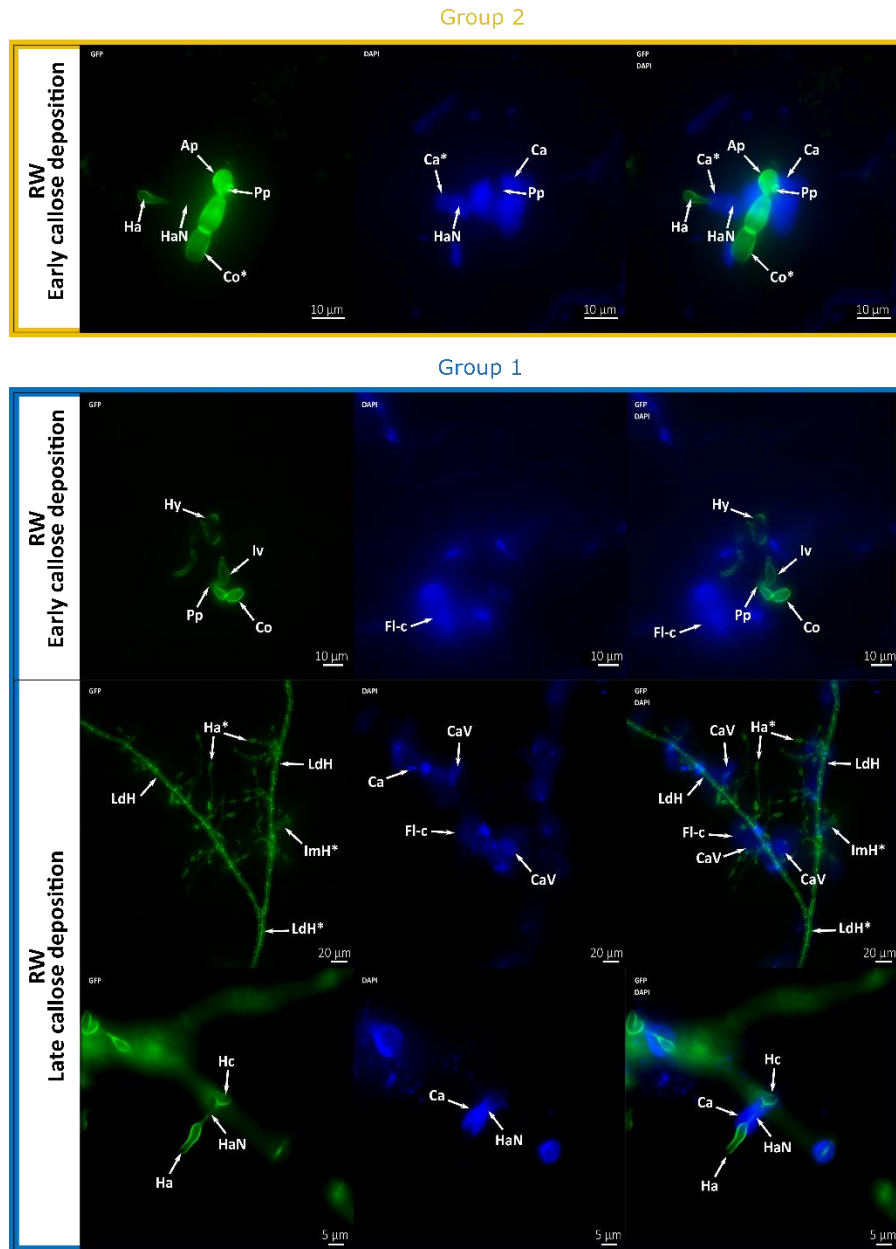


Figure 40: Different types of callose deposition on *R. x wichurana* (RW) old and young leaves at 9dpi in response to *D. rosae* infection

Fluorescence microscopy of RW leaves inoculated with DiFRA67 at 9dpi using a double staining with WGA Alexa Fluor™ 488 that binds to fungal cell wall and aniline blue that visualizes callose deposition. Two filters were used: GFP filter to visualize WGA Alexa Fluor™ 488 and DAPI-Axio filter to visualize aniline blue. Pictures from these separated channels (filters) were merged to localize the callose deposition. In old leaves of RW (group 2), germinated [Co*] that had penetrated the cuticle with a penetration peg [Pp] using an appressorium [Ap] and had produced short structures under the cuticle were observed. Callose deposition at the penetration site [Ca] was observed and, in some cases, callose was also deposited around the haustorial neck [HaN] of the first haustoria [Ha] produced [Ca*]. Two types of response could be observed on RW young leaves (group 1). An early response with fluorescing cells [Fl-c] around the penetration point where a germinated conidia [Co] penetrating the leaf cuticle through a penetration peg [Pp] and growing short hyphae [Hy] and infection vesicle [Iv] could be observed. And a late response with a production of long distance hyphae [LdH*] and some portions of long distance hyphae [LdH] produced intramural hyphae [ImH] and haustoria [Ha] that invaded epidermal cells being invaded. The cells appeared fluorescent [Fl-c] and callose deposition [Ca] on the haustorial neck [HaN]. Haustoria [Ha] under formation were capable of growing through the callose collar [Ca] and mature haustoria [Ha*] exhibited a bottle shape. But, at this stage most of the haustoria were not mature and measured 5-10μm. The hyphal cell swelled before penetrating the epidermal cell [Hc]. In the fluorescing cells, small vesicles of callose could be observed [CaV].

4.4.1. A POST-PENETRATION RESISTANCE IN THE HYBRID SHRUB CV 'GEORGE VANCOUVER' (GV) AND THE TRANSGENIC PC CARRYING THE RESISTANCE GENE *MURDR1A* (PC:*MURDR1A*)

Two types of post-penetration resistance were observed in the hybrid shrub 'Georges Vancouver' (GV) and the transgenic PC::*muRdr1A*. On GV, pathogen penetration was delayed at 9dpi and its development under the cuticle was slowed down until 23dpi whereas in PC::*muRdr1A* leaves, the pathogen already penetrated the host cuticle and developed fungal structures at 9dpi but no further development was observed at a later time point (23dpi).

Indeed, at 9dpi, no visible symptoms were observed on the leaves of the hybrid shrub cv 'George Vancouver' (GV) challenged with DiFRA67 (see Figure 41A) but looking up closer using the magnification 5x, the leaves exhibited small HR-like spots (see Figure 41B-C). Microscopically, a reduced fungal growth was observed on GV leaves with conidia that germinated [Co*] and penetrated the leaf cuticle producing infection vesicle [Iv] and a short hypha [Hy] (see Figure 41D-F-H). A strong fluorescence was observed around the penetration pore [Pp] suggesting callose deposition around it. The epidermal cells beneath the germinated conidia as well as the neighbor cell closest to the hyphae appeared with fluorescent walls [Fl-c] (see Figure 41E-G-I). Fluorescing cells around the penetration point were also observed using the short band emission filter DAPI-Axio (Table 11) (see Supplementary figure 34). At 23dpi, no spots were observed on leaves with a naked eye but, microscopically, further fungal growth happened since 9dpi. Indeed, short hyphae [Hy] were observed under the cuticle with small haustoria [Ha] (see Supplementary figure 32B-C-D-E). Some haustoria exhibited a thin end [Ha*] (see Supplementary figure 32E). Strong fluorescence around the penetration pore [Pp] was observed like at 9dpi. No fungal growth was observed from there but, instead, some conidia germinated again and successfully penetrated the cuticle further away [Pp*] (see Supplementary figure 32B-D). In addition, epidermal cells invaded by haustoria-like structures appeared fluorescent with a granular texture.

At 9dpi, for the transgenic PC carrying the resistance gene *muRdr1A* (PC::*muRdr1A*), no spots were observed at 0.65x magnification but small HR-like spots were observed at 5x magnification (see Figure 42A-B). Microscopically, conidia germinated [Co*] and some penetrated the host cuticle with small hyphae [Hy] growing under the cuticle. Some haustoria [Ha] could be observed growing directly from the hyphae but the size was very reduced compared to susceptible genotypes as haustoria measured around 3 µm long and 2 µm wide whereas in susceptible genotypes haustoria could reach 21 µm in length and 4 µm in width (see Figure 42C-E-F-G-I). A strong fluorescence was observed around the penetration pore [Pp] which suggested, like for GV, a callose deposition at the penetration point. Cells with fluorescent cell walls were also observed where conidia germinated and penetrated (see Figure 42D-F-H-I). Some weak signal using the DAPI-Axio filter was observed around the penetration point as well as the hyphae [Ca] when the conidia were trying to penetrate at 9dpi (see Supplementary figure 34). However, when the conidia already penetrated and produced further fungal structures with cell invasion via haustoria [Ha], no fluorescence could be detected with this filter. At 23dpi, no spots were observed on PC::*muRdr1A* and the fungal growth seemed to have been arrested as the hyphae observed remained very short [Hy] and the size of the haustoria [Ha] (length and width) was unchanged. The fluorescence associated with the callose [Ca] was found to be limited to some parts of the cell walls (see Supplementary figure 33).

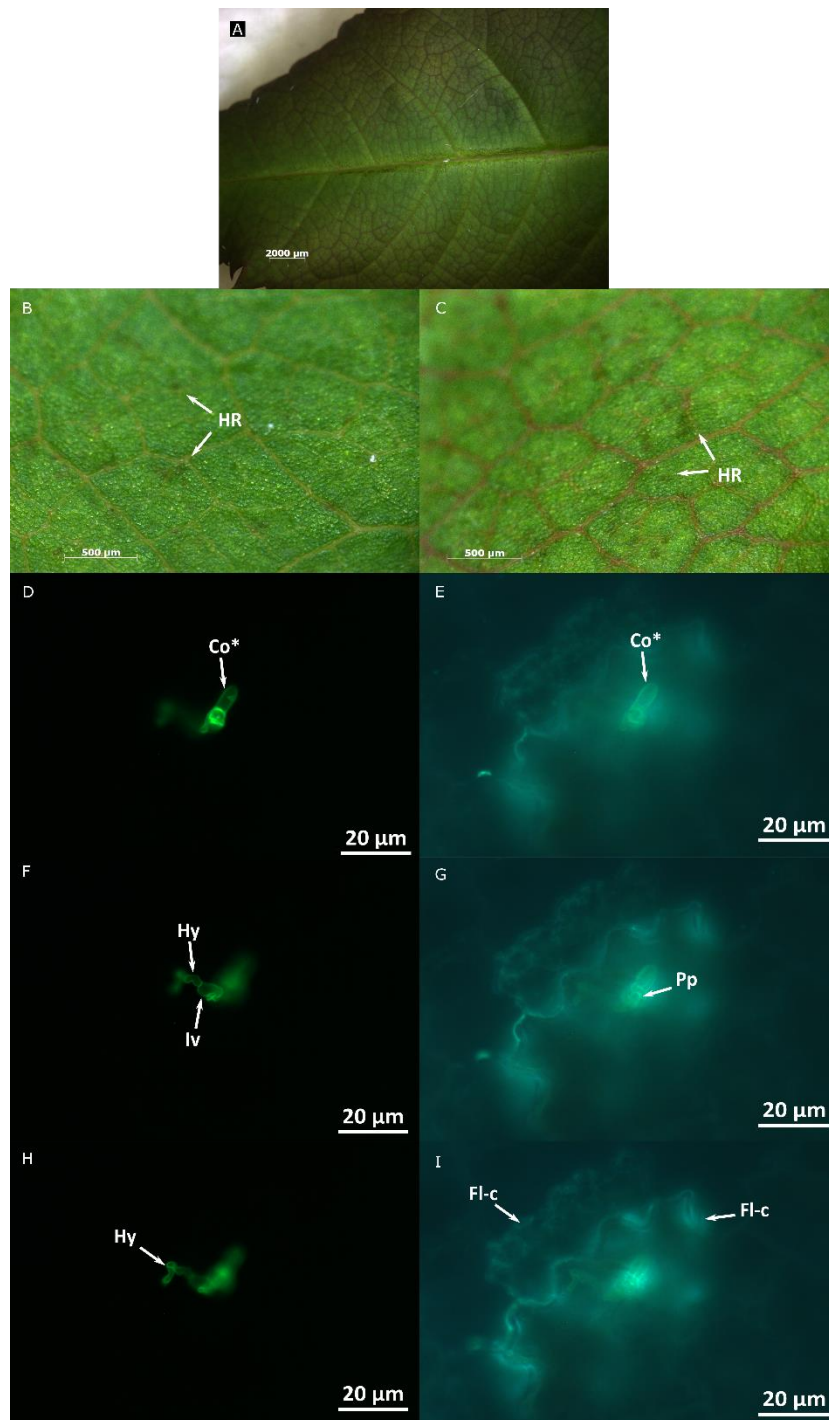


Figure 41: Multiscale investigation of 'Georges Vancouver' (GV) responses to infection by the strain DiFRA67 of *D. rosae*

A: GV leaflet infected by DiFRA67 at 9dpi using the magnification 0.65x; **B-C:** Hypersensitivity-like spots at the infection sites on GV leaflets at 9dpi; **D to I:** Z-stack with both staining methods (Alexa Fluor WGA for D-F-H and aniline blue for E-G-I) showing conidia [Co*] penetrating the leaf cuticle and producing an infection vesicle [Iv] just under the penetration point [Pp] from which a short hypha [Hy] grew. Aniline staining reveals the presence of a fluorescing cell [Fl-c] around the penetration point. The cell right under the penetration point exhibits fluorescing cell walls whereas the neighbor epidermal cell has a granular texture.

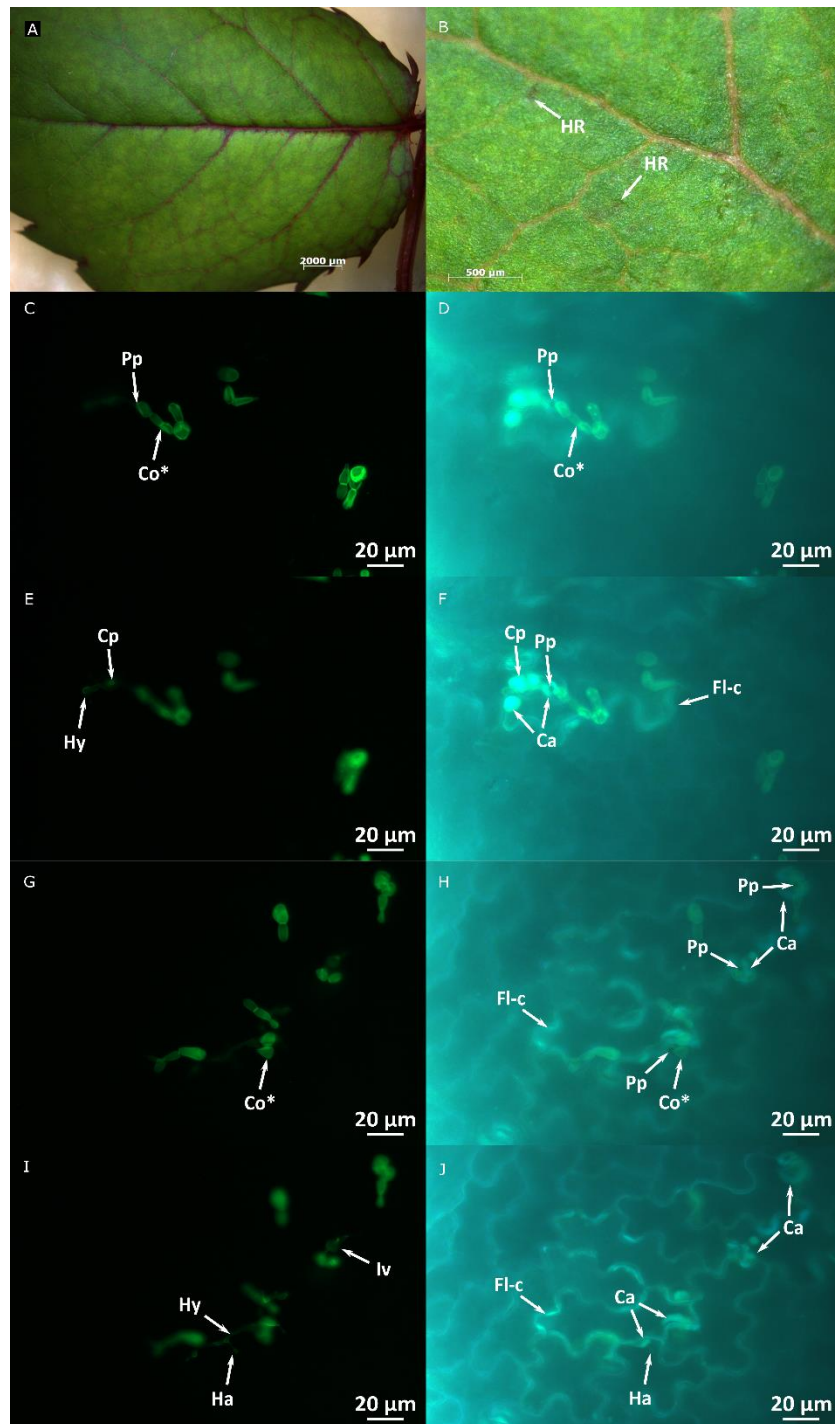


Figure 42: Multiscale investigation of the transgenic PC::muRdr1A responses to infection by the strain DiFRA67 of *D. rosae*

A: PC::muRdr1A leaflet infected by DiFRA67 at 9dpi using the magnification 0.65x; **B:** Hypersensitivity-like spots [HR] on PC::muRdr1A at 9dpi using the magnification 5x; **C-E and D-F:** Two levels on the z-axis using a double staining with WGA-Alexa Fluor™ 488 (C-E) and aniline blue (D-F) showing germinated conidia [Co*] penetrating the cuticle. The penetration pore [Pp] can be observed in D-F as well as callose deposition [Ca] around the penetration site. A short hypha [Hy] could be observed with a clear cell penetration pore [Cp] on E, which was associated with a strong fluorescence on F. The cell near the penetration site appeared fluorescent [Fl-c]; **G-I and H-J:** Two levels on the z-axis showing the penetration and growth of DiFRA67 under the cuticle. Germinated conidia [Co*] penetrated the leaf cuticle via a penetration pore [Pp] producing an infection vesicle [Iv] under the cuticle as well as a short hypha [Hy] with small haustorium [Ha]. The cells around the infection site appeared fluorescent [Fl-c]. Callose depositions [Ca] were observed around the penetration pore as well as at the cell walls of invaded epidermal cells.

4.4.2. PRE-PENETRATION RESISTANCE FOR BOTH CLIMBING ROSE BRITE EYESTM (CV 'RADBRITE') (BE) AND ROSA MAJALIS (RM)

Both climbing rose 'Brite EyesTM' (cv 'RADbrite') (BE) and *Rosa majalis* (RM) did not exhibit symptoms at any magnification of stereomicroscope (see Figure 43A-B-C-D). Both non-germinated [Co] and germinated [Co*] conidia were observed, with sometimes germ tubes [Gt], but no sign of penetration was observed at 9dpi in both genotypes. No callose deposition was observed (see Supplementary figure 34). To observe any signal with the DAPI-Axio filter, strong intensity fluorescence needed to be applied but no callose deposition or cell response with fluorescence was registered on both genotypes (see Supplementary figure 38). However, one replicate of BE exhibited callose deposition at 9dpi but not the other two. At 23dpi, no symptoms were observed on both genotypes (see Supplementary figure 35A-B) but some germinated conidia were associated with a strong callose deposition around the penetration pore for BE (see Supplementary figure 35C-E). No cell reaction with callose deposition could be observed on RM and the conidia were at the same stage of germination than at 9dpi (see Supplementary figure 35D-F). Therefore, we can say that two types of pre-penetration resistance were observed in these two genotypes. In both genotypes, germinated conidia were observed, which indicates that the germination was not impeded but as no quantification of the germination was done, we cannot conclude whether or not the germination rate was affected in both these genotypes. However, observing some penetration at 23dpi on BE leaves indicates that conidia germination could have been slowed down, so penetration only happened at a late time point. Unlike BE, RM seemed to completely prevent pathogen penetration even if conidial germination was observed in some cases.

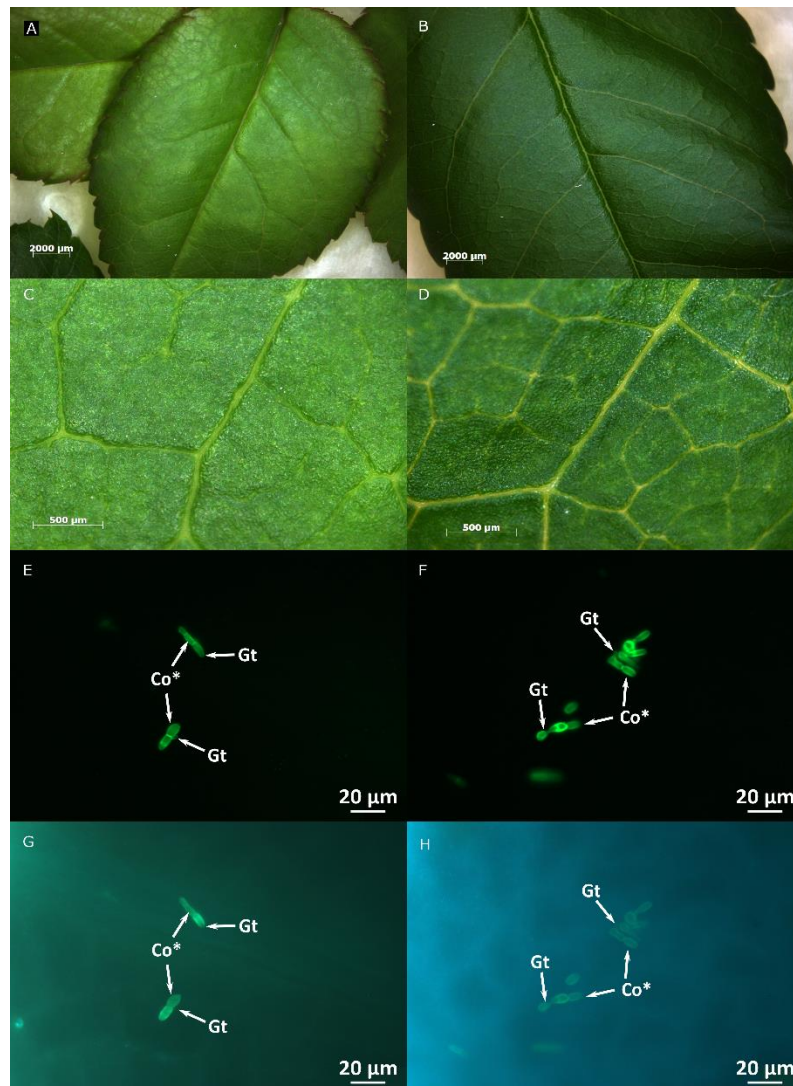


Figure 43: Multiscale investigation of the responses on 'Brite Eyes™' (BE) (left) and *Rosa majalis* (RM) (right) leaves infected with the strain DiFRA67 of *D. rosae* at 9dpi

A-C-E-G: BE response to infection at 9dpi at different levels; **B-D-F-H:** RM response to infection at 9dpi at different levels; **A:** BE leaflet infected by DiFRA67; **B:** RM leaflet infected by DiFRA67; **C-D:** Close up using the 5x magnification showing no visible symptoms at the infection site on BE (C) and RM (D) leaflets; **E-G and F-H:** Double staining with WGA-Alexa Fluor™ and aniline blue showing germinated conidia [Co*] with a small germ tube [Gt] and no apparent callose deposition or cell reactions on BE (E-G) and RM (F-H) leaflets.

4.4.3. DIFFERENT TYPES OF CALLOSE RESPONSE ACCORDING TO THE INTERACTION TYPE

Using the narrow emission band pass filter (DAPI-Axio, see Table 11) from the Zeiss Axio Imager microscope, we were able to classify the fluorescence signal emitted by the aniline blue fluorochrome into three types of signals. Indeed, different UV intensities were needed to be able to observe the DAPI signals and they are represented in three supplementary figures separating the compatible interactions yielding considerable symptoms and infection (PC and OB, Supplementary figure 36), the compatible interaction exhibiting some resistance from the host RW (Supplementary figure 37) and the incompatible interactions (GV, PC::*muRdr1A*, BE and RM, Supplementary figure 38).

First, a strong fluorescence was observed on late callose deposition for PC and OB susceptible genotypes as well as on the young leaves of the partial resistant genotype RW. For these interactions, callose around the haustorial neck and fluorescing cells containing callose vesicles were observed (see A limit on Supplementary figure 36 and on Supplementary figure 37). A particular case of leaves exhibiting an incompatible interaction was observed on some infection sites of young leaves and in all old leaves of RW. This early callose deposition was characterized by a strong callose deposition around the penetration point (see A limit on Supplementary figure 37). Then, an intermediary fluorescence was observed on GV and to early response on PC::*muRdr1A* (see B limit on Supplementary figure 38). Finally, a weak signal that needed a strong intensity of exposure suggesting no callose involved in the response was observed in the genotypes BE and RM as well as PC::*muRdr1A* (when the fungus has already penetrated the host cuticle) at 9dpi (see C limit on Supplementary figure 38).

The same way, using the microscope Axio Imager Z2, we were able to perform colocalization analysis of the signals recovered from the selective DAPI-Axio and the GFP-Axio filters, which is presented in Figure 44.

Different types of callose deposition localized around specific structures were registered according to genotypes. For the partial resistant genotype RW, we described two types of signals in the previous sections. With the co-localization of the signals, we were able to confirm that the penetration peg was surrounded by a strong callose deposition limiting the fungal growth under the cuticle. In some cases, the first haustoria could be observed and a strong but localized callose deposition was observed around the haustorial neck invading an epidermal cell (Supplementary figure 38A).

In the case of the incompatible interaction between GV and DiFRA67, callose was found to be located on cell walls of the epidermal cells right beneath the penetrating conidia (Supplementary figure 38B).

For the transgenic PC::*muRdr1A*, callose was deposited specifically around the penetration pore as well as around the penetrating hyphae (Supplementary figure 38C), but no callose could be observed once the fungus penetrated the cuticle (see C limit on Supplementary figure 38).

Finally, in the case of late responses like for OB, PC and extended infection in RW young leaves, callose was found to co-localize with haustorial neck forming the collar neck observed by many authors, but also some cells appeared fluorescent with dense callose grid forming callose vesicles inside the invaded cells (Supplementary figure 38D).

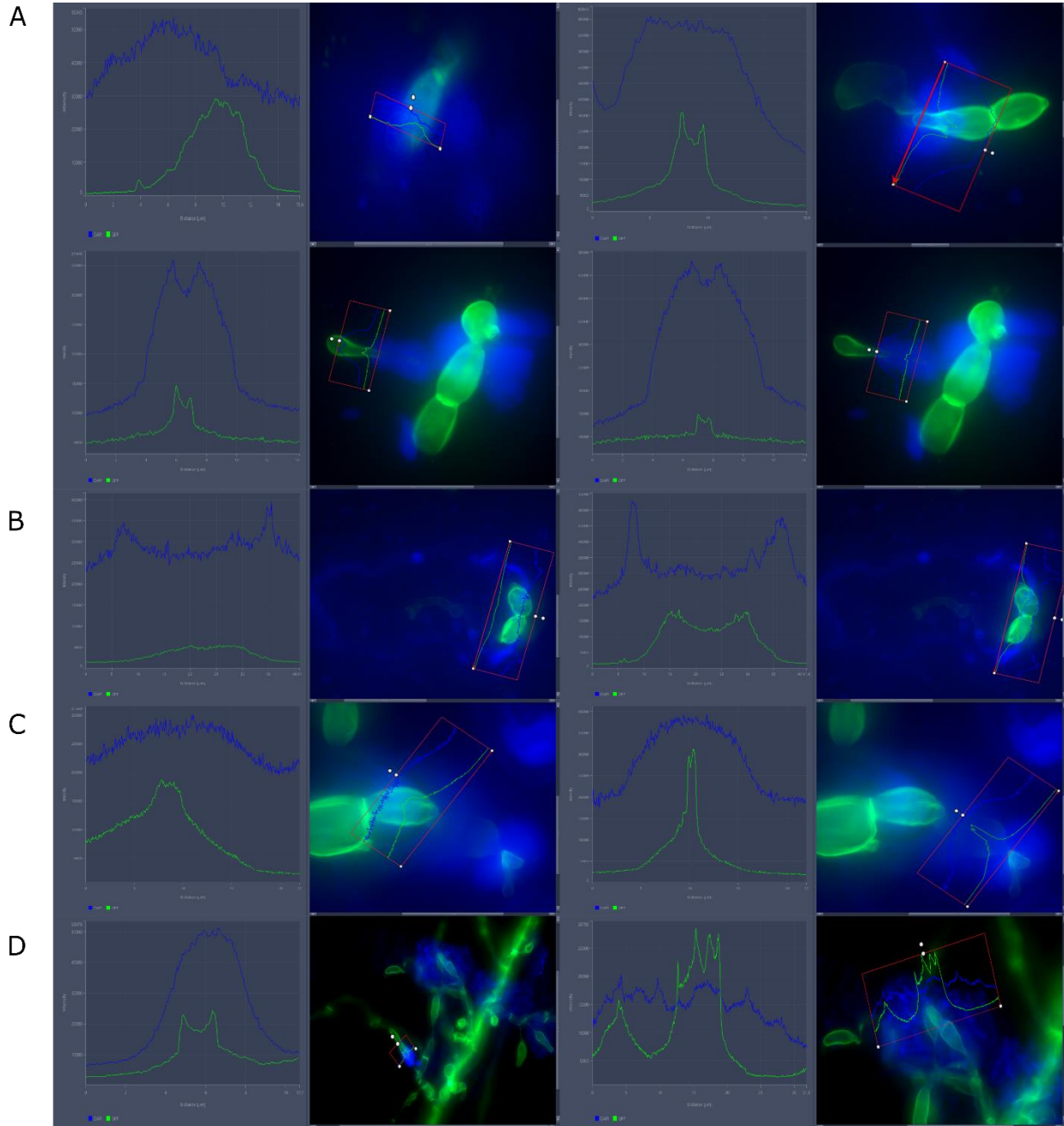


Figure 44: Co-localization of callose responses to *D. rosae* in different types of interaction at 9dpi

This figure shows a graphic with the intensity of the signal received along a line defined by the user on the y-axis and the distance represented by the line in μm was plotted on the x-axis. The picture investigated was associated with the graphic and was reported on the left. The zone studied in the co-localization of both signals (GFP in green and DAPI in blue) were represented by the red arrow. The same graphic was reported on the picture associated with it inside a red rectangle. **A:** Callose deposition at the penetration point in old leaves of RW genotype leading to an incompatible interaction with *D. rosae*. The callose deposition co-localizes with the penetration pore and penetrating hypha on old leaves of RW; **B:** Cell wall fluorescence of the cells beneath the penetrating conidia on GV leaves. The callose is found specifically in the cell call; **C:** Callose deposition at the penetration point (around the penetration pore) and around the invading hyphae on PC::*muRdr1A* leaves leading to an incompatible interaction; **D:** Late callose deposition on OB leaves around the haustorial neck and invaded epidermal cells filled with callose. Similar results were observed for PC and young leaves of RW exhibiting an extended infection.

4.4.4. STRAIN CHARACTERIZATION

According to the expanded rose black spot host differential set describing the 13 races of *D. rosae* identified so far and information gathered in the literature, we can say that DiFRA67 does not belong to race 1, 3, 9, 10, 11 and 12. However, it should be necessary to test this strain with the standard set of hosts proposed by Whitaker et al. (2010b) to be able to clearly identify whether DiFRA67 belongs to race 2, 4, 5, 6, 7 or 8 or if it belongs to a new race not identified yet.

Table 12: Summary of disease responses to DiFRA67 expressed by the studied genotypes

Host	DiFRA67	Disease responses for 13 races ^a
'Pariser Charme' (PC)	+	(-) to race 1 and (+) to all the others
Transgenic PC (PC:: <i>muRdr1A</i>)	-	(+) to R6 (race 7) and AB13 ^b
'George Vancouver' (GV)	-	(+) to race 3-9-10-11 and (-) to all the others
Brite Eyes™ ('RADbrite', BE)	-	(+) to race 12 and (-) to all the others
<i>Rosa majalis</i> (RM)	-	/*
'Old Blush' (OB)	+	/
<i>Rosa wichurana</i> (RW)	+/-	(-) to race 4 and 6 and (+/-) to race 2 ^c

Disease responses are labeled as susceptible (+) or resistant (-). ^a Information about the disease responses to the 13 races described by Whitaker et al. (2010b) and Zlesak et al. (2020). ^b Personal communication of Prof. Debener. ^c Two different representatives of *Rosa wichurana* species exhibited different responses to the strain 2402 E1 (race 2) according to Debener et al. (1998) when leaves from group 1 (young leaves) were used in a detached leaf assay ("fully expanded leaves from the upper part of the shoot"). *The accession 93-09-01 is resistant to many races except AEH10 (see Schulz et al. 2009) but it has not yet been characterized with the strains representing the 13 races.

5. DISCUSSION

Understanding the interaction between *R. wichurana* (RW) and *Diplocarpon rosae* is an important step to better characterize the partial resistance that segregates in the three populations previously studied. Over the years, great attention has been given to the resistance observed in *Rosa wichurana* species but little is still known about the interaction observed between *Rosa wichurana* and *D. rosae*. The difficulty in explaining how *Rosa wichurana* resistance works, considering the different observations made in several studies on different genotypes belonging to this species confirms the idea that partial resistance, whether it is in rose or other species, is a complex mechanism that needs further investigations to be fully understood. So the aim of this chapter was to present new insights on the interaction between *R. wichurana* and *D. rosae* and to prepare the transcriptomic experiment that will be presented in chapter 4. Moreover, the interactions between genotypes carrying *Rdr* genes and *D. rosae* were investigated in detail for the first time, which allowed the comparison between these types of interactions and the interaction between our genotype of *R. wichurana* and *D. rosae*.

5.1. DIPLOCARPON ROSAE INFECTIOUS CYCLE AND IMPORTANT TIME POINTS FOR LATER STUDIES

For that matter, we described the *D. rosae* infectious cycle on the susceptible genotype *Rosa chinensis* 'Old Blush' (OB, parent of OW population). That way, the main steps in the infection were identified and out of the nine time points investigated, three were selected to be investigated in the next chapter. First,

we decided to perform a sampling at “0dpi” that corresponds to 30 minutes after the inoculation to investigate early changes in gene expression when the leaf enters in contact with conidia. Then, 3dpi seems like an interesting time point as the germination has already started and the first penetrations could be observed for both genotypes OB and RW. The time point at 5dpi was only investigated on RW but it gave us the opportunity to study the first stages of the infection after the penetration happened in the susceptible case (OB). It is also when we could observe the callose depositions at the entrance point on RW leaves with low fungal colonization. Then, 7dpi is another interesting time point when the colonization is already advanced in the susceptible case and for which invaded cells are responding by entering in necrosis. We could observe on RW that, after that time point, most of the sites that responded with an early callose deposition did not evolve and stayed at the same stage of infection in later time points. It was the first time that *D. rosae* infectious cycle was described at the same time on partial resistant and susceptible genotypes.

5.2. STRAIN MULTIPLICATION: A STRATEGIC CHOICE

A delay in conidium germination and mature acervulus development was observed compared to the literature. Again, these differences could be due to the differences in rose genotype, fungal isolate, environmental conditions of the experiment and plant growth. However, we suspected that this delay might also be due to the multiplication technique used for the strain. Indeed, our strain DiFRA67 was multiplied in artificial media to obtain highly sporulating cellophanes. But when Prof. Debener team multiplied our strain from cellophanes on PC leaves and used the conidia produced after four cycles of multiplication, they observed that the conidia size slightly increased as well as the strain aggressiveness and that the symptoms started to appear earlier (Prof. Debener personal communication). To study this phenomenon, we inoculated a same leaf with the conidia from both multiplication techniques during an experiment with three independent inoculations on OB and PC genotypes. Overall, the symptoms on OB and PC leaves appeared two days earlier when the drops contained conidia obtained on PC leaves than when the conidia were directly used from the cellophanes (data not shown). Indeed, it was demonstrated that obligate biotrophs lose their pathogenicity and change in morphology when grown in artificial media (Drewes-Alvarez 2003; Gachomo et al. 2006; De Silva et al. 2016; Debener 2019). It would not be impossible that, for the hemibiotroph *D. rosae*, the multiplication on artificial media could have reduced its aggressiveness, which could explain the delay in germination and symptom expression.

Further investigations need to be carried out to better quantify the difference of aggressiveness and conidia size that were observed and if the origin of the conidia (leaf or cellophane) can also affect RW resistance. Furthermore, we could study the influence of the number of multiplication cycles on rose leaves on the strain aggressiveness but also the effect of adding rose leaves extract (from susceptible genotypes) to the artificial media. Actually, plant-based media have been shown to provide good culturing results (Youssef et al. 2016) but might also help to keep the pathogenicity of a fungus like observed with a cabbage media for *A. brassicicola* (supplementary results presented page 141 of Colou PhD thesis (2020)).

Nevertheless, I would like to discuss the choice of strain multiplication according to the type of assay that we want to perform. On one hand, multiplication on artificial media and storage using cellophanes can be interesting since strong sporulation can be obtained with this technique and therefore, large

amounts of inoculum can be prepared with small amount of effort (three large i.e. 6cm or six small i.e. 3cm cellophanes for 300ml at 10^5 conidia per milliliter). This is particularly useful when conducting whole plant assays with several genotypes, high number of plants and more or less developed cuttings (with different sizes) given that the quantities of inoculum needed are very important for this type of assay. Multiplying a strain through inoculation of detached leaves of a susceptible genotype would be very demanding on leaves, time and labor to obtain the same amount of inoculum. Not to mention that the plants used to sample the leaves intended for the isolate multiplication must be sanitized and kept under careful control to avoid contamination of the isolate. However, we need to keep in mind that the artificial medium technique of multiplication eventually leads to a loss of aggressiveness. On the other hand, isolate propagations on rose leaves prove to be interesting when performing detached leaf assays where smaller amounts of inoculum are needed at a time. Seeing the effect of multiplying the pathogen on rose leaves for several cycles, it would be interesting to consider a new approach and mix both types of multiplication to ensure both large inoculum amount for whole plant assay and normal aggressiveness. In that sense, we can multiply the fungus for several cycles on rose leaves and then propagate it for one cycle on artificial media to increase the sporulation. Of course, it is crucial to test whether or not a single propagation on artificial media does not affect the aggressiveness right away.

5.3. AGE-RELATED RESISTANCE TO BLACK SPOT DISEASE IN THE HYBRID OF *ROSA WICHURANA* (RW)

5.3.1. EFFECT OF THE LEAF AGE ON THE COMPONENTS OF PARTIAL RESISTANCE

Several species develop resistance that is restricted to a tissue or organ and that can be more or less efficient according to their maturity or to their position on the plant (rank). It is important to distinguish leaf maturity or “age” and leaf rank as the leaf maturity is directly linked to differences in the physiology of the leaf: the leaf is still growing for immature or young leaves and the leaf finishes its development for mature or old leaves (Develey-Rivière and Galiana 2007). On the contrary, leaves of the same rank (in the absolute sense) on different branches can have different ages if the branches do not develop at the same speed. For example, leaf maturity in rice (*Oryza sativa*) has no effect on the resistance to *Xanthomonas campestris* whereas leaf rank was shown to influence the degree of resistance (Koch and Mew 1991). Another example is the effect of leaf age on the resistance to *Venturia inaequalis* in apple (*Malus atrosanguinea*) with younger leaves being more susceptible than older ones. This age-related resistance is referred to as “ontogenic resistance”. In apple, this resistance is characterized by an increase of resistance (smaller lesion density and longer incubation period) with increased leaf age, and when the leaves are fully expanded, ontogenic resistance starts to have an effect (Li and Xu 2002). In general, ontogenic or age-related resistance describes the ability of whole or parts of plants to better resist as they get older and reach maturity. This type of resistance does not necessarily lead to complete resistance but it can greatly reduce disease severity and sometimes help to avoid infection (Ficke et al. 2002). This type of resistance is commonly found in other pathosystems and for different types of organs such as leaves for resistance against rice blast, *Botrytis fabae* in the faba bean or fruits for the resistance to *Phytophthora capsici* in cucurbit fruits, to grape powdery mildew or to powdery mildew in leaves and fruits for example (Roumen 1992a, b; Li and Xu 2002; Ficke et al. 2002; Bouhassan et al. 2004; Develey-Rivière and Galiana 2007; Asalf et al. 2014; Yamauchi et al. 2017; Hu and Yang 2019). For rose-*D. rosae* pathosystem, limited investigations have been made on the effect of leaf age in the resistance to black spot disease. The effect of leaf maturity

has been briefly mentioned by Dodge in 1931 who observed that both genotypes he studied ('Red Radiance' that was resistant and 'Felicity' that was susceptible) could be infected when "fairly young leaves" were chosen. Later, Aronescu in 1934 reported that young leaves showed 100% of infection and that sometimes infections could be observed in leaves that "had ceased growing before the inoculation" but the spots remained small and with non-mature acervuli. Finally, Knight in 1975 showed an effect of leaf position on the lesion diameter 14 days after inoculation. However, even if he referred to the leaf position as leaf age, it is hard to differentiate leaf age and leaf position in such young cuttings. Indeed, the cuttings he used for the assessment only presented five leaves per shoot.

In our study, the differences observed macroscopically and microscopically in RW leaves led us to consider the existence of an effect of leaf age on the effectiveness of the partial resistance observed in that genotype. Moreover, different components of partial resistance were assessed to characterize the response of young and old leaves separately. The percentage of the leaf that was infected, the leaf area with symptoms, the percentage of the leaf reacting with necrotic spots as well as the number of leaflets exhibiting chlorosis were found to be significantly different between young and old leaves of RW. In contrast, when black spots were observed, no acervuli could be seen at bare eye and the largest lesion length was not found to be significantly different between both leaf ages (Table 13). An interesting fact is that no clear difference could be described on the leaves of the susceptible genotype OB for different ages, and the genotypes carrying major *Rdr* genes remained completely resistant even when young leaves were inoculated as the leaves were found asymptomatic and with some reduced development of the pathogen. So, for the first time in rose-*D. rosae* pathosystem, we demonstrated an effect of leaf age specifically on partial resistance to black spot disease. These results suggest that specific resistance is already implemented and operational in young tissues whereas partial resistance is acquired with leaf maturity. The influence of plant age on disease resistance has been investigated in many plant-pathogen systems (Kus et al. 2002; Develey-Rivière and Galiana 2007; Hu and Yang 2019 and references therein) but in particular, leaf age has been found to affect partial resistance in rice against leaf blast (Roumen 1992a, b), in groundnut against peanut bud necrosis tospovirus (Buiel 1996) and in faba bean against *Botrytis fabae* (Bouhassan et al. 2004).

5.3.2. DIFFERENCE OF INTERACTION TYPE AND HOST RESPONSE ACCORDING TO LEAF AGE IN THE PARTIALLY RESISTANT GENOTYPE RW

Not only several macroscopic components of partial resistance were shown to differ between leaves of different ages but microscopically, the interaction type was shown to be completely different in leaves that were still growing (young) at the moment of inoculation compared to older leaves that were mature when the inoculation happened.

Indeed, young leaves of RW responded very differently to the infection than old ones with a substantial infection that was not observed on older leaves. In advanced stages of infection (15 and 28dpi), black spot-like symptoms on young leaves of RW were always associated with large brown necrotic areas and at 9dpi, only the brown necrotic cells were observed (Table 13). Even if the size of the black spot symptoms were considerably reduced compared to the susceptible genotypes OB and PC, the presence of these reduced black spots suppose that the resistance implemented in these leaves was not sufficient to block the

pathogen at early stages but only to reduce the infection after the colonization was initiated. Besides, microscopically, the extent of the fungal colonization by subcuticular hyphae was reduced and the invasion of epidermal cells by the haustoria was limited (Figure 46 and Table 13). According to Blechert and Debener (2005) classification of interaction types between rose and *D. rosae*, we can say that young leaves of RW exhibit a compatible interaction of type 4. Indeed, this type of interaction is characterized by a weak colonization by only one to three subcuticular hyphae (Blechert and Debener 2005). Like for susceptible cases (OB and PC), the same type of responses with callose depositions around haustorial necks and inside small vesicles was observed in young leaves of RW for which the infection was extended. However, young leaves of RW exhibited very different reactions with a mix of sites where penetration was arrested efficiently and others where penetration and infection were successful like previously described. Interestingly, callose deposition on the cell walls of RW giving these fluorescent cells was not associated with a localized and strong callose deposition around the penetration pore (Figure 46 and Table 13). Similar observations were made when studying the early stage of OB infection as no strong callose deposition was observed around the penetration pore (Figure 45).

On the contrary, the response in old leaves of RW with callose deposition was characterized by cell-wall appositions on a small group of cells around the penetration point but also strong callose deposition localized around the penetration peg. In some cases, callose deposition was also observed around the first haustoria produced after the penetration. So, in the case of old leaves of RW, the infection was limited to the first haustoria and extremely short hyphal development under the cuticle was observed. In addition, macroscopically, these reactions resulted in small necrotic areas on the leaf surface that were only visible at strong magnification of a stereomicroscope. With these observations, we can confirm Blechert and Debener's observations (2005) that the type of interaction observed in *Rosa wichurana*'s old leaves is of type 7 (Table 13).

We can therefore say that for young or old leaves, the partial resistance observed in RW is definitely a post-penetration resistance unlike what was observed by Reddy et al. (1992). Nevertheless, the efficiency of the post-penetration resistance operating in *Rosa wichurana* is age-dependent and the extent of the necrotic responses increases with the invasion of the epidermal cells by the fungus.

It is worth noticing that in Blechert and Debener (2005) study, young leaves of *R. wichurana* were used and the type of interaction observed was similar to the old leaves of our genotype but not to the young ones. The differences observed between our study and the one of Blechert and Debener (2005) could be explained by several factors such as the plant age, the growth conditions, the fungal isolate used or an intraspecific variation in *Rosa wichurana* species like proposed by Debener et al. (1998).

First, the leaves used for artificial inoculation were sampled on plants grown in an experimental field and these plants were probably older than the four-month old cuttings used in our study. In other pathosystems, host plants have been shown to acquire resistance or display an increased resistance at different developmental stages (Dyck 1979; Bouhassan et al. 2004; Develey-Rivière and Galiana 2007; Hu and Yang 2019). Therefore, we could imagine that young leaves of old plants present a similar resistance than old leaves of young cuttings. It would be interesting to compare old leaves from plants that are old

and well installed in the fields to young cuttings and similarly, young leaves of different plant ages for our genotype during the same experiment. Finally, rose responses have been shown to vary according to the strain used. Indeed, several races with different effects on rose varieties were described and as we do not know yet the race of our isolate DiFRA67, we cannot say whether or not it belongs to the same race as DortE4 (race 5) used in Blechert and Debener study (2005). It should be necessary that we better characterize the strain DiFRA67 using the published standard set of rose hosts (Whitaker et al. 2010b; Zlesak et al. 2020).

Table 13: Summary of observations on RW leaves of different ages challenged with DiFRA67

	young leaves	old leaves
9dpi	Fluorescing cells (penetration point) or Haustoria with fluorescent cells and callose around the haustoria	callose deposition (penetration site) and fluorescing cells infection stopped
15dpi	60% of infected leaves Black spot Chlorose Mean of brown spot 60%	0% of infected leaves No black spot No chlorose Mean of brown spot near 1%
23 dpi	Hautoria (callose) + short subcuticular Hyphae showing fungal colonization Some leaves with incompatible symptoms	Brown spot (in contradiction with 15 dpi) All leaves with incompatible symptoms
conclusion	Partial R Interaction Type 4	Total R Interaction type 7

5.4. CUTICLE INTEGRITY AND ITS IMPORTANCE IN PARTIAL RESISTANCE TO BLACK SPOT DISEASE

During our experiments, we also noticed that when RW leaves were punctured to sample the leaf discs for microscopy, they developed black spots after 23dpi no matter if they were young or old at the moment of inoculation. The punching of the leaf leads to a loss of cuticle and tissue integrity that can facilitate the pathogen penetration. Cuticular resistance to black spot disease in rose was reported in the literature (Dodge 1931; Castledine et al. 1981; Walker et al. 1996). Indeed, Castledine et al. (1981) observed that a compromised cuticle can, for some rose species/cultivars that were completely resistant, lead to a successful infection with acervuli production. Other rose cultivars were shown to have an increased susceptibility when the leaf cuticle was abraded. In particular, for *Rosa wichurana* Crép., more leaves exhibited mycelium without acervuli when the cuticle was abraded than when it was intact (4 discs instead of 2). These results suggest the existence of a cuticular resistance for the genotypes that started to be infected after the leaves were abraded, and for *R. wichurana*, the cuticle helped to slow down pathogen penetration but an efficient post-penetration resistance reduced the fungus colonization. On the other hand, some genotypes did not exhibit any mycelium or acervuli even when the cuticle was compromised like 'Allgold', *R. multiflora* Thunb. 'Japonica', *Rosa pendulina* and *Rosa bella* Redh. & Wils. Similar results were observed in our experiments: genotypes GV, BE, PC::muRdr1A and RM did not develop any symptoms around the punctured zone after 23 days. Knowing that these genotypes carry major resistance genes, we can hypothesize that the resistance mechanism controlled by these *Rdr* genes have no link with

cuticle integrity unlike the partial resistance observed on RW genotype for which pathogen colonization seems reduced and slowed down by the presence of an intact cuticle. However, further investigation needs to be done to assess whether or not cuticular resistance is a component of partial resistance. Then, it would be interesting to quantify the pathogen colonization and the importance of the plant's reaction in leaves with a compromised cuticle for both young and old leaves in RW genotype. That way, we could clearly demonstrate the importance of cuticle integrity in the expression of partial resistance to black spot disease.

In addition, several hypotheses can be proposed to explain the cuticular resistance to black spot disease observed in rose. Dodge (1931) proposed that mechanical properties of an intact cuticle were involved in the resistance. However, like mentioned in chapter 1, other studies investigated if the leaf surface properties (epidermal structures or wax apposition) as well as cutin monomers and cuticular wax content had a link with the infection intensity, but no conclusive results were found (Reddy et al. 1992; Goodwin et al. 2007). As Debener (2019) mentioned, these studies lack power to demonstrate such a relationship because a small set of genotypes was used, so the existence of a link between an intact cuticle and resistance cannot be completely ruled out. In my opinion, it would be interesting to investigate to what extent the cuticle is important in the differential expression of partial resistance observed between young and old leaves of RW.

5.5. DIFFERENT TYPES OF CALLOSE DEPOSITION ACCORDING TO THE INTERACTION

Aniline blue staining has been used for a long time to visualize callose deposition at infection sites (Hood and Shew 1996; Bhadauria et al. 2010; Ellinger et al. 2013; Mason et al. 2020). The commercial dye is a heterogeneous mix of fluorophores that binds to different (1-3)- β -D-glucan polymers in cell walls (fungus and plant) and host cell wall depositions. A few fluorophores were isolated from aniline blue dye and characterized. The fluorophores, when bound to (1-3)- β -D-glucan, are excited by UV light and emit wavelengths within the blue range (Smith and McCully 1978; Wood and Fulcher 1984). The fluorophore Sirofluor was extracted from aniline blue dye and demonstrated to specifically bind to (1-3)- β -D-glucan. The fluorophore on itself fluoresces weakly with maximum emission around 455 nm (Smith and McCully 1978), and when it is associated to curdlan (a (1-3)- β -D-glucan), it emits around 495 nm (Wood and Fulcher 1984). However, Smith and McCully 1978 observed that the fluorescence shifts to wavelengths around 500-506 nm, when the fluorophore binds to (1-3)- β -D-glucan, cellulose or mixed-linked glucans. Otherwise, it is believed that a stronger specificity with callose (a (1-3)- β -D-glucan) exists due to a greater accessibility of the polymer (Hood and Shew 1996). In our study, using two types of filter helped us identify different types of plant reactions with callose deposition and cell death. Both filters have an excitation around the same wavelength (365nm for DAPI-Axio and between 330 and 385 nm for DAPI-BH2). The long pass filter DAPI-BH2 retrieves longer wavelengths (after 420 nm to the end of the spectrum) and therefore, autofluorescence of plant tissues and several compounds can be observed like the red/orange color of the cuticle and sometimes the small vacuole inside the conidia. The "strict" filter DAPI-Axio retrieves specific emission wavelengths from 420 nm and stops at 470 nm and therefore, retrieves signals more specific to aniline blue-callose binding. Epidermal cells were found to fluoresce differently according to the

interaction type and the combined use of filters helped us identify specific callose depositions (in papillae and cell walls) and dead cells.

5.5.1. LATE HYPERSENSITIVE RESPONSE AND CALLOSE DEPOSITION UPON EPIDERMAL CELL INVASION BY HAUSTORIAL STRUCTURES

First, we were able to observe two types of fluorescence inside the cells invaded by haustoria on OB and PC: (1) a weak granular fluorescence inside the cells but no strong fluorescence on the cell margins, and (2) circles of strong fluorescence inside the cells that became smooth and continuous around haustorial structures. These two types of cells were found at sites where haustorial colonization had happened but not where subcuticular hyphae alone were growing. The same discs were observed using a filter with narrow emission spectrum (DAPI-Axio) and the first type of cells with granular weak fluorescence (1) were no longer observed while the ones exhibiting circular bodies with strong fluorescence (2) were observed and co-localized with haustorial structures. We hypothesized that these circular bodies could be callose vesicles [CaV] observed inside invaded cells that brought the callose to be deposited in papillae around haustoria structures since the callose deposition around the haustoria neck was characterized by a strong fluorescence using both types of filters.

In addition, the invaded cells that appeared with low fluorescence (1) using BH2 filter (LP, long-pass) seemed to co-localize with the cells found to have collapsed around the subcuticular hyphae in OB and PC. Endogenous fluorophores are particularly abundant in plant tissues and they can fluoresce with excitation at 365 nm (Koga et al. 1988; Bennett et al. 1996; Vleeshouwers et al. 2000; Monici 2005; Donaldson 2020). Dead cells are known to present an autofluorescence and Koga et al. (1988) demonstrated that autofluorescence accompanies hypersensitive response (HR) cell death. Indeed, under an excitation between 320 nm and 490 nm with a peak transmission at 400 nm and an emission filter retrieving signals above 525 nm, these authors demonstrated that the autofluorescence intensity of dying and recently dead cells was weak but increased after death. They proposed that “generation of autofluorescence was a consequence of cell death” and that it might be due to the release or polymerization of cellular compounds upon programmed death and decompartmentalization. The filter sets used in the publications revealing autofluorescence of cells experiencing a HR were similar to the long pass filter DAPI-BH2 (LP420) but not DAPI-Axio. We can, therefore, say that the fluorescence observed in cells invaded by haustoria using the long pass filter DAPI-BH2 is an autofluorescence typical of dying cells or dead cells and is not related to callose. To go further, we can give several hypotheses to explain the epidermal cell death observed when the haustoria invaded them:

- **These cells were exhibiting a late HR-like response upon recognition of invasive haustoria.** However, this HR response seemed ineffective as the pathogen was able to develop further away in OB and PC leaves.
- **The pathogen manipulated the plant responses and induced the cell death via necrotrophic effectors** to enter in its necrotrophic stage.
- **An evolution happened and HR-like responses induced by the plant were overcome by the pathogen by producing intracellular necrotic hyphae to feed on the dead cells.**

The transcriptomic study of differential gene expression on the susceptible genotype can give us some responses. Indeed, if we find genes related to HR-like responses or cell death, we can confirm that cell death was activated upon haustorium recognition by the host. However, to know if these HR-like responses are induced by necrotrophic effectors produced by the pathogen, it will be necessary to study the pathogen transcriptome to identify whether or not the pathogen produces necrotrophic effectors. More specifically, it should be important to study when the shift between biotrophy and necrotrophy happens and if the pathogen produces intracellular hyphae after the invaded cells die or not.

5.5.2. EARLY HYPERSENSITIVE RESPONSE AND CALLOSE DEPOSITION AT THE PENETRATION SITE

On the contrary, for resistance cases like young leaves of RW with early callose deposition and GV, cells responding to the infection right under the penetration point exhibited fluorescence localized at the cell walls and not inside the cells like for the susceptible genotypes. These fluorescent cell walls were observed with both long pass and narrow band emission filters, so we can say with certainty that callose was deposited in these cell walls. Therefore, the fluorescing cells observed in the case of resistant phenotype, which exhibited small necrosis macroscopically, are of different nature than the ones with a fluorescence inside the cells. Then, we can say that in the case of young leaves of RW with early callose deposition and GV, a hypersensitive response was activated at an early stage of infection upon recognition of the first fungal structures and led to cell death (Figure 46). As a result, macroscopic necroses of small size were observed whereas in the case of susceptible genotypes (for which the fluorescence was observed inside the cells), the cell death leading to browning and collapsing of the tissues when the epidermal cells were invaded by haustoria was a late HR-like response. This hypothesis is supported by the observations made by Jacobs et al. (2003) and An et al. (2006) that callose-containing cell wall appositions were found in plasmodesma of cells neighboring the ones undergoing HR and that the dying cells typically became encased by callose (Underwood 2012).

Moreover, strong callose deposition at the penetration site was not observed in susceptible OB at early stages but was observed after 5dpi in RW leaves and was still present with reduced fungal growth in old and young leaves at 9dpi and 23dpi. For GV, a strong callose deposition was observed at 9dpi and was still present at 23dpi while for BE, the same type of callose deposition was not often observed at 9dpi but was frequent at 23dpi (Figure 46). We can say that **RW resistance in old leaves and some sites in young leaves and GV resistance were associated with early callose deposition at the penetration site**. For BE, the observations were less straightforward since a few sites exhibited callose deposition at the penetration site at 9dpi in the first replicate but we could not observe the deposition for the two other replicates. However, at 23dpi all replicates showed callose deposition around the penetration pore, which indicates that callose deposition was also involved in the resistance observed. In many studies, accumulation of callose in papillae is often used as a marker for PAMP-elicited host response (Dong 2005; Kim et al. 2005; Ellinger et al. 2013; Voigt 2014). Rapid formation of papillae was demonstrated to be correlated with enhanced resistance to fungal penetration and in particular, elevated amounts of callose deposited at infection sites at early time points of the infection strongly support penetration resistance (Bayles et al. 1990; Enrique et al. 2011; Ellinger et al. 2013). These observations might be true for genotypes like BE for which no further fungal growth was observed under the cuticle even after 23dpi, but it was less efficient in the case of RW because small hyphae could be observed, and was not sufficient for GV since reduced

fungal development under the cuticle with short subcuticular hyphae and haustoria was observed after 9dpi. For this genotype, a HR limited to a few cells was observed at 9dpi that seemed to have restricted the pathogen development. It would be interesting to investigate the speed of callose deposition for these genotypes as we only used 9dpi to compare these genotypes (Figure 46).

5.5.3. OTHER PLANT RESPONSES

An interesting difference between young leaves of RW and GV is the size of the haustoria that was limited in GV while for RW the haustoria were similar than in susceptible cases. Similarly, the haustoria developed in PC::*muRdr1A* were also small compared to the susceptible cases. It would be interesting to quantify the haustorium size for plants exhibiting different types of resistance such as partial resistance in RW and genotypes with major resistance genes like PC::*muRdr1A* and GV to see if we can identify a significant difference in haustorium size (Figure 46). Finally, RM resistance did not involve any plant response with callose deposition or HR, and might rely on other pre-penetration mechanisms that are yet to be discovered. Indeed, some germination was observed but we could not say if the germination was reduced compared to the other genotypes given that no quantification was done. Also, no observation of penetration attempts was made, which indicates a failure in organization of penetration events in conidia deposited on RM leaves (Figure 46). Existence of germination inhibitors or other toxic substances for the conidia can be hypothesized to be behind RM resistance. We could investigate conidia viability and germination after drops are deposited on the leaf surface for several hours or days but also inoculate the conidia that entered in contact with RM leaves on leaves of susceptible genotypes to see if penetration and infection can be observed. Similar work was done on rose cultivars 'Allgold' and 'Frensham' by Knight and Wheeler (1977). They demonstrated that "diffusates" containing conidia or heat-shock killed conidia, which were deposited on 'Allgold' leaves for 48 hours and then used to germinate new conidia on a slide, exhibited a reduced conidial germination compared to the water control. But when only water with no conidia was deposited on 'Allgold' and 'Frensham' leaves and afterwards conidia were left to grow on them, the germination was increased. The authors hypothesized that presence of fungal inducers (most likely PAMPs) activated the production of germination inhibitors that seemed slow since conidia germinated the first 24 hours on 'Allgold' but no further germination was observed after 48 hours (Knight 1975; Knight and Wheeler 1977).

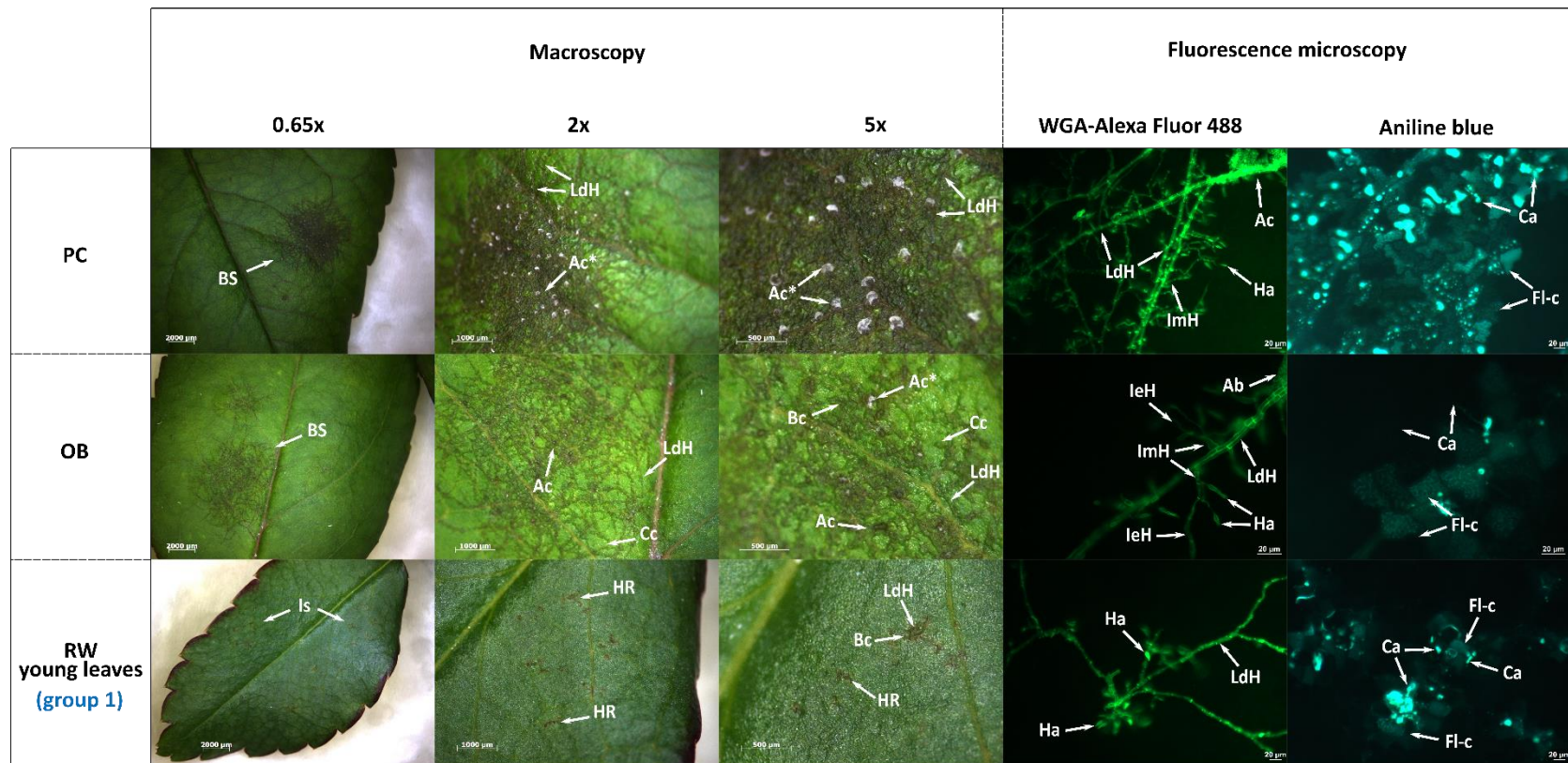


Figure 45: Summary of the compatible interactions between roses and DiFRA-67 investigated in this study

Ac: non-mature acervuli and Ac*: mature acervuli; Bc: brown cells/tissues; BS: black spot; Ca: callose depositions; Cc: cell collapsing; Fl-c: fluorescing cells; Ha: haustoria; HR: hypersensitivity response-like symptoms; Is: infection site; LdH: long distance hyphae (subcuticular hyphae); LeH: intercellular hyphae; ImH: intramural hyphae; .

NB: Young leaves of *Rosa wichurana* (RW) were classified in this section as some acervulus base could be observed at 9dpi in some cases.

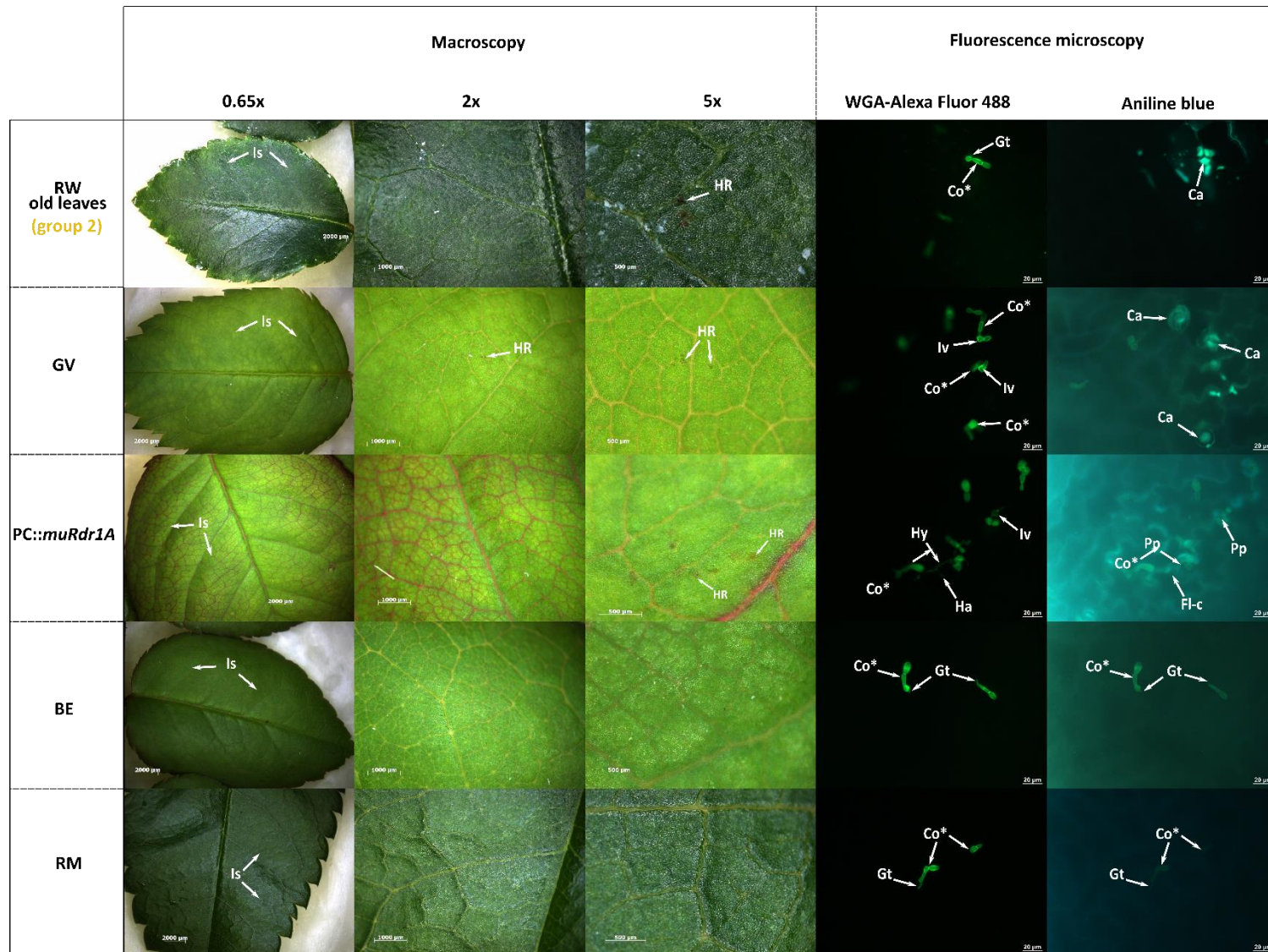


Figure 46: Summary of the incompatible interactions between resistant roses and DiFRA-67 investigated in this study

Is: infection site; HR: hypersensitivity response-like symptoms; Co: non-germinated conidia; Co*: germinated conidia; Gt: germ tube; Ca: callose depositions; Fl-c: fluorescing cells; Ha: haustoria; Hy: hyphae; Pp: penetration pore

Chapter 4 : Comparative transcriptional analysis of compatible and incompatible interactions during *Diplocarpon rosae* infection

Failure is a part of success. There is no such thing as a bed of roses all your life. But failure will never stand in the way of success if you learn from it.

– Hank Aaron



Rosa wichurana and its bed of leaves by M. Tisserand

1. SYNOPSIS

So far, we characterized, at a microscopic level, the interaction between *D. rosae* and two genotypes presenting a contrasted response to black spot infection: ‘Old Blush’ (OB, susceptible) and a genotype of *Rosa wichurana* species (RW, partially resistant). On one hand, the study carried out in chapter 3 showed us that the partial resistance of *R. wichurana* observed in the fields is based on a resistance that becomes more and more efficient as the leaf ages. In general, the partial resistance of our genotype RW resides in a combination of an early callose deposition at the penetration sites and post-penetration resistance involving cell death and something else not observable with the staining used. Also, we described in chapter 2 the existence of two main QTLs controlling black spot resistance in the fields. These QTLs have different effects on the phenotype and influence either the appearance of visible symptoms (QTL B5) or both the appearance and the severity of symptoms (QTL B3). On the other hand, the thorough study of the interaction between *D. rosae* and our susceptible genotype OB showed us a lack of response from OB at the first stage of the infection (before 3dpi), but an increase of reaction from the cells invaded by haustoria happens after 5dpi, with callose deposition and cell death. We could also detect a QTL in this genotype for one year in the field, and the region co-localized with a well-characterized cluster holding the *R*-gene *Rdr1*. However, we do not know anything else about the mechanisms leading to the type of interaction observed under the microscope.

One study demonstrated a medium correlation of three components (number of leaves, lesion length and leaf area with symptoms) between whole plant assay and detached leaf assay by using a single strain on 14 genotypes (Dong et al. 2017). Another study investigated the correlation of disease scores assessed on 19 genotypes between whole plants in a greenhouse assay using cuttings inoculated with 10 different strains (Soufflet-Freslon et al. 2019; Marolleau et al. 2020) and whole plants in fields that were scored at 11 french sites over three years. A good correlation was found between both assays even if a large variability of strains was assessed (10 strains artificially inoculated and 11 french sites with different natural populations of *D. rosae*). Among the genotypes studied, *Rosa wichurana* was found to have similar scores between both types of assay, and the strain DiFRA67, that we have chosen for our transcriptomic assay, was among the strains tested in the greenhouse assay (GDO, personal communication). Besides, the use of the artificial inoculation on whole plants in a greenhouse (Belarosa protocol presented in Soufflet-Freslon et al. 2019 and Marolleau et al. 2020) gives us more hindsight on both ‘Old Blush’ and *Rosa wichurana* behaviors when inoculated under these conditions. Furthermore, and as discussed in [chapter 1](#), plant integrity has been shown to be extremely important in plant-pathogen interactions and especially when studying the interactions at a molecular level (Orłowska et al. 2013). In addition, in non-model plants like apple, tests in detached leaves have yielded inconsistent results when studying plant defense responses to *Venturia inaequalis* in the case of a resistance based on major genes (B. Lecam, personal communication). Therefore, whole plant assay was used in this study to remain the closest to the natural conditions but also to be able to study the partial resistance to black spot disease in RW.

Therefore, to better understand the mechanisms behind RW resistance and to better describe OB compatible interaction, we proceeded to a comparative study of the transcriptomic changes that happen during the infection process for these two genotypes using a time course approach with a multi-series

experiment. The experiments were performed in the greenhouse using the whole plant assay with four times points and three biological replicates.

2. INTRODUCTION

To protect themselves against invaders, plants rely on a complex defense system that recognizes enemy molecules, carries out signals within and outside the invaded cells and initiates defensive responses. Plant immune responses involve many genes and their products that have different natures and functions (Andersen et al. 2018). For an ease of understanding of this complex defense mechanism, pathogen-associated molecular pattern (PAMP)-triggered immunity (PTI) and effector-triggered immunity (ETI) have been described to explain plant immune systems (Jones and Dangl 2006). However, for a long time, PTI and ETI have been considered as two distinct layers of the immune system but in recent studies, they have been shown to work in synergy to fine tune the plant response to invader (Boller and Felix 2009; Pritchard and Birch 2014; Cook et al. 2015).

Each cell of a plant is capable of triggering an immune response that is based on an active perception system recognizing danger signals present in extracellular space or in the host cytoplasm. Plant surveillance system is based on (1) surface detectors like pattern recognition receptors (PRRs) or wall-associated kinases (WAKs) that recognize microbe-associated molecular patterns (MAMPs), damage-associated molecular patterns (DAMPs) or extracellular effectors, and (2) cytoplasmic sensors like nucleotide-binding domains (NBS) and leucine-rich repeats (LRR) resistance proteins that recognize intracellular effectors or endogenous DAMPs (Boller and Felix 2009; Cook et al. 2015; Andersen et al. 2018). On one hand, many surface detectors have been described so far and they can be membrane-bound receptors such as receptor-like kinases (RLKs) or receptor-like proteins (RLPs) that exhibit an external binding domain for detection and internal kinase domain for signaling (Boller and Felix 2009; Andersen et al. 2018). On the other hand, nod-like receptors (NLRs) can directly recognize pathogenic effectors or indirectly by the guard system (example of RIN4 PRR proteins guarded by RPM1 R protein in chapter 1). Then it follows an extensive succession of signal transductions including multiple signaling components such as mitogen-activated protein kinase (MAPK) cascades, G-protein, calcium, ubiquitins or hormones. Hormones systematically regulate resistance responses according to the type of pathogen that has been recognized (biotrophs/necrotrophs). For instance, salicylic acid (SA), jasmonic acid (JA) and ethylene (ET) are involved in defense response to biotrophic pathogens while JA and ET are the main phytohormones involved in the response to necrotrophic pathogens (Derksen et al. 2013; Patkar and Naqvi 2017). Downstream signaling pathways lead to major transcriptional changes in plant cells and these are mediated by various classes of transcription factors that directly regulate responses by binding to promoters or by activation through phosphorylation. The major factors described are ethylene-response element binding factors (ERFs), MYBs, WRKYs or basic-helix-loop-helix (bHLH) proteins (Andersen et al. 2018). Finally, these transcription factors activate sets of genes involved in different immune responses like synthesis of secondary metabolites, cell wall modifications (callose deposition, lignification, etc.), expression of pathogenesis-related (PR) genes or reactive oxygen species (ROS) production and rapid cell death (hypersensitive response).

Many of the mechanisms described in model plants like *Arabidopsis thaliana* were also described in non-model plants like grapevine (*Vitis vinifera*) and in particular, in some members of *Rosaceae* family like strawberry (*Fragaria* genus), apple (*Malus x domestica*) or peach (*Prunus persica*). For example, strawberry fruits infected with *Colletotrichum acutatum* showed upregulation of *PR-5* and *PR-10* genes while *PR-2*, *PR-9* and *PR-13* were downregulated, and ripe and unripe strawberry fruits also exhibited *PR-10* upregulation when infected with *Colletotrichum acutatum* (Casado-Díaz et al. 2006; Guidarelli et al. 2011). Again, major allergens belonging to the *PR-10* family were also found to be highly induced in strawberry roots against the hemibiotroph oomycete *Phytophthora cactorum* (Toljamo et al. 2016). Similarly, several *PR*-genes and in particular *PR-10* were reported to be induced in apple challenged with *Venturia inaequalis* (Pühringer et al. 2000; Poupard et al. 2003; Chevalier et al. 2008; Cova et al. 2017) and in peach challenged with *Taphrina deformans* (Svetaz et al. 2017). ROS accumulation, cell death and callose deposition were reported in response to the filamentous form of *T. deformans* in several genotypes of peach (Svetaz et al. 2017). In addition, SA and JA signaling pathways were shown to be involved in defense response regulation in strawberry (Amil-Ruiz et al. 2016) and in apple, these hormone pathways seemed to be affected differently according to the pathogen (Balan et al. 2018). For example, brassinosteroids were upregulated by fungal pathogens but gibberellins and jasmonates were repressed by them while ethylene was highly affected by the bacterium *Erwinia amylovora*. Also, five different WRKY transcription factors (WRKY33, WRKY35, WRKY40, WRKY70 and WRKY75) were reported to be key regulators of diverse defense responses in apple (Balan et al. 2018). All these studies indicate that many defense mechanisms are similar between model and non-model plants and that conserved mechanisms can be found between members of the *Rosaceae* family.

Aside from major gene identification and some QTL analyses, rose responses to pathogen infection at a molecular level have not been extensively studied. One transcriptomic study reported different mechanisms of defense response to powdery mildew in two wild rose genotypes: the susceptible *Rosa gigantea* and the resistant *Rosa longicuspis* (Xiang et al. 2019). Another one studied the defense responses against *Podosphaera pannosa* (rose powdery mildew) and *Diplocarpon rosae* (black spot disease) during the first stage of compatible interactions (Neu et al. 2019). Both studies reported that the infection of *P. pannosa* in susceptible plants had an inhibitory effect on the photosynthesis and cell wall modification (Neu et al. 2019; Xiang et al. 2019). The infection of both *D. rosae* and *P. pannosa* induced the expression of genes coding for homologues of PR10, chitinase and transcription factors like WKRY and ERFs (Neu et al. 2019; Xiang et al. 2019). In the case of *D. rosae* infection, genes from the phenylpropanoid and flavonoid pathways as well as specific *PR*-genes (*PR1* and *PR5*) were upregulated. Noticeably, inoculation of *P. pannosa* in a susceptible rose genotype did not result in specific upregulation of functional groups related to defense mechanisms in Neu et al. study (2019). However, *RhMLO6* and *RhMLO7* were reported by Xiang et al. (2019) to be key factors in interaction between rose and *P. pannosa*. These studies indicate common responses to both *P. pannosa* and *D. rosae* but also specific pathways activated against each pathogen.

Among the numerous genomic approaches, transcriptomic approaches are the most used nowadays as they have been applied to model and non-model organisms from the plant, animal and fungus kingdoms (Spies and Ciaudo 2015). By tracing the transcripts accumulation, one is capable of studying the complex and dynamic network that is activated upon invader recognition by the host. A transcriptome profiling

aims to give, from the entire range of mRNA molecules of the transcriptome of a specific tissue, the significant changes in gene expression depending on the factors studied (Chakraborty and Basak 2017). Host-pathogen relationships are extremely complex and involve a highly dynamic network of genes for which the transcript accumulation changes over time. Therefore, in plant-pathogen interactions, transcriptomic approaches have helped us unveil many mechanisms of defense responses resulting in significant changes in gene expression within the host but also the pathogen during the infection. RNA-seq is one approach that allows access to a whole transcriptome while providing high reproducibility (Spies and Ciaudo 2015; Chakraborty and Basak 2017). In plant-pathogen interaction, a dynamic study is necessary to unravel the complexity of gene regulations during the infectious process. In this sense, time course (TC) experiments have proven themselves to be very informative to “recapitulate the whole regulatory network involved” (Spies and Ciaudo 2015). For instance, multi-time series comparing the TC data from a specific condition (inoculation for example) to a control TC allows a better control of the external variation due to the time and developmental processes. Indeed, in these multi-time series, controls are sampled at the same time as the tissue placed in a specific condition.

So far, no investigations on the changes in the leaf transcriptome of a partial resistant genotype following *D. rosae* infection has been done. Understanding the mechanism behind such resistance is crucial so we can get more insights in the rose response to *D. rosae*. In this study, we investigated the possible pathways involved in the immune response during *D. rosae* infection for two interaction types: a compatible interaction on OB rose leaves and an incompatible interaction on RW rose leaves. Furthermore, given the importance of systemic signaling in plant resistance (Orłowska et al. 2013) and to remain closer to the natural conditions in which RW partial resistance is well expressed, we decided to use whole plants in our study. Samples from three independent inoculations at four time points of interest in the development of *D. rosae* previously described (see chapter 3) were taken for each one of the two genotypes presenting contrasted levels of resistance. The transcript levels were analyzed following two methods: pairwise comparisons and time course analyses, to provide a comprehensive knowledge on the rose responses in two different contexts: compatible interaction and incompatible interaction.

3. MATERIAL AND METHODS

3.1. EXPERIMENTAL WORK

A transcriptomic approach was chosen to study the genes differentially expressed between the parents that originated the OW population used for QTL mapping: *Rosa wichurana* (RW, known to be partially resistant to *Diplocarpon rosae*) and *Rosa chinensis* ‘Old Blush’ (OB, known to be susceptible to *D. rosae*). The main objective was to investigate the genes involved in the responses of these two genotypes during *D. rosae* infection. Thanks to previous microscopic studies, we chose four time points (0, 3, 5 and 7 dpi, for days post inoculation) of the infectious cycle that seemed to be key moments of the response to the infection for both genotypes (Figure 47).

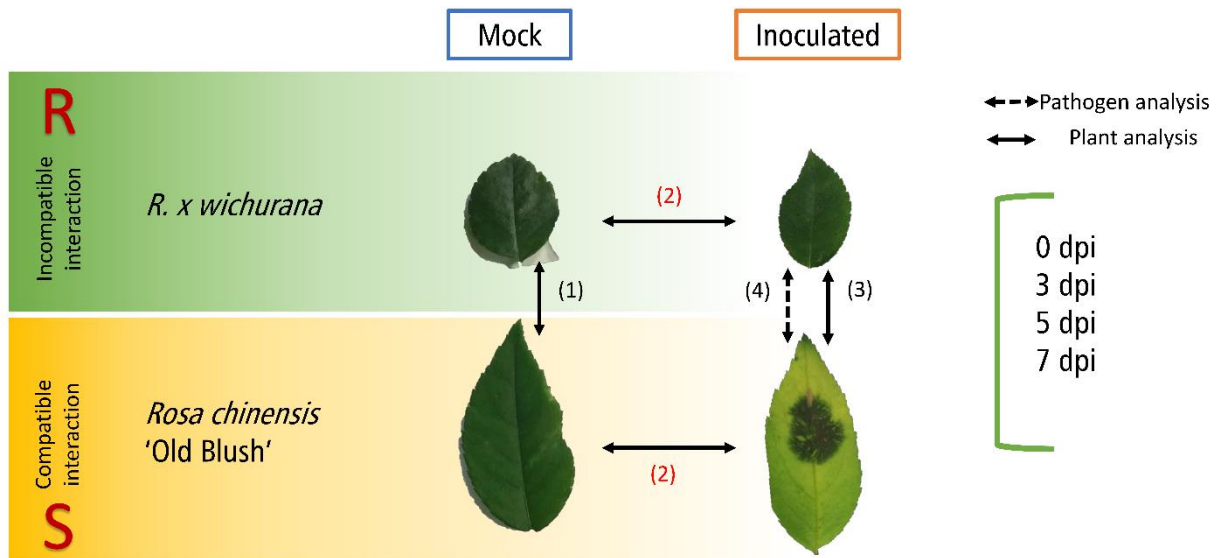


Figure 47: Experimental design for transcriptomic analyses using RNAseq

R. x wichurana is referred to as RW and *R. chinensis* 'Old Blush' is referred to as OB. R for resistant to black spot disease and S for susceptible to black spot disease. Mock are the samples sprayed with distilled water and Infected are the samples inoculated with the strain DiFRA67. Dpi stands for days post inoculation. The numbers in parentheses are the possible comparisons that can be done and in red are the comparisons that will be presented in this manuscript. The arrow with dotted lines (comparison '(4)') refers to the comparative analysis of fungal expression between a compatible interaction and an incompatible one.

Whole plants of each genotype were grown as described in [section 3.3.1](#) of chapter 3. The inoculation procedure for this assay was also described in [section 3.4.1](#) of chapter 3. Three independent inoculations were carried out and used as biological replicates. The plants were scored after 28dpi using the disease scale described in chapter 2. Old leaves were chosen to carry out the experiments as old leaves of RW expressed a true incompatible interaction, which was not the case for young leaves of RW. Moreover, in the fields, the infection starts at the bottom and progresses to the top so young leaves are rarely affected by black spot disease. Several comparisons can be performed but we decided to concentrate on the comparison between mock and infected samples for each type of interaction separately at different time points of the infection. Therefore, as two genotypes were studied under two conditions using three replications and leaves were sampled at four time points during the infection process, 48 samples were prepared in this study (Figure 47).

3.2. RNA PREPARATION

Whole leaves were detached and we removed the petiole just before the samples were flash-frozen in liquid nitrogen. A total of six leaves (two from three different cuttings) were pooled for each sample. The samples were grounded under liquid nitrogen to avoid de-freezing. After that, the samples were maintained at -80°C until RNA extraction. Total RNA was extracted using the kit NucleoSpin® RNA plus from Macherey/Nagel with the following adaptation of the protocol: we used 50mg of frozen tissues and added 600 μL of a solution containing PVP40 at 2% and the buffer LBP preheated. After vortex agitating for 2 min and then centrifuging for 2 min, we treated the pellet a second time to extract as much RNA as possible. After adding the BS buffer and fixing the molecules on the blue filter, we proceeded with a DNase treatment for 30 min (DNase buffer 90 μL + DNase 10 μL) to remove contaminant DNA. The rest of the

protocol was followed as recommended by the supplier. The concentration of RNA in the samples as well as possible contamination of other molecules and degradation were controlled with a Nanodrop™ One machine and an Agilent Bioanalyzer system before sending the samples to the sequencing company.

3.3. TRANSCRIPTOME SEQUENCING AND COMPUTATIONAL ANALYSES

The characteristics of the transcriptome sequencing will be presented in this section and all the computational analyses detailed in the following section are summarized in Figure 48.

3.3.1. LIBRARY PREPARATION AND SEQUENCING CHARACTERISTICS

A minimum of 20 µg of total RNA concentrated at 20ng/ml for each sample was submitted to Novogene Co., Ltd company. They enriched the mRNA using oligo(dT) beads and then fragmented the mRNA randomly in a fragmentation buffer followed by cDNA synthesis using random hexamers and reverse transcriptase. They used TruSeq™ mRNA stranded library preparation kit (Illumina®) and followed the workflow chart presented in Supplementary figure 39. Quality control was performed at each step and the library concentration was first quantified using a Qubit 2.0 fluorometer (from Life Technologies). Insert size was also checked on an Agilent 2100 and quantified using quantitative PCR (qPCR). All 48 samples were laid out in a single lane of Illumina Novaseq 6000 sequencing system. An average of 15G of raw reads per sample was generated with paired-end libraries of 150 base pair (bp) length for each read.

3.3.2. ILLUMINA ADAPTERS TRIMMING IN SAMPLES AND QUALITY CONTROL

Raw reads from Novogene were used for the analysis and a multithreaded command line tool, Trimmomatic (v0.32) was used to trim, cut and remove the adapters from Illumina sequencing (Bolger et al. 2014). The sequencing quality before trimming was assessed and as it was high enough, a gentle trimming was sufficient to obtain good quality data. The parameters used for trimming were:

- adapter and palindrome clipping searching for universal Illumina adapters (TruSeq3-PE) test for two mismatches per seed, a palindrome clip threshold at 30 and an alignment score between read and adapter at 10 (parameter: ILLUMINACLIP:TruSeq3-PE.fa:2:30:10);
- bad end clipping for “LEADING” and “TRAILING” was set at 3 to remove low quality or N bases from the beginning and the end, respectively (parameters: LEADING:3 and TRAILING:3);
- sliding window scan was set at 4 bases checked for quality less than 15 to cut bad quality group of bases (parameter: SLIDINGWINDOW:4:15);
- the minimum length to keep a read was set to half of the total read length, so 75bp.

In general, with these parameters, 4.6% of the reads were trimmed for bad quality and were homogenous for all samples. Quality controls of the data with the duplicated levels, mean quality value across each base position in the read, the number of reads with average quality scores, the GC content and the percent of base calls that were called N for each position on the read (per base N content) were checked using FastQC software (v3) for each sample separately, and Multiqc (1.8) software was used to aggregate the QC results from different samples. Multiqc was run from the Miniconda Prompt shell using conda language.

3.3.3. RNA-SEQ READ MAPPING AND POST-MAPPING QUALITY

The splice-aware alignment tool STAR (v2.7.3, Dobin et al. 2013) was used to perform the read alignment on the rose genome published by Hibrand-Saint Oyant et al. (2018). Before performing the alignment, several tests and calculations were carried out to adapt the parameters to the mapping situations and the genome characteristics (see Annex 5). Indeed, the reference genome corresponds to one parent (OB) whereas RW is another *Rosa* species, and therefore more distant from the reference sequence. So, to improve the mapping efficiency, the mismatches between the reads and the genome were adapted for OB and RW samples with 10 mismatch maximum sets for OB and 16 mismatch sets for RW. The minimum intron length was set to 20bp and maximum intron length was set to 20,000bp (see Annex 5). The intron motifs were removed and the chosen quantification mode was “GeneCounts”. For quantification, STAR uses the same features as htseq-count with default parameters. For each sample, the output was produced as a file “ReadsPerGene.out.tab” with four columns that correspond to different strandness options. Our library being reverse stranded, we used the gene counts given by the fourth column of the count files. The mapping process was looped to run all 48 samples automatically using the server available at the IRHS (characteristics: 16 processor Intel(R) Xeon(R) E5-4620 @ 2.20GHz, RAM 500 Go, operating system Debian GNU/Linux 8 (Jessie))

RSeQC (v3.0.1) offers several packages that can provide useful information about data quality after mapping. A total of 11 modules of RSeQC were used to perform post-mapping quality control. The results of this quality control will not be all developed here but were carefully inspected to detect quality deviations between samples. Bed files for IGV(v2.8.0) visualization were generated using several functions provided by Samtools (v1.10).

3.3.4. DIFFERENTIAL EXPRESSION ANALYSIS OF RNA-SEQ DATA

Two types of analysis are proposed here. First, a pairwise analysis comparing water-sprayed samples (mock) and inoculated ones at each time point separately for both interaction types was carried out using a Wald test. Second, several approaches were explored to perform time course analysis but only the single time series using a Likelihood Ratio Test (LRT) proposed by DESeq2 will be presented here. With the time course approach, we looked at the genes that were differentially expressed over the time and thus exhibited the same pattern of expression over the studied time points. This analysis was carried out separately for inoculated (I) and mock (NI) samples for both genotypes.

3.3.4.1. DATA EXPLORATION AND QUALITY CONTROL

To explore data, a normalization of all 48 samples data was performed using the DESeq2 package (version 1.28.1, Love et al. 2014) available in R (version 4.0.2, R Core Team 2020). DESeq2 package normalizes the counts using a median of ratio method and accounts for the sequencing depth and RNA composition following several steps (row/gene-wise geometric mean, ratio of each sample to the reference, calculation of the normalization factor for each sample and normalization of the count values using a normalization factor). It is important to consider all sources of variation present in our data and to include them in the design formula to remove and/or control them. For our experiment, the three obvious sources of variation were the genotype (OB and RW), the time (0, 3, 5 and 7dpi) and the condition (inoculated and mock). However, knowing that we performed real biological replicates (three separated

inoculations) and that such replicates can represent a source of variation in the data, I decided to include the “rep” effect in the design formula.

Two steps in the data exploration were followed. First, we explored all 48 samples using the data from both genotypes. The design formula used for this step was the following: (1) ‘design = ~ rep + time + genotype + condition’. Then, a per genotype analysis was carried out by separating the samples from each genotype (24 samples per genotype). The design formula used for this step was (2) ‘design = ~ rep + time + condition’. This analysis allowed us to explore the data for each genotype separately. Differences between days post inoculation were found, so I decided to subsequently separate the time points for further pairwise comparison analyses.

The quality controls were performed at sample-level with principal component analysis (PCA) and hierarchical clustering of the normalized data and at gene-level. To proceed with clustering and distance calculations for the PCA and the sample hierarchical visualization, the normalized counts needed to be transformed by moderating the variance across the mean. For this, I used the ‘vst()’ (variance stabilizing transformation) function for the analysis using all the samples (design formula (1)) as it performed better than ‘rlog()’ (regularized log transformation) function for a high number of samples (more than 30). When the genotypes were separated, I used the ‘rlog()’ function to transform the data (less than 30 samples). The hierarchical clustering was performed using the Euclidean distances between samples and was reported using the function ‘heatmap.2()’.

3.3.4.2. PAIRWISE COMPARISONS USING DESEQ2 PACKAGE

The normalized counts obtained for each genotype separately using the formula (2) were used to carry out the pairwise comparisons between inoculated (I) and mock (NI) samples. For each genotype, separated datasets were prepared to study time points independently. So at each time point, I compared (I) samples to (NI) samples for both interaction types (compatible with OB and incompatible with RW). In total, eight pairwise comparisons were made. After normalizing the data, it was important to apply a log fold change (LFC) shrinkage (function ‘lfcShrink()’) to visualize and rank the genes. For example, ranking the genes by LFC to separate up-regulated genes from down-regulated ones for further evaluation as well as enrichment analyses (GSEA, PAGE, etc.). These downstream analyses required shrinkage of log fold change. Indeed, Log fold change shrinkage was shown to improve the DEG detection (Wu, Wang and Wu 2013). Genes with low counts are known to be very variable and have, therefore, higher dispersion. When shrinkage is applied, DESeq2 assumes that genes with similar expression have similar dispersion to generate more accurate estimates of variation and, therefore, tries to address the problem of high dispersion observed in genes with low counts. The shrunken values were used for the following analysis. To test for differential expression in a pairwise comparison approach, a Wald test was used to test the hypothesis of a differential expression across two sample groups ($LFC \neq 0$) against a null hypothesis assuming there is none ($LFC = 0$) for each gene successively. All p-values obtained by single Wald testing were corrected for multiple testing using Benjamini and Hochberg methods and DESeq2 applied a false discovery rate (FDR) of 0.05.

3.3.4.3. TIME COURSE USING A SINGLE TIME SERIES ANALYSIS WITH LRT METHOD AVAILABLE IN DESeq2

An alternative to pairwise comparisons is the analysis of all the levels (here time points) at once and is useful for time course experiments. The likelihood ratio test (LRT) proposed in DESeq2 was used to identify any change of expression across the infection (time). The LRT compares a full model containing the time factor ('design = ~ rep + time') to a reduced model without the time factor ('design = ~ rep') to identify significant genes. In this case, the p-values are determined by the difference in deviance between the 'full' and 'reduced' model formula but not the log2 fold changes like for the pairwise comparison. This test usually yields a larger amount of genes than for the pairwise comparison approach, so an additional step is needed to identify clusters of genes exhibiting particular patterns of expression across time. To do this, I calculated the rlog transformed normalized counts and subsetted the significant differentially expressed genes over the time (with padj<0.05). Using the tool 'degPatterns()', a hierarchical clustering based on pairwise correlations was performed and, then, the hierarchical tree was cut to generate groups (or clusters) of genes exhibiting similar expression profiles over the time. Finally, the list of genes within groups that were generated and that exhibited patterns of interest could be extracted and used in functional enrichment analysis.

3.3.5. COMPLEMENTATION OF ROSA CHINENSIS 'OLD BLUSH' GENOME ANNOTATION AND FUNCTIONAL ENRICHMENT ANALYSES OF RNA-SEQ DATA USING GENE ONTOLOGY

A custom reference annotation of Hibrand-Saint Oyant et al. (2018) genome was prepared. Indeed, only 21,973 genes out of the 44,481 genes predicted were annotated in the gene ontology (GO) annotation file published with the genome. Therefore, to complete the pre-existing gene ontology annotation, we proceeded to different steps using the files provided with the genome publication and that could be downloaded from the GDR website (https://www.rosaceae.org/species/rosa/chinensis/genome_v1.0). First, we gathered the different transcript similarities that were determined by pairwise sequence comparison using the blastx algorithm against various protein databases such as Swissprot, TAIR10 and TrEMBL. When a gene was found in more than one database, we selected the geneID of the database with different priorities. If the Swissprot geneID was available, we chose this one first, if not we chose the gene annotation with the TAIR10 database and if not, we searched in the TrEMBL database. The corresponding geneIDs of the homologues in other species were reported in a file that was used to retrieve the GO annotation using the tool "Retrieve/ID mapping" proposed by Uniprot (<https://www.uniprot.org/uploadlists/>). When genes did not have any similarity with the databases, we used the results of the InterProScan analysis for which GOs were already available. In the end, a total number of 30,729 genes out of 44,481 genes were annotated with this technique which greatly increased our precision in GO enrichment analyses. The new annotation file was prepared to be uploaded on the web-based tool and database for gene ontology AgriGO v2.0 (Du et al. 2010; Tian et al. 2017) for subsequent use as reference background during enrichment analyses (see <http://systemsbiology.cau.edu.cn/AgriGOv2/download.php>).

AgriGO v2.0 was chosen to perform the enrichment analysis of the gene list. AgriGO V2.0 proposes two types of analyses: (1) single enrichment analysis (SEA) that functions like an over representation analysis (ORA) (Du et al. 2010; Tian et al. 2017) and (2) parametric analysis of gene set enrichment (PAGE)

that takes into account expression values of Log2 fold change and that is considered to be a richer alternative to SEA for RNAseq datasets (Kim and Volsky 2005). Therefore, for the pairwise comparison analysis, I used PAGE analysis to perform enrichment analyses on the list of genes that were generated. With this type of analysis, there is no need to separate the up-regulated and down-regulated genes since the Log2 fold changes are taken into account. For each genotype, a joint analysis was carried out which allowed us to browse significant GO terms for all the time points at the same time. The statistical test method selected was Fisher, the multi-test adjustment method used was Hochberg (a less strict adjustment) as the minimum mapping entries proposed by the tool is 10, which is very strict. An interesting feature in the PAGE analysis of AgriGO is that the visualizations with a table and GO trees give information about the GOs being associated with up-regulated or down-regulated genes. Therefore, the results will be presented for each interaction type using the visualizations proposed by AgriGO v2.0. For the time course analysis, as the gene list from each group exhibited similar variation over the time, PAGE analysis was not interesting, so we used SEA analysis instead to explore the GO enriched in each group list keeping in mind the variation described by the group. The statistical test method selected was Fisher, the multi-test adjustment method used was Yekutieli (FDR under dependency), and minimum mapping entries were reduced to three as Yekutieli adjustment is very strict. For both analyses, the reference list of genes used was the newly uploaded GO dataset from our complete annotation of Hibrand-Saint Oyant et al. (2018) genome.

3.3.6. FUNGAL READ MAPPING FOR CONTAMINATION ANALYSIS

The main objective of this part was to test if we could find *Diplocarpon rosae* mRNA in inoculated samples and check if there was no contamination between inoculated and mock samples. Otherwise, some leaflets presented, after 15 days, a slight infection of powdery that remained very limited, so we wanted to know if, within the reads, we had some that aligned to *Podosphaera pannosa* genome. For this purpose, we used the set of reads that did not map to the rose genome (“unmapped reads”).

With several tests of read' blasts, we demonstrated that a significant amount of reads mapped to scaffolds that were mostly rRNA sequences (data not shown). Therefore, I decided to proceed with a computational rRNA removal prior mapping using the software SortMeRNA v4.2.0. SortMeRNA is a sequence alignment tool for filtering, mapping and OUT-picking. A total of eight databases were used to identify reads that corresponded to residual rRNA from the samples: ribosomal RNA from eukaryotes (18s, 28s, 5s and 5.8s), bacterias (16s, 23s and 5s) and archaeas (16s, 23s, 5s and 5.8s). These databases were extracted from SortMeRNA v3.0.4 (see Supplementary table 3). The function generated a log file for each sample separately, so the percent of reads aligning with each database for all samples was gathered in a single file using a shell script. The data were visualized using a 'ggplot2' package on R. As the paired reads that aligned with rRNA databases and the ones that did not align were saved in files with the pair of reads merged together, it was necessary to separate the merged paired-end reads using the shell script 'unmerge-paired-reads.sh' available in SortMeRNA v3.0.4 library before mapping with STAR.

The reads cleaned from rRNA were mapped on the draft genome of DortE4 of *D. rosae* (Neu et al. 2017). Then the same reads were mapped on the genome of *Podosphaera xanthii*, the causal agent of powdery mildew in cucurbits. *P. xanthii* was the closest species to *Podosphaera pannosa*, the causal agent of powdery mildew in rose, which had a published genome (209 Mb, 112 contigs, N50 = 581,650 nt,

https://www.ncbi.nlm.nih.gov/assembly/GCA_010015925.1/). I decided, once again, to adapt the mapping parameter ‘outFilterMismatchNmax’ to the genome where the reads were mapped. Indeed, on one hand, we decided to use 12 mismatches when mapping on DortE4 genome, as we were mapping a different strain (DiFRA67) but that was still the same species (*D. rosae*). On the other hand, we increased the number of mismatches allowed to 16 when mapping on *P. xanthii* genome as rose powdery mildew is a *Podosphaera* but from another species (*P. pannosa* instead of *P. xanthii*). The total number of reads mapping on each one of the fungal genomes tested was counted for all the samples and a statistical analysis was carried out. The percentage of reads mapping on *D. rosae* and *P. xanthii* out of all the unmapped and out of the total number of reads sequenced were also calculated to assess how much of the data they represented.

3.3.7. STATISTICAL ANALYSES

The number of reads mapping on each fungal genome and for all samples was statistically analyzed to identify if there was any difference of read counts between fungus types, conditions (mock and inoculated with DiFRA67), genotypes and time points. For that matter, we tested the normality of the residuals and the homoscedasticity of the raw data with a Shapiro-Wilk normality test and a Bartlett test, respectively. As both assumptions were not met, we searched for the best transformation type using the package ‘bestNormalize’ available in R, and the orderNorm or ORQ transformation was used to transform the data. After that, the normality of residuals and homoscedasticity of the transformed data were tested again and both assumptions were met, which allowed us to proceed with an analysis of variance (ANOVA). The linear model used to perform the ANOVA included an interaction term between the condition, genotype and fungus. The initial formula was:

$$norm.mapping_cts \sim Genotype + Condition + Time + Rep + Fungus + Condition * Genotype * Fungus$$

Among all the interactions tested by this model, only Fungus*Condition was found significant using a likelihood ratio test (LRT) testing the interaction model with a model without interaction. Therefore, the final formula used for the ANOVA analysis was:

$$norm.mapping_cts \sim Genotype + Condition + Time + Rep + Fungus + Fungus * Condition$$

Tukey multiple pairwise comparison was used to assess which group means were different from each other and for this, I used the function ‘TukeyHSD()’ (Tukey honest significant differences) available in R. The graphs were generated using the ggplot2 package.

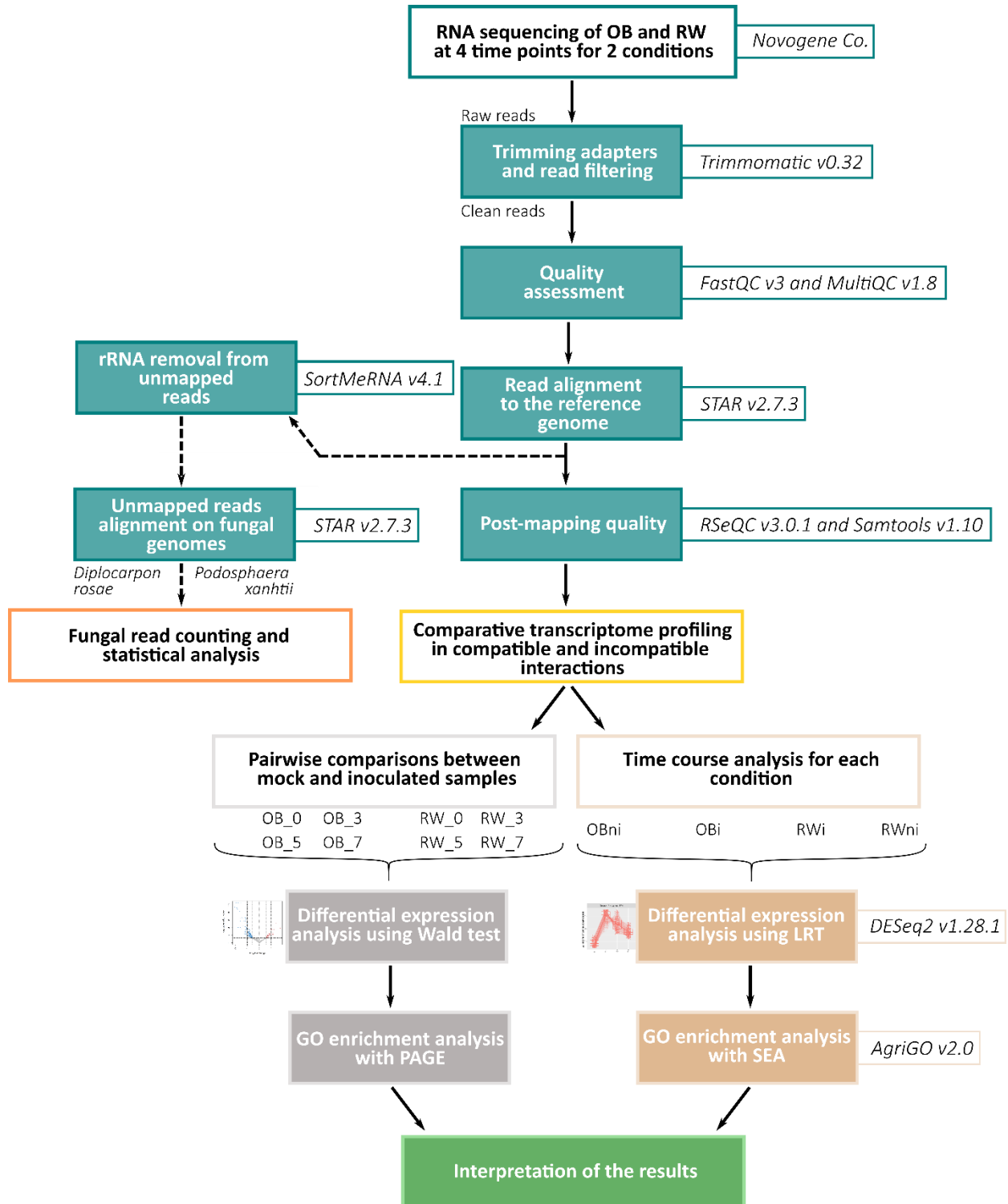


Figure 48: RNAseq analysis workflow followed for the host reads

OBni refers to mock samples of OB genotype and OBi to the inoculated ones; RWni refers to mock samples of RW genotype and RWi to the inoculated ones; LRT stands for likelihood ratio test; SEA stands for single enrichment analysis; PAGE stands for parametric gene set enrichment analysis

4. RESULTS PART 1: MAPPING AND QUALITY ASSESSMENT

4.1. QUALITY CONTROLS

Several quality controls before mapping were performed using the software FastQC but only two QC results for the reads after trimming will be presented here. First, the mean quality scores for all samples were very good and constant along the read length (see Supplementary figure 40A). Then, the GC content was found to be normally distributed with a small difference between forward and reverse reads. The forward reads are displayed in green and the reverse reads are displayed in yellow in the Supplementary figure 40B. According to the sequencing platform, this bias is often observed in stranded libraries like ours.

After the mapping, 11 post-mapping quality controls were carried out using RSeQC. No apparent problem was found in the controls and here, I present the results of the gene body coverage that allowed us to check if the gene coverage was uniform and if there was any 5'/3' bias. In our data, most of the samples exhibited a uniform gene body coverage except for samples RW_I_5_C, RW_N_3_C and RW_N_5_C that showed a lack of coverage at 5' end of the genes (see Supplementary figure 40C). However, to consider that there is a problematic 3'/5' bias (due to RNA degradation, library preparation or computational problem), a dramatic drop or peak needs to be observed, which was not our case. Then, we can conclude that a slight 5' bias was observed for these three samples with no major problem for subsequent analyses. Finally, the read distribution over genomic features did not show any bias in the sequencing. On average 85.6% of the reads mapped to CDS exons and 5.1% to introns. Reads mapping to intergenic regions beyond 10kb from transcription start/end sites (TSS/TES) only represented 4.2%. Separating OB and RW samples, 4.3% were found in intergenic regions for RW compared to 4.1% for OB (see Supplementary figure 40D). Groups of reads mapping in intergenic regions can be due to different reasons: sequencing errors, mapping errors or non-annotated genes. If we consider that the sequencing and mapping errors are very low, the small differences between the percent of tags mapping to intergenic regions between OB and RW means that the difference of genes between OB and RW species is low.

4.2. MAPPING RESULTS

After read alignment, STAR counts the number of reads per gene using the default parameters of HTSeq. For a genome of small size, genes can overlap and it is difficult to count a read as it can belong to one gene or the other one. HTSeq counts the reads with a special care on overlapping genes using the union mode of the overlap resolution modes. With this mode, each exon is considered as a feature so alternative splicing can also be taken into account.

We can see that the percent of reads overlapping genes was similar between RW and OB since on average 83% were assigned to genes. The same observation can be done with the reads that mapped in regions with no annotated genes (i.e. No feature) since on average 5% to 6% of the reads did not overlap genes (see Supplementary figure 41A). Less than 1% of the reads had ambiguous features. A read is considered as ambiguous if it overlaps two genes at the same time. Interestingly, allowing more mismatches for the mapping of RW samples did not significantly increase the percent of reads found to map in multiple locations (i.e. Multimapping feature), indeed 2.73% of the reads were assigned to multimapping features for OB and 3.06% for RW. Finally, the percent of unmapped reads was slightly higher for RW (6.63%) than for OB (6.05%) with sample RW_N_3_C having the highest percentage of

unmapped reads (10.65%) (see Supplementary figure 41B). This might be explained by the small library size observed for that sample (data not shown).

5. RESULTS PART 2: DIFFERENTIAL EXPRESSION ANALYSIS USING RNASEQ

5.1. TRANSCRIPTOMIC CHANGES SPECIFIC TO THE GENOTYPES

To get an overview of the expression level relationship between the different samples, I plotted the transformed normalized counts on principal component analysis (PCA) plot and performed a hierarchical clustering of the samples based on Euclidean distances. Two samples were removed because of quality problems: RW_N_5B and OB_N_7B. Indeed, these samples did not cluster with the rest of the samples and exhibited very different gene expression. In addition, RW_N_5B, a mock sample, exhibited reads from the *D. rosae* (see [section 6.1](#)). The data presented here reports the results for the 46 samples left. Two large groups were visible, clearly separating the genotypes OB and RW (Figure 49A). Indeed, most of the variation observed in the gene expression was driven by the genotype (PC1:91%), and a slight differentiation over the time could be observed along the PC2 axis. In fact, for both genotypes, time points 0dpi and 3dpi were separated, and in the middle the time points 5dpi and 7dpi could be observed (Figure 49A-B). As expected with completely independent inoculations, the replicates were variable. This observation confirms the importance of considering the variation between replicates in the design formula used to normalize the counts. Noticeably, the samples were not well separated between condition types (Figure 49B) even if the black spot disease scoring at the plant level at 28dpi showed a clear difference between inoculated samples and mock ones (see Figure 49C and [Chapter 3](#)). For further analyses, I decided to separate the genotypes so we could have more power to detect differentially expressed genes between inoculated samples and mock ones.

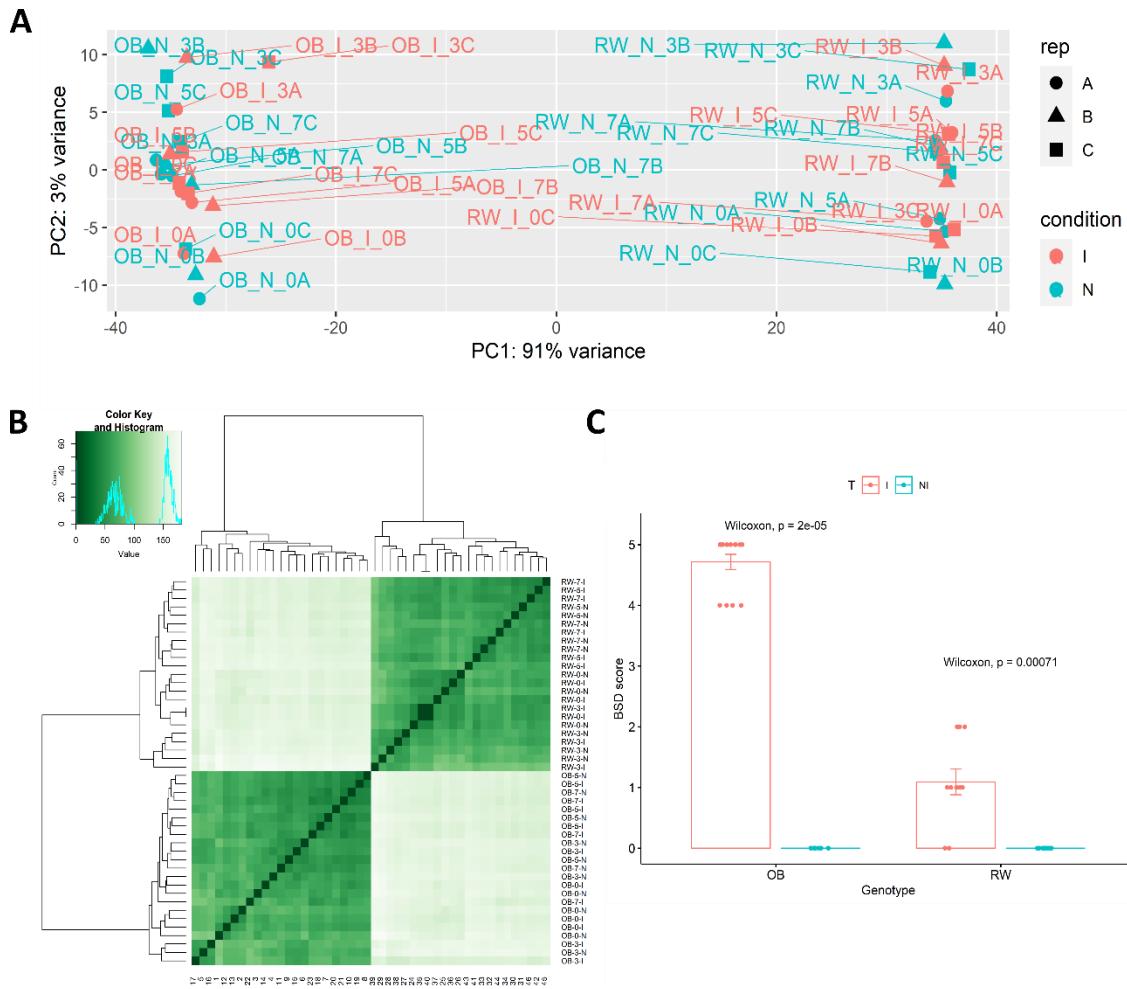


Figure 49: Exploratory data analysis with principal component analysis (PCA) and sample hierarchical clustering for all the samples considering genotype, time, condition and repetition as factors of variation

A: PCA plot of gene expression data in RW and OB leaves challenged by DiFRA67 (I for inoculated) and for the controls sprayed with water (N for mock); **B:** Sample hierarchical clustering using Euclidean distances; **C:** Black spot disease scoring at 28dpi for both genotypes OB and RW and for both conditions (treatments or T): I in pink and NI in blue.

5.2. PAIRWISE COMPARISON BETWEEN MOCK AND INOCULATED SAMPLES FOR A COMPATIBLE INTERACTION

I will first analyze the difference between inoculated and non-inoculated in OB (section 5.2.1) and then in RW (section 5.2.2).

5.2.1. CLUSTERING ACCORDING TO THE TIME AFTER INOCULATION FOR OB SAMPLES

After separating the genotypes, we explored the data once again to reveal differences in gene expression across groups. For OB genotype, the samples were well separated by time: 0dpi (in blue), 3dpi (in yellow) and 5-7dpi (in red), except for the first biological replicate of the mock at 3dpi (OB_N_3A) and the last replicate of the inoculated sample at 0dpi (OB_I_0C) that were both found in the group 5-7dpi. A slight separation between inoculated samples and mock ones was observed for 3dpi and 5-7dpi (Figure 50). However, the difference between inoculated samples and mock ones was relatively small. For subsequent analysis of pairwise comparisons between mock and inoculated samples, I decided to separate the samples by days post inoculation (dpi).

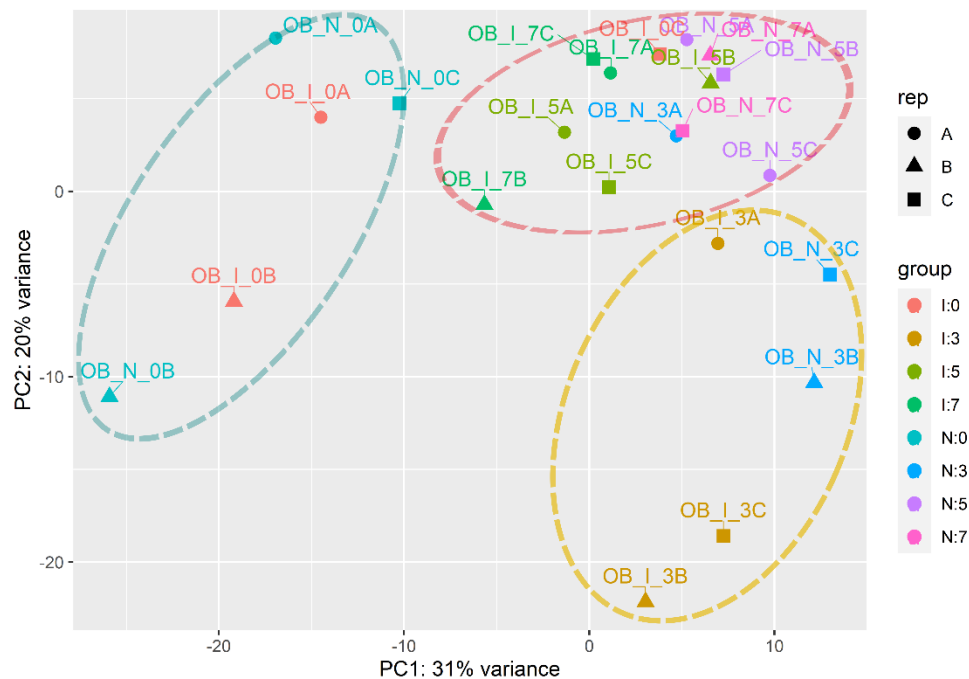


Figure 50: Principal component analysis (PCA) of gene expression data in 'Old Blush' (OB) leaves challenged by DiFRA67 (I) or water-sprayed (N)

5.2.2. NUMBER OF DIFFERENTIALLY EXPRESSED GENES OVER THE INFECTION FOR OB GENOTYPE

A gene was considered differentially expressed if the p-adj was below 0.05 value. I used different values for the log₂FC. First, to count the genes that were differentially expressed between inoculated samples and mock ones for each time point, I set the cut-off at 1 (see Figure 51). Overall, I found 293 genes that were significantly regulated (214 up-regulated and 79 down-regulated) during *Diplocarpon rosae* infection in the susceptible OB. The total number of differentially expressed genes (DEG) varied with the time of infection with interesting patterns: at 0dpi, 47 genes were differentially expressed, the number of DEGs increased at the penetration moment (3dpi) to 104 DEGs, then decreased again when the fungus was growing subcuticular hyphae (5dpi, the asymptotic growth) with only 27 DEGs, and increased again at

7dpi with 115 DEGs when we observed a large amount of cell death at the haustoria invasion sites (see chapter 3). We can see that the same observations can be made for the genes that were specifically up-regulated. However, the number of down-regulated genes decreased over time from 38 genes at 0dpi to six genes at 7dpi. The number of DEG in OB was low when comparing I vs NI samples. This low number could be due to the high variability between the real biological replicates.

Then, to investigate the proportion of genes that had subtle changes in expression, I used two limits of log₂FC at 0.58 and 1 on the volcano plots presented in Figure 52. Interestingly, a high amount of genes was significantly differentially expressed with a log₂FC between 0.58 and 1 especially for time points 0 and 3dpi, but they rarely had a high significance value (low padj).

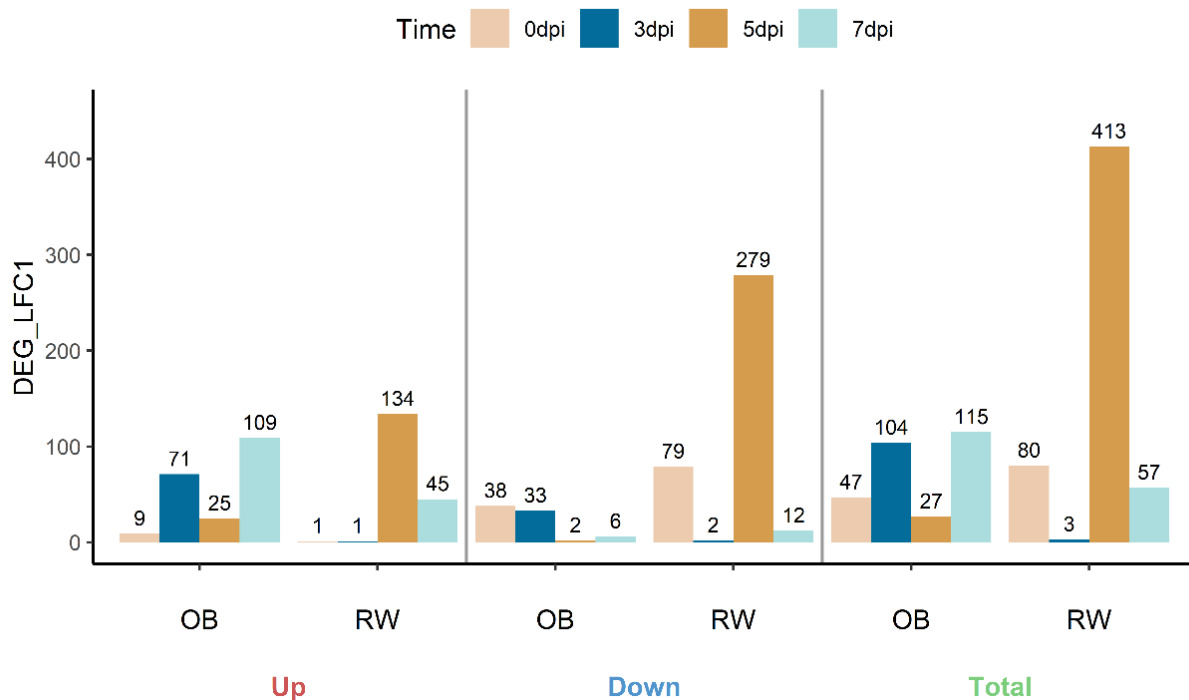


Figure 51: Number of genes differentially expressed (DEG_LFC1) between inoculated and mock samples at each time point of the infection by *Diplocarpon rosae* for both genotypes 'Old Blush' (OB) and *R. x wichurana* (RW)

Indeed, at 0dpi, 101 genes with moderate changes (0.58 to 1) were significantly down-regulated and 36 genes were up-regulated. Similarly, at 3dpi, 45 down-regulated genes and 109 up-regulated genes exhibited moderate changes in expression. However, for 7dpi, most of the up-regulated genes that were differentially expressed exhibited higher changes in expression (more than 1 log₂fold change) and only a small portion of them had moderate changes in expression: only 39 genes had a log₂fold change between 0.58 and 1 while 109 genes had more than 1 log₂fold change between inoculated samples and mock ones. Noticeably, even considering a lower limit of log₂fold change (at -0.58), a very few down-regulated genes could be reported at time points 5 and 7dpi (three and 12 genes with moderate change in expression, respectively).

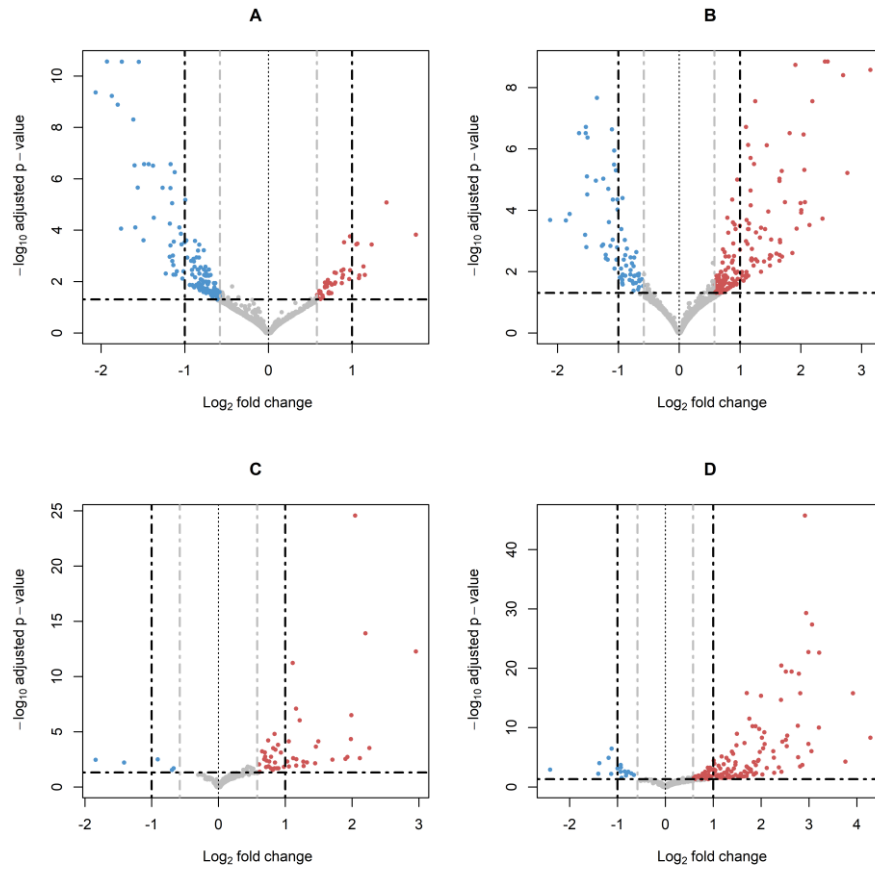


Figure 52: Volcano plots of the genes differentially expressed during *Diplocarpon rosae* infection of the susceptible genotype 'Old Blush' (OB)

Each plot represents the Log2fold change of each gene in function of the $-\log_{10}$ of the p-value adjusted. Genes are considered differentially expressed if the p-adj is below 0.05 (horizontal dashed lines), and two log2fold change limits were used: one at 0.58 (dashed grey vertical line) and another one at 1 (dashed black vertical line). The genes meeting the thresholds are colored in blue if they were down-regulated and in red if they were up-regulated. **A:** Genes differentially expressed at 0dpi; **B:** Genes differentially expressed at 3dpi; **C:** Genes differentially expressed at 5dpi; **D:** Genes differentially expressed at 7dpi.

5.2.3. FUNCTIONAL ANALYSIS USING PARAMETRIC GENE SET ENRICHMENT ANALYSIS (PAGE) OF OB GENES DIFFERENTIALLY EXPRESSED BETWEEN INOCULATED AND MOCK SAMPLES

To run the PAGE enrichment analysis with AgriGO v2, genes with a p-adj below 0.05 in at least one of the time points for OB were selected for the analysis, and the log₂fold change for each gene for all four time points was gathered in a single file and organized following the recommendation of AgriGO v2. In total, 637 genes were found to be significantly expressed in at least one time point, and 539 of them were annotated with the new complete annotation uploaded in AgriGO v2. Overall, 467 GO terms were found to be significantly enriched with 76 GO terms for 0dpi, 56 GO terms for 3dpi, 46 GO terms for 5dpi and 11 GO terms for 7dpi.

Different GO terms enriched for several time points were found to be linked to an up-regulation and the majority of these GO terms were related to defense or immune responses. In Figure 53A, I presented some examples of GO terms found to be enriched for several times points. Defense response genes were found to be up-regulated at 0, 5 and 7dpi with a stronger up-regulation at 7dpi (103 genes were annotated like that at 7dpi). Interestingly, common GO terms were found to be enriched between 0 and 5dpi with, in particular, GO terms associated with plant hypersensitive responses (HR) and cell death upon microbe recognition. Other GO terms indirectly pointing towards cell death preparation were also found to be enriched at 0 and 5dpi such as peptidase activity, proteolysis, protein catabolic process, cellular protein catabolic process, proteolysis, etc. Among the 13 genes annotated with biological process response to UV-B that were found to be up-regulated at 0 and 5dpi, seven genes code for senescence-specific cysteine protease SAG12, and these genes were also annotated as plant HR, defense response to fungus, programmed cell death involved in cell development, response to cytokinins or leaf senescence for the biological process or senescence activated vacuole for cellular components. Finally, three interesting molecular functions were found to be enriched at 0dpi: transmembrane transporter activity (48 genes), active transmembrane transporter activity (26 genes) and kinase activity (51 genes).

GO terms were also found to be enriched at specific time points of the infection and some examples are reported in Figure 53B. No GO term directly related to defense or immune responses was found to be enriched at 3dpi (see Figure 53A) but instead, the GO terms found at 3dpi were linked to regulation of gene expression and transcription (see Figure 53B). Indeed, specific GO terms with regulation of RNA metabolic pathway or biosynthesis were enriched for the biological process and others were linked to different molecular functions like DNA binding, transcription factor activity through sequence specific DNA binding or regulatory region DNA binding. All of these GO terms were associated with up-regulation at 3dpi. The genes associated with these regulations of transcription coded for transcription factors like WKRY24, 40, 41, 46 and 50 or membrane receptor kinases like cystein-rich receptor-like kinase 1 (RLK1) and 27 (RLK27), L-type lectin-domain containing receptor kinase VII.2, lectin-domain containing receptor kinase VI.3 or brassinosteroid-signaling kinase 3 (BSK3). On the contrary, ion homeostasis GO terms were found to be down-regulated at 3dpi (see Figure 53B).

Interestingly, several GO terms associated with cell wall biogenesis were found to be enriched in sets of genes that were down-regulated at 0dpi. Indeed, metabolic processes of cell wall components such as hemicellulose, polysaccharide or xyloglucan were strongly down-regulated at 0dpi (see Figure 53C). Several genes coding for proteins participating in cell wall construction were found among the down-

regulated genes with high significance such as five genes coding for hydrolase proteins 2, 8, 9, 16 or 23 that are xyloglucan endotransglucosylase proteins with some of them being regulated by brassinosteroids, or even three genes coding for exordium proteins that are known to play a role in brassinosteroid-dependent regulation of growth and development (see Supplementary table 5).

Then, two GO terms related to reactions triggered in response to fungus that aim to protect the cell or the organism were specifically enriched at 5dpi (GO:0009817, defense response to fungus, incompatible interaction and GO:0009814, defense response, incompatible interaction). These two GO terms are secondary IDs belonging to the biological process GO:0050832 (defense response to fungus) and GO:0098542 (defense response to other organisms), respectively. These GO terms were associated with an up-regulation at 5dpi (see Figure 53C). Again, GO terms linked to tissue senescence like leaf senescence, aging and cellular macromolecule catabolic processes were found to be specifically enriched among up-regulated genes at 5dpi. Noticeably, at the same time, strongly up-regulated genes were found to be associated with organ development (flower, leaf or phyllome). Finally, specific up-regulation of genes at 7dpi was found to be associated with main GO terms from biological processes such as response to biotic stimulus and response to stress (see Figure 53D). A strong up-regulation at that time point was associated with molecular functions like enzyme regulator activity, enzyme inhibitor activity or molecular regulator. Signaling molecular functions were also found to be up-regulated at 7dpi like, for example, signaling receptor activity or signal transducer activity (see VD). Interestingly, genes coding for pathogenesis-related proteins (PR proteins) were found to be highly up-regulated especially after 5dpi (see Supplementary table 4). Indeed, four genes coding for PR-2 proteins and three genes coding for PR-10 proteins were up-regulated at 5dpi. At 7dpi, 18 PR-genes were up-regulated, and among them five coded for PR-10, five others coded for PR-2, two for chitinases (PR-4 family) and one for PR-1 (see Supplementary table 4). In addition, three genes annotated as "pathogen-related proteins" were also up-regulated specifically at 7dpi. It is worth noticing that three senescence-activated genes 12 (SAG12) were up-regulated (LFC<1) at 5dpi and two other SAG12 genes with a LFC>0.70 were also up-regulated at 5dpi (see Supplementary table 4).

GO Information					CM			
No	GO Term	Onto	Description	OB_0dpi	OB_3dpi	OB_5dpi	OB_7dpi	
1	GO:006952	P	defense response					
2	GO:0034050	P	host programmed cell death induced by symbiont					
3	GO:0009626	P	plant-type hypersensitive response					
4	GO:0012501	P	programmed cell death					
5	GO:0002376	P	immune system process					
6	GO:0045087	P	innate immune response					
7	GO:006955	P	immune response					
8	GO:0008219	P	cell death					
9	GO:0051603	P	proteolysis involved in cellular protein catabolic process					
10	GO:0044257	P	cellular protein catabolic process					
11	GO:0009735	P	response to cytokinin					
12	GO:1990267	P	response to transition metal nanoparticle					
13	GO:0033554	P	cellular response to stress					
14	GO:0048468	P	cell development					
15	GO:0098542	P	defense response to other organism					
16	GO:0030163	P	protein catabolic process					
17	GO:0010224	P	response to UV-B					
18	GO:0009411	P	response to UV					
19	GO:0006508	P	proteolysis					
46	GO:0070011	F	peptidase activity, acting on L-amino acid peptides					
47	GO:0008233	F	peptidase activity					
54	GO:0022857	F	transmembrane transporter activity					
57	GO:0004175	F	endopeptidase activity					
58	GO:0022804	F	active transmembrane transporter activity					
60	GO:0016301	F	kinase activity					

GO Information					CM			
No	GO Term	Onto	Description	OB_0dpi	OB_3dpi	OB_5dpi	OB_7dpi	
78	GO:0010468	P	regulation of gene expression					
80	GO:2000112	P	regulation of cellular macromolecule biosynthetic process					
84	GO:2001141	P	regulation of RNA biosynthetic process					
85	GO:1903506	P	regulation of nucleic acid-templated transcription					
86	GO:0097659	P	nucleic acid-templated transcription					
87	GO:0051252	P	regulation of RNA metabolic process					
88	GO:0032774	P	RNA biosynthetic process					
89	GO:0006355	P	regulation of transcription, DNA-templated					
90	GO:0006351	P	transcription, DNA-templated					
95	GO:0016070	P	RNA metabolic process					
96	GO:0034654	P	nucleobase-containing compound biosynthetic process					
112	GO:0019438	P	aromatic compound biosynthetic process					
121	GO:0003677	F	DNA binding					
124	GO:0003676	F	nucleic acid binding					
125	GO:0043565	F	sequence-specific DNA binding					
126	GO:0046983	F	protein dimerization activity					
127	GO:0003700	F	transcription factor activity, sequence-specific DNA binding					
128	GO:0001071	F	nucleic acid binding transcription factor activity					
129	GO:0044212	F	transcription regulatory region DNA binding					
130	GO:0001067	F	regulatory region nucleic acid binding					
131	GO:0000975	F	regulatory region DNA binding					
116	GO:0055076	P	transition metal ion homeostasis					
118	GO:0050801	P	ion homeostasis					
119	GO:0055080	P	cation homeostasis					
120	GO:0055065	P	metal ion homeostasis					

GO Information					CM			
No	GO Term	Onto	Description	OB_0dpi	OB_3dpi	OB_5dpi	OB_7dpi	
20	GO:0016043	P	cellular component organization					
21	GO:0071840	P	cellular component organization or biogenesis					
22	GO:0005976	P	polysaccharide metabolic process					
23	GO:0044085	P	cellular component biogenesis					
24	GO:0071554	P	cell wall organization or biogenesis					
25	GO:0071555	P	cell wall organization					
26	GO:0045229	P	external encapsulating structure organization					
27	GO:0044036	P	cell wall macromolecule metabolic process					
28	GO:0044262	P	cellular carbohydrate metabolic process					
29	GO:0044264	P	cellular polysaccharide metabolic process					
30	GO:0044042	P	glucan metabolic process					
31	GO:0006073	P	cellular glucan metabolic process					
32	GO:0042546	P	cell wall biogenesis					
33	GO:0010410	P	hemicellulose metabolic process					
34	GO:0010383	P	cell wall polysaccharide metabolic process					
35	GO:0010411	P	xyloglucan metabolic process					

GO Information					CM			
No	GO Term	Onto	Description	OB_0dpi	OB_3dpi	OB_5dpi	OB_7dpi	
142	GO:0009817	P	defense response to fungus, incompatible interaction					
146	GO:0010150	P	leaf senescence					
149	GO:0007568	P	aging					
151	GO:0009814	P	defense response, incompatible interaction					
133	GO:0030154	P	cell differentiation					
135	GO:0048827	P	phyllome development					
137	GO:0009908	P	flower development					
138	GO:0048366	P	leaf development					
140	GO:0044265	P	cellular macromolecule catabolic process					
159	GO:0009607	P	response to biotic stimulus					
160	GO:0006950	P	response to stress					
161	GO:0004857	F	enzyme inhibitor activity					
162	GO:0098772	F	molecular function regulator					
163	GO:0030234	F	enzyme regulator activity					
164	GO:0038023	F	signaling receptor activity					
165	GO:0004871	F	signal transducer activity					

Figure 53: Example of enriched GO terms obtained with a PAGE analysis for the response of ‘Old Blush’ (OB) genotype to *Diplocarpon rosae* infection

Selected GO terms showing specific responses to infection in the susceptible genotype OB are characterized by: a number (No) that can be used to browse the GO terms in the complete table, the GO term number, the ontology (Onto) and the description. PAGE calculates the significance for each time point (named row) given by the user, and each GO term found to be significantly enriched for at least one time point (row) is accompanied with a color. The gradient of colors corresponds to: orange color system means up-regulated, and colors going towards dark blue means down-regulated. The darker the color is, the higher the average log2fold change is. **A:** Subset of GO terms found to be significantly enriched in more than one time point of infection; **B:** Enriched GO terms specific to OB response to infection at 3dpi; **C:** Enriched GO terms specific to OB response to infection at 0dpi; **D:** Enriched GO terms either specific to the response to the infection at 5dpi or at 7dpi.

5.3. PAIRWISE COMPARISON BETWEEN MOCK AND INOCULATED SAMPLES FOR AN INCOMPATIBLE INTERACTION

5.3.1. CLUSTERING ACCORDING TO THE TIME AFTER INOCULATION FOR RW SAMPLES

Like for OB, a majority of the variability in RW transcriptomic data could be explained by the time after inoculation as a clear separation of the time points 0, 3 and 5-7dpi could be observed (see Figure 54). The time point at 3dpi (yellow cluster) was well separated from the others following PC1 (33% explained by this axis), and the time point 0dpi (blue cluster) was also well separated along PC2 with 23% of the variability explained by this component. The same way as for OB, the time points 5dpi and 7dpi were found together (red cluster). Unlike OB, all the replicates for each time point were in the same cluster (see Figure 54). A slight separation along PC1 could be observed between inoculated and mock samples for 0dpi as well as for time points 5 and 7dpi. Nevertheless, the difference between treatments (inoculated with DiFRA67 and water-sprayed) were very small. Noticeably, no separation at all between treatments was observed for the time point at 3dpi (see Figure 54).

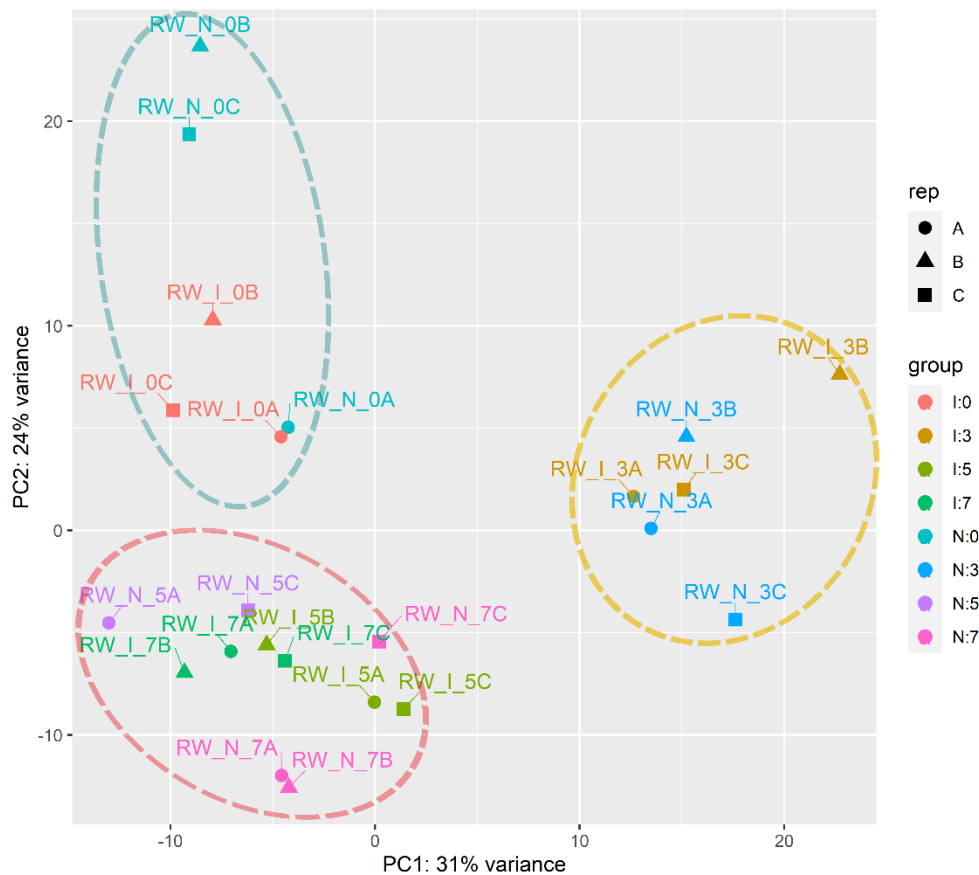


Figure 54: Principal component analysis (PCA) of gene expression data in *R. x wichurana* (RW) leaves challenged by DiFRA67 or water-sprayed

5.3.2. NUMBER OF DIFFERENTIALLY EXPRESSED GENES OVER THE INFECTION FOR RW GENOTYPE

On Figure 51, we can see the number of DEG during the infection for RW genotype if the genes considered as differentially expressed exhibited a p_{adj} below 0.05 and a cut-off of \log_2 fold change at 1. Strangely, the majority of genes found to be differentially expressed between inoculated and mock samples at 0dpi were down-regulated (79 genes) while only one was found to be up-regulated. In addition, at 3dpi, only one gene was up-regulated and two were down-regulated. These odd results can be visualized by the volcano plots A and B of Figure 55. Even considering a lower \log_2 fold change threshold (at 0.58), only an additional small portion of genes were differentially expressed. Indeed, two genes with moderate changes in expression were up-regulated at 0dpi and three additional genes were either up or down-regulated at 3dpi. The lack of differences between treatments on the PCA is observable here with in total three genes that were differentially expressed between the inoculated samples and the mock ones.

A large number of genes (413 DEG) were found to be differentially expressed at 5dpi with 134 up-regulated and 279 down-regulated genes. Interestingly, the majority of genes that were differentially expressed at 5dpi exhibited a \log_2 fold change greater than 1, and 11 down-regulated genes were found with high significance levels (a $-\log_{10}$ of the p_{adj} greater than 20). For 7dpi, 45 DEG were up-regulated and 12 were down-regulated. At this time, two genes were found to be highly up-regulated, and two down-regulated genes had high significance levels compared to the other down-regulated genes found at that time point.

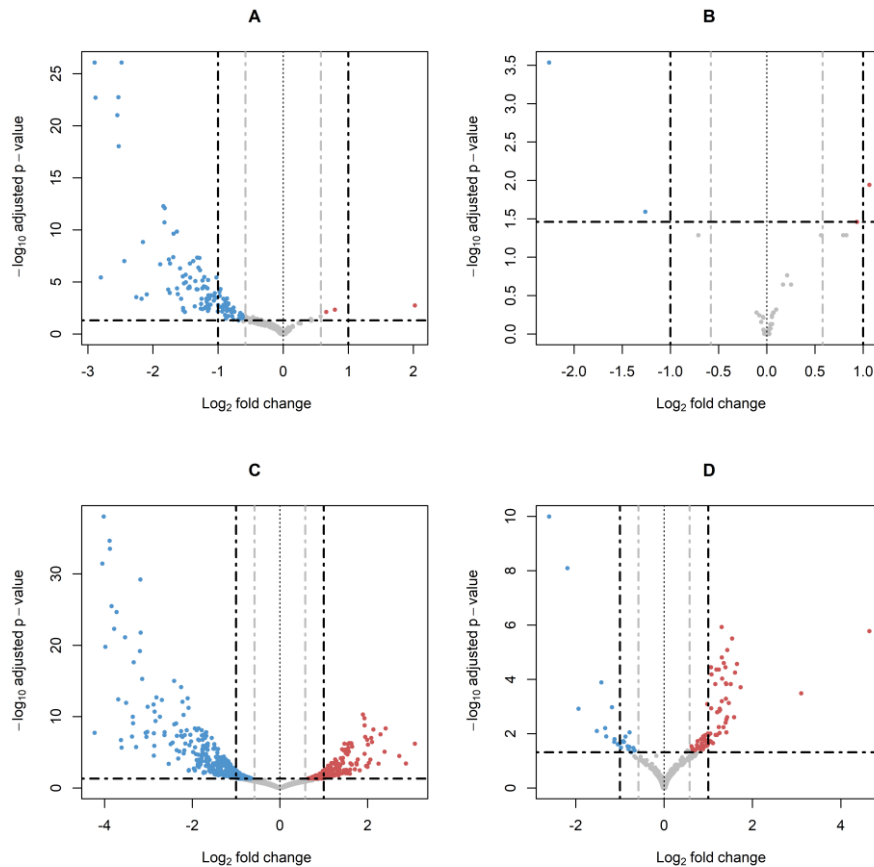


Figure 55: Volcano plots of the genes differentially expressed during *Diplocarpon rosae* infection of the resistant genotype *R. x wichurana* (RW)

Each plot represents the Log₂fold change of each gene in function of the $-\log_{10}$ of the p-value adjusted. Genes are considered differentially expressed if the p-adj is below 0.05 (horizontal dashed lines), and two log₂fold change limits were used: one at 0.58 (dashed grey vertical line) and another one at 1 (dashed black vertical line). The genes meeting the thresholds are colored in blue if they were down-regulated and in red if they were up-regulated. **A:** Genes differentially expressed at 0dpi; **B:** Genes differentially expressed at 3dpi; **C:** Genes differentially expressed at 5dpi; **D:** Genes differentially expressed at 7dpi.

5.3.3. FUNCTIONAL ANALYSIS USING PARAMETRIC GENE SET ENRICHMENT ANALYSIS (PAGE) OF RW DIFFERENTIALLY EXPRESSED GENES BETWEEN INOCULATED AND MOCK SAMPLES

Due to the lack of genes found differentially expressed at 3dpi, I decided to exclude the dataset for 3dpi to run the GO enrichment analysis. Two datasets were then prepared to run the enrichment analysis with genes differentially expressed at 0dpi and 5-7dpi ($p_{adj} < 0.05$ and log₂fold change threshold at 0.58). Examples of the results obtained with this enrichment analysis are presented in Figure 56. First, at 0dpi, only two GO terms from cellular components were found to be significantly enriched and were associated with down-regulation: extracellular region and apoplast (Figure 56A). For 3dpi, no enrichment analysis could be carried out as less than 10 genes were found to be differentially expressed. But the two up-regulated genes code for galactinol synthase 2 (GolS-2) and the two down-regulated genes code for agamous-like MADS-box protein AGL104 and ankyrin repeat domain-containing protein (see Supplementary table 7). For the 5dpi gene list, a large number of GO terms were enriched (Figure 56B). The enriched GO terms associated with up-regulation had a link to defense response, signaling and response to stimulus while the ones associated with down-regulation were mostly linked to the lignin

biosynthesis (phenylpropanoid metabolism), flavonoid production and secondary metabolism (Figure 56B). Among the genes annotated as defense response, three genes coding for SAG12 (senescence-associated gene) proteins, three coding for disease proteins RGA2, one encoding a RPM1 disease protein and two *N* genes coding for TMV resistance protein *N* were found to be significantly up-regulated (see Supplementary table 6). In addition, one gene coding for a pathogenesis-related protein PR-5, two other ones annotated “pathogen-related protein” and “thaumatin-like protein”. Several GO terms were found to be enriched for both 5 and 7dpi such as response to organonitrogen compound that were related to up-regulated genes at 5dpi and down-regulated genes at 7dpi. Another group of GO terms was significantly enriched for both time points and was linked to cell wall biogenesis (plant-type cell wall organization or biogenesis, plant-type secondary cell-wall biogenesis, cell wall macromolecule metabolic process, etc.). These GO terms were associated with genes down-regulated at 5dpi and up-regulated at 7dpi (Figure 56C). Moreover, additional GO terms linked to cell wall biogenesis and production of carbohydrate and polysaccharides were specifically enriched at 7dpi. Other GO terms, found to be associated with down-regulation at 7dpi, were related to responses to abiotic stress such as salt stress, light stimulus, and UV for biological processes but also to gene expression regulation for molecular function (Figure 56D).

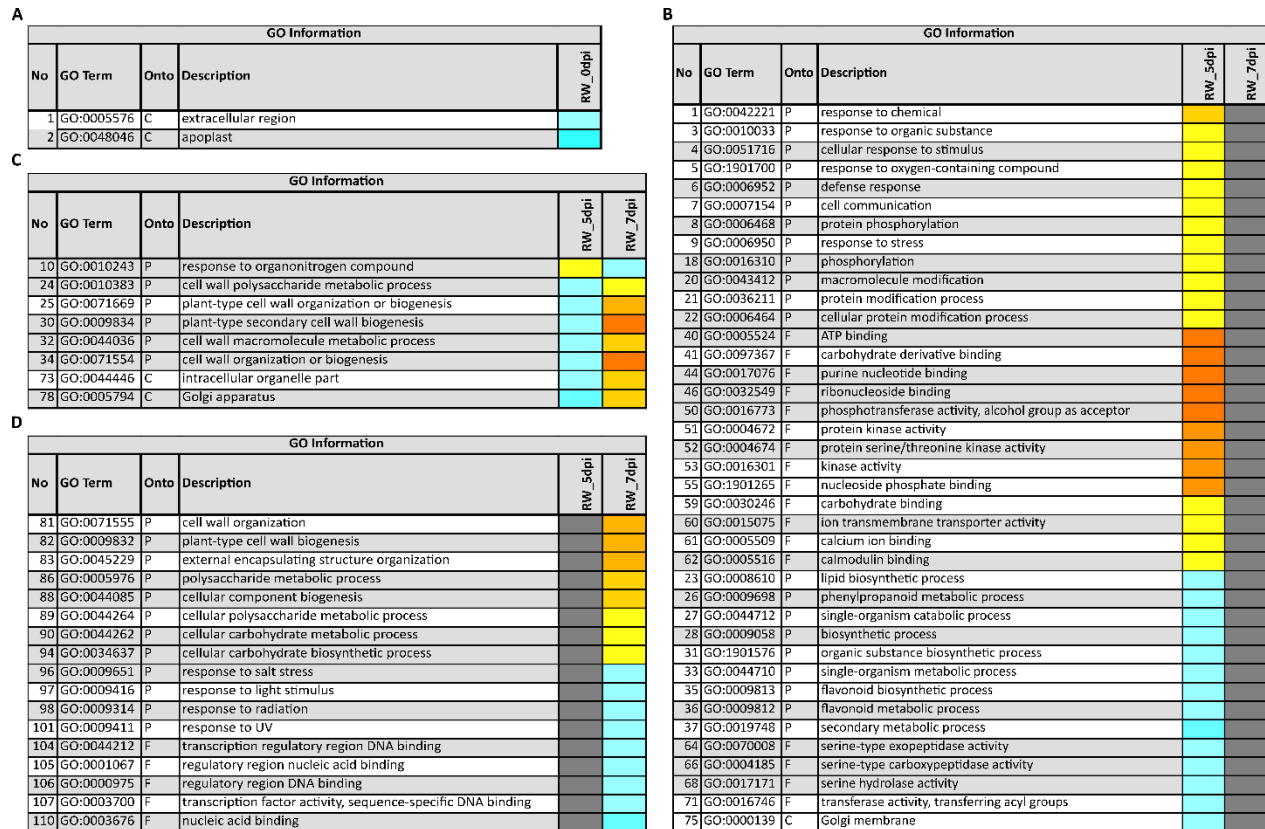


Figure 56: Example of enriched GO terms obtained with a PAGE analysis for the response of *R. x wichurana* (RW) genotype to *Diplocarpon rosae* infection

Selected GO terms showing specific responses to infection in the partial resistant genotype RW are characterized by: a number (No) that can be used to browse the GO terms in the complete table, the GO term number, the ontology (Onto) and the description. PAGE calculates the significance for each time point (named row) given by the user, and each GO term found to be significantly enriched for at least one time point (row) will be accompanied with a color. The gradient of colors corresponds to: orange color system means up-regulated and colors going towards dark blue means down-regulated. The darker the color is, the higher the average log2fold change is. **A:** Subset of GO terms found to be significantly enriched at 0dpi; **B:** Enriched GO terms specific to RW response to infection at 5dpi; **C:** Enriched GO terms common RW response to infection at 5-7dpi; **D:** Enriched GO terms specific to the response to the infection at 7dpi.

6. RESULTS PART 3: INVESTIGATION OF POWDERY MILDEW CONTAMINATION IN RNASEQ SAMPLES

The lack of results for 3dpi as well as the strong down-regulation observed at 0dpi are odd results that are linked to an absence of difference between mock and inoculated samples. As several problems of powdery mildew infection were observed in other experiments before carrying out the transcriptomic assay, and as some leaves were found to present a beginning of powdery mildew infection at 15dpi in our experiment, we hypothesized that some infections of the plants could have happened before the assay and the effect of such infection could be observed in the response of RW. To test this hypothesis, we decided to carry out an investigation of powdery mildew contamination in RNA-seq samples, and this will be presented in the following section. Then, an additional analysis was carried out to study the changes in expression over the time points previously defined by analyzing separately the inoculated and the mock samples using a time course approach.

6.1. QUANTIFICATION OF FUNGAL READS FROM *DIPLOCARPON ROSAE* AND *PODOSPHAERA PANNOSA*

6.1.1. RRNA REMOVAL FROM ROSE UNMAPPED READS AND MAPPING TO FUNGAL GENOMES

To quantify the amount of fungal reads in RNA-seq samples, we used the unmapped reads from the mapping on the host reference genome (*R. chinensis* 'Old Blush', Hibrand-Saint Oyant et al. 2018). The unmapped reads represented around 6.05% and 6.63% of the reads for OB and RW, respectively (see Supplementary figure 42). We detected the presence of rRNA in the unmapped reads. Due to their high level of conservation, we decided to remove and study these rRNA sequences.

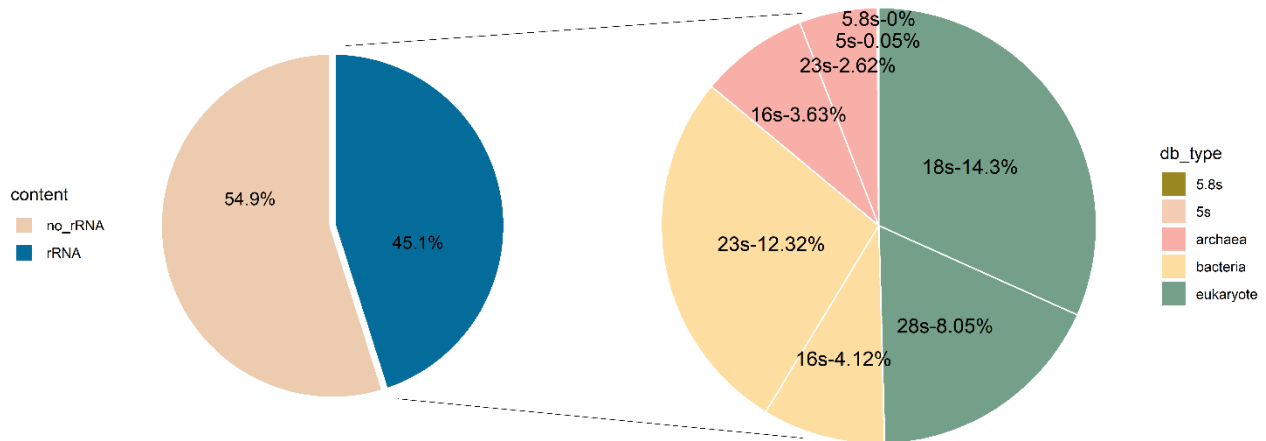


Figure 57: Summary of rRNA composition of unmapped reads (content, pie chart on the left) and the corresponding percent of rRNA aligning with each rRNA database (db_type, pie chart on the right)

45.1% of unmapped reads corresponded to rRNA sequences. Among them, 22.35% were rRNA from eukaryotes (14.3% were 18s rRNA subunit and 8.05% 28s rRNA subunit), 16.44% aligned to bacteria rRNA (12.32% of 23s and 4.12% of 16s), 6.25% corresponded to archaea rRNA (with 3.63% of 16s and 2.62% of 23s) and finally, very small amount to none of the reads aligned to small rRNA subunits like 5s and 5.8s (See Figure 57). We can hypothesize that the unmapped reads consisted of transcripts from organisms present in the phyllosphere. The rRNA, being very conserved between species and even between genera, can interfere with the fungal read counting from the unmapped reads as almost 23% of the rRNA were from eukaryotes, either fungi or plants.

After rRNA removal, less than 0.01% of the total number of reads were mapped on *Diplocarpon rosae* genome which corresponded to less than 0.2% of the unmapped reads (Supplementary figure 43). We observed a higher percentage of reads mapped on *D. rosae* genome for inoculated samples than for mock samples (only RW_N_5B presented a relatively high level of fungal reads). In general, a lower percentage of reads mapped on the *Podosphaera xanthii* genome and it did not seem to vary between samples, treatments or genotypes; these reads represented less than 0.001% of the total number of reads. As we mapped separately the same samples on both genomes, we checked if we had common reads mapping on both genomes, which represented less than 1.5% of the reads mapped on fungal genomes (which corresponded to six reads, data not shown).

6.1.2. STATISTICAL ANALYSES OF FUNGAL READ COUNTS

The study of the number of reads from all samples mapping on both fungal genomes was carried out using an ANOVA, and the significance of each tested interaction was carried out using a likelihood ratio test (LRT). For the multiple pairwise-comparisons of group means that were different from each other according to the ANOVA, we performed a Tukey's honest significant difference test (Figure 58A). The average number of reads mapping on *D. rosae* genome was significantly different between inoculated samples and mock ones with inoculated samples having a higher number of *D. rosae* reads than the mock ones. For inoculated samples with DiFRA67, an average of 2,757 reads were found to map on *D. rosae* genome from OB samples while a mean of 1,860 reads were found in RW samples (see Figure 58B). For non-inoculated samples, no read was found to map on *D. rosae* genome except for RW_N_5B (see Supplementary figure 45A).

That sample has already been removed from the pairwise-comparison analysis due to contamination and bad clustering. Overall, the mapping of fungal reads on *D. rosae* genome reflected the disease scoring observed at 28dpi (see Figure 49 and [Chapter 3](#)).

Concerning *Podosphaera xanthii*, no difference in mapping read counts was found between inoculated and mock samples and between the two genotypes (see Figure 58A). Indeed, for both genotypes and conditions, the average number of reads mapping on *P. xanthii* was similar and around 250 reads but was variable between samples (see Supplementary figure 45B). From this analysis, we can conclude that a contamination with *P. xanthii* was present, but this contamination seems to have been limited and homogenous (same level in all samples).

Even if no significant differences between time points for a specific genotype was detected with the ANOVA, we could observe that the number of *D. rosae* reads in OB inoculated samples decreased between 0dpi and 5dpi, and increased again at 7dpi (with the maximum being at 5,028 reads at 0dpi and the minimum being at 539 reads at 5dpi). As OB, the average number of reads mapping on *D. rosae* for RW decreased from 3,918 reads to 920 reads between 0 and 5dpi, but it remained low at 7dpi (Figure 58A).

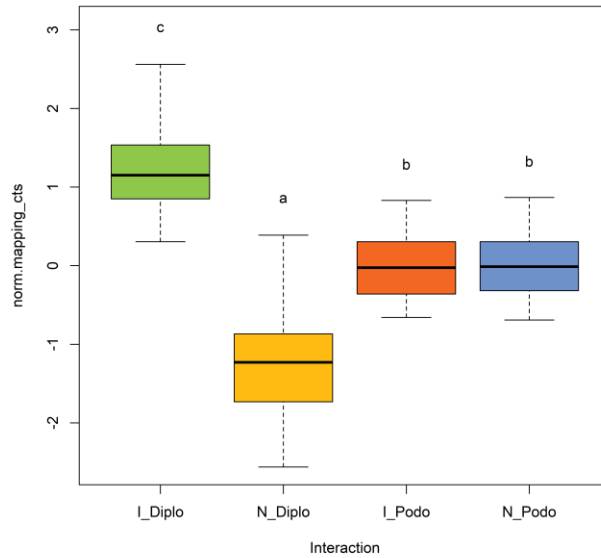


Figure 58: Fungal read counts in RNAseq samples

A: Boxplot of the average fungal read counts according to inoculation condition and fungus with Tukey results. Similar letters show groups of means that were not different from one another, and different letters show a significant difference of group means; **B:** Bar plot of the average fungal read counts from both fungi according to inoculation condition for both genotypes. The bars represent the standard error.

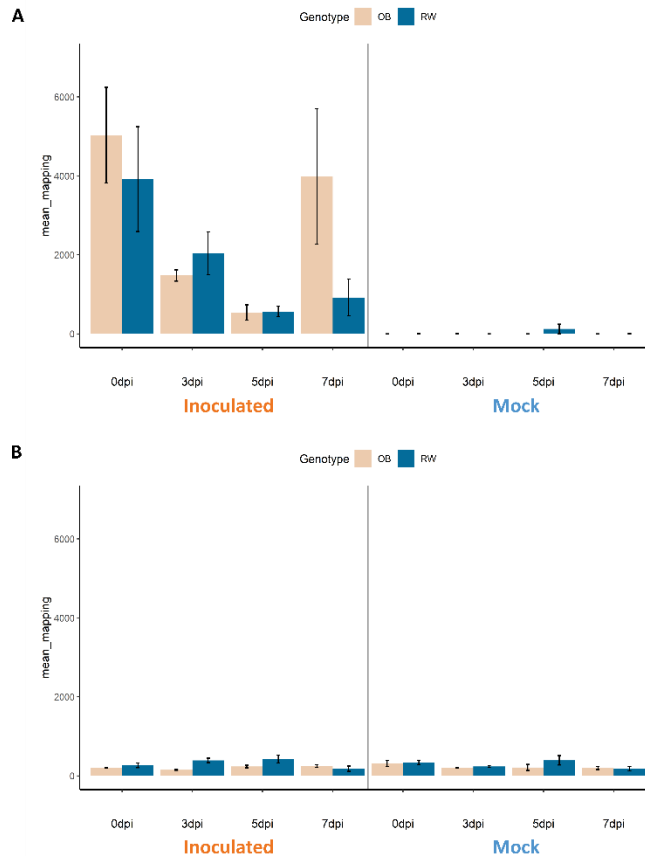


Figure 59: Barplot of fungal read counts from *Diplocarpon rosae* (A) and *Podosphaera xanthii* (B) for 'Old Blush' (OB) and *R. x wichurana* (RW) according to time points and inoculation conditions

6.2. SEPARATED TIME COURSE ANALYSIS FOR INOCULATED AND MOCK SAMPLES FROM THE RNA-DATA

As residual presence of the agent responsible for powdery mildew in rose was found with the previous analyses, I decided to separate the inoculated samples and the mock ones to explore the genotypes' responses under two contexts: (1) inoculation with *Diplocarpon rosae* and a limited presence of powdery mildew, which corresponds to the inoculated samples, and (2) limited presence of powdery mildew, which corresponds to the initial 'mock samples'. A time course analysis was carried out on inoculated and mock samples for RW and OB. The LRT method used in differential expression during a time course analysis yielded a large set of genes differentially expressed over time. To better visualize this large dataset, I proceeded with a clustering by the expression profile of the DEGs obtained in the time course analysis. The Bioconductor (Huber et al. 2015) package DEGreport includes a 'degPatterns' function that uses a hierarchical clustering approach based on pairwise correlations to identify groups of genes with similar patterns of expression as a function of time in our case. Using a single enrichment analysis (SEA), GO enrichment was investigated. For ease of understanding, I focused the presentation of the results on some groups presenting particular patterns of expression across time as well as specific enriched GO terms.

6.2.1. GENE EXPRESSION PROFILES OVER THE INFECTION TIME POINTS AND ASSOCIATED ENRICHED GO TERMS FOR OB GENOTYPE

Here, a total of 4,213 genes for the inoculated samples and 1,971 genes for mock samples were differentially expressed over the time points 0, 3, 5 and 7dpi (padj < 0.05). For inoculated samples, seven groups of genes with different expression profiles were identified with five groups exhibiting from 427 genes to 1,372 genes (groups 1 to 5) and two smaller ones grouping less than 150 genes (groups 6 and 7) (see Figure 60). On the contrary, smaller groups were found for mock samples with only two groups having more than 400 genes (groups 1 and 2), three groups that showed between 150 and 400 genes (groups 4, 5 and 8) and four groups with less than 150 genes (groups 3, 6, 7 and 9, see Figure 60).

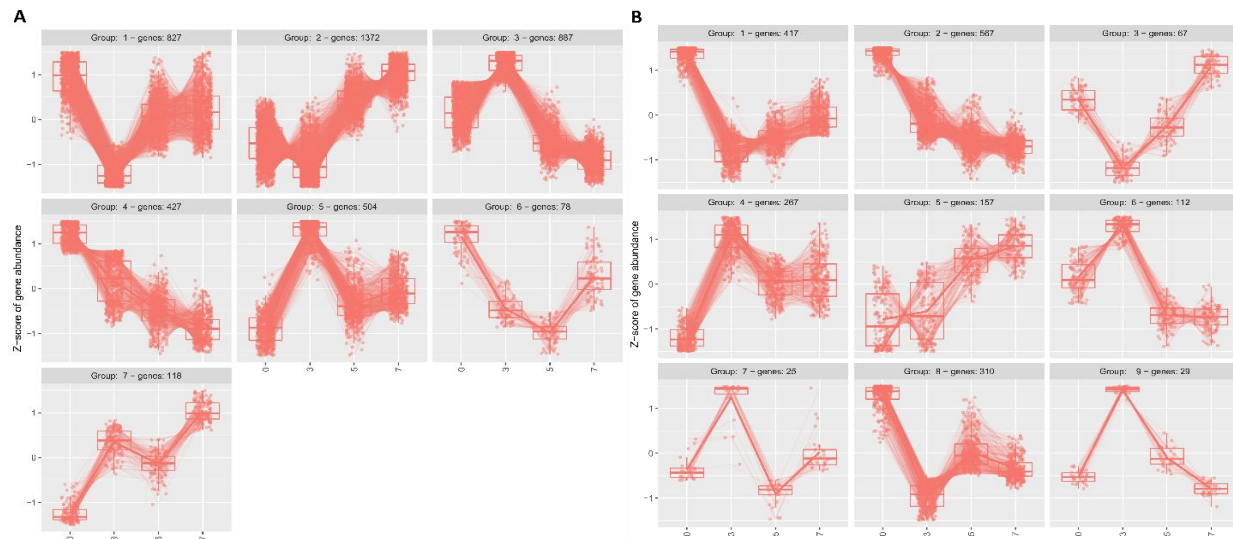


Figure 60: Cluster analysis of genes differentially expressed across time for the inoculated (A) and mock (B) samples for the genotype 'Old Blush' (OB)

The cluster analysis was carried out on 4,213 differentially expressed genes (padj < 0.05) to define temporal differences. These groups or clusters were produced using 'degPatterns' function on the regularized log transformation of the normalized counts. Each group represents differentially expressed genes with similar expression profiles across time. Boxplots are shown for the expression patterns of each group at each time point. The circles over each boxplot represent the expression value of all the genes of that specific group at a given time point.

Comparing the profiles of the different gene groups for both inoculated and mock samples, I was able to identify pairs of groups that exhibited a similar pattern of expression (see below). However, for inoculated samples, group 2 (with 1,176 genes and 302 enriched GO terms) and group 7 (with 118 genes and 42 enriched GO terms) exhibited profiles of expression across time that were not observed for mock samples (see Table 14 and Figure 60). These two groups presented an overall increase in expression of genes linked to gene transcription, and particularly, protein translation and targeting to membrane or organelle (chloroplast or mitochondria).

For the genes presenting the same pattern of expression between mock and inoculated samples, I identified enriched GO terms specific to inoculated or mock conditions and the common ones. The group 1 for inoculated samples and the groups 1 and 8 for mock samples presented a similar profile of expression with a large stepwise decrease in the gene expression at 3dpi (see Figure 60). The majority of enriched GO terms for these groups was associated with cell wall biogenesis (see Figure 61B). The common GO terms between all the groups were due to the 114 and 121 genes shared between the group 1 of inoculated samples and the groups 1 and 8 of mock samples (see Figure 61E). Specific GO terms were found for the group 1 of inoculated samples with GO terms associated with cell wall thickening (see Figure 61A) such as phenylpropanoid metabolic process, lignin metabolic process or lignin biosynthesis but also GO terms associated with ion homeostasis and transport (cation and chemical homeostasis, iron ion transport, transition metal ion transport, etc.). These specific GO terms were also found to be enriched when the list of unique 592 genes from the group 1 of mock samples was used (see Figure 61C). The group 1 of mock samples exhibited a specific enrichment of GO terms associated with photosynthesis and flavonoid biosynthesis (see Figure 61C). The group 8 exhibited overrepresentation of GO terms linked to cell wall biogenesis but also regulation of defense response to virus by the host (see Figure 61D). However, only three genes coding for SAG101 proteins contributed to the enrichment of this GO and the FDR was close to 0.05.

Similarly, the group 2 for mock samples (587 DEGs with 72 enriched GOs) and the group 4 for inoculated samples (427 DEGs with 302 enriched GOs) exhibited a similar pattern of expression with a constant decrease of the DEGs from 0 to 7dpi (see Table 14). These genes showed enrichment in biological processes, molecular functions and cellular components for cell wall biogenesis and organization (see Figure 62B), which corresponds to the 79 common genes found between these two groups (see Figure 62D). In the group 4 of inoculated samples, specific enrichment of GO terms related to response to stress and in particular defense responses was observed in the remaining set of 488 genes. This set of genes was also associated with autophagy (see Figure 62A). Interestingly, out of the 77 genes found to belong to the GO:0006952 (defense response), 54 genes code for R proteins like RGA proteins (1, 3 and 4), TMV resistance proteins or RPP13-like proteins. The other genes code for serine/threonine-protein kinases or other mitogen-activated protein kinases that are important for signaling. For the group 2 of mock samples, the GO terms for the specific 348 genes were also associated with cell wall biogenesis as the genes seem to participate in cell wall components synthesis and secretion. In addition, two GO terms were associated with response to hormone and cell to cell signaling (see Figure 62C).

Four groups for inoculated (groups 3 and 5) and mock samples (groups 4 and 6) exhibited a similar pattern of expression with a peak of expression at 3dpi (Figure 60). However, the group 3 for inoculated

samples and the group 6 for mock samples exhibited a large decrease of expression after 3dpi and the expression remained relatively stable between 5 and 7dpi. In contrast, the group 5 for inoculated samples and the group 4 for mock samples exhibited a large peak at 3dpi followed by a reduced decrease in expression at 5dpi and a slight increase again at 7dpi. When comparing group 3 (inoculated) with 4 (mock) as well as group 5 (inoculated) and 6 (mock), less than 50 genes were found to be in common and no GO term for neither of the comparisons was found to be enriched. Therefore, I decided to compare the group 3 (inoculated) to the group 6 (mock) (see Figure 63), and the group 5 (inoculated) to the group 4 (mock) (see Figure 64).

First, the common set of genes between the group 3 for inoculated samples (with 887 DEGs) and the group 6 for mock samples (with 112 DEGs) was not very high: only 45 genes were found. But this set of genes was linked to defense response and immune response as well as host programmed cell death and plant hypersensitive responses (see Figure 63B). The set of DEGs that was specifically found for mock samples (group 6) only counted 35 genes (see Figure 63D). The overrepresented GO terms in this small set were associated with diverse molecular functions involved in the mannosylation, i.e. the use and production of mannose-containing molecules (see Figure 63C). Interestingly, the group 3 for inoculated samples had 812 specific genes that were differentially expressed over the time (see Figure 63D) and the overrepresented GO terms were associated with two main features: defense response and regulation of gene expression. For the defense response, several GO terms were linked to the regulation of cell death and apoptotic signaling pathway. The others highlighted an immune response to fungus by detection of chitin and regulations of immune response. Noticeably, cell surface receptor signaling pathways with transmembrane receptor serine/threonine and kinase activity were associated with this set of genes (see Figure 63A). In addition, four regulators of defense-related genes via a salicylic acid-dependent signaling pathway were found to be differentially expressed over the time (three genes coding for calmodulin-binding protein 60A that regulates the salicylic acid biosynthetic pathway, and one gene NFXL1 that is a negative regulator of defense genes). For the gene expression regulation, we could see that many GO terms linked to regulation of transcription and RNA biosynthesis but also a lot of terms related to chromatin organization and histone protein demethylation.

Second, the common enriched GO terms between the group 5 for inoculated samples and the group 4 for mock samples were mainly associated with response to abiotic stimuli such as osmotic stress, salt stress and response to oxygen-containing compound (see Figure 64B). Again the GO terms specific to the mock samples were not clearly associated with defense responses (see Figure 64C). However, the 471 genes specifically found in the group 5 for inoculated samples were associated with two types of GO terms: transcription regulation in response to stress and hormone-mediated signaling pathway (see Figure 64A). The ethylene and cytokinin signaling pathways were specifically overrepresented in this group and the gibberellic acid-mediated signaling pathway seemed to be negatively regulated in response to black spot infection. Noticeably, genes associated with rhythmic process and circadian rhythm were differentially expressed.

Table 14: Summary of the separated analysis of mock (NI) and inoculated (I) samples with DiFRA67 for the susceptible genotype *Rosa chinensis* 'Old Blush' (OB)

Sample_Type	TC_Group	DEG	Annotated	GO
OB_NI	gp1	417	379	49
	gp2	567	475	72
	gp3	67	58	5
	gp4	267	164	9
	gp5	157	128	1
	gp6	112	89	24
	gp7	25	22	1
	gp8	310	273	48
	gp9	29	16	0
OB_I	gp1	827	740	64
	gp2	1372	1176	302
	gp3	887	740	257
	gp4	427	385	56
	gp5	504	411	112
	gp6	78	71	13
	gp7	118	91	42

TC_group stands for time course group; DEG stands for differentially expressed genes over time; GO stands for gene ontology and shows the number of GO found to be enriched.

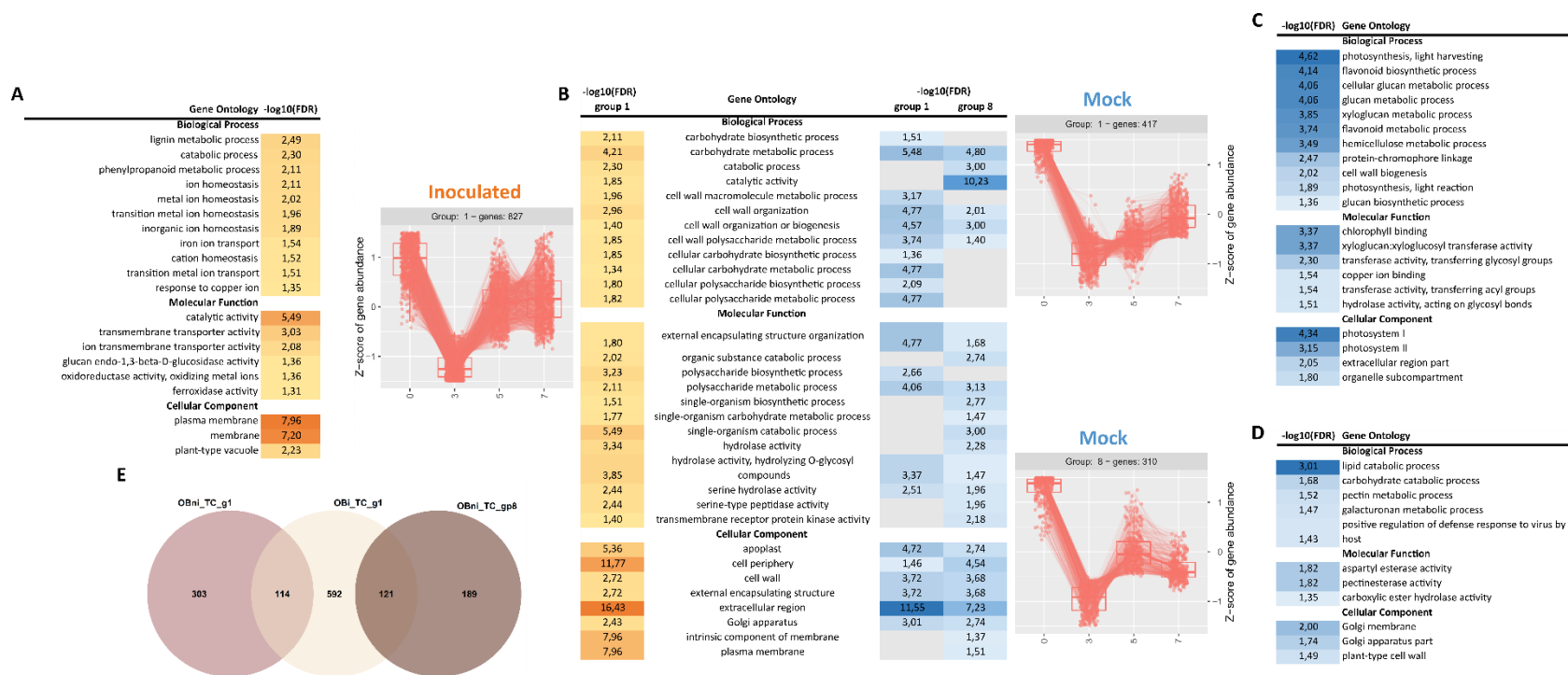


Figure 61: Comparison of time course analyses between the group 1 for inoculated samples and the groups 1-8 for mock samples, all groups exhibiting a drop at 3dpi for the susceptible genotype 'Old Blush' (OB)

The p-values were adjusted with Yekutieli multi-test adjustment method (FDR value) and log transformed for better visualization ($-\log_{10}(\text{FDR})$). Orange color gradient is used for the $-\log_{10}(\text{FDR})$ of inoculated samples and blue color gradient for the mock ones. **A:** Enriched GO terms from group 1 that are specific to inoculated samples; **B:** Enriched GO terms that are common between inoculated and mock samples; **C-D:** Enriched GO terms for mock samples that are specific to group 1 and group 8, respectively; **E:** Venn diagram representing the number of common and specific genes between all three groups (the group 1 for inoculated samples, the groups 1 and 8 for mock samples).

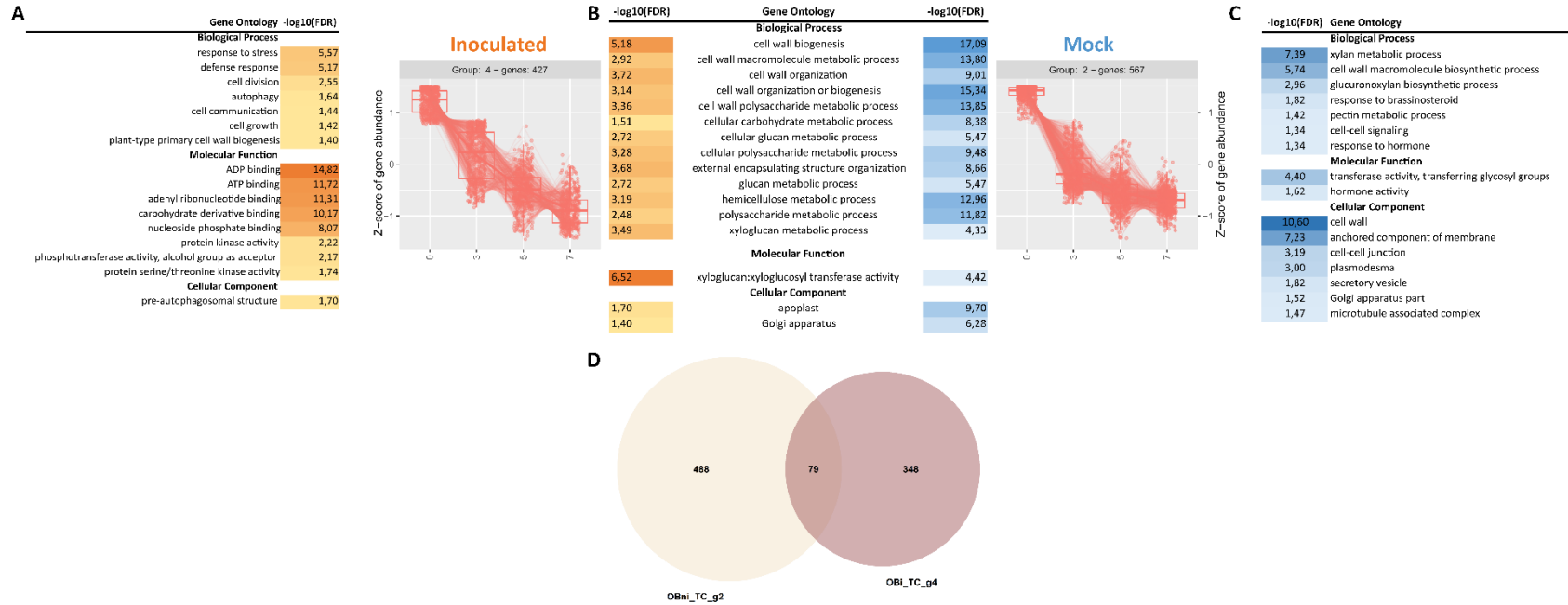


Figure 62: Comparison of time course analyses between the group 4 for inoculated samples and the group 2 for mock samples, both groups exhibiting a gradual decrease in expression for the susceptible genotype ‘Old Blush’ (OB)

The p-values were adjusted with Yekutieli multi-test adjustment method (FDR value) and log transformed for better visualization ($-\log_{10}(\text{FDR})$). Orange color gradient is used for the $-\log_{10}(\text{FDR})$ of inoculated samples and blue color gradient for the mock ones. **A:** Enriched GO terms from group 4 that are specific to inoculated samples; **B:** Enriched GO terms that are common between inoculated and mock samples; **C:** Enriched GO terms for mock samples that are specific to group 2; **D:** Venn diagram representing the number of common and specific genes between both group 4 and group 2.

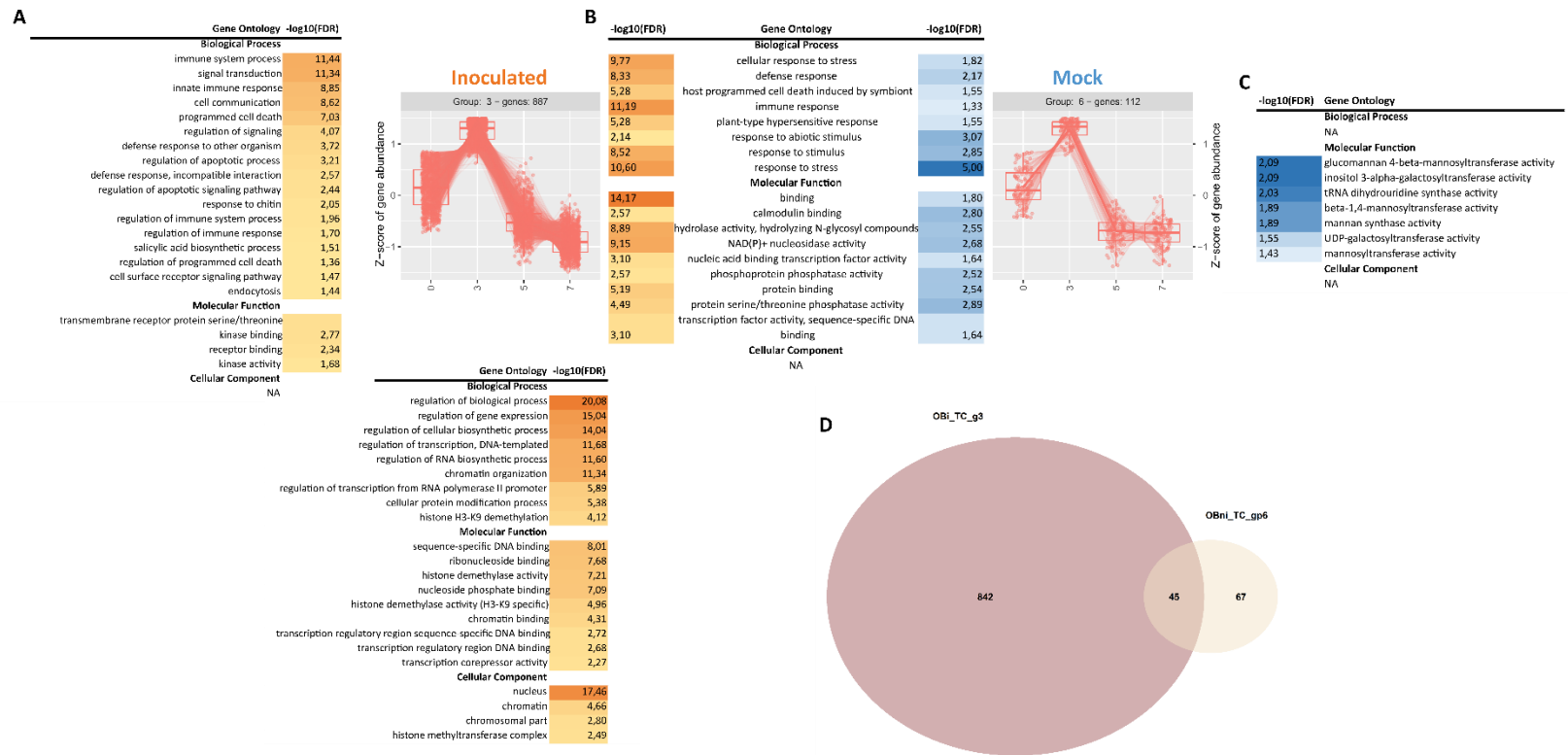


Figure 63: Comparison of time course analyses between the group 3 for inoculated samples and the group 6 for mock samples, both groups exhibiting a large peak at 3dpi and stable expression between 5 and 7 dpi for the susceptible genotype ‘Old Blush’ (OB)

The p-values were adjusted with Yekutieli multi-test adjustment method (FDR value) and log transformed for better visualization ($-\log_{10}(\text{FDR})$). Orange color gradient is used for the $-\log_{10}(\text{FDR})$ of inoculated samples and blue color gradient for the mock ones. **A:** Enriched GO terms from group 3 that are specific to inoculated samples; **B:** Enriched GO terms that are common between inoculated and mock samples; **C:** Enriched GO terms from group 6 that are specific to mock samples; **D:** Venn diagram representing the number of common and specific genes between the group 3 for inoculated samples and the group 6 for mock samples.

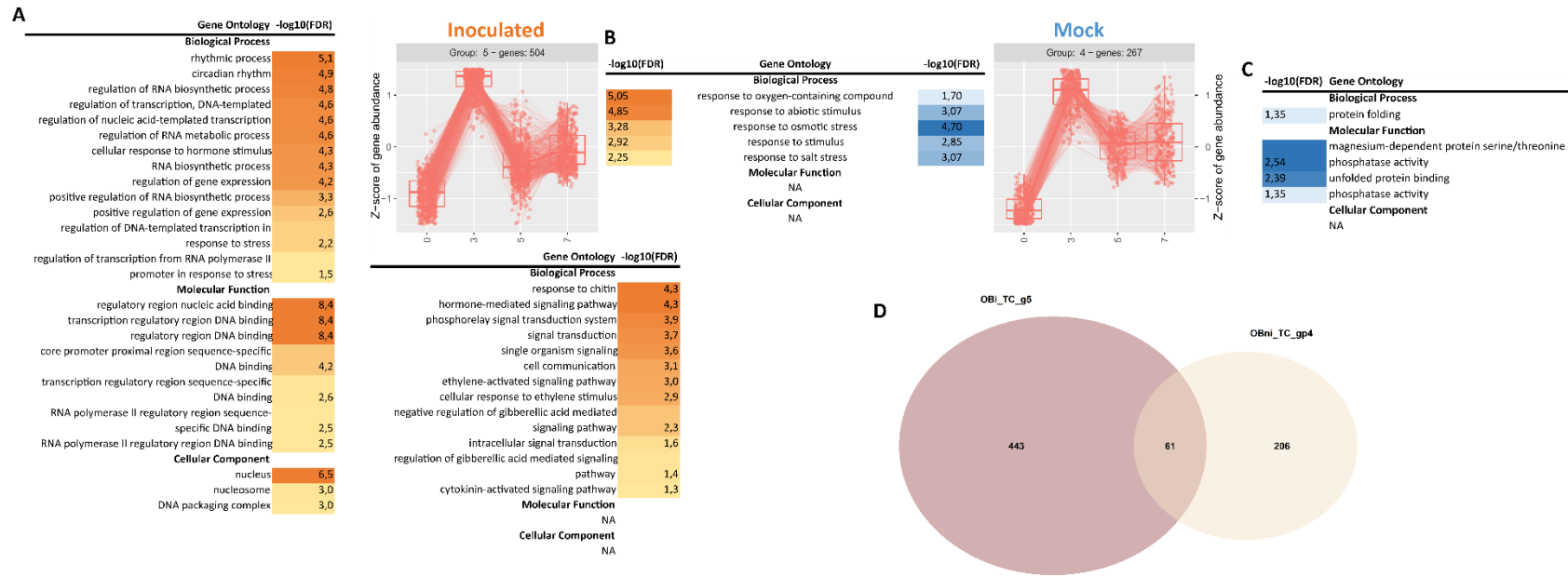


Figure 64: Comparison of time courses analyses between the group 5 for inoculated samples and the group 4 for mock samples, both groups exhibiting a large peak at 3dpi and an increased expression at 7dpi for the susceptible genotype ‘Old Blush’ (OB)

The p-values were adjusted with Yekutieli multi-test adjustment method (FDR value) and log transformed for better visualization ($-\log_{10}(\text{FDR})$). Orange color gradient is used for the $-\log_{10}(\text{FDR})$ of inoculated samples and blue color gradient for the mock ones. **A**: Enriched GO terms from group 5 that are specific to inoculated samples; **B**: Enriched GO terms that are common between inoculated and mock samples; **C**: Enriched GO terms from group 4 that are specific to mock samples; **D**: Venn diagram representing the number of common and specific genes between the group 5 for inoculated samples and the group 4 for mock samples.

6.2.2. GENE EXPRESSION PROFILES OVER THE INFECTION TIME POINTS AND ASSOCIATED ENRICHED GO TERMS FOR RW GENOTYPE

The separated time course analysis of RW mock samples yielded 3,949 genes that were differentially expressed over the four time points studied. Eight groups of genes exhibiting similar patterns of expression were calculated with six groups having more than 400 DEGs (groups 1 to 6) and two smaller groups with less than 200 genes (groups 7 and 8) (see Figure 65B and Table 15). The total number of differentially expressed genes over the time found in the time course analysis of RW inoculated samples was lower as only 3,002 genes were found to be significant. Seven groups of genes with similar patterns of expression were formed with four groups having more than 400 genes and three other groups exhibiting less than 200 genes (see Figure 65A and Table 15).

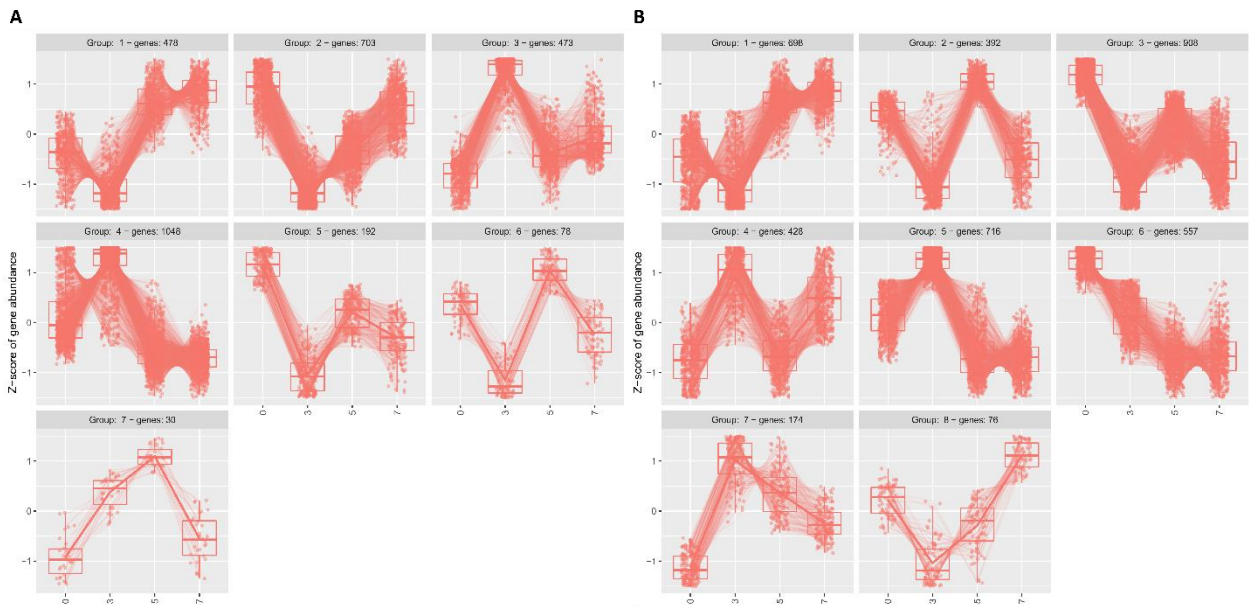


Figure 65: Clustering of genes differentially expressed across time for inoculated (A) and mock (B) samples for the genotype *R. x wichurana* (RW)

Pairing groups from inoculated and mock samples was also possible for RW genotype with the groups 1 for mock and inoculated samples exhibiting similar pattern of expression, the groups 5 (inoculated) and 3 (mock), the groups 4 (inoculated) and 5 (mock) as well as the groups 3 (inoculated) and 4 (mock).

First, both groups 1 for mock and inoculated samples exhibited an increase of expression between 3 and 5dpi (see figure 19), and 199 genes were found in common between these groups (see Figure 66D). Among the common genes, an overrepresentation of GO terms associated with production of precursor metabolites and energy as well as photosynthesis was observed. Indeed, many cellular components were related to chloroplast parts and the photosynthetic membrane. In addition, GO terms associated with translations were also found to be commonly enriched in these two groups 1 with ribonucleoprotein complex biogenesis, RNA binding, translation and structural constituents of ribosomes (see Figure 66B). A total of 279 genes were found to be specifically expressed in the group 1 for inoculated samples and specific GO terms associated with protein production and localization to the mitochondria were found to

be enriched (see Figure 66A). On the contrary, the 499 genes found specifically in the group 1 for mock samples were associated with glucose containing molecule production and energy reserve mobilization for photosynthesis with starch metabolic and catabolic process, pigment, chlorophyll, polysaccharide, carotenoids and glucan metabolic processes (see Figure 66C).

Then, the group 5 for inoculated samples and the group 3 for mock samples exhibited a large drop of expression at 3dpi with a small increase at 5dpi (see figure 19). The group 3 for mock samples counted 908 DEGs with 821 being specifically expressed in mock samples and 87 genes being in common with inoculated samples (see Figure 67D). The GO terms commonly enriched between these two groups were associated with polysaccharide metabolic process and transferase activity probably for the cell wall biogenesis as cell wall, extracellular region and external encapsulating structure GO terms were enriched (see Figure 67B). Many GO terms were specifically enriched in mock samples (group 3) and were in majority related to cell wall biogenesis with the production of its constituents, their transport and secretion. Indeed, many enzymatic activities in relation to cell wall component biogenesis were represented in this set of genes with for example acetyltransferase, ferroxidase, glucosidase, pectin acetyl transferase, cellulose synthase, etc. (see Figure 67C). Interestingly, GO terms like lignin and phenylpropanoid metabolic processes were enriched. Among the 105 genes specifically enriched in the group 5 of inoculated samples, only GO terms in relation to lipid metabolism were found to be overrepresented (see Figure 67A).

The groups 3 (inoculated) and 4 (mock) exhibited a similar pattern of expression (see Figure 65) but also a similar number of genes (473 genes for group 3 and 428 genes for group 4). A total of 116 genes were found to be in common between these two groups and the shared GO terms were related to transcription and expression regulation (see Figure 68B-D). GO terms associated with response to different abiotic stimuli were found to be specifically enriched in the group 3 of inoculated samples (hypoxia, decreased oxygen levels, salt stress and temperature stimulus). Hormone signaling pathways such as cytokinins and gibberellic acid were found among the specific GO terms of this group 3 (see Figure 68A). It is worth noticing that, for the group 4 of mock samples, several molecular functions such as glutamate receptor activity, calcium ion transmembrane transporter activity and calcium channel activity were specifically enriched (see Figure 68C).

The comparison of the group 4 for inoculated samples (1,048 DEGs and 135 enriched GO terms) and the group 5 for mock samples (716 DEGs and 156 enriched GO terms) showed a large portion of common GO terms related to defense and immune response (see Figure 69B). Genes from these two groups showed a higher accumulation at 3dpi, and then a decrease in transcript accumulation at 5 and 7dpi (see Figure 65). A total of 333 genes were found in common between these two groups (see Figure 69E). The commonly enriched GO terms showed an overrepresentation of diverse mechanisms of defense and immune response upon recognition of fungal features (response to chitin). An important regulation of gene expression could be identified in these groups as GO terms associated with molecular functions like nucleic acid binding transcription factor activity and sequence-specific binding or regulatory region DNA binding were enriched. Indeed, GO terms related to regulation of innate immune response, immune system process and immune response could be found in the list but also specific responses to fungus and

wounding were observed. These responses were associated with cell wall thickening and callose deposition on the cell wall. Interestingly, GO terms associated with receptor-mediated endocytosis, receptor activity and transmembrane receptor protein serine/threonine were found in the list showing recognition through membrane receptors. In addition, GO terms like signal transduction and kinase activity of protein serine/threonine pointed out a signal transduction via kinase proteins. Hormone-mediated signaling pathways and cellular response to hormone stimulus were also commonly enriched. A total of 667 genes were found to be specific genes that were differentially expressed over the time in the inoculated group 4 (see Figure 69E). However, a set of 160 genes was identified to have a decrease of expression between 0 and 3dpi instead of increasing in expression like for the majority of other genes of this group but also like for the group 5 of the mock samples. These genes are represented in green in the Figure 69D, and the GO terms significantly enriched from this list were associated with cell wall biogenesis. Indeed, these genes exhibited a similar pattern of expression than the ones of group 1 for which the expression decreased from 0dpi to 7dpi. The 507 genes left in the group 4 were specifically related to defense response during an incompatible interaction and signal transduction (see Figure 69A). Responses to several hormones were overrepresented in this set of genes such as response to brassinosteroid and salicylic acid. Noticeably, genes linked to HR and host programmed cell death induced by symbiont were differentially expressed in mock samples (group 5) and were not found in inoculated samples (group 4). Several GO terms were specifically enriched in group 5 (mock) such as the immune effector process and its regulation, regulation of defense response to oomycetes and response to molecules of fungal origin (see Figure 69C).

Table 15: Summary of the separated analysis of mock (NI) and inoculated (I) samples with DiFRA67 for the partial resistant genotype *R. x wichurana* (RW)

Sample_Type	TC_Group	DEG	Annotated	GO
RW_NI	gp1	698	608	104
	gp2	392	353	68
	gp3	908	789	136
	gp4	428	360	15
	gp5	716	614	156
	gp6	557	495	99
	gp7	174	134	22
	gp8	76	60	20
RW_I	gp1	478	431	113
	gp2	703	594	96
	gp3	473	413	41
	gp4	1048	886	135
	gp5	192	162	14
	gp6	78	59	2
	gp7	30	22	0

TC_group stands for time course group; DEG stands for differentially expressed genes over time; GO stands for gene ontology and shows the number of GO found to be enriched.

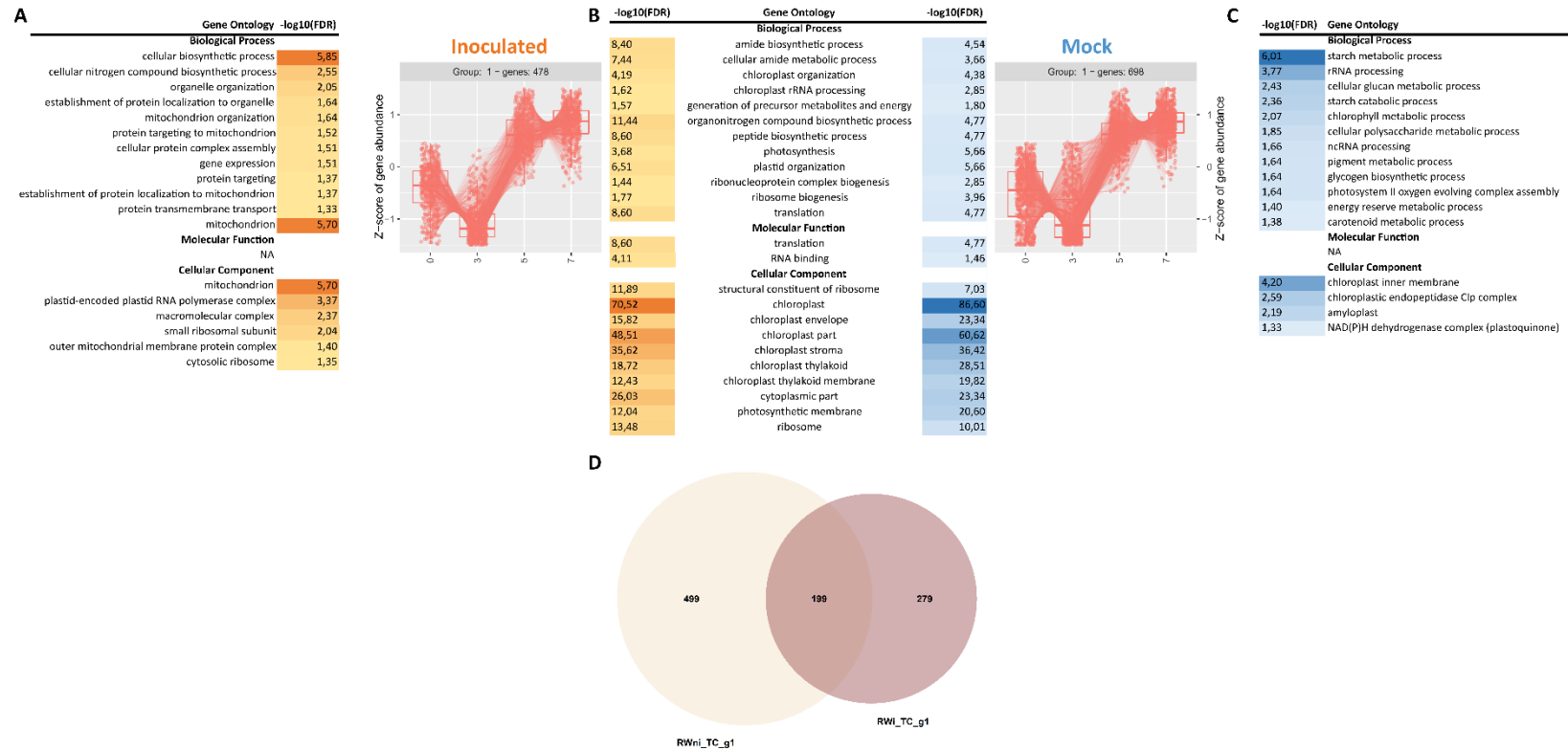


Figure 66: Comparison of time course analyses between the group 1 for inoculated samples and the group 1 for mock samples, both groups exhibiting a drop at 3dpi for the partial resistant genotype *R. x wichurana* (RW)

The p-values were adjusted with Yekutieli multi-test adjustment method (FDR value) and log transformed for better visualization ($-\log_{10}(\text{FDR})$). Orange color gradient is used for the inoculated samples and blue color gradient for the mock ones. **A:** Enriched GO terms from group 1 that are specific to the inoculated samples; **B:** Enriched GO terms that are common between inoculated and mock samples; **C:** Enriched GO terms from mock samples that are specific to group 1; **D:** Venn diagram representing the number of common and specific genes between the group 1 for inoculated samples and the group 1 for mock samples.

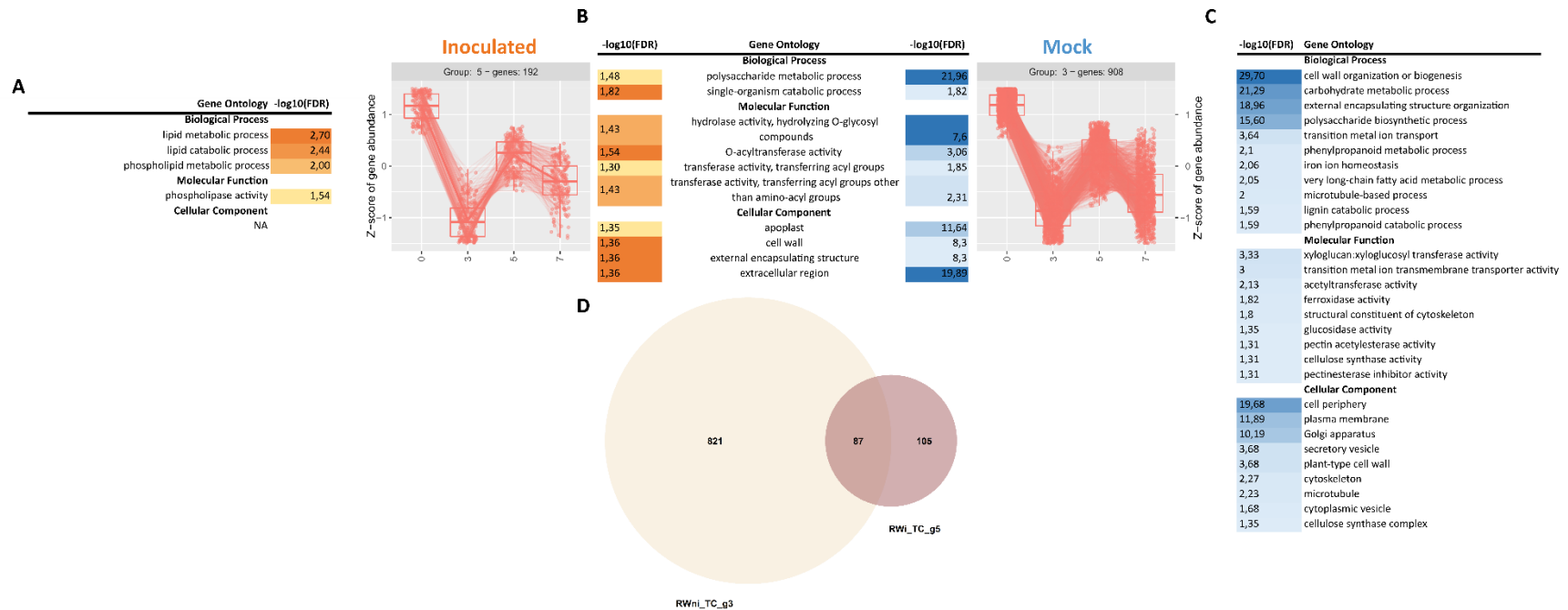


Figure 67: Comparison of time course analyses between the group 5 for inoculated samples and the group 3 for mock samples, both groups exhibiting a decrease of expression at 3dpi and an increased expression at 5 and 7dpi for the partial resistant genotype *R. x wichurana* (RW)

The p-values were adjusted with Yekutieli multi-test adjustment method (FDR value) and log transformed for better visualization ($-\log_{10}(\text{FDR})$). Orange color gradient is used for the $-\log_{10}(\text{FDR})$ of inoculated samples and blue color gradient for the mock ones. **A:** Enriched GO terms from group 5 that are specific to inoculated samples; **B:** Enriched GO terms that are common between inoculated and mock samples; **C:** Enriched GO terms from group 3 that are specific to mock samples; **D:** Venn diagram representing the number of common and specific genes between the group 5 for inoculated samples and the group 3 for mock samples.

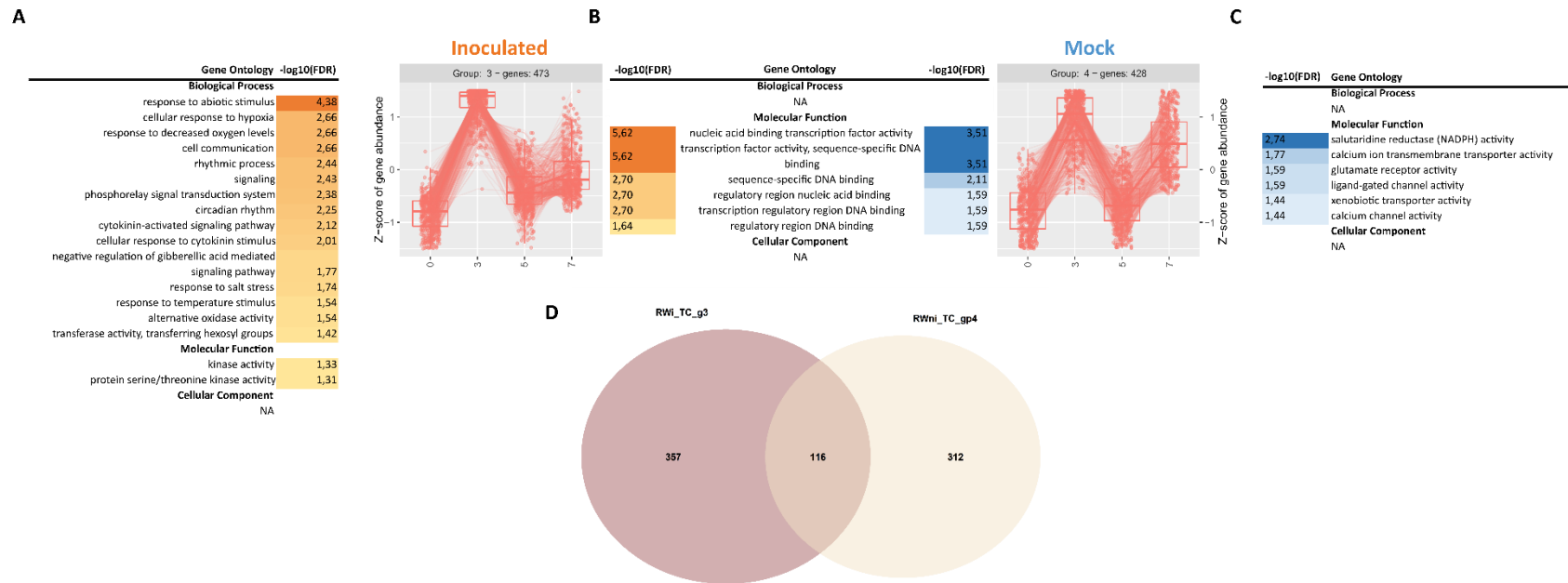


Figure 68: Comparison of time course analyses between the group 3 for inoculated samples and the group 4 for mock samples, both groups exhibiting an increase expression at 3dpi and 7dpi for the partial resistant genotype *R. x wichurana* (RW)

The p-values were adjusted with Yekutieli multi-test adjustment method (FDR value) and log transformed for better visualization ($-\log_{10}(\text{FDR})$). Orange color gradient is used for the $-\log_{10}(\text{FDR})$ of inoculated samples and blue color gradient for the mock ones. **A:** Enriched GO terms from group 3 that are specific to inoculated samples; **B:** Enriched GO terms that are common between inoculated and mock samples; **C:** Enriched GO terms from group 4 that are specific to mock samples; **D:** Venn diagram representing the number of common and specific genes between the group 3 for inoculated samples and the group 4 for mock samples.

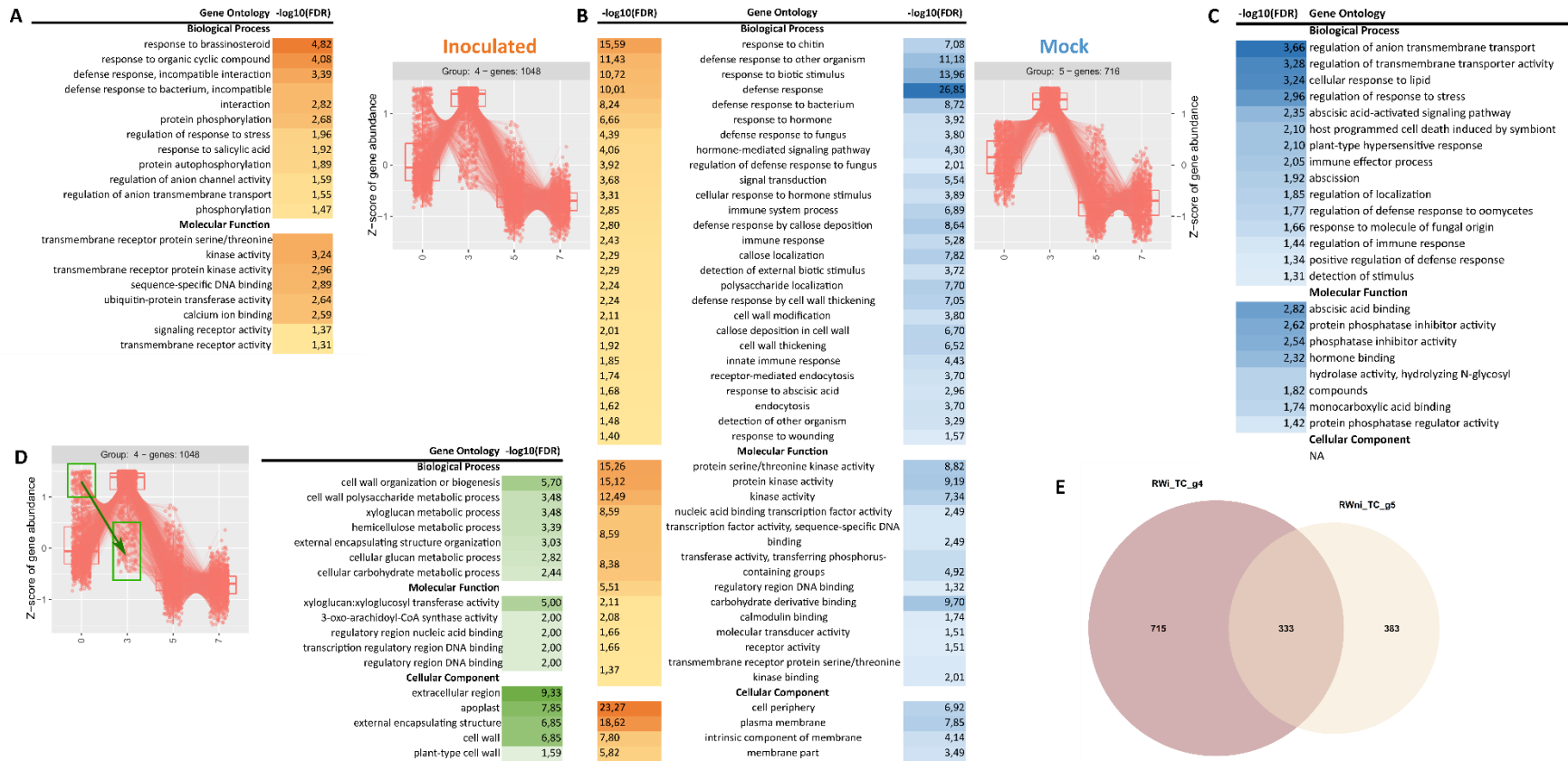


Figure 69: Comparison of time course analyses between the group 4 for inoculated samples and the group 5 for mock samples, both groups exhibiting an increased expression at 3dpi and a stable expression at 5-7dpi for the partial resistant genotype *R. x wichurana* (RW)

The p-values were adjusted with Yekutieli multi-test adjustment method (FDR value) and log transformed for better visualization ($-\log_{10}(\text{FDR})$). Orange color gradient is used for the $-\log_{10}(\text{FDR})$ of inoculated samples and blue color gradient for the mock ones. **A:** Enriched GO terms from group 4 that are specific to inoculated samples; **B:** Enriched GO terms that are common between inoculated and mock samples; **C:** Enriched GO terms from group 5 that are specific to mock samples; **D:** GO analysis for the set of genes for which a decrease in expression was observed between 0 and 3dpi instead of an increase in expression like for the majority of the genes; **E:** Venn diagram representing the number of common and specific genes between the group 4 for inoculated samples and the group 5 for mock samples.

7. DISCUSSION

As presented in chapter 1, detaching leaves for inoculation assays can compromise the plant integrity. Even if good correlations of infection incidence between whole plant and detached leaf assays were reported, several differences in gene expression during plant defense response were also described (Liu et al. 2007; Lieberei 2007; Michel et al. 2010; Orłowska et al. 2012b, a, 2013). In particular, Orłowska et al. (2012a) conducted a thorough experiment where they demonstrated that the lack of systemic reactions in detached leaves of potato inoculated with *Phytophthora infestans* can affect the timing of induction of *PR* genes which can have an impact in the resistance to the pathogen. Rose resistance was demonstrated to be well correlated in both types of assay (Dong et al. 2015). However, Neu et al. (2019) studied the changes in the rose leaf transcriptome during the early stages of compatible interaction with two pathogens, *Diplocarpon rosae* and *Podospaera pannosa*, using a detached leaf assay. They observed that the samples at 0hpi were separated from the rest of the time points and suggested that the experiment procedure (leaf detachment most likely) induced additional stress that was visible in the transcriptome even at later time points (24 and 72 hpi).

In addition, good correlations between whole plant assay in greenhouse and field observations were found by Marolleau et al. (2020). With these considerations in mind, we decided to use the whole plant assay for our transcriptomic experiment using the published test by Soufflet-Freslon et al. (2019). So, in order to study the transcriptomic changes that are involved in the establishment of the partial resistance against black spot disease observed in our genotype of *Rosa wichurana* (RW), we decided to carry out a comparative transcriptional analysis between a compatible interaction represented by the genotype *Rosa chinensis* 'Old Blush' (OB) and an incompatible interaction represented by old leaves of RW. Indeed, we demonstrated in the last chapter that young leaves of RW could be infected by *Diplocarpon rosae* and that the resistance of RW is best expressed in old leaves. Even if Marolleau et al. (2020) found a good correlation between the resistance scored in the field and the one observed for the whole plant assay in greenhouse, two points should be kept in mind: (1) the age of plants were different: young cuttings for the whole plant assay versus well installed plants in the field, and (2) the inoculum was controlled for the whole plant assay whereas in the field it was a natural infection.

Unfortunately, we had to face some sanitary issues and we will first discuss the implications of using RNAseq technology for material coming from semi-controlled conditions and then discuss the results obtained in this context.

7.1. VALIDATION OF *DIPLOCARPON ROSAE* INOCULATION AND ASSESSMENT OF LIMITED PRESENCE OF POWDERY MILDEW THROUGH FUNGAL READ MAPPING

We evaluated our inoculation procedure at two levels. First, we observed that no development of black spot was observed after 28 days on mock plants and that the black spot disease scores were similar to the ones found in the fields. Second, we used the reads that did not map on the rose genome of Hibrand-Saint Oyant et al. (2018), and after cleaning them from residual rRNA reads, we aligned these unmapped reads on the draft genome of *Diplocarpon rosae* published by Neu et al. in 2017. Overall, we observed that the samples inoculated with DiFRA67 exhibited a significantly higher amount of reads than the samples that were water-sprayed (mock). The later ones usually presented less than three reads mapping on the

fungal genome. Moreover, we could observe an evolution of the number of fungal reads across time in samples inoculated with DiFRA67. Interestingly, the number of reads in OB samples were important during the contact point (0dpi), then decreased after the penetration (3dpi) and were low during the asymptomatic growth of subcuticular hyphae (5dpi). And then, when many haustoria started penetrating the host cells and cell death appeared at invasion sites (7dpi), we observed an important increase of transcripts from *D. rosae*. With these results, we observed that *D. rosae* transcript accumulation does not reflect the quantity of fungal structures but its expression over time. Nevertheless, our results at 0dpi and 3dpi do not reflect the observations made by Neu and Debener (2018) as they observed that most of the sequences were expressed at 3dpi. The difference between their study and ours can be explained by many differences between their assay on detached leaves using conidia grown on rose leaves and our study that used conidia from cellophanes that were inoculated on whole plants. It is worth noticing that in both studies, a vaporizer was used to inoculate the leaves and that Neu et al. used an inoculum with a concentration five times higher than in our study (500,000 conidia/ml instead of 100,000 conidia/ml in our study). Several hypotheses can be drawn to explain the differences of expression at 0 and 3dpi between both studies. First, we can imagine that the fact that our inoculum was prepared from frozen and dried conidia could have led to an important expression at 0dpi due to the stress applied to the conidia during the preparation of the inoculum. We shook the cellophane in water in order to release the maximum amount of conidia from it and we rehydrated these conidia for about 30 min to 1 h before inoculation whereas Neu et al. started with fresh conidia that were grown in rose leaves. Second, we can also imagine that the conidia from Neu et al. study were already expressing their virulence genes and were “ready” to infect the leaves while the fungus from cellophanes was growing saprophytically and, thus, many changes in expression could have accompanied the recognition of a host surface. Noticeably, the amount of reads at 7dpi was different in OB and RW samples and that the number of fungal reads in RW samples did not increase again at this time point. This observation can be explained by the fact that the pathogen was stopped at the cuticle penetration in RW leaves (see chapter 3) so it is logical to think that less reads were produced by the pathogen after the time point 3dpi or that the pathogen died after failing to infect its host.

As we obtained odd results for the pairwise comparisons, in RW particularly, with the difference between inoculated samples and mock ones being very low and as a small number of leaves presented a limited infection at 15dpi, we hypothesized that our samples might have been contaminated with powdery mildew. Therefore, we decided to map the same unmapped reads on the genome of *Podosphaera xanthii* that was the genome of the closest species to rose powdery mildew available at the time of the study. Noticeably, very little amount of reads from *P. xanthii* was found in all samples and the amount of reads between mock and inoculated samples was not significantly different for OB and RW. Furthermore, as we mapped the same reads on both fungal genomes, we checked that the residual amount of reads that mapped in *P. xanthii* was not common with the ones mapped on *D. rosae* (data not shown). Only a small fraction of these reads were common with the reads mapped on *D. rosae* (only 1.5% which corresponds to six reads). Given that the fungicide treatment arrived at the end of its effective coverage after two weeks, we think that some residual infection of ambient powdery mildew found in the greenhouse could have started right before our experiment began in all samples (OB/RW, inoculated/mock). As a matter of fact, it is recommended to apply protective fungicidal sprays on a 7-day schedule as long as the conditions

persist, which was not able to be carried out for our black spot assay. But, plants were in a saturating atmosphere under a plastic cover and 100% humidity was maintained with a fine layer of water (with or without conidia) on leaves for three days. Indeed, these conditions are known to not favor powdery mildew development and to kill the conidia (Leus 2005; Horst and Cloyd 2007). A striking example mentioned in Horst and Cloyd (2007) book is that the application of water spray used during 1940s to control spider mites reduced the incidence of powdery mildew in greenhouse but increased black spot disease severity, and when this procedure was replaced by acaricide sprays, black spot was less of a problem but powdery mildew became a serious one. Indeed, powdery mildew conidia are known to not germinate in free-moisture film and when water is deposited on leaves immediately after conidia deposition, it adversely affects its development (Horst and Cloyd 2007).

In addition, the presence of *P. pannosa* conidia at the beginning of the experiment could explain that (1) many differentially expressed genes linked to defense responses were found right at 0dpi due to the presence of powdery mildew (which corresponded to 30min after inoculation or water-spray), but also that (2) the least differences in pairwise comparisons (inoculated/mock) for both genotypes (particularly visible for RW) were found at 3dpi. Therefore, the pairwise comparisons between mock and inoculated samples only showed the genes that were differentially expressed in response to *D. rosae* specifically. Besides, the separate time course analysis gave us more insight in the early response to powdery mildew conidia presence (mock analysis) and in the response to an infection of *D. rosae* in presence of powdery mildew. For the rest of the discussion, I will try to show the specific and common pathways that are activated in response to both pathogens for each genotype separately. Also, I will discuss the limits of this study in relation to the hypothetical unexpected presence of powdery mildew in our assay. Perspectives and current work to validate this data will be addressed.

7.2. RESPONSES TO *D. ROSAE* AND *P. PANNOSA* IN AN INCOMPATIBLE INTERACTION (WITH *R. X WICHURANA*, RW)

Through the alignment of unmapped reads on both *D. rosae* and *P. xanthii* genomes, we assessed the presence of reads from both fungi. In particular, powdery mildew seemed present in relatively small proportions in both mock and inoculated samples while *D. rosae* was specifically found in samples inoculated with DiFRA67 as expected. Genes involved in the recognition of chitin were found to be differentially expressed over the time for both types of sample (inoculated and mock) when we analyzed the samples separately using a time course analysis. Among many other GO terms describing host response to pathogen infection, the GO term “response to molecule of fungal origin” was found to be significantly enriched in mock samples for genes exhibiting an increased expression at 3dpi. This observation is surprising since no inoculation of *D. rosae* was performed in mock samples and no reads of *D. rosae* were found in these samples. This result confirms the presence of a response to powdery mildew in mock samples and explains the lack of genes differentially expressed at 3dpi. Interestingly, this absence of differentially expressed genes between inoculated and mock samples is due to the fact that RW might establish similar responses to powdery mildew infection than to black spot disease infection.

7.2.1. PTI RESPONSE:

First, response to chitin was particularly enriched in both types of sample (mock and inoculated) with 16 genes involved in the response to chitin that were differentially expressed across time. Both host cell surface chitin receptor LYK5 and the gene coding for a mitogen-activated protein kinase (MAPK5) were differentially expressed across time in inoculated and mock samples with a peak of expression at 3dpi. These genes code for proteins that are involved in the recognition of chitin (LYK5) and the cascade of signaling (MAPK5) leading to chitin-induced immunity (Wan et al. 2012; Yamada et al. 2016). Among these 16 genes, five genes coded for E3 ubiquitin-protein ligase or transferase (ATL6, PUB21/23/29). Ubiquitination is particularly important in plant immune signaling as transmembrane receptor-like kinases can phosphorylate ubiquitin proteins. Several ubiquitin proteins intervening in plant immune signaling were described and for example PUB23 was shown to inhibit PTI responses while PUB21 enhanced the ETI responses (Craig et al. 2009; Marino et al. 2012). In addition, many receptor-like kinases such as lectin receptor kinases (LecRKs), cysteine-rich receptor-like kinases (CRKs) or other cell wall receptor-like kinases were found to be differentially expressed in both types of samples with a peak at 3dpi. Two different types of transcription factors were found in common between the inoculated samples and the mock ones: different homologues of WRKY transcription factors (WRKY6, 11, 17, 40, 46) and ethylene-response transcription factors, like the transcriptional activator ERF061 or the repressor ERF4. However, WRKY75, which that was described as the WRKY transcription factor of particular interest in the response of the susceptible genotype 'Pariser Charme' (PC) to both powdery mildew and black spot disease by Neu (2018), was not found to be differentially expressed across time points for inoculated samples (with *D. rosae*). Only one gene (RC4G0344000) coding for WRKY transcription factor 75 was found to be differentially expressed over the time in mock samples. Instead, other WRKYs were found to be significant in both samples, suggesting that RW signaling in response to both fungi might be different than for the susceptible genotype studied by Neu et al. (2019).

The responses triggered by the recognition of both fungus PAMPs lead to the activation of several genes involved in callose deposition in response to infection. Indeed, several GO terms associated with callose deposition in papillae were found to be enriched in both types of samples. These results are supported by microscopic studies on *R. wichurana* reactions against *P. pannosa* and *D. rosae*. Indeed, according to our study presented in chapter 3 and to Blechert and Debener's study (2005), *R. wichurana* resistance to *D. rosae* is associated with large callose deposition in papillae at penetration sites. Similarly, it was shown that *R. wichurana* resistance to *P. pannosa* is mainly based on papilla formation but the constituents of this papillae have not yet been described. Only production of hydrogen peroxide (H₂O₂) was found to be associated with the papillae formed in *R. wichurana* leaves in response to powdery mildew infection (Dewitte et al. 2007). Papilla is a complex structure formed between the plasma membrane and the inside of the plant cell wall. The biochemical composition of these papillae varies between species but the most common compounds are phenolic compounds, reactive oxygen species, cell wall proteins and diverse cell wall polymers. The most abundant polymer commonly found is the (1,3)- β -glucan callose (Ellinger et al. 2013; Voigt 2014). A total of nine DEGs annotated "response by callose deposition" were found in common between mock and inoculated samples. Seven of them coded for LRR receptor-like serine/threonine protein kinases. One gene coding for a mitogen-activated protein kinase kinase kinase 5

(MAPKKK5) and another one coding for MACPF domain-containing protein NSL1 were found in this common set of genes that exhibited an increased expression at 3dpi. Furthermore, Neu et al. (2019) also reported a strong up-regulation of many *PR* genes in the susceptible PC and in particular, many *PR10* genes were highly up-regulated in response to both pathogens. In our case, nine genes coding for *PR10* proteins were found to be differentially expressed over the time in mock samples (seven genes from group 5 with a lower expression at 0-3dpi and two genes from group 6 with a peak at 3dpi) while only one was found to be differentially expressed in the inoculated samples and for which the expression decreased from 0dpi to 7dpi (group 2 of inoculated samples). It is worth noticing that no other *PR* genes were found to be differentially expressed over the time points in the mock and the inoculated samples for RW genotype. These results indicate that the innate immunity in RW seems to be activated in response to PAMPs for both pathogens and leads to the production and deposition of callose. However, the activation of the PTI response in mock samples leads to the production of some *PR* protein which was not the case for the inoculated samples.

Noticeably, one gene (RC2G0339100) coding for callose synthase 12 (or glucan synthase-like 5) was found among the differentially expressed genes in mock samples but not in the inoculated ones. This gene was first described as coding for POWDERY MILDEW RESISTANT 4 (PMR4) protein and is known to be required for wound and papillary callose formation in response to powdery mildew attempt of penetrations (Nishimura et al. 2003; Jacobs et al. 2003; Enns et al. 2005; Dong et al. 2008; Ellinger et al. 2013). Another gene, RCOG0036100, was also found to be a specific DEG of mock samples. This gene codes for LRR receptor-like serine/threonine-protein kinase IOS1 that is involved in BAK1-dependent MAMPs-triggered immunity that leads to defense responses such as callose deposition and MAPK cascade activation against pathogenic bacteria but is also required for chitin-mediated PTI (Yeh et al. 2016). For the inoculated samples, only one gene encoding a LRR receptor-like serine/threonine-protein kinase was found to be differentially expressed during the infection.

In addition, 22 DEGs annotated response to chitin were specifically expressed in the inoculated samples with, for example, nine ERF-like transcription factors (ERF2, 12, 19, 20, 26, 105 and 109), three WRKY transcription factors (WRKY29, 40 and 48), four MYB transcription factors (one MYB40 and three MYB44), three genes coding for scarecrow-like proteins (one AtSCL14 and two AtSCL33). Interestingly, gene coding for MYB44 transcription factors were found to be differentially expressed over the time in the mock samples but in a group that exhibited a decrease of expression between 0 and 7dpi. In particular, MYB44 is known to activate salicylic acid (SA)-mediated defenses and subsequent resistance to biotrophic pathogen *P. syringae* pv. tomato (Shim et al. 2013). These genes are interesting to test as they are found specifically in the samples challenged with DiFRA67 and might be specific markers of response to *D. rosae*.

7.2.2. ETI RESPONSE:

Disease resistance genes were also found to be differentially expressed across time points in both inoculated and mock samples. Some homologs of genes coding for disease resistance protein TAO1 (TARGET OF AVR-B OPERATION1 protein), MLO-like protein 6 or RPP5-like proteins were found in the common DEGs between inoculated and mock sample analyses. Remarkably, MLO-like proteins from clade V (*AtMLO2*, *AtMLO6*, *AtMLO12*) are often associated with susceptibility to powdery mildew and are

therefore considered as susceptibility genes (S-genes). The role of *VvMLO6* in grapevine susceptibility to powdery mildew has not yet been proven as its knock-down alone does not result in any significant reduction of powdery mildew susceptibility. Nevertheless, it seems that it has an additive role with *VvMLO11* and *VvMLO7* as their expression was significantly reduced in all three resistant lines, and when all three genes were knockdown, powdery mildew severity was reduced up to 77% (Pessina et al. 2016). In rose, *RhMLO1* was shown to have a negative role in powdery mildew resistance as mutants with silenced *RhMLO1* exhibited higher resistance levels (Qiu et al. 2015). *RhMLO6* and *RhMLO7* were reported to be key factors in the interaction between rose and *P. pannosa*. Furthermore, genes coding for heat-shock proteins 90 (Hsp90-1) were also found to be differentially expressed in both inoculated and mock samples. Neu et al. (2019) observed that Hsp90 was specifically up-regulated in response to *P. pannosa* in a susceptible rose genotype. But also cytoplasmic Hsp90 are known to be molecular chaperones involved in *R* gene-mediated disease resistance like with *RPS2* gene (Zhang et al. 2019 citing Liu et al. 2004).

Noticeably, Dewitte et al. (2007) observed two other types of interaction during *R. wichurana* response to *P. pannosa* infection: abnormal haustoria with haustorial neck and extra haustorial matrix but also papillae formation associated with cell reaction and sometimes single cell reaction with total cell collapse. In our transcriptomic study, pathways leading to hypersensitive response were found to be enriched in mock samples that probably exhibit a response to *P. pannosa* contamination. The genes intervening in these pathways showed an increase in expression at 3dpi followed by strong down-regulation at 5-7dpi compared to 3dpi. A total of 26 genes were annotated “host programmed cell death induced by symbiont” or “plant-type hypersensitive response” with 16 DEGs specifically found in mock samples. Among these 16 genes, 10 genes were homologous to the *TIR-NB-LRR* resistance gene *N* encoding for a disease resistance protein that is known to trigger a defense mechanism including hypersensitive response to tobacco mosaic virus (TMV) (Dinesh-Kumar et al. 2000). Homologs of this gene were found in several other species and sometimes were reported to be differentially expressed in response to diverse infections and stresses like in mango (Lantican et al. 2020), apple (Zhang et al. 2014; Zhu et al. 2019), strawberry (Barbey et al. 2019) or poplar (Huang et al. 2019) among many others. Two genes coding for senescence-specific cysteine protease *SAG12* were found to be differentially expressed across time points for mock samples. The gene *SAG12* is known to be involved in developmental senescence specific cell death during hypersensitive responses (Pontier et al. 1999; Mukherjee et al. 2010). Remarkably, homologs of the disease resistance gene *RPM1* were found to be differentially expressed over time in mock samples but not in inoculated ones. The disease protein encoded by *RPM1* gene specifically recognizes the AvrRpm1 type III avirulence protein from *P. syringae* and triggers HR response (Gopalan et al. 1996). In *Arabidopsis thaliana*, the oomycete *P. syringae* produces AvrRpm1 to suppress PTI by targeting RIN4 and this way avoids stomatal closure (Anderson et al. 2010 and reference therein). In roses challenged by *P. pannosa*, *RPM1* was found to be induced after 12hpi (Xiang et al. 2019).

The same way, we also observed signs of necrotic cells in response to *D. rosae* inoculation and this cell death was restricted to a small number of epidermal cells around the penetration sites (see chapter 3). However, the genes found to be specifically enriched in the inoculated samples were annotated with “defense response, incompatible interaction” and were different from the ones found to induce cell-death in samples with only powdery mildew (mock samples). A total of 27 genes were found to be involved in

“defense response, incompatible interaction” with 19 specifically found in inoculated samples. Several protein kinases (MAP kinase 4, receptor-like serine/threonine protein kinase or receptor-like protein kinase THESEUS1) and calmodulin binding proteins were found among these 19 genes specific to the inoculated samples. Two genes *ACD6* encoding protein ACCELERATED CELL DEATH 6 were also found to be differentially expressed over time in this list. The protein ACCELERATED CELL DEATH 6 is an activator of the defense responses against many different types of pathogens and it is known to act as a positive feedback loop with the salicylic acid (SA) defense signal. By regulating the SA signaling pathway, it leads to cell death (Rate et al. 1999; Vanacker et al. 2001; Lu 2003).

The presence of genes coding for MLO-like protein 6, RPM1 and Hsp90 among the genes differentially expressed over the time in RW samples (and particularly mock samples) suggests the existence of a response to powdery mildew in our samples. But also, with these results, we can hypothesize that RW induces cell death upon recognition of effectors from both pathogens but that the pathway activated may be different.

Finally, it is worth mentioning that many genes coding for proteins involved in the calcium signaling following recognition of PAMPs were differentially expressed over the time in both inoculated and mock samples with a peak at 3dpi. These genes were either involved in calcium transport (calcium-transporters ATPase 12 and 13 or Calcium permeable stress-gated cation channel 1), calcium/calmodulin binding (calcium-binding protein like PINOID-binding protein 1 or PBP1, calmodulin-binding protein 60 A and E and calmodulin-like protein 3/5 or CML3/5) or Calcium-dependent protein kinase (CDPK2, 10, 12, 21, 28 and 29). Interestingly, more genes coding for proteins involved in this pathway were found to be differentially expressed in the inoculated samples than in the mock ones. In early events of plant defense, calcium concentration increases and is very important for the establishment of defense responses. Indeed, alteration of cytosolic calcium is sensed by different type of proteins like Ca²⁺-binding proteins, including calmodulin (CaMBPs), calcium-dependent protein kinases (CDPK) and calcineurin B-like proteins (Zhang et al. 2014). Calcium signaling with the CaMBPs triggers specific defense responses. The early changes in calcium flux and concentration can be triggered by PAMPs or effector recognition which indicates that calcium signaling might be involved in both PTI and ETI responses (Zhang et al. 2014).

7.3. RESPONSE TO *D. ROSAE* AND *P. PANNOSA* IN A COMPATIBLE INTERACTION (WITH *R. CHINENSIS* ‘OLD BLUSH’, OB)

Several genes linked to disease response were found to be differentially expressed over the time in OB (inoculated and mock samples). However, a smaller number of genes was found in common between inoculated and mock samples for OB compared to RW as 862 genes were common to all differentially expressed genes over the time for OB whereas 1,797 common genes were found for RW. Using the time course analysis, we observed that some responses to *D. rosae* and *P. pannosa* were found to be similar for OB and this could explain the low quantity of differentially expressed genes that we found at 0 and 3dpi. Surprisingly, many more genes linked to defense response were differentially expressed over the time in the samples that were inoculated with DiFRA67 than in mock ones.

7.3.1. RESPONSE TO *D. ROSAE*

Like for RW, several genes encoding kinase proteins (52 kinases encoding genes in total) were found to be differentially expressed between inoculated and mock samples at 0 and 3dpi, with for example an up-regulation of genes coding for different receptor like kinase (RLKs) such as LecRKs, CRKs or other cell wall receptor-like kinases. These genes exhibited an increased expression at 3 and 7dpi in the time course analysis of inoculated samples. Receptor-like kinases are important transmembrane proteins that are used by the plants as pattern recognition receptors (PRRs) that detect microbe- and host-derived molecular patterns. These receptors are of utmost importance as they constitute the first layer of inducible defense (Tang et al. 2017; Andersen et al. 2018). The pairwise comparison analyses between inoculated samples and mock ones showed that several genes coding for PR proteins (PR-1, PR-2, PR-4, PR-5 and PR-10) were up-regulated at 5 and 7dpi. Indeed, in the time course analysis of inoculated samples, these genes were found in groups that exhibited either a low expression at 0 and 3dpi (group 2 for all the *PR10* genes) or an important decrease in expression at 3dpi compared to 0dpi and 7dpi (group 1 for all the *PR2*). These genes were already expressed at 3dpi but to a limited extent and their expression was close to mock samples, which can explain that we did not find them differentially expressed at 3dpi. Neu et al. (2019) reported an important up-regulation of many *PR*-genes at 72hpi in response to both *D. rosae* and *P. pannosa*. In particular, genes coding for PR-10 were found to be up-regulated at 72hpi in response to both pathogens and PR-5 were reported only in response to *D. rosae*. Interestingly, looking at *D. rosae* growth microscopically in Neu et al. study (2019), the time points 24hpi and 72hpi correspond to 3dpi and 5dpi in our study, respectively, in terms of fungal growth. Therefore, the up-regulation of many *PR*-genes found in 'Pariser Charm' (PC) at 72hpi was also observed in our study but at 5dpi. In addition, many GO terms associated with gene expression regulation were found at 3dpi for both inoculated and mock samples. The groups 3 and 5 (with a peak of expression at 3dpi) from the time course analysis of inoculated samples exhibited several enriched GO terms related to regulation of transcription. Then, our results suggest a strong inhibition of the PTI response at 3dpi (when the pathogen is penetrating). Nevertheless, the PTI response seems activated again after 5dpi and is particularly important at 7dpi as seen with the increased expression of different *PR*-genes at 7dpi in the time course analysis but also the high number of *PR*-genes differentially expressed at 7dpi. PR proteins have very different biological functions but among other activities, PR proteins are involved in plant immune responses and for instance, present antifungal activity (PR-2, PR-3, PR-5 and PR-10 for example) or play a role in salicylic acid (SA)-activated signaling pathway against biotrophs (like PR-1, PR-2 or PR-5) or are involved in jasmonic acid (JA)-mediated activation against necrotrophs (like PR-3 or PR-4) (Ali et al. 2018 and reference therein). Surprisingly, we observed that *PR-1*, *PR-2* and *PR-5*, signature genes of the SA signaling pathway, were up-regulated at the same time as *PR-4* genes, which are JA-dependent genes, at 7dpi. These two types of signaling pathway are specifically activated according to pathogen lifestyle: SA pathway for biotrophs or JA pathway for necrotrophs in *Arabidopsis* (Ali et al. 2018 and reference therein). However, in grapevine, *PR-4* was shown to be up-regulated in response to powdery mildew infection (Kortekamp 2006), and an overexpression of *PR-4* gave an increased resistance to powdery mildew (biotrophic fungus) (Dai et al. 2016). In the susceptible rose genotype PC, several chitinases from PR-3 and PR-4 classes were up-regulated at 72hpi in response to two fungi with different lifestyles, *D. rosae* (hemibiotroph) and *P. pannosa* (biotroph) (Neu 2018). This shows that "PR proteins as defense signaling indicators", like often assumed, might be an overstatement that may not necessarily be applicable to non-model plants or plant interactions with hemibiotrophs.

In addition, we observed an up-regulation at 3dpi of genes encoding proteins involved in the indirect or direct recognition of pathogen's effectors like several RGAs, TMV resistance protein N, disease resistance RPP13-like protein, NDR1/HIN1-like protein 10. These genes were annotated as host programmed cell death induced by symbiont in the gene ontology. Similarly, several other genes involved in defense response in incompatible interaction and also in host programmed cell death induced by symbiont were found in the group 3 of the inoculated samples analysis in time course (peak of expression at 3dpi). For example, three genes encoding disease resistance protein TAO1 as well as three other genes coding for disease resistance protein RPM1 were found to have an increased expression at 3dpi. Disease resistance protein TAO1 acts additively with RPM1 to guarantee a full disease resistance of *Arabidopsis thaliana* in response to *P. syringae* by triggering hypersensitive response (Gopalan et al. 1996; Eitas et al. 2008). RPM1 was also found to be up-regulated in response to *L. theobromae* infection in grapevine (Zhang et al. 2019). Some pathogens can secrete effectors that suppress PTI but guard R proteins can sense the degradation of the PRR protein and activate ETI like with the example presented in chapter 1 of the guard R protein RPM1 and RPS2. It is interesting to notice that many RPM1 and other R proteins had an increased expression at 3dpi when most products of PTI presented a low expression. Noticeably, a gene coding for RPM1-induced protein kinase was slightly upregulated at 3dpi. This protein may play a role in PTI. In addition, *HSP90* and *SGT1* genes exhibited an increased expression at 3dpi (for the inoculated sample analysis in time course) as for grapevine response to *L. theobromae* (Zhang et al. 2019). These genes encode important cytosolic chaperones of many R proteins that modulate plant innate immunity (Zhang et al. 2019 citing Liu et al. 2004).

Several mitogen-activated protein kinases (MAPKKK1/5 and MAPK3/4) were found to be differentially expressed in the time course analysis and also exhibited an increased expression at 3dpi. MAPK cascades are a complex module transducer that consists of MAPKKK activating MAPKK by phosphorylation that in turn phosphorylates other MAPKs. This signal transduction regulated the activity of several substrates in response to diverse stresses such as transcription factors and other kinases (Dodds and Rathjen 2010; Jagodzick et al. 2018). Moreover, several other genes involved in salicylic acid-mediated signaling pathway were found to be differentially expressed over the time with an increased expression at 3dpi. Many genes linked to calcium or calmodulin-binding proteins were found to be up-regulated at 3 and 7dpi but also were found to be associated with the group 3 of the inoculated sample time course analysis, which indicates that Ca^{2+} plays a crucial role in the signal transduction in early and late stages of rose response to *D. rosae*. Neu (2018) reported in his PhD thesis that PC responses to *D. rosae* were also linked to "calcium ion binding" and "kinase activity". Furthermore, genes related to other hormone signaling pathways than the salicylic one were overrepresented in group 5 of the inoculated sample time course analysis with, in particular, the ethylene pathway, which was also reported by Neu (2018) in PC responses to *D. rosae*. Noticeably, a negative regulation of the gibberellic acid (GA) pathway was overrepresented in group 5 (inoculated). The four genes found in this overrepresented GO term were transcription repressors that regulate GA signaling pathway. With *Q-DELLA* mutants, GA was reported as a positive regulator of senescence that probably functions upstream of JA, SA and ethylene (Crane et al. 2019). This may indicate an inhibition of the leaf senescence at 3dpi, which correlates well with a decrease in expression of several *SAG12* (group 1 of the inoculated sample time course analysis).

Finally, many *SAG12* genes were found to be up-regulated when comparing inoculated samples and mock ones after 5dpi but they were also found in group 1 for which genes exhibited an increased expression at 5 and 7dpi. *SAG12* proteins are markers of leaf senescence and are also known to be involved in hypersensitive response to pathogen attacks (Pontier et al. 1999; Noh and Amasino 1999; Zhang et al. 2020). These genes seem to play an important role in the defense responses leading to cell death implemented by OB in later time points.

We can then hypothesize that the innate immunity of the susceptible rose ‘Old Blush’ consists of a large network of PRR-proteins and R proteins involved in the recognition of pathogen conserved features and effectors, and that this recognition activates an innate immunity with many cascades of signalization through hormones (SA, ET and CK) and kinase proteins. The response of this rose genotype to *D. rosae* seems to involve both a PTI, repressed at the early stage of infection with an activation of ETI at 3dpi, followed again by a PTI activated response at 5 dpi (?). All this leads to the activation of several genes involved in cell death upon pathogen recognition after 5dpi. Interestingly, a late HR-like response was also observed microscopically after 7dpi, with the cells invaded by haustoria turning necrotic (see chapter 3).

7.3.2. RESPONSE TO *P. PANNOSA*

The rose response to uncontrolled infection of *P. pannosa* can be investigated in the time course analysis of mock samples. Surprisingly, no specific group of genes related to common defense responses was found to be differentially expressed over the time in mock samples. As we mentioned before, the presence of powdery mildew was not controlled and even if it appears that it was pretty much stable between samples, we do not know at which stage the fungus was at the different time points of sampling. We could have therefore missed certain activation of genes. Moreover, Neu et al. (2019) did not find either specific genes that were up-regulated in response to *P. pannosa* in PC genotype. They hypothesized that this result might be due to low inoculation density of the pathogen but also because the pathogen remained restricted to the epidermis. Therefore, the gene expression might remain below a certain threshold not detectable in their analysis. The responses in susceptible genotypes like OB and PC might be reduced; therefore, we cannot see many genes in relation to defense response while the response in a resistant genotype like RW is stronger, and we can consequently observe the genes linked to immunity in all types of samples even with a low infection and unfavorable growth conditions for *P. pannosa*.

Specific GO terms associated with photosynthesis and flavonoid biosynthesis were found among the genes exhibiting a large decrease of expression at 3dpi in mock samples (group 1). In addition, many GO terms were found to be related to cell wall biogenesis and cell wall component production among the genes that exhibited a decrease in expression between 0 and 3dpi (groups 1 and 8 of the mock samples). Neu et al. (2019) also reported many significantly overrepresented GO terms in the down-regulated genes that were associated with photosynthesis and cell wall biogenesis. It is not uncommon to see downregulation of photosynthesis and cell wall biogenesis genes in plant-pathogen interactions (Milli et al. 2012; De Cremer et al. 2013; Balan et al. 2018).

7.4. LIMITS OF THIS STUDY AND PERSPECTIVES

First, the transcriptomic data exhibited a high variability between biological replicates which could, in part, explain the low number of differentially expressed genes between inoculated and mock samples. Indeed, the biological replicates used in the transcriptomic analyses were derived from three independent inoculations at one-day intervals. Highly variable replicates can decrease the power to detect DEGs but this problem can be improved by considering the replicate variability in the experimental design, which was done for our analyses. However, one cannot rule out that only the important differences will be detected with such an approach.

Second, based on the analysis of fungal read mapping and RNASeq analysis and the presence of limited infection of powdery mildew in our plants after 15dpi, we hypothesize that one part of the results we observed is due to a contamination of plants by powdery mildew. The contamination might be present at a low level before the inoculation with the strain DIFRA67 of *D. rosae* and also present in mock samples. Thanks to the mapping of the remaining unmapped reads, we were able to validate that the inoculation of DiFRA67 was well done and that no reads of *D. rosae* were found in mock samples. However, the lack of results when comparing mock and inoculated samples for RW during the pairwise comparison as well as the presence of genes typically expressed in response to fungal infection in mock samples of OB and RW led us to consider that our samples were contaminated by another fungus. As explained in the previous section of this discussion, powdery mildew is a common disease found in greenhouse and in particular, during my PhD, we faced many problems of powdery mildew infection in plants. Therefore, we investigated whether or not the causal agent of powdery mildew (*Podosphaera pannosa*) was found in all samples. At the time of the analysis, the genome of *P. pannosa* was not available, only one genome of *P. xanthii*, causal agent of powdery mildew in cucurbits, was available. However, the genome *P. leucotricha*, causal agent of powdery mildew in apple, is now available (Gañán et al. 2020). *Podosphaera leucotricha* is genetically closer to *Podosphaera pannosa*, the causal agent of powdery mildew in rose, than *P. xanthii* (Nayak et al. 2018). Therefore, I performed the mapping on this new genome and the analyses are under process. The results obtained with this mapping might help us to identify with better precision the extent of the contamination. However, powdery mildew infection being mostly ectopic, the majority of fungal structures of this pathogen are found outside the leaf.

Assuming that the samples in our assay have been contaminated with powdery mildew before the assay took place, there are many points that need to be taken into consideration when interpreting this dataset. First, this contamination results from an uncontrolled “natural” infection from multispore *P. pannosa* present in the greenhouse. Then, we must not forget that the conditions used to guarantee a good germination and development of *D. rosae* are unfavorable conditions for powdery mildew. Indeed, as explained previously, *P. pannosa* conidia do not germinate in free water which is what we applied for three days in our assay. Therefore, we hypothesized that the conidia of *P. pannosa* were killed and it is probably only the roses' response to the first stage of infection that were observed in our samples. Moreover, we do not know at which stage of development *P. pannosa* was when the samples were taken, which makes it difficult to discuss the implication of the responses we observed. Finally, we cannot rule out a possible interaction between both pathogens: does it affect each other's development or aggressiveness? But also, we need to consider the effect of the combined presence of fungi on the rose response at the transcriptomic level. Furthermore, we cannot exclude a priming response due to *P.*

pannosa that will modify the response later to *D. rosae*. Consequently, the responses observed, here, gave us insight on rose responses to both pathogens but the interpretation and discussion remain very much hypothetical. We need to perform further tests to be able to say with certainty that:

- RW responses to black spot disease and powdery mildew infection are part of a similar set of responses including callose deposition and hypersensitive responses;
- OB responses to both infections are rather different with some common pathways.

To do this, we selected 24 genes that are being tested on our samples to validate the RNAseq dataset but that are also tested on new samples that were generated in controlled conditions (with no powdery mildew contamination) in Germany using a detached leaf assay. Among these 24 genes, several genes were selected for the following reasons:

- (1) they were differentially expressed when comparing inoculated and mock samples from the RNAseq dataset,
- (2) they were not differentially expressed between mock and inoculated samples but presented interesting patterns of expression and were involved in molecular functions of interest in RW specifically,
- (3) they were described as markers of rose response to *D. rosae* or *P. pannosa* specifically in Neu et al. study (2019).

Finally, one of the main problems encountered during this study was the difficulty to guarantee good sanitary conditions for plants. Therefore, we have been working on a solution to sanitize plants and to keep them in isolated and clean conditions during their growth to avoid the problem presented here. Another option will be to work on detached leaves for which the sanitary conditions can be controlled easier. But we should not forget that detached leaf assay does not entirely reflect the natural infection in the field.

Chapter 5 : General discussion and perspectives

To the Rose upon the Rood of Time,

*Red Rose, proud Rose, sad Rose of all my days!
Come near me, while I sing the ancient ways: {...}
And thine own sadness, whereof stars, grown old
In dancing silver-sandalled on the sea,
Sing in their high and lonely melody.
Come near, that no more blinded by man's fate,
I find under the boughs of love and hate,
In all poor foolish things that live a day,
Eternal beauty wandering on her way. {...}*

– William Butler Yeats



The resistant rose shrub Knockout® ('Radrazz') by M. Tisserand

It is of high importance to investigate the resistance to black spot disease in the *Rosa* genus to help breeders to develop varieties with increased resistance. Until about 30 years ago, disease resistance was not important in breeding programs. However, a change in consumer demands for varieties with higher degrees of resistance and regulations has led to an increased interest in disease resistance in both breeding companies and research programs. As presented in chapter 1, there is still room for improvement as many more varieties with higher degrees of resistance can be released. In particular, black spot disease is the most important disease worldwide affecting garden roses. On one hand, several studies have been carried out on black spot resistance to identify few resistance genes (*R*-genes). On the other hand, there is still a need of further research on partial resistance to identify genes controlling this type of resistance. Identifying *R*-genes or quantitative loci linked to black spot resistance in rose represents a hope for adapting marker assisted selection in rose breeding programs. Indeed, with the increased availability of genotyping techniques at lower costs, marker assisted breeding can be a future solution to reduce the time of selection in rose breeding programs but also to help screen germplasm for new parents carrying a certain resistance (single or combination of different resistance genes). Consequently, more knowledge on black spot disease resistance and its mechanisms is needed.

The main goal of this thesis research was, then, to study the genetics and genomics of black spot resistance in garden roses with a focus on the resistance exhibited by a genotype belonging to *Rosa wichurana* species, known to present a partial resistance. We proposed, here, a multiscale study integrating genetic (chapter 2), microscopic (chapter 3) and transcriptomic approaches (chapter 4). The outcomes provide a basis for understanding the resistance of *Rosa wichurana* (RW) to black spot disease and reveal some important characteristics observed in this resistance. Furthermore, the study of the susceptible genotype *Rosa chinensis* ‘Old Blush’ brings more information about the mechanisms of defense response to black spot in a compatible interaction. The results from each of the approaches were already discussed at the end of each chapter (chapters 2 to 4). Therefore, the following chapter will focus on integrating these results to (1) discuss the different types of rose resistance to black spot disease (complete and incomplete resistances), (2) propose a model explaining the mechanisms of resistance exhibited by *Rosa wichurana* and (3) discuss the mechanisms of rose defense response to *Diplocarpon rosae* in a compatible interaction. The limiting factors of our approaches and experiments were already discussed in the previous chapters, and will not be developed again here, but additional ideas of investigations shall be proposed as perspectives. To go further in the investigations of black spot disease resistance, I would like to suggest a hypothetical model of *D. rosae* infection on susceptible genotypes that could be the starting point of various experiments designed to better study the transition from one lifestyle to another in this untypical hemibiotroph. Finally, I would like to complete this discussion with a reflection on the consequences of such findings in the development of varieties carrying *Rosa wichurana* resistance.

1. DIFFERENT TYPES OF RESISTANCE TO BLACK SPOT DISEASE IN *ROSA* GENUS

Complete resistance was described in many rose genotypes and is often characterized by the absence of visible symptoms or restricted hypersensitive response. This type of resistance is observed in incompatible interactions that exhibit no sporulation and for which mycelium growth is restricted. Complete resistance was described in genotypes carrying major genes giving a strong resistance to black spot disease. So far, four dominant genes for complete resistance to black spot disease were described on

Rosa multiflora background (*Rdr1*, Malek and Debener 1998; Kaufmann et al. 2010; Terefe-Ayana et al. 2012; Menz et al. 2018 and *Rdr2* Hattendorf et al. 2004; both located in LG1), the shrub rose ‘George Vancouver’ (*Rdr3*, Whitaker et al. 2010; Zurn et al. 2020, not genetically located) and *Rosa hybrida* ‘Radbrite’ or ‘Brite Eyes™’ (*Rdr4*, Zurn et al. 2018, located on LG5). Only the interaction type of the genotype 88/124–46 (*Rdr1* donor) and a transgenic line carrying *Rdr1* gene (PC::*muRdr1A*) was described microscopically (Menz et al. 2018). The effects of the other *Rdr* genes on the outcome of the interaction have not yet been investigated. In addition, *Rosa majalis* was described to be completely resistant to many strains except to AEH10 and was investigated microscopically (Schulz et al. 2009). The interaction type identified by Blechert and Debener (2005) was type 8 with no visible penetration nor plant reaction.

Several genotypes carrying different *Rdr* genes and other complete resistances, which have not yet been identified, were challenged with a monoconidial strain of *D. rosae*. Our study provides the first microscopic characterization of the interaction between *D. rosae* and genotypes carrying *Rdr3* and *Rdr4*. Furthermore, the results observed in the transgenic line PC::*muRdr1A* by Menz et al. (2018) and in a genotype of *Rosa majalis* by Blechert and Debener (2005) were also observed with our strain, which confirms the large spectrum of these two resistances. Our results suggest that different mechanisms of resistance are in place in the genotypes carrying *Rdr* genes since the fungus is stopped at different moments of its infectious cycle, with a much more complex situation than described for *Rdr1*.

First, the transgenic line PC::*muRdr1A* allowed some fungal growth with short subcuticular hypha development but only underdeveloped haustoria were produced at 9dpi. Small necrotic spots can be observed at important magnification and microscopically, necrotic cells were observed with callose deposition at the cell wall and fluorescing epidermal cell wall. It is difficult to classify the interaction type between the transgenic line PC::*muRdr1A* and DiFRA67. No further fungal growth was observed in later time points suggesting that the resistance efficiently stopped the fungus at 9dpi. We can think that it could be type 6 as some haustoria were produced, short hyphal strands that did not develop into long distance hyphae and fluorescent cell-wall appositions were visible (see Figure 70). However, the haustoria were not fully developed and this feature was not described by Blechert and Debener (2005). Several hypotheses can be drawn to explain the mechanism of resistance associated with *Rdr1*: (1) *Rdr1* activates a rapid hypersensitive response blocking the development of haustoria that remain at non-mature stage, (2) *Rdr1* activates a defense mechanism that has a direct effect on the haustorium development but that is not linked to callose deposition on the haustoria or (3) *Rdr1* acts conjointly in the activation of a defense mechanism affecting the haustorium development and leading to a rapid HR response. *Rdr1* locus is associated with several resistance gene analogues (RGAs) coding for NBS-LRR proteins. This family of proteins is known to be involved in recognition of pathogen effectors and the activation of signal cascade that can lead to HR (McHale et al. 2006; DeYoung and Innes 2006; Lee and Yeom 2015). It would be interesting to investigate the production of ROS in the transgenic line, as these molecules are known to participate in the apoptosis process involved in HR responses, and also to quantify the expression of genes related to apoptosis and HR-like responses (Camagna and Takemoto 2018; Balint-Kurti 2019). Then, seeing that the pathogen produced under-developed haustoria that do not develop into full grown haustoria in later time points, we could start investigating the permeability of haustoria membrane using transmission electron micrograph or a specific staining of cell death like with the “LIVE/DEAD fungalLight Yeast” viability

kit (fluorescent Dyes: SYTO 9 dye for live cells in green and propidium iodide for dead cells in red). In addition, if a permeability of the haustoria is observed, it would be interesting to identify the host molecules responsible for the haustoria abortion by for example quantifying pathogen-related proteins like defensins and thaumatins that may compromise pathogen membrane permeability or block ion signaling in the pathogen can also be interesting to investigate (Andersen et al. 2018).

In ‘Georges Vancouver’ (GV) leaves, DiFRA67 was able to develop an infection vesicle with reduced hyphae and sometimes a small haustorium. Callose deposition at the penetration point and fluorescence typical of HR-like responses were observed on a small group of cells around the penetration area. Unlike the transgenic *PC::muRdr1A*, GV delayed the pathogen development until 9dpi but further hyphal development was observed at 23dpi. Indeed, some hyphal growth was observed at 23dpi (similar extent that for *PC::muRdr1A* at 9dpi) with the production of haustoria of small size (smaller than for OB but definitely bigger than *PC::muRdr1A*). However, even if fungal development happened at later time points, the colonization remained extremely limited (see Figure 70). In addition, according to Blechert and Debener (2005), ‘Georges Vancouver’ interaction with DiFRA67 can be classified as type 6 since penetration took place, the short hyphal strands did not develop into long-distance hyphae, large number of necrotic spots was visible and no reproductive structures were observed (see Figure 70). We can hypothesize that the callose deposition at the penetration site and the early HR-like response at the beginning of the infection delayed the pathogen development at least until 9dpi but was not entirely efficient as some fungal growth was observed in later time points.

Conversely, no clear reaction of the plant could be observed at 9dpi on Brite Eyes™ leaves but a strong callose deposition was visible at the penetration point with no fungal growth under the cuticle after 23dpi. Brite Eyes™ interaction with DiFRA67 is of type 8 since no visible fungal structure was observed under the cuticle and at later time points fluorescing papillae was observed (Blechert and Debener 2005). This genotype seems to have delayed pathogen penetration and efficiently stopped the pathogen development very early in the infection process. However, it did not exhibit any HR-like response at the penetration sites (see Figure 70). The responses of ‘Georges Vancouver’ (*Rdr3*) and Brite Eyes™ (*Rdr4*) at microscopic scale are quite different from one another, which suggests that the mechanisms controlled by *Rdr3* and *Rdr4* loci may act at different levels of the pathogen infection as well. On one hand, we can hypothesize that *Rdr4* locus is involved in a strong response both delaying pathogen penetration (maybe some PR proteins?) and/or completely stopping the pathogen by depositing abundantly callose at the penetration site when this one tries to penetrate. On the other hand, *Rdr3* locus seems to act later in the pathogen development because the penetration happened at 9dpi and haustoria can be formed between 9 and 23dpi. This locus might be involved in the recognition of intrinsic effector produced by the pathogen when forming haustoria in epidermal cells. Further investigations need to be done to depict a clear portrait of the mechanisms behind these two loci. For instance, it would be interesting to compare the transcriptomic changes in response to *D. rosae* infection between these two genotypes at different time points of the infection. Moreover, as the *Rdr3* and *Rdr4* loci locations are already identified in these two genotypes, we could look at the expression of the genes around these loci to identify potential candidates using the published genomes of *Rosa chinensis* ‘Old Blush’ (Raymond et al. 2018; Hibrand-Saint Oyant et al. 2018). However, one should not forget that *Rosa* genus consists of a complex hybridization between different

species and that both ‘Georges Vancouver’ and Brite Eyes™ can be rather distant to ‘Old Blush’ and, therefore, some genes in these genotypes might be absent from ‘Old Blush’ sequence.

No visible plant reaction was observed in *Rosa majalis* leaves challenged with DiFRA67. Similarly, to ‘Brite Eyes™’, the type of interaction is type 8 (see Figure 70). Like mentioned in the discussion of chapter 3, this genotype might respond very quickly to the pathogen presence probably by PAMP recognition or DAMP sensing when this one tries to penetrate. At this point, we cannot say if the recognition system is based on efficient PRR proteins and cascade signals or recognition of extracellular effectors damaging the plant cuticle. Indeed, the fact that no fungal structure was observed under the cuticle and that no response with callose deposition happened unlike what was observed for ‘Brite Eyes™’, we are not sure whether or not the pathogen managed to start penetrating. In addition, the resistance from *Rosa majalis* might come from germination inhibitors that impede some conidia of germinating and/or other inhibitors that prevent any organization of the penetration events. Several experiments can be mentioned to better characterize *Rosa majalis* resistance like mentioned in the discussion of chapter 3. A thorough study of the percentage of germinating conidia needs to be conducted but also a counting of penetration attempts. The conidium viability can also be investigated with specific stainings like the already mentioned “LIVE/DEAD fungalLight Yeast” viability kit or phenosafranine stain. For the percentage of germination, it can be done by counting the germinated conidia at different time points between 0 and 3dpi on *Rosa majalis* leaves in comparison to the germination on the leaves of a susceptible genotype (positive control) and in water (negative control). Another interesting option would be to study the presence of diffusible substances like done for ‘Allgold’ by Knight and Wheeler (1977, 1978) by re-collecting the water drops alone or water drops with dead conidia or with chitin polymers that have sit on *Rosa majalis* leaves and use this water drops for conidium germination. The same controls can be done with drops sitting on the leaves of a susceptible genotype and water that has sat the same amount of time on a sterile surface. Several time points should be studied like in Knight's PhD thesis (1975) to assess the time taken for the production of diffusible substances/germination inhibitors if there are. Finally, like in Blechert and Debener's study (2005), we suggested that the fluorescing cells observed microscopically corresponded to the necrotic cells visible macroscopically in all the genotypes presenting them. However, it is necessary to assess whether or not these cells are actually dead by applying a specific staining like trypan blue for cell viability or DAB for ROS accumulation. Noticeably, all the genotypes exhibiting complete resistance and/or carrying *Rdr* genes presented a total resistance even if young leaves were used, unlike for *Rosa wichurana* for which the implementation of a complete resistance seems to be age-related.

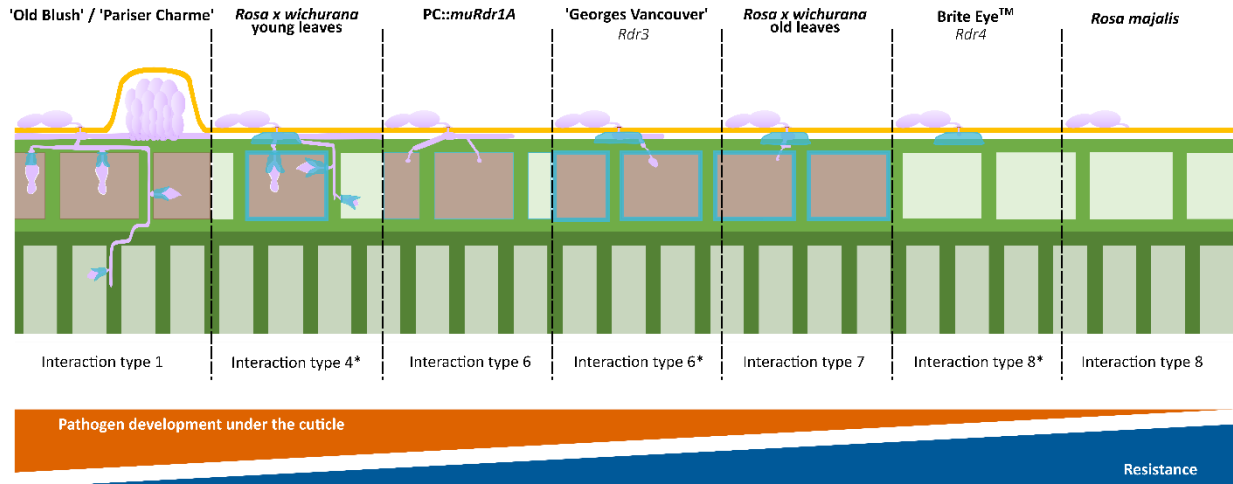


Figure 70: Diagram summarizing the interaction types between different rose genotypes and DiFRA67 observed microscopically

The genotypes are organized from susceptible with important development of fungal structures under the cuticle and for which sporulation happens to resistant ones showing no fungal growth under the cuticle. Callose deposition is represented in blue. Cuticle is in orange. Necrotic cells are represented in brown and healthy cells in green. Fungal structures are in pink. The interaction type is reported under each diagram. The diagram groups the observation made at 9 and 23dpi.

NB (*): For young leaves of *Rosa wichurana*, sporulation was observed in very few cases after 9dpi and for 'George Vancouver', further fungal growth under the cuticle was observed after 9dpi and for Brite Eye™, callose depositions at the penetration sites were observed in some cases at 9dpi and in all samples at 23dpi.

2. *ROSA X WICHURANA* RESISTANCE LEADS TO A COMPLEX INCOMPATIBLE INTERACTION

Transcriptomic changes in old leaves of *Rosa wichurana* upon *D. rosae* infection were analyzed at different time points. Odd results were obtained when comparing inoculated samples to mock ones and we hypothesized that some limited infection of powdery mildew in both inoculated and mock samples was the reason why we obtained these results. The limits of the transcriptomic study were already discussed in chapter 4 so in order to further discuss the results in this chapter, I will consider that the inoculated samples presented a response to *D. rosae* and also a response to the limited presence of *Podosphaera pannosa* while mock samples presented a response to *P. pannosa*. Here, I will review the results for *D. rosae* in order to bring together all the results presented in this study.

Rosa wichurana sp. and genotypes derived from it have been described to present a partial resistance to black spot disease in fields and laboratory assessments (Shupert 2006; Whitaker and Hokanson 2009; Dong 2014; Dong et al. 2017). Our field and greenhouse assays on whole plants confirmed the partial nature of *Rosa wichurana* resistance, and this resistance is quantitatively inherited in segregating populations (Soufflet-Freslon et al. 2019; Lopez Arias et al. 2020). The partial nature of the resistance observed in the genotype *Rosa wichurana* is rather complex. Indeed, old leaves at the base of the plant presented an incompatible interaction of type 7 with a penetration of the cuticle and a reduced development of fungal structures. Conversely, young leaves near the apex presented an interaction between type 4 or 6 with short and long hyphal strands that appear underdeveloped but that were well branched (see Figure 70). Mature haustoria were also produced, but infrequently compared to susceptible genotypes. In some cases, small acervuli were produced at later time points. Young leaves can, therefore, present a compatible interaction unlike old leaves for which the fungal development is completely arrested (see Figure 70). For the first time in rose, age-related resistance to disease was demonstrated. More and

more studies have investigated the plant immune system during plant development. Indeed, as plants or organs grow and mature, “new signals are activated and old processes are attenuated”, which suggests that development and maturity of the plant immune system are inextricably linked to the development and maturation of plants and organs (Li et al. 2020). In our case, the development of *Rosa wichurana* immunity is a function of spatial scale for which the effectiveness of the immune responses increases with the age of the leaf.

The production of callose following *D. rosae* infection observed microscopically on old leaves of *Rosa x wichurana* was also described in the transcriptomic changes with an increased expression of genes involved in callose deposition pathway. Indeed, the PTI response in *Rosa wichurana* seems to be activated with several genes associated with response to chitin (see Figure 71). Noticeably, unlike for mock samples probably exhibiting a response to powdery mildew, no genes directly linked to callose production like callose synthase or other *R* genes activating papillary callose formation were found to be differentially expressed. The genes annotated as “callose deposition on cell wall” were mostly genes coding for LRR receptor-like serine/threonine-protein kinase FLS2. These proteins are known to be pattern-recognition receptors (PPR) that specifically recognize flagellin (flg22). In the microscopic observations of *Rosa wichurana* leaves inoculated with DiFRA67, the callose was already deposited at penetration sites at 3dpi. Then, we can imagine that the signaling pathway leading to this defense response with callose papillae already happened between 0 and 3dpi and, therefore, we could have missed it (see Figure 71). It would be interesting to investigate the expression of genes coding for proteins involved in the callose deposition in papillae following chitin recognition like different glucan synthase-like (GSL5/PMR4 for example), ABC-transporter PEN3 that mediates callose deposition, protein Argonaute1 (AGO1) or RabA4c GTPase, using RT-qPCR for different time points between 0 and 3dpi (Ruano and Scheuring 2020; Wang et al. 2021). Nevertheless, as fungal structures were observed under the cuticle at 9dpi, the PTI response involving callose deposition in papillae at penetration sites was not efficient to block the pathogen. Interestingly, unlike ‘Old Blush’ samples or *Rosa wichurana* mock samples, leaves infected by *D. rosae* do not seem to produce PR proteins that could directly target the pathogen like chitinases. Therefore, *Rosa wichurana* resistance is based on additional mechanisms that stop the pathogen very early in its development under the cuticle but that do not involve chitinases for example.

A clear immune response following effector recognition (ETI) was observed in leaves inoculated with DiFRA67. Indeed, several *R* genes coding for resistance proteins inducing rapid cell death exhibited an increased expression at 3dpi (see Figure 71). Microscopically, 3dpi corresponded to the penetration moment. Effectors can have been secreted at that moment and recognized by receptor-like kinases and NBS-LRR proteins (see Figure 71). This recognition leads to the activation of MAPK cascades that subsequently activate transcription factors like WRK29, 40 or 48. These transcription factors are involved in gene expression regulation. Several genes (like *ACD6* encoding protein ACCELERATED CELL DEATH 6) coding for resistance proteins are involved in the activation of salicylic acid (SA) defense signal that leads to cell death (Rate et al. 1999; Vanacker et al. 2001; Lu 2003). Microscopically, *Rosa wichurana* resistance was also characterized by necrotic cells at the penetration sites that seem to be the results of an early hypersensitive response (HR) (see Figure 70). ETI involves a specific recognition of effectors that are most likely based on a gene-for-gene recognition (see Figure 71). Interestingly, the QTLs linked to *Rosa*

wichurana resistance that were detected seem to have an effect on the penetrance of the disease (QTLs on B5) or on both the penetrance and the severity (QTLs on B3). It is particularly interesting to see that, for example, the right allele at the QTL on B5 will determine whether or not the individual will present symptoms while the ones on B3 will affect the severity as well. In Lopez-Arias et al. (2020), several resistance gene analogues (RGAs) were found to co-localize with the detected metaQTLs. Indeed, the genetic results together with the transcriptomic and microscopic results seem to indicate that the resistance observed on *Rosa wichurana* can be controlled by major *R* genes. Like explained in chapter 1, several authors demonstrated the existence of narrow-spectrum quantitative resistance loci (QRLs) that are involved in a gene-for-gene interaction (Poland et al. 2009 and references therein). Moreover, many speculations were made that quantitative disease resistances are weaker/broken forms of race-specific (*R* gene-mediated) resistances. For rose resistance to black spot disease (BSD), race-specific QRLs were reported by Whitaker et al. (2007b). In addition, several strains were tested on *Rosa wichurana* in previous experiments and we observed that, for some of the strains, *Rosa wichurana* presented higher BSD scores than usual. For example, most of the strains yielded scores of around 1, which indicates that less than 25% of the plant was affected, but with some strains (DiFRA33, DiFRA34 and DiFRA45), the average scores were 2.33, which means that between 25 and 50% of the plant exhibited symptoms (data not shown). As a result, we cannot rule out the possibility that *Rosa wichurana* resistance can be based on *R* genes. This observation could also explain that *Rosa wichurana* resistance is age-dependent given that in other pathosystems, *R* genes inducing HR-like reactions were shown to be effective only at adult plant stage like *Lr22a* and *Lr22b* in wheat (Dyck 1979). However, many other hypotheses can be drawn to explain the age-related resistance in our genotype. For example, constitutive expression of resistance proteins that increase with the leaf age could explain that in old leaves the pathogen is recognized earlier (or more efficiently) and stopped with an HR response while in young leaves the pathogen is not stopped at early stages but its development seems to be slowed down compared to a susceptible genotype. Therefore, it would be interesting to study the transcriptional changes at different time points in old and young leaves of *Rosa wichurana* but also the difference of expression between the ages at different time points. Moreover, the timing of response (ROS burst, HR, Ca²⁺ influx, etc.) between the leaves of different ages should also be investigated to better characterize this age-related resistance.

Finally, the resistance of *Rosa wichurana* seems to be linked to cuticle integrity as old leaves may present black spot symptoms and reduced sporulation when the leaf is wounded. The importance of the cuticle integrity was also observed in other genotypes of *Rosa wichurana* and other rose genotypes (Castledine et al. 1981; Walker et al. 1996). It would be interesting to compare the resistance of *Rosa wichurana* that is based on several genes of small effect to the resistance of the major *Rdr* genes present in the genotypes previously described when their leaves are wounded. Do the *Rdr*-carrying genotypes develop symptoms and exhibit sporulation when the leaf is wounded? Or do they present the same levels of resistance than unwounded leaves? Furthermore, the cuticle being the first physical barrier between a host and a pathogen, its thickness might play an important role in the delay of pathogen entry and therefore, if the cuticle is finer in young leaves, then the entry is not delayed and the host might not have time to implement the defenses before the pathogen penetrates.

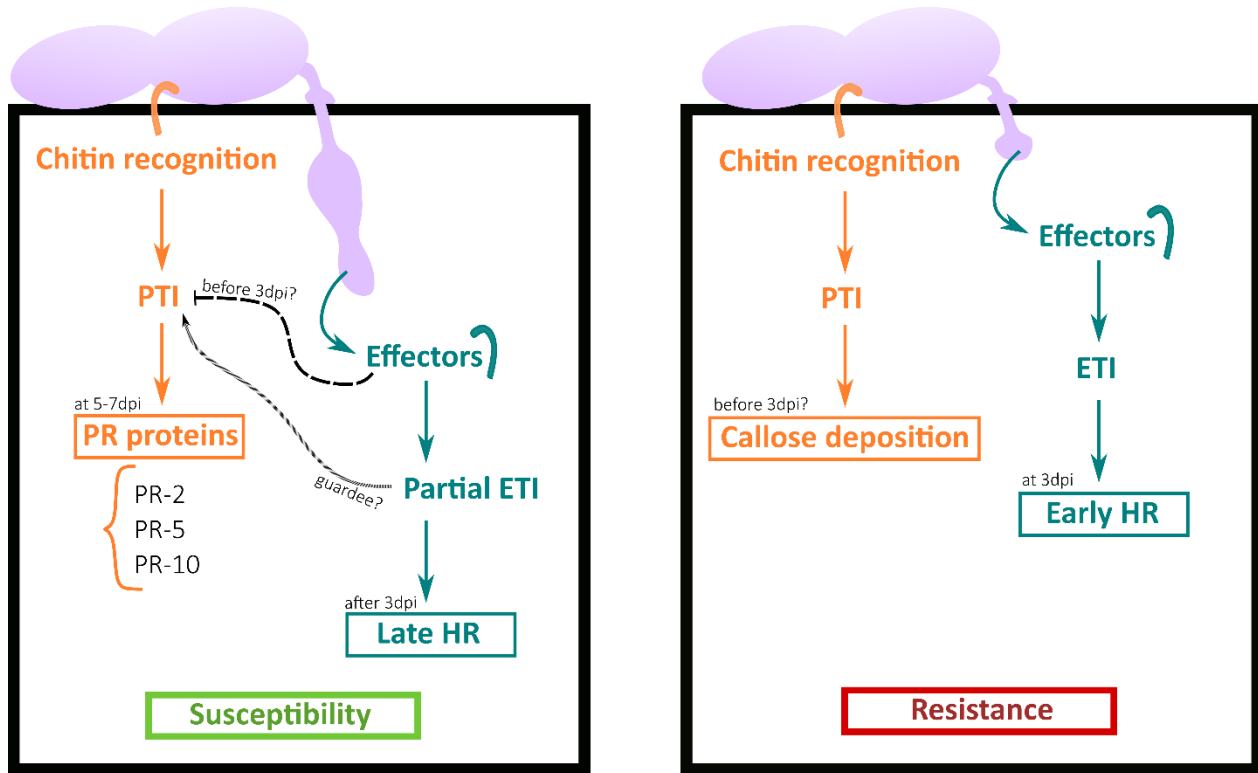
3. *ROSA CHINENSIS* ‘OLD BLUSH’, A SUSCEPTIBLE NOT SO SUSCEPTIBLE

The study of *Rosa chinensis* ‘Old Blush’ in response to *D. rosae* infection in parallel with the resistant genotype *Rosa wichurana* was important so we would be able to compare the genotype responses. As expected, the susceptible genotype ‘Old Blush’ was colonized by DiFRA67 strain and mature acervuli were produced after 7dpi, which shows the completion of *D. rosae* life cycle by 9dpi. Interestingly, no callose deposition at the penetration site was observed at early stages of infection in ‘Old Blush’ unlike for *Rosa wichurana* but was later observed around the haustorium necks that invaded the epidermal cells (see Figure 70). This observation is interesting as we showed with the RNAseq analysis that a strong inhibition of the response associated with PAMP recognition (PTI) happened at an early stage of infection (0 and 3dpi). Indeed, even if many receptor-like kinases bound to the membrane (PRR proteins) were up-regulated at 0 and 3dpi, genes associated with the PTI response like PR proteins exhibited a low expression at these time points and their expression increased after 5dpi. These results suggest an inhibition of the PTI response and we can hypothesize that the pathogen released effectors that can alter/inhibit PTI. However, at the same time as the PTI was inhibited, we observed an increase of expression at 3dpi of genes coding for proteins involved in indirect and direct recognition of effectors from the pathogen (coding for NBS-LRR type of proteins). These genes were involved in the activation of host programmed cell death and HR-like responses. Noticeably, epidermal cells that were invaded by haustoria turned necrotic after 3dpi, which is in line with the observations made in the transcriptomic analysis. Furthermore, some of the genes coding for proteins involved in the guard model (NBS-LRR proteins guarding PRR proteins) like RPM1 were also highly expressed at 3dpi (Anderson et al. 2010; Cook et al. 2015). With these results, we can hypothesize that the recognition of PTI inhibition by the plant through this guard model might have led to the restoration of PTI at later time points (see Figure 71). Moreover, the delayed HR-like response when the fungus invaded the epidermal cells along with the expression of resistance gene analogs (RGAs) suggest the existence of a partial ETI-reaction that happens later than for a resistant plant like *Rosa wichurana* (see Figure 71). Neu (2018) also proposed the existence of a partial ETI-reaction in ‘Pariser Charme’ infected by DortE4. Indeed, similar microscopic observations (cell death in invaded cells) than for ‘Old Blush’ were made during the interaction between ‘Pariser Charme’ and DiFRA67. However, unlike ‘Pariser Charme’, PR-proteins were only produced in later time points, which suggests that some differences of response (particularly the PTI responses) between both genotypes might exist. We also observed that, overall, ‘Old Blush’ leaves presented a smaller black spot than ‘Pariser Charme’ and the production of mature acervuli seemed slightly delayed in ‘Old Blush’ leaves compared to ‘Pariser Charme’. We can, then, imagine that ‘Old Blush’ presents some levels of partial resistance since a delay in pathogen development and reproduction can be observed. In that sense, it would be interesting to perform a quantitative investigation of the components of partial resistance for both susceptible genotypes. The time until sporulation as well as the sporulation capacity should also be studied in order to determine whether or not ‘Old Blush’ carries some resistance reducing pathogen development and sporulation that can be qualified as partial resistance.

Interestingly, ‘Old Blush’ exhibited several QTLs in our field assessments and one was located around the region of *Rdr1* locus. Moreover, in previous experiments, ‘Old Blush’ exhibited lower levels of infection according to the strain used for the infection and in one case, presented no symptoms when inoculated with DiFRA18 (unpublished results from Belarosa project). This strain was not sampled in our region but in

the north of France whereas DiFRA67 was sampled near the institute. This may explain that our field might present strains that are virulent (and perhaps selected over time) in 'Old Blush'. In addition, these observations suggest that 'Old Blush' might be able to recognize effectors from DiFRA18 but not from DiFRA67 and other strains, which in return implies the existence of a possible specific resistance that has been broken by many strains but not by DiFRA18. Effectors recognition is based on resistance proteins coded by *R* genes but some *R* genes can be broken and yield incomplete resistance (see [section 2.2.1](#) of chapter 1). Indeed, *R* genes that are genetically qualitative can cause incomplete resistance that is expressed quantitatively through partial resistance allowing some sporulation (Niks et al. 2015). It would be interesting to investigate the differences of sequence between *Rdr1* locus from the resistant *Rosa multiflora* 88/124–46, the susceptible 'Pariser Charme' also presenting *RGA1*-gene of *Rdr1*-locus and the genotype 'Old Blush' (Kaufmann et al. 2010; Menz et al. 2018, 2020; Neu 2018). That way, different alleles of these *R* genes can be associated to either complete resistance, partial resistance and complete susceptibility.

However, compared to *Rosa wichurana*, 'Old Blush' remains more susceptible regardless of the age of leaves (see Figure 70). We proposed that the delay in response to *D. rosae* infection is mainly due to lack of PTI at the first stage of infection, which gives time to the pathogen to penetrate with less resistance and grow under the cuticle. Chitin being the major elicitor of PTI reaction to fungi, it would be interesting to analyze the response of a resistant and a susceptible rose to an artificial application of chitin. We can hypothesize that chitin alone with no production of the effectors that might inhibit PTI response would lead to an expression of genes related to the activation of a PTI response in 'Old Blush'. Like proposed by Neu (2018), these experiments with artificial chitin inoculation can help to distinguish between mechanisms that are more PTI from the ETI ones and in particular for 'Old Blush', it would be a way to assess whether or not effectors produced by the strain can inhibit the plant PTI response.



Rosa chinensis 'Old Blush'

Rosa x wichurana

Figure 71: Proposed model of defense responses to *Diplocarpon rosae* for the susceptible genotype *Rosa chinensis* 'Old Blush' and the resistant genotype *Rosa wichurana*

In the case of the susceptible 'Old Blush', the recognition of chitin by PRR proteins leads to the induction of a cascade of signaling typical of PAMPs-triggered immunity (PTI) involving several kinases. However, the pathogen quickly penetrates the cuticle and effectors are released into the host cytoplasm and we hypothesized that some inhibited the PTI response before 3dpi. Some R proteins chaperons (HSP90, RPM1, SGT1) in the cytosol might sense the PTI inhibition at 3dpi which leads to the PTI re-activation at 5dpi. PTI signaling leads to the production of pathogenesis-related (PR) proteins (PR-, PR-5 and PR-10). Finally, a late hypersensitive response (through activation of SAG12 genes) might be activated following the activation of a partial ETI by the recognition of effectors through R proteins. These responses lead to susceptibility and the infection of the leaves. The pathogen is capable of producing new conidia. In the case of old leaves of the resistant *Rosa wichurana*, the recognition of chitin by PRR proteins leads to a rapid PTI response consisting of early callose depositions at the penetration points but also at the epidermal cell wall. We hypothesize that this response is activated before 3dpi. However, the callose papillae at the penetration site is not sufficient and the pathogen is capable of invading a single cell. During this invasion, callose is still deposited and effectors are produced by the pathogen. One of these effectors are recognized by an R protein at 3dpi and this activates a full ETI response that leads to a quick HR of the invaded cell and sometimes of the neighbor cells. This rapid response results in a resistance.

4. *DIPLOCARPON ROSAE* DEVELOPMENT IN SUSCEPTIBLE LEAVES, A MIX OF LIFESTYLES?

This section aims to propose a spatial model of *D. rosae* infection that consists of a combination of several feeding behaviors in one single spot following the observations made microscopically, the results obtained from the transcriptomic study and the literature. Indeed, *D. rosae* has been described as a hemibiotroph fungus and it is known that hemibiotrophs have a biotrophic phase during which host cells remain alive and later on switch to necrotrophic phase during which pathogens actively kill the host cells for feeding. Production of haustorial structures in epidermal cells is the sign of the biotrophic stage of *D. rosae*. Several authors believe that the switch between the biotrophic stage and the necrotrophic one is when the fungus starts forming necrotrophic intracellular mycelia (Gachomo et al. 2006). *D. rosae* was also described to be able to grow saprophytically in fallen leaves, which is an important characteristic allowing it to propagate from fallen infected leaves once the winter is done. However, the question of the switch between biotrophic and necrotrophic stages was raised by Debener (2019) in his review. Indeed, Neu and Debener (2018) reported the secretion of biotrophic effectors that are only observed in obligate biotrophs along with two effectors related to necrosis inducers. These two effectors (ricin-b-like lectins) match the apoplastic effector MoCDIP1 from the hemibiotroph *Magnaporthe oryzae* that was shown to induce cell death (Neu 2018). Neu (2018) suggested that these “cell death-inducing genes” are of high importance for the necrotrophic phase of these *M. oryzae* and *D. rosae*. The fact that this necrotrophic effector was highly expressed at early stages supposed to be during the biotrophic phase (24 and 72hpi) suppose that, during the alleged biotrophic stage, the pathogen is already inducing cell death and switching to a necrotrophic stage (Debener (2019)).

In the study of compatible interactions (‘Old Blush’ and ‘Pariser Charme’), we observed that within a same black spot at 9dpi several zones could be delimited. The first zone (A in Figure 72) delimits the asymptomatic growth of the pathogen where subcuticular hyphae and some haustoria are developed. The second zone (B in Figure 72) consists of subcuticular hyphae from which intercellular and intramural hyphae are produced. This zone is characterized by the presence of haustoria inside epidermal cells that appear necrotic. The third and last zone (C in Figure 72) is mainly characterized by large necrotic areas and developed short distance hypha networks (intercellular and intramural hyphae). Acervuli are visible in this old infection site. Gachomo et al. (2006) indicated that the necrotrophic phase was reached after six days under favorable conditions and that intracellular mycelia could be observed at the onset of acervulus formation. In our study, it was difficult to observe intracellular hyphae at 9dpi on ‘Old Blush’ or ‘Pariser Charme’ but these were clearly observed at 15dpi on ‘Old Blush’. Interestingly, when the intracellular hyphae were observed, they were found in the zone C near the acervuli and underneath them. These results indicate that the pathogen might have already switched to a necrotrophic stage at 9dpi. Noticeably, these intracellular hyphae were not observed outside zone C and were found to co-localize with cells appearing necrotic. However, further observations at 7 and 9dpi of leaves infected by *D. rosae* should be required to say with certainty the moment where the pathogen produces the necrotic hyphae (intracellular). We can hypothesize that several feeding behaviors are in place at the same time in a single black spot. Therefore, a progression from biotrophy (zone A) to necrotrophy (zone C) might be happening within the same spot.

Studying each zone separately may bring more information about the necrotrophic switch that happens. Therefore, an interesting study would be to analyze the transcriptomic changes in both pathogen and host tissues in each one of these zones separately. A similar idea was already implemented by Giolai et al. (2019). These authors described an approach for high-throughput spatial transcriptomics at a large scale to spatially characterize the responses of host plants to pathogens. They used GaST-seq (Grid-assisted, Spatial Transcriptome sequencing) method and were able to obtain both host and pathogen spatial transcriptomes while reducing the costs compared to existing sequencing-based methods. This approach is interesting as it allows to study responses through differential gene-expression analysis similarly to a single-cell without the additional experimental procedures to remove plant cell wall and cell sorting (fluorescent activated cell sorting (FACS) assays). Indeed, the authors explained that these manipulations could compromise the characterization of cell-type transcript and differential expression studies. Moreover, these techniques lose spatial information when the protoplasts are extracted from a tissue (Giolai et al. 2019). Other methods like fluorescent in-situ hybridization (FISH), laser-capture microdissection (LCM) or the SPATIAL TRANSCRIPTOMICS can also be used and a high resolution can be obtained (Giolai et al. 2019 and reference therein). However, they are difficult to implement in most laboratories, which is not the case with the GaST-seq workflow since standard laboratory equipment can be used (Giolai et al. 2019). It seems very interesting to implement this technique in our pathosystem so we can spatially investigate the transcriptional changes by using the different zones described in Figure 72.

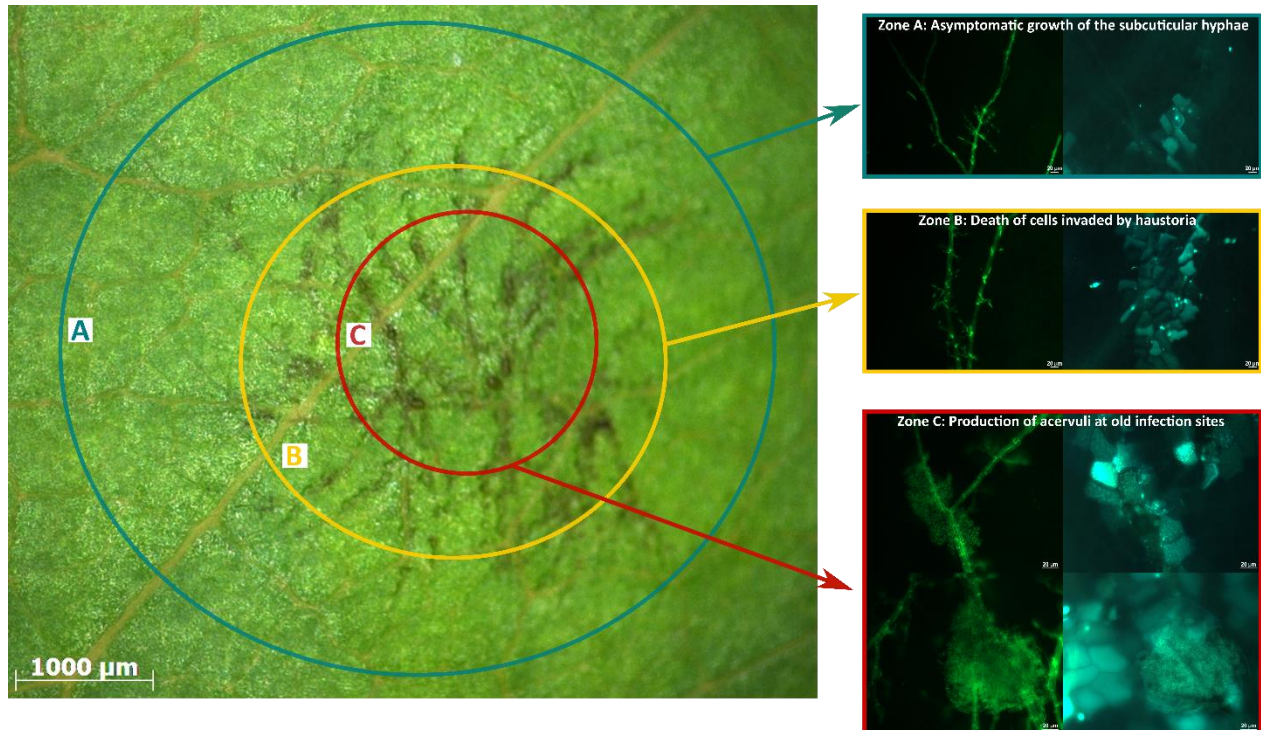


Figure 72: Proposition of a spatial model of infection for the hemibiotroph fungus *Diplocarpon rosae*

5. BREEDING FOR BLACK SPOT RESISTANCE IN GARDEN ROSES

The genotype used in this study is a hybrid of *Rosa wichurana* that is heterozygous at the locus controlling recurrent blooming located on chromosome 3 (Iwata et al. 2012). Indeed, at that locus (*RoKSN* gene), *Rosa wichurana* exhibits both a wild type allele responsible for once flowering and an allele responsible for continuous flowering (Iwata et al. 2012). Recurrent blooming is a highly desirable character in rose and was introduced in the European roses by the Chinese background like explained in chapter 1. *Rosa wichurana* is particularly interesting for breeding because it presents black spot resistance in the field and a large spectrum of efficiency (several locations for field assessments and strains used for laboratory/greenhouse assays) but also because this genotype is heterozygous at the recurrent blooming locus. Therefore, it is, in theory, easier to get the right allele of continuous flowering combined with resistance than from a true wild type *Rosa wichurana* that is homozygous wild type at that locus of interest. However, this locus is located near the major QTL B3 linked to black spot resistance and sometimes the confidence intervals overlap with the recurrent blooming locus. The QTL on B3 is particularly important as it is found for all the years scored in all three populations (OW, FW and HW) and it has an effect on the penetrance and the severity of disease. If we only want to introgress the major QTL B3 and at the same time obtain a continuous flowering genotype, it could be problematic as both loci seem physically linked. In that case, two situations need to be considered:

- (1) The continuous-flowering allele is linked to the resistance allele of the QTL on B3 and in this case, there is no problem to get both continuous flowering and resistance;
- (2) The once-flowering wild type allele is linked to the resistance allele of the QTL on B3 and in this case, it will be difficult to separate these loci and so more individuals in the progeny will be necessary to be able to have the right genetic combination.

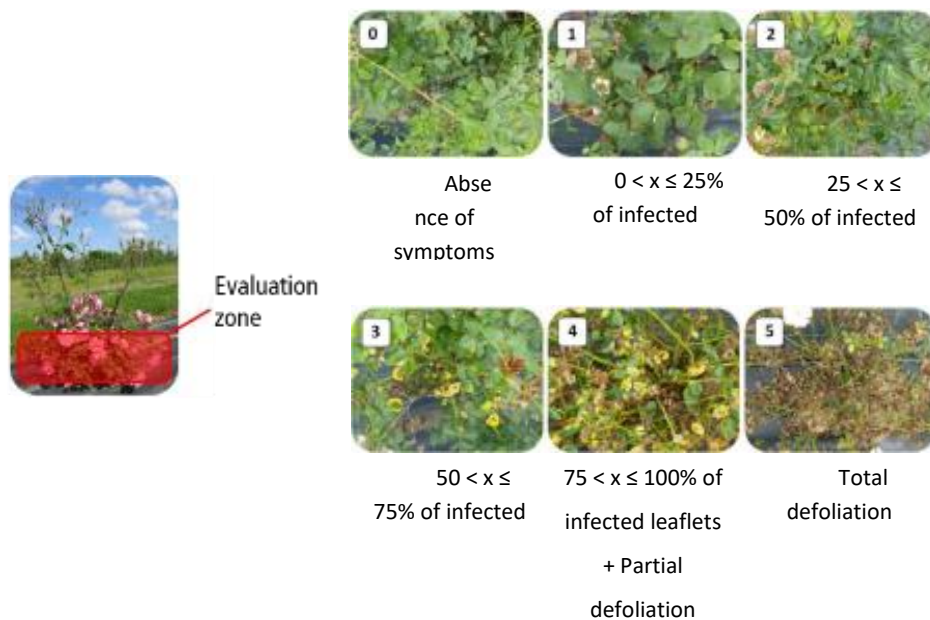
The next step in our investigation shall be to determine which allele from the recurrent blooming locus is linked to the resistance allele of the QTL on B3. An easy analysis is to study the disease resistance presented by individuals from the OW population that present the continuous-flowering allele and compare the resistance to the ones presenting the once-flowering wild type allele. Indeed, with the marker KSN, we can identify which individual carries the continuous-flowering allele from the ones carrying the wild type allele that does not give continuous-flowering. These analyses are under process. Furthermore, we started a collaboration with a private company that is currently working on the phasing of our genotype *Rosa wichurana* using artificial intelligence. The outcome of this collaboration will be to obtain the phasing of each chromosome of *Rosa wichurana* and to generate a new map that will present a higher marker density than the one used in chapter 2 (more than a thousand of markers per chromosome). Subsequently, we shall run the QTL analyses with this new map so a more precise location can be identified. In addition, our team is currently building a high-quality genome for the heterozygous *Rosa wichurana*. Genome generation of highly heterozygous genotypes is particularly complicated, but with the phasing made by the artificial intelligence and the combination of long reads (PacBio) and optical mapping (Bionano), we hope to be able to clearly construct each homologous chromosome with more precision. With all this additional data generated, we could identify with more precision the location of the QTLs linked to black spot disease as well as the genes underlying them but also we could investigate more precisely whether or not the continuous-flowering allele is linked to the resistance allele of the QTL on B3.

Nonetheless, we should not forget that resistance in *Rosa wichurana* is also controlled by loci of smaller effect like B5, B4 or B6 (Lopez Arias et al. 2020). In particular, studying the effect of each QTL separately can give us information on their specific effect on the phenotype. A project which aims at studying the effects of the QTLs B3 and B5 has been initiated in our team. We selected and multiplied in 2019 several individuals from OW population that presented 1) the resistance allele at the metaQTL1 and the metaQTL2 on chromosome 3 without the resistance allele on the metaQTLs on chromosome 5 and the QTLs on chromosome B4 and A1, 2) the resistance allele at the metaQTL1 on chromosome 5, or both metaQTLs on chromosome 5 without the resistance allele on the metaQTLs on chromosome 3 and neither QTLs on chromosome B5 or A1. The purpose is to study the individuals' resistance in whole plant inoculation and detached leaf assays with the strain DiFRA67 but also to determine the interaction types with microscopic observations like the ones presented in this study. The individual QTLs will also be characterized in detached leaf assays for their behavior towards the international race collection of *D. rosae*. That project can give us more insights on the individual effect of each QTL detected in our study (Lopez Arias et al. 2020). We can imagine that if the QTL on B5 gives a good level of resistance to black spot disease on its own, it could be used in breeding programs, which would be easier than the QTL on B3 because it is not physically linked to the recurrent blooming locus. It could also be interesting to go further on the genetic characterization of these loci by cloning the genes.

These findings are the starting point of various investigations on black spot resistance in our team. New collaborations and techniques were either developed or transferred from foreign teams and will be useful in this quest of understanding. Several points remain unclear and need further validation in particular in the RNAseq analysis. Nevertheless, a lot of information has been brought to light with this study even if more knowledge about genetics and genomics of rose resistance to black spot disease is yet to be discovered. In a context of constant change in consumer's expectations about disease resistance and in legislation becoming more and more strict about the use of chemicals, rose industry must adapt to release varieties with higher degrees of resistance. Helping breeders is the final outcome of these long research projects and we hope that we will be able to provide them with markers linked to both *R* genes and loci controlling quantitative resistance in the future.

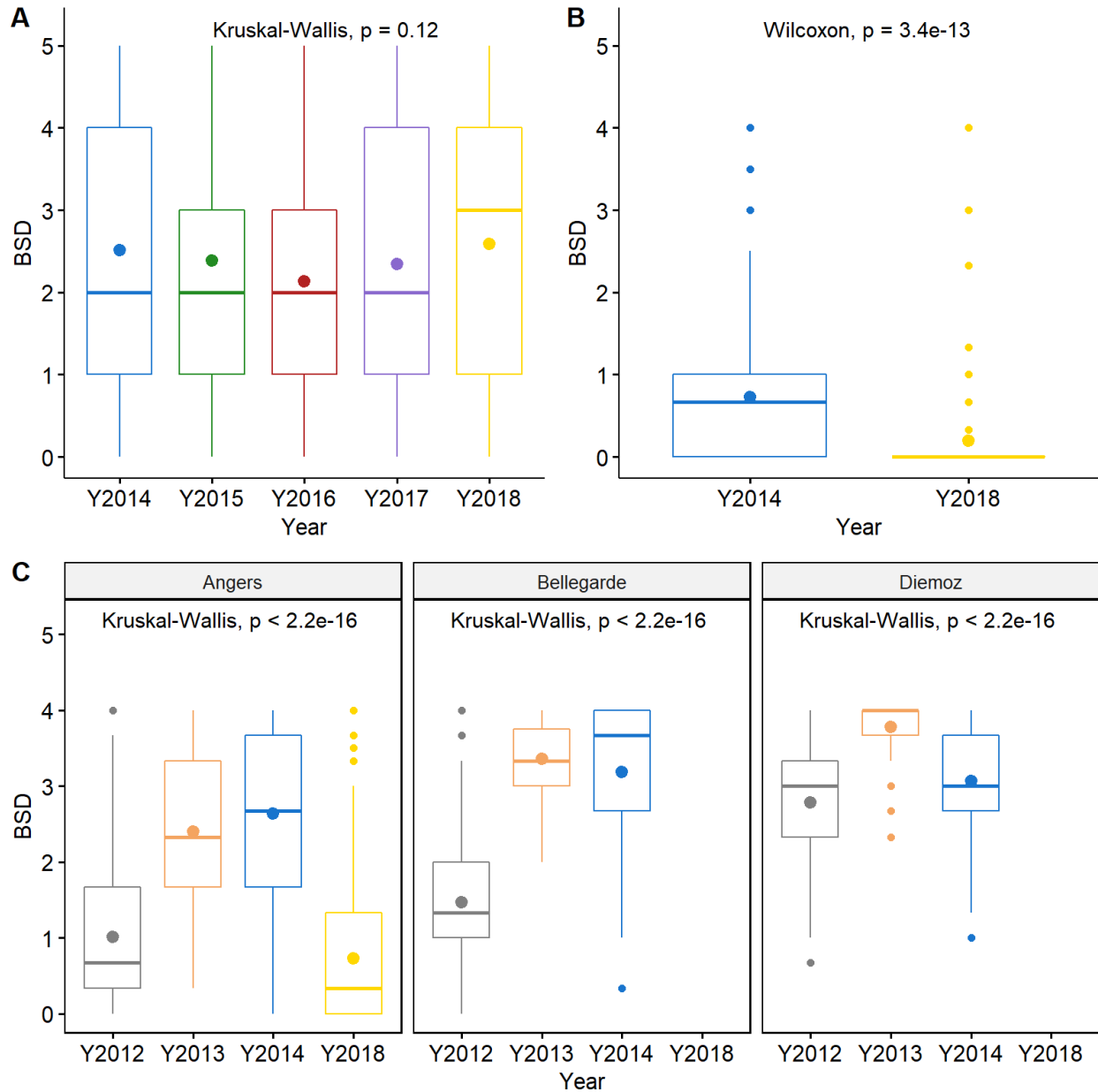
Appendixes

Appendix A : Supplementary figures and tables of chapter 2 - Article



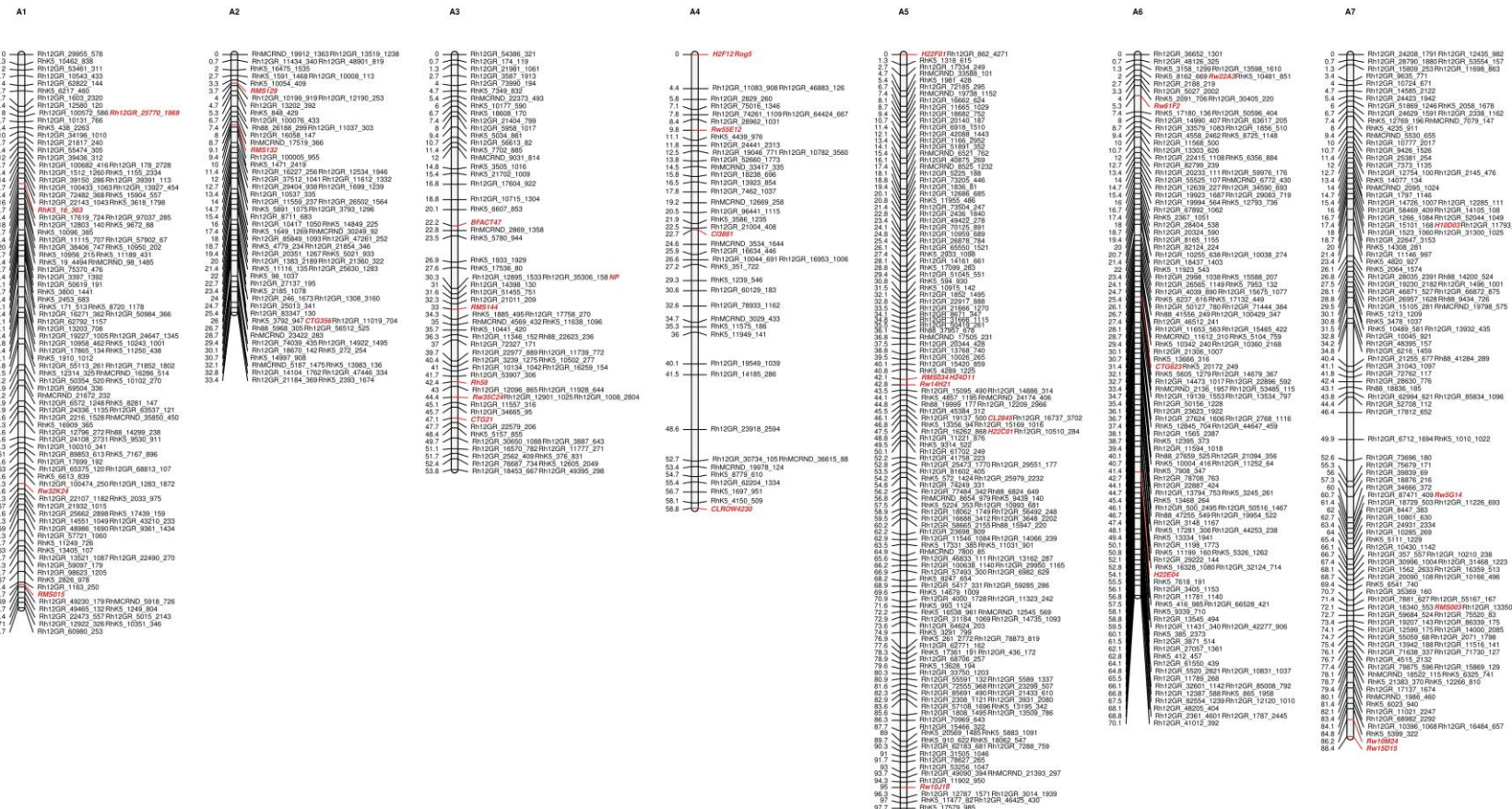
Supplementary figure 1: Evaluation zone and rating scale of black spot disease in rose

From 0 (no symptoms) to 5 (total defoliation of the plant) with a score of 1 for less than 25% of infected leaflets, a score of 2 for infection between 25 and 50%, a score of 3 for infection between 50 and 75% of infected leaflets and 4 for infection of 75% to 100% and partial defoliation.



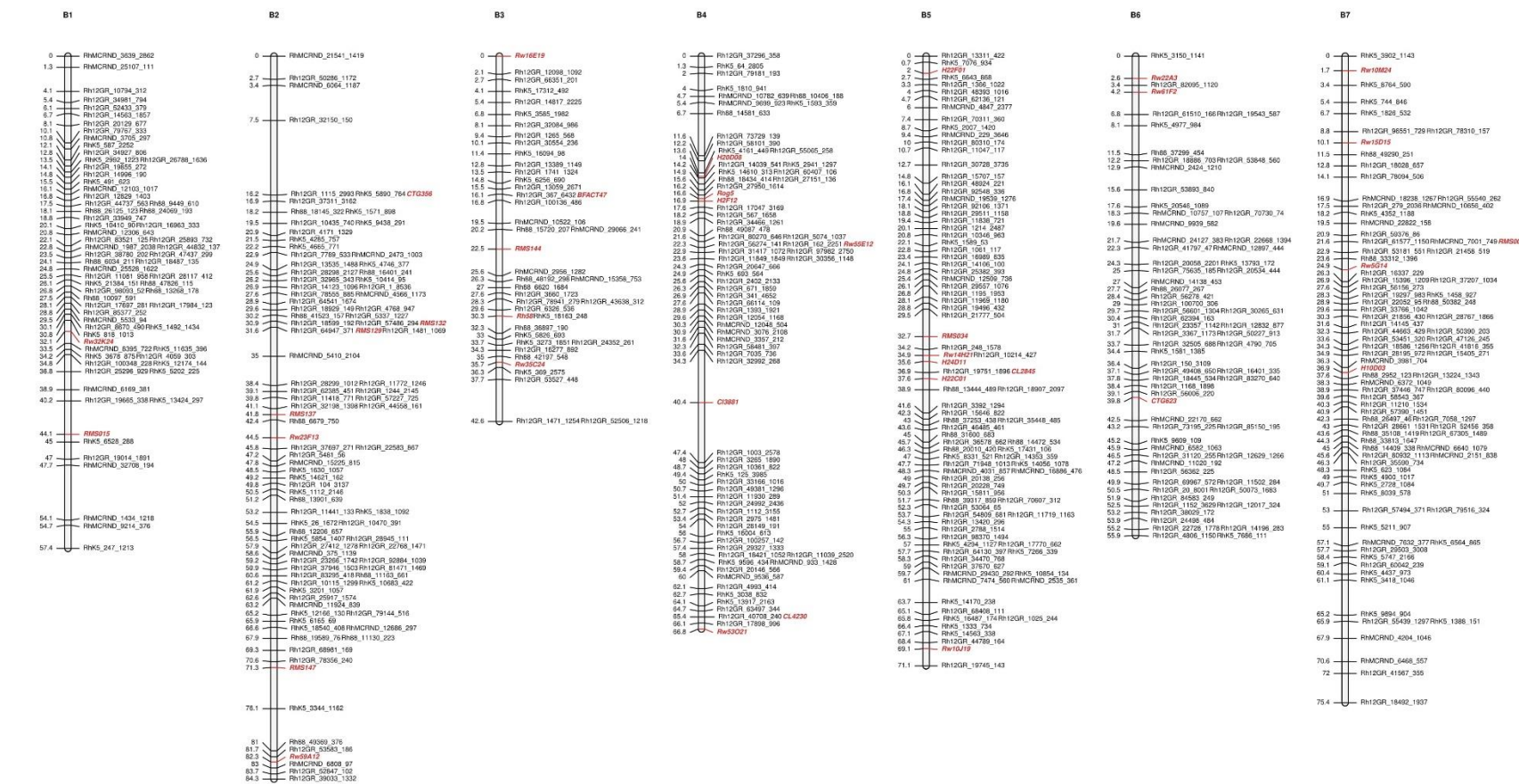
Supplementary figure 2: Overall mean of black spot disease (BSD) scores for three rose populations over several locations and years under natural infections in field

In the box plots, the boundaries of the box indicate the 25th percentile (on the lower part) and the 75th percentile (on the upper part). A thick line within the box marks the median, and a dot within the box marks the mean. Lines above and below the box indicate the 10th and 90th percentiles. Points above and below the whiskers indicate outliers outside the 10th and 90th percentiles. **A:** Data description for different years for OW population in Angers, **B:** Data description for different years for FW population in Angers, **C:** Data description for different years for HW population in Angers, Bellegarde and Diémoz. A Kruskal-Wallis test was used to compare the scoring years for HW and OW populations, and a Wilcoxon test was used to compare the two scoring years 2014-2018 for FW. For HW population, locations were considered separately. P-values of the tests are displayed on the graphs for all populations.



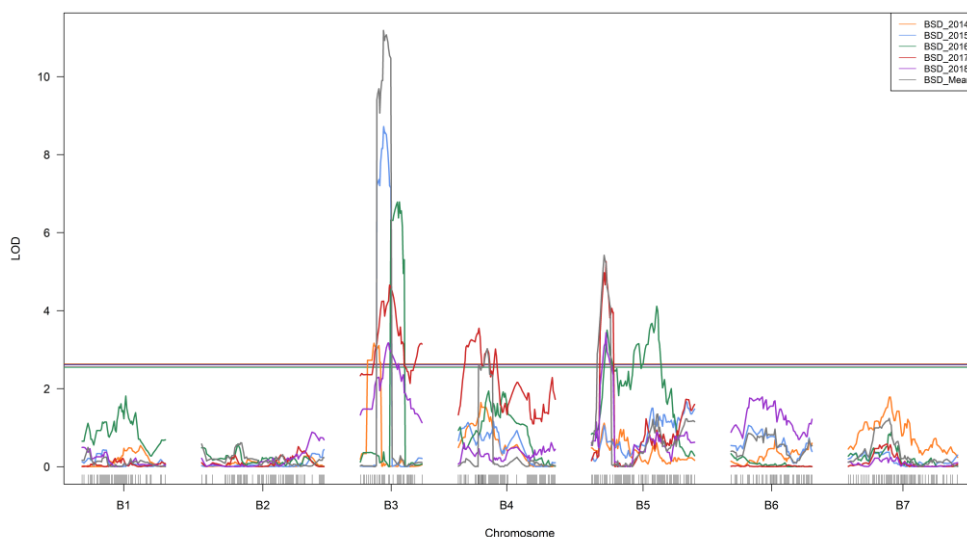
Supplementary figure 3: Genetic linkage map of the female parent, *Rosa chinensis* 'Old Blush', for OW population

Linkage groups (LG) names for the female map (A1 to A7) are placed above the corresponding linkage groups. Locus names are indicated on the right side of each LG. When several markers were mapped at the same position, one or two markers were reported corresponding to the unique loci or markers with different phases. SSR markers are indicated in red. Genetic distances (cM) are indicated on the left side of each LG.



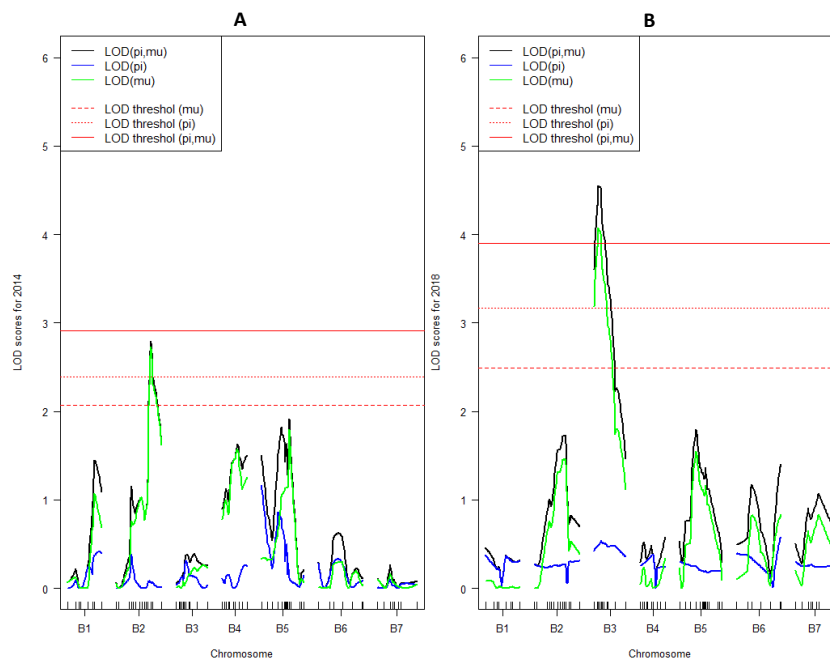
Supplementary figure 4: Genetic linkage map of the male parent hybrid, *Rosa wichurana*, for OW population

Linkage groups (LG) names for the male map (B1 to B7) are placed above the corresponding linkage groups according to Spiller et al. 2011. Locus names are indicated on the right side of each LG. When several markers were mapped at a same position, one or two markers were reported corresponding to the unique loci or markers with different phases. SSR markers are indicated in red. Genetic distances (cM) are indicated on the left side of each LG.



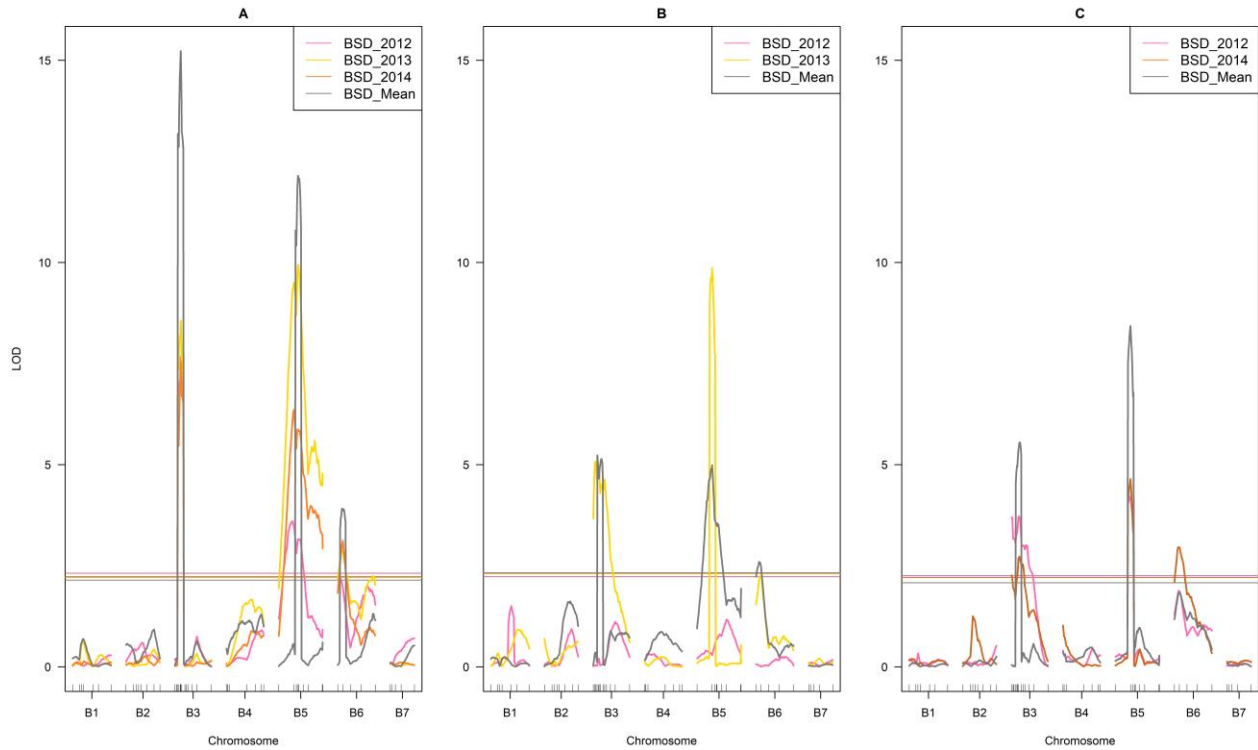
Supplementary figure 5: QTL mapping associated with black spot disease (BSD) resistance using a normal model with an CIM analysis for OW population for the male map

Linkage groups are named as follows: “B” for the male map and the number of the linkage group. LOD score for each year and the mean of all years are calculated using a Composite Interval Mapping method (CIM) and are displayed with different colors. The same set of colors is used to represent the $\alpha=0.05$ LOD threshold for declaring significant QTL based on 1,000 permutations.



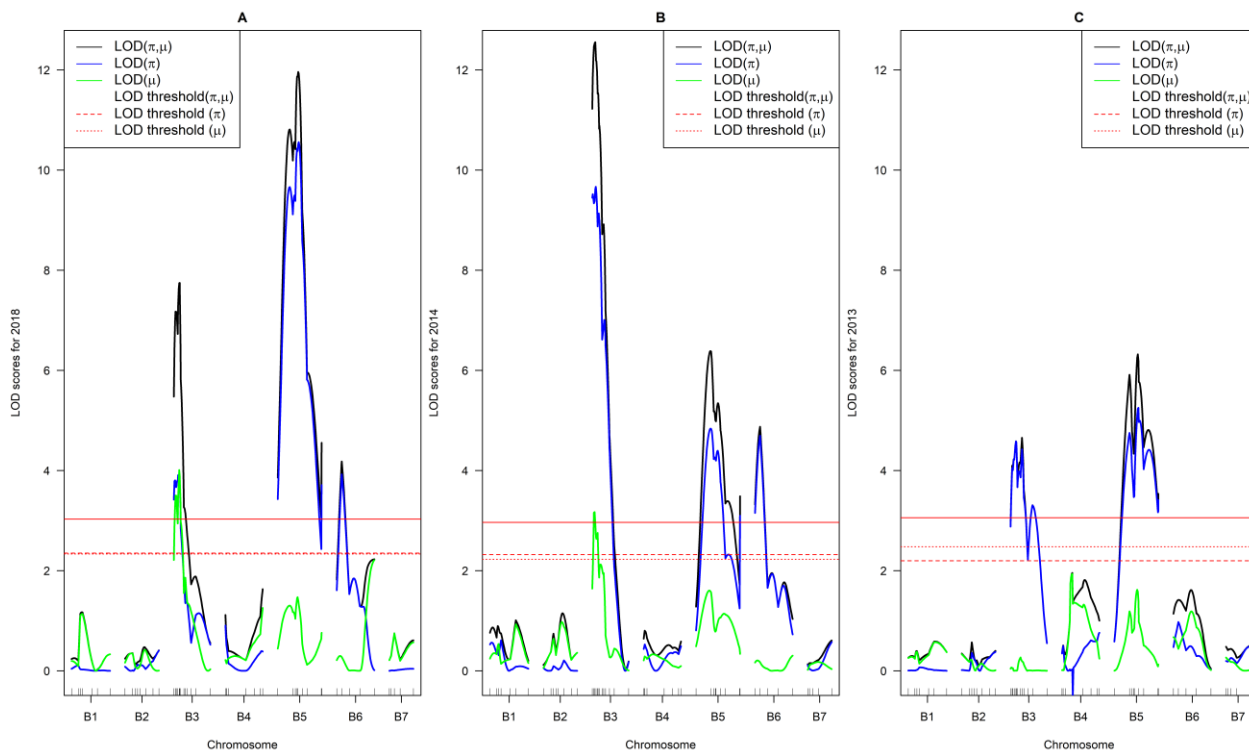
Supplementary figure 6: QTL mapping associated with black spot disease resistance using a two-part model approach for non-normally distributed data of FW population for the male map

A and B: LOD curves for the two-part model for 2014 (A) and 2018 (B); LOD. π (penetrance, equivalent to binary model) displayed in blue, LOD. μ (severity, equivalent to normal model for non-spike phenotypes) displayed in green and LOD. $\pi.\mu$ (sum, representing the complete model) displayed in black; LOD thresholds are displayed in red with $\alpha=0.05$ for declaring significant QTL based on 1,000 permutations.



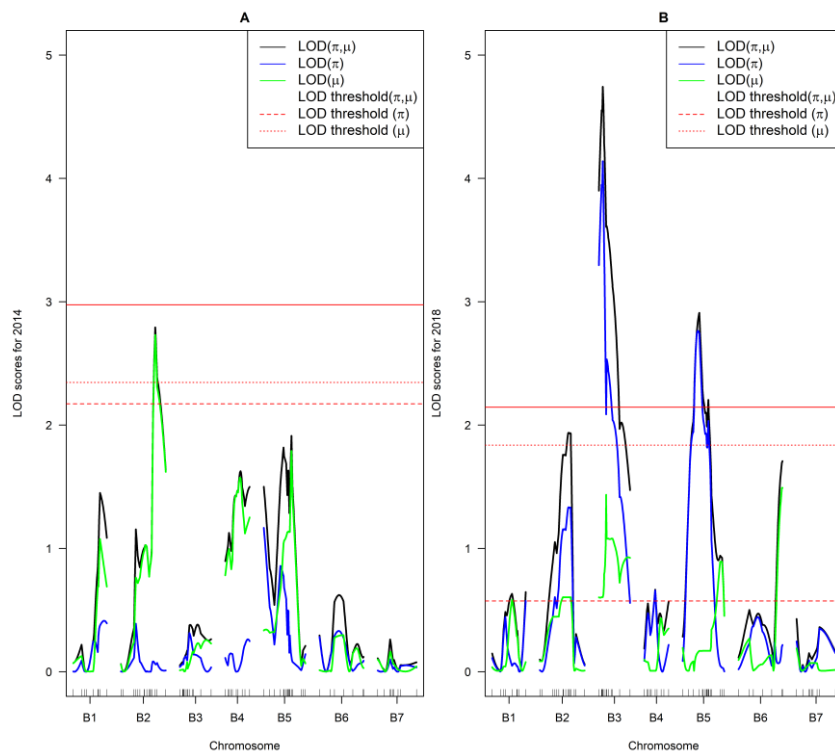
Supplementary figure 7: QTL mapping associated with black spot disease (BSD) resistance for normally distributed data of HW population using a normal model with CIM analysis for the male map

Linkage groups are named as follow: “B” for the male map and the number of the linkage group. For HW population, BSD was scored in three locations: **(A)** Angers, **(B)** Bellegarde and **(C)** Diémoz. LOD score for each year and the mean of all years were calculated using a Composite Interval Mapping (CIM) method. The same set of colors is used to represent the different scoring years in the different locations. $\alpha=0.05$ LOD threshold was used for declaring significant QTL based on 1,000 permutations.



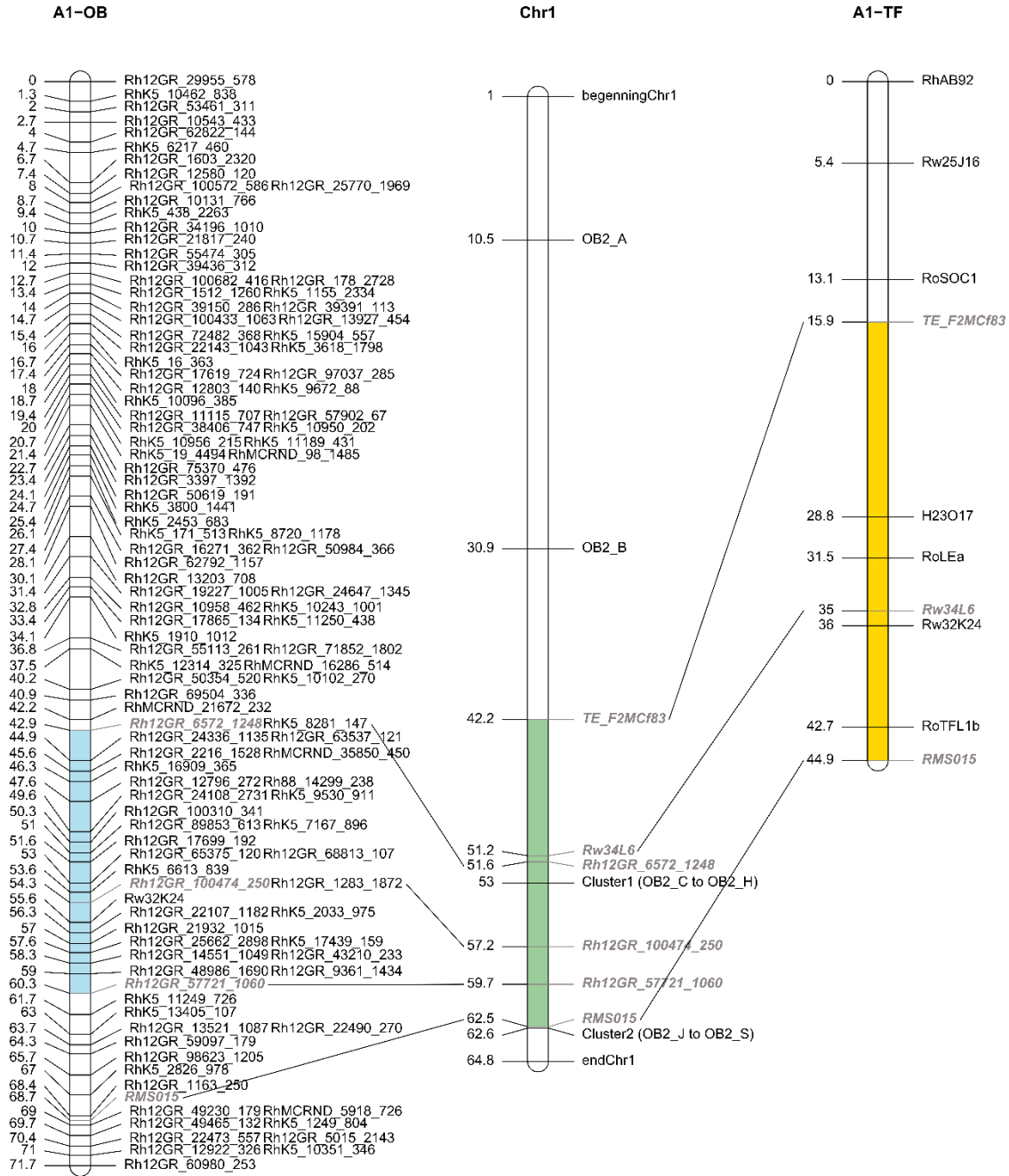
Supplementary figure 8: QTL mapping with black spot disease (BSD) resistance using a two-part model approach for non-normally distributed data of HW population for the male map

Linkage groups are named as follows: “B” for the male map and the number of the linkage group. A to C: LOD curves of the two-part model analysis for spike-like distribution of HW BSD scoring years (Angers-2018 (A), Bellegarde-2014 (B) and Diémoz-2013 (C)); $LOD.\pi$ (penetrance, equivalent to binary model) displayed in blue, $LOD.\mu$ (severity, equivalent to normal model for non-spike phenotypes) displayed in green and $LOD.\pi.\mu$ (sum, representing the complete model) displayed in black; LOD thresholds are displayed in red with $\alpha=0.05$ for declaring significant QTL based on 1,000 permutations.



Supplementary figure 9: QTL mapping with black spot disease resistance using a two-part model approach for non-normally distributed data of FW and HW populations for the female maps

A: LOD curves for the two-part model for FW population using 2018 scoring year in Angers; B: LOD curves for the two-part model for HW population using scoring year 2014 in Bellegarde; LOD. π (penetrance, equivalent to binary model) displayed in blue, LOD. μ (severity, equivalent to normal model for non-spike phenotypes) displayed in green and LOD. $\pi.\mu$ (sum, representing the complete model) displayed in black; LOD thresholds are displayed in red with $\alpha=0.05$ for declaring significant QTL based on 1,000 permutations.



Rendered by L³PageMio3V²ve

Supplementary figure 10: Co-localization of the Rdr1 genes cluster with the QTLs on A1 from OW and FW female maps

Linkage groups (LG) names from female genetic maps are placed above the LG and named A1 - “population name” and the corresponding chromosome is placed in the middle. Names of markers are on the right and the genetic distances (in cM) on the left. For the chromosome from the physical map, physical distances are expressed in mega-base (Mb). TNLs genes and clusters (OB2-A, OB-B, Cluster1 and Cluster2, Menz et al. 2020) are shown in black. The markers peaks of each QTL are displayed in grey. The active form of Rdr1 resistance gene (muRdr1A) is located on the cluster2 (Menz et al. 2020). QTLs widest confidence intervals are represented in plain colors on the linkage groups: blue for the OW female map, yellow for the FW female map and green for the equivalent common widest region on the physical map.

Supplementary table 1: Common marker list for all populations for the female and male maps

Male maps					Female maps				
Markers ^a	LG ^b	OW	HW	FW	Markers ^a	LG ^b	OW	HW	FW
<u>RMS015</u>	B1	X	X	X	RMS015	A1	X		X
Rw25J16	B1		X	X	Rw32K24	A1	X		X
<u>Rw32K24</u>	B1	X	X	X	Rw25J16	A1		X	X
CTG329	B2		X	X	<u>RMS132</u>	A2	X	X	X
CTG356	B2	X	X		CTG356	A2	X		X
RMS129	B2	X		X	RMS147	A2		X	X
<u>RMS132</u>	B2	X	X	X	Rw59A12	A2		X	X
<u>RMS137</u>	B2	X	X	X	Rw23F13	A2		X	X
<u>RMS147</u>	B2	X	X	X	RMS137	A2		X	X
Rw23F13	B2	X		X	CTG329	A2		X	X
<u>Rw59A12</u>	B2	X	X	X	Rh80	A2		X	X
<u>BFACT47</u>	B3	X	X	X	BFACT47	A3	X	X	
RoAP2	B3		X	X	<u>Rh58</u>	A3	X	X	X
Rh50	B3		X	X	Rw35C24	A3	X		X
<u>Rh58</u>	B3	X	X	X	CTG21	A3	X		X
RMS144	B3	X		X	Rh50	A3		X	X
RoIAA	B3		X	X	Rog5	A4	X	X	
RoVIP3	B3		X	X	Rw55E12	A4	X	X	
<u>Rw16E19</u>	B3	X	X	X	Cl3881	A4	X		X
<u>Rw35C24</u>	B3	X	X	X	<u>Rh98</u>	A4	X	X	X
<u>Cl3881</u>	B4	X	X	X	H22F01	A5	X	X	
H20D08	B4	X	X		H24D11	A5	X	X	
H2F12	B4	X	X	X	<u>Rw14H21</u>	A5	X	X	X
Rog5	B4	X		X	<u>CL2845</u>	A5	X	X	X
<u>Rw53O21</u>	B4	X	X	X	Rw10J19	A5	X		X
<u>Rw55E12</u>	B4	X	X	X	Rw22A3	A6	X		X
<u>CL2845</u>	B5	X	X	X	Rw61F2	A6	X		X
H17C12	B5		X	X	<u>CTG623</u>	A6	X	X	X
H22C01	B5	X	X		<u>RMS003</u>	A7	X	X	X
<u>H22F01</u>	B5	X	X	X	Rw10M24	A7	X	X	
H24D11	B5	X		X	<u>Rw15D15</u>	A7	X	X	X
RMS034	B5	X		X					
<u>Rw10J19</u>	B5	X	X	X					
<u>Rw14H21</u>	B5	X	X	X					
<u>CTG623</u>	B6	X	X	X					
<u>Rw22A3</u>	B6	X	X	X					
Rw61F2	B6	X	X						
H10D03	B7	X	X						
<u>RMS003</u>	B7	X	X	X					
Rw10M24	B7	X		X					
<u>Rw15D15</u>	B7	X	X	X					

^a Only SSR markers are listed, the markers shared by all three populations are displayed in emphasized green; ^b A1-A7 for the female maps and B1-B7 for the male maps.

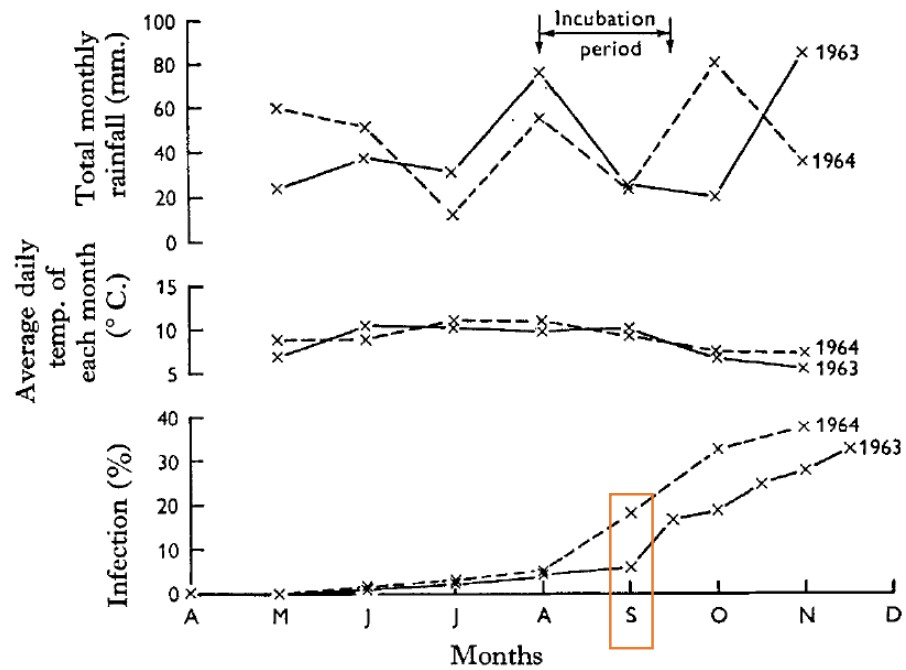
Supplementary table 2: NB-encoding genes information and position in Rose genome

Gene ID	Chromosome	Start	End	Classification	Non-canonical domains	Configuration of subdomains within NB-ARC	Detailed domain configuration, including E-values from Pfam analysis
RC0G0129500	rc00	15921725	15925651	NBS-LRR		P-loop[465-473] Kin-2[546-553] RNBS-B[573-576] GLPL[629-635]	[440-721]NB-ARC:6.8e-40 [872-926]LRR_8:4.7e-07
RC0G0129700	rc00	15936605	15940195	NBS-LRR		P-loop[491-499] Kin-2[572-579] RNBS-B[599-605] GLPL[661-667]	[467-747]NB-ARC:1.3e-38 [908-964]LRR_8:9.6e-08
RC0G0157500	rc00	20165214	20168978	NBS		P-loop[100-108] Kin-2[181-188] RNBS-B[209-215] GLPL[276-282]	[76-370]NB-ARC:6.2e-73 [4-135]RPW8:8.3e-22
RC0G0174400	rc00	22640609	22644651	NBS	RPW8	P-loop[186-194] Kin-2[267-274] RNBS-B[292-298] GLPL[347-353]	[165-435]NB-ARC:1.7e-34 [3-113]RPW8:7e-17 [165-429]NB-ARC:5.1e-34
RC0G0176800	rc00	22873190	22878387	NBS-LRR	RPW8	P-loop[184-192] Kin-2[263-270] RNBS-B[288-294] GLPL[343-349]	[628-684]LRR_8:1.2e-05 [724-763]LRR_4:0.00046 [172-194]AAA_16:0.0003 [196-458]NB-ARC:7.2e-61 [578-
RC0G0200900	rc00	26709295	26713250	NBS-LRR		P-loop[205-213] Kin-2[280-287] RNBS-B[310-316] GLPL[369-375]	615]LRR_8:0.0026 [620-656]LRR_8:0.0064 [172-194]AAA_16:1.9e-05 [196-455]NB-ARC:2.2e-
RC0G0201600	rc00	26778236	26782002	NBS-LRR		P-loop[205-213] Kin-2[280-287] RNBS-B[310-316] GLPL[369-375]	60 [576-613]LRR_8:0.0037 [83-105]AAA_16:0.00016 [107-367]NB-ARC:7e-63
RC0G0202800	rc00	26907214	26909933	NBS-LRR CC-		P-loop[116-124] Kin-2[191-198] RNBS-B[221-227] GLPL[280-286]	[490-527]LRR_4:0.0038 [528-564]LRR_8:0.006 [184-464]NB-ARC:1.4e-
RC0G0283700	rc00	44426071	44428206	NBS-LRR		P-loop[205-213] Kin-2[282-289] RNBS-B[313-319] GLPL[376-382]	59 [574-623]LRR_8:2e-07 [630-652]LRR_4:8.3e-05
RC1G0009500	rc01	1503964	1506714	NBS		P-loop[26-34] Kin-2[104-111] RNBS-B[132-138] GLPL[191-197]	[2-263]NB-ARC:6.7e-37

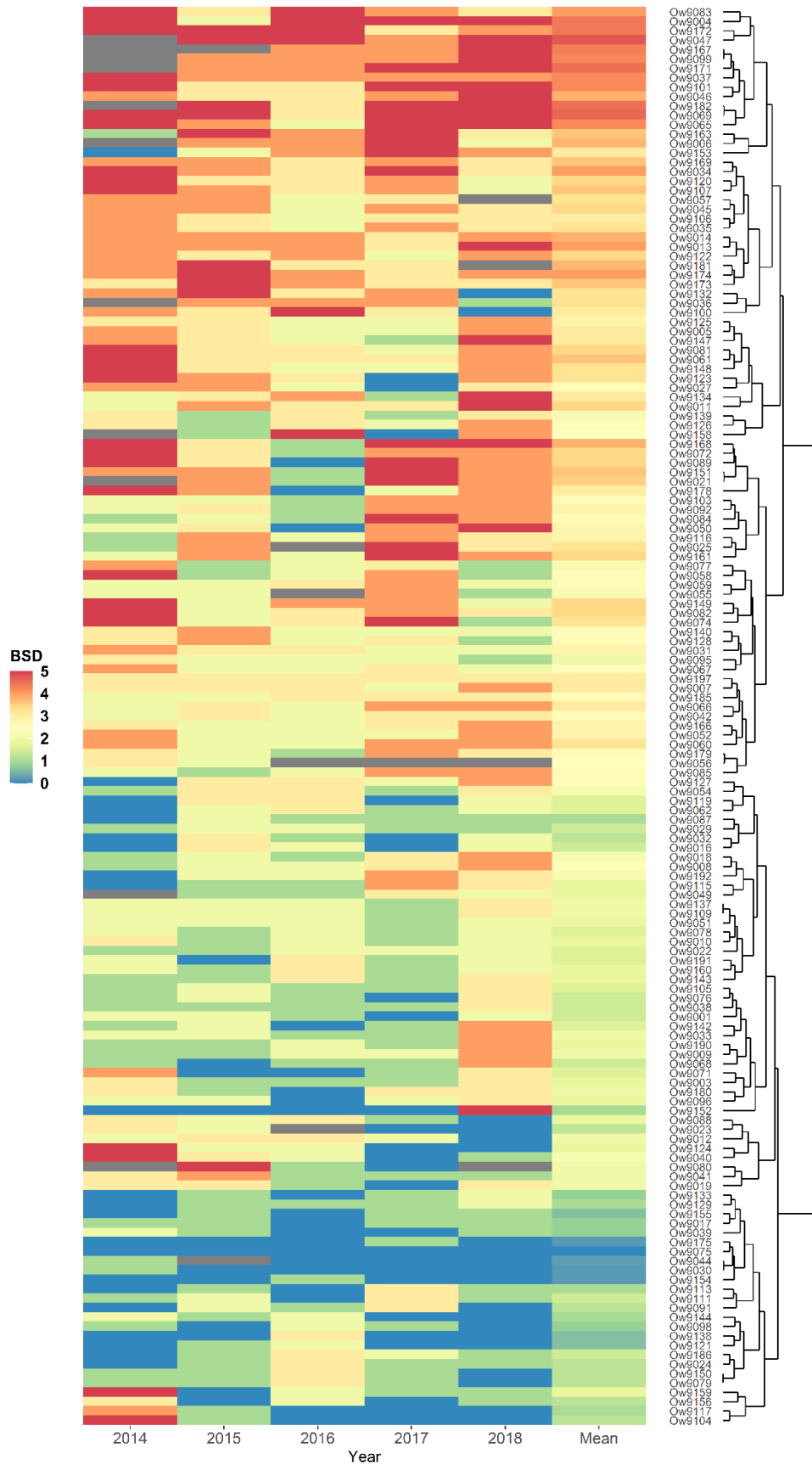
Summary of NB-encoding genes identified in manual annotations. Listed are gene ID names, chromosomal affiliation, end and start positions, classification (CC=Coiled Coil; LRR=Leucine Rich Repeat; NBS=Nucleotide Binding Site; TIR=Toll Interleukin Like Receptor); non-canonical domains (i.e., conserved protein domains that are atypical of NBS-LRR proteins); configuration of identified conserved NB-ARC subdomains; and detailed domain configurations, complete with reported e-values from a Pfam analysis.

NB: This an example of 10 first lines of the file. If you need the complete file, please download it here: <https://drive.google.com/file/d/1DhOpvevYq-kUPOh83FaaH02Fb1mbUIOu/view?usp=sharing>.

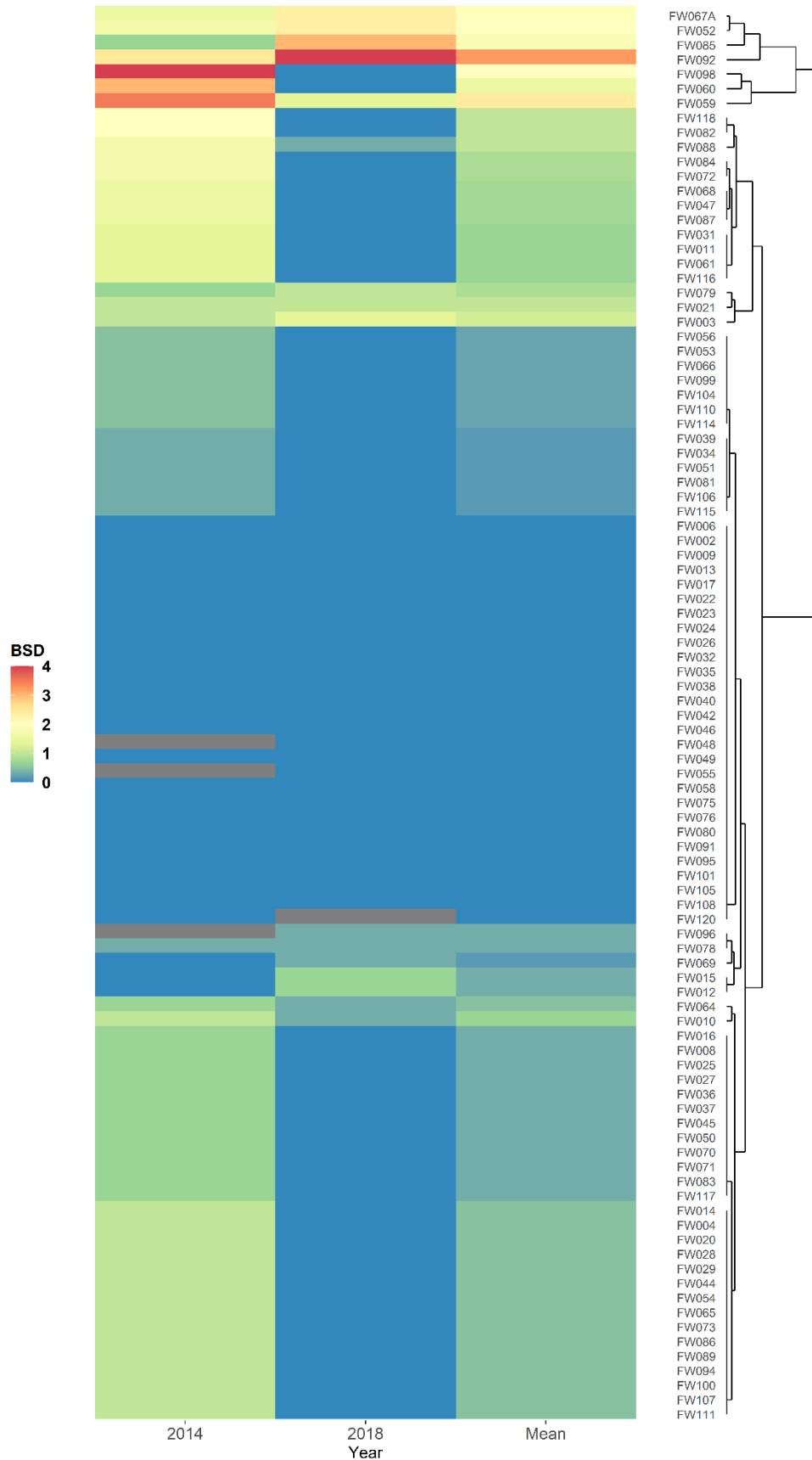
Appendix B : Supplementary figures of chapter 2 – Additional results



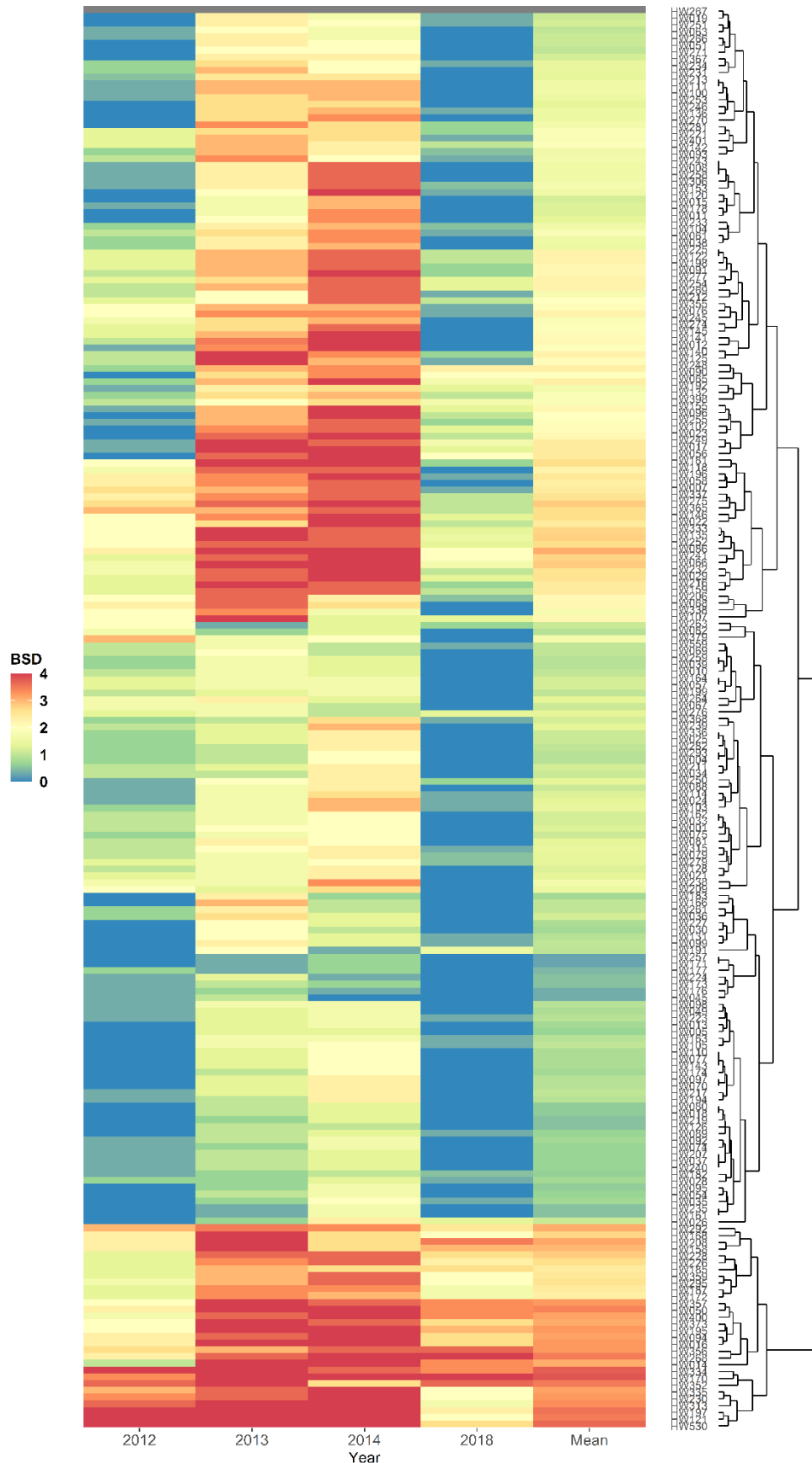
Supplementary figure 11: Influence of rain and temperature upon build-up of infection in H.T. roses at Alphington in 1963 and 1964
 Extracted from Saunders 1966



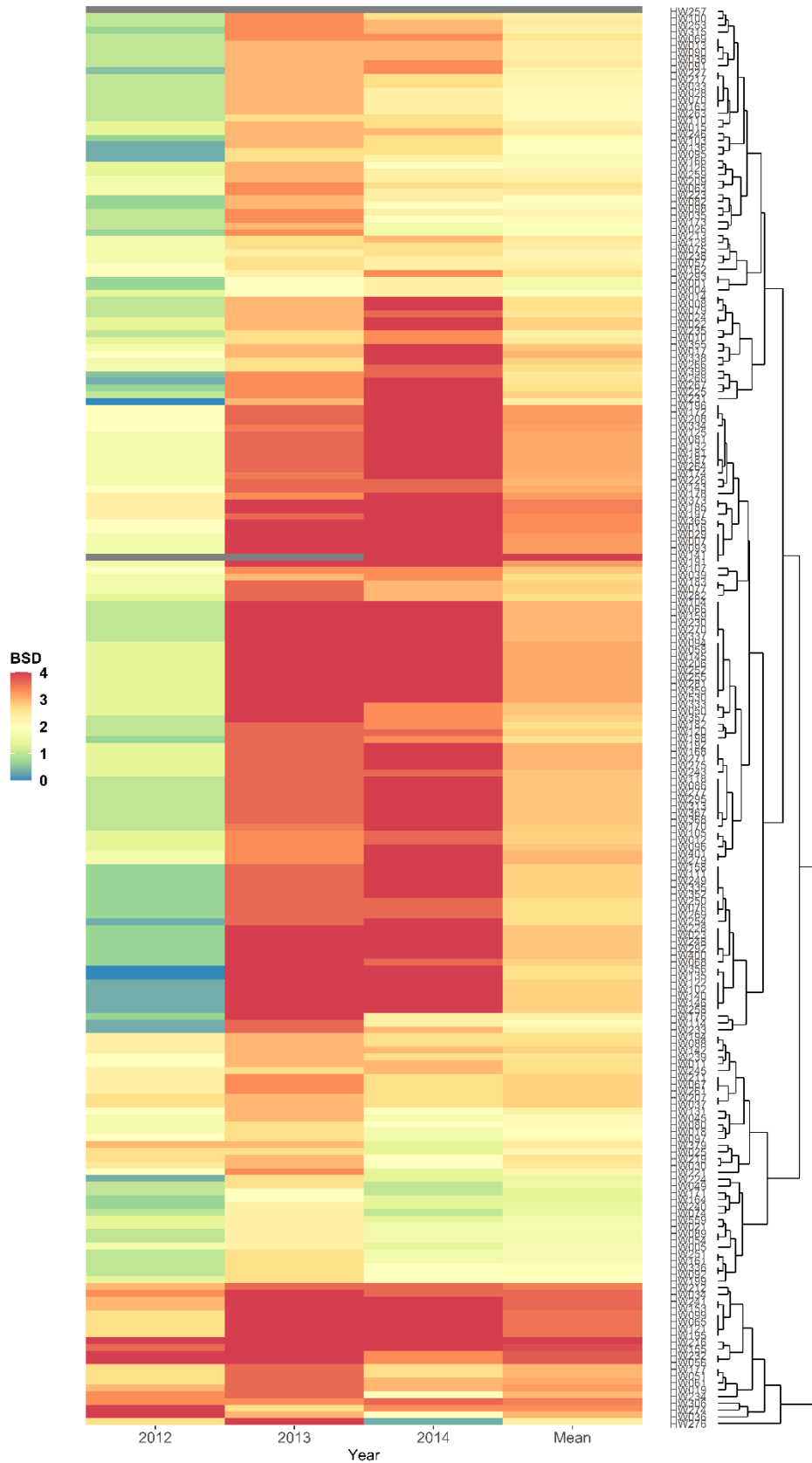
Supplementary figure 12: Heatmap of disease score evolution for hybrids of OW population (from 2014 to 2018)



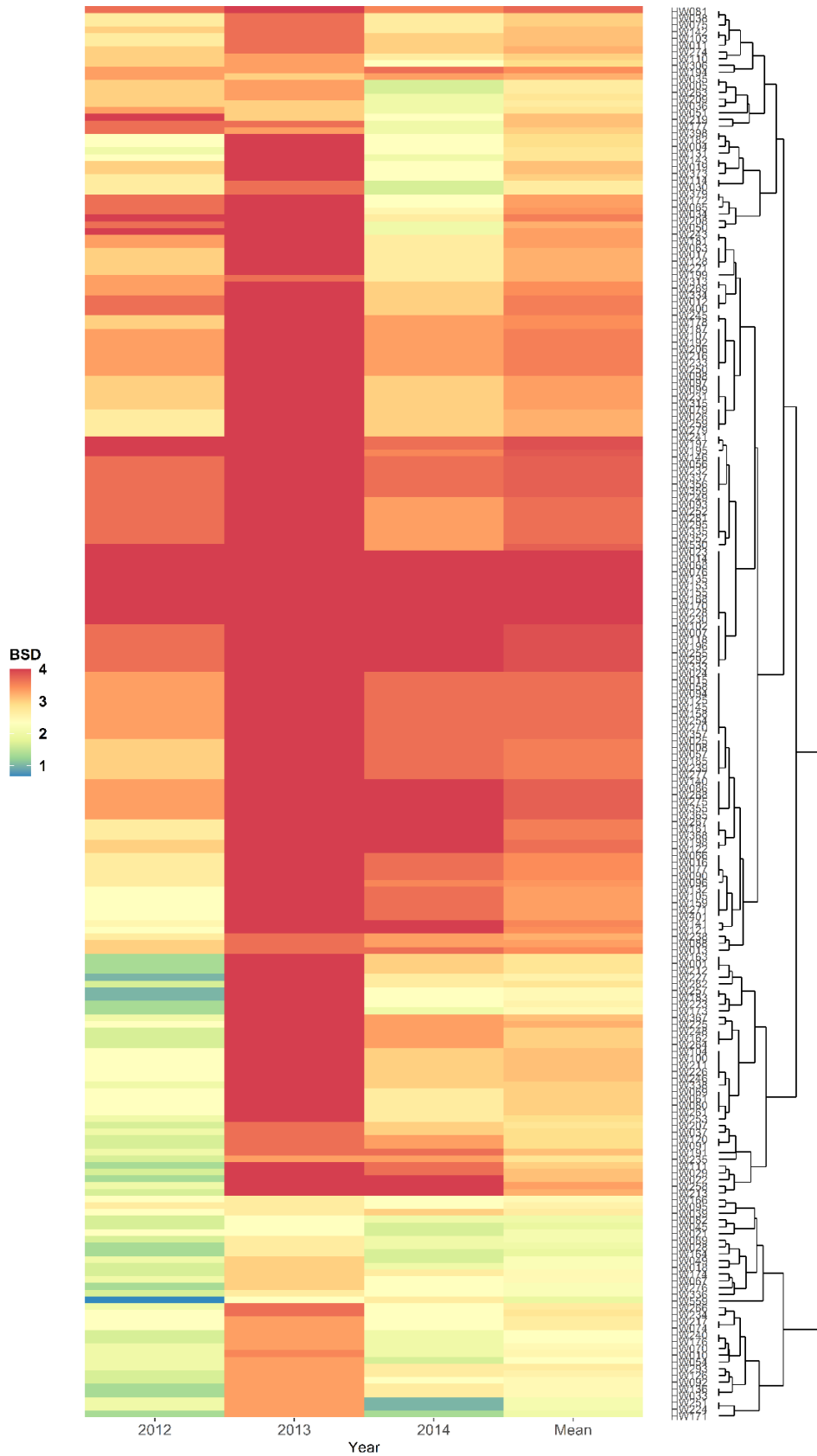
Supplementary figure 13: Heatmap of disease score evolution for hybrids of FW population (for 2014 and 2018)



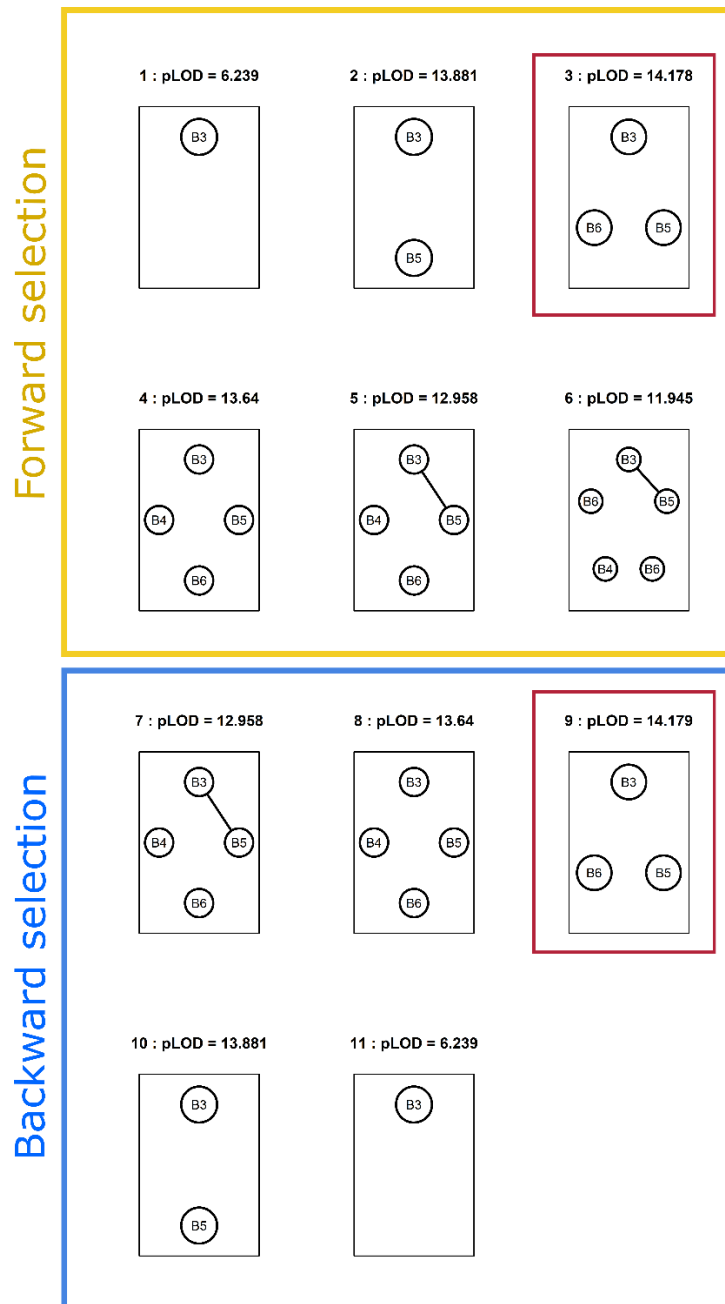
Supplementary figure 14: Heatmap of disease score evolution for hybrids of HW population planted in Angers (from 2012 to 2014 and for 2018)



Supplementary figure 15: Heatmap of disease score evolution for hybrids of HW population planted in Bellegarde (from 2012 to 2014 and for 2018)

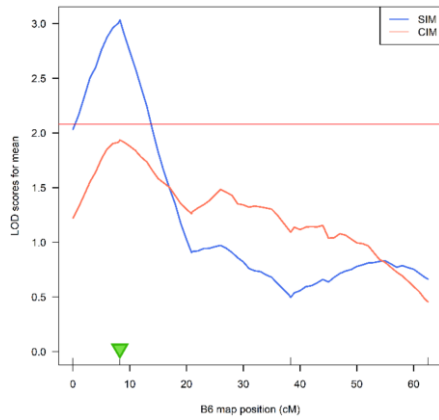


Supplementary figure 16: Heatmap of disease score evolution for hybrids of HW population planted in Diémoz (from 2012 to 2014 and for 2018)



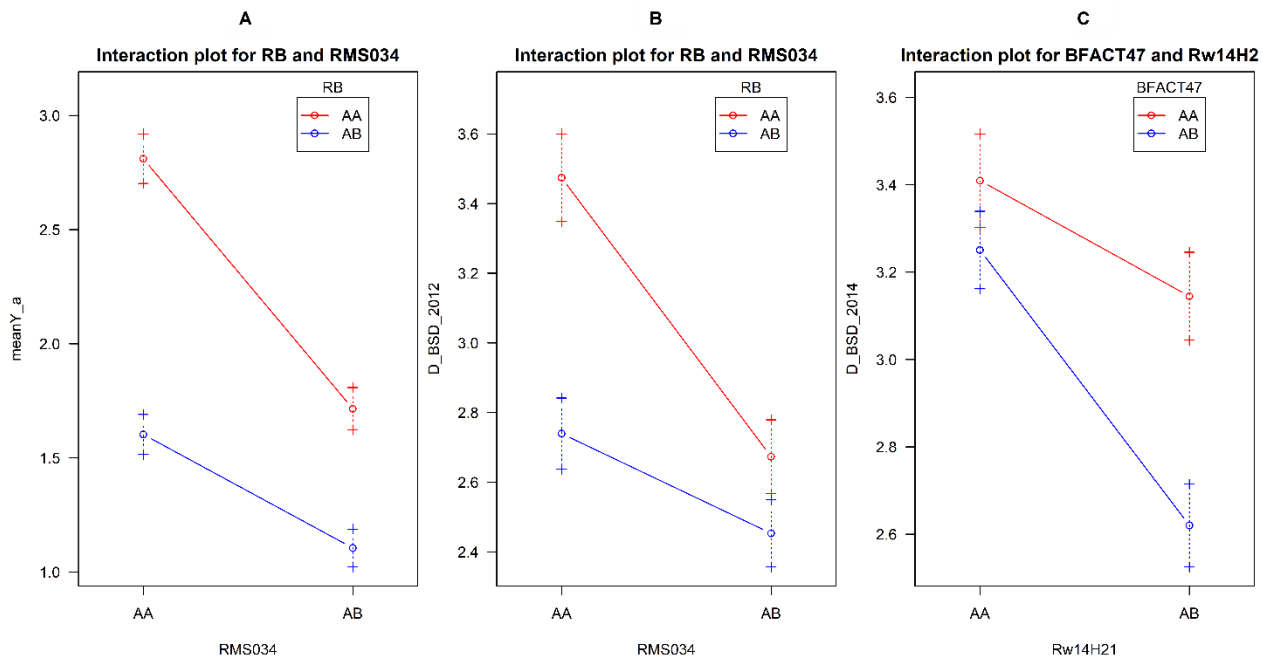
Supplementary figure 17: Example of the sequence of models visited by the forward/backward selection of the *stepwiseqtl* function for HW population scored in 2013 in Angers

The model chosen is the one with the highest LODscore and is framed in red. Each circle represents a QTL and the linkage group where it was detected is mentioned in the center of the circle. Links between circles represent the interaction between loci and means that the algorithm is allowing interaction between specific loci.



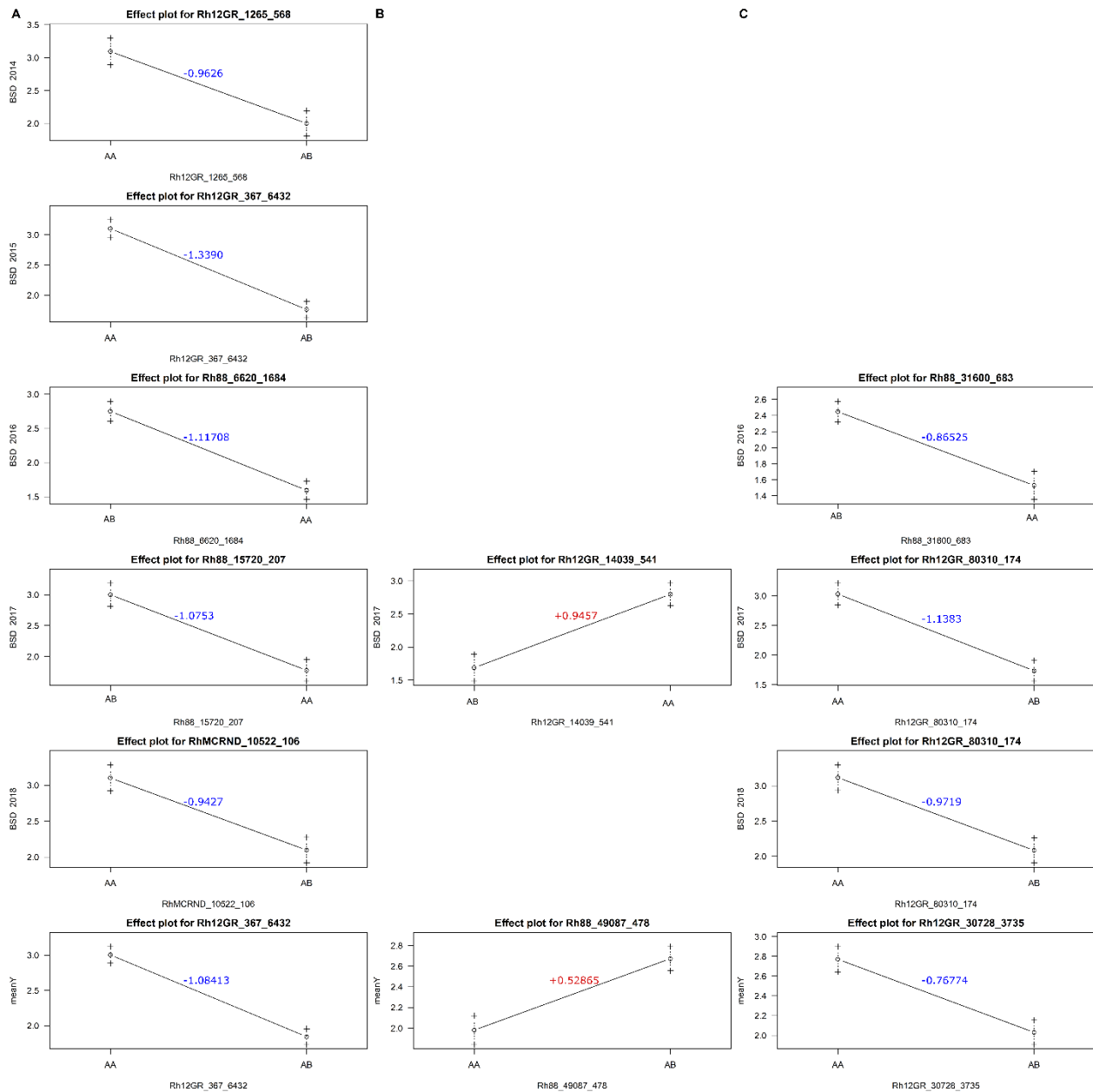
Supplementary figure 18: Comparison of LOD curves for the simple interval mapping (SIM) and composite interval mapping (CIM) for HW population for the mean of the scored years in Diémoz

LOD curves for each analysis are reported in different colors: blue for SIM and orange for CIM. The LOD thresholds are reported as a red line. QTL locations found with the CIM analysis and published in the article are reported with orange arrow heads. Possible positions for the QTLs found with the multiple-QTL model fitting are reported with a green arrow head. No QTL was detected with the CIM analysis.



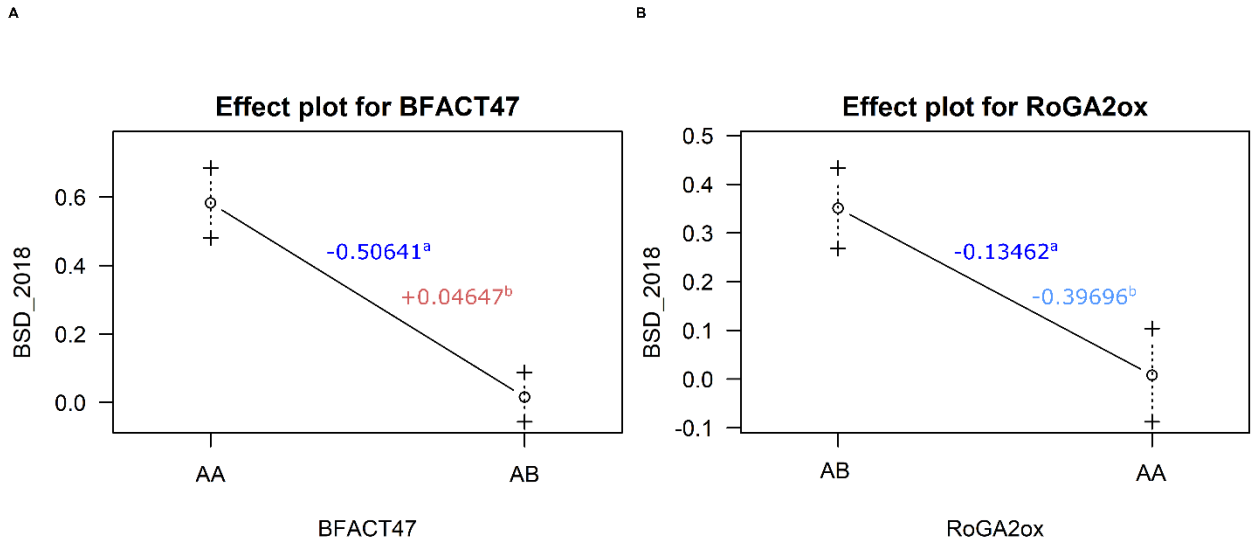
Supplementary figure 19: Example of interaction plots between detected QTLs to assess evidence for epistasis

A: Interaction plot between the QTL on B3 (RB) and the QTL on B5 (RMS034) for the average of the scored years in Angers for HW population, **B:** Interaction plot between the QTL on B3 (RB) and the QTL on B5 (RMS034) for Diémoz in 2012 for HW population, **C:** Interaction plot between the QTL on B3 (BFACT47) and the QTL on B5 (Rw14H21) for Diémoz in 2014 for HW population.



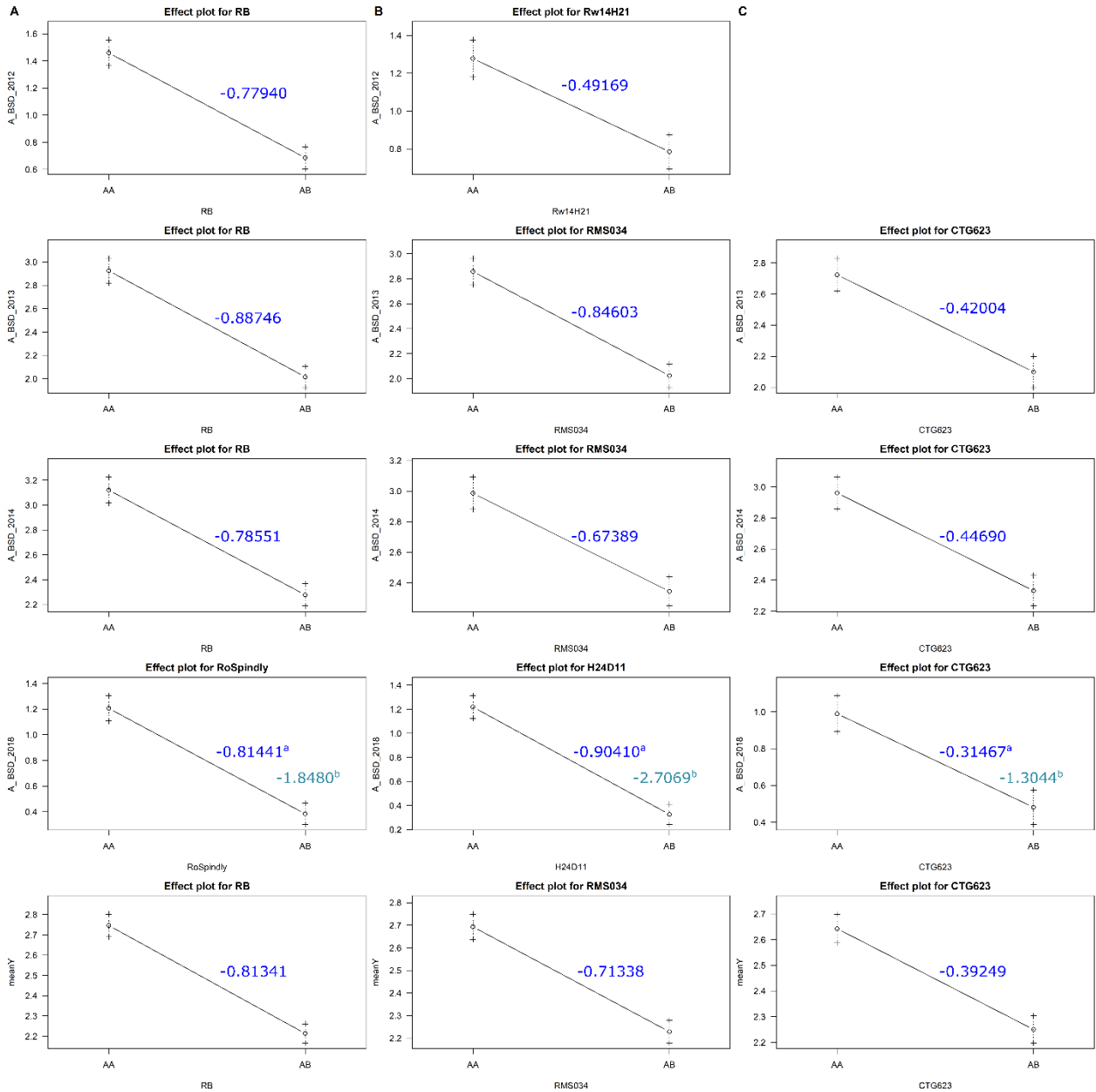
Supplementary figure 20: Effect of putative QTLs detected on linkage groups 3, 4 and 5 of the male map for OW population.

The average BSD score for each scoring year was plotted against the genotype at the marker peak of each QTL using the *effectplot* function of R/qtl package, and the estimated effects are added in color from *fitqtl* function. The effects of the QTLs detected on B3 are plotted on column (A), B4 on column (B) and B5 on column (C). Each row represents a scoring year from 2014 to 2018 as well as the mean at the last row. A blank was left when no QTLs were detected on one of the three linkage groups at a specific year. AA and AB represent the alleles of the closest marker to the QTL peak. That marker is mentioned on the top of each plot as well as the names of x-axes. The estimated effects obtained with *fitqtl* function are added in blue for negative estimated effect and in red for positive estimated effect.



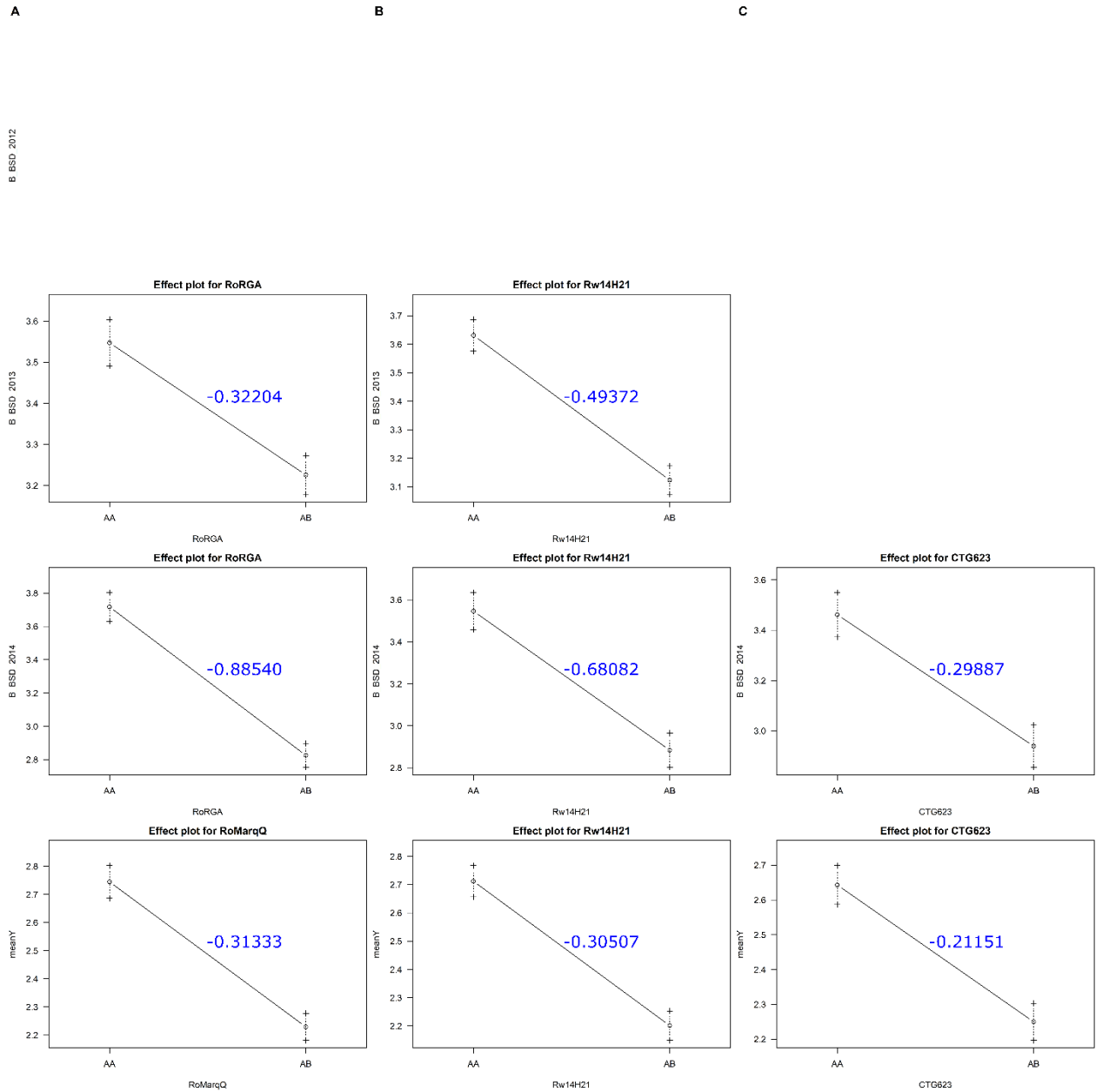
Supplementary figure 21: Effect of putative QTLs detected on linkage groups 3 and 5 of the male map for FW population.

The average BSD score for 2018 was plotted against the genotype at the marker peak of each QTL using the *effectplot* function of R/qtl package. The effects of the QTLs detected on B3 are plotted on column (A) and B5 on column (B). AA and AB represent the alleles of the closest marker to the QTL peak. That marker is mentioned on the top of each plot as well as the names of x-axes. The estimated effects obtained with *fitqtl* function are added in blue for negative estimated effect and in red for positive estimated effect. (a) represents the estimated effects calculated with a normal model in *fitqtl* function and (b) the estimated effects calculated with a binary model.



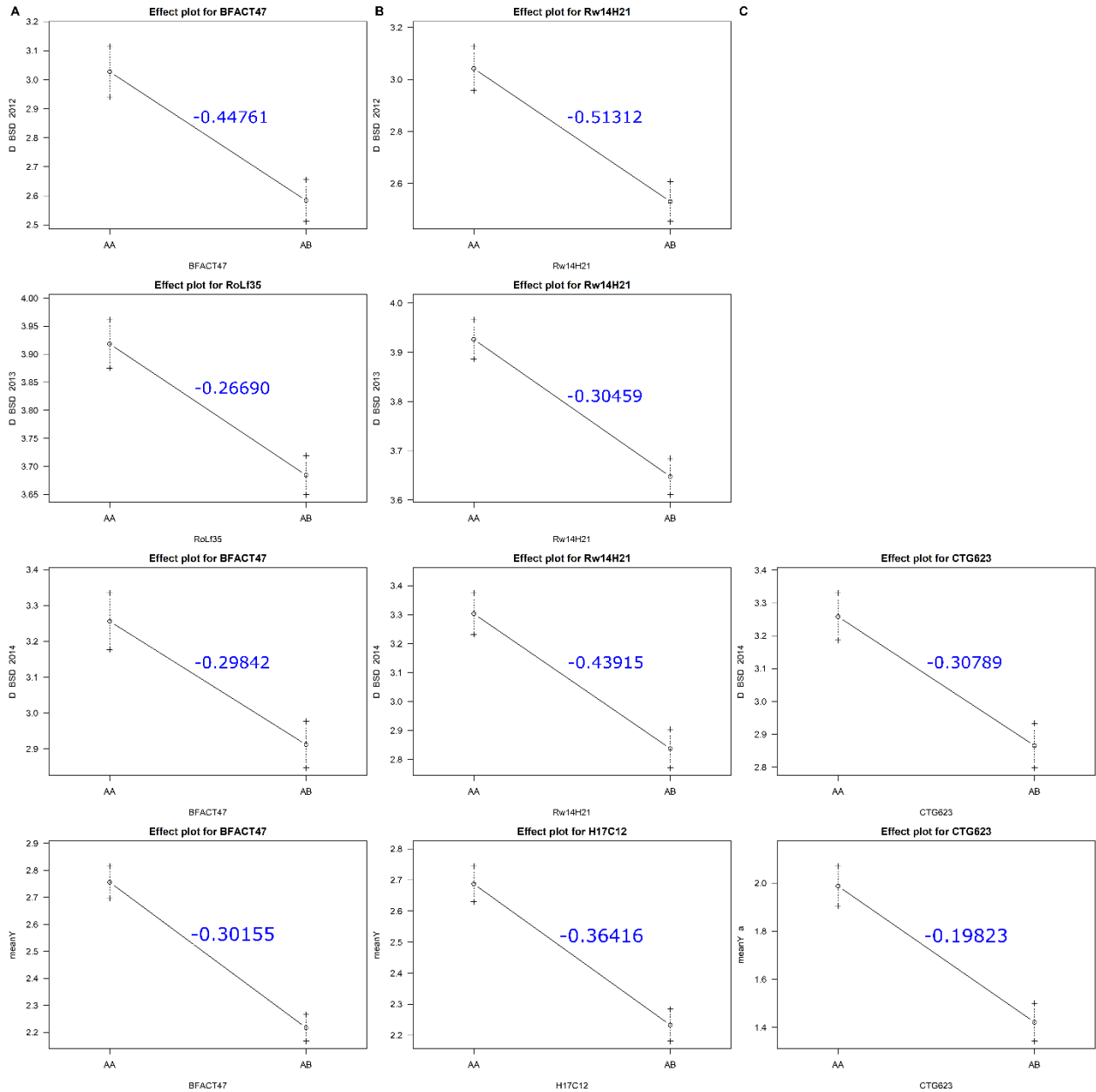
Supplementary figure 22: Effect of putative QTLs detected on linkage groups 3, 5 and 6 of the male map for HW population localized in Angers.

The average BSD score for each scoring year was plotted against the genotype at the marker peak of each QTL using the *effectplot* function of R/qtl package. The effects of the QTLs detected on B3 are plotted on column (A), B5 on column (B) and B6 on column (C). Each row represents a scoring year from 2012 to 2014, 2018 as well as the mean at the last row. A blank was left when no QTLs were detected on one of the three linkage groups at a specific year. AA and AB represent the alleles of the closest marker to the QTL peak. That marker is mentioned on the top of each plot as well as the names of x-axes.



Supplementary figure 23: Effect of putative QTLs detected on linkage groups 3, 5 and 6 of the male map for HW population localized in Bellegarde.

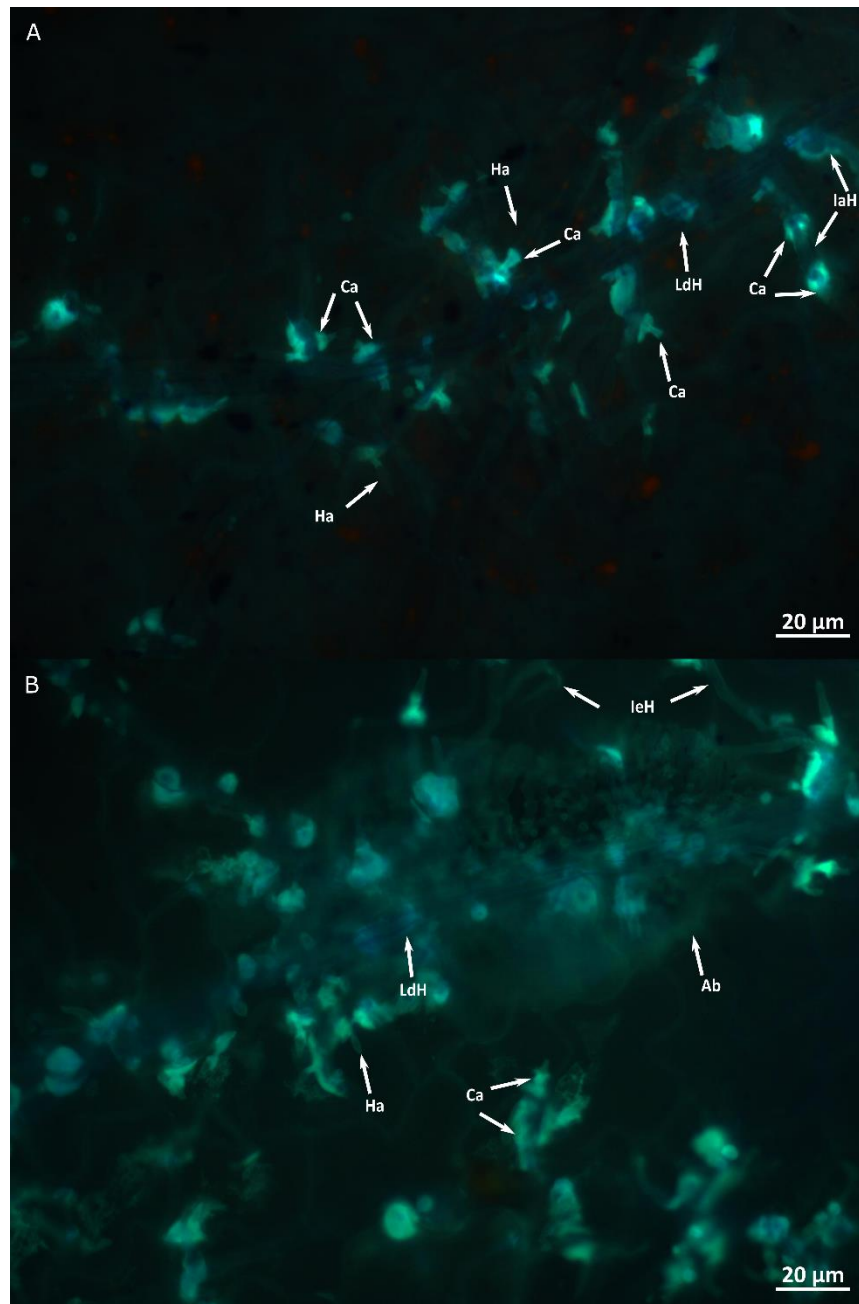
The average BSD score for each scoring year was plotted against the genotype at the marker peak of each QTL using the effectplot function of R/qtl package. The effects of the QTLs detected on B3 are plotted on column (A), B5 on column (B) and B6 on column (C). Each row represents a scoring year from 2012 to 2014 as well as the mean at the last row. A blank was left when no QTLs were detected on one of the three linkage groups at a specific year. AA and AB represent the alleles of the closest marker to the QTL peak. That marker is mentioned on the top of each plot as well as the names of x-axes.



Supplementary figure 24: Effect of putative QTLs detected on linkage groups 3, 5 and 6 of the male map for HW population localized in Diémoz. The average BSD score for each scoring year was plotted against the genotype at the marker peak of each QTL using the *effectplot* function of R/qtl package

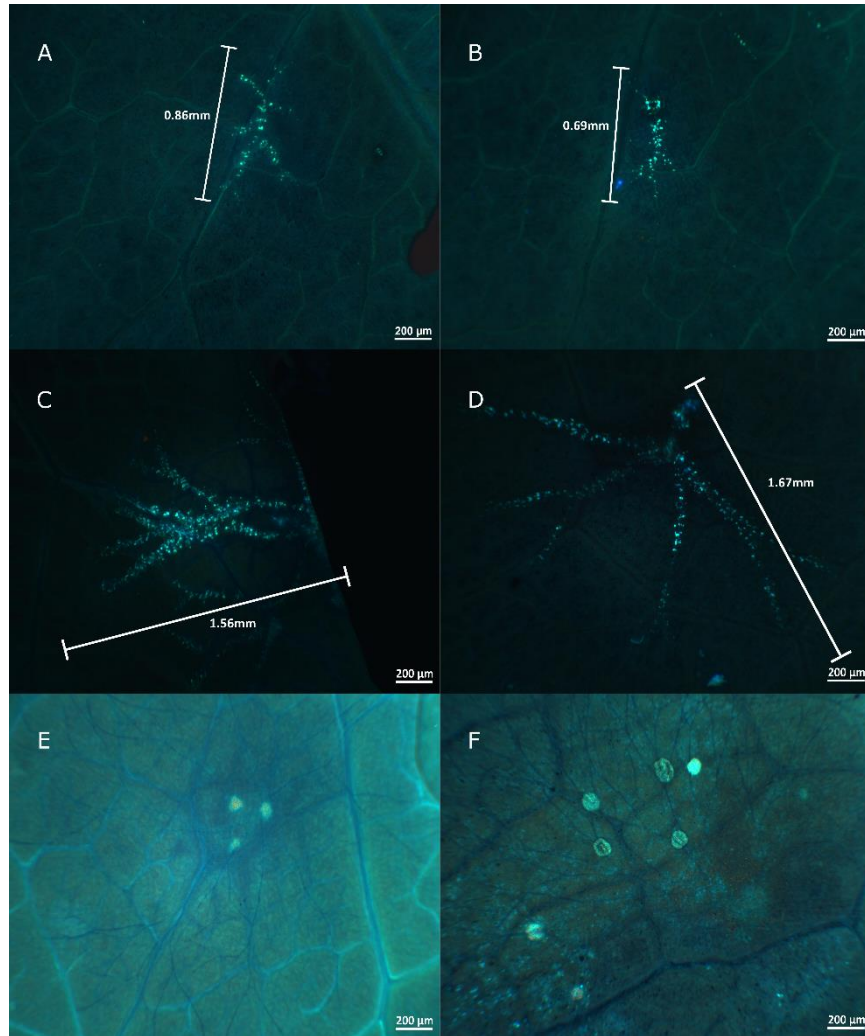
The effects of the QTLs detected on B3 are plotted on column (A), B5 on column (B) and B6 on column (C). Each row represents a scoring year from 2012 to 2014 as well as the mean at the last row. A blank was left when no QTLs were detected on one of the three linkage groups at a specific year. AA and AB represent the alleles of the closest marker to the QTL peak. That marker is mentioned on the top of each plot as well as

Appendix C : Supplementary figures of chapter 3



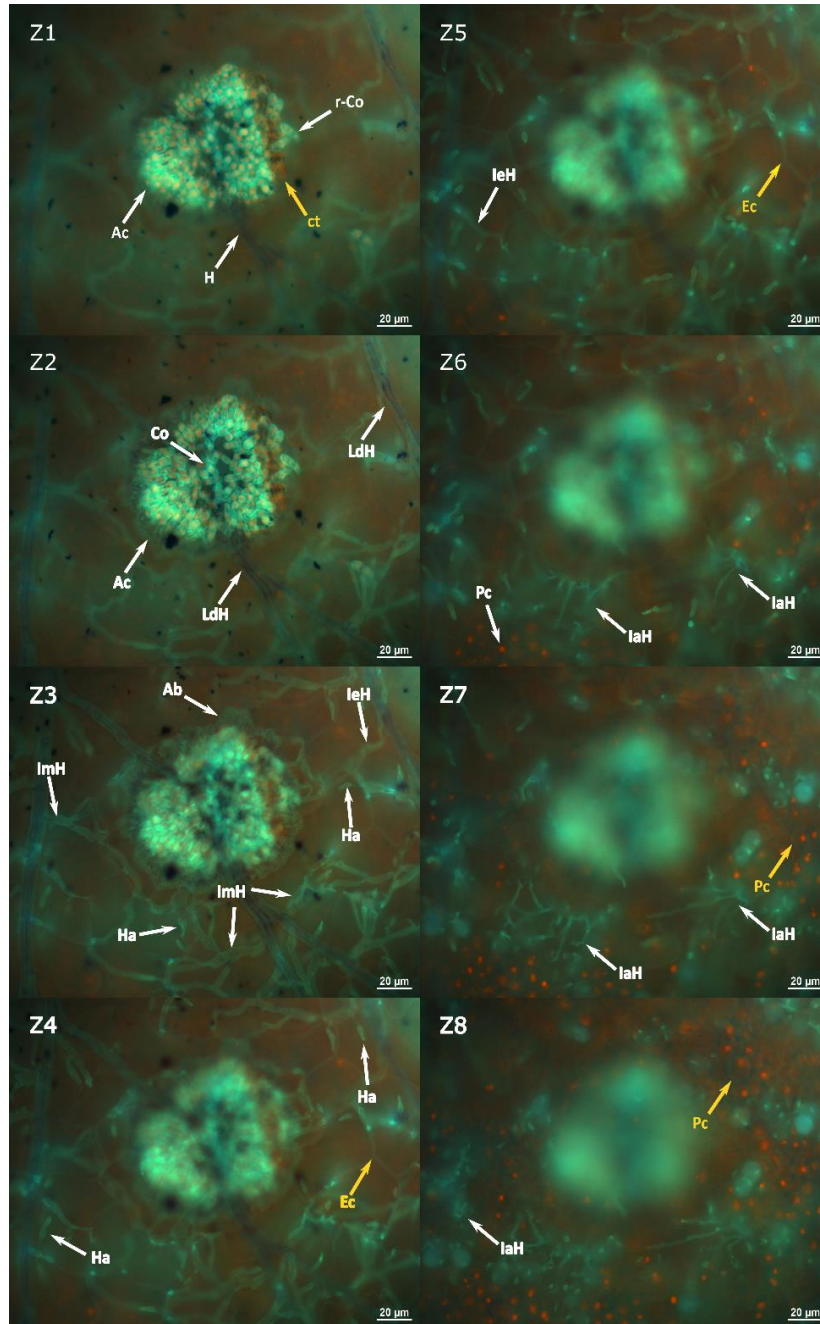
Supplementary figure 25: Callose deposition after *D. rosae* invasion in 'Old Blush' (OB) leaf tissue at 9dpi

A: Callose deposition on haustorial neck [Ca], long distance hyphae [LdH], haustoria [Ha], presence of intracellular hyphae [IaH] growing inside epidermal cells and callose deposition surrounding them; **B:** Acervuli in formation with acervulus base stroma development [Ab] on long distance hyphae (subcuticular hyphae, [LdH]) from which haustoria [Ha] grow to invade the cells. Callose deposition [Ca] on long distance hyphae and presence of intercellular hyphae [IeH] (hyphae that grow between the cells to colonize lower levels of the leaf mesophyll. It is often difficult to get a clear picture of them as they grow vertically through the Z-axis while subcuticular hyphae grow horizontally).



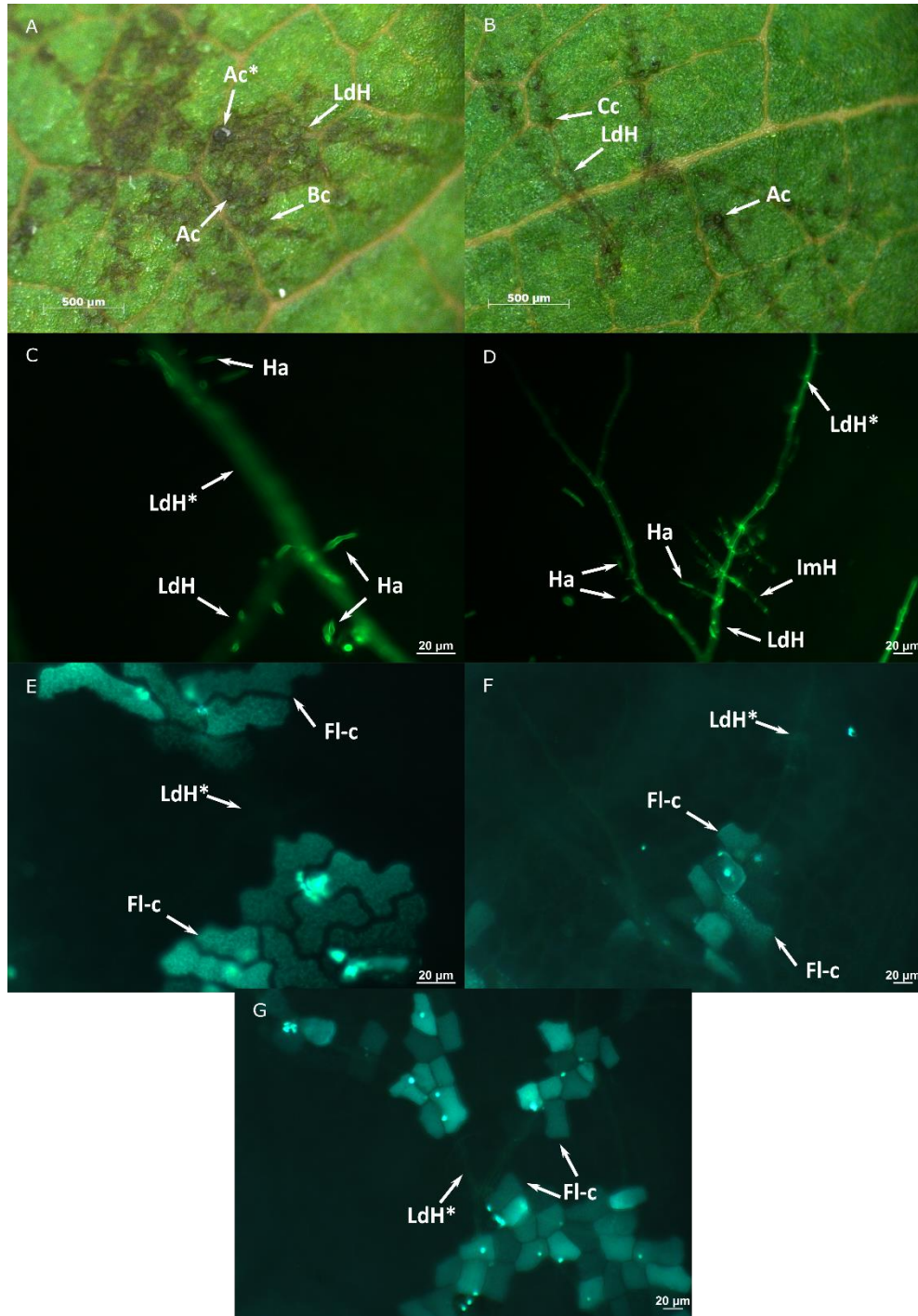
Supplementary figure 26: Evolution of *D. rosae* hyphal network during the infection of the susceptible host 'Old Blush' and extent of the reacting area in host tissues upon infection by *D. rosae*

A-B: Reacting area at an infection site at 7dpi, the bright blue shows the presence of intense callose deposition and a star-like structure of the hyphal colonization can be observed, the extent of the hyphal network is much more important than the reacting area but the extremities of long distance hyphae are difficult to observe at this magnification due to the brightness of the callose deposition near the penetration point; **C-D:** Reacting area at an infection site at 9dpi, the area is more extensive and more branches can be observed; **E:** Three acervuli under development and hyphal network at 9dpi, with a brighter field to see the extent of the subcuticular hyphal colonization; **F:** Mature acervuli and extensive hyphal colonization and ramification in host leaf tissue.



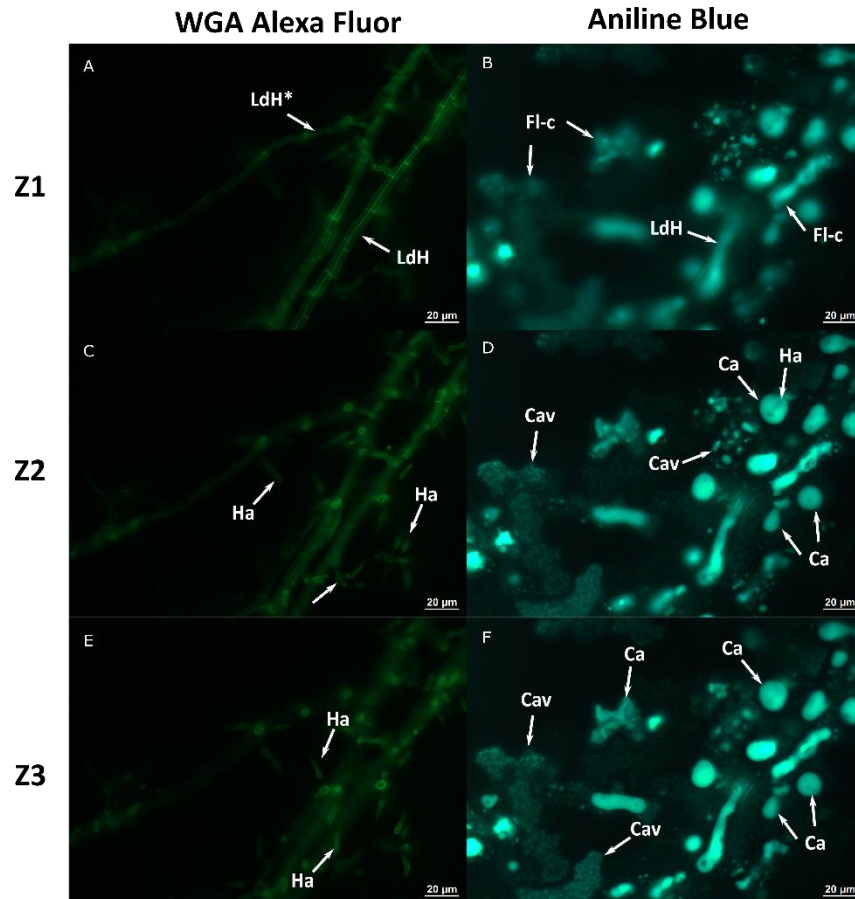
Supplementary figure 27: Fluorescence microscopy Z-stack of an acervulus in an old infection site at 15dpi on 'Old Blush' (OB) leaves

Manual Z-stack of an acervulus to assess the depth of fungal infection at 15dpi on a susceptible genotype. **Z1** corresponds to the view of a mature acervuli [Ac] on top of a long distance hyphae [LdH] from outside the cuticle [Ct] where newly released conidia [r-Co] can be found and **Z2 to Z8** correspond to the different levels inside the leaf on the Z-axis that can be seen thanks to the discoloration of the leaf tissue. **Z2** corresponds to the view just underneath the cuticle and **Z8** the view just before the palisade parenchyma. **Z2**: Just under the cuticle, subcuticular hyphae [LdH] can be seen as well as the well-developed acervulus base stroma [Ac] and the inside of the acervulus with the new conidia [Co] can be seen through the ripped cuticle; **Z3**: View of the top layer of the epidermal cell wall where intramural hyphae [ImH] grow inside the epidermal cell wall to invade epidermal cells with haustoria [Ha]. Some intercellular hyphae [IeH] can be observed as well as the acervuli base [Ab]; **Z4**: Layer just below the top epidermal cell wall where we can see epidermal cell delimitation (adjacent cell walls, [Ec]) and haustoria [Ha] inside the epidermal cells can be well distinguished; **Z5**: View from the inside of the epidermal cells [Ec] with intercellular hyphae [IeH] that can be seen but that grow down in deeper layers to colonize the leaf tissue; **Z6-Z7**: View deeper inside the epidermal cells where intracellular hyphae [IaH] can be seen and at **Z7**, the palisade cells [Pc] start to be visible; **Z8**: View from the palisade cells layer where further fungal growth of intracellular hyphae [IaH] can be described inside the palisade cells [Pc].



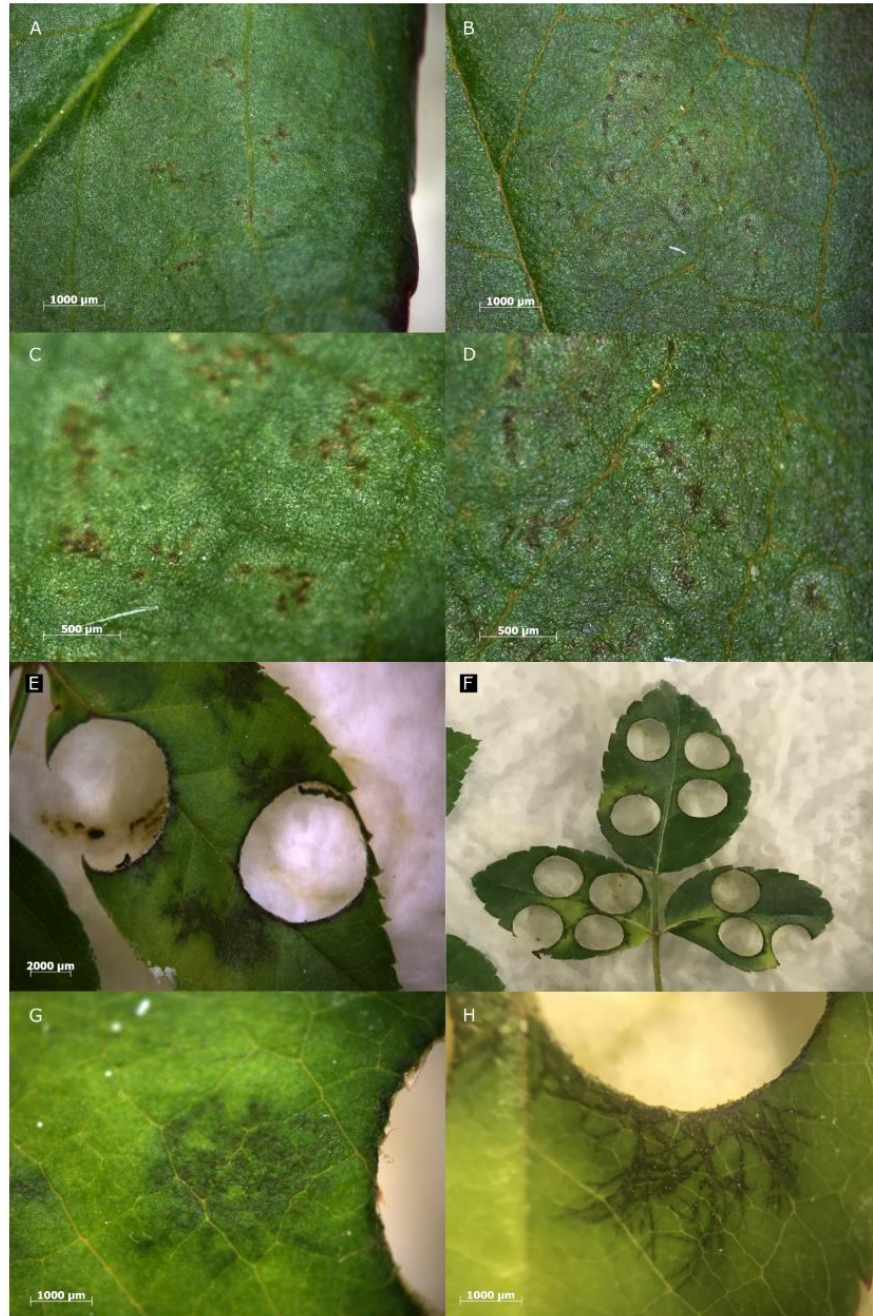
Supplementary figure 28: Epidermal cells fluorescing when invaded by haustorial structures of DiFRA67

A-B: Close up of PC and OB symptoms revealing subcuticular hyphae [LdH] and cells around them browning [Bc] and collapsing [Cc]. Mature [Ac*] and non-mature acervuli [Ac] can be observed on PC leaves at 9dpi and only non-mature acervuli could be observed on OB leaves at 9dpi; **C-E and D-F-G:** Fluorescence microscopy of the same region with GFP filter (C-D) and DAPI filter (E-F-G) to visualize both fungal structures (long distance hyphae [LdH], intramural hyphae [ImH], and haustoria [Ha]) and callose depositions, respectively. Fluorescing epidermal cells [Fl-c] co-localize with their invasion by haustoria [Ha], and the epidermal cells do not react to long distance hyphae alone (subcuticular hyphae [LdH*]). **C-F:** Example on PC leaves. **E-F-G:** Example on OB leaves.



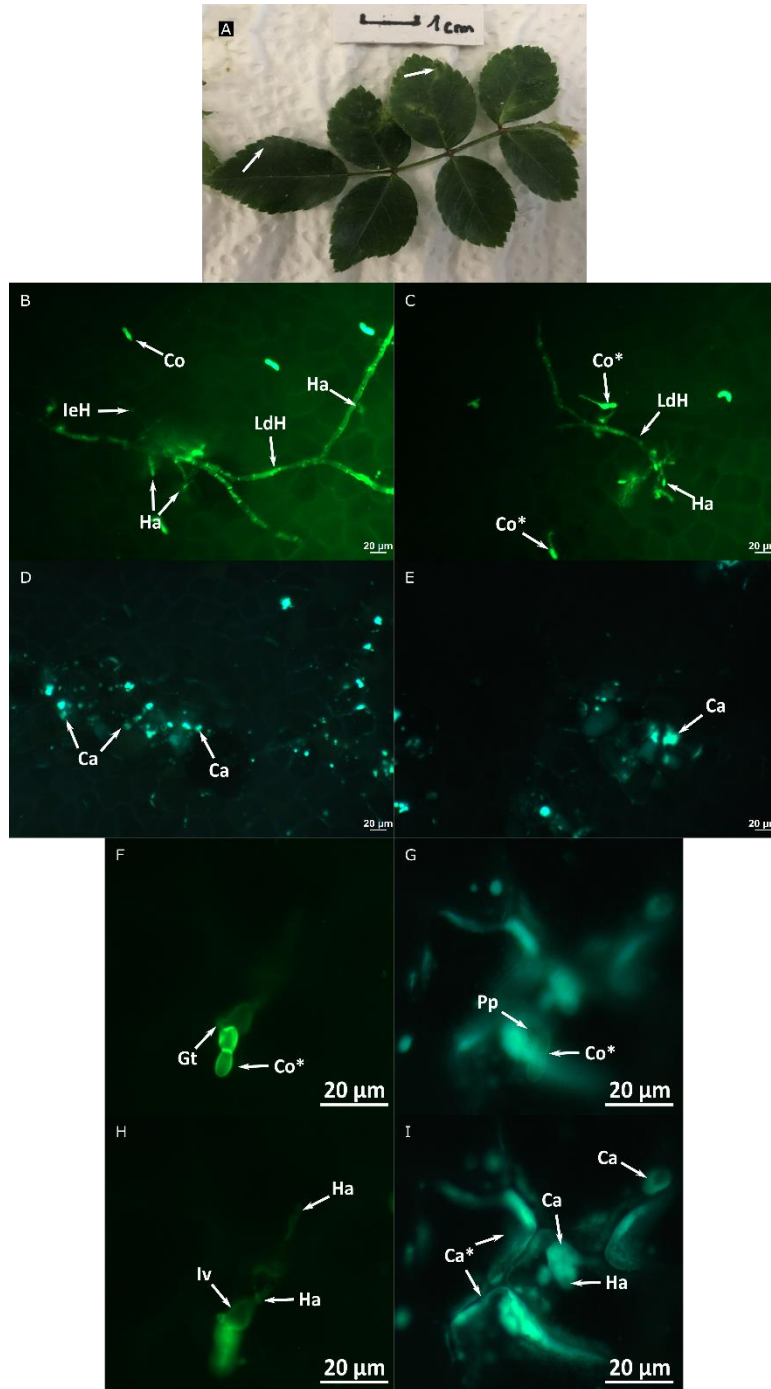
Supplementary figure 29: Z-stack of an infection site on PC leaves inoculated with DiFRA67 using a double staining of WGA-Alexa Fluor™ 488 and Aniline blue

A-C-E: Fungal structures stained with WGA-Alexa Fluor™ 488 and visualized using a GFP filter at different levels in the leaf surface. Z1: Long distance hyphae [LdH] from which short distance hyphae like intramural and intercellular hyphae grow to start the invasion of the epidermal cells. Near these long distance hyphae, haustoria [Ha] can be seen invading the epidermal cells (Z2-Z3). Some long distance hyphae do not exhibit any haustoria [LdH*]; **B-D-F:** Long distance hyphae can be observed on B and haustoria [Ha] on C. Callose depositions [Ca] and fluorescing epidermal cells [Fl-c] observed at the same levels than the fungal structures described previously. Some epidermal cells neighboring invaded cells exhibit granular texture with small callose vesicles [Cav] and other exhibit a clear deposition [Ca] around fungal structures. Some cells also exhibit bigger patches of callose that are not found continuous around a fungal structure like on Z2.



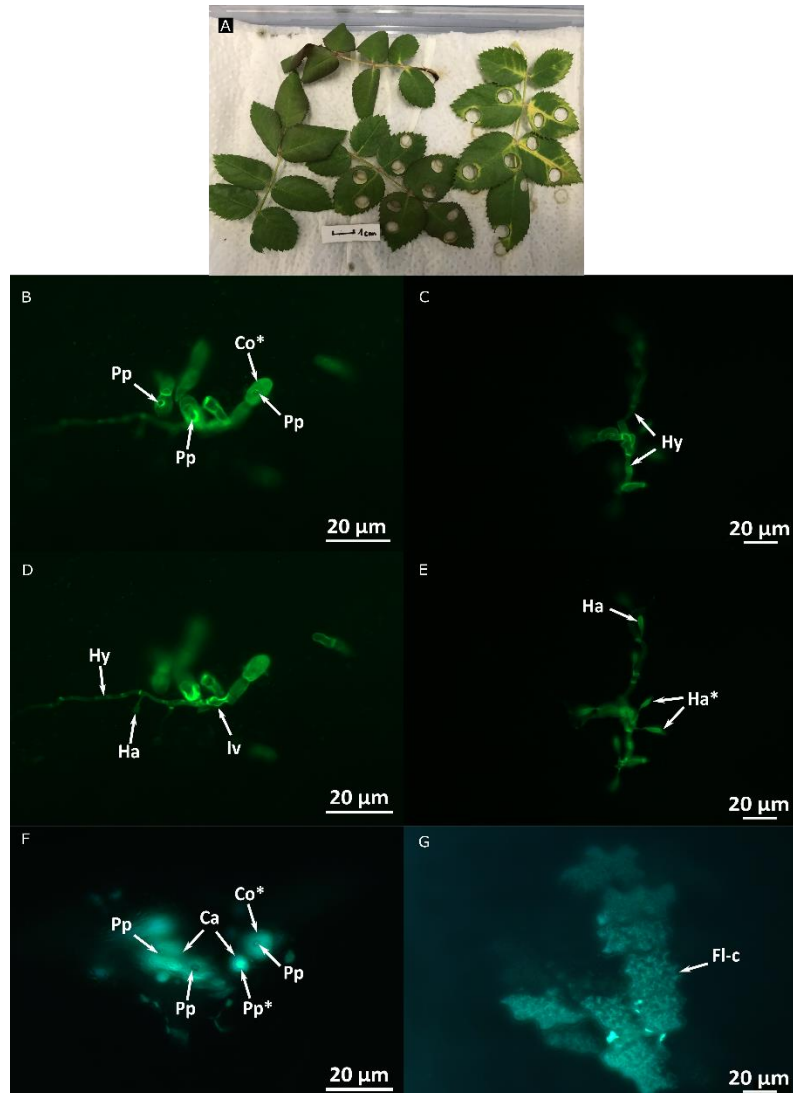
Supplementary figure 30: Hybrid of *Rosa wichurana* (RW) leaves infected with the strain DiFRA67 at 9dpi and 23dpi and effect of sampling on the resistance to *D. rosae*

A-B: Infection site on RW leaf showing the discoloration around the brown spots (HR-like spots) using the magnification 2x at 9dpi; **C-D:** A close up of the infection sites (5x) where the spots and the discoloration can be seen; **E-F-G-H:** A young leaf (E) and an old leaf (F) from which the discs were sampled at 9dpi developed black spots whereas the ones left untouched only exhibited HR-like spots like A-B-C-D; **G:** The sampled leaf exhibiting black spots at 0.65x; **H:** A leaf with early chlorosis at 0.65x (top middle leaf in E-F); **G-H:** Close up of black spot symptoms on RW punctured leaf (sampled leaf) for young (G) and old leaves (H) at 23dpi.



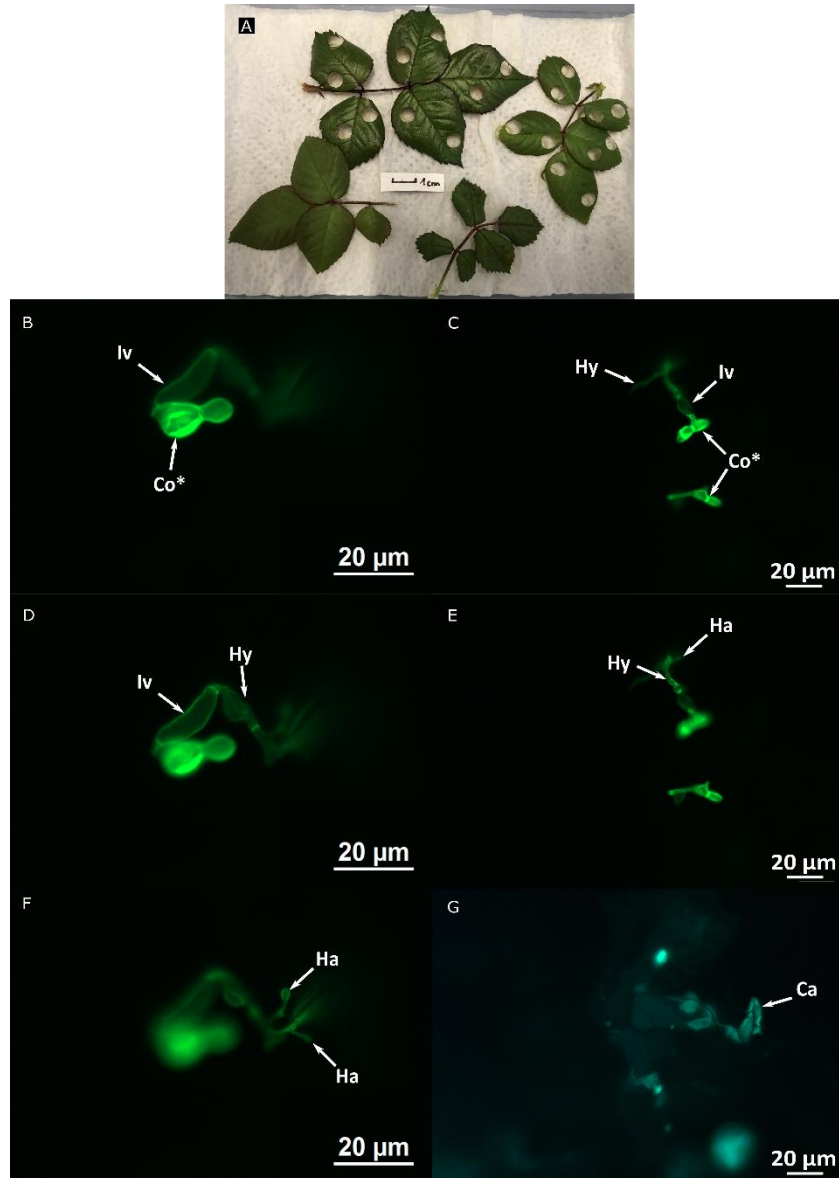
Supplementary figure 31: Hybrid of *Rosa wichurana* (RW) young leaves inoculated with *D. rosae* at 23dpi

A: Example of young leaf of RW inoculated with DiFRA67 at 23dpi. The arrows show infection sites that developed some symptoms. The other infection sites only exhibit small HR-like spots; **B-C-F-H:** Examples of fungal structures found in RW leaves at 23dpi with an extended fungal network (B-C) and a small hyphal network (F-H), both with long distance hyphae [LdH] branching, a few haustoria [Ha] and intercellular hyphae [IeH]. Some conidia germinated [Co*] but did not penetrate the leaf cuticle. Clear callose deposition (D-E) was observed but no fluorescing cells were observed at this late stage of infection; **F-G-H-I:** An example of fungal growth arrested very early in the infection at two levels on the z-axis that show in the first level (F-G) the conidia germinating [Co*] and penetrating the cuticle via a short germ tube [Gt], and a penetration pore can be observed on G with the aniline blue staining. At this time point, the cells did not appear completely fluorescent with a granular texture like at 9dpi but the callose depositions were smooth and localized. Indeed, in the second level, an infection vesicle [Iv] with two haustoria can be observed on H and callose depositions on the cells walls [Ca*] near the entry point as well as around the haustorial structures [Ca] can be seen.



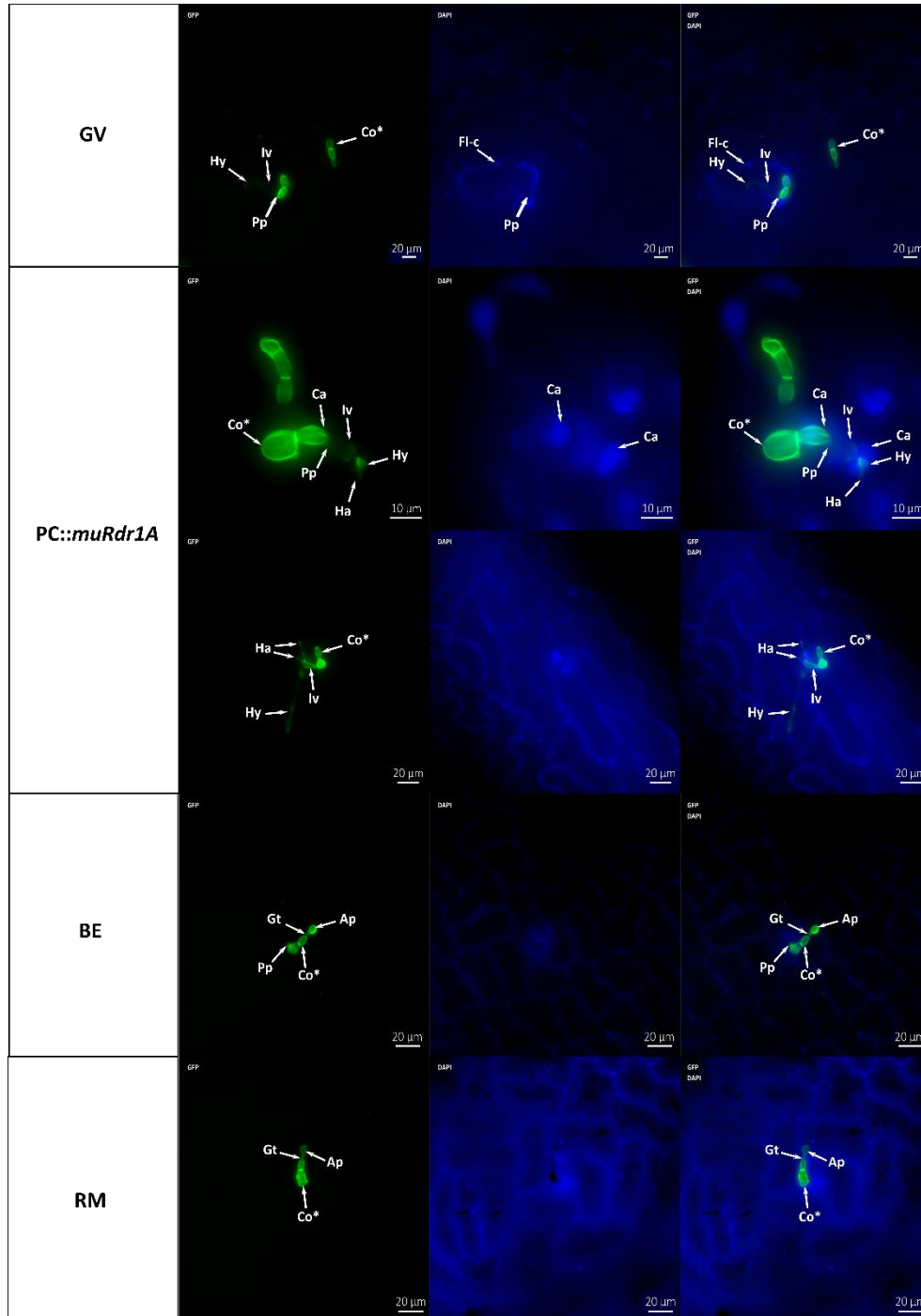
Supplementary figure 32: 'George Vancouver' (GV) leaves inoculated with *D. rosae* at 23dpi

A: Photograph of one of the boxes with GV leaves at 23dpi; **B-D-F:** Three attempts of penetration by a germinated conidia [Co*] arrested by a strong callose deposition [Ca] around the penetration pore [Pp] and on successful penetration with development of an infection vesicle [Iv], hyphae [Hy] and small haustoria [Ha] under the cuticle. Callose deposition was also observed around the successful penetration site [Pp*]; **C-E-G:** Successful penetration site with development of hyphae [Hy] and bigger haustoria [Ha]. Some haustoria exhibited a fine end [Ha*]. The epidermal cells invaded by haustoria appeared fluorescent [Fl-c].



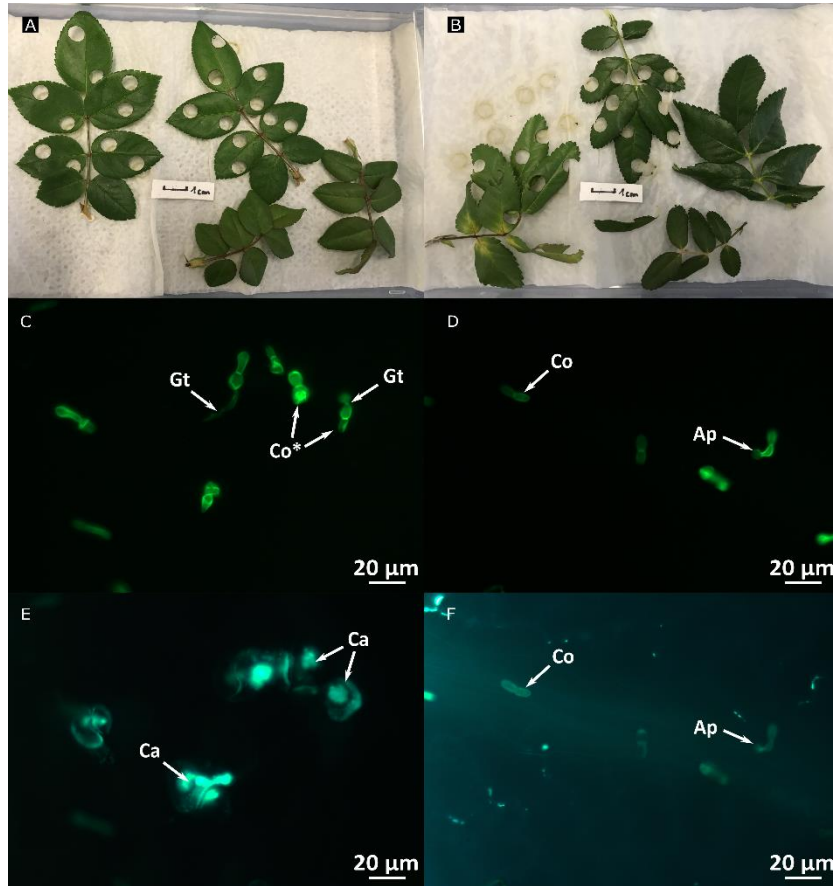
Supplementary figure 33: *PC::muRdr1A* leaves inoculated with *D. rosae* at 23dpi

A: Photograph of one of the boxes with *PC::muRdr1A* leaves at 23dpi; **B-D-F and C-E:** Conidia [Co*] that had penetrated the *PC::muRdr1A* cuticle producing an infection vesicle [Iv] and a short hypha [Hy] that enlarged before penetrating the epidermal underneath the conidia to produce haustoria [Ha] of small size inside the epidermal cells; **G:** Callose deposition [Ca] on the cell wall of the invaded epidermal cell.



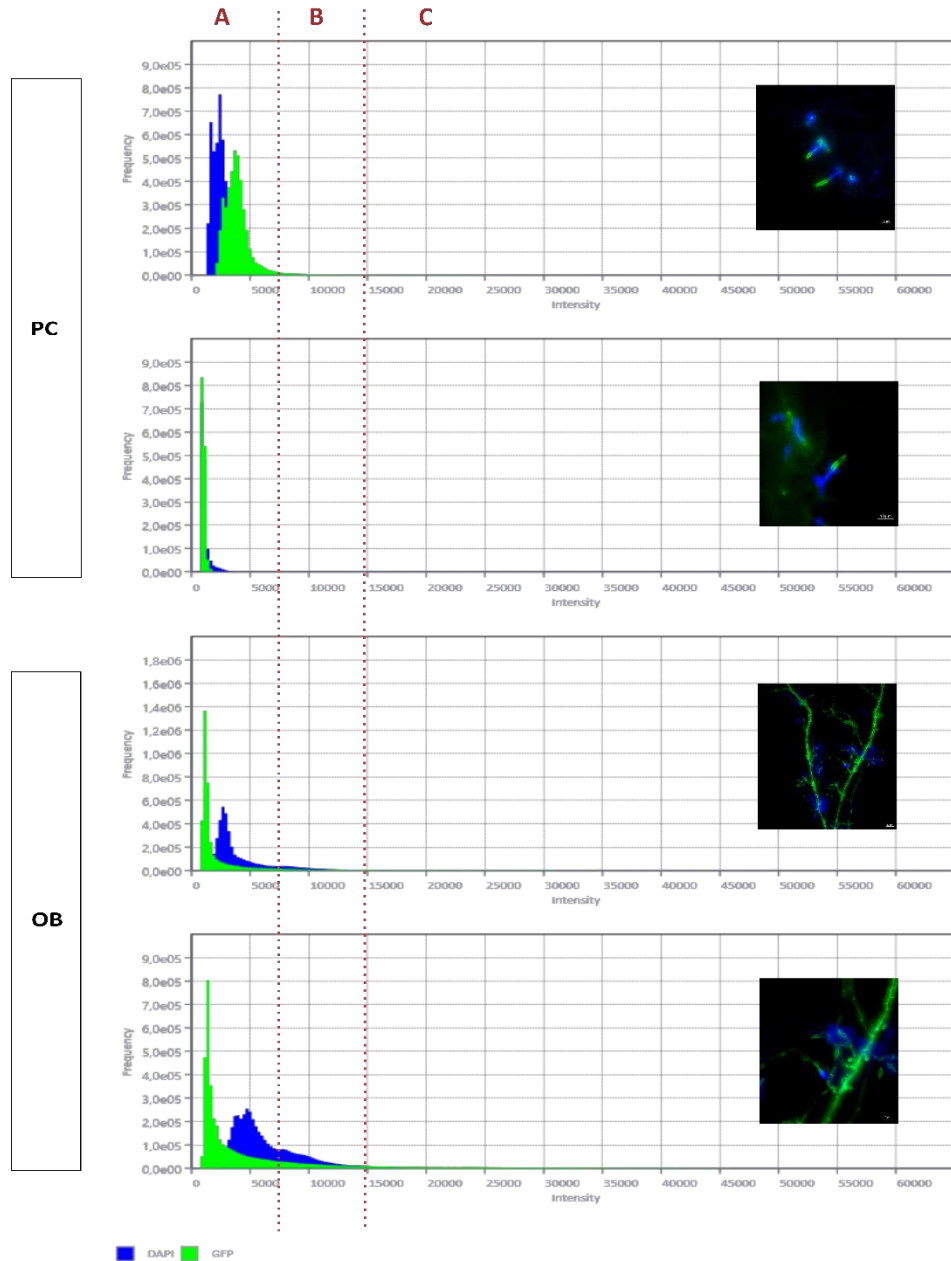
Supplementary figure 34: Callose deposition in incompatible interactions between rose and *D. rosae* at 9dpi

Fluorescence microscopy of GV, PC::muRdr1A, BE and RM leaves inoculated with DiFRA67 at 9dpi using a double stained with WGA Alexa Fluor™ 488 that binds to fungal cell wall and aniline blue to visualize callose deposition. Two filters were used: GFP filter to visualize WGA Alexa Fluor™ 488 and DAPI-Axio filter to visualize the aniline blue. Pictures from these separated channels (filters) were merged to localize the callose deposition. Conidia germinated [Co*] and penetrating the host cuticle of GV and PC::muRdr1A. Infection vesicles [Iv] as well as short hyphae [Hy] were observed with a few haustoria-like structures of small size [Ha]. Weak fluorescence was emitted from the samples stained with aniline blue and was found on the cell wall to GV and around the penetration pore [Pp] and the hyphae in PC::muRdr1A leaves. In the cases of PC::muRdr1A as well as BE and RM, no clear callose deposition was observed with the short emission band filter DAPI-Axio. For BE and RM, appressoria [Ap] were observed in some cases from germinated conidia with a defined germ tube [Gt]. None of the conidia found on BE and RM penetrated the host cuticle.



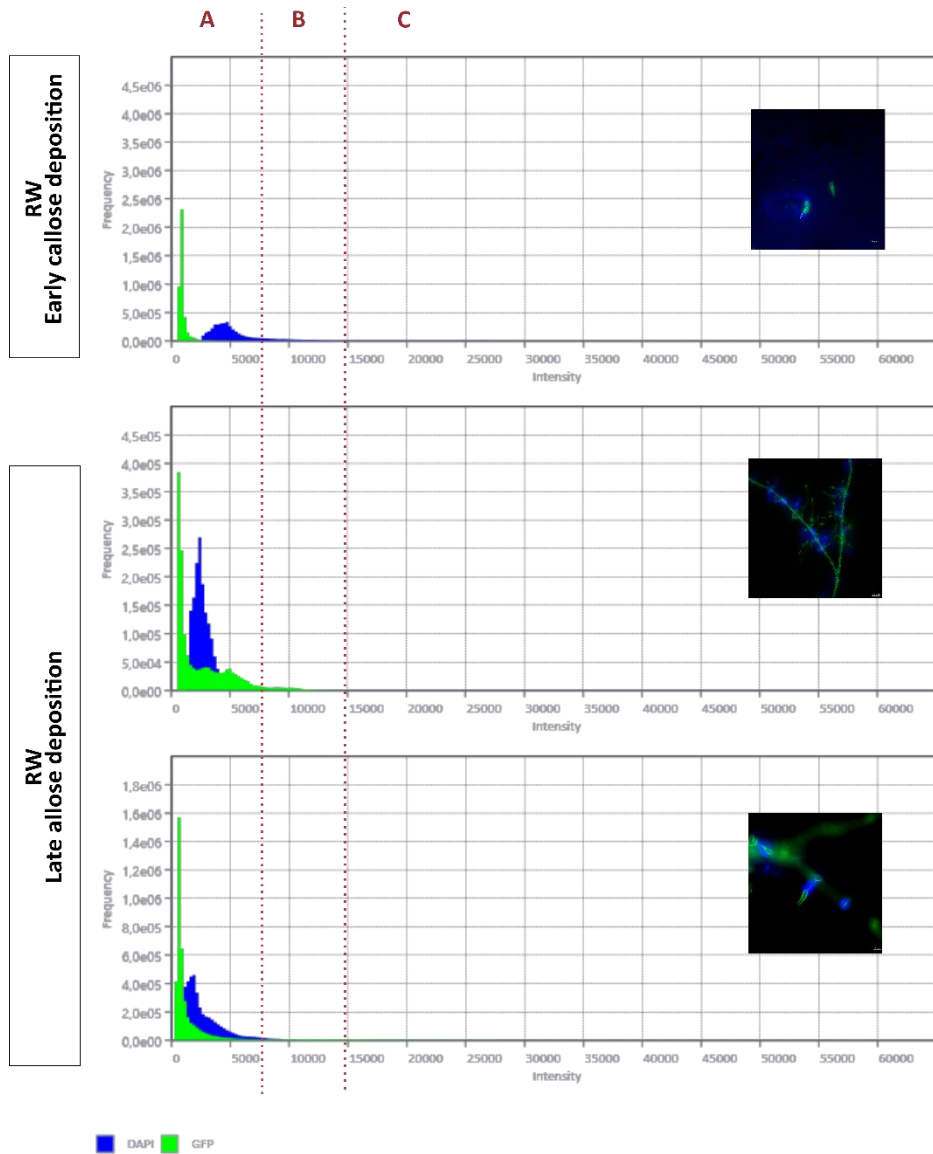
Supplementary figure 35: 'Brite Eyes™' (BE, right) and *Rosa majalis* (RM, left) leaves inoculated with *D. rosae* at 23dpi

A-B: Photographs of one of the boxes with BE (A) and RM (B) leaves at 23dpi; **C-E:** Germinated conidia [Co*] with germ tubes [Gt] that tried to penetrate BE cuticle but a strong callose deposition [Ca] was observed at the site of penetration; **D-F:** Non-germinated conidia [Co] and germinated conidia could be observed on RM leaves. No sign of cell response with callose deposition was observed upon infection. Some conidia grew appressoria-like structures [Ap] that appear round and lighter stained.



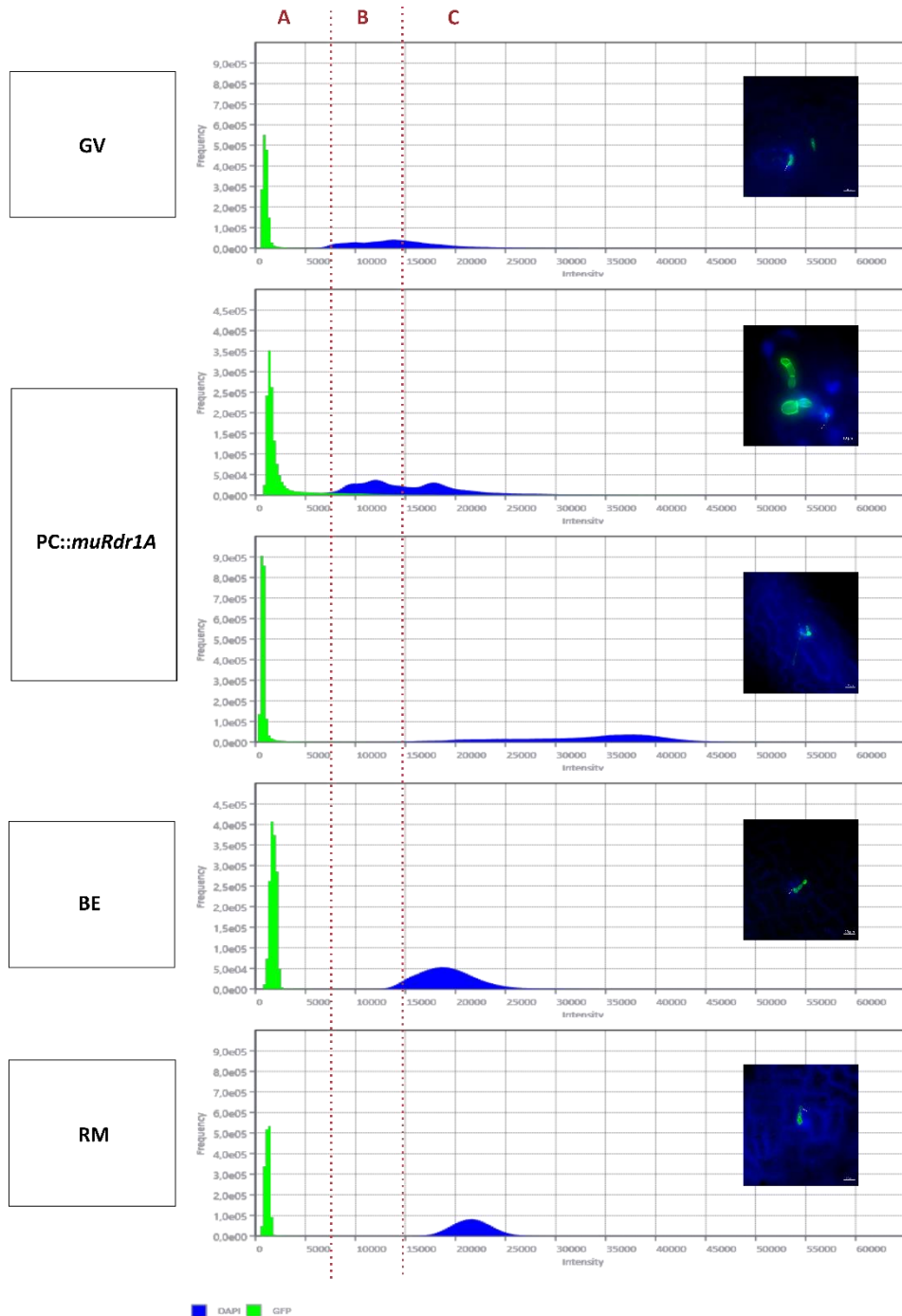
Supplementary figure 36: Fluorescence intensity used to observe the signals on ‘Pariser Charme’ (PC) and ‘Old Blush’ (OB) leaves challenged with DiFRAG.

These pictures were acquired with the Axio Imager microscope with multichannel images using both filters GFP-Axio and DAP-Axio. The graphs show the intensity of the lamp used to visualize the signal on the x-axis and the frequency of photons received in the range of intensity applied for the whole picture. The picture for which the graph reports the frequency of photons observed for the intensity applied was added on the left. Zone A corresponds to low intensity applied to observe the signals (less than 10% of the lamp intensity), which means that the signals are strong. Zone B corresponds to intermediate intensity applied to observe the signals (between 10 and 30% of the lamp intensity), which indicates the presence of signals with moderate intensity. Zone C corresponds to very high intensity applied to observe the signals (more than 50% of the lamp intensity), which indicates low to no signal observed.



Supplementary figure 37: Fluorescence intensity used to observe the signals on the hybrid of *Rosa wichurana* (RW) leaves challenged with DiFRA67

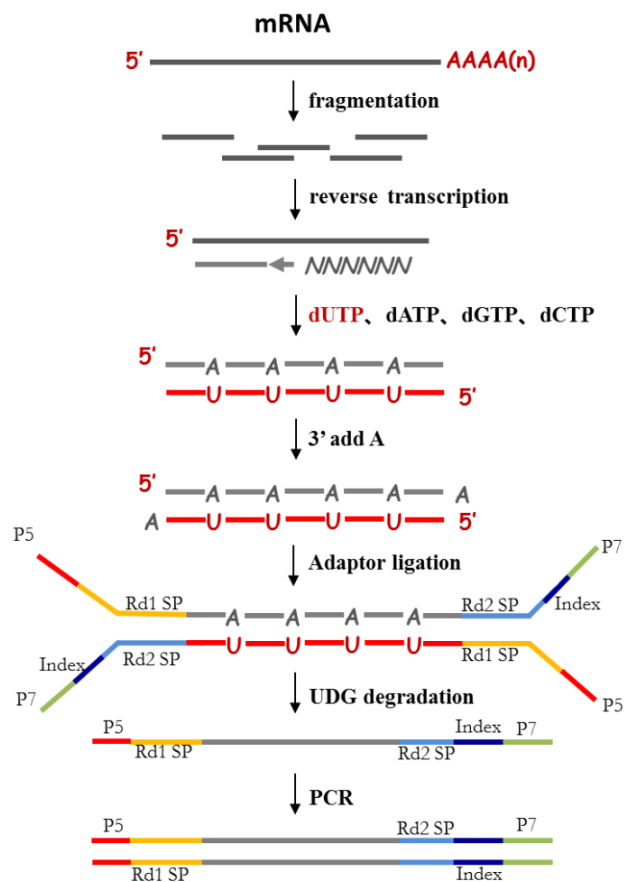
These pictures were acquired with the Axio Imager microscope with multichannel images using both filters GFP-Axio and DAP-Axio. The graphs show the intensity of the lamp used to visualize the signal on the x-axis and the frequency of photons received in the range of intensity applied for the whole picture. The picture for which the graph reports the frequency of photons observed for the intensity applied was added on the left. Zone A corresponds to low intensity applied to observe the signals (less than 10% of the lamp intensity), which means that the signals are strong. Zone B corresponds to intermediate intensity applied to observe the signals (between 10 and 30% of the lamp intensity), which indicates the presence of signals with moderate intensity. Zone C corresponds to very high intensity applied to observe the signals (more than 50% of the lamp intensity), which indicates low to no signal observed.



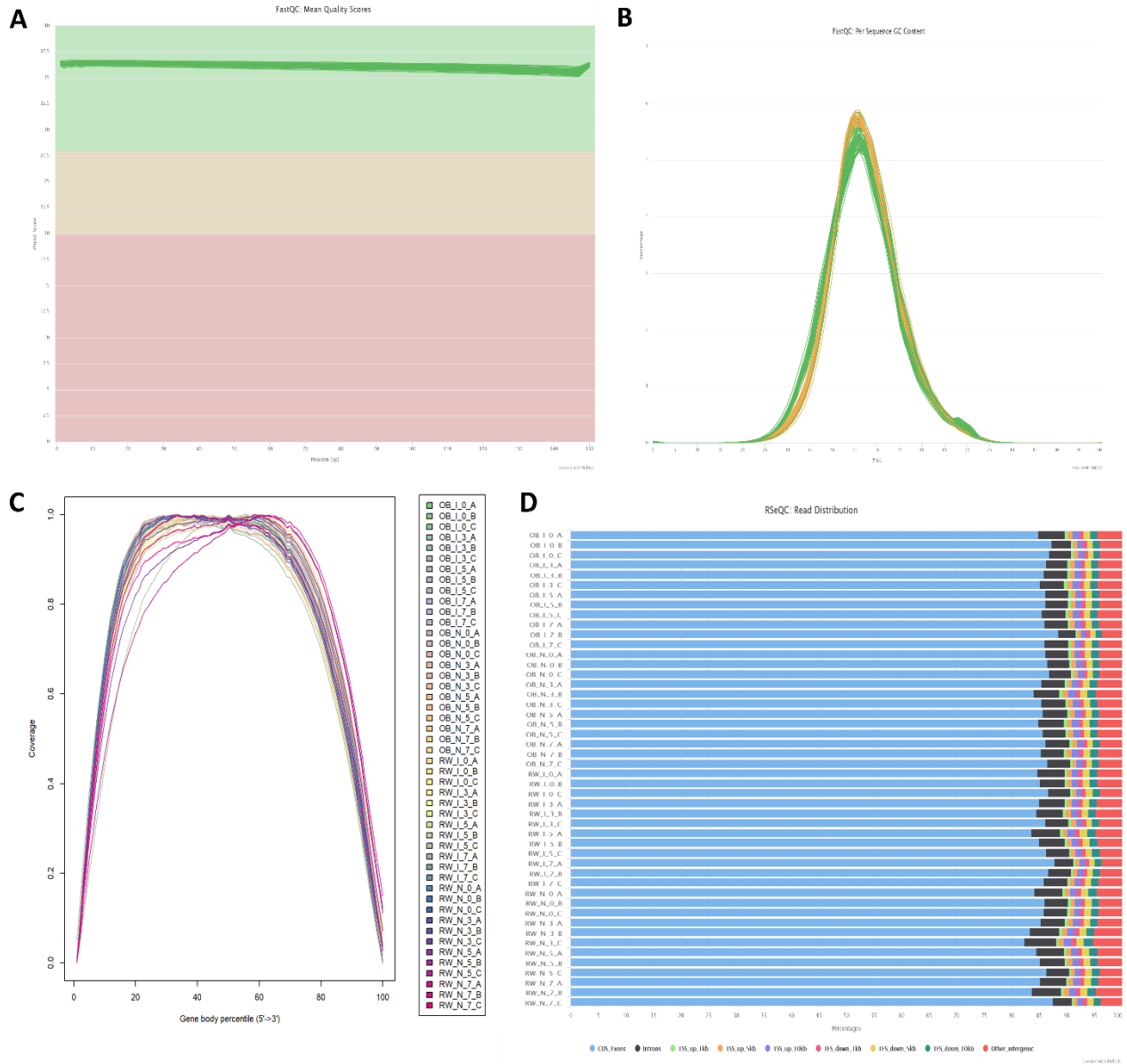
Supplementary figure 38: Fluorescence intensity used to observe the signals on ‘Georges Vancouver’ (GV), *PC::muRdr1A*, Brite Eyes™ (BE) and *Rosa majalis* (RM) leaves challenged with DiFRA67

These pictures were acquired with the Axio Imager microscope with multichannel images using both filters GFP-Axio and DAP-Axio. The graphs show the intensity of the lamp used to visualize the signal on the x-axis and the frequency of photons received in the range of intensity applied for the whole picture. The picture for which the graph reports the frequency of photons observed for the intensity applied was added on the left. Zone A corresponds to low intensity applied to observe the signals (less than 10% of the lamp intensity), which means that the signals are strong. Zone B corresponds to intermediate intensity applied to observe the signals (between 10 and 30% of the lamp intensity), which indicates the presence of signals with moderate intensity. Zone C corresponds to very high intensity applied to observe the signals (more than 50% of the lamp intensity), which indicates low to no signal observed.

Appendix D : Supplementary figures of chapter 4

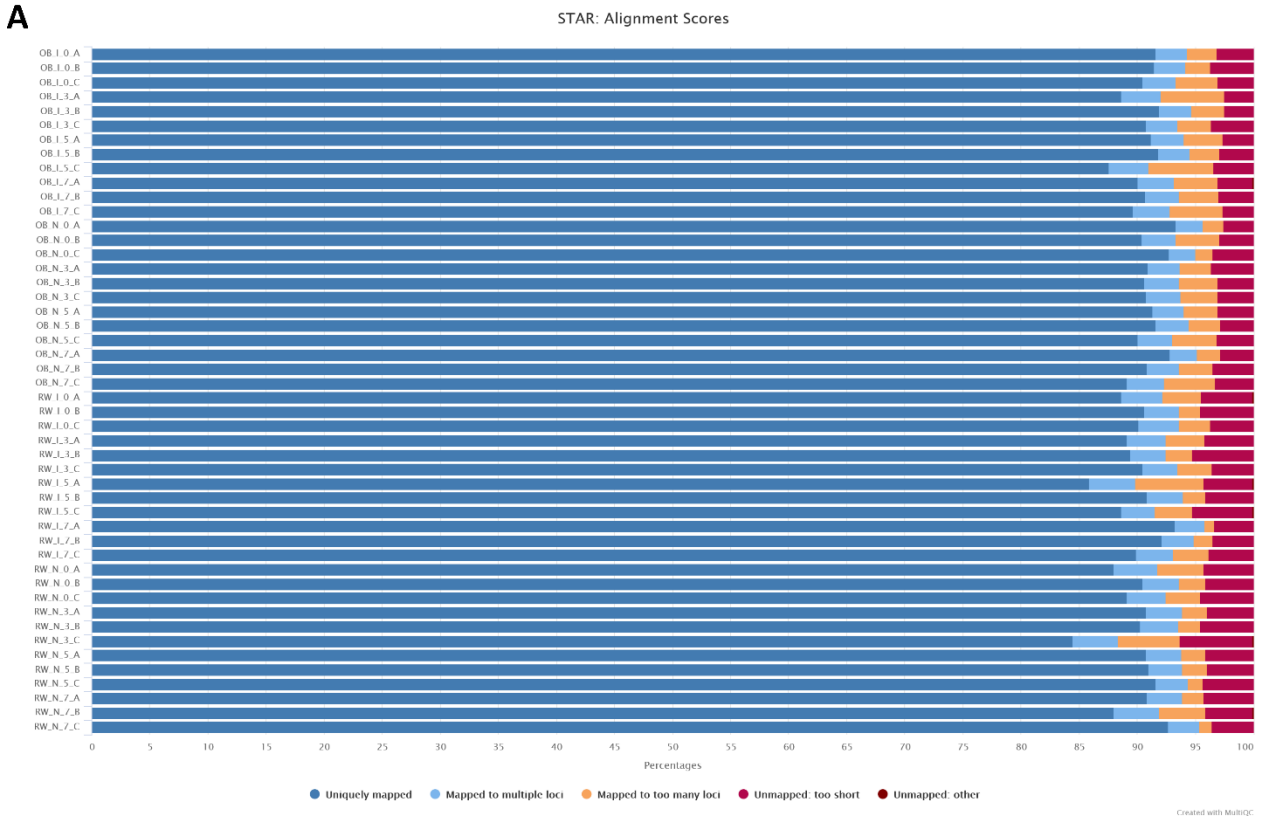


Supplementary figure 39: Library preparation by Novogene company using TruSeq™ RNA sample preparation kit from Illumina®



Supplementary figure 40: Alignment results and QC results after trimming and mapping

A: Mean quality score (Phred score, on y-axis) of each sample over the read length (on x-axis) with high quality scores in green (from 28 to 40), medium quality scores in yellow (from 20 to 28) and bad quality scores in red (from 0 to 20); **B:** GC content per sequence for all samples with the reads separated (forward in green and reverse in yellow); **C:** Gene body coverage after mapping for each sample; **D:** Read distribution over the genome features with CDS_exons in blue, introns in black, TSS_up_1kb in green, TSS_up_5kb in orange, TSS_up_10kb in purple, TES_dwn_1kb in pink, TES_down_5kb in yellow, TES_down_10kb in dark blue-green and other intergenics in red.

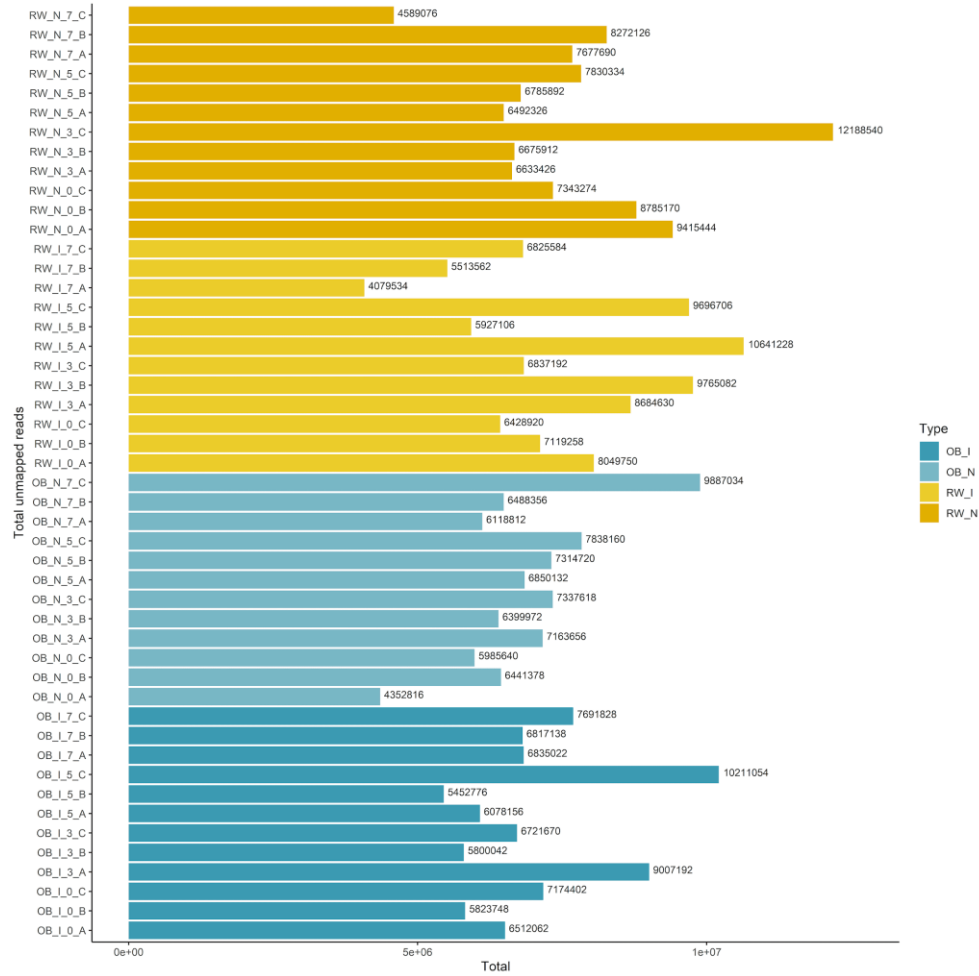


B

Feature	Genotype	count	Min	Max	Mean	sd
Overlapping genes	OB	24	80.4736450	86.378232	83.7328455	1.3786124
	RW	24	76.3157001	87.732779	83.0417465	2.4861309
No features	OB	24	4.5397385	8.054251	5.9834562	0.7686789
	RW	24	3.9425305	6.968588	5.5913837	0.8189304
Ambiguous features	OB	24	0.7297167	1.073477	0.8897166	0.1112831
	RW	24	0.7784330	1.408096	0.9748417	0.1829017
Multimapping	OB	24	2.0816434	3.657010	2.7340006	0.3709494
	RW	24	2.1570844	3.793558	3.0578788	0.4354600
Unmapped	OB	24	3.8028479	8.920686	6.0537178	1.1552238
	RW	24	3.5640102	10.647906	6.6342854	1.6405752

Supplementary figure 41: Summary of mapping results

A: Barplot of the mapping results for all samples separately with the percentage of uniquely mapped reads in dark blue, the percentage of reads mapping to multiple loci in light blue, the percentage of reads mapping to too many loci in orange, the percentage of loci that were unmapped because the seed was too short and the percentage of reads that were unmapped for other reasons; **B:** Table summarizing the percentage of reads assigned to genes, with ambiguous count, no count, mapping to multiple genes and unmapped reads.



Supplementary figure 42: Number of reads that did not map on rose genome (Hibrand et al. 2018) for all sequenced samples

Supplementary table 3: Information concerning the eight databases of SortMeRNA software

representative database	%id	# seq (clustered)	origin	# seq (original)
silva-bac-16s-id90	90	12798	SILVA SSU Ref NR v.119	464618
silva-arc-16s-id95	95	3193	SILVA SSU Ref NR v.119	18797
silva-euk-18s-id95	95	7348	SILVA SSU Ref NR v.119	51553
silva-bac-23s-id98	98	4488	SILVA LSU Ref v.119	43822
silva-arc-23s-id98	98	251	SILVA LSU Ref v.119	629
silva-euk-28s-id98	98	4935	SILVA LSU Ref v.119	13095
rfam-5s-id98	98	59513	RFAM	116760
rfam-5.8s-id98	98	13034	RFAM	225185

Source : [https://github.com/biocore/sortmerna/wiki/2.-User-manual-\(todo\)](https://github.com/biocore/sortmerna/wiki/2.-User-manual-(todo))

Supplementary table 4: Example of the most highly up-regulated genes according to their $-\log_{10}(\text{padj})$ and their mean \log_2 fold change at each time point for 'Old Blush' (OB) genotype

GeneID	log2FoldChange	padj	$-\log_{10}(\text{padj})$	GeneID	Description
UP_7dpi_OB					
RC3G0223600	2,914378446	1,78E-46	45,74839649	Q9FSG7	Thaumatococcus protein 1a (Mdt1) (Pathogenesis-related protein 5a) (PR-5a) (allergen Mal d 2); PR5
RC1G0372500	2,939031355	4,84E-30	29,31501088	P50694	Glucan endo-1,3-beta-glucosidase (EC 3.2.1.39) ((1->3)-beta-glucan endohydrolase) ((1->3)-beta-glucanase) (Allergen Pru a 2) (Beta-1,3-endoglucanase) (Thaumatococcus protein) (TLP) (allergen Pru av 2); PR2
RC4G0172700	3,065081866	4,17E-28	27,37960983	O24248	Major allergen Pru av 1 (Allergen Pru a 1) (allergen Pru av 1); PR10
RC5G0257300	2,987284367	1,77E-23	22,7521929	Q9LMU2	Kunitz trypsin inhibitor 5 (AtKT15) (Kunitz trypsin inhibitor 2) (AtKT12)
RC3G0105000	3,213158781	2,29E-23	22,64045768	P52408	Glucan endo-1,3-beta-glucosidase, basic isoform (EC 3.2.1.39) ((1->3)-beta-glucan endohydrolase) ((1->3)-beta-glucanase) (Beta-1,3-endoglucanase) (PpGns1); PR2
RC0G0198300	2,420929868	3,41E-21	20,46712476	A7PQW3	Glucan endo-1,3-beta-glucosidase (EC 3.2.1.39) ((1->3)-beta-glucan endohydrolase) ((1->3)-beta-glucanase) (Beta-1,3-endoglucanase); PR2
UP_5dpi_OB					
RC3G0104700	2,046831847	2,69E-25	24,56945074	P52408	Glucan endo-1,3-beta-glucosidase, basic isoform (EC 3.2.1.39) ((1->3)-beta-glucan endohydrolase) ((1->3)-beta-glucanase) (Beta-1,3-endoglucanase) (PpGns1); PR2
RC4G0475100	2,199694005	1,23E-14	13,90885635	O48676	UDP-glycosyltransferase 74B1 (N-hydroxythioamide S-beta-glucosyltransferase) (EC 2.4.1.195) (Thiohydroximate S-glucosyltransferase)

RC0G0225700	2,956306802	5,33E-13	12,27311539	Q3ZPN4	Methanol O-anthraniloyltransferase (EC 2.3.1.232) (Anthraniloyl-CoA:methanol acyltransferase) (Benzyl alcohol O-benzoyltransferase) (EC 2.3.1.196)
RC3G0104800	1,110090247	6,03E-12	11,21995242	P50694	Glucan endo-1,3-beta-glucosidase (EC 3.2.1.39) ((1->3)-beta-glucan endohydrolase) ((1->3)-beta-glucanase) (Allergen Pru a 2) (Beta-1,3-endoglucanase) (Thaumatococcus-like protein) (TLP) (allergen Pru av 2); PR2
UP_3dpi_OB					
RC4G0113600	2,395866229	1,42E-09	8,848549265	Q9SS87	Protein SIEVE ELEMENT OCCLUSION B (AtSEOb) (Protein SIEVE ELEMENT OCCLUSION-RELATED 1) (AtSEOR1)
RC1G0559900	2,441597053	1,42E-09	8,848549265	Q8H0Y8	Probable WRKY transcription factor 41 (WRKY DNA-binding protein 41)
RC4G0082700	1,910819103	1,83E-09	8,738260753	O03376	Alternative oxidase 3, mitochondrial (EC 1.10.3.11); May increase respiration when the cytochrome respiratory pathway is restricted
RC5G0672600	3,144494472	2,64E-09	8,579152764	Q7XKV4	Beta-glucosidase 12 (Os4bglu12) (EC 3.2.1.21)
RC6G0048600	2,696141184	3,93E-09	8,405779844	O48651	Panax ginseng (Korean ginseng); Catalyzes the first oxygenation step in sterol biosynthesis and is suggested to be one of the rate-limiting enzymes in this pathway
UP_0dpi_OB					
RC2G0158000	1,410085936	8,32E-06	5,079938685	Q8L7A0	Sulfite exporter TauE/SafE family protein 3; Protein ubiquitination
RC3G0330800	1,762243123	0,000149027	3,826735324	C7G304	Galactinol synthase 2 (GolS-2) (SIGoIS2) (EC 2.4.1.123); May promote plant stress tolerance

Supplementary table 5: Example of the most highly down-regulated genes according to their $-\log_{10}(\text{padj})$ and their mean \log_2 fold change at each time point for 'Old Blush' (OB) genotype

GeneID	log2FoldChange	padj	$-\log_{10}(\text{padj})$	GeneID	Description
DOWN_7dpi_OB					
RC4G0411200	-1,122440544	3,41E-07	6,467793136	Q93ZR8	Cell wall organization; Rhamnogalacturonan I rhamnosyltransferase 1 (EC 2.4.1.351) (O-fucosyltransferase 21) (O-FucT-21) (O-fucosyltransferase family protein)
RC2G0139800	-1,185975038	1,19E-05	4,923192043	M5VUN2	VOC domain-containing protein
RC5G0597400	-1,379773086	9,40E-05	4,026675945	Q93Z81	Ion transport/homeostasis; Vacuolar cation/proton exchanger 3 (Ca(2+)/H(+)) antiporter CAX3 (Ca(2+)/H(+)) exchanger 3 (Protein CATION EXCHANGER 3)
DOWN_3dpi_OB					
RC2G0158000	-1,352333463	2,16E-08	7,666305104	Q8L7A0	Sulfite exporter TauE/SafE family protein 3
RC5G0731500	-1,535078081	1,93E-07	6,714721164	Q9LHN7	Probable polyamine transporter At3g13620
RC4G0402900	-1,10777626	2,30E-07	6,63842573	NoMatch	NoMatch
RC5G0580500	-1,647295989	3,06E-07	6,513704551	NoMatch	NoMatch
RC6G0561000	-1,536765546	3,06E-07	6,513704551	NoMatch	NoMatch
RC5G0579600	-1,506773725	4,26E-07	6,37078413	M5W5L9	Uncharacterized protein
RC2G0139800	-1,069783845	1,13E-06	5,948710336	M5VUN2	VOC domain-containing protein
RC7G0169800	-1,071806803	3,26E-06	5,487110712	NoMatch	NoMatch
RC4G0082300	-1,041066721	5,00E-06	5,301420363	Q8L730	Protein SULFUR DEFICIENCY-INDUCED 2
RC5G0554500	-1,517856489	7,83E-06	5,106168892	NoMatch	NoMatch
RC2G0445500	-1,249493379	9,33E-06	5,030293516	O95372	Acyl-protein thioesterase 2 (APT-2) (EC 3.1.2.-) (Lysophospholipase II) (LPL-II) (LysoPLA II)
RC5G0597400	-1,370910048	1,09E-05	4,964461448	Q93Z81	Vacuolar cation/proton exchanger 3 (Ca(2+)/H(+)) antiporter CAX3 (Ca(2+)/H(+)) exchanger 3 (Protein CATION EXCHANGER 3)
RC5G0476600	-1,165730216	1,99E-05	4,700708114	Q9SSK5	MLP-like protein 43; defense response
RC7G0289000	-1,513268496	3,05E-05	4,515859054	Q9LQL2	Protein NRT1/ PTR FAMILY 7.3 (AtNPF7.3) (Nitrate transporter 1.5); leaf senescence

RC1G0156100	-1,016580888	4,48E-05	4,348890602	O82089	Copper transport protein CCH (Copper chaperone CCH)
RC5G0181600	-1,092048871	4,48E-05	4,348890602	D0R6I7	Phloem protein 2
RC4G0403000	-1,014490595	9,48E-05	4,023238396	NoMatch	NoMatch
DOWN_0dpi_OB					
RC5G0117000	-1,930520147	2,73E-11	10,56376856	Q8LG58	Participates in cell wall construction of growing tissues; Probable xyloglucan endotransglucosylase/hydrolase protein 16 (At-XTH16) (XTH-16) (EC 2.4.1.207)
RC3G0382600	-1,752124714	2,75E-11	10,56046291	Q9FJT7	Protein NDL1 (Protein N-MYC DOWNREGULATED-LIKE 1)
RC2G0554200	-1,55058862	2,81E-11	10,551079	Q8LDW9	Participates in cell wall construction of growing tissues; Xyloglucan endotransglucosylase/hydrolase protein 9 (At-XTH9) (XTH-9) (EC 2.4.1.207)
RC1G0221000	-2,06625039	4,36E-10	9,360884499	Q9LQL2	Protein NRT1/ PTR FAMILY 7.3 (AtNPF7.3) (Nitrate transporter 1.5)
RC5G0036500	-1,871332915	5,94E-10	9,225870103	Q8L9A9	Participates in cell wall construction of growing tissues; Probable xyloglucan endotransglucosylase/hydrolase protein 8 (At-XTH8) (XTH-8) (EC 2.4.1.207)
RC6G0313300	-1,80169798	1,31E-09	8,882411705	Q9SII5	Protein EXORDIUM-like 5
RC3G0078600	-1,615769773	4,94E-09	8,305933908	P27492	Chlorophyll a-b binding protein 16, chloroplastic (LHCII type I CAB-16) (LHCP)
RC0G0131300	-1,486235002	2,69E-07	6,570319747	Q9ZRA4	Auxin-binding protein ABP19a
RC3G0303800	-1,432742727	2,69E-07	6,570319747	Q94AK6	Senescence associated gene 20 (Protein WOUND-INDUCED 12) (AtWI-12)
RC2G0192700	-1,169913077	2,70E-07	6,568635093	M5VUS8	Remorin_C domain-containing protein
RC7G0548700	-1,601101029	3,00E-07	6,523561482	Q9ZPE7	Protein EXORDIUM; Brassinosteroid response, required for cell expansion in leaves
RC6G0521900	-1,379149653	3,07E-07	6,512574378	Q93X17	Snakin-2; antimicrobial activity

RC6G0520200	-1,120831235	5,48E-07	6,260886931	Q94CH6	Lipid catabolic process; GDSL esterase/lipase EXL3 (EC 3.1.1.-) (Family II extracellular lipase 3) (Family II lipase EXL3)
RC4G0194600	-1,562578243	2,20E-06	5,657443747	P35694	Participates in cell wall construction of growing tissues; Xyloglucan endotransglucosylase/hydrolase 2 (EC 2.4.1.207) (Brassinosteroid-regulated protein BRU1)
RC7G0490400	-1,266314573	2,24E-06	5,649286907	M5XBL1	Uncharacterized protein
RC5G0262300	-1,171153714	2,31E-06	5,636670104	Q6DR10	May be involved in the specific O-acetylation of cell wall polymers; Protein trichome birefringence-like 43
RC5G0737300	-1,151231099	8,95E-06	5,047938075	NoMatch	NoMatch
RC4G0096600	-1,371088317	3,29E-05	4,483171882	Q38910	Participates in cell wall construction of growing tissues; Probable xyloglucan endotransglucosylase/hydrolase protein 23 (At-XTH23) (XTH-23) (EC 2.4.1.207)
RC0G0115400	-1,179013081	5,53E-05	4,256951328	NoMatch	NoMatch
RC3G0273700	-1,065282448	7,79E-05	4,108440213	Q94748	Probable dynein light chain (T-cell-stimulating antigen SM10)
RC7G0548200	-1,591491096	7,79E-05	4,108440213	Q9ZPE7	Protein EXORDIUM; Brassinosteroid response, required for cell expansion in leaves
RC0G0035600	-1,761182371	8,73E-05	4,05922298	Q8S3D2	Transcription factor bHLH87 (Basic helix-loop-helix protein 87) (AtbHLH87) (bHLH 87) (Transcription factor EN 121) (bHLH transcription factor bHLH087)

Supplementary table 6: Example of the most highly up-regulated genes according to their $-\log_{10}(\text{padj})$ and their mean \log_2 fold change at each time point for *R. x wichurana* (RW) genotype

GeneID	log2FoldChange	padj	$-\log_{10}(\text{padj})$	GeneID	Description
UP_7dpi_OB					
RC3G0223600	2,914378446	1,78E-46	45,74839649	Q9FSG7	Thaumatococcus protein 1a (Mdt1) (Pathogenesis-related protein 5a) (PR-5a) (allergen Mal d 2); PR5
RC1G0372500	2,939031355	4,84E-30	29,31501088	P50694	Glucan endo-1,3-beta-glucosidase (EC 3.2.1.39) ((1->3)-beta-glucan endohydrolase) ((1->3)-beta-glucanase) (Allergen Pru a 2) (Beta-1,3-endoglucanase) (Thaumatococcus protein) (TLP) (allergen Pru av 2); PR2
RC4G0172700	3,065081866	4,17E-28	27,37960983	O24248	Major allergen Pru av 1 (Allergen Pru a 1) (allergen Pru av 1); PR10
RC5G0257300	2,987284367	1,77E-23	22,7521929	Q9LMU2	Kunitz trypsin inhibitor 5 (AtKT15) (Kunitz trypsin inhibitor 2) (AtKT12)
RC3G0105000	3,213158781	2,29E-23	22,64045768	P52408	Glucan endo-1,3-beta-glucosidase, basic isoform (EC 3.2.1.39) ((1->3)-beta-glucan endohydrolase) ((1->3)-beta-glucanase) (Beta-1,3-endoglucanase) (PpGns1); PR2
RC0G0198300	2,420929868	3,41E-21	20,46712476	A7PQW3	Glucan endo-1,3-beta-glucosidase (EC 3.2.1.39) ((1->3)-beta-glucan endohydrolase) ((1->3)-beta-glucanase) (Beta-1,3-endoglucanase); PR2
UP_5dpi_OB					
RC3G0104700	2,046831847	2,69E-25	24,56945074	P52408	Glucan endo-1,3-beta-glucosidase, basic isoform (EC 3.2.1.39) ((1->3)-beta-glucan endohydrolase) ((1->3)-beta-glucanase) (Beta-1,3-endoglucanase) (PpGns1); PR2
RC4G0475100	2,199694005	1,23E-14	13,90885635	O48676	UDP-glycosyltransferase 74B1 (N-hydroxythioamide S-beta-glucosyltransferase) (EC 2.4.1.195) (Thiohydroximate S-glucosyltransferase)

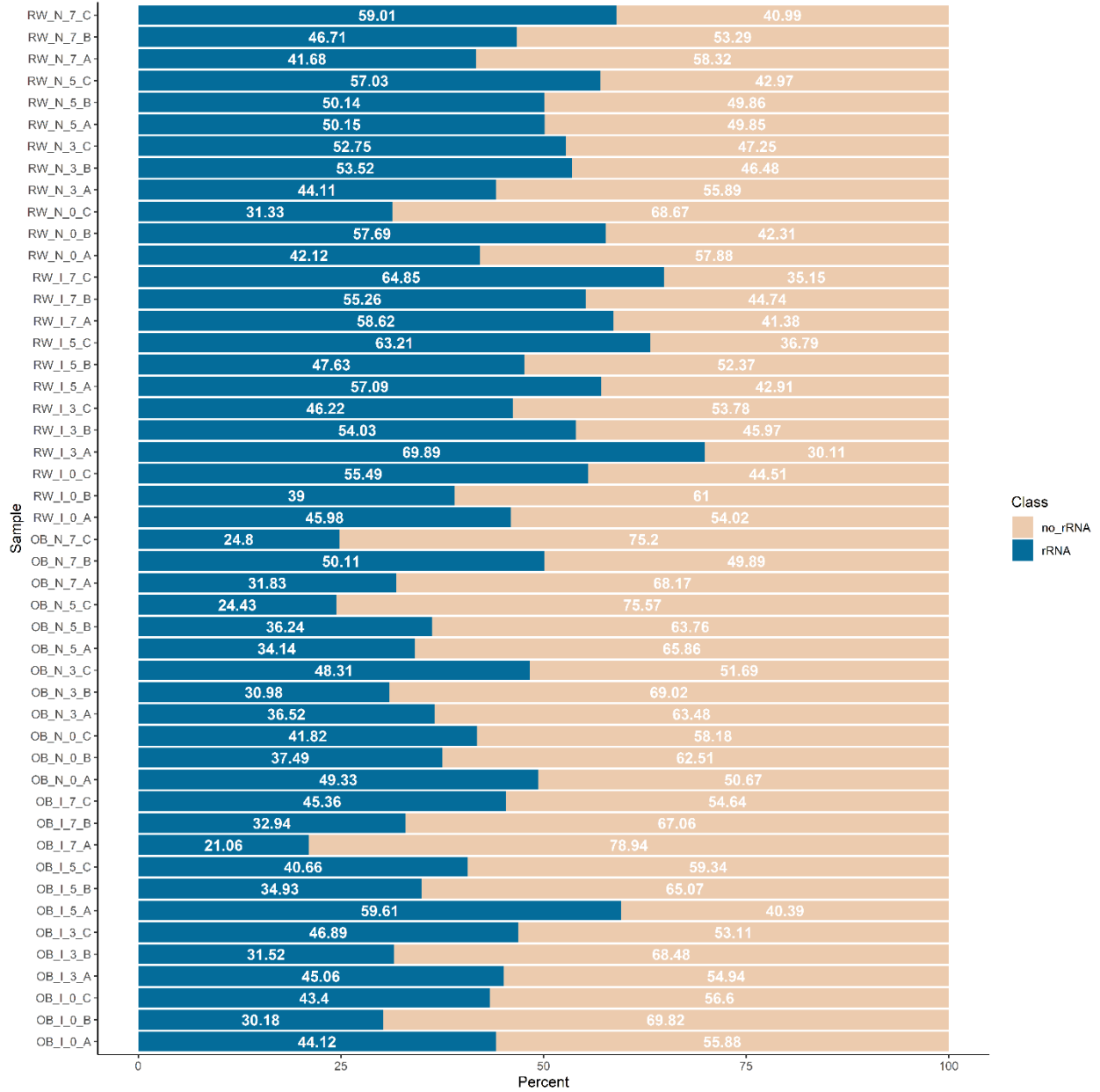
RC0G0225700	2,956306802	5,33E-13	12,27311539	Q3ZPN4	Methanol O-anthraniloyltransferase (EC 2.3.1.232) (Anthraniloyl-CoA:methanol acyltransferase) (Benzyl alcohol O-benzoyltransferase) (EC 2.3.1.196)
RC3G0104800	1,110090247	6,03E-12	11,21995242	P50694	Glucan endo-1,3-beta-glucosidase (EC 3.2.1.39) ((1->3)-beta-glucan endohydrolase) ((1->3)-beta-glucanase) (Allergen Pru a 2) (Beta-1,3-endoglucanase) (Thaumatococcus-like protein) (TLP) (allergen Pru av 2); PR2
UP_3dpi_OB					
RC4G0113600	2,395866229	1,42E-09	8,848549265	Q9SS87	Protein SIEVE ELEMENT OCCLUSION B (AtSEOb) (Protein SIEVE ELEMENT OCCLUSION-RELATED 1) (AtSEOR1)
RC1G0559900	2,441597053	1,42E-09	8,848549265	Q8H0Y8	Probable WRKY transcription factor 41 (WRKY DNA-binding protein 41)
RC4G0082700	1,910819103	1,83E-09	8,738260753	O03376	Alternative oxidase 3, mitochondrial (EC 1.10.3.11); May increase respiration when the cytochrome respiratory pathway is restricted
RC5G0672600	3,144494472	2,64E-09	8,579152764	Q7XKV4	Beta-glucosidase 12 (Os4bglu12) (EC 3.2.1.21)
RC6G0048600	2,696141184	3,93E-09	8,405779844	O48651	Panax ginseng (Korean ginseng); Catalyzes the first oxygenation step in sterol biosynthesis and is suggested to be one of the rate-limiting enzymes in this pathway
UP_0dpi_OB					
RC2G0158000	1,410085936	8,32E-06	5,079938685	Q8L7A0	Sulfite exporter TauE/SafE family protein 3; Protein ubiquitination
RC3G0330800	1,762243123	0,000149027	3,826735324	C7G304	Galactinol synthase 2 (GolS-2) (SIGoIS2) (EC 2.4.1.123); May promote plant stress tolerance

Supplementary table 7: Example of the most highly down-regulated genes according to their $-\log_{10}(\text{padj})$ and their mean \log_2 fold change at each time point for *R. x wichurana* (RW) genotype

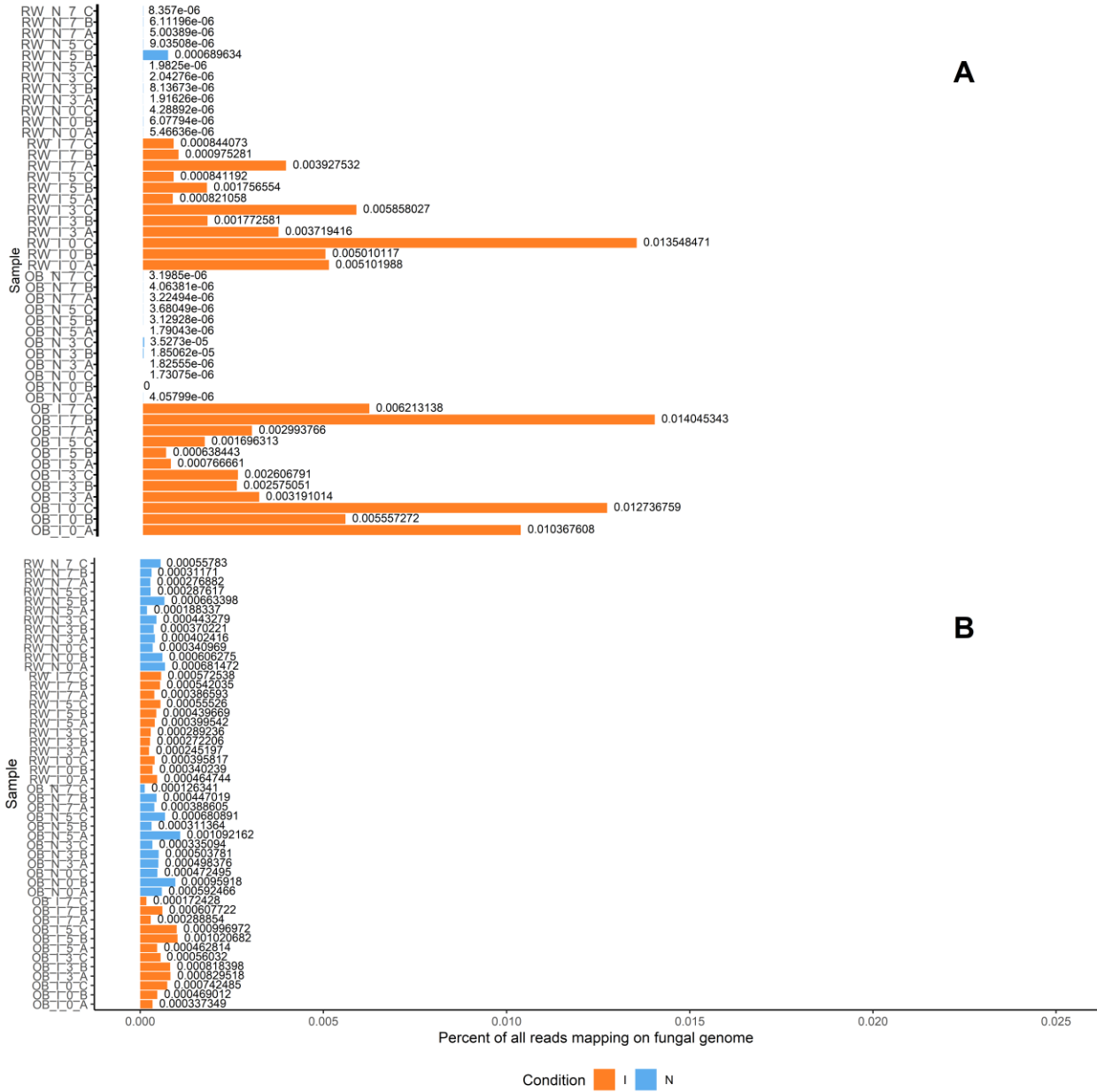
GeneID	log2FoldChange	padj	$-\log_{10}(\text{padj})$	GeneID	Description
DOWN_7dpi_OB					
RC4G0411200	-1,122440544	3,41E-07	6,467793136	Q93ZR8	Cell wall organization; Rhamnogalacturonan I rhamnosyltransferase 1 (EC 2.4.1.351) (O-fucosyltransferase 21) (O-FucT-21) (O-fucosyltransferase family protein)
RC2G0139800	-1,185975038	1,19E-05	4,923192043	M5VUN2	VOC domain-containing protein
RC5G0597400	-1,379773086	9,40E-05	4,026675945	Q93Z81	Ion transport/homeostasis; Vacuolar cation/proton exchanger 3 (Ca(2+)/H(+)) antiporter CAX3 (Ca(2+)/H(+)) exchanger 3 (Protein CATION EXCHANGER 3)
DOWN_3dpi_OB					
RC2G0158000	-1,352333463	2,16E-08	7,666305104	Q8L7A0	Sulfite exporter TauE/SafE family protein 3
RC5G0731500	-1,535078081	1,93E-07	6,714721164	Q9LHN7	Probable polyamine transporter At3g13620
RC4G0402900	-1,10777626	2,30E-07	6,63842573	NoMatch	NoMatch
RC5G0580500	-1,647295989	3,06E-07	6,513704551	NoMatch	NoMatch
RC6G0561000	-1,536765546	3,06E-07	6,513704551	NoMatch	NoMatch
RC5G0579600	-1,506773725	4,26E-07	6,37078413	M5W5L9	Uncharacterized protein
RC2G0139800	-1,069783845	1,13E-06	5,948710336	M5VUN2	VOC domain-containing protein
RC7G0169800	-1,071806803	3,26E-06	5,487110712	NoMatch	NoMatch
RC4G0082300	-1,041066721	5,00E-06	5,301420363	Q8L730	Protein SULFUR DEFICIENCY-INDUCED 2
RC5G0554500	-1,517856489	7,83E-06	5,106168892	NoMatch	NoMatch
RC2G0445500	-1,249493379	9,33E-06	5,030293516	O95372	Acyl-protein thioesterase 2 (APT-2) (EC 3.1.2.-) (Lysophospholipase II) (LPL-II) (LysoPLA II)
RC5G0597400	-1,370910048	1,09E-05	4,964461448	Q93Z81	Vacuolar cation/proton exchanger 3 (Ca(2+)/H(+)) antiporter CAX3 (Ca(2+)/H(+)) exchanger 3 (Protein CATION EXCHANGER 3)
RC5G0476600	-1,165730216	1,99E-05	4,700708114	Q9SSK5	MLP-like protein 43; defense response

RC7G0289000	-1,513268496	3,05E-05	4,515859054	Q9LQL2	Protein NRT1/ PTR FAMILY 7.3 (AtNPF7.3) (Nitrate transporter 1.5); leaf senescence
RC1G0156100	-1,016580888	4,48E-05	4,348890602	O82089	Copper transport protein CCH (Copper chaperone CCH)
RC5G0181600	-1,092048871	4,48E-05	4,348890602	D0R6I7	Phloem protein 2
RC4G0403000	-1,014490595	9,48E-05	4,023238396	NoMatch	NoMatch
DOWN_0dpi_OB					
RC5G0117000	-1,930520147	2,73E-11	10,56376856	Q8LG58	Participates in cell wall construction of growing tissues; Probable xyloglucan endotransglucosylase/hydrolase protein 16 (At-XTH16) (XTH-16) (EC 2.4.1.207)
RC3G0382600	-1,752124714	2,75E-11	10,56046291	Q9FJT7	Protein NDL1 (Protein N-MYC DOWNREGULATED-LIKE 1)
RC2G0554200	-1,55058862	2,81E-11	10,551079	Q8LDW9	Participates in cell wall construction of growing tissues; Xyloglucan endotransglucosylase/hydrolase protein 9 (At-XTH9) (XTH-9) (EC 2.4.1.207)
RC1G0221000	-2,06625039	4,36E-10	9,360884499	Q9LQL2	Protein NRT1/ PTR FAMILY 7.3 (AtNPF7.3) (Nitrate transporter 1.5)
RC5G0036500	-1,871332915	5,94E-10	9,225870103	Q8L9A9	Participates in cell wall construction of growing tissues; Probable xyloglucan endotransglucosylase/hydrolase protein 8 (At-XTH8) (XTH-8) (EC 2.4.1.207)
RC6G0313300	-1,80169798	1,31E-09	8,882411705	Q9SII5	Protein EXORDIUM-like 5
RC3G0078600	-1,615769773	4,94E-09	8,305933908	P27492	Chlorophyll a-b binding protein 16, chloroplastic (LHCII type I CAB-16) (LHCP)
RC0G0131300	-1,486235002	2,69E-07	6,570319747	Q9ZRA4	Auxin-binding protein ABP19a
RC3G0303800	-1,432742727	2,69E-07	6,570319747	Q94AK6	Senescence associated gene 20 (Protein WOUND-INDUCED 12) (AtWI-12)
RC2G0192700	-1,169913077	2,70E-07	6,568635093	M5VUS8	Remorin_C domain-containing protein
RC7G0548700	-1,601101029	3,00E-07	6,523561482	Q9ZPE7	Protein EXORDIUM; Brassinosteroid response, required for cell expansion in leaves

RC6G0521900	-1,379149653	3,07E-07	6,512574378	Q93X17	Snakin-2; antimicrobial activity
RC6G0520200	-1,120831235	5,48E-07	6,260886931	Q94CH6	Lipid catabolic process; GDSL esterase/lipase EXL3 (EC 3.1.1.-) (Family II extracellular lipase 3) (Family II lipase EXL3)
RC4G0194600	-1,562578243	2,20E-06	5,657443747	P35694	Participates in cell wall construction of growing tissues; Xyloglucan endotransglucosylase/hydrolase 2 (EC 2.4.1.207) (Brassinosteroid-regulated protein BRU1)
RC7G0490400	-1,266314573	2,24E-06	5,649286907	M5XBL1	Uncharacterized protein
RC5G0262300	-1,171153714	2,31E-06	5,636670104	Q6DR10	May be involved in the specific O-acetylation of cell wall polymers; Protein trichome birefringence-like 43
RC5G0737300	-1,151231099	8,95E-06	5,047938075	NoMatch	NoMatch
RC4G0096600	-1,371088317	3,29E-05	4,483171882	Q38910	Participates in cell wall construction of growing tissues; Probable xyloglucan endotransglucosylase/hydrolase protein 23 (At-XTH23) (XTH-23) (EC 2.4.1.207)
RCOG0115400	-1,179013081	5,53E-05	4,256951328	NoMatch	NoMatch
RC3G0273700	-1,065282448	7,79E-05	4,108440213	Q94748	Probable dynein light chain (T-cell-stimulating antigen SM10)
RC7G0548200	-1,591491096	7,79E-05	4,108440213	Q9ZPE7	Protein EXORDIUM; Brassinosteroid response, required for cell expansion in leaves
RCOG0035600	-1,761182371	8,73E-05	4,059222298	Q8S3D2	Transcription factor bHLH87 (Basic helix-loop-helix protein 87) (AtbHLH87) (bHLH 87) (Transcription factor EN 121) (bHLH transcription factor bHLH087)

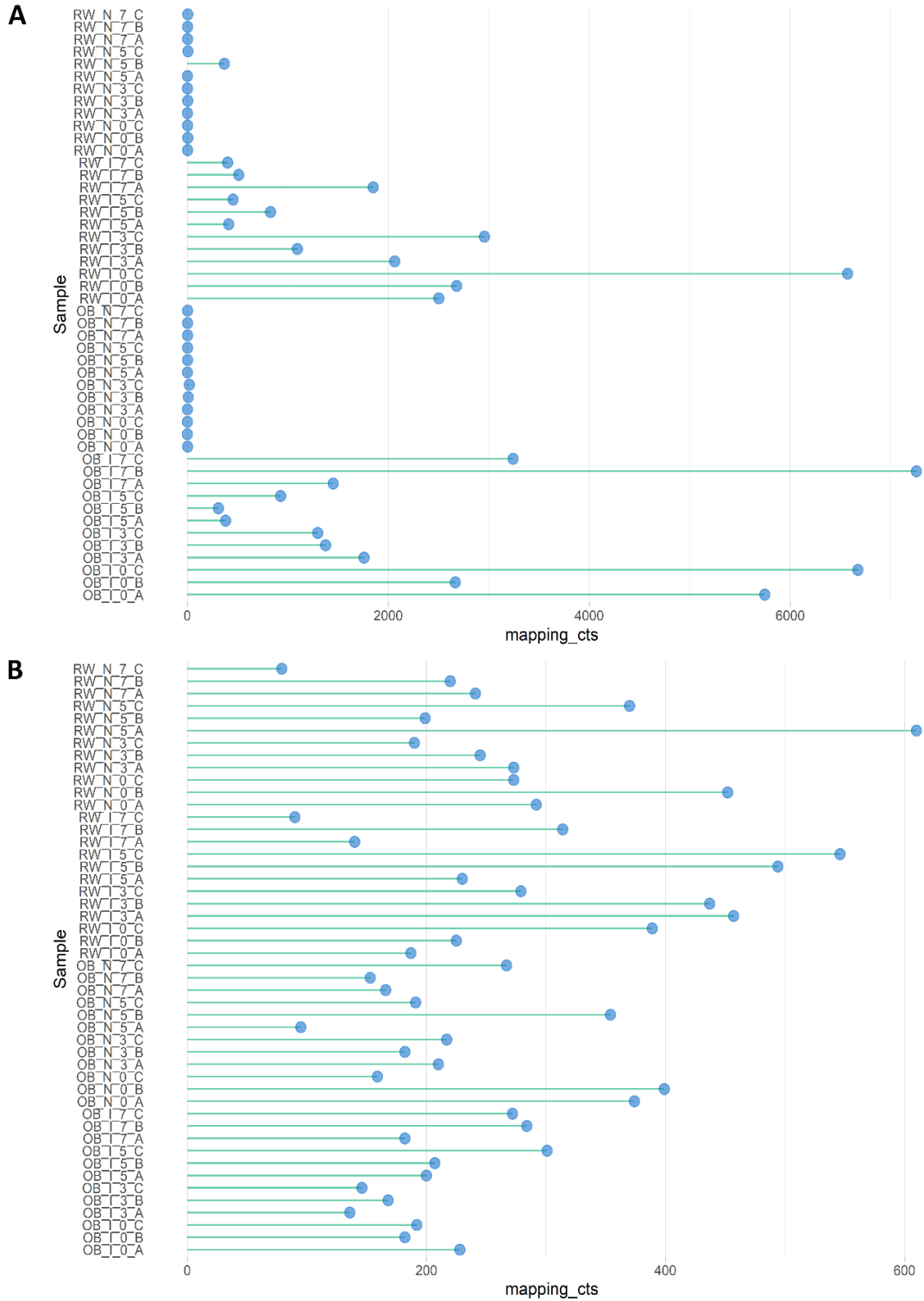


Supplementary figure 43: Percentage of reads unmapped on the rose genome and aligning with the rRNA database (in blue, rRNA) and not aligning with it (in beige, no-rRNA)



Supplementary figure 44: Percentage of fungal reads out of the total number of reads for each sample

A: Percentage of cleaned unmapped reads mapping on *Diplocarpon rosae* genome for all samples; B: Percentage of cleaned unmapped reads mapping on *Podosphaera xanthii* genome; I stands for inoculated samples and N for mock samples.



Supplementary figure 45: Plot by sample of fungal read counts for both genotypes

A: Number of reads mapping on *Diplocarpon rosae* genome; **B:** Number of reads mapping on *Podosphaera xanthii* genome.

REFERENCES

- Adam-Blondon A-F, Martinez-Zapater J-M, Kole C (2016) Genetics, genomics, and breeding of grapes. CRC Press
- Allum JF, Bringloe HD, Roberts AV (2010) Interactions of four pathotypes of *Diplocarpon rosae* with species and hybrids of *Rosa*. Plant Pathol 59:516–522. <https://doi.org/10.1111/j.1365-3059.2009.02222.x>
- Arcade A, Labourdette A, Falque M, et al (2004) BioMercator: integrating genetic maps and QTL towards discovery of candidate genes. Bioinforma Oxf Engl 20:2324–2326. <https://doi.org/10.1093/bioinformatics/bth230>
- Becker HF (1963) The Fossil Record of the Genus *Rosa*. Bull Torrey Bot Club 90:99–110. <https://doi.org/10.2307/2483008>
- Black WA, Byrne DH, Pemberton HB (1994) Field study of black spot resistance in rose. HortScience 29:
- Blechert O, Debener T (2005) Morphological characterization of the interaction between *Diplocarpon rosae* and various rose species. Plant Pathol 54:82–90. <https://doi.org/10.1111/j.1365-3059.2005.01118.x>
- Boontiang K (2003) Breeding of black spot disease resistance of garden and florist rose. PhD Thesis, 愛媛大学
- Bourke PM, Gitonga VW, Voorrips RE, et al (2018) Multi-environment QTL analysis of plant and flower morphological traits in tetraploid rose. TAG Theor Appl Genet Theor Angew Genet 131:2055–2069. <https://doi.org/10.1007/s00122-018-3132-4>
- Broman K, Sen S (2009) A Guide to QTL Mapping with R/qlt. Springer-Verlag, New York
- Broman KW (2003) Mapping quantitative trait loci in the case of a spike in the phenotype distribution. Genetics 163:1169–1175
- Broman KW, Wu H (2019) Qtl: tools for analyzing qtl experiments. Version 1.44-9URL <https://CRAN.R-project.org/package=qtl>
- Bruneau A, Starr JR, Joly S (2007) Phylogenetic relationships in the genus *rosa*: new evidence from chloroplast dna sequences and an appraisal of current knowledge. Syst Bot 32:366–378
- Byrne DH, Pemberton HB, Holeman DJ, et al (2019) Survey of the rose community: desired rose traits and research issues. Acta Hort 189–192. <https://doi.org/10.17660/ActaHortic.2019.1232.28>
- Carlson-Nilsson BU (2001) Evaluation of rose species and cultivars for resistance to *Marssonina rosae* (*Diplocarpon rosae*). Acta Hort 413–417. <https://doi.org/10.17660/ActaHortic.2001.547.53>
- Cheema J, Dicks J (2009) Computational approaches and software tools for genetic linkage map estimation in plants. Brief Bioinform 10:595–608. <https://doi.org/10.1093/bib/bbp045>

- Chu KT, Ng TB (2003) Isolation of a large thaumatin-like antifungal protein from seeds of the Kweilin chestnut *Castanopsis chinensis*. *Biochem Biophys Res Commun* 301:364–370. [https://doi.org/10.1016/S0006-291X\(02\)02998-4](https://doi.org/10.1016/S0006-291X(02)02998-4)
- Corbeil RR, Searle SR (1976) Restricted maximum likelihood (REML) estimation of variance components in the mixed model. *Technometrics* 18:31–38. <https://doi.org/10.2307/1267913>
- Corwin JA, Kliebenstein DJ (2017) Quantitative resistance: more than just perception of a pathogen. *Plant Cell tpc.00915.2016*. <https://doi.org/10.1105/tpc.16.00915>
- Covarrubias-Pazarán G (2019) Sommer: solving mixed model equations in R. Version 4.0.1URL <https://CRAN.R-project.org/package=sommer>
- Debener T (2017) Inheritance of characteristics. In: Reference Module in Life Sciences. Elsevier, Hannover, Germany, pp 1–7
- Debener T, Drewes-Alvarez R, Rockstroh K (1998) Identification of five physiological races of blackspot, *Diplocarpon rosae* Wolf, on roses. *Plant Breed* 117:267–270. <https://doi.org/10.1111/j.1439-0523.1998.tb01937.x>
- Debray K (2020) Phylogénomique du genre Rosa : hybridation et polyploidie comme facteurs de diversification. These en préparation, Angers
- Debray K, Marie-Magdelaine J, Ruttink T, et al (2019) Identification and assessment of variable single-copy orthologous (SCO) nuclear loci for low-level phylogenomics: a case study in the genus Rosa (Rosaceae). *BMC Evol Biol* 19:. <https://doi.org/10.1186/s12862-019-1479-z>
- Doerge RW, Churchill GA (1996) Permutation tests for multiple loci affecting a quantitative character. *Genetics* 142:285–294
- Dong Q, Wang X, Byrne DH, Ong K (2017) Characterization of partial resistance to black spot disease of *Rosa* Sp. *HortScience* 52:49–53. <https://doi.org/10.21273/HORTSCI11349-16>
- Dong X (2005) Functional investigation of *Arabidopsis* callose synthases and the signal transduction pathway. The Ohio State University
- Dong X, Hong Z, Chatterjee J, et al (2008) Expression of callose synthase genes and its connection with *Npr1* signaling pathway during pathogen infection. *Planta* 229:87–98. <https://doi.org/10.1007/s00425-008-0812-3>
- Edgar RC (2010) Search and clustering orders of magnitude faster than BLAST. *Bioinformatics* 26:2460–2461. <https://doi.org/10.1093/bioinformatics/btq461>
- Edgar RC (2004) MUSCLE: Multiple sequence alignment with high accuracy and high throughput. *Nucleic Acids Res* 32:1792–1797. <https://doi.org/10.1093/nar/gkh340>
- Ellinger D, Naumann M, Falter C, et al (2013) Elevated early callose deposition results in complete penetration resistance to powdery mildew in *Arabidopsis*. *Plant Physiol* 161:1433–1444. <https://doi.org/10.1104/pp.112.211011>

- Enns LC, Kanaoka MM, Torii KU, et al (2005) Two callose synthases, GSL1 and GSL5, play an essential and redundant role in plant and pollen development and in fertility. *Plant Mol Biol* 58:333–349. <https://doi.org/10.1007/s11103-005-4526-7>
- Enrique R, Siciliano F, Favaro MA, et al (2011) Novel demonstration of RNAi in citrus reveals importance of citrus callose synthase in defence against *Xanthomonas citri* subsp. *citri*. *Plant Biotechnol J* 9:394–407
- Feenstra B, Skovgaard IM (2004) A quantitative trait locus mixture model that avoids spurious LOD score peaks. *Genetics* 167:959–965. <https://doi.org/10.1534/genetics.103.025437>
- Felsenstein J (1989) PHYLIP - Phylogeny Inference Package (Version 3.2). *Cladistics* 5:164–166. <https://doi.org/10.1111/j.1096-0031.1989.tb00562.x>
- Finn RD, Clements J, Arndt W, et al (2015) HMMER web server: 2015 update. *Nucleic Acids Res* 43:W30–W38. <https://doi.org/10.1093/nar/gkv397>
- Finn RD, Coghill P, Eberhardt RY, et al (2016) The Pfam protein families database: towards a more sustainable future. *Nucleic Acids Res* 44:D279–D285. <https://doi.org/10.1093/nar/gkv1344>
- Fischer BM, Salakhutdinov I, Akkurt M, et al (2004) Quantitative trait locus analysis of fungal disease resistance factors on a molecular map of grapevine. *Theor Appl Genet* 108:501–515. <https://doi.org/10.1007/s00122-003-1445-3>
- Fougère-Danezan M, Joly S, Bruneau A, et al (2015) Phylogeny and biogeography of wild roses with specific attention to polyploids. *Ann Bot* 115:275–291. <https://doi.org/10.1093/aob/mcu245>
- Fu Y, van Silfhout A, Shahin A, et al (2017) Genetic mapping and QTL analysis of Botrytis resistance in *Gerbera hybrida*. *Mol Breed* 37:.. <https://doi.org/10.1007/s11032-016-0617-1>
- Gachomo EW (2005) Studies of the life cycle of *Diplocarpon rosae* Wolf on roses and the effectiveness of fungicides on pathogenesis. Cuvillier Verlag
- Gachomo EW, Dehne H-W, Steiner U (2006) Microscopic evidence for the hemibiotrophic nature of *Diplocarpon rosae*, cause of black spot disease of rose. *Physiol Mol Plant Pathol* 1–3:86–92. <https://doi.org/10.1016/j.pmpp.2007.02.002>
- Gachomo EW, Kotchoni SO (2007) Detailed description of developmental growth stages of *Diplocarpon rosae* in *Rosa*: a core building block for efficient disease management. *Ann Appl Biol* 151:233–243. <https://doi.org/10.1111/j.1744-7348.2007.00167.x>
- Gachomo EW, Seufferheld MJ, Kotchoni SO (2010) Melanization of appressoria is critical for the pathogenicity of *Diplocarpon rosae*. *Mol Biol Rep* 37:3583–3591. <https://doi.org/10.1007/s11033-010-0007-4>
- Gartner GAL, McCouch SR, Moncada MDP (2013) A genetic map of an interspecific diploid pseudo testcross population of coffee. *Euphytica* 192:305–323. <https://doi.org/10.1007/s10681-013-0926-y>
- Goffinet B, Gerber S (2000) Quantitative trait loci: a meta-analysis. *Genetics* 155:463–473

- Grattapaglia D, Sederoff R (1994) Genetic linkage maps of *Eucalyptus grandis* and *Eucalyptus urophylla* using a pseudo-testcross: mapping strategy and RAPD markers. *Genetics* 137:1121–1137
- Griffiths S, Simmonds J, Leverington M, et al (2009) Meta-QTL analysis of the genetic control of ear emergence in elite European winter wheat germplasm. *TAG Theor Appl Genet Theor Angew Genet* 119:383–395. <https://doi.org/10.1007/s00122-009-1046-x>
- Guo B, Sleper DA, Lu P, et al (2006) QTLs associated with resistance to soybean cyst nematode in soybean: meta-analysis of QTL locations. *Crop Sci*
- Guo J, Chen L, Li Y, et al (2018) Meta-QTL analysis and identification of candidate genes related to root traits in maize. *Euphytica* 214:223. <https://doi.org/10.1007/s10681-018-2283-3>
- Hamon C, Coyne CJ, McGee RJ, et al (2013) QTL meta-analysis provides a comprehensive view of loci controlling partial resistance to *Aphanomyces euteiches* in four sources of resistance in pea. *BMC Plant Biol* 13:45. <https://doi.org/10.1186/1471-2229-13-45>
- Harp DA, Zlesak DC, Hammond G, et al (2009) Earth-Kind® rose trials – identifying the world’s strongest, most beautiful landscape roses. 10
- Harville DA (1977) Maximum likelihood approaches to variance component estimation and to related problems. *J Am Stat Assoc* 72:320–338. <https://doi.org/10.2307/2286796>
- Hattendorf A, Linde M, Mattiesch L, et al (2004) Genetic analysis of rose resistance genes and their localisation in the rose genome. *Acta Hortic* 123–130. <https://doi.org/10.17660/ActaHortic.2004.651.14>
- Hibrand-Saint Oyant L, Crespel L, Rajapakse S, et al (2007) Genetic linkage maps of rose constructed with new microsatellite markers and locating QTL controlling flowering traits. *Tree Genet Genomes* 4:11. <https://doi.org/10.1007/s11295-007-0084-2>
- Hibrand-Saint Oyant L, Ruttink T, Hamama L, et al (2018) A high-quality genome sequence of *Rosa chinensis* to elucidate ornamental traits. *Nat Plants* 4:473–484. <https://doi.org/10.1038/s41477-018-0166-1>
- Ho VSM, Wong JH, Ng TB (2007) A thaumatin-like antifungal protein from the emperor banana. *Peptides* 28:760–766. <https://doi.org/10.1016/j.peptides.2007.01.005>
- Holland JB, Coles ND (2011) Qtl controlling masculinization of ear tips in a maize (*zea mays* l.) intraspecific cross. *G3 GenesGenomesGenetics* 1:337–341. <https://doi.org/10.1534/g3.111.000786>
- Holland JB, Nyquist WE, Cervantes-Martínez CT (2010) Estimating and interpreting heritability for plant breeding: an update. *Plant Breed Rev* 9–112. <https://doi.org/10.1002/9780470650202.ch2>
- Horst RK, Cloyd RA (2007) *Compendium of rose diseases and pests*. APS Press
- Iwata H, Gaston A, Remay A, et al (2012) The TFL1 homologue KSN is a regulator of continuous flowering in rose and strawberry. *Plant J* 69:116–125. <https://doi.org/10.1111/j.1365-313X.2011.04776.x>

- Kao C-H, Zeng M-H (2010) An investigation of the power for separating closely linked QTL in experimental populations. *Genet Res* 92:283–294. <https://doi.org/10.1017/S0016672310000273>
- Kaufmann H, Mattiesch L, Lörz H, Debener T (2003) Construction of a BAC library of *Rosa rugosa* Thunb. and assembly of a contig spanning *Rdr1*, a gene that confers resistance to blackspot. *Mol Genet Genomics* 268:666–674. <https://doi.org/10.1007/s00438-002-0784-0>
- Kaufmann H, Terefe D, Yasmin A, et al (2010) Cloning and analysis of *Rdr1*, a black spot resistance gene from roses. *Acta Hort* 191–196. <https://doi.org/10.17660/ActaHortic.2010.870.25>
- Kawamura K, Hibrand-Saint Oyant L, Crespel L, et al (2011) Quantitative trait loci for flowering time and inflorescence architecture in rose. *TAG Theor Appl Genet Theor Angew Genet* 122:661–675. <https://doi.org/10.1007/s00122-010-1476-5>
- Kawamura K, Hibrand-Saint Oyant L, Thouroude T, et al (2015) Inheritance of garden rose architecture and its association with flowering behaviour. *Tree Genet Genomes* 11:1–12. <https://doi.org/10.1007/s11295-015-0844-3>
- Kelly JD, Vallejo V (2006) Qtl analysis of multigenic disease resistance in plant breeding. In: Tuzun S, Bent E (eds) *Multigenic and Induced Systemic Resistance in Plants*. Springer US, Boston, MA, pp 21–48
- Khowaja FS, Norton GJ, Courtois B, Price AH (2009) Improved resolution in the position of drought-related QTLs in a single mapping population of rice by meta-analysis. *BMC Genomics* 10:276. <https://doi.org/10.1186/1471-2164-10-276>
- Kirst M, Myburg A, Sederoff R (2004) Genetic mapping in forest trees: markers, linkage analysis and genomics. In: Setlow JK (ed) *Genetic Engineering: Principles and Methods*. Springer US, Boston, MA, pp 105–141
- Knight C (1975) Development of *Diplocarpon rosae* on different rose cultivars. PhD Thesis, London University
- Koopman WJM, Wissemann V, De Cock K, et al (2008) AFLP markers as a tool to reconstruct complex relationships: A case study in *Rosa* (*Rosaceae*). *Am J Bot* 95:353–366. <https://doi.org/10.3732/ajb.95.3.353>
- Krzywinski M, Schein J, Birol I, et al (2009) Circos: An information aesthetic for comparative genomics. *Genome Res* 19:1639–1645. <https://doi.org/10.1101/gr.092759.109>
- Labbé J (2014) LOI n° 2014-110 du 6 février 2014 visant à mieux encadrer l'utilisation des produits phytosanitaires sur le territoire national
- Lacape J-M, Llewellyn D, Jacobs J, et al (2010) Meta-analysis of cotton fiber quality QTLs across diverse environments in a *Gossypium hirsutum* x *G. barbadense* RIL population. *BMC Plant Biol* 10:132. <https://doi.org/10.1186/1471-2229-10-132>
- Lanaud C, Fouet O, Clément D, et al (2009) A meta-QTL analysis of disease resistance traits of *Theobroma cacao* L. *Mol Breed* 24:361–374. <https://doi.org/10.1007/s11032-009-9297-4>

- Lander ES, Botstein D (1989) Mapping mendelian factors underlying quantitative traits using RFLP linkage maps. *Genetics* 121:185–199
- Lespinasse D, Rodier-Goud M, Grivet L, et al (2000) A saturated genetic linkage map of rubber tree (*Hevea* spp.) based on RFLP, AFLP, microsatellite, and isozyme markers. *Theor Appl Genet* 100:127–138. <https://doi.org/10.1007/s001220050018>
- Leus L, Hosseini Moghaddam H, Van Huylenbroeck J, De Riek J (2015) Qtls associated with powdery mildew resistance responses in roses. *Acta Hortic* 287–293. <https://doi.org/10.17660/ActaHortic.2015.1064.34>
- Liorzou M (2016) Impact de la sélection au XIXe siècle sur la diversité génétique du rosier cultivé en France (*Rosa* sp.) Nineteenth century French rose (*Rosa* sp.) germplasm shows a shift over time from a European to an Asian genetic background. These de doctorat, Angers
- Liorzou M, Pernet A, Li S, et al (2016) Nineteenth century French rose (*Rosa* sp.) germplasm shows a shift over time from a European to an Asian genetic background. *J Exp Bot* 67:4711–4725. <https://doi.org/10.1093/jxb/erw269>
- Liu S, Hall MD, Griffey CA, McKendry AL (2009) Meta-analysis of qtl associated with fusarium head blight resistance in wheat. *Crop Sci* 49:1955–1968. <https://doi.org/10.2135/cropsci2009.03.0115>
- Lopez Arias DC, Chastellier A, Thouroude T, et al (in press) High density SNP and SSR linkage map and QTL analysis for resistance to black spot in segregating rose population. *Acta Hortic*
- Lui S, Luo C, Zhu L, et al (2017) Identification and expression analysis of WRKY transcription factor genes in response to fungal pathogen and hormone treatments in apple (*Malus domestica*). *J Plant Biol* 60:215–230. <https://doi.org/10.1007/s12374-016-0577-3>
- Lupas A, Van Dyke M, Stock J (1991) Predicting coiled coils from protein sequences. *Science* 252:1162–1164. <https://doi.org/10.1126/science.252.5009.1162>
- Lynch M, Walsh B (1998) *Genetics and analysis of quantitative traits*. Sunderland, Mass. : Sinauer
- Malek B von, Debener T (1998) Genetic analysis of resistance to blackspot (*Diplocarpon rosae*) in tetraploid roses. *Theor Appl Genet* 96:228–231. <https://doi.org/10.1007/s001220050731>
- Malek B von, Weber WE, Debener T (2000) Identification of molecular markers linked to *Rdr1* blackspot in roses. *Theor Appl Genet* 101:977–983. <https://doi.org/10.1007/s001220051570>
- Marolleau B, Petiteau A, Bellanger MN, et al (2020) Strong differentiation within *Diplocarpon rosae* strains based on microsatellite markers and greenhouse-based inoculation protocol on *Rosa*. *Plant Pathol*
- Marriott M (2003) History of roses in cultivation | Modern (post-1800). In: Roberts AV (ed) *Encyclopedia of Rose Science*. Elsevier, Oxford, pp 402–409
- Menz I, Lakhwani D, Clotault J, et al (2020) Analysis of the *Rdr1* gene family in different *Rosaceae* genomes reveals an origin of an R-gene cluster after the split of *Rubeae* within the *Rosoideae* subfamily. *PLOS ONE* 15:e0227428. <https://doi.org/10.1371/journal.pone.0227428>

- Menz I, Straube J, Linde M, Debener T (2018) The TNL gene *Rdr1* confers broad-spectrum resistance to *Diplocarpon rosae*. *Mol Plant Pathol*. <https://doi.org/10.1111/mpp.12589>
- Meynet J (Institut N de la RA, Barrade R, Duclos A, Siadous R (1994) Dihaploid plants of roses (*Rosa x hybrida*, cv “Sonia”) obtained by parthenogenesis induced using irradiated pollen and in vitro culture of immature seeds. *Agron Fr*
- Morant M, Bak S, Møller BL, Werck-Reichhart D (2003) Plant cytochromes P450: tools for pharmacology, plant protection and phytoremediation. *Curr Opin Biotechnol* 14:151–162. [https://doi.org/10.1016/S0958-1669\(03\)00024-7](https://doi.org/10.1016/S0958-1669(03)00024-7)
- Münnekhoff A-K, Linde M, Debener T (2017) The gene diversity pattern of *Diplocarpon rosae* populations is shaped by the age, diversity and fungicide treatment of their host populations. *Plant Pathol* 66:1288–1298. <https://doi.org/10.1111/ppa.12681>
- Nakamichi R, Ukai Y, Kishino H (2001) Detection of closely linked multiple quantitative trait loci using a genetic algorithm. *Genetics* 158:463–475
- Niks RE, Qi X, Marcel TC (2015) Quantitative resistance to biotrophic filamentous plant pathogens: concepts, misconceptions, and mechanisms. *Annu Rev Phytopathol* 53:445–470. <https://doi.org/10.1146/annurev-phyto-080614-115928>
- Pandey SP, Somssich IE (2009) The role of wrky transcription factors in plant immunity. *Plant Physiol* 150:1648–1655. <https://doi.org/10.1104/pp.109.138990>
- Patterson HD, Thompson R (1971) Recovery of inter-block information when block sizes are unequal. *Biometrika* 58:545–554. <https://doi.org/10.2307/2334389>
- Pilet-Nayel M-L, Moury B, Caffier V, et al (2017) Quantitative resistance to plant pathogens in pyramiding strategies for durable crop protection. *Front Plant Sci* 8:1838. <https://doi.org/10.3389/fpls.2017.01838>
- Plomion C, Durel C (1996) Estimation of the average effects of specific alleles detected by the pseudo-testcross QTL mapping strategy. *Genet Sel Evol* 28:223. <https://doi.org/10.1186/1297-9686-28-3-223>
- Poland JA, Balint-Kurti PJ, Wisser RJ, et al (2009) Shades of gray: the world of quantitative disease resistance. *Trends Plant Sci* 14:21–29. <https://doi.org/10.1016/j.tplants.2008.10.006>
- Qi Z, Sun Y, Wang J, et al (2011) Meta-Analysis of 100-Seed Weight QTLs in Soybean. *Agric Sci China* 10:327–334. [https://doi.org/10.1016/S1671-2927\(11\)60011-4](https://doi.org/10.1016/S1671-2927(11)60011-4)
- Rawat N (2016) Approaches for disease resistant candidate genes identification in plants: recent techniques and trends. *Austin Food Sci* 1:1010
- Raymond O, Gouzy J, Just J, et al (2018) The *Rosa* genome provides new insights into the domestication of modern roses. *Nat Genet* 50:772. <https://doi.org/10.1038/s41588-018-0110-3>

- Rehder A (1940) Manual of cultivated trees and shrubs hardy in North America, exclusive of the subtropical and warmer temperate regions,. Macmillan Co., New York
- Roman H, Rapicault M, Miclot AS, et al (2015) Genetic analysis of the flowering date and number of petals in rose. *Tree Genet Genomes* 11:85. <https://doi.org/10.1007/s11295-015-0906-6>
- Roux F, Voisin D, Badet T, et al (2014) Resistance to phytopathogens *e tutti quanti*: placing plant quantitative disease resistance on the map. *Mol Plant Pathol* 15:427–432. <https://doi.org/10.1111/mpp.12138>
- Said JI, Lin Z, Zhang X, et al (2013) A comprehensive meta QTL analysis for fiber quality, yield, yield related and morphological traits, drought tolerance, and disease resistance in tetraploid cotton. *BMC Genomics* 14:776. <https://doi.org/10.1186/1471-2164-14-776>
- Saunders (1966) Epidemiological aspects of blackspot disease of roses caused by *Diplocarpon rosae* Wolf. *Ann Appl Biol* 58:115–122. <https://doi.org/10.1111/j.1744-7348.1966.tb05076.x>
- Schuler MA, Duan H, Bilgin M, Ali S (2006) Arabidopsis cytochrome P450s through the looking glass: a window on plant biochemistry. *Phytochem Rev* 5:205–237. <https://doi.org/10.1007/s11101-006-9035-z>
- Schuler MA, Werck-Reichhart D (2003) Functional genomics of P450s. *Annu Rev Plant Biol* 54:629–667. <https://doi.org/10.1146/annurev.arplant.54.031902.134840>
- Schulz DF, Linde M, Bleichert O, Debener T (2009) Evaluation of genus *Rosa* germplasm for resistance to black spot, downy mildew and powdery mildew. *Eur J Hortic Sci* 74:1–9
- Semagn K, Beyene Y, Warburton ML, et al (2013) Meta-analyses of QTL for grain yield and anthesis silking interval in 18 maize populations evaluated under water-stressed and well-watered environments. *BMC Genomics* 14:313. <https://doi.org/10.1186/1471-2164-14-313>
- Shupert DA (2006) Inheritance of flower, stem, leaf, and disease traits in three diploid interspecific rose populations. Texas A&M University
- Singh NK, Kumar KRR, Kumar D, et al (2013) Characterization of a Pathogen Induced Thaumatin-Like Protein Gene AdTLP from *Arachis diogeni*, a Wild Peanut. *PLOS ONE* 8:e83963. <https://doi.org/10.1371/journal.pone.0083963>
- Smith IM, Dunez J, Philips DH, et al (1989) European handbook of plant diseases. *Q Rev Biol* 64:200–200. <https://doi.org/10.1086/416271>
- Smulders MJM, Arens P, Bourke PM, et al (2019) In the name of the rose: a roadmap for rose research in the genome era. *Hortic Res* 6:65–65. <https://doi.org/10.1038/s41438-019-0156-0>
- Sosnowski O, Charcosset A, Joets J (2012) BioMercator V3: an upgrade of genetic map compilation and quantitative trait loci meta-analysis algorithms. *Bioinforma Oxf Engl* 28:2082–2083. <https://doi.org/10.1093/bioinformatics/bts313>

- Soufflet-Freslon V, Marolleau B, Thouroude T, et al (2019) Development of tools to study rose resistance to black spot. *Acta Hort* 213–220. <https://doi.org/10.17660/ActaHortic.2019.1232.31>
- Spiller M, Linde M, Hibrand-Saint Oyant L, et al (2011) Towards a unified genetic map for diploid roses. *Theor Appl Genet* 122:489–500. <https://doi.org/10.1007/s00122-010-1463-x>
- St Clair DA (2010) Quantitative disease resistance and quantitative resistance Loci in breeding. *Annu Rev Phytopathol* 48:247–268. <https://doi.org/10.1146/annurev-phyto-080508-081904>
- Stamatakis A (2014) RAxML version 8: a tool for phylogenetic analysis and post-analysis of large phylogenies. *Bioinformatics* 30:1312–1313. <https://doi.org/10.1093/bioinformatics/btu033>
- Terefe-Ayana D, Yasmin A, Le TL, et al (2011) Mining disease-resistance genes in roses: functional and molecular characterization of the *Rdr1* locus. *Front Plant Sci* 2:. <https://doi.org/10.3389/fpls.2011.00035>
- Tomljenovic N, Pejić I (2018) Taxonomic Review of the Genus *Rosa*. *Agric Conspec Sci* 83:139–147
- Trognitz F, Manosalva P, Gysin R, et al (2002) Plant defense genes associated with quantitative resistance to potato late blight in *Solanum phureja* x dihaploid *S. tuberosum* hybrids. *Mol Plant-Microbe Interact* 15:587–597. <https://doi.org/10.1094/MPMI.2002.15.6.587>
- Tsuchiya T, Eulgem T (2011) EMSY-like genes are required for full *RPP7*-mediated race-specific immunity and basal defense in *Arabidopsis*. *Mol Plant-Microbe Interact* 24:1573–1581. <https://doi.org/10.1094/MPMI-05-11-0123>
- Uggla M, Carlson-Nilsson BU (2005) Screening of fungal diseases in offspring from crosses between *Rosa* sections *Caninae* and *Cinnamomeae*. *Sci Hortic* 104:493–504. <https://doi.org/10.1016/j.scienta.2004.11.001>
- VAL'HOR (2017) Bilan complet achats de végétaux. Val'hor & France AgriMer
- van Oijen (2019) JoinMap® 5.0 - Software for the calculation of genetic linkage maps in experimental populations of diploid species. Version 5.0. Kyazma B.V., Wageningen. URL <https://www.kyazma.nl/index.php/JoinMap/General/>
- Van Ooijen JW (2011) Multipoint maximum likelihood mapping in a full-sib family of an outbreeding species. *Genet Res* 93:343–349. <https://doi.org/10.1017/S0016672311000279>
- Vasconcellos RCC, Oraguzie OB, Soler A, et al (2017) Meta-QTL for resistance to white mold in common bean. *PLOS ONE* 12:e0171685. <https://doi.org/10.1371/journal.pone.0171685>
- Veyrieras J-B, Goffinet B, Charcosset A (2007) MetaQTL: a package of new computational methods for the meta-analysis of QTL mapping experiments. *BMC Bioinformatics* 8:49. <https://doi.org/10.1186/1471-2105-8-49>
- Voigt CA (2014) Callose-mediated resistance to pathogenic intruders in plant defense-related papillae. *Front Plant Sci* 5:. <https://doi.org/10.3389/fpls.2014.00168>

- Voigt CA (2016) Cellulose/callose glucan networks: the key to powdery mildew resistance in plants? *New Phytol* 212:303–305. <https://doi.org/10.1111/nph.14198>
- Voigt CA, Somerville SC (2009) Chapter 4.4.5 - Callose in Biotic Stress (Pathogenesis): Biology, biochemistry and molecular biology of callose in plant defence: callose deposition and turnover in plant–pathogen interactions. In: Bacic A, Fincher GB, Stone BA (eds) *Chemistry, Biochemistry, and Biology of 1-3 Beta Glucans and Related Polysaccharides*. Academic Press, San Diego, pp 525–562
- Waliczek TM, Byrne DH, Holeman DJ (2015a) Growers’ and consumers’ knowledge, attitudes and opinions regarding roses available for purchase. *Acta Horti*
- Waliczek TM, Byrne DH, Holeman DJ (2015b) Growers’ and consumers’ knowledge, attitudes and opinions regarding roses available for purchase. *Acta Horti* 235–239. <https://doi.org/10.17660/ActaHort.2015.1064.26>
- Wang H, Yang Y, Li M, et al (2017) Residents’ preferences for roses, features of rose plantings and the relations between them in built-up areas of Beijing, China. *Urban For Urban Green* 27:1–8. <https://doi.org/10.1016/j.ufug.2017.06.011>
- Weber CA, Moore GA, Deng Z, Gmitter FG (2003) Mapping Freeze Tolerance Quantitative Trait Loci in a *Citrus grandis* × *Poncirus trifoliata* F1 Pseudo-testcross Using Molecular Markers. *J Am Soc Hortic Sci* 128:508–514. <https://doi.org/10.21273/JASHS.128.4.0508>
- Whitaker VM, Bradeen JM, Debener T, et al (2010a) *Rdr3*, a novel locus conferring black spot disease resistance in tetraploid rose: genetic analysis, LRR profiling, and SCAR marker development. *TAG Theor Appl Genet Theor Angew Genet* 120:573–585. <https://doi.org/10.1007/s00122-009-1177-0>
- Whitaker VM, Debener T, Roberts AV, Hokanson SC (2010b) A standard set of host differentials and unified nomenclature for an international collection of *Diplocarpon rosae* races. *Plant Pathol* 59:745–752. <https://doi.org/10.1111/j.1365-3059.2010.02281.x>
- Whitaker VM, Hokanson SC (2009) Partial resistance to black spot disease in diploid and tetraploid roses: general combining ability and implications for breeding and selection. *Euphytica* 169:421–429. <https://doi.org/10.1007/s10681-009-9976-6>
- Whitaker VM, Hokanson SC, Bradeen J (2007) Distribution of rose black spot (*Diplocarpon rosae*) genetic diversity in Eastern North America using amplified fragment length polymorphism and implications for resistance screening. *J Am Soc Hortic Sci* 132:534–540
- White MA, Steffy B, Wiltshire T, Payseur BA (2011) Genetic dissection of a key reproductive barrier between nascent species of house mice. *Genetics* 189:289–304. <https://doi.org/10.1534/genetics.111.129171>
- White MA, Stubbings M, Dumont BL, Payseur BA (2012) Genetics and evolution of hybrid male sterility in house mice. *Genetics* 191:917–934. <https://doi.org/10.1534/genetics.112.140251>
- Wiggers RJ, West JG, Taylor J (1997) Conidial germination and infection by *Diplocarpon rosae* on susceptible and resistant rose species. *Mycologia* 89:103–108. <https://doi.org/10.2307/3761178>

- Wissemann V (2003) CLASSIFICATION | Conventional Taxonomy (Wild Roses). In: Encyclopedia of Rose Science. pp 111–117
- Wissemann V, Ritz CM (2007) Evolutionary patterns and processes in the genus *Rosa* (*Rosaceae*) and their implications for host-parasite co-evolution. *Plant Syst Evol* 266:79–89. <https://doi.org/10.1007/s00606-007-0542-1>
- Wylie AP (1955) The history of garden roses, Part 2. *J R Hort Soc* 80:77–87
- Xue AG, Davidson CG (1998) Components of partial resistance to black spot disease (*Diplocarpon rosae* wolf) in garden roses. *HortScience* 33:96–99
- Yadava SK, Arumugam N, Mukhopadhyay A, et al (2012) QTL mapping of yield-associated traits in *Brassica juncea*: meta-analysis and epistatic interactions using two different crosses between east European and Indian gene pool lines. *TAG Theor Appl Genet Theor Angew Genet* 125:1553–1564. <https://doi.org/10.1007/s00122-012-1934-3>
- Yagi M, Kimura T, Yamamoto T, et al (2012) QTL analysis for resistance to bacterial wilt (*Burkholderia caryophylli*) in carnation (*Dianthus caryophyllus*) using an SSR-based genetic linkage map. *Mol Breed* 30:495–509. <https://doi.org/10.1007/s11032-011-9639-x>
- Yagi M (National I of FS, Onozaki T, Taneya M, et al (2006) Construction of a genetic linkage map for the carnation (*Dianthus caryophyllus*) by using RAPD and SSR markers and mapping quantitative trait loci (QTL) for resistance to bacteria wilt caused by *Burkholderia caryophylli*. *J Jpn Soc Hortic Sci Jpn*
- Yan M, Byrne DH, Klein PE, et al (2019) Black spot partial resistance in diploid roses: QTL discovery and linkage map creation. *Acta Hortic* 1232:135–141. <https://doi.org/10.17660/ActaHortic.2019.1232.21>
- Yang B, Jiang Y, Rahman MH, et al (2009) Identification and expression analysis of WRKY transcription factor genes in canola (*Brassica napus* L.) in response to fungal pathogens and hormone treatments. *BMC Plant Biol* 9:68. <https://doi.org/10.1186/1471-2229-9-68>
- Yang Q, Balint-Kurti P, Xu M (2017) Quantitative disease resistance: dissection and adoption in maize. *Mol Plant* 10:402–413. <https://doi.org/10.1016/j.molp.2017.02.004>
- Yokoya K, Kandasamy KI, Walker S, et al (2000) Resistance of roses to pathotypes of *Diplocarpon rosae*. *Ann Appl Biol* 136:15–20. <https://doi.org/10.1111/j.1744-7348.2000.tb00003.x>
- Zhang J, Wang F, Liang F, et al (2018) Functional analysis of a pathogenesis-related thaumatin-like protein gene *TaLr35PR5* from wheat induced by leaf rust fungus. *BMC Plant Biol* 18:76. <https://doi.org/10.1186/s12870-018-1297-2>
- Zhu M, Zhao S (2007) Candidate gene identification approach: progress and challenges. *Int J Biol Sci* 3:420–427
- Zlesak DC, Nelson R, Harp D, et al (2017) Performance of landscape roses grown with minimal input in the north-central, central, and south-central united states. *HortTechnology* 27:718–730. <https://doi.org/10.21273/HORTTECH03681-17>

- Zlesak DC, Whitaker VM, George S, Hokanson SC (2010) Evaluation of roses from the Earth-Kind® trials: black spot (*Diplocarpon rosae* wolf) resistance and ploidy. HortScience 45:1779–1787. <https://doi.org/10.21273/HORTSCI.45.12.1779>
- Zurn JD, Zlesak DC, Holen M, et al (2018) Mapping a novel black spot resistance locus in the climbing rose Brighth eyes™ ('radbrite'). Front Plant Sci 9:1730. <https://doi.org/10.3389/fpls.2018.01730>
- Zurn JD, Zlesak DC, Holen M, et al (2020) Mapping the black spot resistance locus Rdr3 in the shrub rose 'George Vancouver' allows for the development of improved diagnostic markers for DNA-informed breeding. Theor Appl Genet. <https://doi.org/10.1007/s00122-020-03574-4>

Annexes

Annex 1 : Short explanation of two dimensional scan

The main objective of the two dimensional scan is to investigate the possible QTL models by scanning the genome for pairs of QTLs explaining the data. The two dimensional scan can be performed with normal model (for normally distributed phenotypes) and with a binary model (for binary traits). Two dimensional scan is performed using the *scantwo* function provided by the R/qtl package. Like for *scanone*, this function performs the genome scan as well as the data permutation to calculate the LOD thresholds. But unlike one dimensional scan, the two-QTL scan tests several possible models and calculates the LOD scores comparing the fit of the four models tested: H_i , the full model where two QTLs are allowed to interact; H_a , the additive model where QTLs assumed to act additively; H_1 , all the possible the single-QTL models and H_0 , the null model with no QTL explaining the data (see equation 1 extracted from Broman and Sen (2009)). Four principal LOD scores are then calculated: LOD_i that measures the improvement in fit of the two-locus model over the null model, LOD_a that measures the improvement in fit of two additive loci over the null model, LOD_i that measures specifically the improvement of the model by adding the interaction (full model over additive only) and the LOD_1 that is the LOD score for a one dimensional scan. If the LOD scores previously described are high, evidence of additivity (LOD_a), interaction (LOD_i) or both (LOD_i) between two QTLs can be demonstrated.

$$H_f: y = \mu + \beta_1 q_1 + \beta_2 q_2 + \gamma(q_1 \times q_2) + \varepsilon$$

$$H_a: y = \mu + \beta_1 q_1 + \beta_2 q_2 + \varepsilon \quad (\text{Equation 1 extracted from Broman and Sen (2009)})$$

$$H_1: y = \mu + \beta_1 q_1 + \varepsilon$$

$$H_0: y = \mu + \varepsilon$$

With y the observed phenotype, μ the average phenotype, β_1 and β_2 the effect of QTL q_1 and q_2 respectively, γ the effect of the interaction between q_1 and q_2 and ε the residual variance.

However, if the *scanone* shows evidence for a QTL on a linkage group, the LOD_i and LOD_a will be large, which will not necessarily tell us if there is evidence of a second QTL in that same linkage group. That is why, LOD_{i1} and LOD_{a1} were described in R/qtl. They compare the full model to the single-QTL model (LOD_{i1}) and the additive model to single-QTL model (LOD_{a1}). Therefore, LOD_{i1} is used instead of LOD_i to assess the evidence for second QTL allowing epistasis as well as LOD_{a1} instead of LOD_a to assess the evidence of a second QTL that is additive and assuming no epistasis. To control for false positives that can detect spurious QTLs in the genome, a permutation test is performed. However, the permutation test performed in the case of two dimensional scan requires an important computation time and was, therefore, run on the server available at the institute. That way, 20 processors were used to split the job and to perform the 1,000 permutations quicker for each scoring year of all populations. The output of the permutation test gives estimated thresholds for all the LODs mentioned above at 5% and 10% significance levels (Broman and Sen 2009). To assess evidence for additional QTLs detected with the two-QTL scan, I decided to use

5% significance levels. The *summary* function will give all the pairs of loci that meet the permutation test thresholds at the chosen significance level.

REFERENCES:

Broman K, Sen S (2009) A Guide to QTL Mapping with R/qtI. Springer-Verlag, New York

Annex 2 : Explanation of two-way pseudo-testcross strategy and phasing in heterozygous genotypes

Two-way pseudo-testcross mapping strategy was designed for map generation of highly heterozygous individuals. This strategy is based on the selection of single-dose markers present in one parent and absent in the other. Therefore, to build the parental genetic maps, two “pseudo backcrosses”-like populations are artificially generated with the genotyping of the markers from one parent for which the phasing is known, and the other parent will be considered as homozygous “aa” for which the phasing is not known (Grattapaglia and Sederoff 1994; Plomion and Durel 1996).

In the figure, one homologous chromosome pair is represented for each genotype with the genotyping and phasing known at six loci. The crossing (X) includes meiosis steps for each parent (with possible recombinations between the chromosomes of the homologous pair) and the hybridization step. The individuals of the mapping population inherit one chromosome from the gamete of female parent and one chromosome from the gamete of male parent. Parental alleles can be followed in the pseudo-backcross progeny on the basis of testcross markers inherited from either of the two parents of the hybrid. Therefore, only markers heterozygous in one parent are used to build separated parental genetic maps (colored homologous chromosome pair), which sets artificially the other parent as homozygous (gray homologous chromosome pair). In this manuscript, we call male map, the genetic map built with the markers heterozygous in the male parent (here the hybride of *Rosa wichurana*, called RW), and the female map refers to the genetic map built with the markers heterozygous in the female parent (here either *Rosa chinensis* ‘Old Blush or OB, *Rosa hybrida* ‘The Fairy’ or TF or the genotype H190). For the female map, markers of type <abxaa> were used while for the male map, markers of type <aaxab> were used.

JoinMap software V4.1 was used to build separated parental linkage maps and to determine the parental phases (van Oijen 2019). The codification of the phases in JoinMap uses two numbers, 0 or 1, and inside the braces, we can find information about the phases from the parental genotypes. In the case the genotyping of both parents is known, the phases can be calculated and JoinMap will note the phase with two numbers: {10} or {01} or {00} or {11} according to the phases of both parents. However, in our case, one parental genotype was considered “aa”, therefore the phasing could not be calculated and was noted with a dash (“-”). So for markers like <abxaa>, only the phases of the markers from the female parent were known, i.e. {1-} or {0-}, and conversely for markers like <aaxab>, only the phases from the male parents were known, i.e. {-1} or {-0}.

To load the genetic maps in R and to be able to use Rqtl package for QTL mapping, it is necessary to convert the genotypes with the coding presented in the figure that corresponds to a backcross-like situation (Broman and Sen 2009). However, the software is no longer “aware of the phases”, so when the effect plots are generated, the software will calculate the mean score for the genotype “AA”

(corresponding to code 1) and “AB” (corresponding to code 2) at a specific marker. But with coding we had to do, if the phase was {1-} or {-1}, what was noted “AA” and “AB” in the effect plot actually corresponded to the opposite as 2 refers to genotyping “aa” and 1 to genotyping “ab”. Therefore, it is important to check the phases at the locus of interest and to switch the alleles if necessary.

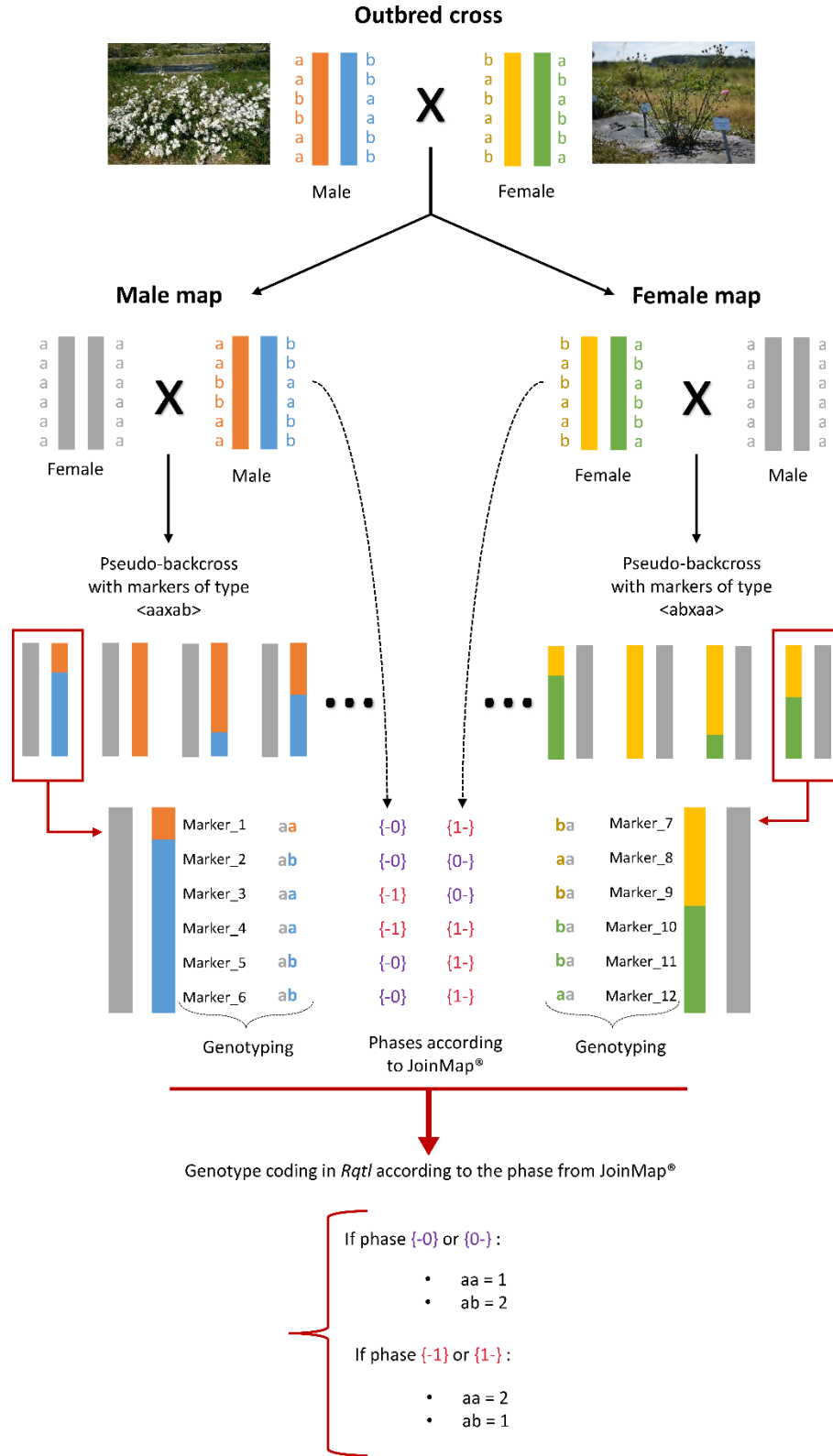


Figure 1: Two-way pseudo-testcross strategy and phasing illustration to introduce the coding used for the maps in *RqtI* (Picture credits: T. Thouroude and M. Tisserand)

REFERENCES:

Broman K, Sen S (2009) A Guide to QTL Mapping with R/qtl. Springer-Verlag, New York

Grattapaglia D, Sederoff R (1994) Genetic linkage maps of *Eucalyptus grandis* and *Eucalyptus urophylla* using a pseudo-testcross: mapping strategy and RAPD markers. *Genetics* 137:1121–1137

Plomion C, Durel C (1996) Estimation of the average effects of specific alleles detected by the pseudo-testcross QTL mapping strategy. *Genet Sel Evol* 28:223. <https://doi.org/10.1186/1297-9686-28-3-223>

van Oijen (2019) JoinMap® 5.0 - Software for the calculation of genetic linkage maps in experimental populations of diploid species. Version 5.0. Kyazma B.V., Wageningen. URL <https://www.kyazma.nl/index.php/JoinMap/General/>

Annex 3 : Diplocarpon rosae infectious cycle on the leaves of the hybrid of Rosa wichurana RW with different ages

The infectious cycle on *R. x wichurana* (RW) leaves was described with leaves that were randomly sampled on the shoots. This experiment allowed us to observe the differences between leaves of different ages at macroscopic and microscopic levels. The leaves sampled for this experiment were indeed at different stages of their development which can explain the differences of fungal growth observed on the leaves of the partial resistant genotype RW. This result was surprising as it was not observed on the leaves of the susceptible genotype OB. Because of problems growing plants, we could not carry out the experiment for all the time points again by separating the leaves by age but subsequent experiments were carried out to further investigate this phenomenon on whole plants inoculated for the transcriptomic assay and also using a single time point during a detached leaf assay. The results on the effect of the leaf age on the partial resistance observed on RW were presented in chapter 3.

An additional time point at 5dpi for RW was studied to investigate the time point of appearance of callose deposition around the penetration point in some leaves. At 5dpi, callose was deposited in almost all the sites observed, which was not the case at 3dpi. This time point was therefore considered for the transcriptomic analysis of [chapter 4](#).

The aniline blue staining visualized with a long pass filter (LP420, DAPI-BH2) was used to describe the cycle (see [chapter 3](#)). The orange color of the cuticle is due to the wide range of photons that are caught with this long pass filter.

A brown hole was often associated with callose deposition and fungal growth on whole plants inoculated with DiFRA67 for all the independent inoculations and for different experiments but this feature was not observed during detached leaf assay. Further analyses need to be carried out to identify the origin of such features.

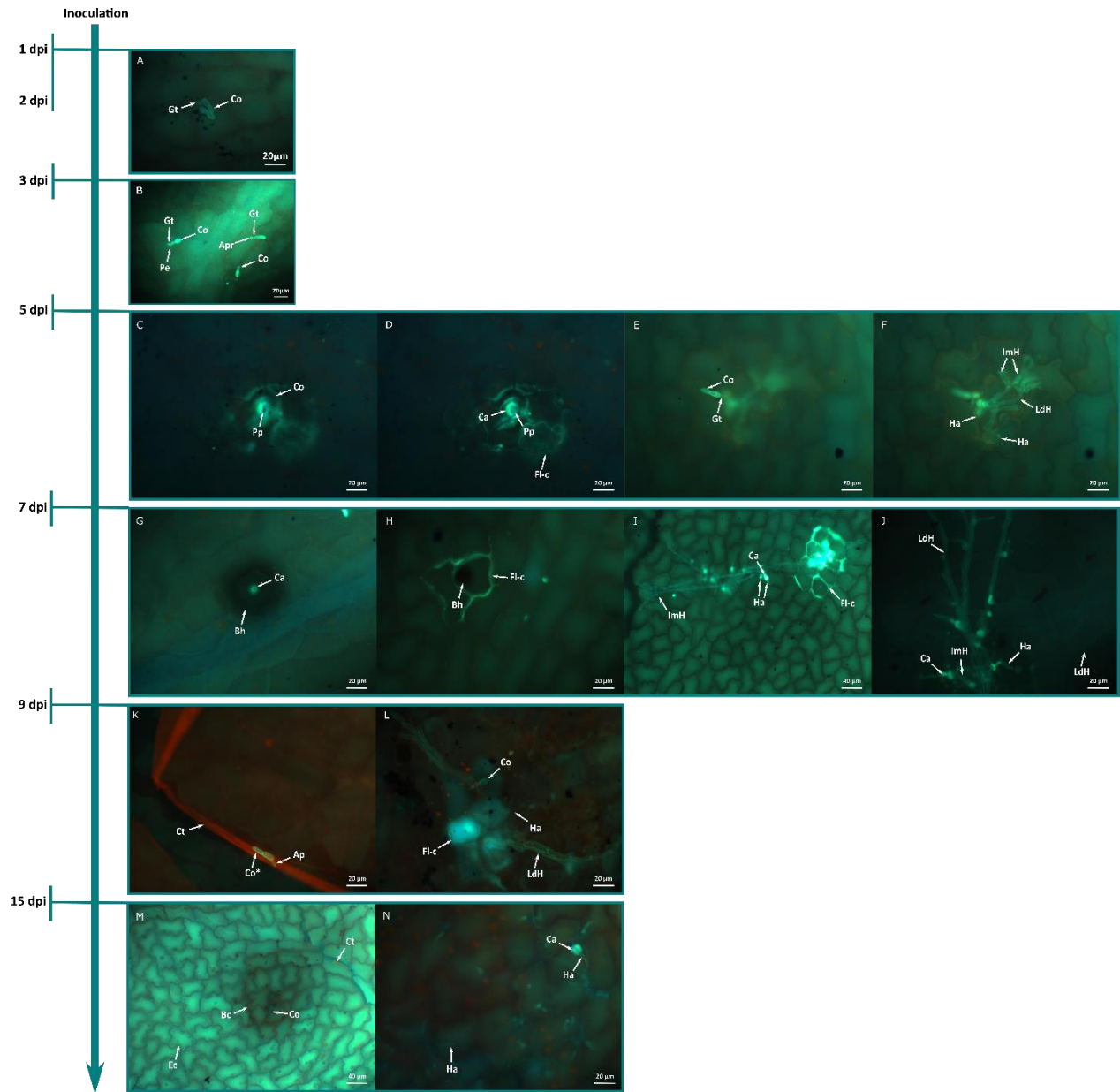


Figure 1: Fluorescent microscope photographs of *Diplocarpon rosae* infectious cycle on the resistant genotype *R. x wichurana* (RW)

A: Germinated conidium [Co] with a well-defined germ tube [Gt] at 2dpi; **B:** Two germinated conidia [Co] at 3dpi with a germ tube [Gt] and with one showing an appressorium [Apr] and another one showing a penetration peg [Pe]; **C-D and E-F:** Two z levels showing the germination [Gt] of conidia [Co] through the cuticle on RW at 5dpi. The penetration was associated with callose deposition [Ca] around the penetration pore [Pp] (C-D). In some leaves further fungal growth was observed with short subcuticular hyphae [LdH] from which intramural hyphae [ImH]. Haustoria [Ha] can be observed in these infected leaves; **G-H and I-J:** The infection sites at 7dpi on RW leaves exhibited very different types of fungal growth and plant responses. Callose deposition [Ca] at the penetration point was often associated with a black hole [Bh] in whole plant inoculations (G). Black holes [Bc] were also found associated with a small number of fluorescing cells [Fl-c] (H). In some leaves, extended fungal development under the cuticle was observed with short subcuticular hyphae [LdH] from which short intramural hyphae [ImH] and small haustoria [Ha] mounted with a callose deposition [Ca] around the haustorial neck (I-J); **K-L:** Leaves of RW at 9dpi showed again two situations. The first was fungal penetration arrested at a very early stage with germinated conidia [Co*] attached to a broken cuticle [Ct] thanks to an appressorium [Ap] (K). The second type of situation was found in leaves exhibiting extended fungal growth with fluorescing cells [Fl-c] at the penetration site, long distance hyphae [LdH] and haustoria [Ha]; **M-N:** Two contrasted types of leaves were found at 15dpi with some exhibiting conidia associated with no fungal growth under the cuticle [Ct] but areas exhibiting brown epidermal cells [Bc] were observed (M), and others exhibiting a fungal growth that reached lower levels of mesophyll with haustoria [Ha] and callose [Ca] around the haustorial neck (N). [Ec] stands for epidermal cells.

Annex 4 : Limited effect of leaf age on Diplocarpon rosae development on 'Old Blush' leaves

Different components of partial resistance were assessed on two groups of leaves with different ages challenged with a monosporial isolate DiFRA67 during a whole plant inoculation (group 1 with leaves that were still growing and group 2 with leaves that finished their growth). No significant differences in the percentage of the leaf infected by DiFR67 was observed between young (group 1) and old (group 2) leaves for OB plants with an average of 70% (see Figure 36A). Among the infected leaves, the leaflet area with symptoms (LAS) was similarly important for young and old leaves of OB with in average 10 to 25% of the leaflet infected, and no difference between the number of leaflets exhibiting chlorosis or that were prematurely drop was observed (see Figure 36B-E-F).

However, the largest lesion length (LL) was significantly more important on young leaves of OB than on old ones with in average 6.1mm on leaves from group 1 whereas the largest lesion measured 4.6mm on leaves from group 2 at 15dpi (see Figure 36C). Indeed, macroscopically, we observed the same difference of lesion length between leaves of different ages that were sampled from OB plants and inoculated with DiFRA67 using a detached leaf assay. Young leaves of OB exhibited, on average, larger black spots with a more complex hyphal network than old leaves (see Figure 1A-B-C). In both cases, long distance hyphae [LdH] were developed but the ones found in old leaves were shorter. Cell collapse [Cc] was described on young leaves of OB as well as on old ones. However, the area collapsing around the long distance hyphae seemed wider on old leaves but it should be necessary to quantify it to be sure (see Figure 1F-H-I).

Microscopically, no clear difference of pathogen development as well as leaf reaction was observed between the leaves of different ages of OB genotype challenged with DiFRA67 (see Figure 2A-C-E-G). In both cases, long distance hyphae [LdH] were observed with intramural hyphae [ImH] and short intercellular hyphae [IeH]. Full-grown haustoria and haustoria under development [Ha] were observed in both types of leaves as well as epidermal cell fluorescence [FI-c] when they were invaded. Some fluorescent cells also exhibited granular texture and others clear circles of fluorescence [FI-c*] were observed probably corresponding to callose vesicles [Cav]. Callose deposition [Ca] around the haustorial neck was also observed in both cases (see Figure 2B-D-F-H).

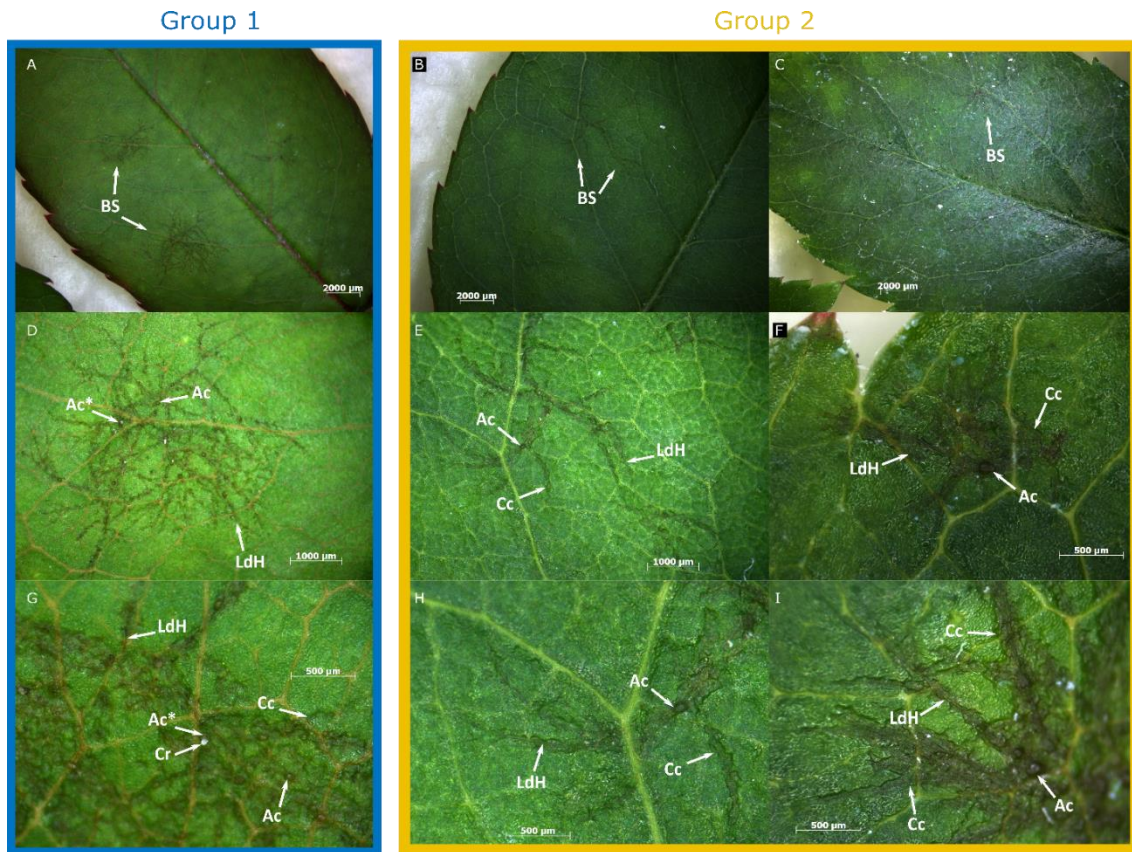


Figure 1: Macroscopic observations of ‘Old Blush’ (OB) leaves with different ages (young: group 1, and old: group 2) at the time of inoculation with DiFRA67

A: Black spots [BS] on young leaves of OB (group 1) at magnification 0.65x; **B-C:** Black spots [BS] on old leaves of OB (group 2) at magnification 0.65x; **D-G:** Close up of black spots on young leaves of OB (2x and 5x magnification) where long distance hyphae [LdH], non-mature [Ac] and mature acervuli [Ac*] with conidia released [Cr] can be observed as well as epidermal cell collapsing [Cc] around the hyphae; **E-F-H-I:** Close up of black spots observed on old leaves of OB with long distance hyphae [LdH], non-mature [Ac] and epidermal cell collapsing [Cc] around the hyphae.

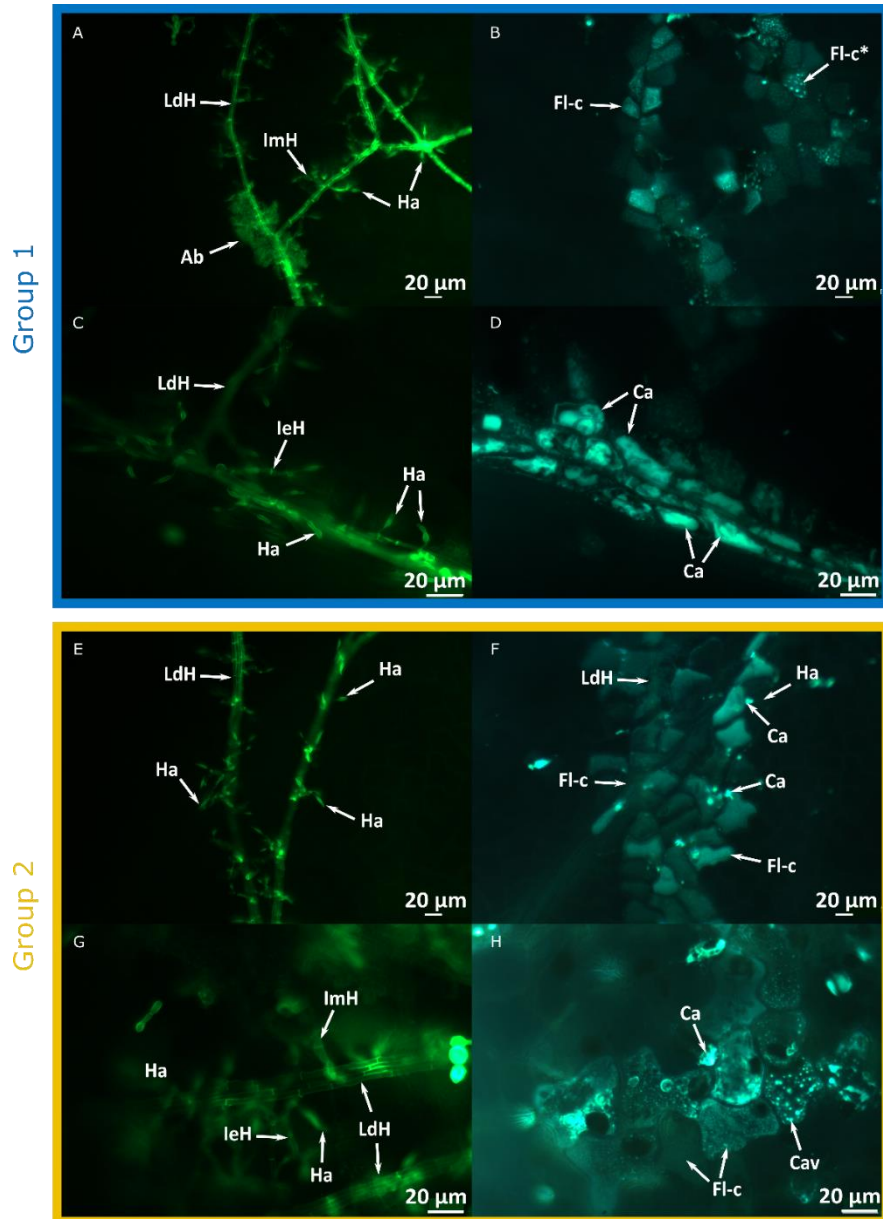


Figure 2: Fluorescence microscopy with a double staining of 'Old Blush' (OB) leaves of different ages (young: group 1, and old: group2)

A-C and E-G: Photographs of fluorescence microscopy using the GFP-BH2 filter to visualize the fungal development under the cuticle after infection of young leaves (Group 1, A-C) and old leaves (Group 2, E-G) of OB. Different fungal structures can be observed like long distance hyphae (or subcuticular hyphae) [LdH], intramural hyphae [ImH], intercellular hyphae [IeH], acervulus base [Ab] and haustoria [Ha]; **B-D and F-H:** Photographs of the same zone using DAPI-BH2 filter to visualize the plant response with callose around the long distance hyphae [LdH]. Callose deposition [Ca] around the haustorial neck of full grown haustoria [Ha] and inside the epidermal cells (D) were observed as well as two types of fluorescing epidermal cells. Fluorescing cells with a granular texture [Fl-c] and others with defined callose vesicles [Cav] in them [Fl-c*].

Annex 5 : Mapping parameter choice for STAR software

Special care on the choice of the parameters for mapping was taken as we had two types of situation during the mapping: reads from a heterozygous *Rosa chinensis* 'Old Blush' (OB) were mapped on a homozygous *R. chinensis* 'Old blush' (HapOB) genome for the samples describing a compatible interaction, and reads from the hybrid of *Rosa wichurana* (RW) were mapped on HapOB genome for samples describing an incompatible interaction. Indeed, we needed to consider these two situations separately since the possible mismatches between OB against HapOB (mapping of the same species) would be different than the ones between RW and HapOB (mapping of different species) and, therefore, required specific parameters of mismatch ("outFilterMismatchNmax").

Several tests were performed where I used a different number of mismatches that were allowed during the mapping. Only two samples were used from both of the genotypes to investigate the best mismatch parameters. From tests T1 to T4, parameters of minimum intron length and maximum number of mismatches recommended by other colleagues were tested. From tests T5 to T10, the intron length was set to 20 and I tested different mismatch parameters to find the most suitable one for each genotype.

Table 1: Mapping parameters tested and effect on the percent of reads mapped in each category (Unique mapping, Multiple mapping, Too many, Too short) for both genotypes ('Old Blush', OB and *R. x wichurana*, RW)

Test	Mapping Parameters			Genotype											
	alignIntronMin	outFilterMismatchNmax	Percent of mismatch	OB					RW						
				Time (min)	Total ^a	Unique ^b	Multiple ^c	Too many ^d	Too short ^e	Time (min)	Total ^a	Unique ^b	Multiple ^c	Too many ^d	Too short ^e
T1	10	6	2.00	26	93.28	90.71	2.57	2.54	4.16	19	89.10	85.82	3.28	3.35	7.50
T2	10	10	3.33	27	94.30	91.61	2.69	2.54	3.14	21	91.13	87.62	3.51	3.36	5.46
T3	20	6	2.00	26	93.30	90.72	2.58	2.54	4.13	30	89.14	85.85	3.29	3.35	7.46
T4	20	10	3.33	27	94.32	91.62	2.70	2.54	3.11	32	90.91	87.65	3.26	3.37	5.41
T5	20	12	4.00	27	94.54	91.81	2.73	2.54	2.90	29	91.63	88.05	3.58	3.36	4.94
T6	20	14	4.67	28	94.68	91.93	2.75	2.54	2.76	32	91.94	88.32	3.62	3.36	4.64
T7	20	16	5.33	28	94.77	92.01	2.76	2.54	2.65	21	92.19	88.54	3.65	3.36	4.40
T8	20	18	6.00	NA	94.85	92.08	2.77	2.54	2.58	NA	92.37	88.70	3.67	3.36	4.22
T9	20	30	10.00	39	95.02	92.23	2.79	2.54	2.41	48	92.80	89.09	3.71	3.36	3.79
T10	20	50	16.67	32	95.06	92.27	2.79	2.54	2.37	NA	92.90	89.18	3.72	3.36	3.68

Note: All the tests were performed on OB_I_0_A and RW_I_0_A to gain time as the mapping for one sample took an hour.

The final parameters chosen for each genotype are displayed in red.

a Percent of all the reads mapped on the reference genome from the trimmed data;

b Percent of reads mapped at a unique location in the genome;

c Percent of reads mapping in several locations with high scores (between 1 and 10);

d Percent of reads which seed alignment was too short to be considered as a real mapping, i.e. by default, here, less than 2/3 of the total read length (forward + reverse).

The most suitable mismatch parameter is the one that allows a high number of reads to map without increasing the number of reads that have multi-mapping. So for each genotype separately, I choose the smallest number of mismatches after which the number of unique mapping did not increase significantly (Table 1). Interestingly, the number of multi-mapping reads did not increase too much (less than 0.5%) for OB after 12 mismatches while for RW, it stabilized after 16 mismatches. Moreover, it seems that by increasing the number of mismatches, we were able to decrease the percent of reads that were considered as unmapped because the alignment length was too short (see (e) in Table 1).

The parameters that were chosen for each genotype are reported in red in Table 1. To conclude, a maximum of 10 mismatches were set for OB and 16 for RW.

Moreover, specific minimum (`AlignIntronMin`) and maximum (`AlignIntronMax`) intron lengths were adapted to the genome characteristics using two scripts to extract introns from the “.gff3” files (`extract_intron_gff3_from_gff3.py` from Chanaka Mannapperuma) and to calculate the maximum and minimum intron lengths from the reference genome (`intron_length.akw` from Nathan Weeks). The minimum intron length found was **39bp** and the maximum **15,670bp**. An additional test (not represented on Table 1) was carried out to see the effect of a large intron length on the reads mapped with the default parameter of 60,000bp compared to a more moderate maximum intron length of 20,000bp that was close to the maximum calculated. In figure 1, an example of spanned reads reported in chromosome 3 was shown. The first window displays the results of a test where 60,000bp maximum intron length was used and the second panel when 20,000bp was used. Spanned reads can be observed in the first panel that starts around 10,030kb and ends after 10,050kb (spanned over a distance greater than 20,00bp). We can see that the maximum intron length is important as reads can be spanned from one gene to the next one if the maximum intron length is set too high and is particularly important for the cases where the distance between two genes is smaller than the maximum intron length set for the mapping. In the end, the maximum intron length chosen was **20,000bp** (close to the real intron length of the genome but allowing the discovery of new genes with longer but reasonable intron length). The minimum intron length was set to **20bp**.



Figure 1: Effect on mapping of the parameter 'AlignIntronMax' visualized by IGV software

The first panel shows a zone on chromosome 3 that was mapped with the default intron length parameter (60,000bp) of the sample OB_I_0_A, and the second panel shows the same zone using the calculated intron length of 20,000bp. The green lines on the first panel show the reads that were spanned over the second gene as the maximum intron length was higher than the distance between the genes.

Titre : Génétique et génomique de la résistance à la maladie des taches noires chez le rosier de jardin

Mots clés : Maladie des taches noires, *Diplocarpon rosae*, *Rosa*, résistance partielle, QTL, RNAseq.

Résumé : La maladie des taches noires (TN, causée par *Diplocarpon rosae*) représente une menace majeure pour la filière des rosiers de jardin. En effet, avec la réduction voire l'interdiction de l'utilisation de produits phytosanitaires et la demande croissante de rosiers résistants, il est essentiel d'étudier les mécanismes de résistance à cette maladie. Jusqu'à présent, les recherches se sont principalement concentrées sur l'étude des gènes majeurs (gènes *Rdr*) mais ce type de résistance est connu pour être moins durable. Une résistance partielle à la TN a été décrite chez les génotypes associés à *Rosa wichurana* dont la ségrégation quantitative est mal connue. Cette thèse a permis d'étudier les bases génétiques et moléculaires de la résistance partielle de *Rosa x wichurana* (RW) à la TN. Tout d'abord, il a été montré que la résistance partielle de ce génotype est principalement contrôlée par deux loci quantitatifs (QTL) situés sur les groupes de liaison B3 et B5 ; les intervalles de confiance de ces QTL ont été réduits à 10cM en utilisant une approche de méta-analyse sur trois populations interconnectées. Les QTL en B3 semblent affecter la pénétrance et la sévérité de la maladie alors que

les QTL en B5 n'affectent que la pénétrance. La résistance à la TN chez RW dépend aussi de l'âge de la feuille. Par une approche histologique, un dépôt de callose autour du point de pénétration du pathogène a été observé sur les feuilles jeunes et vieilles mais une réponse rapide d'hypersensibilité (HR) n'a été observée que sur les vieilles feuilles. Une étude transcriptomique a permis de caractériser la réponse de RW : dans un premier temps, une réponse rapide de type PTI (immunité basale) conduit à l'activation de gènes impliqués dans le dépôt de callose, puis une réponse ETI (immunité déclenchée par des effecteurs) conduit à une HR. Au contraire, la réponse PTI du génotype sensible *Rosa chinensis* 'Old Blush' (OB) est inhibée aux premiers stades de l'infection et une ETI partielle se met en place, impliquant probablement une reconnaissance spécifique d'effecteurs fongiques. Cette étude nous a permis de caractériser finement l'interaction entre *D. rosae* et un génotype sensible (OB) d'une part, et un génotype résistant (RW) d'autre part, ce qui ouvre la voie au clonage de gènes et à la sélection assistée par marqueurs.

Title: Genetics and genomics of black spot disease resistance in garden roses

Keywords: Black spot disease, *Diplocarpon rosae*, *Rosa*, partial resistance, QTL, RNAseq.

Abstract: Black spot disease (BSD, caused by *Diplocarpon rosae*) represents a major threat for garden roses. Indeed, with the reduction or even sometimes the prohibition of agrochemical use and the increasing demand for roses with a higher degree of resistance, it is essential to investigate the mechanisms of resistance to BSD in roses. So far, research has mainly focused on the study of major genes (*Rdr* genes), but this type of resistance is known to be less durable. Partial resistance to black spot disease was described in *Rosa wichurana* genotypes for which quantitative segregation is not well known. This thesis allowed us to study the genetic and molecular bases of BSD resistance in *Rosa x wichurana* (RW). First, we showed that the partial resistance to black spot disease is mainly controlled by two quantitative trait loci (QTLs) located on linkage groups B3 and B5; the confidence intervals of the QTLs were reduced to 10cM using a meta-analysis approach of three interconnected populations. The QTL on B3 seems to affect the penetrance and the severity of

the disease while the QTLs on B5 only affects the penetrance. The disease resistance of RW is leaf age-dependent. By histological approach, callose deposition at pathogen penetration sites was observed in both young and old leaves but a quick hypersensitive response (HR) was only found in old leaves. A transcriptomic analysis made it possible to characterize the RW defense response: first, a quick immune response (PTI) leads to the activation of genes involved in callose deposition in papillae, and then an effector-specific response (ETI) results in a HR. On the contrary, the PTI response is inhibited at the first stages of infection in the susceptible genotype *Rosa chinensis* 'Old Blush', which exhibited a partial ETI probably involving specific recognition of fungal effectors. This study allowed us to precisely characterize the interaction between susceptible (OB) and resistant (RW) genotypes, which paves the way for gene cloning and for marker-assisted selection.